

FOURTH INTERNATIONAL CONFERENCE
ON
STABILITY OF SHIPS AND OCEAN VEHICLES

STAB '90

VOL. I

SEPTEMBER 24 - 28, 1990
NAPLES (ITALY)

FOURTH INTERNATIONAL CONFERENCE
ON
STABILITY OF SHIPS AND OCEAN VEHICLES

STAB '90

SEPTEMBER 24 - 28, 1990

NAPLES (ITALY)

ORGANIZED BY

DEPARTMENT OF NAVAL ENGINEERING - UNIVERSITY «FEDERICO II» OF NAPLES

UNDER THE HIGH PATRONAGE OF THE PRESIDENT OF THE ITALIAN REPUBLIC

UNDER THE PATRONAGE OF THE:

- Ministry of Balance and Economic Programming;
- Ministry of Defense;
- Ministry of the Education;
- Ministry of the University and the Scientific Research;
- Ministry of the Mercantile Marine;
- Campania Region;
- Municipality of Naples;
- University «Federico II» of Naples;
- Naval University Institut of Naples.

PROCEEDINGS

Published by

Department of Naval Engineering of the University «Federico II» of Naples

QUARTA CONFERENZA INTERNAZIONALE
SULLA
STABILITÀ DELLE NAVI E DEI MEZZI OFFSHORE

STAB '90

NAPOLI, 24 - 28 SETTEMBRE 1990

ORGANIZZATA DAL

DIPARTIMENTO DI INGEGNERIA NAVALE DELL'UNIVERSITÀ «FEDERICO II» DI NAPOLI

SOTTO L'ALTO PATRONATO DEL PRESIDENTE DELLA REPUBBLICA

SOTTO IL PATRONATO:

- del Ministero del Bilancio e della Programmazione Economica;
- del Ministero della Difesa;
- del Ministero della Pubblica Istruzione;
- del Ministero dell'Università e della Ricerca Scientifica;
- del Ministero della Marina Mercantile;
- della Regione Campania;
- del Comune di Napoli;
- dell'Università «Federico II» di Napoli;
- dell'Istituto Universitario Navale di Napoli.

The National Research Council and Tecnomare S.p.A., with hearty cooperative attitude, enabled us to publish the Proceedings by providing the funds to cover expenses needed for printing.

The Organizing Committee expresses here his sincerest gratitude to National Research Council and Tecnomare S.p.A.

The Organizing Committee expresses also his sincerest gratitude to following sponsors of the Conference:

<ul style="list-style-type: none">- ARMARE S.R.L.- AUGUSTEA S.p.A.- AZIENDA AUTONOMA DI CURA, SOGGIORNO E TURISMO - NAPOLI- BANCA NAZIONALE DELL'AGRICOLTURA- CAMERA DI COMMERCIO, INDUSTRIA, ARTIGIANATO E AGRICOLTURA DI NAPOLI- CAREMAR- CE.TE.NA. S.p.A. GENOVA- CONSORZIO ESERCENTI PICCOLE IMPRESE ARMATORIALI DEL MEZZOGIORNO- CONFITARMA- CONSIGLIO NAZIONALE DELLE RICERCHE- FRATELLI D'AMICO ARMATORI- I.N.S.E.A.N. - ROMA- ISTITUTO UNIVERSITARIO NAVALE - NAPOLI- MARNABI S.R.L.	<ul style="list-style-type: none">- ASSESSORATO AL TURISMO DELLA REGIONE CAMPANIA- MINISTERO DELLA PUBBLICA ISTRUZIONE- NAVALTEC PAOLILLO S.a.S - NAPOLI- NAVARMA S.p.A.- ORDINE DEGLI INGEGNERI DELLA PROVINCIA DI NAPOLI- RIMORCHIATORI NAPOLETANI- SOCIETÀ ESERCIZIO RIMORCHI E SALVATAGGI S.r.L.- SPERRY MARINE S.p.A.- STARGAS S.p.A. VENEZIA- STUDIO TECNICO NAVALE - ING. ANDALÒ- NAPOLI- TECNOMARE S.p.A.- TIRRENIA SOCIETÀ DI NAVIGAZIONE- UNIONE DEGLI INDUSTRIALI DELLA PROVINCIA DI NAPOLI- UNIVERSITÀ DEGLI STUDI DI NAPOLI
---	---

TECNOMARE S.p.A.

Tecnomare performs applied research, engineering and systems supply in the marine field. Primary activities cover the application of innovative technologies to the knowledge, protection, exploration and exploitation of the marine and submarine resources.

Among the areas of interest are offshore platforms, subsea production, remote control; subsea trenching vehicles, NDT machines; modelling, monitoring and protection of the marine environment; large marine civil works and tunnelling; simulation, software. .

COMITATO D'ONORE

HONORARY COMMITTEE

S.E. Cardinale MICHELE GIORDANO	Arcivescovo Metropolita di Napoli
On. FERDINANDO CLEMENTE di S. LUCA	Presidente della Giunta Regione Campania
On. PAOLO CIRINO POMICINO	Ministro del Bilancio e Programmazione Economica
On. MINO MARTINAZZOLI	Ministro della Difesa
On. ANTONIO RUBERTI	Ministro Università e Ricerca Scientifica
On. SERGIO MATTARELLA	Ministro della Pubblica Istruzione
On. CARLO VIZZINI	Ministro della Marina Mercantile
Ammiraglio FILIPPO RUGGIERO	Capo di Stato Maggiore Marina Militare
Dott. ANGELO FINOCCHIARO	Prefetto di Napoli
Dott. VITO MATTERA	Questore di Napoli
Prof. CARLO CILIBERTO	Rettore Università degli Studi «Federico II»
Prof. GENNARO FERRARA	Rettore Istituto Universitario Navale
On. AMELIA CORTESE ARDIAS	Assessore P. I. e Cultura Regione Campania
On. RAFFAELE COLUCCI	Assessore Turismo, Sport e Spettacolo Regione Campania
On. PIETRO LEZZI	Sindaco di Napoli
Dott. SALVATORE SCOGNAMIGLIO	Assessore al Provveditorato Generale Economato e Giardini Comune di Napoli
Ing. GIANDOMENICO LOMBARDI	Capo Ispettorato Tecnico Marina Mercantile
Cav. SALVATORE D'AMATO	Presidente Unione Industriali Provincia di Napoli
Dott. FRANCO PECORINI	Amministratore Delegato Tirrenia S.p.A.
Com.te LUIGI FIORENTINO	Amministratore Delegato CAREMAR
Prof. GIAMPIERO PUPPI	Presidente Tecnomare S.p.A.
Prof. ARMANDO ALBINI MARINI	Presidente Ordine Ingegneri Provincia di Napoli
Ammiraglio VITTORIO MARULLO	Presidente CE.TE.NA. S.p.A.
Ammiraglio LUIGI RICCIARDI	Presidente I.N.S.E.A.N.
Ing. SALVATORE PIANURA	Presidente STARGAS S.p.A.

INTERNATIONAL PROGRAMME COMMITTEE

Prof. A. ALAEZ	Director, Canal de Experiencia Hidrodinamicas of Madrid - Spain
Prof. R. BHATTACHARYYA	Superintendent, United States Naval Academy of Annapolis - U.S.A.
Dr. P. BLUME	Head of Seakeeping Depart., Hamburg Ship Model Basin - F. R. of Germany
Dr. P. BOGDANOV	Director, Bulgarian Ship Hydrodynamics Centre of Varna - Bulgaria
Prof. A. CARDO	Director, Institute of Naval Architecture, University of Trieste - Italy
Prof. P. CASSELLA (Chairman)	Department of Naval Engineering, University «Federico II» of Naples - Italy
Dr. J. C. DERN	Director, Bassin d'Essais des Carenes of Paris - France
Prof. M. GU	Director, China Ship Scientific Research Center of Wuxi - China
Prof. S. KASTNER	Bremen Polytechnic - F. R. of Germany
Prof. L. KOBYLINSKI	Director, Ship Research Institute of Gdansk - Poland
Prof. C. KUO	Director, Marine Technology Centre, University of Strathclyde, Glasgow - United Kingdom
Prof. A. LOUKAKIS	Director, Department of Naval Architecture and Marine Engineering, University of Athens - Greece
Prof. I. A. MANUM	Director, Norwegian Maritime Directorate of Oslo - Norway
Prof. S. MOTORA	Head, Japan Foundation Shipbuilding Advancement of Tokyo - Japan
Prof. J. R. PAULLING	Director, College of Engineering Naval Architecture and Offshore Engineering, University of California - U.S.A.
Dr. N. RAKHMANIN	Head of Seakeeping Laboratory, Krilov Shipbuilding Research Institute of Leningrad - U.S.S.R.
Dr. J. S. SPENCER	Head, Naval Architecture Branch, Marine Technical and Hazardous Materials Division, U.S. Coast Guard, Washington - U.S.A.
Dr. A. DI LORENZO	Director, Engine Institute of Research Council of Naples - Italy

ORGANIZING COMMITTEE

Prof. PASQUALE CASSELLA Full Professor, University «Federico II» of Naples
Chairman

Prof. ANTONIO FIORENTINO Full Professor, University «Federico II» of Naples

Dr. ERNESTO FASANO Doctor Researcher, University «Federico II» of Naples

Dr. ELIO ABATINO Doctor Researcher, Engine Institute of National Research Council of Naples

CONTENTS

Welcome and Introductory Addresses	
Address by Prof. P. Cassella	pag. XI
PAPERS	
Latest Work of the International Maritime Organization related to the Stability of ships	
F. Plaza and V.Y. Semenov	» 1
A Capsizing Experiment of a Small Fishing Boat in Breaking Waves	
S. Ishida T. Yoshifumi	» 10
Numerical Simulation of the Rolling Motion of a Ship in Quartering Sea	
Ho Van Binh and M. Frackoviak	» 19
Simulation of Control Functions for Ship Stability: A User Oriented Flexible tool	
R. Molinari, C. Penno and C. Rezzoagli	» 26
Influence of Main Form Parameters on stability Margin of Ship Rolling in Beam Synchronous Waves	
A. Zborowski and M. Taylan	» 32
On Ship Stability EN-Route	
V. Sizov, Yu. Vorobyov and E. Pergaev	» 40
A simplified Lower-Bound Criterion for Stable Rolling Motion	
N.L. Virgin	» 45
Model Tests on Rolling Behaviour under Damaged Conditions	
Jin Hao and Yuan Don Lei	» 51
Sloshing of Water on Deck of Small Vessels	
Pantazopoulos	» 58
Problem of the Stability Control of Transport Ships in Operation	
V. B. Lipis and N. Y. Salov	» 66
Stability of Ship's Rolling in waves	
V. A. Nekrasov	» 74
Experiments into Capsize of ships in head seas	
R. K. Burkner	» 82
A Guideline to Avoids the Dangerous Surf-Riding	
M. Kan	» 90
Stability and Rolling of a ship with shifting Cargo	
Yu. Remez and V. Shestopal	» 98
A Study of Stability Criterion for Ships in Irregular Following Sea Way	
D. L. Huang	» 102

Model tests on Capsizing of a Ship in Quartering Waves M. Kan, Y. Takaishi, H. Taguchi, T. Saruta and M. Yasuno	pag. 109
The Probability of Compartment and Wing Compartment Flooding in the Case of Side Damage - New Formulas for Practical Application W. Abicht	» 117
Theoretical Analysis of Motion and Stability of Nonlinear Ship Rolling in Random Beam Seas P. Kaplan	» 125
Stability of Damaged Ship During Ship Motions in Waves N. N. RaKhmarin	» 132
Design Excitations for Dynamic Ship Stability Assessment J. G. M. Alexander	» 142
On the Dynamics of Ship Instability R. Bishop, W. G. Price, P. Temarel and E. H. Twizell	» 150
Experimental Investigation of Roll Damping Characteristics of a Destroyer Model D. Cumming	» 159
The Transverse Stability of a Patrol Boat Travelling in Following Waves Z. Cao	» 167
Safety Limits for Small Fishing Vessels at Sea K. Amagai and N. Kimura	» 175
An Analysis of Ship Stability Based on Transient Motions M. S. Soliman	» 183
The Effect of Wind on Small Vessels E. A. Dahle, D. Myrahaug and S. J. Dahl	» 191
The Amplitude Motion Calculations for VW-Type Hull in Waves Yu. L. Vorobyov	» 200
Survival Testing, A Tool and Technique to Establish the Safety level of Marine Floating Structures; Smaller Vessels to large Offshore Structures T. Nedrelid	» 208
An Investigation of Vessel Stability in Waves by means of Numerical Motion Simulations J. S. Pawlowski and D. W. Bass	» 217
On the Determination of Ship Stability during Service H. Kaps and S. Kastner	» 226
Consideration of the Influence of a Ship's own Wave System on Ship Stability when Moving in Following Seas A. V. Lipis and Y. I. Voikounski	» 232
A Control of an Unstable Motion of a Semisubmersible Platform with a Large List Angle M. Takaki and Y. Higo	» 239

Research Towards Criteria of Stability of Civil Deck Bulk Cargo Ships Y. Dibang, H. Weiping, J. Quilan and Wu Zhi	pag. 247
A Theoretical and Experimental Investigation of Large Roll Damping A. K. Brook and R. G. Standing	» 253
A note on Surging and Loss of Control of Small Fishing Vessels in Severe Following Seas M. R. Renilson and G. A. Thomas	» 261
Determination of Capsizing Safety of Damaged Ships by means of Motions Simulations in Waves F. Petey	» 267
Series Stand Tests with Passiv Stabilizing Tanks V. Rakitin, R. Natchev and T. Tzetanov	» 275
Approximate Method for Stability Arm Evaluation at Initial Ship Design Stages S. Dimitrova and R. Kishev	» 283
On Large Rolling in Following Directional Spectrum Waves S. Takezawa, T. Hirayama and S. Acharya	» 287
Damping Effects of Sails on Roll Motion and Effect of Sail on Capsizing of Sail Ship in Gusts and Waves Y. Inoue	» 295
A Fast Numerical Solver for Large Amplitude Ship Motions Simulations B.K. King	» 299
Review of the New Solas Damage Stability Requirements for Passenger Ship P. L. Carrigan and J. S. Spencer	» 307
Turbulent Winds and Forces for Consideration of Stability of Marine Systems M. K. Ochi	» 315
Stability of High Speed Vessels E. Jullumstroe	» 322
Probabilistic Study on Ship Capsizing Due to Pure Loss of Stability in Irregular Quartering Seas N. Umeda, Y. Yamakoshi and T. Tsuchiya	» 328
Probabilistic Study on Surf - Riding of a Ship in Irregular Following Seas N. Umeda	» 336
On the Stability of a Swath Ferry in calm Water and In Waves A. Papanikolaou, C. Kostinas, J. Savvas and G. Zaraphonitis	» 344
An Analitical Approach to Capsizing of a Ship in Following Seas M. Hamamoto and N. Wakiyama	» 354
On the Pure Loss of Stability of Ship in a Following Sea H. Tatano, Y. Soo Kim and J. Ahn Kim	» 362
Loss of Stability of Ships in Following Waves in Relation to their Design Characteristics H. Vermeer	» 369

A New Program Investigating Survival Requirements for All Anticipated Conditions of Small-Sized Tank Vessels	
M. Fujino, I. Fujii, S. Higashi, M. Nakato, Y. Okuyama and I. Suzuki	pag. 378
Prediction of Critical Wave Conditions for Extreme Vessel Response in Random Seas	
K. K. Tikka and J. R. Paulling	» 386
The Role of Numerical Simulation in the Study of Extreme Platform Response	
J. R. Paulling and J. S. Shin	» 395
On the Stability of Antisymmetric Motions of a Ship Equipped with Passive Antirolling Tanks	
A. Francescutto and V. Armenio	» 401
On the Influence of Restoring Moment Changes in Waves on Stability Estimations	
P. Bogdanov, S. Dimitrova and R. Kishev	» 409
Aspects on the Damaged Stability in the Computer Augmented Design Process for Swath Vessels	
A. F. Miller	» 416
System- Cybernetic Approach to the Ship's Stability Problem	
J. T. Stasiak	» 424
An Experimental Investigation into the Stability and Motions of a Damaged Swath Model	
B. C. Nehrling	» 433
Ship Stability in Waves: on the Problem of Righting Moment estimations for Ships in Oblique Waves	
I. K. Boroday	» 441
On the Influence of Variation of Righting Levers in Waves on Stability Requirements	
P. Blume	» 452
Design Consequences of Practical Ship Stability Criteria	
R. Ozkan	» 460
Hidrodinamyc Phenomenon Generated by Bulwark Submergence and its Influence on Ship Susceptibility to Capsizing	
S. Grochowalski	» 470
The Prediction of Deck Wetness in Oblique Waves and Effects of Shipping Water on Stability of Ships	
C. Shin	» 479
Computers on Board. A General Challenge	
B. Arndt	» 487
An Expert Loading System for Chemical and Product Carriers	
L. Bardis, T. A. Loukakis and C. A. Vorous	» 493
On the Possibility of Establishing Rational Stability Criteria	
L. Kobylinsky	» 501
Instrumental Control of Stability and Operational Safety of Seagoing Ships	
M. Alexandrov, Yu. Zhukov and A. Gal	» 512
An Investigation into the Combined Effects of Trasverse and Directional Stabilities on Vessel Safety	
D. Vassalos and K. Spyrou	» 519

Advances in the Stability Assessment of semisubmersibles	
D. Vassalos and C. Kuo	pag. 527
Intact Stability Standards for Large Sailing Vessels	
R.R. Gilbert and W. M. Hayden	» 535
Stability Criteria for Container Ships	
G. Helas	» 543
Stability of Dry Cargo Ships. State of the art, Intact and Damage Requirements, Implementation In Practice	
H. Hormann	» 548
Ridgely-Nevitt Fishing Vessel Series Stability in Longitudinal Waves	
G. Boccadamo and P.Cassella	» 556
Application of Modern Geometric Methos for Dynamical to the Problem of Vessel Capsizing with Water-on deck	
J. M. Falzarano and A. W. Troesh	» 565
Fire and Stability	
R. Balestrieri, D. Impagliazzo and C. Vassallo	» 565
Sensitivity of Ship Motion Predictions to Wave Climate Descriptions	
G. C. Soares and M. F. S. Trovao	» 582
The Assessment of Damaged Stability Criteria Using Model Tests	
A. Graham	» 591
Small Vessel Optimization for Increased Seakeeping and Stability Performance	
R. Nabergoj	» 597
Some Large Roll Motion Simulations Using Multiple Time Scales	
S. B. Hodges	» 604
The Transient Capsize Diagram - A Route to Soundly Based New Stability Regulations	
R. C. T. Rayney, J. M. T. Thompson, G. Tam and P. G. Noble	» 613
A Review of the Stability Characteristics of Smaller Commercial Fishing Vessels of The United States	
B. H. Adee	» 620
Subdivision and Damage Stability of Dry Cargo Ships; An Approval Authority View	
D. J. Holland and C. M. Magill	» 629
Safety for Damaged Vessels as Probability of Non-Capsizing in Following Seas	
G. Trincas	» 637
Bifurcation Analysis of A Vessel Slowly Turning In Waves	
J. Falzarano, A Steindl, H. Troger and A. Troesh	» 647
A Preventive Framework for Achieving Effective Safety	
C. Kuo	» 653

Panel Discussion N. 1
Operational Safety and Avoidance of Accidents pag. 660

Panel Discussion N. 2
Inclusion of Theoretical Achievements in the Field of Stability in the Ship design
Process » 676

List of Participants » 687

Author’s Index » 697

OPENING ADDRESS BY PASQUALE CASSELLA
CHAIRMAN OF STAB '90

Ladies and Gentlman,

I would firstly like to welcome you all, both personally and on behalf of the Organizing Commitee and the Department of Naval Engineering of The University «Federico II» of Naples.

I would also like to express my gratitude to all the interest in the matters that will be discussed at Coference.

STAB 90 is the 4th Conference on the Stability of Ships and Offshore Vessels and follows the three previous events held in Glasgow in the 1975, organized by Professor Kuo who has also acted as the promoter of these conference, the second in Tokyo in 1982 and third in Gdansk in 1986.

STAB 90, I think, has two goals, which also are the same of those set by Prof. Kuo at the first Conference in Glasgow: to stimulate further researches and studies on the various aspect of ship stability and capsizing and to discuss the results of researches and studies carried out by leading international experts and accademic staff so as to find practical applications for theme.

The I. M. O. has been working for many years now on the complex problems of possible heeling actions on ships and on the stability characteristics for the ships.

Recent developments in seakeeping theory and experimental techiques along with the use of powerful computers has made possible to adopt more realistic sability criteria. Nevertheless, the level currently reached is insufficient: capsizing is still a frequent phenomenon, especially with smaller ships such as fishing vessels and car ferries, with consequential losses of human life. We must, therefore, move faster so as to make ships safer in the future.

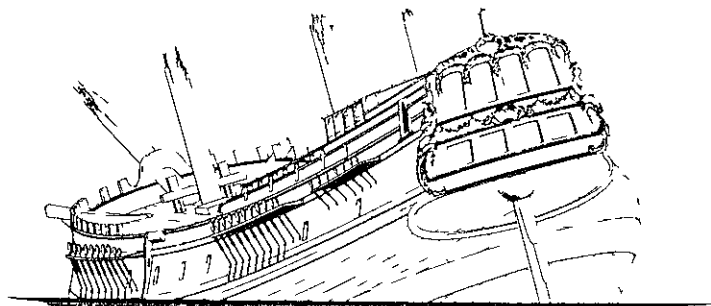
I hope that the papers presented at STAB 90 will increase our actual knowledge of ship stability and capsizing mechanisms and, above all, suggest pratical applications for the knoledge acquired so that we can define new and better stability criteria trough the I. M. O. in order to reduce the loss of human life at sea.

Before I finish, I would like to express my thanks to the President of the Italian Republic for the grant of the high patronage to the Conference and also to the Ministry of Finance, the Ministry of Defence, the Ministry for education, the Ministry for the Merchant Marine, the Ministry for University Education and Research, the Campania Regional Authority, the University «Federico II» of Naples and the University Naval Institute for their Patronage.

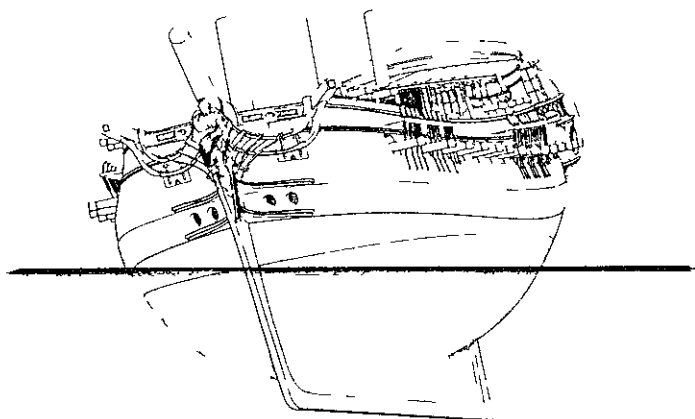
I would also like to thank all the firms, Organizations, Shipowners and naval designer for their help in making this Conference possible and I apologize to them for having perhaps been so troublesome.

Finally I would like to wish you all a pleasant stay in our city which, with its many negative points, still has a charismatic and enchanting beauty.

Thank you.



PAPERS



LATEST WORK OF THE INTERNATIONAL MARITIME ORGANIZATION
RELATED TO THE STABILITY OF SHIPS

F. PLAZA AND V.Y. SEMENOV

ABSTRACT

One of the specialized bodies of the International Maritime Organization (IMO) - the Sub-Committee on Stability and Load Lines and on Fishing Vessels Safety (SLF) - is inter alia entrusted to deal with matters related to the intact and damage stability of ships and other marine installations within the scope of various IMO international conventions, codes, guidelines and recommendations. Previous work of this Sub-Committee covering the period 1962 to 1986 has already been presented at STAB '82 in

Tokyo and STAB '86 in Gdansk respectively. Since 1986 the Organization has developed further stability standards for ships, mobile offshore drilling units (MODUs) and sea-going pontoons.

The main aim of this paper is to outline the results of the work carried out by the SLF Sub-Committee since 1986 to date related to stability and to give an insight into the future work of the International Maritime Organization in this regard.

1 PREAMBLE

One of the main purposes of the Organization consists of promoting the highest practical standards of maritime safety and navigation, and the Sub-Committee on Stability and Load Lines and on Fishing Vessels Safety (hereunder referred to as SLF) in its current, as well as in its previous, work undertakes all possible effort to incorporate the latest achievements related to both design and theoretical areas into its existing standards as well as in regulations actually being developed. So far, intact stability requirements and recommendations have been developed for passenger ships, cargo ships, fishing vessels, dynamically supported craft, mobile offshore drilling units, offshore supply vessels, special purpose ships and sea-going pontoons, thus covering the overwhelming majority of the world's merchant fleet.

Standards of damage stability were introduced for the first time for passenger ships in the 1948 SOLAS Convention and re-adopted by the 1960 and 1974 SOLAS Conventions [1, 2]. For some specific categories of ships, such as tankers, chemical tankers

and gas carriers, IMO developed sets of requirements and recommendations based on the principle of prevention of massive spillage of their cargo into the sea; the current "state of the art" for other types of ships is given below.

The detailed description of IMO's activities related to the development of stability standards within the period 1962 to 1986 was given in papers presented at the Second and Third International Conferences on Stability of Ships and Ocean Vehicles held in 1982 in Tokyo and in 1986 in Gdansk, respectively. This paper summarizes the progress achieved by the SLF Sub-Committee since 1986.

2 LATEST STABILITY STANDARDS ADOPTED BY IMO

2.1 Intact stability: weather criterion for fishing vessels having a length of 24 metres and over

As is known, the severe wind and rolling criterion (weather criterion) could become a governing stability criterion for certain types of ships and maritime installations, depending on design features such as large

lateral projected windage area, shallow draught, unconventional hull shape, etc. On these grounds, weather criterion was introduced in international stability requirements for passenger and cargo ships, dynamically supported craft and mobile offshore drilling units (MODUs). With respect to fishing vessels in particular, the Organization pointed out in resolution A.562(14) "Recommendation on a severe wind and rolling criterion (weather criterion) for the intact stability of passenger and cargo ships of 24 metres in length and over", adopted in November 1985 [3], that the requirements of the recommendation could be applied also to fishing vessels of 45 m in length and over in unrestricted service. In the same resolution, IMO requested its Members to review the adopted parameters of weather criterion aiming at their possible harmonization with those for other types of ships and, in particular, for fishing vessels under 45 m in length. In pursuance of this task, the SLF Sub-Committee assessed the possibility of applying the recommendation contained in resolution A.562(14) to fishing vessels in the length range of 24m to 45m and concluded that the approach given therein could be valid for these vessels with some modifications as to the values of wind pressure (which should take account of the wind velocity gradient versus the distance "h" between the centroid of windage area and the level of the ship's waterline) and the values of the so-called "rolling period factor" ("C") which should preferably be determined in an experimental way or, in case of the absence of such data, be found in the FAO/ILO/IMO Code of Safety for Fishermen and Fishing Vessels, Part B [4] (for vessels in the length range from 24m to 45m) or determined in accordance with the equation $C=0.373+0.023(B/d)-0.043(L/100)$ for ships having a length of 45 metres and over.

The corresponding values of the wind pressure depending on the distance "h" referred to above appear in the following table:

h(m)	1	2	3	4	5	6 and over
$P(N/m^2)$	315.5	386.1	429.2	459.7	485	504.2

The weather criterion as specified above is covering all fishing vessels having a length of 24 metres and over thus overlapping with resolution A.562(14) regarding ships having a length of 45 m and over, for which both methods are the same. Since the approach developed by the SLF Sub-Committee for ships of 24 m in length and over is more universal and therefore more preferable, it is expected to be applied in conjunction with a future protocol to the 1977 Torremolinos International Convention for the Safety of Fishing Vessels, now being developed whilst resolution A.562(14) is expected to be incorporated in an intact stability code for all types of ships covered by IMO instruments currently being developed in IMO as referred to in section 3.1 below, thus superseding it in the future.

2.2 Intact stability: application of resolution A.167(ES.IV) to ships above 100m in length

Aiming at the adoption of an international standard for intact stability of passenger and cargo ships above 100 m in length (apart from the requirements on weather criterion referred to in section 2.1 above) the SLF Sub-Committee considered in detail the possibility of application of resolution A.167(ES.IV) "Recommendation on intact stability for passenger and cargo ships under 100 m in length" [5] to these vessels. Experience from the application of resolution A.167(ES.IV) to passenger and cargo ships having lengths of 100 m and above showed that satisfactory results could be achieved provided that the ships are of conventional hull type and therefore it was recommended to apply resolution A.167(ES.IV) as a basic minimum standard to these vessels.

The need for special consideration to be given to ships having non-conventional hull types, like catamarans, has been emphasized and with respect to ships with unconventional geometric proportions resulting from special operational features, such as

offshore supply vessels and pontoons, specific criteria are applicable [6, 7]. For ships involved in specialized operations, like tugs and trawlers (e.g. those ships the stability of which could be seriously impaired by excessive external forces and moments), special consideration should be given to the application of a general principle that such forces and moments must not exceed dangerous limits. The restriction of external forces and moments could be achieved, for example, by the fitting of "weak links" in towing lines or by other means to prevent overloading to the satisfaction of the Administration.

2.3 Intact stability: new requirements for mobile offshore drilling units (MODUs)

The IMO Assembly in 1989 adopted by resolution A.649(16) the revised Code for the Construction and Equipment of Mobile Offshore Drilling Units (1989 MODU Code) for MODUs whose keels are laid or which are at a similar stage of construction on or after 1 May 1991 [8]. The new Code will supersede the existing MODU Code contained in the annex to resolution A.414(XI) regarding these units.

Among other amendments reflecting the progress achieved since the date of the adoption of the existing MODU Code in 1979 there are two major changes relating to intact stability, namely a provision concerning the ability of a unit to withstand a severe storm condition without the removal or relocation of solid consumables or other variable load, and an option permitting the use of alternative stability criteria instead of those given in section 3.3 of the Code.

The first provision referred to above contains a relaxation allowing a unit to be loaded beyond the point at which solid consumables would have to be removed or relocated in order to withstand severe storm conditions, provided that the allowable KG is not exceeded, weather conditions in a

geographic area of operation permit it and any extra deck load in the unit is carried well within the bounds of a favourable weather forecast.

The alternative intact stability criteria referred to earlier apply only to twin-pontoon column-stabilized drilling units in severe storm conditions.* The stability of the unit should meet the requirements of the two criteria, the first being the capsize criterion which is expressed by the relation (area 'B'/area 'A') > 0.10 (see figure 1), where

area 'B' is the reserve energy area under the righting arm curve within the range from

$$(\theta_1 + 1.15 \theta_{dyn}) \text{ to } \theta_2$$

area 'A' is the dynamic response area under the righting arm curve from

$$\theta_1 \text{ to } (\theta_1 + 1.15 \theta_{dyn})$$

θ_1 and θ_2 are the angles of the first and second intercepts of the righting moment curve with the

100-knot wind moment curve, and

θ_{dyn} is the dynamic response angle due to waves and fluctuating wind, determined as a function of the unit's main dimensions, the vertical distance from the metacentre to the centre of buoyancy of the unit in upright position and the metacentric height which gives the minimum restoring energy ratio 'B'/'A'.

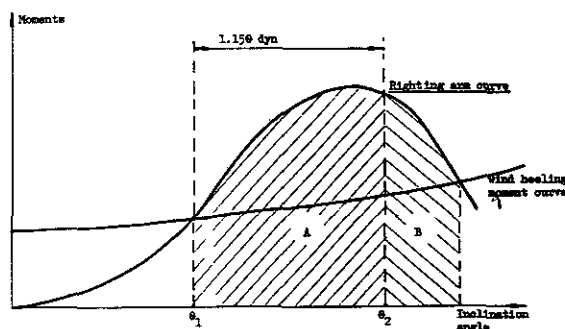


Fig.1 Capsize criterion for MODUs: righting moment and heeling moment curve.

* provided that some of their geometrical parameters meet specific conditions indicated in the annex to resolution A.650(16) [9]

The second criterion is the downflooding one; it is based on the actual geometric dimensions of the unit and its relative motion about static inclination due to a 75 knot wind measured at the survival draught. The initial downflooding distance DFD_0 should be greater than the reduction in downflooding distance RDFD at the survival draught, i.e. the condition $DFD_0 > RDFD$ should be met (see figure 2)

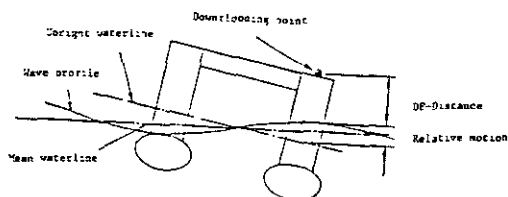


Fig.2 Downflooding criterion for MODUs:
definition of downflooding distance
and relative motion

The value of RDFD is to be determined analytically as a function of the geometrical dimensions of the unit and two variable vertical distances, the first being the difference between DFD_0 and quasi-static downflooding distance at θ_1 , the second being relative motion due to waves about θ_1 in metres, taking account of correlation existing between these two distances and uncertainties not taken into consideration (such as non-linear effects, etc.)

In the future the Organization plans to give further consideration to the alternative criteria of intact stability described above, based on experience gained from their application.

2.4 Damage stability: flooding protection of passenger ships

A series of amendments to SOLAS 74 has been adopted by IMO since 1986; a number of them resulted from serious casualties which occurred to passenger vessels (in particular ro-ro vessels) and the corresponding amendments are chiefly of an operational nature (provision of indicators on the bridge signalling the closure of doors or ramps

ensuring the watertight integrity etc.). However, the most important measure taken within IMO regarding the damage stability of passenger ships is the adoption of amendments to regulation II-1/8 of the 1974 SOLAS Convention "Stability of passenger ships in damaged condition", which entered into force on 29 April 1990[10] applicable to all passenger ships. The new requirements significantly enlarge the range of controlled parameters of a damaged passenger ship as follows:

- .1 the positive residual righting lever curve shall have a minimum range of 15° beyond the angle of equilibrium;
- .2 the area under the righting lever curve shall be at least 0.015 m-rad in the range from the angle of equilibrium to the angle corresponding to the progressive flooding or 22° (for one-compartment flooding) or 27° (for two or more adjacent compartments), whichever is less;
- .3 a residual righting lever is to be obtained by means of calculating the moments due to the crowding of passengers the launching of survival craft or wind pressure (whichever results in greater values of GZ) but in no case shall it be less than 0.10 m,

and the required values of all three parameters should be met simultaneously (i.e. none of these parameters could substitute another) see figure 3.

The residual righting lever shall be determined as:

$$GZ = (\text{heeling moment/displacement}) + 0.04(m)$$

The heeling moment referred to in the above formula for GZ shall be either a moment due to the crowding of all passengers towards one side or a moment due to the launching of all fully-loaded davit-launched survival craft on one side, or a moment due to wind pressure (120 N/m^2 applied to the projected windage area), whichever is greater.

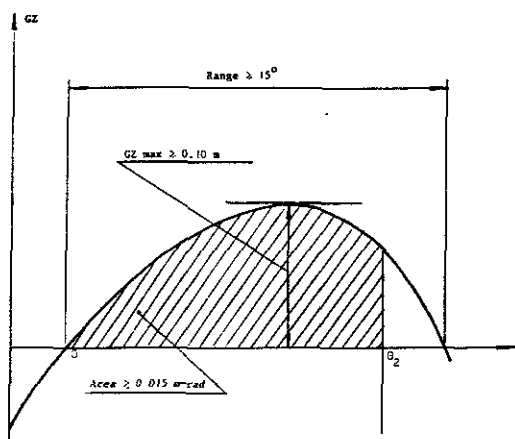


Fig.3 Residual stability criteria for passenger ships

- θ_1 - angle of equilibrium
 θ_2 - angle equal to:
 22° for one-compartment flooding
 27° for flooding of two or more adjacent compartments; or
 angle corresponding to the progressive flooding,
 whichever is less.

New requirements were developed also with regard to intermediate stages of flooding. They envisage the minimum GZ-value of 0.05m in conjunction with the range of positive righting levers of at least 7°.

A new provision regarding the maximum permissible value of 15° of the angle of heel after flooding but before equalization was introduced in the text of regulation II-1/8; to ensure consistency with resolution A.265(VIII) with regard to unsymmetrical flooding, the obsolete requirements of the existing regulation II-1/8 were replaced with the provisions permitting to reach a heel of not more than 7° for the case of one-compartment flooding and not more than 12° for the simultaneous flooding of two or more adjacent compartments.

The SLF Sub-Committee at its 34th session held in February this year gave further consideration to the new residual stability requirements and agreed that the Administrations should be given some further instructions aimed at the uniform

application of amended regulations II-1/8 and II-1/20 which deal with watertight integrity of the ship's hull ensured by cargo loading doors located above the margin line and contain mainly operational requirements with regard to these doors. These instructions cover those enclosed spaces which are included in the damage stability calculations and prescribe that these spaces may have weathertight subdivision if they do not submerge during any stage of flooding, otherwise the subdivision should be watertight. With regard to spaces located above the bulkhead deck it was agreed that they should have watertight subdivision to the extent required by amended regulation II-1/8 in case they have been included in the damage stability calculation. As an example partial watertight bulkheads and their adjacent structures should be constructed in such a way as to restrict progressive flooding in the range of the required residual stability. The watertight doors located in the same area should meet requirements of amended regulation II-1/15 for power-operated sliding watertight doors with a number of reasonable relaxations.

Besides that, a number of operational measures aimed at ensuring appropriate intact and damage stability parameters of passenger ships have also been introduced in SOLAS 74 (stability information for masters; provision of a draught indicating system; use of loading instruments such as mini computers; use of effective systems for the opening and closing of the doors, ensuring the watertight integrity; and the lightweight survey of ships, as contained in further amendments to regulations II-1/8 and 20 already dealt with earlier and also in the amendments to regulation 22 [10].

The methods of assessment of survivability of passenger ships after sustaining damage are expected to be subject to further research within IMO; such aspects as survivability of damaged ships in waves, which is still beyond the scope of the above-described regulations, as well as

investigation of other factors associated with specific operational factors which might affect survivability characteristics deserve further consideration in the 1990s.

2.5 Damage stability: regulations on subdivision and damage stability of dry cargo ships including ro-ro ships

In May 1990 the Maritime Safety Committee, the senior technical body of the Organization, adopted a set of amendments to the 1974 SOLAS Convention in the form of a new part B-1 of chapter II-1 "Subdivision and damage stability of cargo ships" [11]. These amendments are expected to enter into force on 1 February 1992 and are to be applied to dry cargo ships, including ro-ro ships having a subdivision length of 100 m or more. These new requirements are based on the so-called "probabilistic concept of survival", similar to that used in IMO resolution A.265(VIII) [12] for passenger ships, but it should be emphasized that the probabilistic approach with respect to cargo ships will appear in SOLAS for the first time. The main principle of the regulations could be expressed by the condition $A > R$ to be met by a ship, where

A is the attained Subdivision Index, determined as a function of the degree of the ship's subdivision, parameters of the initial stability, ship's main particulars, permeability of spaces assumed flooded and some other factors. It is based on the concept of the probability of survival of the ship in case of collision. Numerically, the value of A indicates, in terms of probability, the level of safety of the ship breached as a result of damage. The probability of survival is the sum of the products for each compartment or group of compartments of the probability that a space is flooded, multiplied by the probability that the ship will not capsize or sink with the considered space flooded.

R is the Required Subdivision Index; its value is obtained by means of the following formula, depending on the

ship's subdivision length L_s :

$$R = \sqrt[3]{(C_1 + C_2 L_s)}, \text{ where}$$

$C_1 = 0.002$ and $C_2 = 0.0009$ are the empiric coefficients determined in such a way as to obtain the highest practical levels of the attained Index A, based on the analysis of a large number of existing ships. The value of R does not depend on the ship's type.

The value of A should cover only those cases of flooding which contribute to the value of A and should be taken over the ship's length for all cases of flooding in which a single compartment or two or more adjacent compartments are involved. In a case where wing compartments are fitted, contribution to the summation should be taken at first for all cases of flooding in which wing compartments are involved and, in addition, for all cases of simultaneous flooding of wing compartment(s) and adjacent inboard compartment(s), assuming a rectangular penetration which extends to the ship's centreline but excludes damage to any centreline bulkhead. The assumed vertical extent of damage is to extend from the baseline upwards to any watertight horizontal subdivision above the waterline, or higher. If a lesser extent will give a more severe result, such extent is to be assumed. If pipes, ducts or tunnels are situated within assumed flooded compartments, arrangements are to be made to ensure that progressive flooding cannot extend to compartments other than those assumed flooded. At the same time, the Administration may permit minor progressive flooding on condition that its effects could be easily controlled and the safety of the ship is not impaired.

The new regulations prescribe to have on board ships reliable stability information which includes a curve of GM min (or KG max) versus draught and incorporates also data reflecting damage stability requirements, instructions concerning the operation of cross-flooding arrangements and all other relevant data and aids which may be necessary to maintain stability after damage. The new regulations also prescribe that all external openings below the final damage

waterline which lead to intact compartments (as assumed in the damage analysis) should be watertight. They should have adequate strength and should be fitted with indicators on the bridge (with the exception of cargo hatch covers). Any openings in the shell plating below the deck which limits the vertical extent of damage should be kept permanently closed while at sea, but when they are accessible during the voyage they shall be fitted with a device which prevents unauthorized opening.

The SLF Sub-Committee recognized the need to give further consideration to the method to improve it on the basis of experience gained from its application. Possibly some operational and design aspects of various types of ships could also affect in certain cases the value of the Required Subdivision Index (R) together with the ship's subdivision length (L_s), which is the only parameter determining R in the present regulations (i.e. the possibility of a parametric study could be envisaged for the purpose of the improvement of the method).

2.6 Damage stability: new requirements for MODUS

A number of new requirements constituting substantially stricter levels of safety for column stabilized units were introduced in the text of the 1989 MODU Code [8] referred to in section 2.3 above. These new requirements are as follows:

- .1 the angle of heel after damage (vertical extent 3.0 m occurring at any level between 5.0 m above and 3.0 m below operational draughts of the unit; horizontal penetration 1.5 m) should not be greater than 17° ;
- .2 any opening below the final waterline should be made watertight and openings within 4 m above the final waterline should be made weathertight;
- .3 the righting moment curve after damage referred to in .1 should have, from the first intercept to the lesser of the extent of weathertight integrity

specified in .2 and the second intercept a range of at least 7° . Within this range the righting moment curve should reach a value of at least twice the wind heeling moment curve, both being measured at the same angle, as shown in figure 4.

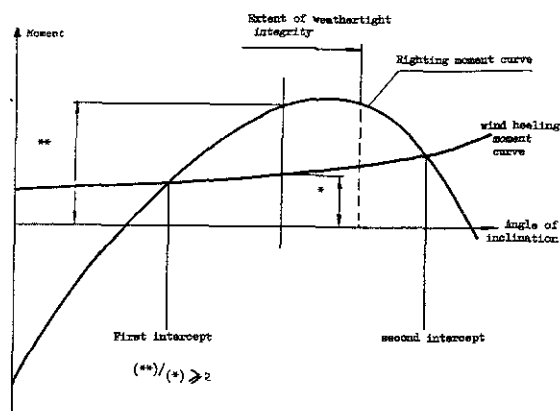


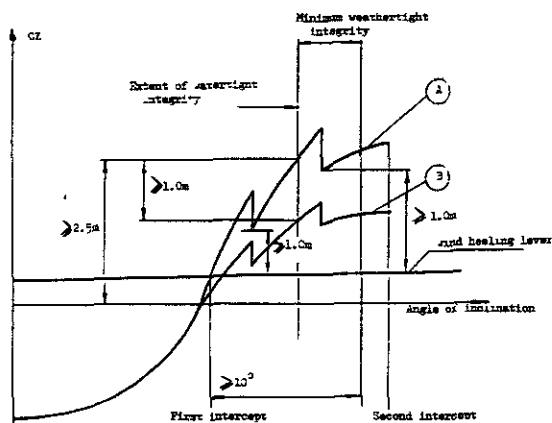
Fig.4 Damage stability of column-stabilized units: righting moment and wind heeling moment curves.

In addition to the above requirements, it was agreed that the unit should provide sufficient buoyancy and stability to withstand, in any operating or transit condition, the flooding of any watertight compartment wholly or partially below the waterline in question, which is a pump room, a room containing machinery with a salt water cooling system or a compartment adjacent to the sea, considering that the angle of heel after flooding should not exceed 25° ; any opening below the waterline should be made watertight; and a range of positive stability beyond the calculated angle of inclination must be at least 7° .

At the same time the Organization, by resolution A.651(16) [13], adopted an example of alternative damage stability criteria for column-stabilized semi-submersible units which could substitute criteria specified in the 1989 MODU Code. These criteria are:

- .1 the righting lever curve after damage or flooding should, before the second intercept angle, reach a value of at least 2.5 m (see fig.5); at least 1.0 m of this righting lever should arise from enclosed watertight volumes above watertight flats positioned at or above the lowest continuous deck;

- .2 the righting lever curve after damage or flooding should have a positive range of at least 10^0 between the first and second intercepts;
- .3 for the purpose of calculating the righting lever curve, buoyancy may be assumed from all spaces which are closed in a manner specified in .4 below. If the lower edge of any opening not closed as set forth in .4 is submerged, the corresponding space shall be excluded from the buoyancy beyond the angle at which this opening is submerged, but it should be included up to this angle. Any such loss of buoyancy should not cause the righting lever to fall below 1.0 m above the wind heeling moment curve within the range of 10^0 specified in .2;
- .4 any opening submerged before the angle at which the righting lever required in .1 is reached should be fitted with a remotely operated means of closure, including those of a self-activating type;
- .5 any opening submerged after the angle in .4 and within the range specified in .2 should be fitted with means of closure required in .4 or an easily operable weathertight means of closure.



- A GZ curve including enclosed volumes above watertight flats or above the lowest continuous deck
- B GZ curve excluding enclosed volumes above watertight flats at or above the lowest continuous deck.

Fig.5 Alternative damage criteria for column stabilized semi-submersible units: requirements for righting lever curves.

3 CURRENT WORK ON INTACT AND DAMAGE STABILITY

3.1 Intact stability: code to cover all types of ships

At the present time, numerous international conventions, codes, guidelines etc. containing mandatory requirements as well as recommendations related to intact stability are given in different formats although they could be set forth in a more generalised form, provided that specific design and operational parameters governing one or another way to specify stability criteria are clearly indicated. As a consequence of this situation it was agreed that the SLF Sub-Committee should develop an "all-embracing" code which would contain both the mandatory and voluntary stability requirements contained in existing IMO documents as well as future standards yet to be developed by the Organization. The future code should also contain instructions on operational procedures together with comprehensive and explicit requirements of a technical nature covering all aspects of intact stability ensuring safe operation of ships.

3.2 Damage stability: probabilistic concept of survival to be applied to dry cargo ships below 100 m in length

Since the amendments to SOLAS 74 referred to in section 2.5 above [11] only cover ships having a length of 100 m and over, IMO undertook to investigate the applicability of the probabilistic concept of survival to ships of lesser sizes in order to develop possibly a uniform approach regarding vessels of both size categories. Work on this item as well as on the development of explanatory notes to regulations on subdivision and damage stability of dry cargo ships, including ro-ros, is now in progress within the Organization.

REFERENCES

- [1] International Convention on Safety of Life at Sea, 1960, including the International Convention for the Safety of Life at Sea, 1960
- [2] International Convention for the Safety of Life at Sea (consolidated edition, published 1986)
- [3] Recommendation on a severe wind and rolling criterion (weather criterion) for the intact stability of passenger and cargo ships of 24 metres in length and over (resolution A.562(14))
- [4] Code of Safety for Fishermen and Fishing Vessels, Part B - Safety and Health Requirements for the Construction and Equipment of Fishing Vessels
- [5] Recommendation on Intact Stability for Passenger and Cargo Ships under 100 m in length (resolution A.167(ES.IV)) as amended by resolution A.206(VII))
- [6] Guidelines for the Design and Construction of Offshore Supply Vessels (resolution A.469(XII))
- [7] Intact Stability Requirements for Pontoon (MSC/Circ.503 of 17 April 1989)
- [8] Code for the Construction and Equipment of Mobile Offshore Drilling Units (MODU Code 1989) (resolution A.649(16))
- [9] An Example of Alternative Intact Stability Criteria for Twin Pontoon Column Stabilized Semi-submersible Units (resolution A.650(16))
- [10] Amendments to regulation II-1/8 of the 1974 SOLAS Convention (resolution MSC.12(56))
- [11] Amendments to the 1974 SOLAS Convention (new Part B-1 of chapter II-1 - "Subdivision and damage stability of dry cargo ships") (resolution MSC.16(58))
- [12] Regulations on Subdivision and Stability of Passenger Ships as an equivalent to Part B of chapter II of the International Convention for the Safety of Life at Sea, 1960 (resolution A.265(VIII))
- [13] An Example of Alternative Stability Criteria for a Range of Positive Stability After Damage or Flooding for Column Stabilized Semi-submersible Units (resolution A.651(16))

FERNANDO PLAZA, a Spanish national, graduated in naval architecture and marine engineering from the Superior Technical School at Madrid University. He then entered Lloyd's Register of Shipping as a Ship Surveyor and after some years he joined the International Maritime Organization (IMO) in 1975. He is presently Head of the Sub-Division for Technology and Senior Deputy Director of the Maritime Safety Division of IMO.

VLADIMIR SEMENOV is a Technical Officer of the Maritime Safety Division of IMO and is the Secretary of the Sub-Committee on Stability and Load Lines and on Fishing Vessels Safety. He graduated in naval architecture in 1976 from the Shipbuilding Institute in Leningrad. Before joining IMO in 1988 he held a position as a Principal Surveyor with the USSR Register of Shipping.

A CAPSIZING EXPERIMENT OF A SMALL FISHING BOAT IN BREAKING WAVES

Shigesuke Ishida¹, Yoshifumi Takaishi¹

ABSTRACT

This paper deals with the capsizing of a small fishing boat in beam seas at zero forward speed. In a basin four patterns of capsizing could be seen in concentric transient waves having a couple of crests, some of which were so called spilling breakers. The maximum wave heights were comparable to the model breadth. An optical position sensing device was used to measure the ship motion free from disturbance by an experimental apparatus. The contributions of KG, initial heel and initial position of the model relative to the wave to the rolling motion and capsizing were also investigated.

As for the mechanism of capsizing it is clarified that the model was heeled over the stability vanishing angle in a large amplitude rolling motion which was mainly excited by a non-impulsive wave exciting force. The spilling breakers only gave her a small impulsive moment for capsizing, but they played a significant role in terms of changing the conditions, i.e. heeling angle, angular velocity and so on, to encounter the following critical waves. It is interesting to say that the breakers worked to prevent capsizing in some cases.

INTRODUCTION

It is well known that one of the major reasons of maritime accidents is capsizing caused by a couple of large successive (breaking) beam waves. In recent research works on capsizing in beam seas it was reported that capsizing could be caused by an impulsive overturning moment due to a sudden attack of a breaking wave. For example, Dahle and Kjærland [1] reported that a research vessel ($L_{OA} = 34.7m$) was forced to heel over 80 degrees to capsize mainly by a impulsive force of a breaker which worked on the higher part of the ship side. On the other hand, Hirayama and Yamashita [2] conducted an experiment using a model of a fishing boat ($L_{OA} = 42m$) and concluded that a large impulsive overturning moment worked on the ship when the breaker pushed up the weather side bottom of the ship. Other than those papers, for example, Matora et al. [3] and Morral [4] reported more complicated capsizing patterns.

In spite of these efforts the mechanism of capsizing in breaking waves has not been fully clarified. Moreover, the hull shapes and ship length in these papers were somewhat different from the ones of small ships, those are less than or around 10 m long and frequently reported to have capsized in the record of maritime accidents. Being characteristic to have a small draft and a large bulwark, those small ships can have a peculiar capsizing mechanism. It is of importance and of emergency to study the capsizing mechanism of those ships from the viewpoint of sea safety. The purpose of this paper is to study dangerous conditions for capsizing of small boats and to grasp the mechanism of it.

EXPERIMENT

Model Ship

The principal particulars and conditions of the fishing boat model are shown in Table 1 and 2, respectively. GM values were altered by moving dead weights vertically. The characteristic of the stability curves of all conditions, see Fig.1, was that GZ value became negative over 39 degrees because of the bulwark top immersion.

The body plan and the arrangement of sensors are shown in Fig.2. Two spot lights on the mast were traced by an optical position sensing device, which was used not to disturb the ship motion. Acceleration of vertical and lateral directions was measured at the almost CG position. Two water level gauges, one on the house side and one on the bulwark side, and six pressure gauges were fitted on the weather side of the model.

Experiment

The experiment was carried out in a tank of 50 m long, 8 m wide and 4.5 m deep, see Fig.3. The model was set free abeam to the wave. The ship motions, i.e. roll, heave and sway, were measured by an optical position sensing device, whose sampling frequency was 60 Hz. Nine wave gauges, named WG1, WG2, ..., WG9 were arranged with 30 cm distance along the wave propagation direction. The initial position of the model ship was varied from WG2 to WG6.

Waves

The signals to the flap type wave maker were made with the Ohmatsu's method [5], which can generate waves of an arbitrary time history at a point

¹Ship Research Institute, Mitaka, Tokyo, Japan

under the assumption that linear theory is valid. In this experiment wave time histories were intended to have triangle shape at WG5. The duration time T of the triangles were intended to be 1.5 sec., 2.0 sec. and 2.5 sec., each wave is called W1.5, W2 and W2.5 hereafter. The amplitude of the flap motions was controlled for the waves not to break before they reached WG1 and to break after that position, because after breaking a wave shape gets distorted from the intended one by a non-linear effect. The wave of W2.5, however, didn't have a breaking crest because of the capacity of the wave maker. We used another wave for $T=2$ sec. named W2S whose height was slightly smaller than W2, intended to have a similar time history to W2 but not to break.

Fig.4 shows the time histories of the four waves. Sharp crests, for example wave W2 at gauge WG2, mean spilling breakers. Maximum wave heights of W1.5, W2, W2S and W2.5 were 30 cm, 43 cm, 40 cm and 48.5 cm respectively. Those heights are comparable to the breadth of the model ship, that is commonly said [6] to be the critical wave height for capsizing.

CONDITION OF CAPSIZING

The result of the experiment, capsized or not capsized, is shown in Table 3. The ship didn't capsize in the model conditions out of the table. Plural marks at the same column show that repeatability was confirmed in critical conditions. When the record of the wave gauge on the bulwark got over the bulwark top, which didn't mean much shipping water but some impulsive force, each mark has a flag.

From this table we can lead the following remarks:

1. The higher CG became, in the more various initial positions she capsized.
2. The difference of 30 cm, 1.82 m for the real ship, of the initial position had much influence on capsizing.
3. Without initial heel, capsizing didn't take place in almost single-crested waves like W2.5 at WG5, but in double-crested ones whose first crest was breaking capsizing was easily occurred.
4. With initial heel, especially to lee side, the ship was apt to capsize even with larger GM value.
5. The model only capsized to weather side in the shortest wave W1.5 and in the heeled condition to weather side. In both cases the water over the bulwark top was measured.
6. Comparing the results in the wave W2 (with breaker) and W2S (without breaker), it is interesting to say that the model capsized only in W2S in many conditions when she had initial heel.

CLASSIFICATION OF CAPSIZING

The processes of capsizing seems to be classified to four patterns by the initial heel, the existence of a breaker and the direction of capsizing like Table 4. We show the ship motion of each pattern hereafter with the record of pressure and lateral acceleration. In the following figures symbols ϕ , x and y denote roll (positive to lee side), sway (weather side) and heave (upward) respectively. The contribution of the gravity acceleration is included in the record of lateral acceleration, but that is not of importance as long as impulsive phenomenon is concerned.

Pattern-A, Capsize to Lee Side without Initial Heel

Fig.5 shows an example of the typical capsizing pattern in this experiment. The model of the condition C7 capsized to lee side after she encountered the wave of W2 at the position of WG2. As shown in Fig.4(b) the wave W2 at WG2 had two crests and the first one was a spilling breaker. In Fig.5(a) the ship is represented by a straight line and are drawn from the time S to the time E with frequency of 3 Hz. The curve means the trajectory of CG. Fig.5(b) also shows the ship motion with the wave profiles from the time S to E . When the rolling motion was drawn on the $\phi - d\phi/dt$ plane the trajectory had a spiral shape like Fig.5(c).

Seeing the capsizing sequence step by step,

1. Being hit by the first breaker the ship swayed to lee side with little heeling angle.
2. In the trough the ship heeled to weather side.
3. Again she heeled to lee side swaying heavily on the non-breaking second crest.
4. At last she capsized just after the wave train had passed her.

At the moment or just before capsizing the water surface was of almost calm condition and the rolling angle was close to the static stability vanishing angle, 34 degrees. So, it is clear that capsizing was not brought about by a large impulsive moment directly but by a large amplitude rolling motion which was excited in the wave train. From Fig.5(c) also we can see the gradual development of the rolling motion in one and a half cycle.

This kind of capsizing is apparently different from the ones dealt by Dahle and Hirayama which were mainly caused by a large impulsive moment. It looks rather similar to the one of Morrall's experiment, but we cannot affirm it because there is no detailed description on the capsizing process in his paper.

The pressure and lateral acceleration is shown in Fig.6. The impulse of the breaker, evaluated by the lateral acceleration, was about $0.3 \text{ kg} \cdot \text{sec.}$. The impulsive moment was supposed to be about $0.05 \text{ kg} \cdot \text{m} \cdot \text{sec.}$ if we assume that the impulse worked around the water line of the ship. This moment is

rather small compared to the dynamic righting moment. But it is interesting that in W2S, which had almost the same shape as W2 but no breaker, the vessel did not capsize. Sadakane et al. pointed out in their papers [7][8] that "the initial condition for encountering the critical wave plays a significant role for capsizing". In this case, too, the small impulse by the breaker might change the condition to encounter the second wave. Further study on this point will be discussed later.

Pattern-B, Capsize with Initial Heel to Lee Side

Fig.7 shows an example of Pattern-B. The model of condition CL capsized to lee side in the non-breaking wave W2S. Looking at the latter half of the trajectory of CG and also the trajectory on the phase plane, it can be told that the ship motion before capsizing was similar to the one of Pattern-A. But these two patterns made a remarkable contrast because Pattern-B only occurred in the non-breaking waves while a breaker was a necessary condition for Pattern-A. In other words the condition to go into the motion, which leads to capsizing in the end, was different in these two patterns.

The ship motion in the same condition as Fig.7 but in the different wave W2, with breaker, is shown in Fig.8. She did not capsize because of the effect of the breaker. It is interesting that a small breaker modified the ship motion to prevent capsizing.

Pattern-C, Capsize to Weather Side Being Hit by a Breaker

Fig.9 and 10 show an example of Pattern-C in the breaking wave W1.5 and the initial position WG3. In this case the vessel had an initial heeling angle to weather side, but even without initial heel, e.g. wave W1.5, ship condition C8, initial position WG2, the pattern of capsizing was almost the same as shown in Fig.9.

The ship swayed with little rolling motion like Pattern-A after the breaker, but after that she rapidly heeled to weather side and in the trough the bulwark top almost immersed. So she was heeled further by the second wave to weather side, which is the opposite direction to Pattern-A and B, and capsized at the second crest. The trajectory in the phase plane is characteristic to indicate a fast development of the rolling motion leading to capsizing in a half cycle, while in the previous two patterns it developed gradually.

The acceleration and pressure show two impulse, the first one by the breaker and the second one in the trough. The magnitude of the first one was about $1.3 \text{ kg} \cdot \text{sec.}$, which was about four times larger than Pattern-A. However the impulsive moment was too small to make her capsize alone in this pattern, too. Instead that moment is supposed to have contributed to the fast development of the rolling motion.

Pattern-D, Capsize to Weather Side Without a Breaker

The typical pattern of weather-side-capsizing

was mentioned in the previous section, but that also occurred without a breaker as shown in Fig.11 and 12. In Fig.11 a phase plane is omitted because the trajectory was similar to the one of Pattern-B.

In this example the experiment started at WG5, where the first crest of W2S was small. It is characteristic that the non-breaking second crest hit the ship causing an impulse like Fig.12. The impulse was observed to push the vessel and to make it under a kind of surf-riding condition on the second crest, which seemed to lead to capsizing. In W2, which had a deeper trough at around WG5, no impulse, no surf-riding and no capsizing were observed.

As shown above and in previous sections, impulse sometimes worked at the moment when the relative wave slope was large even if the crest was not breaking. This kind of impulse also have a possibility to have given much effect on the ship motion.

FURTHER STUDY ON THE MECHANISM OF CAPSIZING

In this section the mechanism of capsizing will be studied further using phase planes and a simulation program, focused on Pattern-A.

Phase Planes

Ship motion which corresponds to Fig.5 is represented by two phase planes, i.e. $y-\phi$ and $\phi-d\phi/dt$, in Fig.13. The result in the same experimental conditions but in the non-breaking wave W2S, leading to no capsizing, is also shown in Fig.14. The effect of the breaker will be discussed comparing these two figures.

Every trajectory started from the origin because the model came across the waves in upright condition. When she capsized, the trajectories went out of the figures in plus ϕ direction. The symbols A , B , C and D denote the moments when the ship was on the top of the first crest, in the bottom of the trough, $y = 0$ on the front slope of the second wave and on the top of the second crest respectively. Note that this ship was so light that y , heave of her, almost agreed with the displacement of water surface.

In Fig.14(a), without impulse, the trajectory drew a straight line till point B , the trough. So the rolling motion and the heaving motion, or the water elevation and the rolling motion, were in phase. We could see the same kind of straight trajectories in regular non-breaking waves [9], in which she didn't capsize in upright conditions. On the other hand in Fig.13(a), it drew an oval because of phase difference which was caused by the impulse. As a result the condition to encounter the second wave, for example the rolling velocity at point B , was changed from the one in non-breaking waves.

Looking at the point C in Fig.13 the rolling angle was almost zero and the rolling velocity was at the maximum, moreover the wave slope was almost at the maximum, so the rolling motion seems to have been in a kind of resonant condition. As a result the rolling amplitude continued to develop in the second wave and finally she exceeded the stability vanishing angle. On the other hand in Fig.14 the model

heeled to weather side at C , which means larger relative wave slope and larger moment to lee side than Fig.13. But the rolling velocity had not developed enough to absorb much energy from that wave exciting moment. So the growth of roll was limited in the second wave.

Simulation

A simulation was carried out in order to confirm the discussion in the previous section. The only unknown variable in the equation of motion was ϕ_a , the relative rolling angle to the wave slope ϕ_w . For evaluating the contribution from sway x and heave y the experimental result was used because the purpose of the simulation was to investigate the effect of impulsive moment. The change of sway and heave by the impulse was not considered at this stage. The equation of motion was,

$$\begin{aligned} & I_\phi \ddot{\phi} + \Delta I_\phi \ddot{\phi}_a + B_\phi \dot{\phi}_a + W \cdot GM f(\phi_a) \\ & + A_x l_{Ax} \cos \phi \cdot \ddot{x} + B_x l_{Bx} \cos \phi \cdot \dot{x} + C_x l_{Cx} \cos \phi \cdot \dot{x} | \dot{x} | \\ & + A_y l_{Ay}(\phi_a) \cos \phi \cdot \ddot{y} \\ & = IM(t) \end{aligned} \quad (1)$$

where ϕ denotes the rolling angle like,

$$\phi = \phi_a + \phi_w \quad (2)$$

and the coefficients I_ϕ , ΔI_ϕ , B_ϕ and W are the moment of inertia, the added moment of inertia, the linear damping coefficient and the weight of the ship respectively. The fourth term means the restoring moment and the experimental results (see Fig.1) was used for it. The coefficients for the contribution of sway and heave, from the fifth to eighth terms, are roughly evaluated using Lewis form table and so on. The lever of moment at the last term $l_{Ay}(\phi_a)$ is the horizontal distance between CG and the center of buoyancy. $IM(t)$ in the right hand side means the impulsive moment. The equation was solved by Runge-Kutta-Gill method with the time step of 1/60 second.

In Fig.15 the calculated rolling motion and the measured one was compared for an example in W2S, the non-breaking wave. The wave slope was also shown. The conformation between (a) and (b) shows the validity of this simplified simulation.

The rolling motion of Pattern-A, presented in Fig.5 and Fig.13, was calculated and shown in Fig.16. When impulse was not taken into consideration the calculated time history of roll was far from the experiment like Fig.16(b). When we added an impulse of $IM_1 = -0.05 kg \cdot m \cdot sec$. (weather side, evaluated before) at the moment the breaker hit the model, the motion became closer to the experiment till the trough like Fig.16(c), but she recovered in the end. The reason for the recovery is not clear at this stage, but we could recognize a small impulse in Fig.6 when encountering the second wave. With $IM_2 = -IM_1/2$, which was temporarily added, the ship capsized like Fig.16(d) and had a similar time history to the experiment.

From the investigation above using phase planes and simulations the capsizing mechanism of Pattern-A can be explained as follows:

The impulse caused by the first spilling breaker worked to modulate the ship motion. As a result she encountered the second wave in a kind of resonant condition in which she absorbed much energy from the wave to develop the rolling motion. In the end, heeling over the stability vanishing angle, she capsized when the wave train had almost passed her. Moreover, the small impulse which was measured when running across the second non-breaking wave might further the development of roll.

As for other patterns the capsizing mechanism has not been fully studied. At this stage we can only mention that the equation of motion (1) cannot give a complete explanation for other patterns. One solution might be including another roll-heave interaction term because a rolling moment due to relative heave in a inclined condition cannot be neglected as Tamiya pointed out [10]. Moreover the program should be improved to make it possible to simulate heaving and swaying motions in order to evaluate the effect of impulse to these motions.

CONCLUDING REMARKS

The shape of the model ship in this experiment represented the ones of small ships and has characteristics such as small draft, big bulwark and negative rightening arm when her bulwark immersed. The experiment was conducted in four kinds of waves varying the KG value and the initial position. From the experimental results and the simulation we could have following helpful conclusions to the safety of small ships.

As for critical conditions for capsizing,

1. In wave trains having a few crests with the heights of the order of the model breadth the vessel frequently capsized. The higher the CG was, the more frequently she capsized. The limiting value of GM against capsizing was $GM/B \approx 0.18$.
2. In the wave W2.5, the highest wave but with small wave slope, capsizing seldom happened.
3. Without initial heel, capsizing didn't take place in almost single-crested waves but in double-crested ones. Receiving an impulse from a breaker was a necessary condition for capsizing. The capsizing direction was mainly lee side but rarely weather side in the short steep wave, W1.5.
4. For weather-side-capsizing also an impulse by a breaker was a necessary condition regardless of initial heel.
5. With initial heel, especially to lee side, the ship was apt to capsize even with large GM value. Comparing the result in wave W2 (with breaker) and W2S (without breaker), the model capsized

only in W2S in many cases.

6. The difference of 30 cm of the encountering position to the wave had much influence on the occurrence of capsizing.

As for capsizing patterns and mechanism,

7. The process of capsizing were classified to four patterns by the initial heel, the existence of a breaker and the direction of capsizing. They could be divided into two groups, one which was characterized by a rapid growth of roll as Pattern-C and the other by a gradual growth as Pattern-A, B and D.
8. In any patterns capsizing was not caused by a large impulsive overturning moment directly. The ship capsized because she heeled over the (static) stability vanishing angle at the last stage of a large rolling motion. The moment which excited the motion could be explained mainly by a wave slope and partly by a breaker.
9. Capsizing happened in or just after the second wave. So the encountering condition to it, which could be changed by the first wave, was a fatal factor for capsizing.
10. Impulse was measured not only when a breaker hit the ship but also when the relative wave slope was large in a trough. The impulsive moment was rather small compared to the rightening moment of the ship, but it played a significant roll as mentioned above. It is noticeable that impulse acted to prevent capsizing in some cases.
11. Capsizing mechanism of most frequently seen Pattern-A was investigated using phase planes and a simplified simulation program. It was clarified that being hit by the first breaker the ship encountered the second wave in a kind of resonant condition resulting in a large heeling angle over the stability vanishing angle when the wave train had almost passed her. Moreover the small impulse which worked when running across the second wave might further the development of the rolling motion.

The waves used in this experiment should not be called "freak waves" because the ships in service can conceivably encounter the wave train of this length and this height. So, this kind of capsizing sequence is supposed to be rather common in capsizing accidents of small vessels. The authors are planning to study the capsizing mechanism of other patterns than Pattern-A and the characteristics of "critical wave trains" through improving the simulation program.

ACKNOWLEDGEMENTS

This investigation was carried out collaborated with Japan Craft Inspection Organization. The authors would like to thank the organization and the members of the Research Committee on the Seakeep-

ing Capability of Small Vessels in that organization.

REFERENCES

1. Dahle, E.A. and Kjærland, O. : The Capsizing of M/S HELLAND HANSEN, J-RINA, (1980)
2. Hirayama, T. and Yamashita, Y. : On the Capsizing Process of a Fishing Vessel in Breaking Waves, Journal of the Kansai Society of Naval Architects, Japan, No.196, (1985)
3. Motora, S., Shimamoto, S. and Fujino, M. : Capsizing Experiment on a Totally Enclosed Life Boat, Second International Conference on Stability of Ships and Ocean Vehicles, (1982)
4. Morrall, A. : Capsizing of Small Trawlers, RINA Spring Meetings, (1979)
5. Ohmatsu, S. : Une Méthode Simple pour Générer une Houle Arbitraire dans un Bassin d'Essais, Papers of the Ship Research Institute, No.65, (1981)
6. Hirayama, T. and Sadakane, H. : Capsizing of Ships in Breaking Waves and Irregular Waves, Safety and Stability of Ships and Offshore Structures, (1986)
7. Sadakane, H. : On the Rolling of a Ship on a Billow (2nd Report), (3rd Report), Journal of the Kansai Society of Naval Architects, Japan, No.173(1979), No.180(1981)
8. Sadakane, H. and Yamamoto, K. : An Examination on Capsizing Condition of Ships in Beam Waves, Journal of the Kansai Society of Naval Architects, Japan, No.194, (1984)
9. Japan Craft Inspection Organization : Report of the Research on the Seakeeping Capability of Small Vessels, (1989)
10. Tamiya, S. : A Calculation of Non-linear, Non-symmetric Rolling of Ships, Journal of the Society of Naval Architects of Japan, Vol.126, (1969)
11. Ishida, S. and Yasuno, M. : Model Experiment on Capsizing in Breaking Waves, Abstract Note of the General Meeting of Ship Research Institute, No.52, (1988)
12. Ishida, S., Yasuno, M. and Takaishi, Y. : Model Experiment on the Mechanism of Capsizing of a Small Ship in Beam Seas, Journal of the Society of Naval Architects of Japan, Vol.167, (1990)

Table 1 Principal particulars

	SHIP	MODEL
L _{oa} (m)	7.87	1.300
B (m)	2.47	0.408
D (m)	1.17	0.193
d (m)	0.27	0.053
W (kg)	2500	11.20
GM (m)	0.69	0.082~0.055
Tr (sec)	3.41	1.28 ~ 1.74

Tr : Rolling Period

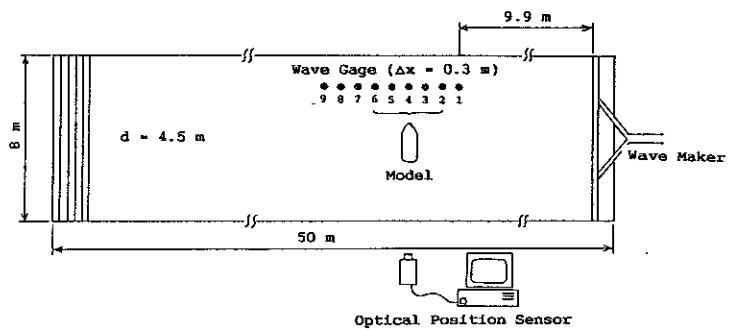


Fig. 3 Experimental apparatus

Table 2 Model conditions

NO.	GM(cm)	Tr(sec)	K	heel(deg)
C1	8.19	1.28	0.401	0
C2	7.74	1.31	0.408	0
C3	7.30	1.34	0.413	0
C4	6.85	1.38	0.417	0
C5	6.40	1.44	0.416	0
C6	6.40	1.46	0.434	0
C7	5.96	1.53	0.433	0
C8	5.51	1.74	0.448	0
CL	8.07	1.41	0.400	7.5 l.side
CW	8.07	1.41	0.400	7.5 w.side

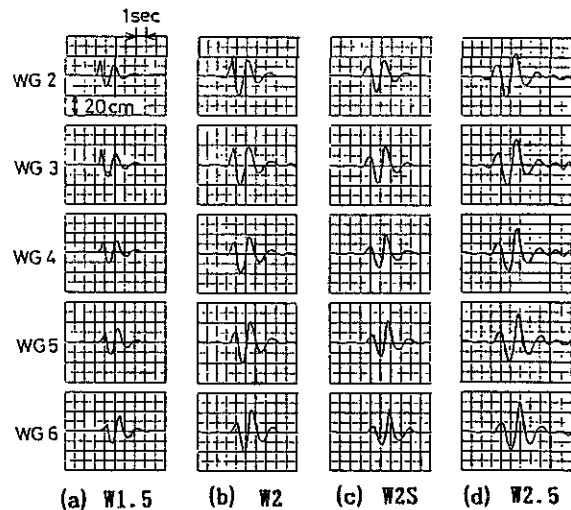


Fig. 4 Wave time histories

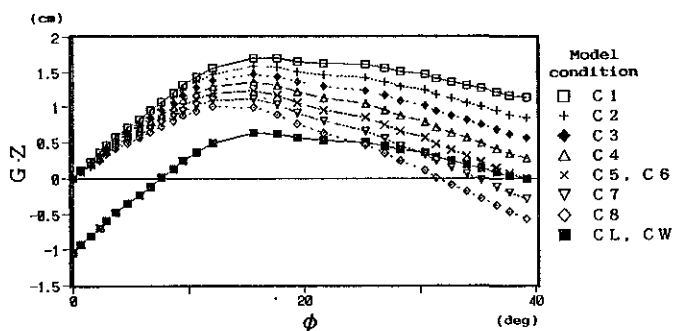


Fig. 1 GZ curves

Table 3 Conditions of capsizing

		Wave & Model Condition																		
		W1. 5				W2				W2 S				W2. 5						
		7	8	L	W	5	6	7	8	L	W	7	8	L	W	7	8	L	W	
Initial Position	2	○	▲	○		●	●	●	●	○		○	○	●	●		○	○	●	
	3	○	▲	○	▲	○	○	○	○	○	○		○	○	○	○	○	○	○	
	4	○	○	○	○	○	○	○	○	●	○	○	○	○	○	▲	○	○	○	
	5	○	○	●	○				○	○	○			○	○	○	○	○	○	
	6	○	○	●	○	○	○	○	○	○	○	○		○	○	○	○	○	○	

○ : No Capsize ● : Capsize(L.Side)
 ▲ : Capsize(W.Side) ○●▲ : Water over Bulwark

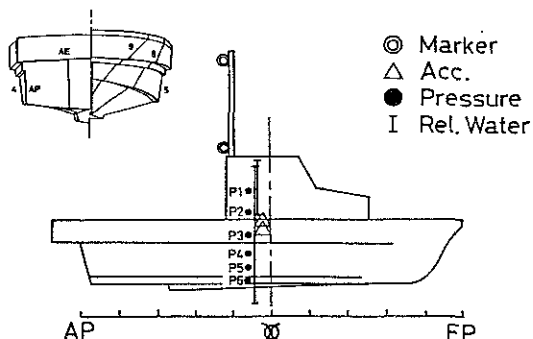
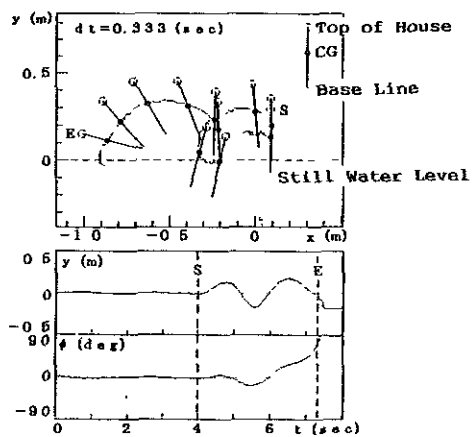


Fig. 2 Layout of sensors and body plan

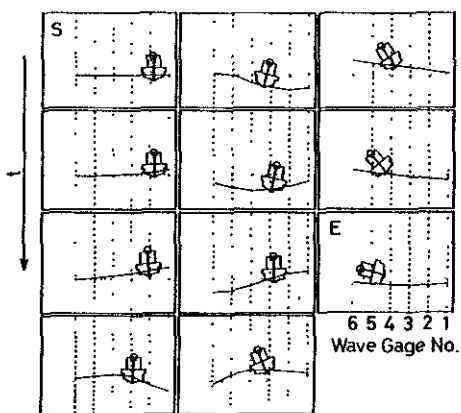
Table 4 Classification of capsizing

		Breaking		Non breaking	
		●	▲	●	▲
Initial heel	7.5°L	—	—	B	—
	0	A	C	—	—
	7.5°W	—	C	—	D

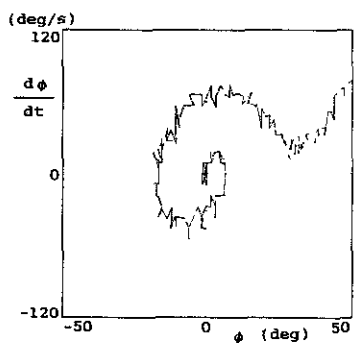
● : Capsize to Lee Side
 ▲ : Capsize to Weather Side



(a) Trajectory of CG

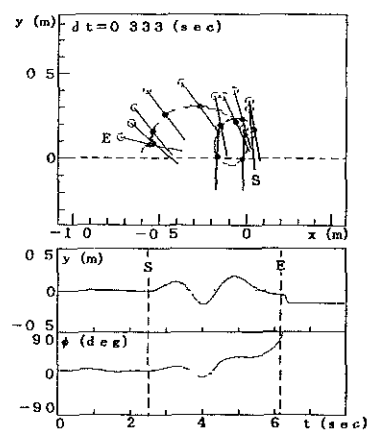


(b) Animation

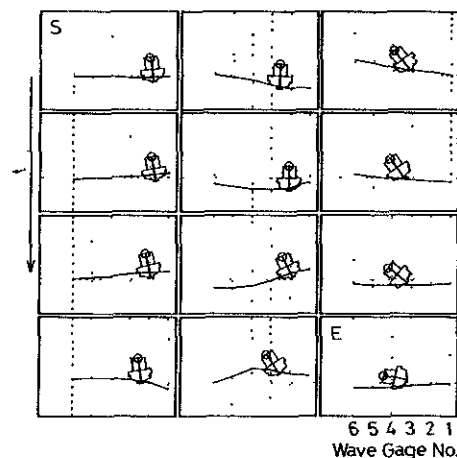


(c) Phase plane ($\phi - d\phi/dt$)

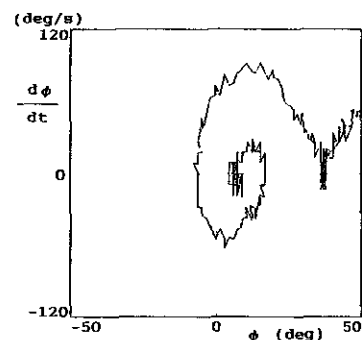
Fig.5 Ship motion, Pattern-A
(Wave:W2, Condition:C7, Position:WG2)



(a) Trajectory of CG



(b) Animation



(c) Phase plane ($\phi - d\phi/dt$)

Fig.7 Ship motion, Pattern-B
(Wave:W2S, Condition:CL, Position:WG2)

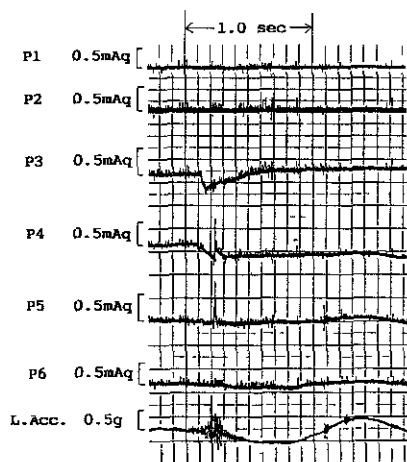


Fig.6 Pressure and lateral acceleration
(Wave:W2, Condition:C7, Position:WG2)

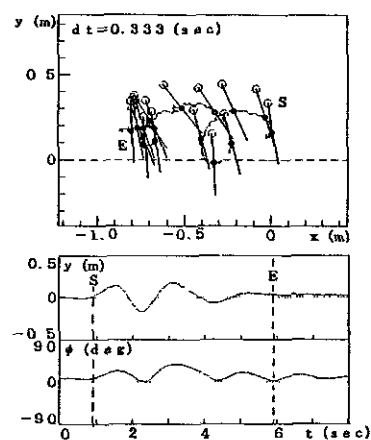


Fig.8 Ship motion
(Wave:W2, Condition:CL, Position:WG2)

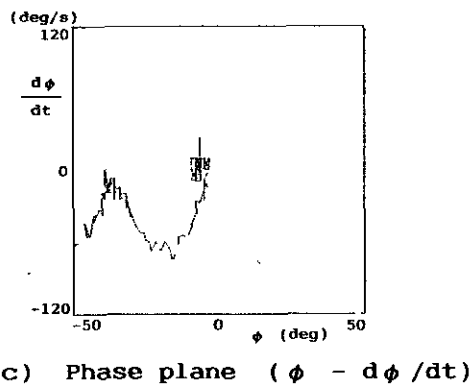
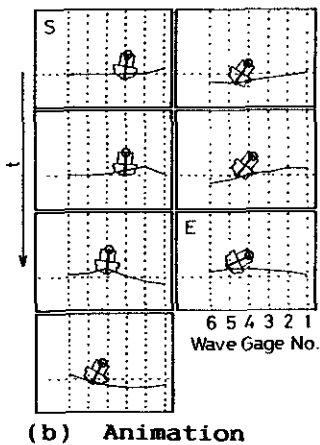
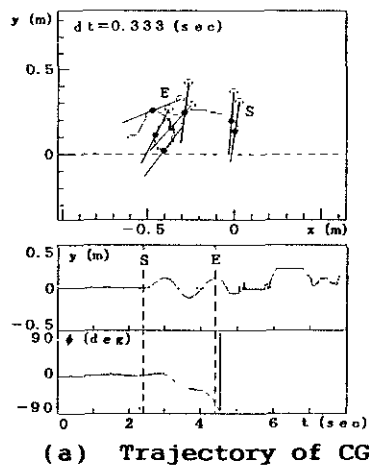


Fig.9 Ship motion, Pattern-C
(Wave:W1.5, Condition:CW, Position:WG3)

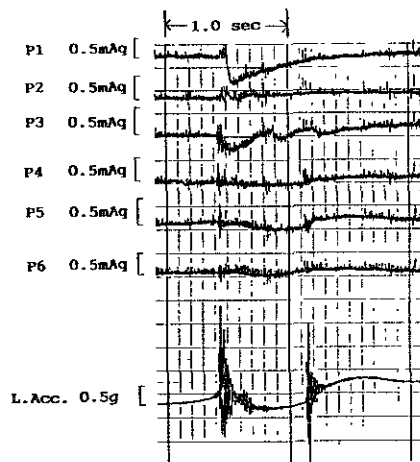


Fig.10 Pressure and lateral acceleration
(Wave:W1.5, Condition:CW, Position:WG3)

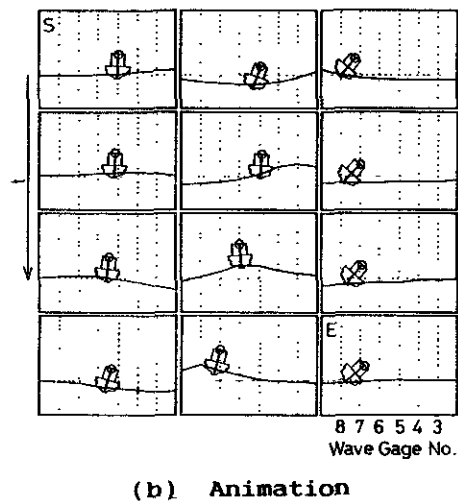
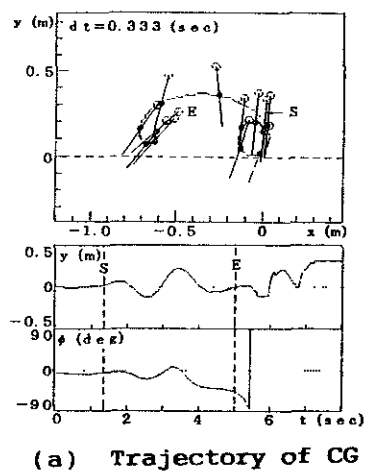


Fig.11 Ship motion, Pattern-D
(Wave:W2S, Condition:CW, Position:WG5)

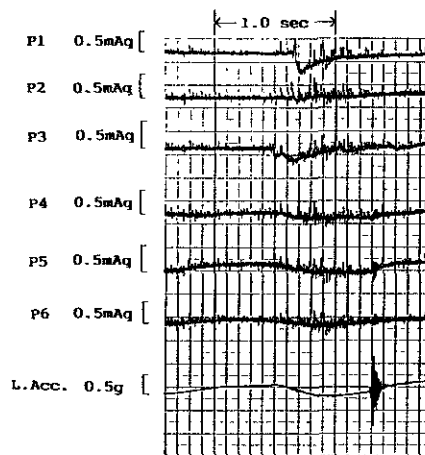
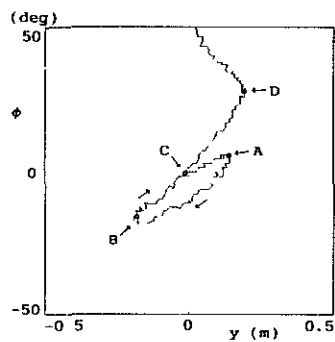
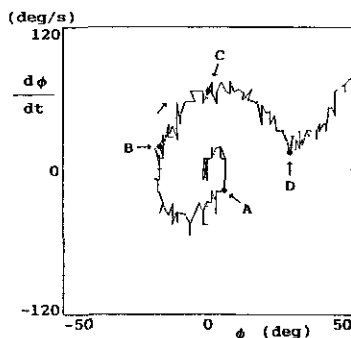


Fig.12 Pressure and lateral acceleration
(Wave:W2S, Condition:CW, Position:WG5)

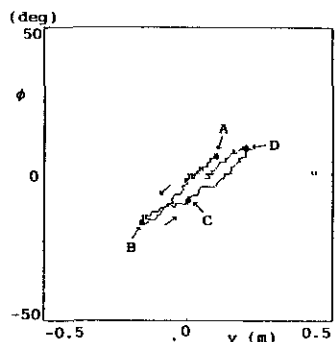


(a) $y - \phi$ plane

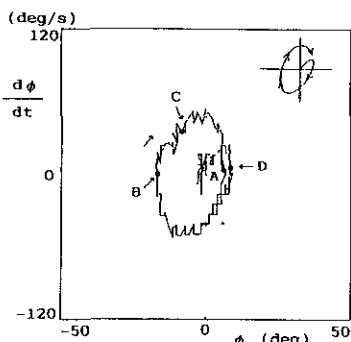


(b) $\phi - d\phi/dt$ plane

Fig.1 3 Phase planes
(Wave:W2, Condition:C7,
Position:WG2)

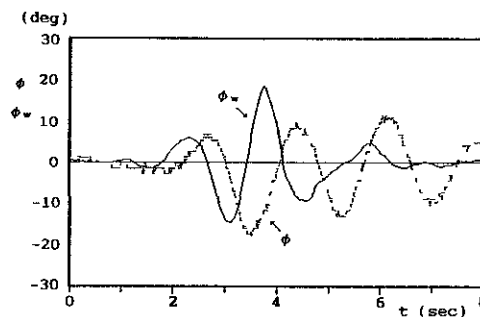


(a) $y - \phi$ plane

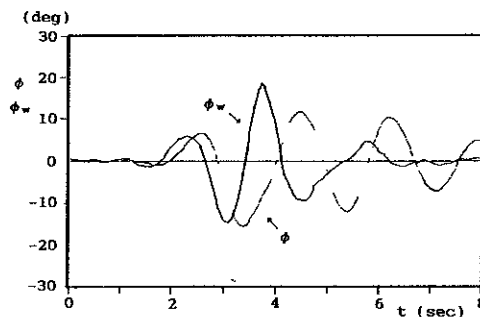


(b) $\phi - d\phi/dt$ plane

Fig.1 4 Phase planes
(Wave:W2S, Condition:C7,
Position:WG2)

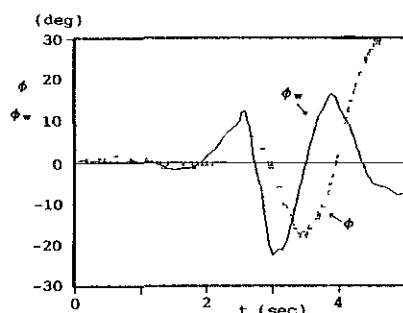


(a) Experiment

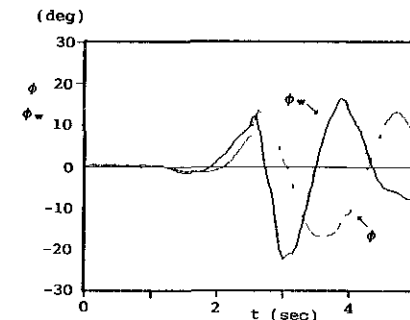


(b) Simulation

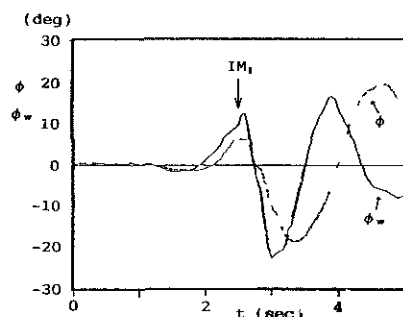
Fig.1 5 Time histories of roll and wave slope
(Wave:W2S, Condition:C7, Position:WG2)



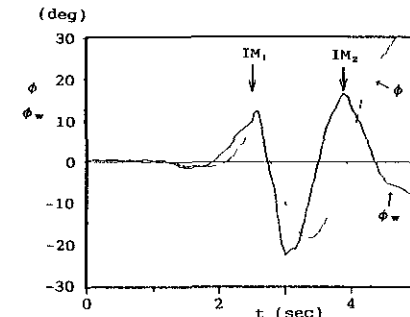
(a) Experiment



(b) Simulation with
no impulsive moment



(c) Simulation with
impulsive moment IM_1



(d) Simulation with
impulsive moment
 IM_1 and IM_2

Fig.1 6 Time histories of roll and wave slope
(Wave:W2, Condition:C7, Position:WG2)

NUMERICAL SIMULATION OF THE ROLLING MOTION OF A SHIP IN QUARTERING SEAS

*
Ho V.B.

**
Frackowiak M.

ABSTRACT

This paper deals with the numerical simulation of the rolling motion of a ship in quartering seas. The roll-sway motions of a ship can be described by differential equations with nonlinear damping, nonlinear time-dependent righting arm functions and sway, roll exciting functions. The numerical simulation is realized on Af 386-EMPAC with the ship of 59m length.

The results of simulation show us:

-When the stability demands of IMO are satisfied, the ship in loaded condition is safe but in ballast condition may be capsized;

-The main reason of capsizing is the exciting moment of wave in ballast condition. The great distance of gravity centre of a ship above exploitation waterline caused this increase of exciting moment;

-The couple of roll-sway in ballast condition has no influence on ship capsizing.

The conclusions show us the way of further investigation of ship stability in following and quartering seas, especially for small ships.

INTRODUCTION

The capsizing of ship in quartering seas is still actual. The ship may suffer from capsizing caused by the pure loss of righting arm, parametric resonance or broaching. Usually these phenomena take place together. Ship may also be capsized because of roll-sway coupling in connection with pure loss of righting arm (5). In this paper, the roll-sway coupling in connection with change of righting arm is investigated by simulation of ship motion in quartering seas.

FORMULATION OF THE EQUATIONS

Systems of coordinates

Three systems of coordinates are used (see fig.1):

-system $O\xi\eta\zeta$ fixed to the earth;

-system $Oxyz$ fixed to the ship and has the centre coincided with the gravity centre of the ship G ;

-system $\bar{O}\bar{x}\bar{y}\bar{z}$ moving with steady forward-speed V in relation with system $O\xi\eta\zeta$.

Equations of motion

Based on the fundamental principle of rigid body dynamics, the

equations describing the five degrees of freedom motion taking into consideration nonlinear term of damping and nonlinear, time-dependent term of righting arm are as follows:

$$m\ddot{y} = Y_{\dot{y}}\dot{y} + Y_{\dot{y}}\dot{y} + Y_y y + Y_{\phi}\dot{\phi} + Y_{\phi}\dot{\phi} + Y_{\phi}\dot{\phi} + Y_{\psi}\dot{\psi} + Y_{\psi}\dot{\psi} + Y_{\psi}\dot{\psi} + Y(t)$$

$$m\ddot{z} = Z_{\dot{z}}\dot{z} + Z_{\dot{z}}\dot{z} + Z_z z + Z_{\theta}\dot{\theta} + Z_{\theta}\dot{\theta} + Z_{\theta}\dot{\theta} + Z(t)$$

$$I_x\ddot{\phi} = K_{\dot{y}}\dot{y} + K_{\dot{y}}\dot{y} + K_y y + K_{\dot{\phi}}\dot{\phi} + K_{\dot{\phi}}\dot{\phi} + K_{\psi}\dot{\psi} + K_{\phi}\dot{\phi} + \frac{1}{6}K_{\phi^3}\dot{\phi}^3 + K_R(\phi, t) + K(t)$$

$$I_z\ddot{\psi} = N_{\dot{y}}\dot{y} + N_{\dot{y}}\dot{y} + N_y y + N_{\dot{\phi}}\dot{\phi} + N_{\dot{\phi}}\dot{\phi} + N_{\phi}\dot{\phi} + N_{\dot{\psi}}\dot{\psi} + N_{\dot{\psi}}\dot{\psi} + N_{\psi}\dot{\psi} + N(t)$$

$$I_y\ddot{\theta} = M_{\dot{z}}\dot{z} + M_{\dot{z}}\dot{z} + M_z z + M_{\dot{\theta}}\dot{\theta} + M_{\dot{\theta}}\dot{\theta} + M_{\theta}\dot{\theta} + M(t) \quad (1)$$

where $K_R(\phi, t) = \Delta[l_{av} + \Delta l \cos(\omega_e t + \xi_0)]$

$$l_{av} = (l_{cr} + l_{tr})/2$$

$$\Delta l = (l_{tr} - l_{cr})/2$$

l_{cr} - righting arm - wave crest amidship;

l_{tr} - righting arm - wave trough amidship;

ω_e - encounter frequency;

ξ_0 - phase angle.

* Associate head of Ship Mechanics Department, the Research and Design Institute of Mechanical Engineering of Communication and Transport - Hanoi.

** Associate professor, Ship Hydromechanic Division, Ship Research Institute Technical University of Gdansk.

With supposition that in quatering seas the most important motion is the sway-roll coupling, we can reduce system [1] to:

$$\begin{aligned}\ddot{y} &= \lambda_1 \dot{y} + \lambda_2 y + \lambda_3 \dot{\phi} + \lambda_4 \phi + \gamma(t) \\ \ddot{\phi} &= \beta_1 \dot{y} + \beta_2 y + \beta_3 \dot{\phi} - g(\phi) - f(\phi) + \bar{K}(t)\end{aligned}\quad (2)$$

where $g(\phi) = a\phi + b\phi^3$
 $f(\phi) = d\phi + e\phi^3 + f\phi^5 + \delta \cos(\omega_e t + \varepsilon_0)$

NUMERICAL ANALYSIS

Simulation of ship is based on polish MS B-57 with main characteristics in table Nr1.

Calculation of differential equation coefficients

The coefficients in [2] are calculated as follows:

-linear coefficients are calculated by known methods in ship hydrodynamics, e. g. program LATAS by the author (3);

-nonlinear damping coefficients are calculated on the base of ship model test data (6);

-nonlinear coefficients of righting arm are approximated by 5-order polynomial on the base of righting arm curves;

-coefficients taking into consideration the influence of the change of righting arm in waves are calculated according to author's program (7).

Some results of simulation

System [2] is high nonlinear. The resolution is realized on microcomputer AT 386 EMFAC with procedure of resolution of differential equation MERSON.

Initial data for simulation

Data for waves

Wave height : $H = 5$ m
 Wave length : $\lambda = 100$ m
 Angle of heading: $\chi = 30^\circ$
 Ship speed : $V = 10$ knots
 Encounter frequencies:
 $\omega_e = 0.51$ 1/s

Data for ship

Ship in loaded condition with $GM = 0.194 - 0.65$ m

Ship in ballast condition with $GM = 0.573 - 0.97$ m (see tabl.1-3).

Righting arm curves in loaded and ballast conditions see fig.4,5.

Results

Fig. 6,7,8 : the time history from the simulation

Fig.9,10,11: the participation of different exciting moments

Fig.12: the final result of the simulation (see tabl.6-8).

CONCLUSIONS

The following conclusions are drawn:

-When IMO stability criteria are satisfied, ship in ballast condition may be capsized, but ship in loaded condition is not capsized (see fig.12):

-The influence of changes of righting arm in wave on roll amplitude is not significant when wave length is much longer than ship length. The decreasing of 75% of righting arm not causes the increasing of roll amplitude (see fig.6,7,8):

-The influence of sway on roll is controversial. On the figures 9-11, participation of every kind of exciting moments in common excitation are shown:

$$\phi + g(\phi) + f(\phi, t) - w(\dot{y}, y, \dot{y}) - \bar{K}(t) = 0 \quad (3)$$

where:

$g(\phi)$ - damping function;
 $f(\phi, t)$ - righting arm function;
 $w(\dot{y}, y, \dot{y})$ - exciting moment of sway on roll;
 $\bar{K}(t)$ - exciting moment of wave.

In ballast condition, the coupling of sway-roll is not very large and not causes the ship to capsize:

-The main reason of capsizing of ship is the wave exciting moment. In the case of ballast condition, this moment is 3,4 times bigger than the case of loaded condition. Large distance between centre of gravity and actual waterline on still water 0b causes the increasing of this moment.

Besides, in ballast condition, because of small draft, damping function is smaller than in loaded condition.

Ship in ballast condition may be capsized in quatering seas because of large exciting moment of wave. The roll-sway coupling does not cause the capsizing. It is the particular case of Ms B-57. We are unable to be sure that it is true for all cases.

These conclusions demand us further investigation of the problem of ship stability in quatering seas.

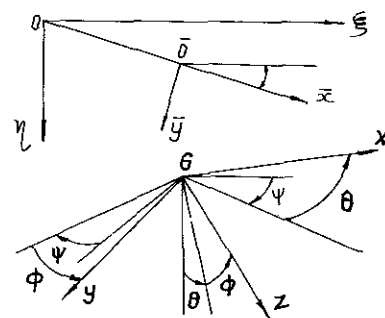


Figure 1. Coordinate systems

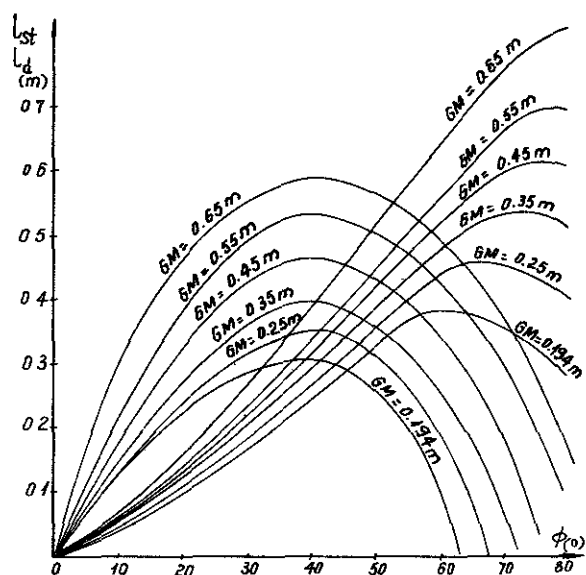


Figure 2. Static and dynamic righting arm curves. Loaded condition.

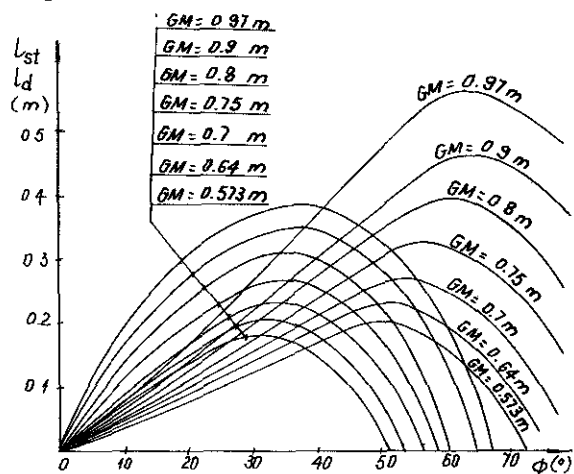


Figure 3. Static and dynamic righting arm curves. Ballast condition.

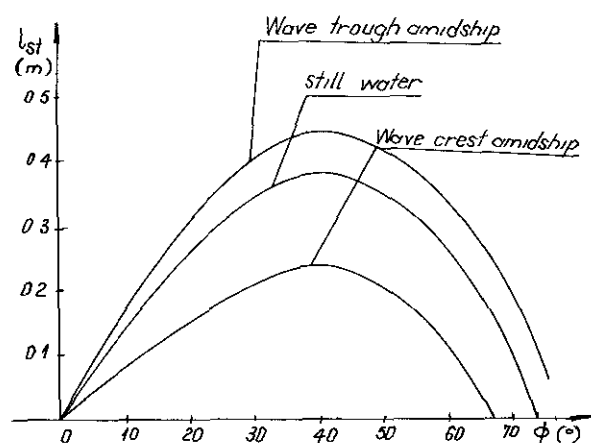


Figure 4. Righting arm curves in seas. Loaded condition.
Wave height $H = 5\text{m}$;
Wave length $\lambda = 100\text{m}$;
Heading angle $\chi = 30^\circ$;
Metacentric height $GM = 0.35\text{m}$.

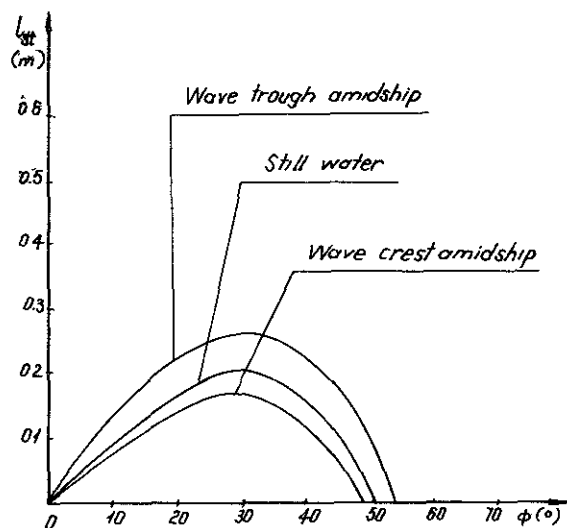


Figure 5. Righting arm curves in seas. Ballast condition.
Wave height $H = 5\text{m}$;
Wave length $\lambda = 100\text{m}$;
Heading angle $\chi = 30^\circ$;
Metacentric height $GM = 0.573\text{m}$.

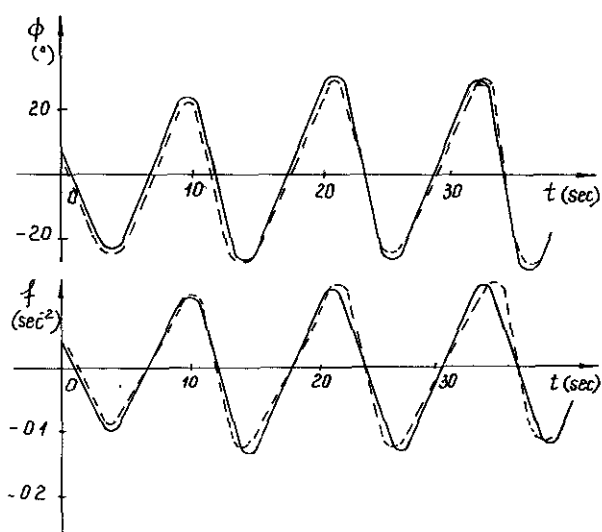


Figure 6. Runs of simulation of ship behaviour in 5m high waves. Loaded condition.
 ϕ - roll angle;
 f - righting arm function;
--- with changes in waves;
— without changes in waves;
Wave height $H = 5\text{m}$;
Wave length $\lambda = 100\text{m}$;
Heading angle $\chi = 30^\circ$;
Metacentric height $GM = 0.35\text{m}$.

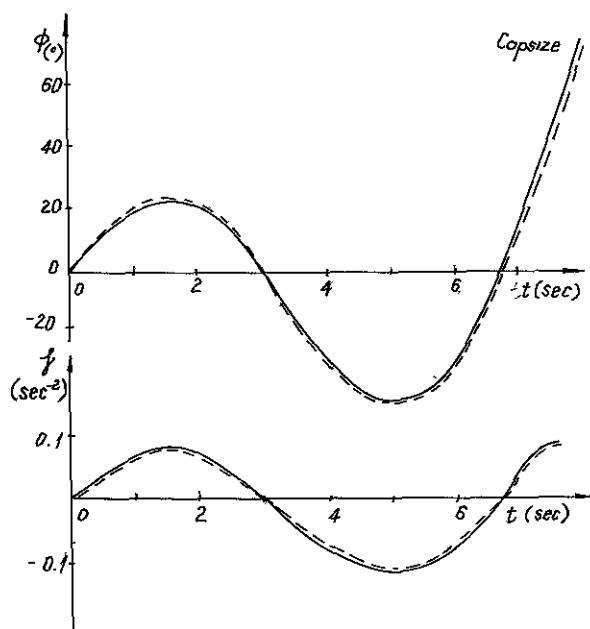


Figure 7. Runs of simulation of ship behaviour in 5m high waves. Ballast condition.

ϕ - roll angle;
 f - righting arm function;
 --- with changes in waves;
 — without changes in waves;
 Wave height $H = 5\text{m}$;
 Wave length $\lambda = 100\text{m}$;
 Heading angle $\chi = 30^\circ$;
 Metacentric height $GM = 0.573\text{m}$.

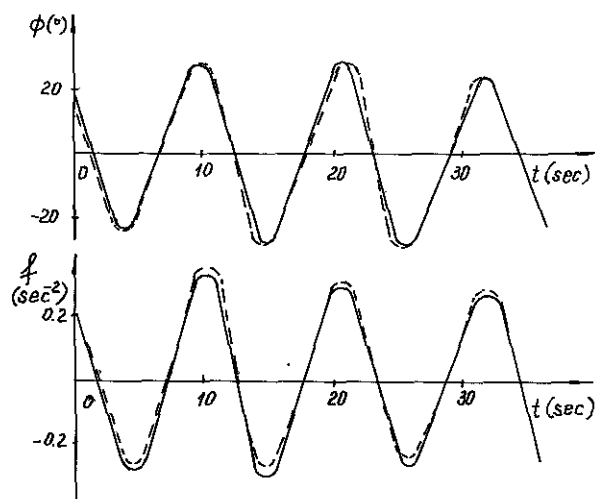


Figure 8. Runs of simulation of ship behaviour in 5m high waves. Ballast condition.

ϕ - roll angle;
 f - righting arm function;
 --- with changes in waves;
 — without changes in waves;
 Wave height $H = 5\text{m}$;
 Wave length $\lambda = 100\text{m}$;
 Heading angle $\chi = 30^\circ$;
 Metacentric height $GM = 0.97\text{m}$.

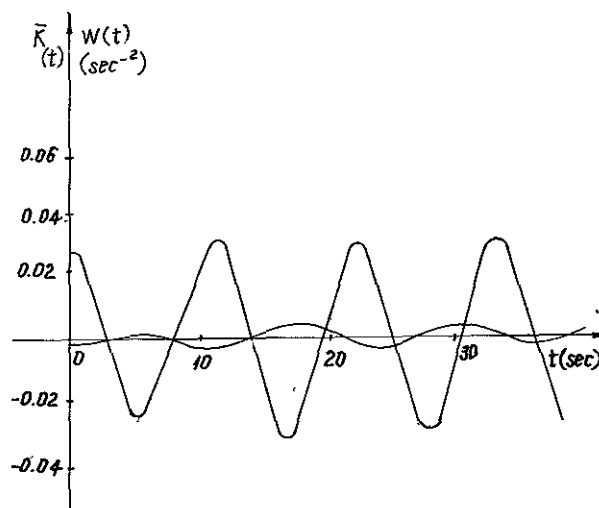


Figure 9. Runs of simulation of ship behaviour in 5m high waves. Loaded condition.

$\bar{K}(t)$ - wave exciting moment;
 $W(t)$ - sway exciting moment;
 Wave height $H = 5\text{m}$;
 Wave length $\lambda = 100\text{m}$;
 Heading angle $\chi = 30^\circ$;
 Metacentric height $GM = 0.35\text{m}$.

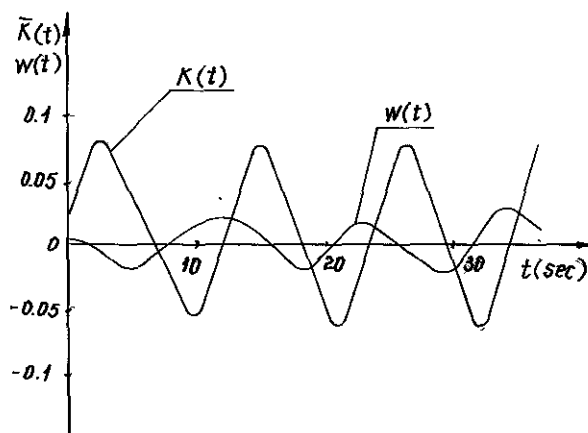


Figure 10. Runs of simulation of ship behaviour in 5m high waves. Ballast condition.

$\bar{K}(t)$ - wave exciting moment;
 $w(t)$ - sway exciting moment;
 Wave height $H = 5\text{m}$;
 Wave length $\lambda = 100\text{m}$;
 Heading angle $\chi = 30^\circ$;
 Metacentric height $GM = 0.573\text{m}$.

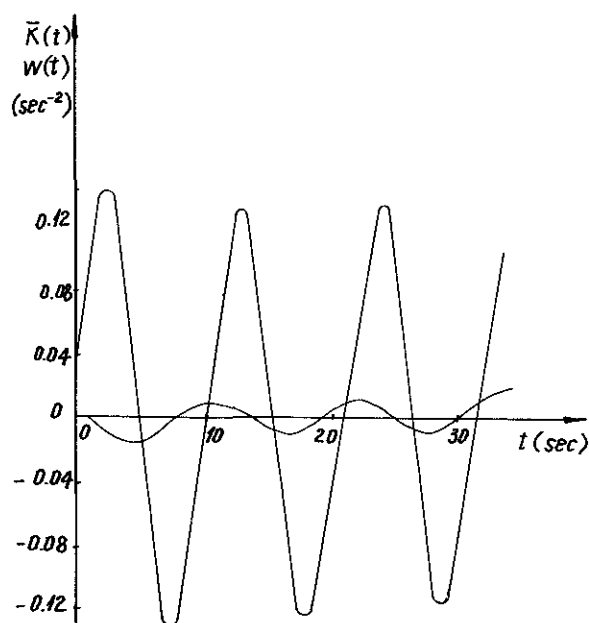


Figure 11. Runs of simulation of ship behaviour in 5m high waves. Ballast condition.

$K(t)$ - wave exciting moment;
 $w(t)$ - sway exciting moment;
 Wave height $H = 5m$;
 Wave length $\lambda = 100m$;
 Heading angle $\chi = 30^\circ$;
 Metacentric height $GM = 0.97m$.

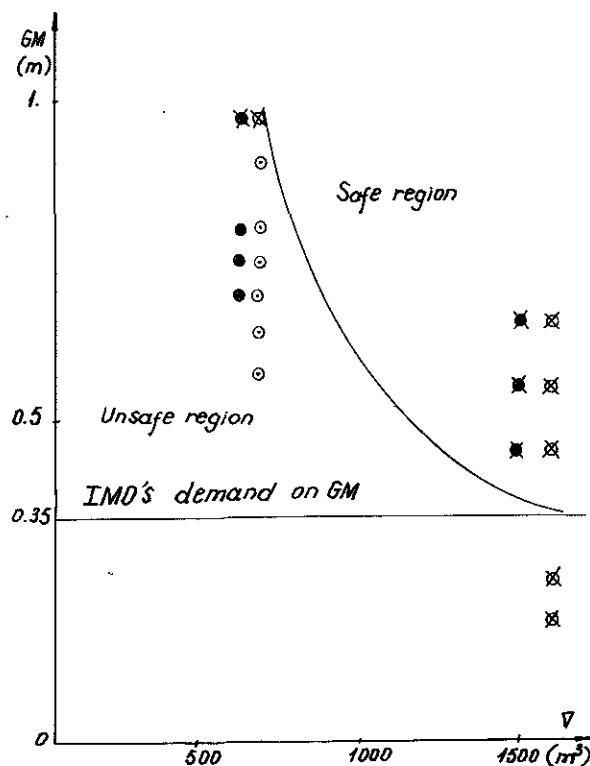


Figure 12. The results of the simulation.

⊗ - no capsize (simul.);
 ⊗ - no capsize (model test);
 ○ - capsize (simul.);
 ● - capsize (model test).

TABLE 1
Main characteristics of ships

Name of ship				B-57	Edith Terkol
Length between perpendiculars	Lpp	m		59.0	58.6
Breadth	B	m		9.9	9.65
Depth	D	m		5.95	4.95
Speed	V	kn.		10.0	10.0

TABLE 2
Characteristics in ballast condition

Name of ship				B-57	Edith Terkol
Volume displacement	V	m ³		690.0	645.0
Draft aver.	d	m		1.99	1.64
Metacentric height	GM	m		0.64	0.64

TABLE 3
Characteristics in loaded condition

Name of ship			B-57	Edith Terkol
Volume displacement	V	m ³	1566.0	1561.0
Draft aver.	d	m	3.715	-
Metacentric height	GM	m	0.65	0.65

TABLE 4
Dynamic righting arm curves in ballast condition

	e30 m.rad	e40 m.rad	e40-e30 m.rad	Gzmax m	$\phi(Gzmax)$	GM m
B-57	0.067	0.099	0.032	0.218	30	0.64
Edith Terkol	0.096	0.135	0.039	0.32	27	0.64
IMO's demands	0.055	0.09	0.030	0.20	30	0.15

TABLE 5
Dynamic righting arm curves in loaded condition

	e30 m.rad	e40 m.rad	e40-e30 m.rad	Gzmax m	$\phi(Gzmax)$	GM m
B-57	0.107	0.198	0.091	0.586	40	0.65
Edith Terkol	0.055	0.098	0.043	0.29	46	0.65
IMO's demands	0.055	0.09	0.030	0.20	30	0.15

TABLE 6
Simulation results in ballast condition

GM (m)	B-57 Number of simulations	Number of capsizes	Model Edith Terkol Number of runs	Number of capsizes
0.575	1	1	-	-
0.64	1	1	5	2
0.70	1	1	3	2
0.75	1	1	3	1
0.80	1	1	-	-
0.90	1	1	-	-
0.97	1	0	6	0

TABLE 7
Simulation results in loaded condition

GM (m)	B-57 Number of simulations	Number of capsizes	Model Edith Terkol Number of runs	Number of capsizes
0.194	1	0	-	-
0.25	-	-	-	-
0.35	1	0	-	-
0.45	1	0	3	0
0.55	1	0	10	0
0.65	1	0	4	0

TABLE 8

Exciting amplitude in relation with initial metacentric height and distance between ship centre of gravity and actual waterline

	GM (m)	ZG (m)	OG (m)	Exciting amplitude
Loaded condition	0.194	3.970	0.255	0.0267
	0.350	3.814	0.099	0.0427
	0.450	3.714	-0.001	0.0536
	0.550	3.614	-0.101	0.0647
	0.650	3.514	-0.201	0.0757
Ballast condition	0.573	5.213	3.223	0.1090
	0.640	4.573	2.583	0.1120
	0.700	4.513	2.523	0.1150
	0.750	4.463	2.473	0.1180
	0.800	4.413	2.423	0.1210
	0.900	4.313	2.323	0.1270
	0.970	4.243	2.253	0.1320

REFERENCES

1. Ho V. B., The Stability Safety of a Ship in Quartering Seas. Doctor Thesis, Ship Research Institute, Gdansk, 1980.
2. Raff A.I., Program SCORES - Ship Structural Response in Waves. Ship Structural Committee Report SSC - 230, July 1972.
3. Ho V. B., Le H. H., Program LATAS - Ship Structural Response in Waves. Science and Technics of Transportation Engineering Nr 3, Hanoi, 1986 (in vietnamese).
4. Bishop R.E., Price W.G., Temarel P. The Influence of Load Condition in the Capsizing of a Ship. STAB'86 - Gdansk 1986.
5. Kure K., Pang C.J., The Ultimate Half Roll. International Conference on Stability of Ship and Ocean Vehicles - Glasgow 1975.
6. Dudziak J., Frackowiak M., Współczynnik tłumienia kołysan bocznych. Publ. Nr 277, Ship Research Institute, Gdansk 1974.
7. Ho V. B., Calculation of Cross Curves in Wave. Publ. Nr 1029 /78 Ship Research Institute, Gdansk 1978.

ABOUT THE AUTHORS

Ho Van Binh, graduated in naval architecture from the Technical University of Gdansk in 1971. Since then he has been working as a researcher at Shipmechanic Department of the Research and Design Institute of Mechanical Engineering of Communication and Transport in Hanoi. He completed his Ph.D. thesis in 1980 at the Ship Research Institute, Technical University of Gdansk.

Frackowiak Milosz, graduated in naval architecture from Technical University of Gdansk in 1956 and since then started his work at the Ship Hydromechanic Division and has been working there till now. Ph. D. in 1966, since 1970 assistant professor. In the period 1970-1973 professor at Marine Engineering Department, Basra (Iraq) and in 1981 - 1983 Marine Engineering Department, Port Harcourt (Nigeria).

**SIMULATION OF CONTROL FUNCTIONS FOR SHIP STABILITY:
A USER ORIENTED FLEXIBLE TOOL.**

R.Molinari (*), C.Penno (#), C.Rezzoagli (#)

ABSTRACT

Ship stability requires flexible and reliable tools for the simulation of effects produced by the control actions.

Stability problems represent a fundamental issue especially in semisubmersible vessels, where the variability of operating conditions covers a wide range of values.

A simulator has been developed in order to face two important problems. Viz working out the expected changes in stability conditions as consequence of load, crane and ballast operations and, on the other hand, obtaining an advice related to the modality of ballasting operations to achieve the target condition.

A mathematical model has been developed to compute the vessel position with respect to pitch, roll and heave; the displacement and the stability margin have also been worked out.

The system checks if stability requirements are satisfied in the actual simulated condition and analyses the hydraulic network system.

Three automation levels have been taken into account: manual, semi-automatic and fully automatic level.

Great care has been taken in providing the system with a user-friendly interface.

INTRODUCTION

Design and control technology, applied to offshore semisubmersible vessels, has been recently considerably innovated in order to increase the operative time by allowing transport of higher quantities of loads and keeping the operativeness also in critical sea conditions.

Operativeness can be increased by the use of advanced automatic systems able to control the six freedom degrees of movement of the vessel, that is modelled as a rigid body.

While a Dynamic Positioning System handles the three horizontal movements (surge, sway and yaw), the other degrees of freedom (pitch, roll and heave) are controlled by a Ballast System.

The latter is the object of this study and operates in order to maintain the draught, heel and trim angles within pre-defined user constraints.

This system monitors the values of the controlled variables. In case of necessity, it advises the user and, when the automatic mode is switched on, this acts the hydraulic ballast system. The Ballast System verifies also the stability conditions.

A ballast control system simulator has been developed to support the user's actions and relieve him of the heaviest stability calculations.

Three automation levels (manual, semi-automatic, automatic) have been distinguished, according to the kind of function requested by the user.

RESEARCH PROGRAM OBJECTIVES

The purpose of the present study is the development of an instrument aimed to the automatic verification of stability conditions and to the optimal loads distribution.

Furthermore, other functions are provided to simulate loading and ballasting operations and their influence on stability parameters.

This tool can be usefully employed by an operator or by a designer who deals with ballast strategies or hydraulic network layouts.

An operator can use the simulator off-line as a training tool, or on-line as an advisory tool.

In the first case the operator can become familiar with: ballasting techniques, hydraulic network topology, vessel's response to loading/unloading and crane's operations.

In the second case, he can simulate an operation before doing it and verify if the results are really the expected ones.

A ballast designer can use the simulator trying different automatic ballast strategies in order to find the best one. Besides he can verify if the designed hydraulic network topology and its conventional use, are suitable.

(*) Ansaldo Industria, Genova, Italy

(#) Ansaldo Ricerche, Genova, Italy

The simulator provides several functions.

Displacement and ship inclination can be changed by:

- loading/unloading solid and liquids weights
- moving cranes
- setting heel and trim angles' offsets due to unknown forces
- acting on the ballast tanks' content (manually or automatically).

The system has four operative modes: heeling elements setting and three ballast levels (manual, semiautomatic and automatic).

In the "heeling elements setting" mode, the open-loop vessel is simulated.

Menu choices allow to execute loading/unloading operations, crane movements, or select trim and heel offsets due to unknown causes.

At the "manual level" the user can open/close valves or start/stop valves and pumps using cursor control on the graphic display reproducing the vessel's hydraulic network.

On the synoptic, vessel's response to the chosen operation is shown, updating the tanks' contents.

At the "semiautomatic level" the user can choose tanks' level set-points. The simulator acts on the hydraulic network devices in order to achieve the required configuration.

The network state evolution is graphically displayed and, at every moment, the user can stop the current actions.

The "automatic level" represents the highest automation level: the user can only require certain values of draught, trim and heel angles.

The program establishes which tanks fill/drain and how much fill/drain them, to obtain the selected draught, trim and heel angles.

On the graphic display the user can again control the hydraulic system evolution, following the sequence of operations chosen by the simulator's ballast strategies.

This sequence is the result of an optimization algorithm.

THEORETICAL APPROACHES

A fundamental issue in the development of a Ballast Control System concerns the vessel's model, which underlies the functions regarding ship stability and ballast operations.

The simulation model has been based essentially on static criteria [1],[2],[3]: only the static vessel's behaviour has been reproduced, while dynamic transients have been neglected.

Given a certain load condition (including deckloads, deadweights, cranes, ballast and various tanks), the vessel's state is estimated, calculating heel and trim angles, draught, total center of gravity, stability margin.

In addition, other important parameters are derived, in order to simulate the behaviour of the hydraulic ballast system, such as water level in the tanks and valves' and pumps' state.

Transients due to crane's movements or ballast operations are approximated by subsequent steady conditions, coming between the initial and the final stable states.

Namely the evolution of the system is described as a succession of intermediate steady states, that correspond to a real forces configuration. The static hypothesis allows to consider null angular and linear velocities in each state.

The static approach can be justified by considering that the Ballast System has to handle forces that are nearly time invariant.

The sequence of such "photograms" allows to verify stability conditions during the above mentioned operations, in order to find at which step of cranes' rotation or ballasting they are violated.

The dynamic response delays of the vessel at the ballast control actions permit to suppose that the controlled system behaves like an open loop system.

That hypothesis comes true when a transient produced by a certain new heeling moment ends before the beginning of the control reaction caused by the moment itself.

On the basis of this feature a static model is suitable.

A discrete event simulation has been worked out. Heeling causes can be set simultaneously or separately, and the final vessel's condition is generated.

Only cranes' rotations and ballasting operations are virtually split into subsequent steps. In fact they are supposed to need more time than loading/unloading operations and, above all, they can be interrupted, whenever a harmful situation happens.

In the next paragraphs, some theoretical aspects are pointed out.

THE MATHEMATICAL MODEL

The model used to simulate the vessel static behaviour is simply given by the mathematical equation representing the equilibrium between the heeling moment and the righting moment [1],[2],[3].

The distribution of loads can change the position of the center of gravity, moving it away from the vertical line passing through the center of buoyancy.

A heeling moment is generated, making the vessel to change heel and trim angles, with corrections also of the draught as side effect, until the buoyancy center and the gravity center lie again on the same vertical line.

A loads' definition is requested as precise as possible, specifying the weight and the coordinates of each load.

A particular description is needed by liquid loads, whose tipology can change in dependence on the kind of vessel dealt with.

The definition of the liquid's level in a tank makes unique the other meaningful variables related to that load, by means of tables expressing such dependency.

Among those variables, the longitudinal and transversal free surface inertial moments are displayed. They allow the estimation of the metacentric height reduction, that affects the righting moment.

In addition, the availability of the even keel table and the cross curves table is supposed.

In particular from the even keel table the discrete definition of the longitudinal and transversal righting arm has been used. The cross curves table has provided the correspondence of draught with displacement and longitudinal and transversal metacenter vertical coordinates.

Given the coordinates of the center of gravity and the displacement, whether the righting moment is known, the values of draught and of trim and heel angles are uniquely determined.

Interaction between pitch and roll movements has been considered negligible, so that the estimation of the longitudinal heeling moment can be superimposed on the transversal heeling moment, and viceversa.

The heel angle p can be obtained (fig.1) from the following geometrical expression:

$$\begin{aligned} Y_G - Y_B(0) \\ \text{tg}(p) = \frac{\quad}{z_M(p) - z_G} \end{aligned} \quad (1)$$

where:

- Y_G : transversal coordinate of the actual center of gravity
- $Y_B(0)$: transversal coordinate of the center of buoyancy at even keel
- $z_M(p)$: vertical coordinate of the center of gravity at the heel angle p
- z_G : vertical coordinate of the actual center of gravity

The difference $z_M(p) - z_G$ takes into account the metacentric height due to the free surface of liquid loads. More precisely, the reduction has been added to the real vertical coordinate of the center of gravity.

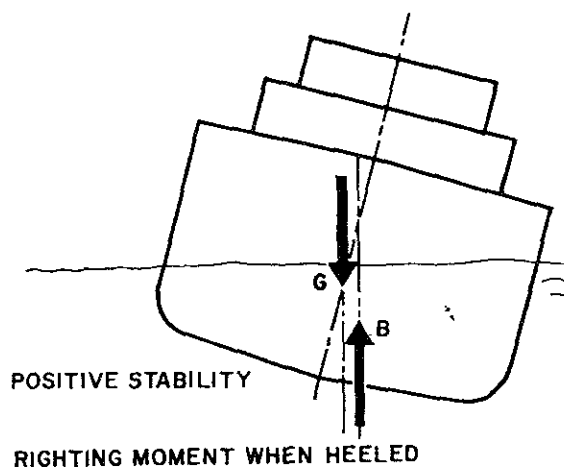


FIG.1

The expression (1) can be rewritten:

$$\begin{aligned} z_M(p) * \sin(p) &= \quad (2) \\ &= z_G * \sin(p) + (Y_G - Y_B(0)) * \cos(p) \end{aligned}$$

Note that $z_M(p) * \sin(p)$ is the arm of the righting moment ($KN_1(p)$).

The hull intrinsic characteristics, represented by the even keel table and the cross curves table, provide the value of the righting arm (KN) as a discrete function of the heel angle p :

$$KN_2(p) = f(p)$$

The actual value of p is determined by the intersection of the two curves $KN_1(p)$ and $KN_2(p)$.

REGULATOR

Using the fully automatic level of the system, the user is only requested to declare the desired values of draught and of heel and trim angles.

This level aims at hindering only time invariant moment and forces, acting on the vessel.

A control strategy of this kind can be applied to a ballast system, whose operations are so slow that compensations of brief deviations are unfeasible, or at least useless.

Therefore the difference between the set-point and the real values of draught and trim and heel angles is integrated and the result is compared with a fixed threshold.

When the threshold is exceeded, the suitable amount of ballast water for each tank is allotted.

The threshold's value must be chosen so that it represents a good compromise between the vessel's safety and insensibility to time variant heeling moments.

To avoid that a meaningless deviation, constant for a long time, produces an unuseful ballast reaction, the mean error is compared with another threshold, which represents the minimum constant deviation that has to be hindered.

Whenever the ballast allotment is activated, the integral error is reset, so that hystorical information is deleted, after the generation of right control actions.

BALLAST ALLOTMENT

Ballast allotment consists in a procedure that assigns the right amount of ballast water to the tanks.

It is mainly used by the automatic ballast system, but it can be very helpful also as an advisory function.

It works out a suitable tanks' configuration, in order to produce the values of draught, heel and trim angles.

Changes of such variables are translated in an equivalent heeling moment, that the ballast system try to obtain by moving or flowing in/out a suitable amount of ballast water.

Then a new center of gravity is calculated.

A linear programming algorithm (the simplex method [4]) has been chosen to find an optimal allotment of the required changes in tanks' water.

There are essentially two targets, both regarding the center of gravity:

- 1) the whole change in ballast water must be as close as possible to the change of displacement required;
- 2) the new center of gravity must lie as close as possible to its ideal position.

The following constraints are imposed:

- a) in each tank the water amount must not exceed the limits of full/empty tank;
- b) ballast water must be allotted with preference to pontoon (column tanks are used only when pontoon tanks do not allow to reach the target);
- c) the horizontal distance between the vessel's center of gravity and the center of gravity of tanks' water must be minimum, to avoid structural stress;
- d) tanks' contents are preferably changed if they have large free surface, as to possibly reduce it.

To express linearly the b),c),d) constraints, for each tank a penalty cost is computed.

To avoid numerical problems, conversion factors are used. In this way the algorithm deals with values, that are homogeneous in magnitude.

HYDRAULIC BALLAST SYSTEM

The hydraulic network is represented by a set of connections between single ballasting devices and the sea.

Moreover operational constraints are provided, in order to allow the user to execute only correct operations and to permit the automatic system to select feasible choices.

Additional features support the graphic representation of the ballast hydraulic system.

The network model consists in an oriented graph ($G = \langle N, L \rangle$) [5], where:

$N = \{ \text{arcs representing pipes} \};$

$L = \{ \text{nodes representing sea chests, outlets, tanks and all those points in which two or more pipes are connected} \};$

The adjacency matrix represents all the connections between the nodes and is, in general, not symmetric.

If a pipe contains a valve/pump, its ends will be considered connected only if the device is open/active.

Further information are added, establishing conventional constraints of the hydraulic network exploitation.

They are used either for user's input checking (manual level) or automatic path retrieving (semiautomatic and automatic levels).

UNDETERMINED FORCES

A special problem arises dealing with the real difficulty of defining the right weight and, above all, the exact coordinates of the center of gravity of each load on board.

To cope with this aspect, the user has been given the possibility to define the real values of heel and trim angles, so that the simulator can correct the computed values.

This is done by adding two virtual loads, that lie in symmetrical positions with respect to the center of gravity. They both have the same weight, with different sign, so that they produce a heeling moment equivalent to the moment that had been neglected.

Although this compensation method could be considered rough, it provides efficient corrections of errors related to unavoidable inaccuracy of the loads' parameters definition.

STABILITY CRITERIA

The following stability criteria have been taken into account in order to check stability conditions. They are synthesized by the maximum allowable VCG curve, that is obtained by taking the lowest values of a set of curves referred to the following principles:

- 1) the first interception between the heeling moment and the righting moment must not be less than 15°;
- 2) the second interception between the heeling moment and the righting moment must be greater than 30°;
- 3) the area under the righting moment curve must be greater than 30% in excess of the heeling area from 0° to 30°, or from 0° to downflooding angle, if it is less than 30°;
- 4) the righting arm must be positive over the entire range of definition;
- 5a) the metacentric height must be greater than 0.3 m. for temporary conditions;
- 5b) the metacentric height must be greater than 1.0 m. for stationary conditions.

The 5a) and 5b) criteria are applied to different vessel's conditions. The vessel is supposed to stay at some predefined draught (transit, survival and operational); in this case the 5b) criterion is used. On the contrary, during passages between predefined states, the 5a) criterion is applied.

SIMULATOR'S FUNCTIONAL OVERVIEW

A simulator has been implemented, using a high level language (C) on personal computer.

An accurate friendly interface has been developed, in order to simplify parameters settings and ballast management.

Main stability values are continuously displayed, using a clear graphic.

The user interface as well as the program are menu structured. This structure has been implemented as a finite state automata [6].

In this way a high modularity level has been achieved.

As consequence, the program structure allows for an adaptable configuration of the system, in case the vessel in question were to be a different one.

Loads on board have been defined, using three data bases, dedicated respectively to movable solid, fixed solid and fixed liquid loads.

The user can act on them directly.

List functions are provided to display the actual values of the main simulation parameters.

To lighten the data definition, a special function has been given. It consists in the possibility of using predefined system configuration, that are particularly significant for ship stability. Moreover the user can store critical configuration during the development of real operations.

Afterwards, selecting these configuration, the user can try new actions, or execute them in a different order, until the optimal sequence is achieved.

Effects of these operations on the stability values are displayed in a window that is present in all the menu pages.

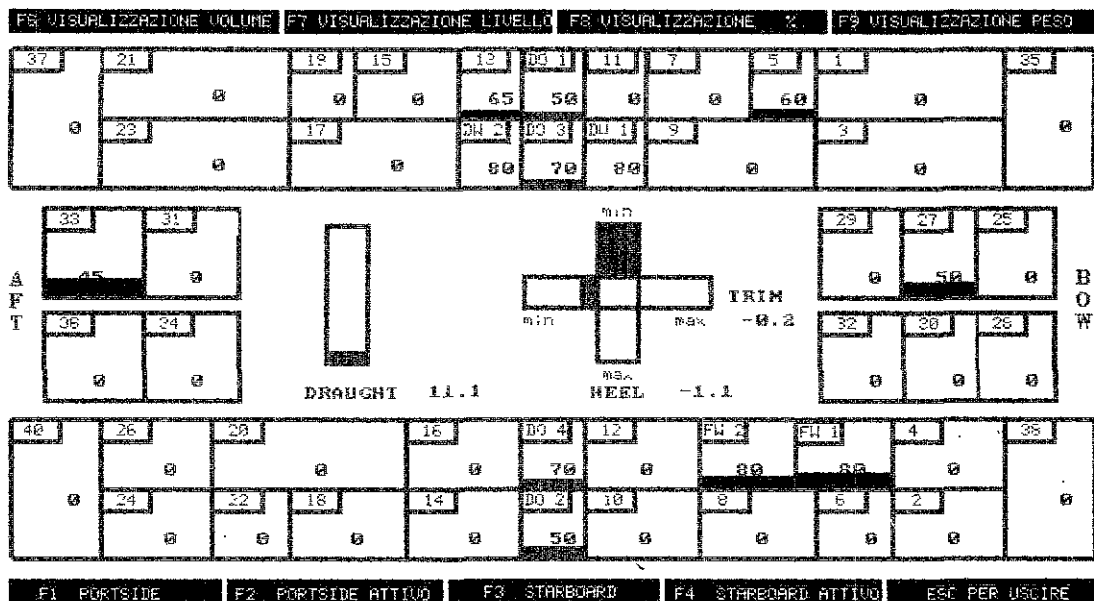


FIG.2

Moreover, an alarm window displays warning messages when security levels, i.e. heel and trim, draught or stability limits have been exceeded.

An example of the clear graphics, used in synoptic pages, is given in fig.2. It shows the tanks inside the hull, their contents and the actual values of draught, trim and heel angles.

EXPERIMENTAL RESULTS

The simulation has been based on data concerning the semisubmersible vessel Scarabeo 5, a drilling rig operated by the oil company SAIPEM.

The hull is formed by two pontoons and six columns. Each pontoon contains 15 ballast tanks, while 10 tanks are distributed inside four columns.

The hydraulic network is fully redundant in order to improve the system's reliability, in case of fault.

Pontoon tanks are filled by gravity, while pumps are used in all the other operations.

The behaviour of the simulated system is close to the real one that has been observed on board, during sea-trials.

Experimental tests have been made on the model, reaching vessels' configurations in agreement with theoretical documented results, that have been worked out by the shipyard [7].

CONCLUSIONS

The activity here presented follows the general trend increasing the degree of automation employed on board, freeing the user from the heaviest jobs and supporting him on his decisions.

The developed tool helps the user in taking vision on the whole plant. Then he can either simulate operations before the real actions or control the operation's effect on ship inclination and stability parameters.

These possibilities give the system a higher level of reliability, making easier, at the same time, the user interaction.

On the other hand a ballast system designer can take advantage from the implementation of a vessel's mathematical model, in order to compare different ballast strategies.

REFERENCES

- [1] C.S. Moore
PRINCIPLES OF NAVAL ARCHITECTURE
Chapter II: INTACT STABILITY
SNAE, 1969
- [2] G. Gazzo
LEZIONI DI ARCHITETTURA NAVALE
Poligrafico Accademia Navale Livorno, 1974
- [3] A. Di Bella
APPUNTI DI STATICA DELLA NAVE
Universita' di Genova, 1984
- [4] W.H. Press, B.P. Flannery, S.A. Teukolsky, W.T. Vetterling
NUMERICAL RECIPES IN C
Chapter 10: LINEAR PROGRAMMING AND THE SIMPLEX METHOD
Cambridge University Press, 1988, pp.329-343
- [5] Elaine Rich
ARTIFICIAL INTELLIGENCE, Chapter 3
Mc Graw-Hill Ed., U.S.A., 1983
- [6] David Gries
COMPILER CONSTRUCTION FOR DIGITAL COMPUTERS, Chapter 3
J.Wiley & Sons, N.Y., U.S.A., 1984
- [7] FINCANTIERI
BALLASTING FROM TRANSIT TO SURVIVAL - OPERATING DRAFT
Booklet MC/CAL N.174
FINCANTIERI, Trieste, 1989

INFLUENCE OF MAIN FORM PARAMETERS ON STABILITY MARGIN OF SHIPS ROLLING IN BEAM SYNCHRONOUS WAVES

Andrew Zborowski¹ and Metin Taylan²

ABSTRACT

The objective of the paper is to compare the statical and dynamical stability characteristics of a dozen of small vessels forms. For the purpose of comparison a ship stability merit and a procedure to calculate it have been proposed. The suggested stability merit is in a form of the stability margin which includes roll motion responses in beam synchronous waves. The applied nonlinear roll motion prediction model introduces a number of ship dynamic characteristics along with the basic environmental parameters into the conventional statical stability approach. The rolling amplitude has been calculated for the conditions for which the forms analyzed meet the stability standards. The analysis reveals how any stability standards, particularly the IMO criteria, may affect the stability margin of various ship design alternatives defined by a given combination of the main form parameters.

1. INTRODUCTION

One of the fundamental features of the engineering philosophy widely applied in naval architecture since the field had fully emerged last century, is the known iterative approach which involves various levels of sophistication in development of marine vehicle design and prediction of its performance. The number of iterations and sophistication of the adopted methods depend on the type of vessel, but first of all they are affected by the available technology. Nowadays the progress in research and application of computers make it possible to develop and apply highly advanced approaches in design of ships and more realistic prediction methods.

The iterative approach and application of different levels of sophistication are common in preliminary

design, in ship hydrodynamics, in structural mechanics, and are justified by complexity of the ship and the environment interaction. Fig.1 illustrates this point by emphasizing the three levels: basic, standard (or comparative) and advanced.

The most powerful tool will probably be furnished by the advanced level of sophistication once the research in progress provides us with the verified methods of design and prediction for particular applications. But even if it happens there will always be a need for comparative evaluation of the design in hand against already existing designs. Realization of this need by naval architects over last century led to the formulation of a number of useful methods and procedures that helped enhance the progress in marine technology and verifying new developments before they could be implemented with full confidence. There has been a feed-back, particularly between the comparative and advanced method of approaches, through which both have been verified and improved.

It is believed that the importance of such a comparative method of approach should, also be emphasized in the field of ship and marine vehicles stability safety. The present work offers one of, possibly, a number of ways by which such an approach can be developed. The proposed way is looking for a comparative measure of ship stability safety by which various designs can be evaluated against each other and eventually against new stability criteria that will be developed in the future.

2. BACKGROUND

It is suggested that a suitable basis for comparison of ship stability in waves can be provided by the so-called stability margin which is based on the righting and upsetting moments balance [1].

In Fig 2, the stability margin is represented by the area A_s , and the total upsetting energy is represented by the area A_2 . The ship's position with respect to the wind and waves is shown in Fig.3, which ex-

¹Professor of Ocean Engineering, Florida Institute of Technology, 150 W. University Blvd. Melbourne, Fl, 32901. U.S.A.

²Doctoral candidate, Department of Oceanography and Ocean Engineering, Florida Institute of Technology.

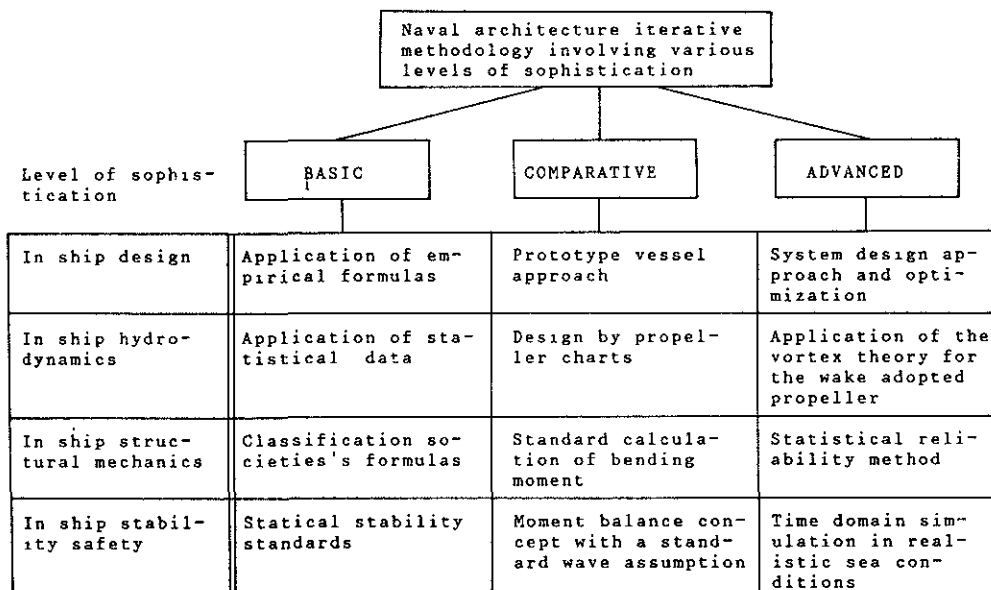


Fig.1 Methodological breakdown of Naval Architecture approach

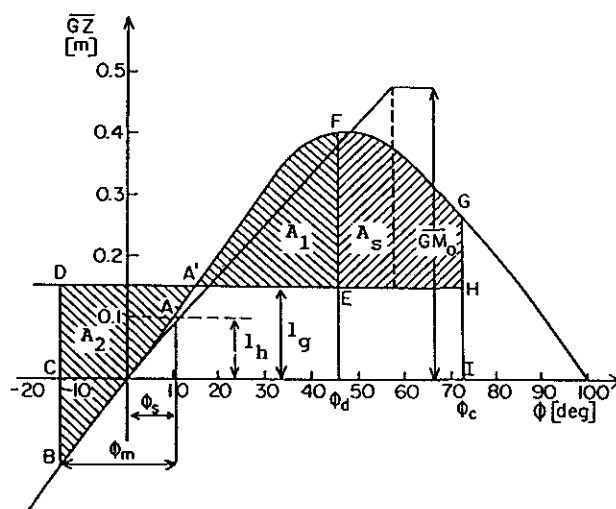


Fig.2 Definition of stability margin.

plains the basic terms of Fig.2. The ship is poised on a wave of a maximum slope, α_m . Due to steady-state wind of a speed V_w , the wind moment (with the moment arm, l_h) causes the ship to assume a static heel angle ϕ_s . The ship rolls around this angle with the amplitude ϕ_m . In the case of a gusting wind, the wind moment will be larger and the corresponding wind moment arm is l_g . The area A'BCD in Fig.2 represents the total upsetting energy due to the gusting wind and waves (roll motion). The wind moment can be calculated by one of many methods available in the literature. To calculate the wave effect, the maximum rolling amplitude, ϕ_m , must be known.

The method for calculating the roll response suggested in [2] applies a nonlinear single-degree-of-freedom equation for rolling motion which includes the nonlinearity of the damping and restoring moments. The equation derived in [2] is as follows;

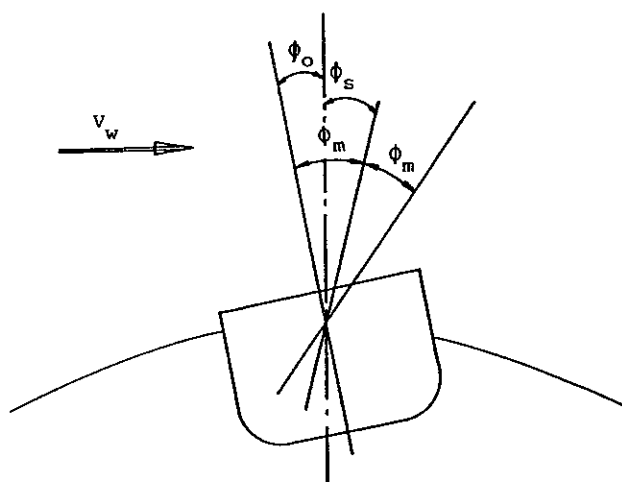


Fig.3 Ship's position with respect to wind and waves.

$$\ddot{\phi} + b_1 \dot{\phi} + b_2 \phi |\dot{\phi}| + \omega_\phi^2 \phi + m_3 \phi^3 + m_5 \phi^5 = \lambda \alpha_m \omega_w^2 \cos(\omega_w t + \delta) \quad (1)$$

Using this equation and the concept of rolling stability illustrated in Fig.2, a number of ship dynamic and environmental parameters can be included into the analysis of ship stability safety in waves, such as;

- the actual (nonlinear) righting arm curve,
- the rolling amplitude ϕ_m with respect to the wave slope,
- the ship mass moment of inertia, I_{xx} ,
- the added mass moment of inertia, δI_{xx} ,
- the damping characteristics of the hull and appendages, b_1 , and b_2 ,
- the natural period of roll, $T_\phi = 2\pi/\omega_\phi$,
- the wave period, T_w ,
- the wave height, H_w , and the wave length, L_w ,
- the wind speed, V_w ,
- the gusting wind speed, V_g , and
- the maximum wave slope, α_m .

the solution to the equation (1) has been found using the perturbation method. The solution obtained provides the relationship between the roll amplitude ϕ_a , the encountering frequency ω_e and the maximum wave slope α_m .

To find the roll amplitude ϕ_a the following parameters should be known:

1. The restoring moment coefficients m_3 and m_5 .
2. The added mass moment of inertia I_{xx} to calculate

$$\lambda = \frac{I_{xx}}{I_{xx} + \delta I_{xx}}$$
3. The linear and the nonlinear damping coefficients b_1 and b_2 , equation.
4. The maximum wave slope, α_m . This can be calculated with the given wave height, H_w , and the wave length, L_w .

2.1 Restoring moment

The restoring moment of a vessel is equal to the righting arm (GZ) times the displacement. The GZ-curve is an odd function and therefore an odd order polynomial has been used to represent it. Due to mathematical complexity and the difficulties involved in using higher order polynomials, the roll motion model used in the present study has been restricted to a fifth order polynomial representation. Thus, the righting arms GZ-curve can be expressed as

$$GZ = C_1 \phi + C_3 \phi^3 + C_5 \phi^5 \quad (2)$$

It should be noted that application of the quintic polynomial to represent the righting arm curve has also been reported in [3].

2.2 Hydrodynamic moments coefficients

The added mass moment of inertia and damping coefficients were calculated by the ship seakeeping characteristics program (SSCP) which is a mi-

crocomputer adaptation of the known ship motions program (SMP)[4]. The way the SSCP output was used to come up with the linear, b_1 , and nonlinear, b_2 , damping coefficients for equation (3) is discussed in [1].

2.3 Environmental data

The maximum wave slope α_m for equation (3) was calculated for a wave of the period equal the ship's natural period, $T_w = T_\phi$ (resonance condition) using the following formula;

$$\alpha_m = \frac{\pi H_w}{L_w}$$

where

H_w : the wave height

L_w : the wave length

The ship rolling period T_ϕ and the roll natural frequency ω_ϕ are provided in the output of the SSCP program.

The environmental data used in the present study are depicted in Fig.4 [5]. The figure was entered with the calculated roll period and the wave height, H_w and the so-called wind stress factors U_A were read off for the maximum fetch.

A computer program WSTAB in Pascal has been developed to calculate the roll responses. The responses are calculated for a range of encountering frequencies from 0.2 rad/sec. to 2.0 rad/sec. with the increments of 0.01 rad/sec.

2.4 Wind heeling moment

The wind heeling moment arm l_h was calculated using the following formula

$$l_h = \frac{0.004 V_w^2 a A}{2240 \Delta} \quad [\text{ft.}] \quad (3)$$

where

A : projected sail area,

a : the lever arm from half draft to the centroid of

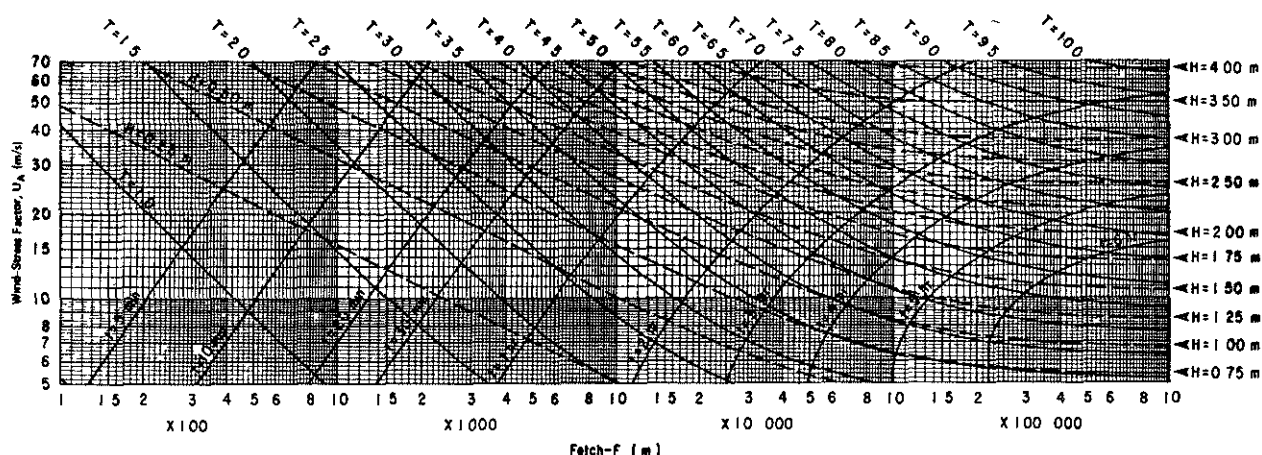


Fig.4 Environmental data.

the sail area,
 V_w : the wind speed

$$V_w = (U_A / 0.71)^{0.81},$$

U_A : the wind stress factor,
 from Fig.4.

The gusting wind moment arm was taken as $l_g = 1.5l_h$. Fig.5 summarizes the whole concept of roll motion stability, and the stability margin, and defines all the required parameters to implement it.

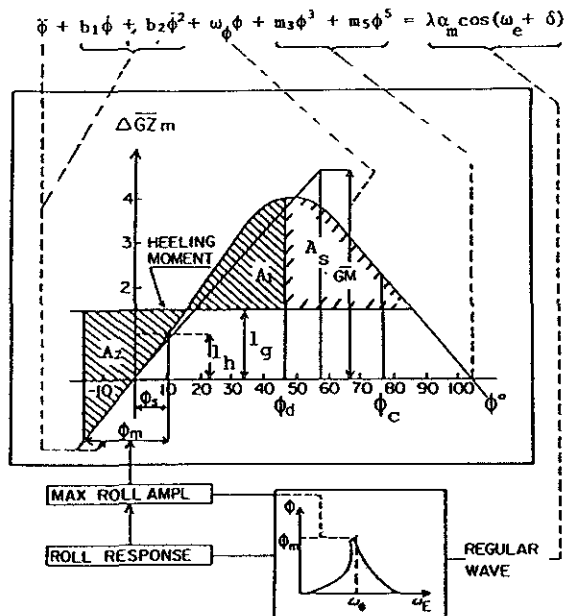


Fig.5 Concept of roll motion stability.

2.5 Upper limit of the stability margin

It should be pointed out that the ultimate purpose of the implementation of the roll motion stability concept is to arrive at the stability reserve or stability margin that the ship, which meets the IMO stability standards, possesses after external moments (due to wind and waves) are applied, area A_s in Fig.5. The upper limit of the stability margin or the maximum dynamic heel angle (referred to as the critical heel angle), ϕ_c , the vessel can theoretically be heeled to, is evaluated using the concept of dynamical metacentric stability and depends entirely on the $GZ(\phi)$ curve. The way by which the angle ϕ_c is evaluated can be explained by Fig.6.

3. CALCULATION OF STABILITY MARGIN FOR SERIES OF FORMS

The stability margin was calculated for twelve forms which were derived from the BSRA trawler series [6] [7]. The original series of nine forms was extended to include additional forms SZ, LZ, and JZ. These forms were de-

veloped in the process of optimization of the trawler forms for good seakeeping performance [8] [9]. Fig.7 depicts the spatial arrangement of the geometrically related forms. As it can be seen from the figure three form parameters were varied, i.e. the beam-draft ratio, the block coefficient, and the length-displacement ratio. All the forms have the same displacement $\Delta = 200$ T, a constant freeboard of $F_b = 1.28$ m, and the radius of gyration $k_{xx} = 0.35B$. The calculation of the stability margin was carried out for a ship speed of 10 knots. Table 1. provides the main parameters of the forms discussed.

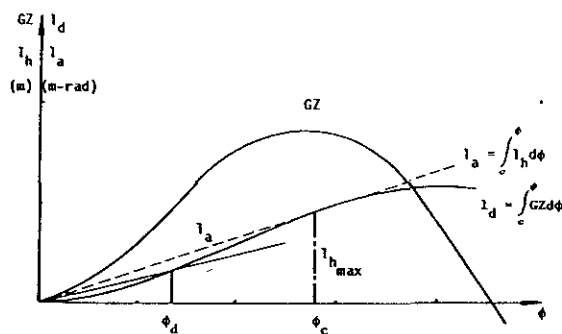


Fig.6 Dynamical and critical heel angles.

3.1 Calculation of statical stability curve

Values of the righting arms KN with respect to the keel were calculated by the Ship Hull Characteristics Program, SHCP [10]. The KN values for a displacement of 200 tons are given in Tab.2. Next, the maximum position of the center of gravity KG_{max} was evaluated to satisfy the IMO Stability Standards.

Tab.1 gives the KG_{max} values for all the forms tested and Fig.7 shows the effect of the form parameters on KG. Tab.3 provides the characteristics of the statical stability arms $GZ(\phi)$ for tested forms compared with the IMO standards.

Tab.4 includes the input to WSTAB program and the calculated roll responses ϕ_m for all the forms tested.

4. PRESENTATION OF RESULTS

It should be recalled that the ultimate goal of the present study is to assess the stability qualities of the test forms as represented by their stability margin the forms possess when rolling in beam synchronous waves.

The stability margin has been suggested as a measure of merit of

Table 1 Hull form parameters

Ship	L_{PP} (m)	B (m)	T (m)	$L/\nabla^{1/3}$	B/T	C_B	L/B	KM (m)	A_T (m ²)	a (m)	T_ϕ (sec)	KG (m)
XF	29.01	4.97	2.51	4.85	1.98	0.546	5.70	2.344	114.2	4.297	6.21	1.993
XG	28.26	5.24	2.37	4.85	2.22	0.546	5.38	2.429	114.2	4.224	6.56	2.078
WO	28.28	5.55	2.24	4.85	2.47	0.546	5.10	2.542	114.2	4.163	6.92	2.191
WP	28.28	5.82	2.14	4.85	2.72	0.546	4.86	2.676	114.2	4.111	7.28	2.325
WS	25.34	5.55	2.50	4.35	2.22	0.546	4.57	2.573	114.2	4.347	6.90	2.222
WR	26.80	5.40	2.43	4.60	2.22	0.546	4.97	2.493	112.3	4.283	6.72	2.142
WQ	29.72	5.12	2.31	5.10	2.22	0.546	5.80	2.374	116.2	4.167	6.39	2.023
ZQ	27.76	4.88	2.46	4.76	1.98	0.596	5.70	2.298	113.4	4.284	6.07	1.947
ZP	28.96	5.09	2.58	4.97	1.97	0.522	5.70	2.408	115.5	4.315	6.38	2.057
LZ	30.68	5.40	2.19	5.10	2.47	0.564	5.49	2.481	116.3	4.104	6.77	2.131
JZ	31.18	5.24	2.13	5.35	2.47	0.564	5.91	2.420	119.8	4.031	6.60	2.069
SZ	29.81	5.52	2.01	4.85	2.75	0.600	5.39	2.560	116.4	4.017	6.95	2.209

Note: constant displacement = 200 Tons.

Table 2 Righting arm KN for the test forms

ϕ (deg)	10	20	30	40	50	60	70	80	90
XF	0.409	0.820	1.235	1.598	1.871	2.061	2.171	2.207	2.179
XG	0.425	0.852	1.281	1.635	1.893	2.058	2.142	2.153	2.100
WO	0.444	0.892	1.337	1.684	1.921	2.063	2.124	2.111	2.036
WP	0.468	0.939	1.399	1.734	1.951	2.071	2.110	2.076	1.979
WS	0.449	0.902	1.352	1.713	1.973	2.140	2.224	2.233	2.100
WR	0.435	0.874	1.311	1.666	1.922	2.087	2.170	2.180	2.125
WQ	0.415	0.831	1.251	1.604	1.858	2.024	2.108	2.120	2.069
ZQ	0.402	0.807	1.218	1.575	1.843	2.026	2.129	2.160	2.126
ZP	0.420	0.842	1.266	1.636	1.918	2.114	2.230	2.271	2.247
LZ	0.423	0.871	1.308	1.653	1.888	2.030	2.090	2.079	2.006
JZ	0.433	0.849	1.278	1.621	1.855	1.996	2.056	2.046	1.975
SZ	0.448	0.897	1.339	1.665	1.873	1.986	2.020	1.983	1.886

Note : KN in meters.

Table 3 Characteristics of statical stability curves for tested forms compared with IMO standards

Stan. No.	1	2	3	4	5	6
	A	B	C	D	E	F
	$\int_0^{30} GZ d\phi$ (m-rad)	$\int_0^{40} GZ d\phi$ (m-rad)	$\int_0^{60} GZ d\phi$ (m-rad)	GZ_{max} (m)	$\phi @ 4$ (deg)	GM (m)
IMO req.	0.055	0.090	0.030	0.200	>30°	0.35
XF	0.056	0.104	0.048	0.430	50	0.351
XG	0.057	0.104	0.047	0.305	44	0.351
WO	0.057	0.103	0.046	0.275	40	0.351
WP	0.057	0.098	0.041	0.252	35	0.351
WS	0.057	0.103	0.046	0.285	42	0.351
WR	0.057	0.103	0.046	0.290	43	0.351
WQ	0.056	0.104	0.047	0.310	46	0.351
ZQ	0.057	0.107	0.050	0.350	50	0.351
ZP	0.056	0.104	0.048	0.340	52	0.351
LZ	0.057	0.105	0.048	0.285	40	0.351
JZ	0.057	0.104	0.047	0.280	39	0.351
SZ	0.056	0.098	0.042	0.357	35	0.351

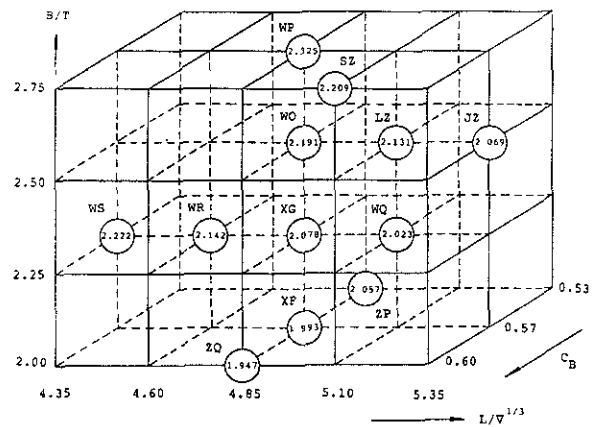


Fig.7 Effect of form parameters on KG_{max} calculated to meet IMO stability standards.

Table 4 Input to WSTAB program and stability margin

	λ	ω_ϕ (1/s)	b_1 (1/s)	b_2 (1/rad)	ϕ_v (deg)	GM (m)	α_m (rad)	A_{ϕ_v} (m-rad)	ϕ_m (deg)	A_{ϕ_m} (m-rad)
XF	0.879	1.01	0.101	0.833	115	0.35	0.108	0.400	17.5	0.268
XG	0.908	0.96	0.107	0.871	92	0.35	0.109	0.282	17.1	0.166
WO	0.903	0.92	0.114	0.856	76	0.35	0.110	0.205	16.8	0.107
WP	0.880	0.85	0.124	0.909	65	0.35	0.110	0.153	15.6	0.071
WS	0.908	0.92	0.114	0.800	85	0.35	0.110	0.241	17.3	0.126
WR	0.908	0.94	0.110	0.833	86	0.35	0.109	0.254	17.2	0.147
WQ	0.908	0.99	0.104	0.887	95	0.35	0.106	0.296	16.9	0.183
ZQ	0.884	1.02	0.098	0.841	117	0.35	0.109	0.408	17.6	0.273
ZP	0.852	0.99	0.104	0.820	120	0.35	0.107	0.406	16.8	0.253
LZ	0.901	0.94	0.112	0.971	78	0.35	0.110	0.222	16.2	0.121
JZ	0.903	0.96	0.107	1.131	80	0.35	0.109	0.231	15.3	0.129
SZ	0.871	0.93	0.117	1.047	60	0.35	0.109	0.159	15.1	0.071

Note : b_1 and b_2 are calculated for $V = 10$ knots.

the ship stability qualities. To obtain the margin for a particular form a number of static and dynamic features have to be calculated along with the environmental characteristics as defined in Fig.5 and Section 2. These features and characteristics can be grouped as follows:

- 1.The statical stability curve,
- 2.The hydrodynamic coefficients of the rolling motion equation, i.e moment of inertia, and linear and nonlinear damping coefficients,
- 3.The roll exciting moment parameters including maximum wave slope and,
- 4.The wind speed generating the synchronous wave, and steady and gusting wind moment.

The statical stability have been already discussed in section 3.2. The relevant features of the stability of form and the statical stability curve $GZ(\phi)$ for the forms analyzed are provided in the following tables:

- The position of the metacenter above the keel, KM , Tab.1,
- The values of KN , Tab.2,
- The area under the GZ curve, A_{ϕ} , the angle of vanishing stability, and the metacentric height GM , Tab.4,
- The areas under the GZ curve up to 30 and 40 degrees, the maximum righting moment arm GZ_{max} and the corresponding heel angle, Tab.3.

The effect of form parameters on the position of initial metacenter KM is shown in Fig.8. The added mass moment of inertia δI_{xx} , the linear b_1 and nonlinear damping coefficients b_2 from Tab.4 were plotted in Figures 9, 10, and 11 respectively to show how

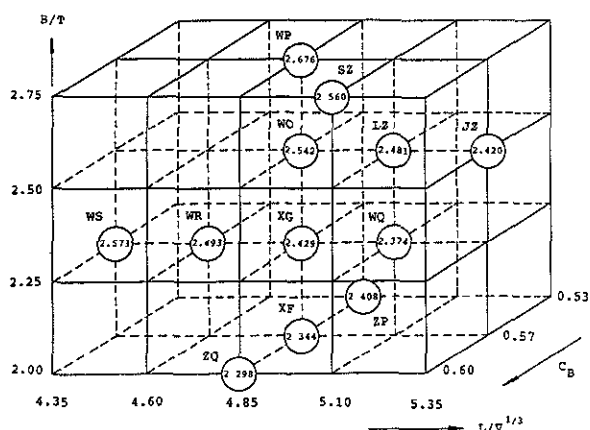


Fig.8 Effect of form parameters on position of initial metacenter KM .

they vary with the main form parameters. The effect of the form parameters on the resonant wave height H_w is shown in Fig.12. The roll amplitudes for the resonance condition calculated by WSTAB program as discussed in section 2 are given in Tab.4 and are plotted in Fig.13. The stability margin A_s is provided in Tab.4 and is plotted in Fig.14.

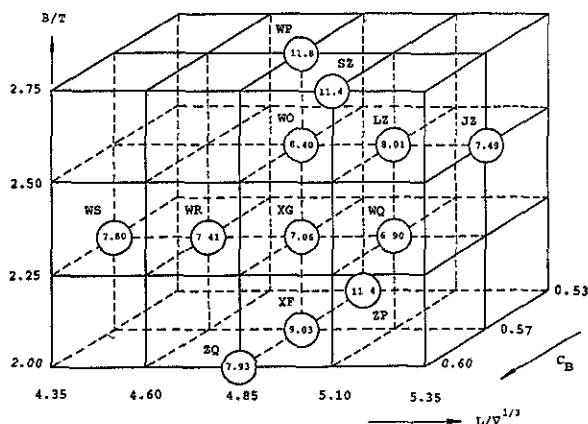


Fig.9 Effect of form parameters on added mass moment of inertia δI_{xx} .

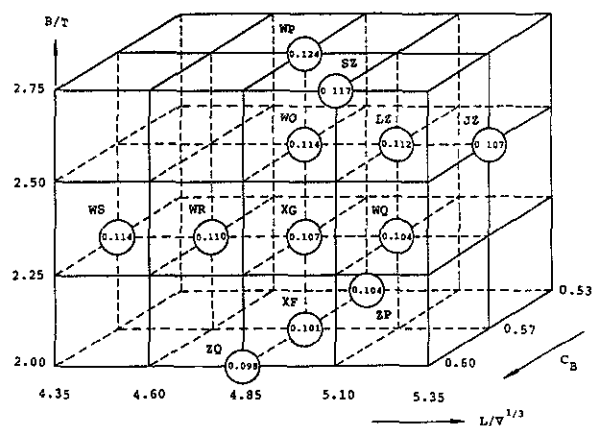


Fig.10 Effect of form parameters on linear damping coefficient b_1 .

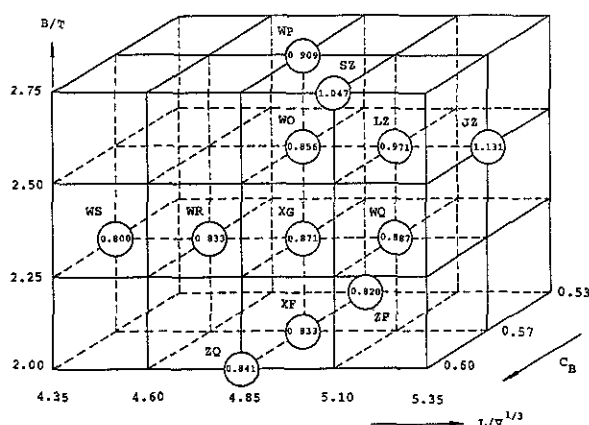


Fig.11 Effect of form parameters on nonlinear damping coefficient b_2 .

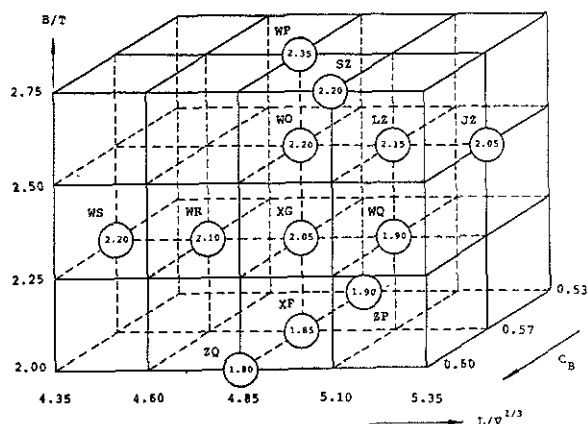


Fig.12 Effect of form parameters on resonant wave height H_w .

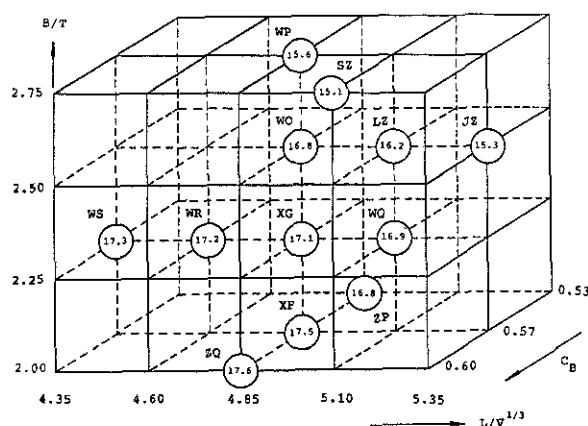


Fig.13 Effect of form parameters on maximum roll amplitude ϕ_m .

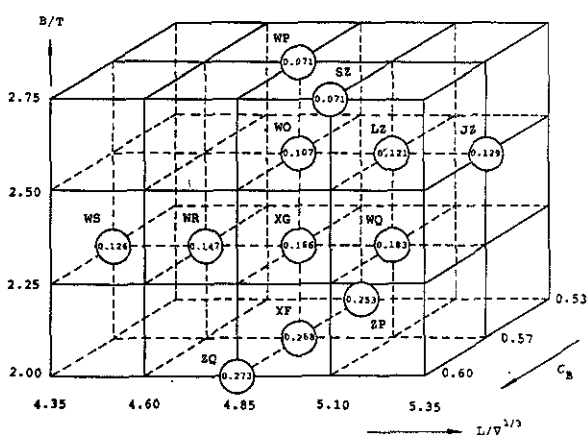


Fig.14 Effect of form parameters on stability margin A_s .

5. FINAL REMARKS

The paper suggests a measure of merit of ship stability in waves in a form of the stability margin. The stability margin is the difference between the ship righting energy and upset-

ting energy due to wind and wave action. The wave effect in the proposed approach is accounted for by an uncoupled nonlinear equation of roll motion which includes the nonlinearities of the damping and restoring moments. The way to calculate the terms of the equation has been suggested.

The concept has been applied to a dozen of geometrically related models with varying the beam-draft ratio, the block coefficient and the length displacement ratio. The effect of these form parameters on the statical and dynamical characteristics of the ship rolling in beam synchronous waves has been calculated and results presented in the paper. The present study has shown that in the roll motion stability the righting moment is the key factor affecting the ship safety even in the resonance condition where damping and excitation are assumed to play an important part. It can again be concluded that the possibility of capsizing as a result of excessive rolling depends to a large extent on the characteristics of the righting moment. This conclusion applies both to beam and following wave situations. In the latter case the variations of the righting moment with a wave passing the ship seems to have much larger effect than the variation of other moments involved in the ship motion process. This has been shown by the recent study by de Kat and Paulling [11].

The righting moment or righting arms curve depends on the hull form parameters and the vertical position of the center of gravity KG . A ship designer can consider for his design various hull geometrical configurations (defined for instance, by different combinations of B/T , C_B and $L/V^{1/3}$). In such a case the position of the center of gravity, KG which was calculated to meet the minimum IMO stability requirements, provides different level of stability safety for each variant depending on the combination of the main form parameters, Fig.14. For instance the application of the IMO standards to a design of the same displacement and freeboard but of different B/T ratios, 2.0 and 2.75, results in a vertical position of the center of gravity 1.99 m and 2.33 m, respectively. In such a case the decision which variant has been selected for the final design is at the same time the decision made on ship stability safety. The IMO criteria differentiate too much various design configuration which otherwise might be equivalent from the intact stability safety view point.

REFERENCES

1. Zborowski, A. and Taylan, M.,
Evaluation of Small Vessels' Roll
Motion Stability Reserve for
Resonance Conditions, The society
of Naval Architects and Marine
Engineers, Spring Meeting/STAR
Symposium, New Orleans, 1989.
2. Singh, D., Effect of Nonlinear
Stiffness on Roll Motion of Ships
in Regular Beam Seas, M.S Thesis,
Department of Oceanography and
Ocean Engineering, Florida
Institute of Technology, 1986.
3. Brook, A.K., The Role of
Simulation in Determining the
Roll Response of a Vessel in an
Irregular Sea-way", Int. Conf. on
SafeShip Project : Ship Stability
and Safety, RINA, 1986, London,
4. Sainsbury, S.R., Adoption and
Evaluation of a Ship Motion
Prediction Program for the Use on
Microcomputers, M.S Thesis,
Department of Oceanography and
Ocean Engineering, Florida Insti
tute of Technology, 1986.
5. Shore Protection Manual, Waterways
Experiment Station, Corps of
Engineers, Coastal Engineering
Research Center, 1984.
6. Pattullo, R.N.M. and Thomson, G.R.
The BSRA Trawler Series (Part 1)-
Beam/Draft and Length/Displacement
Ratio Series Resistance and
Propulsion Tests", Trans. RINA,
1965.
7. Pattullo, R.N.M., "The BSRA
Trawler Series (Part II)-Block
Coefficient and Longitudinal
Centre of Buoyancy Variation
Series", Trans. RINA, 1968.
8. Zborowski, A. and Sainsbury, S.R.,
Small Vessel Hull Form
Optimization for Heave and Pitch
Performance, Marine Technology,
October 1988.
9. Liu, S.J., Seakeeping
Consideration in Design of Small
Displacement Vessels, M.S Thesis,
Department of Oceanography and
Ocean Engineering, Florida
Institute of Technology, 1989.
10. Ship Hull Characteristics Pro
gram-SHCP", User's Manual, Naval
Ship Engineering Center, 1976.
11. de Kat, J.O and Paulling J.R.,
The Simulation of Ship Motions
and Capsizing in Severe Seas,
Transactions SNAME, 1989.

SIZOV V., VOROBYOV Yu., PERGAEV E.

The hydrodynamic problem concerning the ship stability during its movement in calm water was studied by prof. V.G. Sizov [1]. This report deals with obtaining the principal integral equation determining pressure distribution over central longitudinal plane by means of the potential acceleration method and the ways to its simplification were established.

Then E.V. Pergaev in the thesis worked out under the guidance of prof. Yu.L. Vorobyov extended this solution for the case of ship's movement on the following waves. He made use of a number of assumptions further improved the principal equation to the possibility of its numerical solution.

In the following report only the case of ship's proceeding in calm waters is studied. Let a ship propagating in calm water with constant speed v having a small angle of heel θ . Then we add a uniform flow with constant speed $-v$, and the ship becomes stationary. We apply coordinate plane XOY on the undisturbed liquid surface and axis Y directed vertically downward. Let the surface of the ship in the straight position is described by the equation

$$y = \pm f(x, z) \quad (1)$$

Assume the ship to be thin (so called Michell-type hull). Due to the heel the waterline symmetry will be broken. Ordinates in the direction of the listed side will be

$$y_1 = f(1 - \theta \frac{\partial f}{\partial z}), \quad (2)$$

and the opposite side

$$y_2 = -f(1 + \theta \frac{\partial f}{\partial z}). \quad (3)$$

The velocity field disturbed by the presence of the ship in the flow will be determined by the potential function $\varphi(x, y, z)$. This function should satisfy the Laplace equation and the following boundary conditions: on the free surface the linearized condition

$$\frac{\partial \varphi}{\partial z} - \gamma \frac{\partial^2 \varphi}{\partial x^2} = 0, \quad (\gamma = \frac{v^2}{g}), \quad (4)$$

which should be fulfilled when $z=0$; on hull surface

$$\frac{\partial \varphi}{\partial y} = -v \frac{\partial y_1}{\partial x}, \quad \frac{\partial \varphi}{\partial y} = -v \frac{\partial y_2}{\partial x}, \quad (5)$$

which will be considered to be fulfilled at $y = +0$ and $y = -0$ respectively; and the condition on the infinity

$$\Delta \varphi \rightarrow 0 \quad \text{when} \quad \sqrt{x^2 + y^2 + z^2} \rightarrow \infty. \quad (6)$$

Taking advantage of the expressions (2) and (3), the conditions (5) may be expressed in the form

$$\frac{\partial \varphi}{\partial y} \Big|_{y=\pm 0} = \pm \frac{1}{2} q(x, z) + w(x, z), \quad (7)$$

where the items express

$$q = -v \frac{\partial (y_1 + y_2)}{\partial x} = -2v \frac{\partial f}{\partial x}, \quad (8)$$

$$w = -\frac{v}{2} \frac{\partial (y_1 - y_2)}{\partial x} = -v \theta \left[\frac{\partial f}{\partial x} \frac{\partial f}{\partial z} + f \frac{\partial^2 f}{\partial x \partial z} \right], \quad (9)$$

and represent symmetric and antisymmetric components of $\frac{\partial \varphi}{\partial y}$ respectively.

Analytically extending potential φ to the volume occupied by the ship hull, it is possible to conclude that the source layer with density $q(x, z)$ and the dipole layer generating velocity $w(x, z)$ are located in the submerged part of diametral plane limited by the center line of a ship.

We shall write down the total potential of disturbances in the form of the sum of the potentials generated by the mentioned above layers of singularities:

$$\varphi(x, y, z) = \varphi_1(x, y, z) + \varphi_2(x, y, z). \quad (10)$$

For φ_1 and φ_2 potentials the boundary conditions at $y \pm 0$ will be:

$$\frac{\partial \varphi_i}{\partial y} \Big|_{y=\pm 0} = \mp v \frac{\partial f}{\partial x}, \quad (11)$$

$$\frac{\partial \varphi_2}{\partial y} \Big|_{y=0} = -v\theta \left[\frac{\partial f}{\partial x} \frac{\partial f}{\partial z} + f \frac{\partial^2 f}{\partial x \partial z} \right] \quad (12)$$

It is evident that φ_1 is a well known Michell's velocity potential corresponding to the ship in a straight position:

$$\varphi(x, y, z) = \int_D q(\xi, \zeta) G(x, y, z, \xi, 0, \zeta) d\zeta,$$

where G is the potential of a point source, located in the point $(\xi, 0, \zeta)$. This potential produces the force and the moment acting in the ship's longitudinal plane.

The hydrodynamic moment of stability which is of a particular interest for us arises due to the presence of potential φ_2 .

However the difficulty is connected with producing a picture of distribution of dipole singularities in the flow that sets up the necessary current.

That's why we have to introduce the acceleration potential connected with the pressure p and potential φ_2 in the following way:

$$\chi(x, y, z) = \frac{1}{\rho} p = -v \frac{\partial \varphi_2}{\partial x}. \quad (13)$$

Evidently that potential φ_2 expressed by means of χ as an integral of equation (13) turns into zero when $x \rightarrow \infty$:

$$\varphi_2(x, y, z) = -\frac{1}{v} \int_x^\infty \chi(s, y, z) ds \quad (14)$$

Potential φ_2 is continuous function everywhere in the flow except the submerged part of the ship's longitudinal plane where the potential function has a jump and a vortex shed φ which consists of vortices distributed continuously. This vortex shed starts from the stern perpendicular and extends to the infinity. Potential χ as well as pressure p are continuous all over the flow except the mentioned above longitudinal plane, where the jump of the potential χ occurs:

$$\chi_{0-} - \chi_{0+} = v \theta p(x, z), \quad (15)$$

In this case it can be represented as a potential of conventional dipoles distributed over D .

The concept of conventional dipoles used here for the description of the acceleration potential differs by the physical sense and dimensional representation from the corresponding concepts for the velocity potential.

The free surface condition may be taken in a form including dissipative forces

$$\frac{\partial \chi}{\partial z} - \mu \frac{\partial \chi}{\partial x} - \nu \frac{\partial^2 \chi}{\partial x^2} = 0, \\ \text{when } z = 0, \left(\mu = \frac{\mu_1}{g} \right),$$

Then the Green function for χ - potential may be found from the same boundary value problem as for potential, so we get

$$\chi(x, y, z) = \\ = v\theta \int_D p(\xi, \zeta) \frac{\partial}{\partial \eta} G(x, y, z, \xi, 0, \zeta) d\zeta \quad (16)$$

and for φ_2 potential we find

$$\varphi_2(x, y, z) = \\ = -\theta \int_D \int_x^\infty p(\xi, \zeta) \frac{\partial}{\partial \eta} G(s, y, z, \xi, 0, \zeta) ds d\zeta \quad (17)$$

For getting the $p(x, z)$ function that presents the pressure jump over region D we use the condition (12) and have an integral equation for the named function in a form

$$v \left[\frac{\partial f}{\partial x} \frac{\partial f}{\partial z} + f \frac{\partial^2 f}{\partial x \partial z} \right] = \\ = - \int_D \int_x^\infty p(\xi, \zeta) \frac{\partial^2}{\partial y^2} G(s, 0, z, \xi, 0, \zeta) ds d\zeta. \quad (18)$$

After introducing the Green function in the integral equation (18), this equation may be divided into two independent integral equations as soon as the following assumptions are made:

- the ship velocity is high enough as soon as such conditions are of a special interest;
- pressure distributions over the hull length and draft are independent:

$$p(x, z) = p_1(x) \cdot p_2(z).$$

In such a case the pressure distribution over the draft can be found from the solution of the singular integral equation:

$$p(z) = \frac{1}{\pi} \int_0^1 \frac{dP_2(\zeta)}{d\zeta} \left(\frac{1}{z-\zeta} + \frac{1}{z+\zeta} + \right. \\ \left. + 2u \int_0^\infty \sqrt{1 - \frac{1}{t^2}} e^{-u(z+\zeta)t} dt \right) d\zeta, \quad (19)$$

$$\text{where } u = \lambda \omega; \lambda = \frac{T}{L}; \omega = \frac{1}{Fr^2}.$$

In this case we also accept that the hull shape equation is represented in the form:

$$f(x, z) = f_1(x) \cdot f_2(z) \quad (20)$$

Assuming the load distribution over the draft to be elliptical we get the integral equation for $p_1(x)$:

$$p_1(x) \cdot q + u^2 \psi \int_0^x p_1(\xi) \int_{-1}^{\infty} t \sqrt{t-1} e^{-ut} * \sin\left[\frac{\omega(x-\xi)\sqrt{t}}{2}\right] dt d\xi = \frac{df_1(x)}{dx}, \quad (21)$$

where:

$$q = 1 + \frac{1}{\pi} \left[\psi - u \psi e^{-u/2} K_1\left(\frac{u}{2}\right) \right],$$

$$\psi = \int_0^1 p_2(\xi) d\xi,$$

$K_1\left(\frac{u}{2}\right)$ - McDonald function.

The kernel of equation (21) was approximated on the base of the results of numerical calculations, so the equation (21) converted to convolution type and its solution was received by operational calculus technique.

The practical method of restoring moment and lateral force determination is based on the results of computer calculations for different ship hulls. The hull forms are given in the form:

$$y = f(x, z) = \frac{B}{2} \left[1 - \left(\frac{2x}{L} \right)^m \right]^k * \left[1 - \left(\frac{z}{T} \right)^n \right], \quad (22)$$

where L , B , T - ship length, breadth and draft respectively; $k = 1$ for fishing vessels and $k = 1/2$ is for transport vessels. Powers m and n are connected with waterline and midship section coefficients α and β in the following manner:

$$m = \frac{\alpha}{1-\alpha}, \quad n = \frac{\beta}{1-\beta}.$$

The lateral hydrodynamic force and its application point are determined by formulae

$$R_y = \int v^2 \theta B^2 \lambda K_x K_z, \\ Z_R = \int \frac{K_z''}{K_z'} \quad (23)$$

The hydrodynamic restoring moment is determined by the formula:

$$M_x = 2 \int v^2 \theta \frac{(BT)^2}{\pi} K_x [K_z - \theta^2 \left(\frac{B}{T} \right)^4 K_z'' \phi_z], \quad (24)$$

where:

$$K_z = \alpha (\gamma K_z'' - Z_g K_z');$$

$$K_z' = \alpha K_z'; \quad K_x = \psi_x K_x,$$

Z_g - center of gravity applicate.

The values of the functions participating in formulae (23) and (24) are given in tables 1 and 2, where $\beta_{cp} = \frac{\sigma}{\alpha}$. One needs to keep in mind that in the table 2 K_x is determined by means of α , while the rest of the values are determined by β_{cp} . One must bear in mind that function ϕ_z is oscillating.

Fig. 1 shows the comparison of the model test results obtained in the Scotch experimental tank /3/ with the calculated data (24). The values of α and β coefficients for ship hulls investigated in /3/ are not given in this issue. So these coefficients were determined by approximate formulae and taken $\alpha = 0.76$; $\beta = 0.98$.

The described method was also applied for calculations of hydrodynamic forces acting on a ship that moves with a drift angle, as well as to catamarane ships and for determination of additional wave resistance due to the hull of a ship.

REFERENCES

1. SIZOV V. G. Hydrodynamic Problem of Ship's Stability En-Route/Reports to XVI Scientific-Technical Conference on Ship Theory. Ed. 73. L., 1966, p. 207-210.
2. PERGAEV E. V. Investigation of Hydrodynamic Restoring Moment Acting on a Ship Moving in Calm Water and Following Waves/ Dissertation Paper, Odessa, 1973, 122 p.
3. The Effect of Forward Motion on the Transverse Stability of a Displacement Vessel/ Transaction of the Institution of Eng. and Shipb. in Scotland, vol. 113, 1969-1970,

Table 1

Fr	T/L = 0.04			T/L = 0.06			T/L = 0.08		
	φ_x	α	β	φ_x	α	β	φ_x	α	β
0	1.0	1.0	1.0	1.0	1.0	1.0	1.0	1.0	1.0
0.1	0.940	1.0	1.0	0.875	1.0	1.0	0.940	1.0	1.0
0.15	0.930	0.985	1.015	0.770	0.986	1.0	0.845	0.995	1.010
0.20	0.990	0.950	1.020	0.675	0.982	1.010	0.750	0.990	1.015
0.25	0.965	0.910	1.025	0.675	0.950	1.020	0.640	0.980	1.018
0.30	0.725	0.870	1.039	0.760	0.904	1.025	0.600	0.941	1.021
0.35	0.575	0.838	1.043	0.925	0.880	1.035	0.810	0.912	1.027
0.40	0.650	0.820	1.045	1.035	0.841	1.040	1.020	0.880	1.038
0.45	0.976	0.810	1.046	0.700	0.830	1.042	0.630	0.855	1.040
0.50	0.720	0.800	1.048	0.530	0.815	1.045	0.525	0.830	1.042

Table 2

α	0.65	0.68	0.70	0.73	0.75	0.78	0.80	0.83	0.85
K _x	4.00	4.20	4.50	5.00	5.50	6.15	7.00	8.75	12.50
β_{cp}	0.45	0.50	0.55	0.60	0.65	0.70	0.75	0.80	0.85
K _z ^I	0.184	0.196	0.206	0.214	0.218	0.220	0.217	0.207	0.190
K _z ^{II}	0.066	0.084	0.097	0.107	0.114	0.119	0.119	0.117	0.110
Φ_z	-0.05	-0.036	-0.02	-0.04	0.017	0.045	0.078	0.120	-

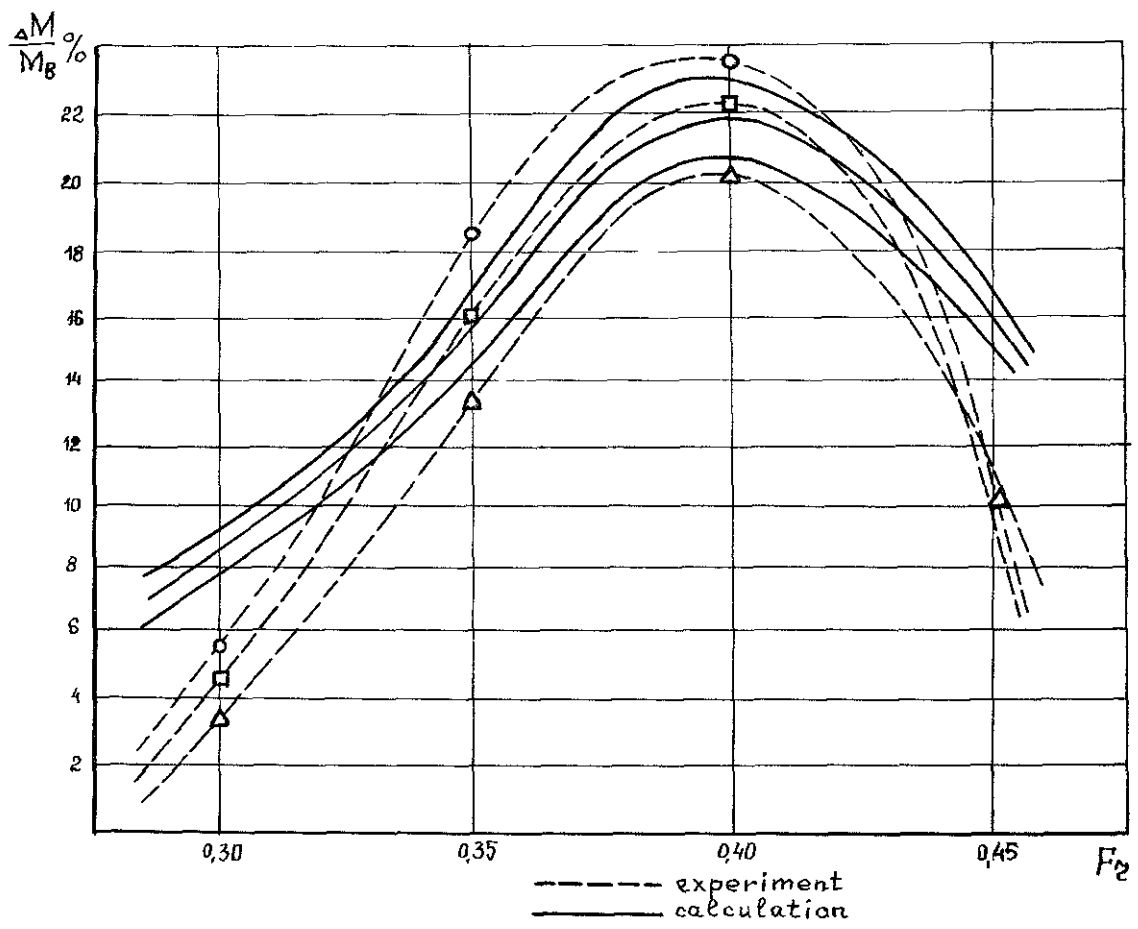


Fig 1

A SIMPLIFIED LOWER-BOUND CRITERION FOR STABLE ROLLING MOTION

Lawrence N. Virgin¹

Abstract

This paper develops an ad hoc criterion for stable rolling motion of a floating vessel in regular waves under slowly changing conditions. The total energy associated with the angle of vanishing stability is compared with the total energy of the harmonic response. Incorporation of a factor of safety enables the determination of critical forcing parameters which delineate 'safe' regions where stable rolling motion persists. An alternative measure of stability is also presented which is applied to an idealised version of a biased floating vessel and the results are compared with the dynamic instabilities obtained from numerical integration in previous studies.

Introduction

A ship at rest in a calm sea is an archetypal example of a dynamical system in stable equilibrium. The system will return to this position, dynamically, given some small perturbation due to the combined effects of (positive) damping and restoring force. For small-amplitudes the comparison with the free response of a simple spring-mass-damper mechanical oscillator is clear. A further analogy extends to consider the motion of a ball rolling on a locally parabolic track, where the shape of the track represents the underlying potential energy of the system. Trajectories in the phase portrait spiral towards the equilibrium position, and all possible initial conditions cause transients which decay on to this point attractor [1].

The static stability of a floating vessel is typically limited by the angle of vanishing stability resulting from the softening spring characteristic of the GZ curve. For a symmetric hull geometry these large-angle unstable equilibria are represented by saddle points in the phase portrait [2]. The unstable equilibria give rise to separatrices which now divide the plane of initial conditions into domains of attraction. Transient motion may no longer be captured by the attractor and initial conditions lying outside of the domain of attraction or basin boundary will lead to unstable, growing oscillations. This is a familiar scenario from ship dynamics where a floating vessel inclined to a large angle will lose its stability resulting in a rapid roll to an inverted position [3]. This is properly viewed in the two-dimensional phase portrait of displacement and velocity so that it can be seen that it is the combination of roll angle and roll velocity that may lead to capsize.

In this unforced (autonomous) case the effects of rapidly applied loads, for example modeled by impulse, pulse or step inputs, can be assessed. This has obvious relation to ocean wave slam loading. This paper is restricted to the consideration of *periodic* excitation which might arise for example as a regular wave train from a distant storm. Furthermore, the forcing parameters are assumed to change slowly so that transient effects are negligible [4].

Returning to the analogy of the ball rolling on the potential energy surface, the angle of vanishing stability is manifested as two 'hilltops' on either side of the stable 'well' at the origin. Under the action of harmonic excitation, the steady-state forced response will depend on the magnitude of the forcing amplitude and frequency, including the familiar resonance feature [5]. This is akin to oscillating the track on which the ball is rolling; a horizontal projection of this nonautonomous behavior now occupying a three-dimensional phase space with time as the third axis. It is clear that under certain circumstances, especially proximity to resonance, the forcing may be such that the ball will 'escape' from the potential well corresponding to a capsize situation.

For large-amplitude motion the nonlinear restoring force causes a variety of complex instability phenomena preceding escape [6]. The total energy of the response increases with the amplitude and this is used as a measure of proximity to capsize, i.e. the total energy (kinetic and potential) of the response is required to be somewhat less than the total energy associated with the angle of vanishing stability. A safety factor is incorporated to ensure that this criterion is satisfied in terms of the forcing parameters. Previous studies have indicated where typical ordinary differential equations lose their stability leading to escape [6,7]. The present paper outlines a simplified ad hoc criterion based on considerations of limiting the total energy of a system, and deriving conditions under which stable rolling motion persists.

¹ Assistant Professor
School of Engineering
Duke University
Durham, NC 27706, USA.

Free rolling motion

In order to convey the underlying principle of the new criterion consider the free roll motion of a floating body described by

$$\ddot{\theta} = f(\theta, \dot{\theta}). \quad (1)$$

Initially damping is ignored so that the ordinary differential equation of motion is of the form

$$\ddot{\theta} + V'(\theta) = 0 \quad (2)$$

where a prime denotes differentiation with respect to the roll angle θ and a dot denotes differentiation with respect to time t .

A first approximation to a typical restoring force (GZ curve) experienced by a body inclined to an angle θ is

$$V'(\theta) = \theta - \alpha \theta^3 \quad (3)$$

This type of system is often referred to as a softening spring characteristic. It can be seen that equilibrium points correspond to stationary values of the underlying potential energy, i.e.

$$\theta_e = 0, \theta_e = \pm \frac{1}{\sqrt{\alpha}}. \quad (4)$$

The saddle points associated with the second two equilibria of equation (4) correspond to the angle of vanishing stability.

Returning to the analogy of the rolling ball, the underlying potential energy curve is given by

$$V(\theta) = \frac{1}{2} \theta^2 - \frac{\alpha}{4} \theta^4 + c \quad (5)$$

and trajectories in the phase portrait are given by contours of constant total energy, i.e.

$$\begin{aligned} E &= \frac{1}{2} \dot{\theta}^2 + V(\theta) \\ &= \frac{1}{2} \dot{\theta}^2 + \frac{1}{2} \theta^2 - \frac{\alpha}{4} \theta^4 + c \end{aligned} \quad (6)$$

where the constant depends on the initial conditions.

The value of the total energy at the saddle points is

$$E = \frac{1}{2} \left(\pm \frac{1}{\sqrt{\alpha}} \right)^2 - \frac{\alpha}{4} \left(\pm \frac{1}{\sqrt{\alpha}} \right)^4 \quad (7)$$

where the arbitrary constant c is taken as zero, giving

$$E = \frac{1}{4\alpha}. \quad (8)$$

The restoring force of equation (3) is shown plotted in figure 1(a) together with the underlying potential energy function of equation (5) in figure 1(b). The phase trajectories for this conservative system describe ellipses as given by equation (6) and are illustrated in figure 1(c).

The safety factor ρ can be incorporated into the analysis to give a limiting total energy value of

$$E = \frac{\rho}{4\alpha} \quad (9)$$

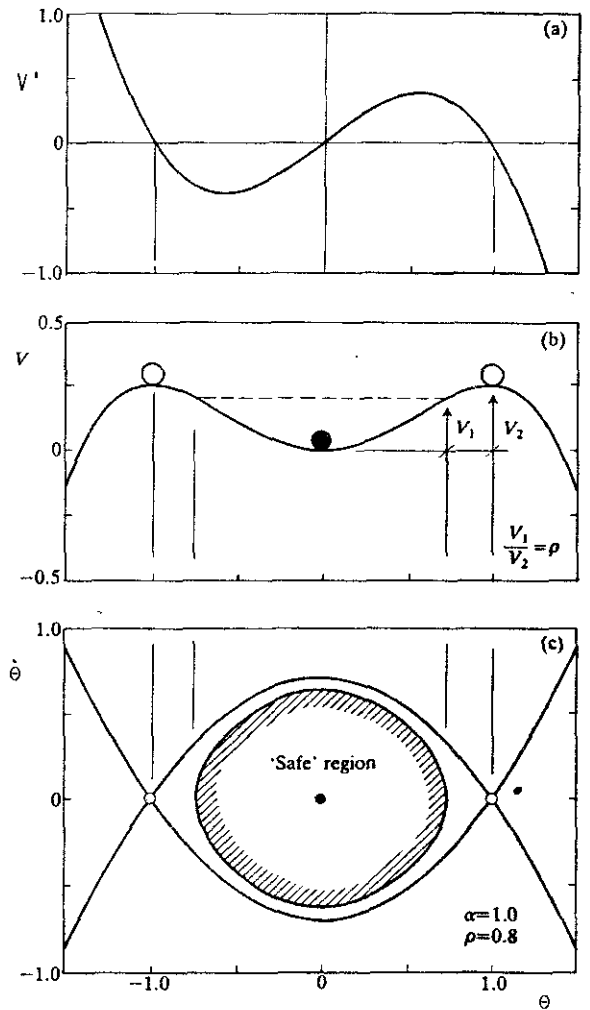


Figure 1. (a) Restoring force; (b) potential energy; and (c) phase portrait for a softening spring. The ad hoc boundary for stable rolling is shown for $\rho=0.8$. ($\alpha=1.0$, $\beta=0.0$)

and this is shown in figure 1(c) for $\rho = 0.8$. In other words, the motion of the vessel should remain at least within the shaded region for stability.

Forced rolling motion (Linear)

Harmonically excited roll motion can be approximately described by

$$\ddot{\theta} + \beta \dot{\theta} + \theta - \alpha \theta^3 = F \sin \omega t \quad (10)$$

where the forcing amplitude F and frequency ω can be thought of as sinusoidally perturbing the potential energy function.

For relatively small amplitude motion the nonlinearity in the restoring force is negligible, so that the roll motion can be described by

$$\ddot{\theta} + \beta \dot{\theta} + \theta = F \sin \omega t \quad (11)$$

and the steady-state response is given by

$$\theta = A \sin(\omega t - \phi) \quad (12)$$

where

$$A = \frac{F}{\sqrt{(1 - \omega^2)^2 + (\omega \beta)^2}}$$

and

$$\tan \phi = \frac{\omega \beta}{1 - \omega^2}.$$

The familiar amplification of the response near resonance ($\omega = 1$) can be seen.

There are a number of ways in which this response can be compared with the static stability features of the underlying GZ curve [4]. Firstly, the maximum total energy of the response can be used as a 'measure of proximity to the total energy associated with the angle of vanishing stability. Later, the amplitude and maximum velocity of the forced response is used as a measure of proximity to the amplitude and maximum velocity associated with the angle of vanishing stability.

Maximum total energy bound

The total energy associated with the forced response is

$$E = \frac{1}{2} \dot{\theta}^2 + \frac{1}{2} \theta^2 \quad (13)$$

where θ is given by equation (12). Therefore, for a given F and β the total energy will depend primarily on ω , i.e.

$$E = \frac{1}{2} (A \omega)^2 \cos^2(\omega t - \phi) + \frac{1}{2} A^2 \sin^2(\omega t - \phi) \quad (14)$$

which, for low damping, is a maximum at resonance ($\omega = 1$), giving a maximum total energy of

$$E = \frac{1}{2} A^2$$

$$= \frac{1}{2} \left(\frac{F}{\beta} \right)^2. \quad (15)$$

For example, for a damping coefficient of $\beta = 0.1$, nonlinearity parameter of $\alpha = 1$, and a safety factor of $\rho = 0.8$, a forcing amplitude of $F = 0.0632$ would result in an oscillation whose maximum total energy is equal to a prescribed proportion of the total energy associated with the angle of vanishing stability, i.e.

$$\frac{1}{2} \left(\frac{F}{\beta} \right)^2 \leq \frac{\rho}{4 \alpha}. \quad (16)$$

A forcing frequency less than or greater than the resonant value will result in an oscillation with less total energy and therefore would require a greater level of forcing to violate the condition of equation (16). With $\omega = 0.8$, $F^c = 0.233$ and with $\omega = 1.2$, $F^c = 0.2405$.

Figure 2 shows the maximum total energy of the forced linear response (equation (14)) for $\beta = 0.1$ and $F = 0.05, 0.07$. Also plotted on this diagram is the total energy associated with the angle of vanishing stability (equation (9)). This illustrates that the limiting condition is reached between $F = 0.05$ and $F = 0.07$, thus confirming the value of $F^c = 0.0632$ for equation (16). The relative contributions of the displacement and velocity terms in equation (14) depend on ω but the light damping present in the system results in the symmetric nature of the curves.

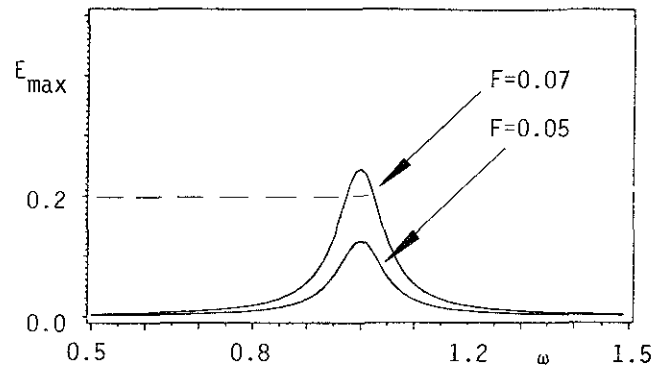


Figure 2. Variation of the maximum total energy with frequency for the linear response of a harmonically oscillating system. ($\beta = 0.1$).

However as the amplitude of the motion grows then the effect of the nonlinear restoring force will grow. In this case the response must be based upon the solutions to equation (10) rather than the assumed form of equation (11). The criterion of equation (16) can be summarized as

$$\text{Energy (response)} < \rho \text{ Energy (instability)}$$

The next section obtains expressions for the total energy of the response based on nonlinear (i.e. larger amplitude) motion.

Forced rolling motion (Nonlinear)

The use of small oscillation theory which leads to the linear response of equation (12) results in amplitudes which would simply grow indefinitely with no instability. For consistency the forced response must be based on the same equation as the unforced or free response with the addition of external excitation: i.e. equation (10) must be solved to obtain the nonlinear response which can then be compared with the approach to instability. An approximate solution can be obtained to equation (10) using various methods [8]. Here, a harmonic balance approach is used whereby a solution is assumed of the form

$$\theta = a \sin \omega t + b \cos \omega t \quad (17)$$

which can then be substituted into equation (10) and after equating sine and cosine coefficients leads to the following algebraic equations

$$-a \omega^2 - b \omega \beta + a - \frac{3}{4} a^3 - \frac{3}{4} a b^2 = 0$$

$$-b \omega^2 - a \omega \beta + b - \frac{3}{4} b^3 - \frac{3}{4} a^2 b - F = 0 \quad (18)$$

which can be rearranged to give

$$F^2 = A^2 \left[\left(1 - \omega^2 - \frac{3}{4} A^2 \right)^2 + (\beta \omega)^2 \right] \quad (19)$$

where A is the amplitude of the response, i.e.,

$$A = \sqrt{a^2 + b^2}. \quad (20)$$

Given F and β , equation (19) can be solved for A in terms of ω . Figure 3 shows typical amplitude response diagrams with $F = 0.2$ and $F = 0.3$, and $\beta = 0.6$.

The familiar softening spring effect can be clearly seen although with this relatively high level of damping the jump in resonance feature is not observed.

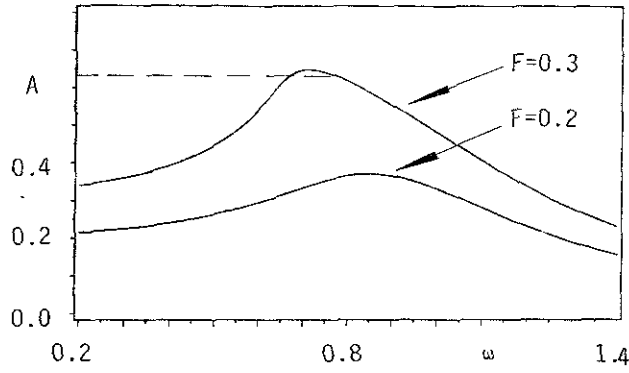


Figure 3. Amplitude response diagram for the fully nonlinear system. ($\beta=0.6$).

Again the total energy associated with the response is given by equation (14) where now the (nonlinear) frequency-amplitude relationship is governed by equation (19). Figure 4 illustrates the total energy of the harmonic response for $\alpha=1$, $\beta=0.6$ and $\omega=0.8$ through a complete cycle of motion. It can be seen that the maximum total energy occurs at

$$(\omega t - \phi) = \frac{n\pi}{2}. \quad (21)$$

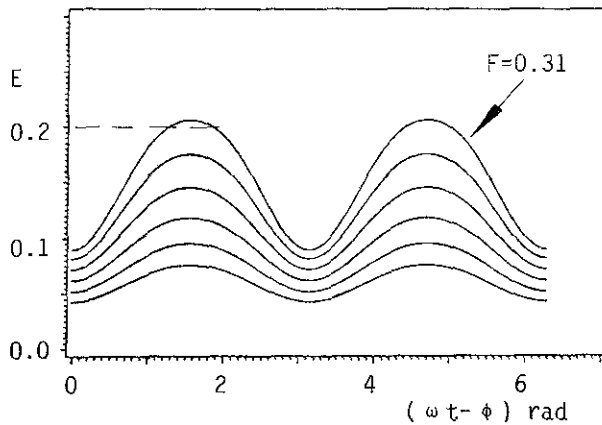


Figure 4. Variation of the total energy of the harmonic response through a complete cycle. ($\beta=0.6$, $\alpha=1.0$, $\omega=0.8$ and F increments by 0.02 from 0.21 to 0.31).

The curves in this figure start with $F=0.21$ and increment by 0.02 to the value of $F=0.31$ giving a maximum total energy greater than the $E=0.2$ obtained from equation (9). This is confirmed by the upper curve in figure 3 reaching amplitudes greater than

$$E = \frac{1}{2} A^2, \text{ i.e. } A = 0.632$$

corresponding to a safety parameter of $\rho=0.8$.

In this way, the maximum total energy of the nonlinear response can be obtained for different values of ω given F and β . This is shown in figure 5 for $\rho=0.6$ and $\rho=0.8$. It can be seen that a larger forcing amplitude F can be tolerated for $\rho=0.8$ than for $\rho=0.6$ for the total energy criterion to be met. The curves in figure 5 thus represent levels of forcing which ensure that the magnitude of the response is constrained to remain somewhat below the loss of stability [9].

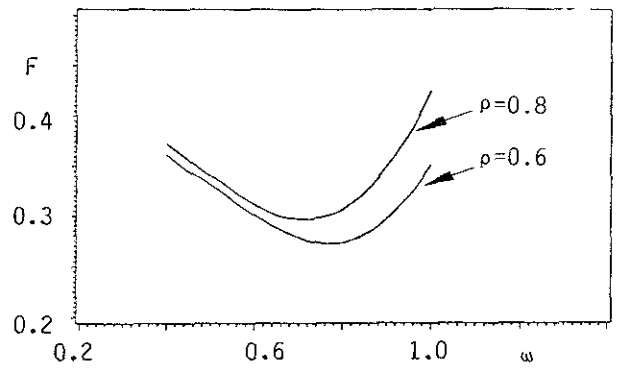


Figure 5. Limiting values of the forcing parameters. ($\beta=0.6$, $\alpha=1.0$).

So far no mention has been made of the mechanisms by which a system such as equation (10) will typically lose its stability. This is a subject of current research. It is important for the curves of figure 5 to be below the forcing levels at which these nonlinear phenomena occur in order for the total energy criterion to be lower bound and useful [10]. As mentioned earlier it is also possible to limit the response by the amplitude and maximum velocity associated with the total energy of the angle of vanishing stability. This approach has been successfully used by the author and is briefly introduced here to show that such ad hoc criteria can ensure stable rolling motion [4].

Amplitude and maximum velocity bound

An alternative measure of proximity to instability was developed in reference [4]. The separatrix joining the saddle points in figure 1 is given by equation (6) with $c=-1/4\alpha$. Rearranging equation (6) leads to

$$\dot{\theta} = \pm \left[-\theta^2 + \frac{\alpha}{2} \theta^4 + \frac{\rho}{2\alpha} \right]^{\frac{1}{2}} \quad (22)$$

where ρ is again used as a safety margin.

From this alternative form for constant total energy it is possible to obtain the maximum velocity as

$$\dot{\theta}_{\max} = \pm \left(\frac{\rho}{2\alpha} \right)^{\frac{1}{2}} \quad (23)$$

and the maximum displacement

$$\theta_{\max} = \pm \left[\frac{1}{\alpha} \left(1 \pm (1-\rho)^{\frac{1}{2}} \right) \right]^{\frac{1}{2}}. \quad (24)$$

The alternative criterion for stable oscillations now requires that the maximum velocity and amplitude of the forced response to be less than the maximum velocity (equation (23)) and maximum displacement (equation (24)) respectively for the undamped, unforced conservative system.

Assuming the linear forced rolling model of equation (11) leads to the following condition to limit the amplitude

$$F_c = \left[\frac{1}{\alpha} \left(1 \pm (1-\rho)^{\frac{1}{2}} \right) \left((1-\omega^2)^2 + (\beta\omega)^2 \right) \right]^{\frac{1}{2}} \quad (25)$$

and the maximum velocity

$$F_c = \left[\frac{\rho}{2\alpha\omega^2} \left((1-\omega^2)^2 + (\beta\omega)^2 \right) \right]^{\frac{1}{2}} \quad (26)$$

which are plotted in figure 6(a) for $\beta=0.1$, $\rho=0.8$ and $\alpha=1.0$ (for the unforced system), $\alpha=0.0$ (for the forced system). The response of the nonlinear equation (10) leads to the condition limiting the amplitude as

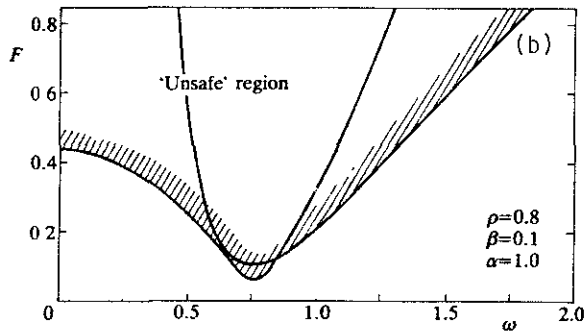
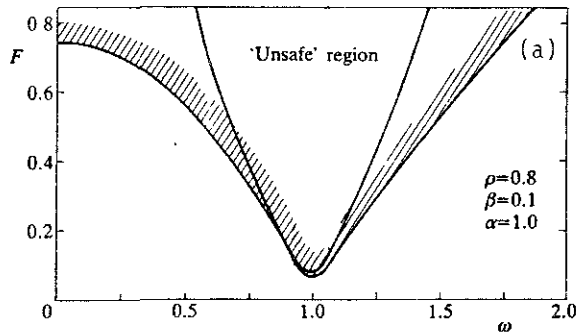


Figure 6. (a) Stability criterion based on the assumption of linear resonance. ($\beta=0.1$, $\rho=0.8$). (b) nonlinear resonance.

$$F_c = \left[\frac{1}{\alpha} \left(1 \pm (1-\rho)^{\frac{1}{2}} \right) \left(\left(1 - \omega^2 - \frac{3}{4} (1 \pm (1-\rho)^{\frac{1}{2}}) \right)^2 + (\beta\omega)^2 \right) \right]^{\frac{1}{2}} \quad (27)$$

and limiting the maximum velocity as

$$F_c = \left[\frac{\rho}{2\alpha\omega^2} \left(\left(1 - \omega^2 - \frac{3\rho}{8\omega^2} \right)^2 + (\beta\omega)^2 \right) \right]^{\frac{1}{2}} \quad (28)$$

which are plotted in figure 6(b) for $\beta=0.1$, $\rho=0.8$ and $\alpha=1.0$, now for both the unforced and forced systems. The effect of the softening spring can now be observed, resulting in frequencies around $\omega=0.75$ producing oscillations with the greatest energy for fixed forcing and damping. The two conditions of maximum displacement and maximum velocity are both required because of the effect of the frequency on the response. This is related to the relative contributions of the two terms on the right hand side of equation (14).

A static bias, due perhaps to a constant wind loading or shifted cargo has been shown to have a marked effect on the dynamics of a rolling ship. This effect can be incorporated into the dynamic model with the addition of a constant term in the equation of motion. The criteria suggested in this paper can include this effect with relative ease.

Bifurcational behavior

Considerable research has been conducted into the loss of stability of forced mechanical oscillators [1]. These inherently nonlinear phenomena can be

investigated in one of two ways. Firstly, an analytical method such as the Routh-Hurwitz criterion or Floquet theory [9] may be used to study stability characteristics of small perturbations about the steady-state solutions as described by equation (17). For example, equation (10) has been shown to lose its stability close to resonance in one of two generic ways: a jump to resonance at a saddle-node bifurcation; or a flip bifurcation leading to subharmonic oscillations initiating a sequence of period-doubling bifurcations leading to chaos and escape [6]. For slowly changing conditions both of these events have been shown to occur after the critical conditions of equations (27) and (28) have been reached, with a suitable choice for ρ .

The second approach to studying the dynamic stability of nonlinear oscillators involves extensive numerical integration. As an example of an asymmetric mechanical oscillator consider the following equation:

$$\ddot{\theta} + \beta \dot{\theta} + \theta - \theta^2 = F \sin \omega t \quad (29)$$

which has a potential of

$$V(\theta) = \frac{\theta^2}{2} - \frac{\theta^4}{4} + c \quad (30)$$

Solutions to this equation may 'escape' over the lower of the two hilltops analogous to figure 1(c). Figure 7 shows instabilities obtained by the numerical integration of equation (29) which lead to escape or capsize, together with the proposed ad hoc criterion suggested here [4]. For a given damping ratio and safety factor, forcing parameters within the shaded region have been shown to lead to escaping solutions[6]. The ad hoc criterion of equations (27) and (28) is also plotted indicating a conservative estimate of stable rolling motion. Instabilities such as a relatively small jump in amplitude may occur below these forcing levels but do not lead to escape for this system. For further details on these instabilities see reference [4].

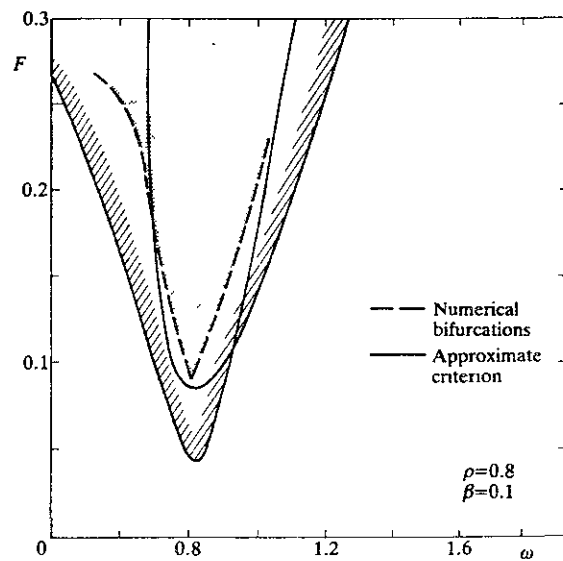


Figure 7. A comparison between the maximum velocity and amplitude bounds and the numerically determined bifurcations leading to escape (for an unsymmetrical system). ($\beta=0.1$, $\rho=0.8$).

Conclusions

This paper describes the early stages of research into a possible new criterion for quantifying the stability of a rolling vessel in a regular and slowly changing environment. Although the suggested method is based on simplistic equations and takes no account of transient motion it is a useful way of introducing important dynamic effects: in contrast to much of the existing stability criteria based on static concepts [11]. A particular advantage of the proposed method is the inclusion of a factor of safety which can be adjusted to different circumstances and improved information. Further developments would include coupling with other degrees of freedom, improvements in the modeling process, more realistic forcing conditions and incorporation of transient motion effects to take account of wave conditions which are not slowly changing.

Acknowledgement

The author would like to express his appreciation to Raymond Plaut of Virginia Polytechnic Institute and State University, and Michael Thompson of University College London for useful discussions.

References

1. Thompson, J.M.T. and Stewart, W.B. Nonlinear Dynamics and Chaos, 1986, Wiley:London.
2. Caldwell, J.B. and Yang, Y.S. Risk and reliability analysis applied to ship capsizing : a preliminary study. Proceedings, International Conference, The Safeship Project : Ship Stability and Safety, 1986, R.I.N.A.
3. Kuo, C. and Odabasi, A.Y. Application of dynamic systems approach to ship and ocean vehicle stability. Proceedings of the International Conference on Stability of Ships and Ocean Vehicles, 1975, Strathclyde.
4. Virgin, L.N. Approximate criterion for capsizing based on deterministic dynamics. Dynamics and Stability of Systems, 1989, 4, 55-70.
5. Bishop, R.E.D. and Johnson, D.C. The Mechanics of Vibration, 1960, Cambridge University Press.
6. Thompson, J.M.T. Chaotic phenomena triggering the escape from a potential well, Proceedings of the Royal Society, A421, 1989, 195-225.
7. Virgin, L.N. The nonlinear rolling response of a vessel including chaotic motions leading to capsizing in regular seas. Applied Ocean Research, 1987, 9, 89-95.
8. Hayashi, C. Nonlinear oscillations in physical systems. McGraw-Hill:New York, 1964.
9. Virgin, L.N. and Cartee, L.A. A note on the escape from a potential well. International Journal of NonLinear Mechanics, submitted.
10. Wellicome, J.F. An analytical study of the mechanism of capsizing. Proceedings of the International Conference on Stability of Ships and Ocean Vehicles, 1975, Strathclyde.
11. International Maritime Organisation. Intact stability criteria for passenger and cargo ships, 1987, London, IMO

MODEL TESTS ON ROLLING BEHAVIOURS UNDER DAMAGED CONDITIONS

Jin Hao, *

Yuan Don Lei **

ABSTRACT

A series of model tests has been conducted for a ship model under two displacements, to investigate its zero-speed rolling behaviours under intact and various damaged conditions. The results, which are introduced in this paper, are thought to be helpful to ship designers for understanding ship rolling behaviour characteristics, evaluating its stability and taking measures to ensure its safety, under damaged conditions.

A brief introduction of the make-up of the test model is also given for the reference of tank personnel in preparing test models of this kind.

Proposals for further developing the studies on rolling behaviours under damaged conditions are also suggested in the paper.

INTRODUCTION

A ship may sustain damage on its underwater portion when underway or even at mooring. It is greatly expected that the flooded ship still maintain its sea worthiness and safety to some degree. In view of the fact that little is known about the characteristics of ship rolling behaviors under damaged conditions, it is highly desirable that a study should be made in this field. To begin with, zero-speed rolling conditions are chosen for simplicity and directness.

The test model is made of tin plates. The positions of decks, bulkheads and holds are imitated after the prototype ship. As a result, the freeboard and hold capacities are also in scale. A number of round holes are drilled at the bottom of the model and can be opened and closed by easily operated valves. Besides, about 10 elliptical openings have been fitted above the waterline along the sides from the fore to the aft, and are equipped with close-fitting covers, which can be dismantled to allow the inflow of outboard water. These openings are employed to simulate the possible interchange of water flow between the flooded holds and the outboard water.

Since it is not possible to predict the exact shapes of damage openings, it is only appropriate to simulate the durations of the flooding process in determining the shapes and

dimensions of the holes. The diameters of the round holes which are 50 in number drilled both at the bottom and at the sides, are chosen to be 10mm, and the size of the elliptical openings to be 15 × 40mm.

The set-ups of valve-rod for operating the valves are shown in Fig. 1.

Before each test, the model is ballasted to the required displacement, and adjusted to the correct KG and transverse moment of inertia, the latter is adjusted by placing the model in calm water and checking its free rolling periods.

A TC-3 angular displacement gyro is fitted at the gravity of the model.

Tests are conducted at zero speed in beam waves.

The main principals of the test model are as shown in Table 1.

RESEARCH PROGRAM OBJECTIVES

Owing to the fact that theoretical investigations for ship rolling behaviours under damaged conditions are so scarce as to be of practical use, and it is out of question to attack this problem on full-sized ship, the only way feasible is to conduct model tests under damaged conditions.

The objectives of this project are;

a. To have some knowledge about the characteristics of rolling behaviours under damaged conditions.

b. To provide test results for the purpose of evaluating ship stability and safeness under damaged conditions.

c. To accumulate experience in the design and fabricating of models for tests under damaged conditions.

* China Ship Science Research Centre, Wuxi, China.

** Wuhan Ship Design & Development Institute, Wuhan, China.

TABLE 1
Main principals of the test model

	Displacement-I	Displacement-II
LWL, m	3.160	3.140
B, m	0.310	0.310
Mean draft, m	0.107	0.092
Displacement, kg	55.13	44.25
LCG, m	0.040 aft	0.025 aft
KG, m	0.122	0.138
GM, m	0.025	0.017
Freeboard, fore, m	0.173	0.188
Freeboard, middle, m	0.083	0.096
Freeboard, aft, m	0.081	0.094

TABLE 2
Details of various flooding conditions

	Displacement-I		Displacement-II					
	[1]	[2]	[3]		[4]		[5]	
	4 holds, fore	4 holds, aft	3 holds, before mid.		3 holds, middle		3 holds aft mid.	
Heeling angle, deg	—	—	5.96	19.66	2.44	10.94	4.20	15.6
Trimming angle, deg	-2.3	+1.6	-1.3	-1.1	~0	~0	+0.9	+1.0
Amount of flooding water, kg	14	15	18.2	16.6	17.8	17	19.3	18.5
GM, cm	3.025	1.450	1.35	1.075	0.875	0.60	1.0	0.725
Min. residual freeboard, cm	4.7	2.45	5.0	1.55	0.65	0.438	3.75	1.25
Location of min. res. fbd.	1/4L from FP	aft	~mid	~mid	~mid	~mid	aft	aft

TABLE 3
Damping characteristics for 10 test conditions

	Displacement-I			Displacement-II						
	intact	[1]	[2]	intact	[3]		[4]		[5]	
					Small heeling	Large heeling	S.h	L.h	S.h	L.h
$2\phi_{i-1}/2\phi_i$	0.625	0.118	0.294	0.544	0.274	0.254	<0.100	0.254	<0.100	0.200
$\frac{\text{intact-flooded}}{\text{intact}}, \%$	/	81%	53%	/	50%	53%	>82%	53%	>82%	63%

EXPERIMENTAL TESTS

10 tests have been conducted for the test model, including: 3 tests for displacement-I (intact, fore symmetrical flooding and aft symmetrical flooding), and 7 tests for displacement-II (intact, and 6 variants of unsymmetrical flooding). Prior to each test, free rolling experiment is carried out in calm water to ascertain the respective natural rolling period of the model.

After completing the experiment for the intact condition, a group of valve rods is operated so as to flood certain pre-determined holds and simulate a certain flooding condition. Experiment for that condition having finished, the water in the holds is removed and another group of valve rods are operated to flood other holds and simulate another flooding condition. This process is repeated until all tests have been carried out for that displacement. Then the model is ballasted to displacement-II condition and the whole process is renewed.

Obviously, in the shift from one flooding condition to another, it is inevitable that a small amount of water will be remained in the holds. But this amount is so small in comparison with the new flooding water, its influence is negligible.

In these tests, large heeling conditions are caused by heavily unsymmetrical flooding, and small heeling conditions are caused by flooding the opposite holds of the already flooded holds in large heeling conditions.

The details of various flooding conditions, such as holds being flooded, amount of flooding water, metacentric height, initial heeling angle and longitudinal inclination, minimum residual freeboard etc., are given in Table 2.

Experiments are conducted in regular beam waves with constant wave height and various wave lengths. Owing to great differences in the natural rolling periods of 10 test conditions (i.e. 1.59 sec. to 3.59 sec.), the ranges of wave frequencies to be produced in the tank also differ widely, with the maximum wave length as long as 22 m. For a tank of 4 m in depth, the profile of this 22 m wave is obviously distorted as expected.

For each experiment, wave heights and rolling movements are recorded. Rolling movements are measured by an angular displacement gyro of TC-3 type installed in the model. Wave heights are measured by a wave probe of capacity type located at a distance of about 20 m from the wavemakers, and kept an appropriate distance from the model under test so as to avoid the wavemaking interferences from the model. Wave heights, rolling movements and time signals are all recorded simultaneously.

In order to prevent water from washing the deck, the undamaged side of the model is made to face the direction of the wavemakers.

RESULTS & ANALYSIS

a. Nondimensional response curves for rolling movements

For rolling movements and wave heights recorded during different experiments, response curves have been calculated for the corresponding conditions. With $T\phi/\tau$ as the abscissa and $\Phi a/\chi$ as the ordinate, nondimensional roll response

curves can be plotted, here $T\phi$ is the natural rolling period, τ the wave exciting period, Φa the double amplitude rolling angle, χ the wave number and τa the wave height.

Fig. 2 through Fig. 11 are curves of nondimensional rolling angle versus $T\phi/\tau$, for these 10 conditions of different displacements and various conditions of both intact and flooding.

From these 10 curves, it can be seen that the curves in Fig. 2 to Fig. 5 are mono-crested. These results indicate that response curves of symmetrically flooded model are similar to that of intact model. When wave exciting periods approach the natural rolling period, synchronizing rolling will take place. But the response curves in Fig. 6 to Fig. 11 display a different trend. The response curve in Fig. 7 is double crested, while the curves in Fig. 6 and in Fig. 8 to Fig. 11 are even triple crested.

For the rolling movements of the intact model, the model can be regarded as a system with single degree of freedom and has naturally a response curve with only one crest. When the model is damaged and flooded, it becomes a system with multiple degrees of freedom. When several holds are flooded, they can be regarded as water chambers, each with its own natural period. The greater is the number of holds flooded, the greater is the number of degrees of freedom. In this series of experiments, the number of holds flooded is greater than 1, causing the model-chamber system to be a system of multiple degrees of freedom. When the wave frequencies vary in a wide range, synchronizing rolling may appear at several wave frequencies. Thus, we have a double crested response curve in Fig. 7 and triple-crested response curves in Fig. 8 to Fig. 11.

It also can be seen that the response curves in Fig. 9 to Fig. 11 are quite similar in shape with the curve shown in Fig. 12 which is taken from Ref. (1), and the curve in Fig. 8 is even more alike. From these resemblances, it can be deduced that response curves with triple crests are a feature pertaining to rolling movements of ship model with several flooded holds. As to the locations and magnitudes of these crests, they are governed by the natural periods and dampings of these water chambers.

From the response curve with triple crests, it can be seen that there is a prominent peak at $T\phi/\tau$ about 1. It illustrates the strong influence of the natural rolling period of the ship model on the response curve of the model-chamber system.

As to the response curves in Fig. 4 and 5 which correspond to the fore and aft symmetrical flooding conditions for displacement-I respectively, the results are mono-crested, though there are 4 holds flooded. Besides, this peak locates at the natural period of the model-chamber system. It indicates that the influence of the natural periods of these 4 holds on response curves is so weak as to be detected, and only the peak values are subdued owing to the increase in rolling dampings.

b. Free rolling motion curves

Free rolling motions in calm water have been recorded before each experiment, and are also shown in Fig. 2 to Fig. 11. From these curves shown in Fig. 4 to 11, it is obvious that under damaged conditions they decay very quickly, totalling less than 2 complete cycles. As a result,

normal method for calculating damping coefficient cannot be employed. The dampings are characterized through the ratios of successive double amplitude values, and are tabulated in Table 3. From Tab. 3, it can be seen that rolling dampings are increased under damaged conditions.

CONCLUSIONS AND PROPOSALS

a. Series of model tests of rolling behaviours under damaged conditions is for the first time conducted in CSSRC. As an effort to investigate the rolling behaviour characteristics, the tests are thought to be successful. Considerations given to the locations of damages and heeling due to flooding during the tests are of practical interest to the designers. The results obtained from the experiments are beneficial to the designers for understanding the characteristics of rolling behaviours and evaluating ship stability and safety under damaged conditions.

b. After damage, the ship becomes a ship-chamber system with multiple degrees of freedom. Under the action of waves, its rolling response may be mono-, double- or even triple-crested. The locations and magnitudes of the peaks are dictated by the locations of the flooded holds and the amount of water flooding. If the damage is incurred at the fore or aft portion of the ship and is far from the middle, the natural period of the water chamber may have

little contribution to the response curve. The sole influence is the increase of rolling damping.

c. Though the whole test is thought to be successful, there are however some shortcomings. The round holes at the bottom seem to be not big enough, and the time for flooding is not adequate.

Another point is, the model is made to face the wavemakers with its undamaged side to ensure safety during experiments. But, actually, if the damaged side of the model is made to face the wavemakers, it will be more typical.

d. It is suggested to develop further research projects on the basis of these model tests, such as:

i. Further experiments to be conducted under the combined actions of winds and waves, and with model fitted with superstructures;

ii. Experiments be extended to non-zero-speed condition and preferable in irregular waves.

ACKNOWLEDGEMENTS

The author is grateful to the Ship Hydrodynamics Laboratory of Shanghai Jiao Tong University for their support and help rendered.

REFERENCES

1. N.Y. Marnichev, Theory of Floodability of Ships, Chinese translation by Mou Chi. Defense Publishing House, 1977.

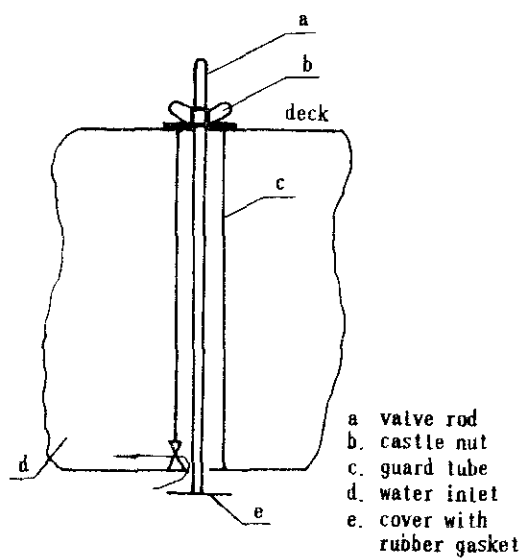


fig.1 Set-up of Valve-rod

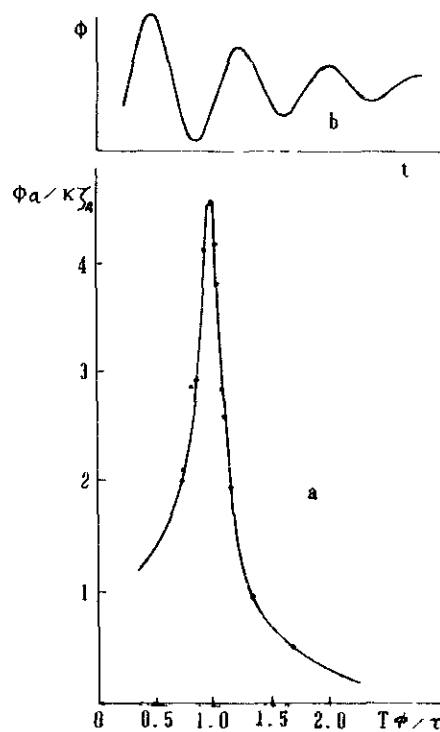


fig. 3 Displ-II, intact, $T = 1.91\text{sec}$
a. roll response; b. free rolling

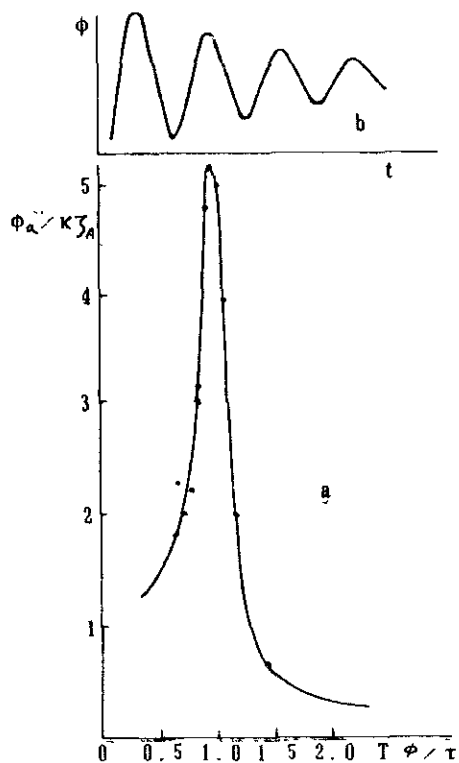


fig.2 Displ-I, intact, $T = 1.59\text{sec}$
a. roll response; b. free rolling

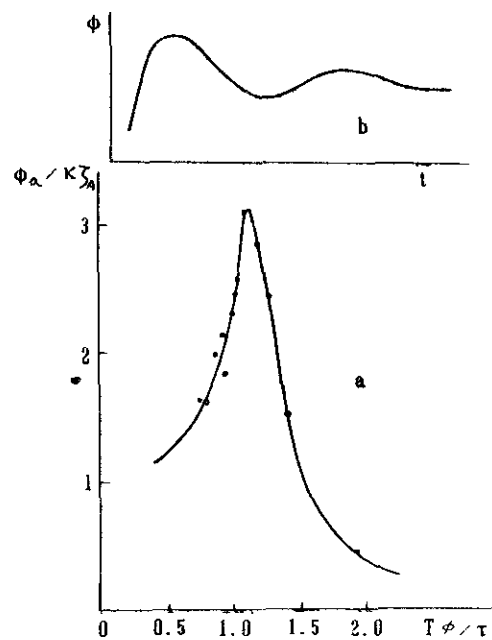


fig. 4 Displ-I, fore sym. fl., $T = 1.77\text{sec}$
a. roll response; b. free rolling

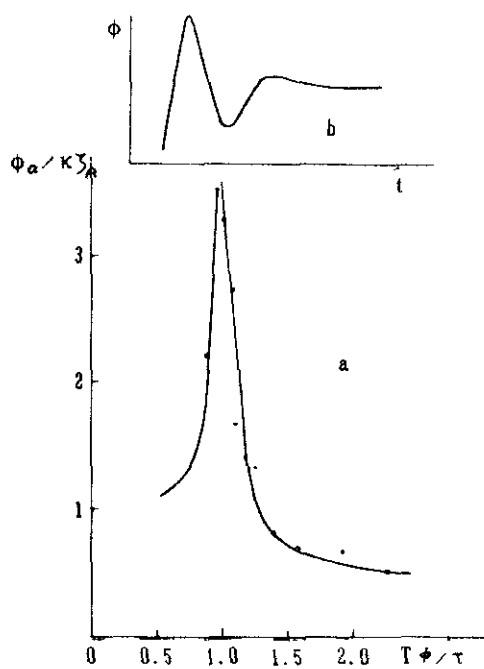


fig. 5 Dispt-I, aft sym. fl., $T = 3.59\text{sec}$
a. roll response; b. free rolling

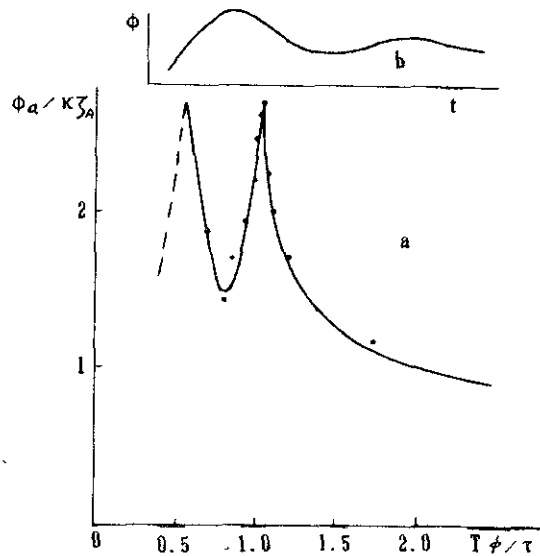


fig. 7 Dispt-II, case[3], L.h., $T = 1.94\text{sec}$
a. roll response; b. free rolling

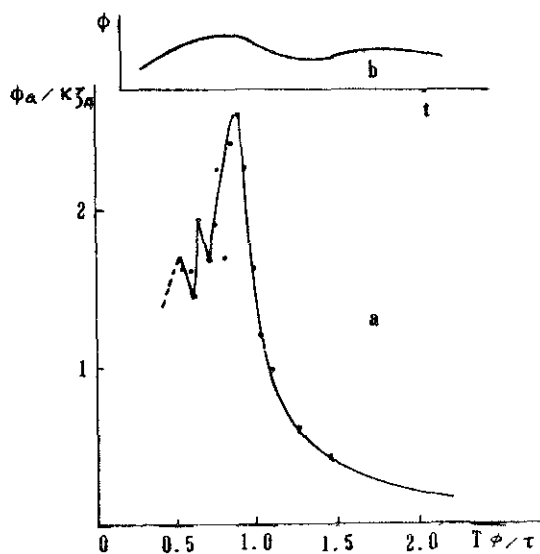


fig. 6 Dispt-II, case[3], S.h., $T = 1.72\text{sec}$
a. roll response; b. free rolling

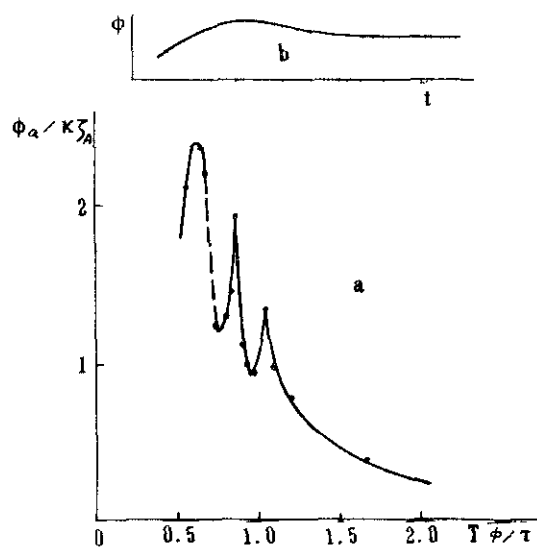


fig. 8 Dispt-II, case[4], S.h., $T = 1.95\text{sec}$
a. roll response; b. free rolling

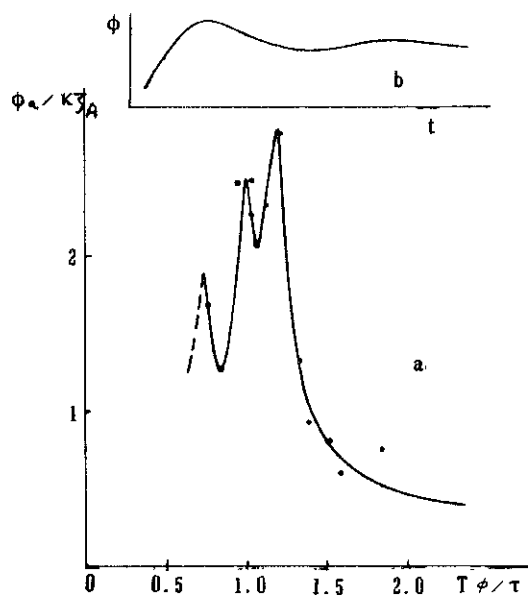


fig. 9 Displ-II, case[4], L.h., $T = 2.40\text{sec}$
a. roll response; b. free rolling

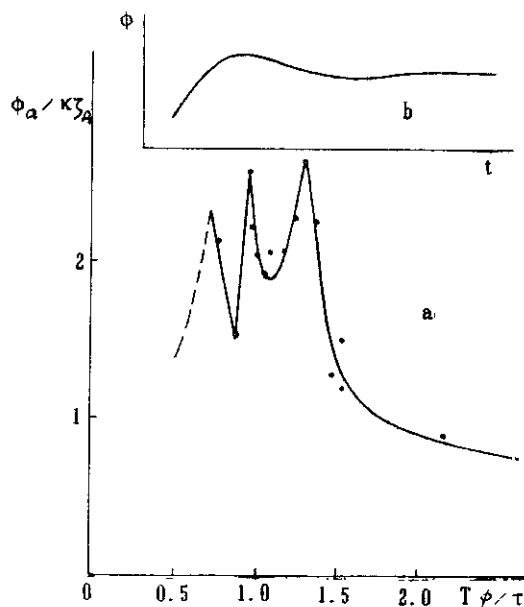


fig. 11 Displ-II, case[5], L.h., $T = 2.46\text{sec}$
a. roll response; b. free rolling

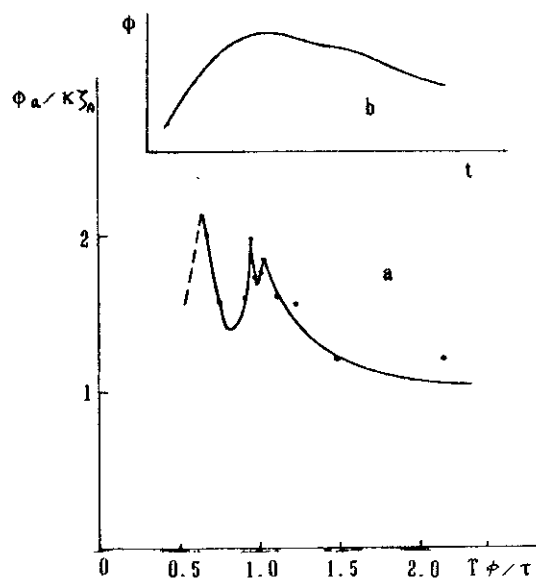


fig. 10 Displ-II, case[5], S.h., $T = 2.37\text{sec}$
a. roll response; b. free rolling

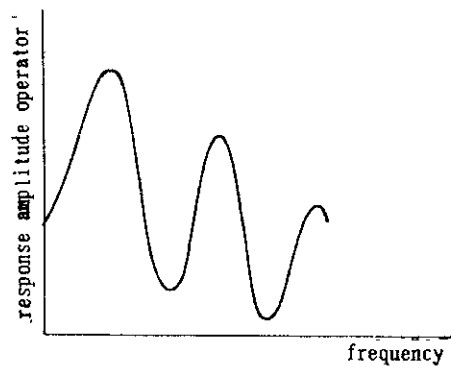


fig. 12 Roll response for a ship with
fluid loads, ref.(1)

SLOSHING OF WATER ON DECK OF SMALL VESSELS

Dr. Michael S. Pantazopoulos¹

A methodology is proposed to solve the problem of the three dimensional flow of water sloshing on the deck of a vessel, and to calculate the resulting forces and moments at the center of gravity. The Eulerian equations of motion of the water particle for incompressible inviscid shallow water flow are formulated with respect to a system attached to the oscillating vessel. The system of the nonlinear hyperbolic equations of motion is solved numerically using Glimm's method (random choice method). Complex flow patterns consisting of oblique bores and "swirling" motions of the water on deck were revealed, for a vessel oscillating in roll and pitch motions, for a wide range of excitation frequencies. Large accumulation of water is occurring at the corners while parts of the deck become dry. Significant rolling moments due to sloshing are exerted on the vessel. These must be taken into account when the dynamic response of the vessel is studied.

INTRODUCTION

Liquid sloshing on decks or in tanks of vessels has been a difficult problem to model in order to formulate guidelines for the design and analysis of marine vessels and structures. The sloshing of water on the deck of small vessels in combination with other factors has contributed to capsizing. The sloshing of liquid in containers in large carriers has caused failure of structural members supporting the container. Both types of failures have resulted in severe financial losses, human losses, and environmental damages. Human loss is considered to have the most significant impact in the community when it occurs.

Analysis and examination of recent fishing vessel losses suggested that the sloshing of water on the decks contributed to the tragic losses of the vessels and in some cases the total number of the crew [1]. These casualties raised public concern over the safety of fishing vessels and their crews, which motivated the organization of the 1984 Fishing Industry Safety and Health Conference [2].

While the effect of sloshing water on the static stability of a vessel is a straightforward and extensively studied problem, the dynamic effect of sloshing on the response and the stability of a vessel has not been investigated adequately. Early attempts to study the problem have been reviewed by Storch and Caglayan [3].

Most of these studies were based on empirical or experimental investigations. A very limited number of analytical and computational studies have been performed to date on the dynamics of water sloshing, the flow calculation and its effect on the response and stability of the vessel [4-6]. Most of these studies were limited to the two dimensional sloshing problem, where the water sloshes from side to side on the deck of a vessel, which undergoes two dimensional harmonic oscillations in sway, heave and roll and small amplitudes of excitation.

In the early eighties a number of studies were performed for two dimensional motions of large amplitudes but they were limited to side to side sloshing [8-9].

The objective of this study is to analyze the flow of the water on deck in the general three dimensional case and to calculate the resulting forces and moments, due to sloshing, at the center of gravity of the vessel. Thus a qualitative comparison can be made between the wave excitation forcing functions and the forces and moments that are induced by sloshing. Because of the complexity of the problem only the problem of the flow of the water on deck is approached assuming the motions of the vessel to be given.

The problem of water sloshing in an oscillating vessel is idealized as a shallow water wave problem. This is particularly true on the deck of small fishing vessels or on the deck of slightly

¹ Senior Research Engineer, Exxon Production Research Company, P.O. Box 2189, Houston, Texas 77252-2189

submergible bodies (platforms, etc.) where the deck area is large and the water depth is small compared to the breadth of the vessel and the wavelength of the waves traveling across the deck. The Eulerian equations of motion of the water particle for incompressible inviscid fluid flow are formulated. The equations of motion are transformed to a system attached to the oscillating vessel. The vessel undergoes sinusoidal motions in the six degrees of freedom except for yaw motion.

The nonlinear hyperbolic equations derived for shallow water waves are solved using Glimm's method. The solution is approximated by piecewise constant functions constructed as a superposition of locally theoretical solutions of the dam breaking problem and random sampling techniques. This method is particularly attractive because it handles complex flows with multiple shocks and hydraulic jumps without any special treatment of discontinuities, and the case where the deck becomes partially dry. Horizontal velocity components and the depth are obtained at each time step.

Performed studies revealed complex flow patterns consisting of oblique bores and "swirling" motion of the water on deck for a vessel oscillating in roll and pitch motions for a wide range of excitation frequencies. The presence of bores is not only a steady state solution as was thought by other investigators [9], but also they appear during the transient stage of the solution.

Sloshing induced forces and moments are of significant magnitudes when compared to the wave excitation (buoyant part) forces and moments. They must be calculated and taken into account in the analysis of the vessel response, because they can result in very dangerous situations during the seagoing operations of fishing vessels.

The magnitude of the sloshing induced forces and moments increases dramatically as the center of rotation moves further below the free surface. This again presents a dangerous situation since the center of rotation (gravity) in fishing vessels is below the free surface of the water on deck.

WATER ON DECK EFFECT ON FISHING VESSELS

Statistics related to vessel casualties in the United States over many years indicate that the fatality rate of commercial fishermen is approximately seven times that of the overall US-industry average. A Coast Guard survey, Table 1, shows fishing vessel total losses and deaths for the period 1970-1987 classified by nature of casualty [10,11]. The single greatest contributor is the category of foundering, flooding, and capsizing, accounting for 40% of the total losses. The greatest loss of

life also occurred because of foundering, flooding and capsizing, 69% of total lives.

Analysis of documented casualties suggests that losses rarely result from a single cause; instead, they stem from a combination of human error, vessel failure and environmental effects [1].

Table 1.
U.S. Documented Total Losses
of U.S. Fishing Vessels

	<u>Total Loss</u>		<u>Deaths /</u>
	1970-79	1980-87	<u>Injuries</u> 1980-87
Collision	227	173	23/23
Fire & Explosion	309	372	14/41
Grounding	335	232	22/12
Founder Flooding Capsize	567	807	311/34
Heavy Weather	14	29	64/5
Material Failure	223	130	11/14
Other	22	53	9/1

Notes:

- 1) Between 1970 and 1973 many of foundering, floodings, and capsizings were coded as material failures.
- 2) Statistics are including only documented fishing vessels of about 10 to 500 tonnage.

Fishing vessels, in general, have low freeboard and high bulwarks around the deck for crew protection. Freeing ports are provided along the bulwarks to allow water to be cleared from the deck. If the freeing ports are small, a considerable amount of water may remain on the deck. The volume of the accumulated water may sometimes be 20 to 30 percent of initial displacement [12]. It is apparent that the entrapped water poses a stability problem and may contribute to the capsizing of some of these vessels.

Caglayan [13], and also this investigator [14], performed two dimensional model tests at the Harris Hydraulic wave channel using typical midship sections of fishing vessels. Statical stability of the model and the amount of water on deck were varied in these studies. Both studies resulted in similar conclusions about the effect of water on deck on the model response.

For high metacentric height, which translates into a very stable vessel, and a small amount of water on deck the model roll response was reduced. However, for intermediate and low metacentric height, which translates into a marginally stable or unstable vessel, the effect of water on deck was detrimental, increasing the model

roll response. In the experiments capsizing occurred under a combination of low metacentric height and large amounts of water on deck. It also occurred for large slopes of incident waves, and in all cases additional water came over the top of the bulwark onto the deck before the model capsized.

A phenomenon which occurs when water is trapped on deck is the vessel heeling to a pseudostatic angle. This is a quasistatic angle of heel that the vessel assumes because of the effect of the movement of water on deck. The vessel then oscillates about the pseudostatic angle in a seaway. The magnitude of the pseudostatic angle depends on the initial statical stability conditions and the amount of water on deck. A vessel in a seaway assuming such an angle is more susceptible to capsizing for marginal statical stability conditions and large amount of water on deck.

Dillingham, in numerical parametric studies [4], concluded that the water on deck acts upon the ship response as a damping mechanism in all cases, except when more water was flowing onto the deck than flowing off the deck. Apparently the effect of the pseudostatic angle in the response and the stability of the vessel was not considered in the analysis.

THEORETICAL ANALYSIS OF SLOSHING IN AN OSCILLATING VESSEL

The problem of determining the movement of water on the deck of an oscillating vessel is formulated assuming that the water depth is small, the undisturbed free surface of the water on deck is the x, y plane and the z axis is directed vertically upward. The water depth is $-h(x, y, t)$ and the free surface elevation is $\eta(x, y, t)$, measured from $z = 0$.

Stoker's [15] one dimensional formulation of the shallow water wave equations is expanded in the present two dimensional problem while averaging over the vertical dimension. By integrating the continuity equation over the depth while imposing the kinematic and dynamic boundary conditions, one finds:

$$\begin{aligned} u_t + uu_x + vu_y &= -g\eta_x, \\ v_t + uv_x + vv_y &= -g\eta_y, \end{aligned} \quad (1)$$

$$[u(\eta+h)] + [v(\eta+h)] = -\eta_t. \quad (2)$$

These equations represent the movement of water in a stationary and level vessel. To introduce the motion of the vessel into the problem, the equations must be transformed into a coordinate system attached to the moving vessel. This introduces apparent body forces which arise as a result of the accelerations and rotations of the vessel. A complete derivation is given by Pantazopoulos [16], while a summary is presented here.

Let $\bar{x}, \bar{y}, \bar{z}$, define the coordinate system fixed in space and x, y, z define a coordinate system originating at the point about which the vessel oscillates. Fluid particle velocities u, v , and w are expressed in the x, y, z system. The coordinate systems are shown in Figure 1. The components of the absolute acceleration of a water particle expressed in the x, y , and z directions respectively are:

$$\begin{aligned} a(x) = & \ddot{n}_1 \cos\theta + \ddot{n}_2 \sin\phi \sin\theta - \ddot{n}_3 \sin\theta \cos\phi \\ & + 2\omega_1 \omega_2 x \sin\phi \sin\theta \cos\theta + \omega_1 \omega_2 y \cos\phi \cos\theta \\ & - \omega_1 \omega_2 z_d \sin\phi (\cos^2\theta - \sin^2\theta) - \omega_1^2 x \\ & \times \sin^2\theta + \omega_1^2 z_d \sin\theta \cos\theta - \omega_2^2 x \\ & \times (1 - \sin^2\theta \sin^2\phi) + \omega_2^2 y \sin\phi \sin\theta \cos\phi \\ & - \omega_2^2 z_d \sin\theta \sin^2\phi \cos\theta - 2\omega_1 v \sin\theta + 2\omega_2 v \\ & \times \sin\phi \cos\theta - \dot{\omega}_1 y \sin\theta + \dot{\omega}_2 y \sin\phi \cos\theta \\ & + \dot{\omega}_2 z_d \cos\phi - g \sin\theta \cos\phi + \dot{u} \end{aligned} \quad (3a)$$

$$\begin{aligned} a(y) = & \ddot{n}_2 \cos\phi + \ddot{n}_3 \sin\phi + \dot{v} - \omega_1^2 y + \omega_2^2 x \\ & \times \sin\phi \sin\theta \cos\phi - \omega_2^2 y \sin^2\phi - \omega_2^2 z_d \\ & \times \sin\phi \cos\phi \cos\theta + \omega_1 \omega_2 x \cos\phi \cos\theta \\ & + \omega_1 \omega_2 z_d \sin\theta \cos\phi - 2\omega_1 u \sin\theta \\ & - 2\omega_2 u \sin\phi \cos\theta + \dot{\omega}_1 x \sin\theta - \dot{\omega}_1 z_d \\ & \times \cos\theta - \dot{\omega}_2 x \sin\phi \cos\theta - \dot{\omega}_2 z_d \sin\theta \sin\phi \\ & + g \sin\phi \end{aligned} \quad (3b)$$

$$\begin{aligned} a(z) = & \ddot{n}_1 \sin\theta - \ddot{n}_2 \sin\phi \cos\theta + \ddot{n}_3 \cos\phi \cos\theta \\ & + \omega_1 \omega_2 x \sin\phi (\sin^2\theta - \cos^2\theta) + \omega_1 \omega_2 y \\ & \times \sin\theta \cos\phi - 2\omega_1 \omega_2 z_d \sin\phi \sin\theta \cos\theta \\ & + \omega_1^2 x \sin\theta \cos\theta - \omega_1^2 z_d \cos^2\theta - \omega_2^2 x \\ & \times \sin\theta \sin^2\phi \cos\theta - \omega_2^2 y \sin\phi \cos\phi \cos\theta \\ & - \omega_2^2 (1 - \sin^2\phi \cos^2\theta) + 2\omega_1 v \cos\theta + 2\omega_2 v \\ & \times \sin\phi \sin\theta - 2\omega_2 u \cos\phi + \dot{\omega}_1 y \cos\theta \\ & - \dot{\omega}_2 x \cos\phi + \dot{\omega}_2 y \sin\phi \sin\theta + g \cos\phi \cos\theta \end{aligned} \quad (3c)$$

where: n_1 = surge displacement
 n_2 = sway displacement
 n_3 = heave displacement
 ϕ = roll angle
 θ = pitch angle
 ω_1 = roll rotation
 ω_2 = pitch rotation

The left side of the shallow water wave equations (1) and (2) contain the x and y components of the absolute acceleration of a fluid particle and are replaced by (3a) and (3b) for the moving coordinate frame. The vertical acceleration g in the right side of equations (1) is replaced by the local acceleration (3c). Then, the equations of motion of the water particle in the moving coordinate frame x, y, z are written:

$$\begin{aligned} u_t + uu_x + vu_y &= -a(z) \eta_x + f_1(x) \\ v_t + uv_x + vv_y &= -a(z) \eta_y + f_2(y) \\ [u(\eta+h)]_x + [v(\eta+h)]_y &= -\eta_t \end{aligned} \quad (4)$$

where $f_1(x)$ and $f_2(y)$ are defined:

$$\begin{aligned}
f_1(x) = & \ddot{n}_1 \cos\theta - \ddot{n}_2 \sin\phi \sin\theta + \ddot{n}_3 \sin\phi \sin\theta \\
& - 2\omega_1 \omega_2 x \sin\phi \sin\theta \cos\theta - \omega_1 \omega_2 y \cos\phi \cos\theta \\
& - \omega_1 \omega_2 z_d \sin\phi (\sin^2\theta - \cos^2\theta) + \omega_1^2 x \sin^2\theta \\
& - \omega_1^2 z_d \sin\theta \cos\theta + \omega_2^2 x (1 - \sin^2\theta \sin^2\phi) \\
& - \omega_2^2 y \sin\theta \sin\phi \cos\phi + \omega_2^2 z_d \sin\theta \sin^2\phi \cos\theta \\
& + 2\omega_1 v \sin\theta - 2\omega_2 v \sin\phi \cos\theta + \dot{\omega}_2 y \\
& \times \sin\phi \cos\theta - \dot{\omega}_2 z_d \cos\phi + g \sin\theta \cos\phi
\end{aligned} \quad (5)$$

$$\begin{aligned}
f_2(y) = & \ddot{n}_2 \cos\phi - \ddot{n}_3 \sin\phi + \omega_1^2 y - \omega_2^2 x \\
& \times \sin\theta \sin\phi \cos\phi + \omega_2^2 y \sin^2\phi + \omega_2^2 z_d \\
& \times \sin\phi \cos\phi \cos\theta - \omega_1 \omega_2 x \cos\phi \cos\theta \\
& - \omega_1 \omega_2 z_d \sin\theta \cos\phi - 2\omega_1 u \sin\theta + 2\omega_2 u \\
& \times \sin\phi \cos\theta - \dot{\omega}_1 x \sin\theta + \dot{\omega}_1 z_d \cos\theta \\
& + \dot{\omega}_2 x \sin\phi \cos\theta + \dot{\omega}_2 z_d \sin\phi \sin\theta \\
& - g \sin\phi
\end{aligned}$$

These equations represent the shallow water waves in a reference frame attached to the moving vessel. However, rotation about the z axis is assumed to be zero in this formulation.

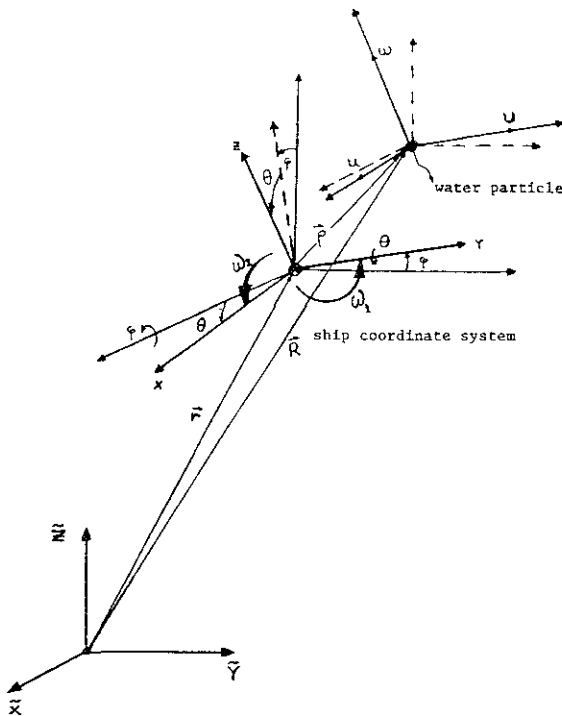


Figure 1. Coordinate System Configuration.

METHOD OF SOLUTION

The shallow water wave equations are solved by the random choice method (Glimm's method) [17]. This solution was developed by Holt and Li [18], and Dillingham [4] for the one dimensional case. Glimm's method is particularly attractive because it handles relatively complex flows with multiple shocks and hydraulic jumps without any special treatment of the discontinuities, and the case

where the deck becomes partially dry. Solution of the inhomogeneous nonlinear partial differential equations yields the water depth, and the velocities u and v with respect to the x and y axes at each grid point at each time step.

Equations (4) are solved efficiently using the technique of fractional steps as presented by Yanenko [19]. Using fractional steps, a multidimensional problem is reduced to a series of steps each of which involves differential approximations in only one dimension. Then, each of the one dimensional problems is solved using the random choice method. This gives a sequence of Riemann problems or dam breaking problems which are solved by the method of characteristics given by Stoker [15]. For an extensive discussion on the random choice method and step by step calculations, see Pantazopoulos [16].

CALCULATION OF SLOSHING FORCES AND MOMENTS

Water sloshing on the deck of a vessel exerts on it forces and moments. Here, forces and moments are calculated with respect to a moving coordinate system x, y, z with origin at the center of gravity of a stationary and level vessel, Figure 1. Then, they are transformed to a fixed coordinate system whose origin coincides with the initial position of the center of gravity of the vessel. The force exerted on the vessel walls and deck is given by:

$$\vec{F}(x, y, z) = \int_s \int p(x, y, z) \vec{n} ds \quad (6)$$

where:

$p(x, y, z) = \rho a(z)(x, y)z$ "hydrostatic" pressure
 n = unit exterior normal to wall
 s = interior deck surface area (underwater).

The moment about the origin is:

$$\vec{M}(x, y, z) = \int_s \int p(x, y, z) \vec{r} \times \vec{n} ds \quad (7)$$

where: \vec{r} = location of point with respect to origin.

NUMERICAL VERSUS EXPERIMENTAL STUDIES

The problem of liquid sloshing in containers has been the subject of experimental studies by many investigators in the last three decades. Unfortunately, a very limited number of experiments were performed for fill depth less than 20 percent, which is considered "shallow." Moreover, there have not been any experimental studies for excitation in six degrees of freedom: surge, sway, heave, roll, pitch, and yaw. This makes comparison of numerical predictions and experimental results difficult. Therefore, comparisons of numerical results with one-dimensional experimental studies were performed.

The most extensive experimental study on liquid sloshing was performed by Det Norske Veritas [20]. They used prismatic and spherical tanks excited harmonically in sway, planar roll, planar pitch, and diagonal roll, with fill depths up to 50 percent and for different liquids, i.e. water, glycerol-water, etc. We compared numerical and experimental results for shallow fill depths when the tank is filled with water in sway, planar and diagonal roll.

Sway Experiments

The depth to beam ratio was 0.12, and the sway amplitude to beam ratio was 0.10. The tank undergoes sinusoidal excitations with periods of 1.40 to 3.0 seconds. Figure 2 shows a qualitative comparison of the wave patterns between numerical analysis and results. There is good agreement. Comparison of the total maximum horizontal force, shown in Figure 3, also indicates good agreement. There is a discrepancy around the resonance frequency region in both the experimental and numerical results. This is probably due to the non-linear nature of the sloshing problem.

Planar Roll Experiments

A depth to beam ratio of 0.15 produced the most severe sloshing motion and loads and it was used in the numerical analysis. The sinusoidal roll excitation amplitude was 0.3 radians and periods ranged between 1.0 and 2.0 seconds. Wave mode comparison is shown in Figure 4. The region of transformation from a travelling wave pattern to a bore does not coincide exactly. However, there is some question about the definition of the travelling wave in the experiments [20]. It appears that the wave mode results from a combination of a weak bore and a "forced" surface wave caused by the tank oscillation.

Wave displacements or total force were not recorded during this experiment so no comparison was possible. Instead, pressure was recorded at several points in the tank near the walls. Reference [20] cites that these pressures were of impulsive type. No meaningful comparison can be made because the numerical algorithm cannot predict impact pressures but only non-impulsive hydrostatic pressures.

Diagonal Roll Experiments

A roll excitation with amplitude of 0.28 radians and a pitch excitation with amplitude of 0.1 radians were combined in the diagonal roll experiments. The observed wave modes in this case are identical to these of the planar roll investigation. The orientation of the appearing bore is oblique to the physical grid with varying orientation angle between 3.5 to 8.0 degrees. This agrees well with the experiments, Figure 5. Only impulsive pressure were recorded in the experiments so that no meaningful comparison can be made.

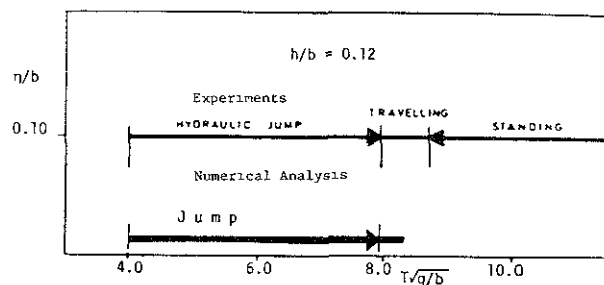


Figure 2. Wave Modes - Sway.

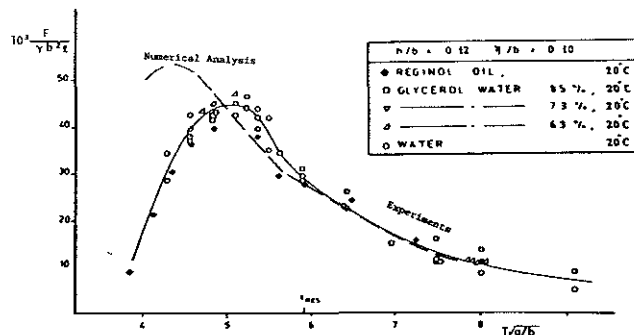


Figure 3. Maximum Horizontal Force - Sway.

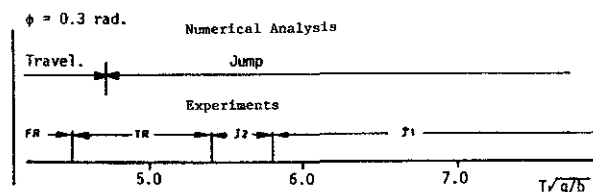


Figure 4. Wave Mode - Planar Roll.

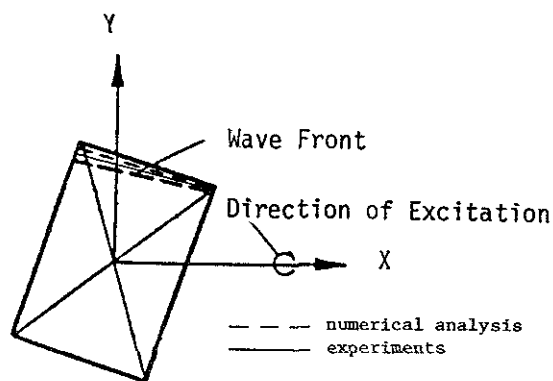


Figure 5. Oblique Bore - Diagonal Roll.

SMALL VESSEL EXAMPLE

An example of the flow of water on the deck of a typical small vessel is presented in this section to discuss some of the results that were similar in most of the studied cases. First, some qualitative results are presented which describe the wave patterns of the flow of water on deck. Second, quantitative and qualitative results are presented which show the magnitude of the forces and moments that the sloshing of water produces.

than the magnitude of the buoyant part of the wave exciting moment. This presents an additional forcing function that acts on the vessel at all times and should be taken into account when the equation of motion is solved.

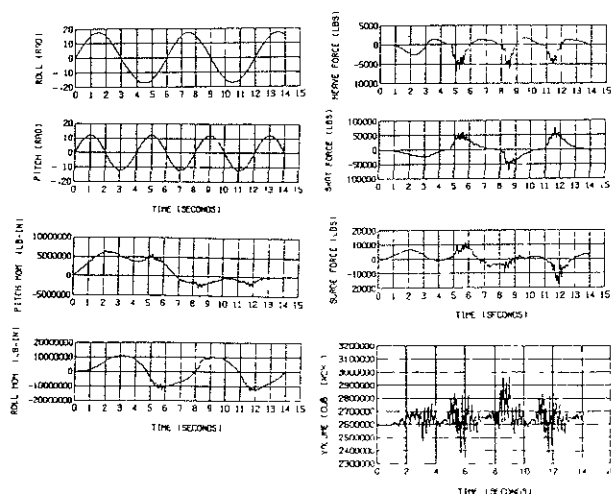


Figure 7. WOD Induced Forces and Moments.

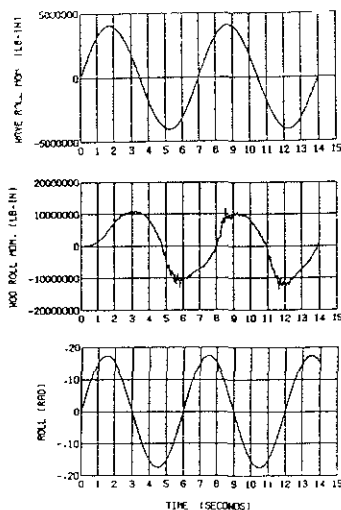


Figure 8. Wave Exciting (buoyant part) and Sloshing Moments.

Effect of Location of Center of Rotation

Faltinsen [7], using two dimensional deep water sloshing and assuming small roll motion, concluded that the severity of the sloshing increases as the location of the center of rotation moves further below the undisturbed free surface.

Similar parametric studies were performed to evaluate the severity of sloshing loads for shallow water depths. A vessel was given a roll excitation of 0.10 radians amplitude and the location of the roll axis was varying from positive values (below the undisturbed free surface) to negative values (over the free surface). The severity of sloshing was examined using the magnitude of the resulting sloshing rolling moment at the center of motion.

Qualitatively, the results agreed with Faltinsen's conclusions. Larger moments were registered as the distance increased

in the positive direction, while the opposite is true when moving in the negative direction. Figure 9 shows the quantitative effect of the roll axis location on the induced rolling moment for 10 percent fill depth. It appears that such behavior is expected because of reinforcement of the effects of a "forced" surface wave and a free wave, i.e., a bore, when moving further below the undisturbed free surface. When moving in the opposite direction the effects of the two waves oppose one another, resulting in a reduction of the sloshing loads.

The situation described above becomes particularly dangerous in real world conditions because the center of motion for fishing vessels is located below the free surface of the water on deck.

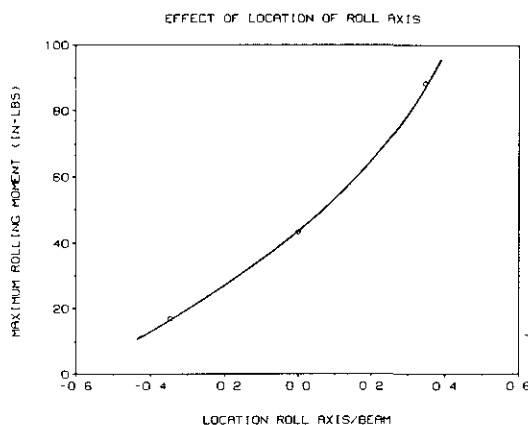


Figure 9. Effect of Roll Axis Location on Sloshing Rolling Moment.

CONCLUSIONS

This study suggests a methodology for the solution of the problem of the three dimensional flow of shallow water sloshing on the deck of a vessel or in tanks, and the calculation of the resulting forces and moments due to sloshing. Conclusions are summarized as follows:

- 1) The numerical scheme based on the random choice method provides a satisfactory tool for the calculation of the flow of the shallow water on deck sloshing problem. Complex flow patterns consisting of oblique bores, "swirling" motions, and dry bed conditions are handled without any difficulties.
- 2) Forces and moments due to sloshing are of significant magnitude when compared with the "wave exciting" forcing functions. They should be taken into account when the equation of motion of the vessel response is solved.
- 3) The suggested methodology produces results in an accurate manner for a broad range of initial conditions, excitation amplitudes and frequencies. The calculation of forces and moments due to sloshing at the center of gravity can assist the designer in stability, structural and dynamical analysis studies.

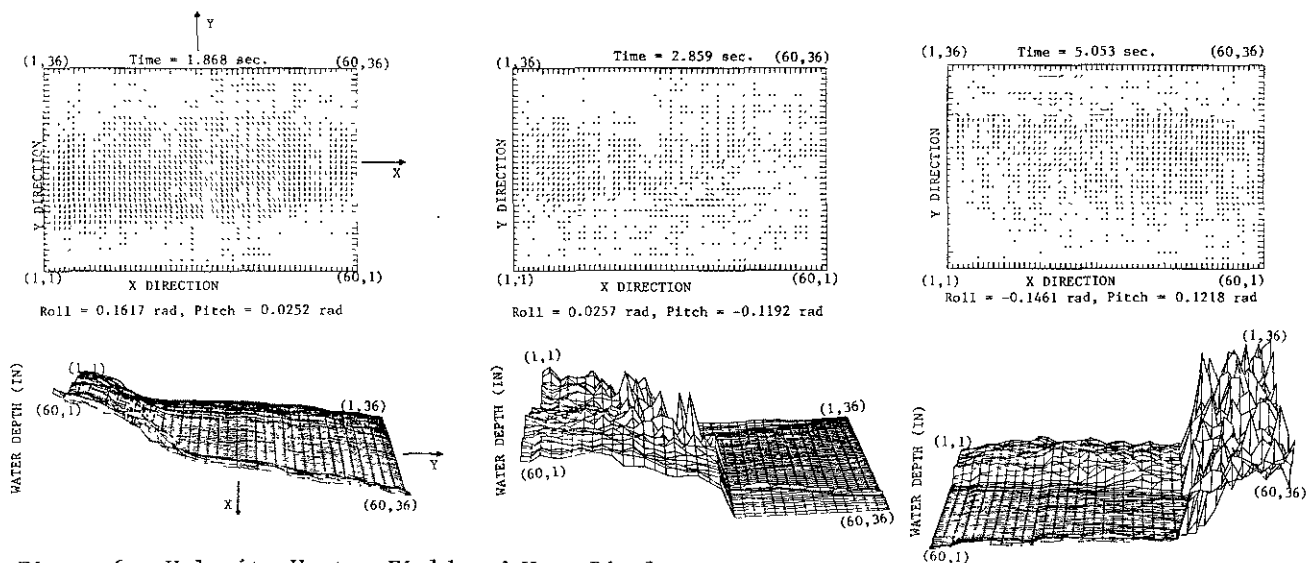


Figure 6. Velocity Vector Field and Wave Displacement.

Typical dimensions and input data are presented in Table 2. No water is allowed to escape from the deck or to be added on the deck. The vessel sits in the upright position at time $t = 0.0$. The flow field and the wave elevation are shown in the sequence of pictures in Figure 6. As the motion begins water runs smoothly from one corner of the diagonal to the corner across. The flow field appears as if a source is created at one corner and a sink at the corner where the water is accumulating. As the motion continues the profile of the wave surface steepens and after a finite time a sharp wave profile is created. The wave is oriented obliquely to the physical grid. Reflections from the walls result in secondary waves that travel on the deck. Local effects create a rotating flow pattern, especially around the corners. Water jets are formed that run around the circumference of the deck in a "swirling" motion. The interaction of "forced" surface waves and free waves is very clear during some instances. Large accumulations of water are occurring at the corners, while parts of the deck become almost dry.

Forces and moments are calculated about the center of gravity of the vessel. Forces and moments as a function of time are shown in Figure 7. The rolling moment and the roll displacement are not in phase for this particular example. However, in other cases they were in phase. The sloshing rolling moment approaches steady state after one excitation cycle on the average.

Forces and moments induced by sloshing are of significant magnitude, when compared with the buoyant part of the wave exciting roll moment, for unresisting harmonic rolling motion, (Principles of Naval Architecture, pp. 672-673 [21]). The buoyant part of the wave exciting moment in roll is given by:

$$M_w = \Delta \cdot GM \cdot 2 \cdot \pi \cdot (j_\alpha / L_w) \cdot \sin \omega_w t$$

Table 2.
Dimensions and Input Data

Length Overall:	30.480 m.	(100.000 ft.)
Beam:	9.144 m.	(30.000 ft.)
Draft:	3.048 m.	(10.000 ft.)
Depth:	4.267 m.	(14.000 ft.)
KG:	3.658 m.	(12.000 ft.)
GM:	1.219 m.	(4.000 ft.)
Deck Length:	15.240 m.	(50.000 ft.)
Displacement:	304.810 mtons	(300.000 itons)
Undisturbed WOD Depth:	0.305 m.	(1.000 ft.)
WOD Depth/Beam Ratio:	0.033	
WOD Weight/Displacement:	0.139	
Natural Slosh Per.(1st)	10.598 sec.	(10.598 sec.)
Roll Amplitude:	0.175 rad.	(10.000 deg.)
Roll Period:	7.000 sec.	(7.000 sec.)
Pitch Amplitude:	0.122 rad.	(4.000 deg.)
Pitch Period:	4.000 sec.	(4.000 sec.)
Center of Motion		
(below deck):	0.609 m.	(2.000 ft.)
Wave Amplitude:	1.524 m.	(5.000 ft.)
Wave Period:	6.000 sec.	(6.000 sec.)
Wave Length:	76.200 m.	(250.000 ft.)
Number of Cells:	60 x 36	
Sweeping Mode:	X - Y	
Time Step (Dt initial):	0.079 sec.	
Random Number Sequences:	(5,3) (5,3)	

where: Δ = displacement
 GM = metacentric height
 j_α = wave amplitude
 L_w = wave length
 ω_w = wave frequency

Figure 8 shows the buoyant part of the wave exciting rolling moment, the sloshing induced rolling moment and the roll displacement as a function of time. As may be seen the magnitude of the sloshing moment is significantly larger than that of buoyant part of the wave exciting moment and they are in-phase. However, they are out of phase with the roll displacement. The phase difference is about 70-80 degrees. In other examples the moments and the roll displacement were in phase. This is a dangerous situation when it occurs in real world operations. The net sum of the magnitudes of the two moments is greater

FURTHER RESEARCH

There is considerable room for further study in the area of water sloshing on the deck of an oscillating vessel. Some possibilities of extension of the present work are as follows:

- 1) Combination of the numerical algorithm for the flow of water on deck with a solver of the equation of motion of a vessel is a logical extension of the present research.
- 2) Time variation of flow with addition and

subtraction of water onto and off the deck will idealize better real world conditions in applications where the combined responses of a vessel with water on deck are to be determined.

- 3) The numerical scheme developed in this study can be used with minor modifications in problems of flows of liquids in tanks with fill depth ratios less than 20 percent, to calculate sloshing loads on supporting structural elements of the container.

REFERENCES

1. Adee, B. H., "A Review of Some Recent Stability Casualties Involving Pacific Northwest Fishing Vessels," International Conference on Fishing Vessels, Melbourne, Florida, May 1984.
2. 1984 Fishing Industry and Health Conference, Videotape, Seattle, December 11-12, 1984.
3. Caglayan, I. H. and Storch, R. L., "Stability of Fishing Vessels with Water on Deck: A Review," Journal of Ship Research, pp. 106-111, June 1982.
4. Dillingham, J. T., "Motion Studies of a Vessel with Water on Deck," Marine Technology, Vol. 18, pp. 38-50, Jan. 1981.
5. Caglayan, I. H., "Effect of Water on Deck on the Motion and Stability of Small Ships," Ph.D. Dissertation, University of Washington, Seattle, August 1983.
6. Van den Bosch, J. J., and Vugts, J. H., "On Roll Damping by Free Surface Tanks," Transactions RINA, pp. 345-361, March 1966.
7. Faltinsen, O. M., "A Numerical Method of Sloshing in Tanks with Two Dimensional Flow," Journal of Ship Research, Vol. 22, pp. 193-202, Sept. 1978.
8. Lou, Y. K., Wu, M. C., and Lee, C. K., "Further Studies on Liquid Sloshing," Maritime Administration Report No. MA-RD-760-85009, March 1985.
9. Vergagen, J. H. G., and Van Wijngaarden, L., "Nonlinear Oscillations of Fluids in a Container," Journal of Fluid Mechanics, Vol. 22, Part 4, pp. 737-751, 1965.
10. Hart, T. E., and Perrini, F., "Analysis of U.S. Commercial Fishing Vessels Losses, 1970-1982," U.S. Coast Guard Report, Seattle, 1984.
11. Casualty Update for Documented Fishing Vessels in 1983-1987, U.S. Coast Guard Report, Feb. 1990.
12. Numata, E., "Subdivision Standards Based on Probability Studies - A Progress Report," IMCO, SDS IV/5, 1965.
13. Adee, B. H., and Caglayan, I. H., "The Effect of Free Water on Deck on the Motions and Stability of Vessels," Second International Conference on Stability of Ships and Ocean Vehicles, Tokyo, Oct. 1982.
14. Pantazopoulos, M. S., and Adee, B. H., "An Experimental Investigation of a Vessel Response with Water Trapped on Deck," Third International Conference on the Stability of Ships and Ocean Vehicles, Gdansk, Poland, Sept. 1986.
15. Stoker, J. J., Pure and Applied Mathematics, Vol. ix, Water Waves, The Mathematical Theory with Applications, Edited by Courant, R., Bers, L. and Stoker, J. J., Interscience Publishers, Inc., New York, 1957.
16. Pantazopoulos, M. S., "Numerical Solution of the General Shallow Water Sloshing Problem," Ph.D. Dissertation, Department of Mechanical Engineering, University of Washington, Seattle, August 1987.
17. Chorin, A. J., "Random Choice Solutions of Hyperbolic Systems," Journal of Computational Physics, Vol. 22, pp. 517-533, Dec. 1976.
18. Li, K. M., and Holt, M., "Numerical Solutions to Water Waves Generated by Shallow Underwater Explosions," Physical Fluids, Vol. 24, No. 5, May 1981.
19. Yanenko, N. N., The Method of Fractional Steps, Springer-Verlag, New York, Berlin/Heidelberg, 1971.
20. Olsen, H. and Hysing, T., "A Study of Dynamic Loads Caused by Liquid Sloshing in LNG Tanks," Maritime Administration Report No. MA-RD-920-75040, Det Norske Veritas Report No. 74-276-C, Dec. 1974.
21. Principles of Naval Architecture, "The Motions of Ships in Waves," 1967 edition, pp. 672-674.

PROBLEM OF THE STABILITY CONTROL OF TRANSPORT SHIPS IN OPERATION

Lipis V.B.*, Salov V.Y.**

SUMMARY

Ways to achieve a more reliable control of ships' actual stability in operation are discussed. An analysis of the calculation method errors is made based on the full-scale trial results. Proposals aimed at a better quality of actual stability definition are given in order to standardize the requirements for reliability of stability evaluation.

1. INTRODUCTION

The requirements of national and international stability standards allow to provide a high level of structural safety of transport ships in their design and construction 1. At the same time, any ship optimally designed and having sufficient stability can be brought to a dangerous inclination or even to capsizing if her crew does not take necessary measures for stability control and maintaining when loading in harbour or operating at sea. This is clearly demonstrated by casualty statistics. Every year, 15 to 20 ships of total capacity of up to 100,000 grt are lost worldwide because of a capsizing.

Of course, our knowledge of the intricate mechanism of the wind

and waves action on ships should be updated to improve the stability standard criteria; however, it is known that the main cause of accidents for today (more than 70 percent of all disasters) is insufficient information and improper actions of sailors. The situation seems absurd in the context of today's development of shipboard diagnostics and automation equipment. Employing this equipment in stability control seems one of the primary steps towards accident-free shipping.

2. METHODS OF SHIP STABILITY CONTROL IN OPERATION

Fig.1 is a scheme endeavoring to show, without any pretence to completeness, the long history of the ship stability control problem, the principal methods, and the variety of proposals [2], [3]. The quality of control using this or that method is defined by sufficient accuracy of the values obtained for the ship stability parameters and trim under actual operating conditions.

2.1. Calculation method

The basis for any methods of calculated ship stability control in operation is the designer's documentation forming 'The Information on Ship Stability for the Master'. 'The Information' serves to define the stability characteristics in typical and unspecified cases of ship loading based on the

* Head of Department

** Research Scientist

Central Marine Research and Design
Institute

Krasnoy konnitsy str.6

Leningrad, USSR

data of masses and static moments for the deadweight components with regard to the influence of liquid cargo free surfaces.

In design calculations for hypothetical typical cases of ship loading and present values of mass and of light ship center of gravity coordinates, the standard error of metacentric height calculation with a 99.9% confidence does not exceed 2 or 3% [4], [5]. It can be said that the same accuracy is achieved in the preparation of a preliminary Cargo Plan which is presently supplied by the shore service to all ships prior to loading in harbour.

The calculated ship stability control when drawing up the executive Cargo Plan for the moment of termination of loading, when checking the worst possible case in a voyage, when taking measures to provide a stability margin, and in other practical cases is carried out by the Navigation Officer for particular non-typical loading cases. Of course, in doing so, the specified accuracy of design calculations cannot be provided.

As is well known from practice, the actual weights of many categories of cargo including containers may differ significantly from those specified in the documentation. Our investigations made on modern container-carrying transport ships have shown that the average error in the weight of one standard container may be about 2 tons. The actual weight was defined either by variation in the total displacement mass of cargo or, in some cases, by weighting the containers. Table 1 presents, for demonstration purposes, the data for one voyage of a ship of 'Khudozhnik Saryan' type.

TABLE 1
Containers weight errors
during the voyadje

Number of containers loading in the port	Total cargo data errors in conoasment (t)	One container weight error (t)
84	88	1,05
99	-13	-0,13
44	91	2,07
47	142	3,02
88	99	1,13
280	-414	-1,48
65	-103	-1,58
105	-120	-1,14
32	-213	-6,66
109	-104	-0,95
46	91	1,98
134	-271	-2,02

When 3 or 4 tiers of containers are carried on deck and the weight errors of all containers loaded are of the same sign, maximum errors in metacentric height (h) are on the average 25 to 35 percent (in some cases, up to 100-120%).

Important is also the error of the basic data on the cargo center of gravity coordinates. According to navigators' estimates the error in the definition of center of gravity heights is 0.2 to 0.5 m. The container certificate documentation does not specify the center of gravity, and in calculations, the center of volume coordinates are usually introduced.

Errors in the amount of ballast also contribute. These errors in tank level measuring by sounding rod are 3 to 4 percent and result in maximum errors in the metacentric height calculations of about 0.04 to 0.05 m.

Fig.2 shows a direct comparison of actual values h_m measured on ships and calculated h_c based on the results of observations on 12 ships. It is evident that the calculation method of stability control does not satisfy with permissible parameters and therefore can-

not always guarantee safety of navigation.

With this in mind, shipmasters either have to take unjustified risks or to provide higher stability margins which generally leads to excess ship ballasting, underloading and increased fuel consumption.

Automation of calculation, i.e. the use of personal computers and specializing computing instruments, facilitates navigation officers' work, reduces time and decreases the probability of coarse errors in computations but does not permit to increase accuracy of stability control. This can be solved by transition to diagnosis of actual stability characteristics using instrument measurements.

2.2. INSTRUMENTAL/CALCULATION METHOD

The problem of instrument/calculation stability control comprises two principal tasks:

- ship stability control at the berth or in the outer roads,
- ship stability control at sea.

Let us dwell on the first task the solution of which is based on the operational heeling method.

The definition of stability on the basis of an operational heeling experiment assumes the possibility to create a moment to heel the ship to an angle down to 3° , and control of ship displacement, heeling angle increment, and heeling moment values. The displacement D is defined by the draft measurement results. The value of h is calculated using the metacentric formula.

The method is rather widely used on ships carrying deck cargo. Most container ships and Ro-Ro ships have graduated tanks and level inclinometers specially designed for such experiments. The accuracy of

heeling moment definition at the design calculation level is reached by checking the liquid ballast pressing into a gage tank. Of considerable importance for the quality of experiment is the use of pumps having sufficient capacity to make the required number of inclinations within a limited time. On ships with special inclination equipment, it is possible to make up to 4-5 inclinations in 1 hour, while on ships without such equipment one inclination can only be made in 0.5 to 1.5 hours. In the latter case it is difficult to ensure high quality measurements and stable external conditions.

Fig. 3 shows the block diagram of an automated trim and stability control system using the instrument/calculation method and the operational heeling principle.

For an ideal system with Klimmchen-type tanks the error of measurement of stability factor D_h is determined by the error of measurement of heeling angle θ . If, for example, an r.m.s. error $(D_h) = (3+5)\%$ is preset, and the inclination is for $\theta = 1^\circ$, the heeling angle must then be measured with an absolute error at the level of 0.01° - 0.02° .

Thus, the requirements for measurement accuracy of the sensors comprised in the system follow from the evaluation of the operational inclination quality and the standards of permissible errors for D and h .

3. EVALUATION OF QUALITY OF SHIP STABILITY CONTROL IN OPERATION

Methodically, the requirements for an operational inclination experiment are similar to those adopted for shipyard heeling experiments at ships' deliveries. Maximum permissible error must be

established to eliminate faults at particular measurements and to limit cumulative probable error in Retaining the maximum permissible errors as in a shipyard experiment one cannot obtain the same reliability level of stability control for operational heeling experiment. Nevertheless, the results of the shipyard heeling experiment are used in stability calculations in each of the hundreds of voyages of this and the next 4 ships in the series throughout their service life; while the result of an operational heeling experiment is needed only to define h in a single particular voyage. It is evident that the requirements for the reliability of this latter result may be not so high as former one.

The probable error of the inclination experiment is set according to the relationship

$$T_{\alpha n} \sigma_h / n^{1/2} \leq B \quad (1)$$

where

B = standard by a confidence interval,

α = confidence probability /reliability/,

$T_{\alpha n}$ = safety factor at the confidence probability and the number of measurements n ,

σ_h = r.m.s. deviation from the mean value h_k ,

$$\sigma_h = (n-1)^{-1} \sum (h_i - h_k)^2 \quad (2)$$

$$h_k = n^{-1} \sum h_i \quad (3)$$

where h_i is the value of h in the i -th dimension.

According to the USSR Register for a shipyard heeling experiment [1], [6].

$$B = \beta \cdot (1 + h_k), \quad \beta = 0.02 \quad (4)$$

at $h_k \leq 2.0 \text{ m}$

The values of $T_{\alpha n}$ are assumed according to Student's distribution, for a high set confidence $\alpha = 0.999$ at a limited number of inclinations $n \geq 8$.

A question arises as applied to operational heeling experiments: how will the set values of α and $T_{\alpha n}$ change if the same regulatory value (4) and estimates at $n < 8$ are considered. The answer can be obtained on the basis of a statistical analysis of experiment results on ships in operational voyages. Such experiments were made on six transport vessels [7].

Employed in the analysis were the results of 27 experiments made at metacentric heights of 0.2 m to 2.0 m, at the berth or in the roads lead, at wind velocities up to 5 m/s and sea states up to 3. Inclinations as such took about 100 hours disregarding the time used for preliminary operations. Both standard shipboard equipment and special instruments (Amayev's recording inclinometer, SAMS system sensors etc.) were used for measurements.

The measurements were made with the following limit errors:

- for ship draft: $\pm 0.02 \text{ m}$ (up to 1%)
- for heeling angle increments: $\pm 0.04^\circ$ (up to 1.5%)
- for heeling moment: $\pm 5 \text{ t}$ (up to $\pm 3\%$).

The number of inclinations n in some heeling experiments varied from 3 to 17. The distribution of the number of inclinations N as related to the n is given in the Table 2.

TABLE 2

n	3	4	5	6	7	8
N	27	23	19	18	16	16

Statistical relationships $\alpha = f(n)$ and $T_{\alpha n} = f(n)$ were defined based on relationship (1), standard value (4), experimental estimates for G_h and confidence probability by Student's law.

Fig.4 shows the results for an average value of α_k and the corresponding confidence interval of 95%. With decreasing number of experiments n the confidence of definition h naturally decreases. It is significant that no considerable difference is obtained in the estimated mean values of safety factor $T_{\alpha n k}$ at various $n < 8$. These results are presented in Table 3 with corresponding standard errors (in %) $\varepsilon_\alpha = G_\alpha / \alpha n^{1/2}$ and $\varepsilon_T = G_T / T_{\alpha n k} n^{1/2}$, the confidence probabilities of which are known to be about 75%.

TABLE 3

Mean value and standard errors of reliability and safety factor for various $n < 8$

n	α		$T_{\alpha n}$	
	α_k	$\varepsilon_\alpha \%$	$T_{\alpha n k}$	$\varepsilon_T \%$
3	0,87	1,45	4,79	11,4
4	0,92	1,00	4,75	9,5
5	0,96	0,43	4,50	5,5
6	0,97	0,38	4,70	5,6
7	0,98	0,22	4,80	5,5
8	0,99	0,12	5,24	5,7

As can be seen from Fig.4 and Table 3, the empirical results have a proper trend to an asymptotic transition to the high level of $\alpha > 0,99$ at $n \geq 8$, which is foreseen in the USSR Register Rules for shipyard heeling experiments ($T_{\alpha n} = 5.4$ at $n = 8$ and $\alpha = 0.999$).

Proceeding to equally accurate evaluation of reliability of operational heeling experiments at differing number of $n < 8$ one should bear it in mind that three inclinations to an angle down to 3° , on

transport ships equipped with stability control facilities, take about one hour. Therefore, guided by the experimentally obtained level $\alpha = 0.85$ for $n = 3$, let us compare the values of $T_{\alpha n}$ for $\alpha = 0.85$ at all $n < 8$, and empirical estimate of $T_{\alpha n}$ at variable α along the lower border of the 95% - confidence interval. The results are given in Fig.5. It can be seen that when setting $T_{\alpha n}$ by the constant value of $\alpha = 0.85$ with increasing $n > 3$, there is an actual safety factor for measurements of 17% (at $n = 4$) to 80% (at $n = 7$).

For specified conditions of $\alpha = 0.85 = \text{const}$ with the factor $\beta = 0.02$ value (4) and h_k in the range of 0.2 to 1.0 m, the permissible values of standard error ε_h for h_k are of the order of 2% to 7% at $n = 3$ to 8, being slightly dependent on n for $n > 6$ (see Fig. 6). These conditions of standard setting actually will not change if we adopt a more convenient standard combining $\alpha = 0.90$ and $\beta = 0.025$ (lines 1 and 2 in Fig.6 can be compared). Fig.6 shows also standard errors for shipyard inclination experiments, i.e. at $\alpha = 0.999$, $\beta = 0.02$, and $n \geq 8$. It seems logical that permissible values of standard error in this case are considerably lower and do not exceed 3%.

As to the elimination of faults in particular measurements, a differentiated approach based on the estimates employing well-known criteria of Chauvin, Romanovsky and others can be applied to experimental result processing with various $n < 8$. However, the analysis allows to adopt a single standard at the level of two standard deviations from the mean (with a 95% confidence according to the normal law of distribution).

Thus, for actual conditions of operational heeling of transport ships the result of metacentric height definition may be considered satisfactory when the following requirements are met:

- for each observation with a result for h_i :

$$|h_i - h_k| \leq 2 \left[\sum (h_i - h_k)^2 / (n-1) \right]^{1/2} \quad (5)$$

Measurements that do not meet this condition must be excluded from processing.

- for a probable experimental error:

$$T_{\alpha n} \left[\sum (h_i - h_k)^2 / n(n-1) \right]^{1/2} \leq 0,025(1+h_k) \quad (6)$$

at $h_k \leq 2$ m.

The factor $T_{\alpha n}$ is assumed as a function of n according to Student's law of distribution with a 90% confidence (Table 4).

TABLE 4

n	3	4	5	6	7	8
$T_{\alpha n}$	2,92	2,35	2,13	2,02	1,94	1,90

The total number of satisfactory inclinations must be not less than 3.

4. CONCLUDING REMARKS

On the basis of the foregoing the following remarks could be made.

The analysis of ship stability definition methods under operational conditions shows the necessity to apply modern automated instrument means of diagnostics of actual characteristics.

Experimental research carried out onboard allowed to provide statistical evaluation of the quality of stability control using the operational heeling method and to put forward the requirements ensuring sufficient accuracy of actual stability control system has confirmed the feasibility to use the proposed standards as a basis for require-

ments for such systems to be set by the USSR Register.

As automated ship stability control systems are being constructed in many countries and their use on ships becomes more and more widespread, it seems advisable also to prepare and approve international recommendations aimed at the improvement of operational heeling quality.

Acknowledgements

The authors feel it is their pleasant duty to acknowledge the assistance rendered by the USSR Register to this research at Central Marine Research & Design Institute.

References

(published in Russian)

1. Rules for the Classification and Construction of Sea-Going Ships. USSR Register of Shipping. - L., 'Transport', 1985. - 928 pp.
2. Kozlov K.S. Advanced Methods of Ship Trim and Stability Assessment. L., 'Morskoy Transport', 1963.
3. Naidenov Y.V. Ship Trim and Stability Control. M., 'Transport', 1983.
4. Krylov A.N. Lectures on Approximate Calculations. Coll. Works, Vol. 3, part I. M.-L., Acad. Sc. USSR, 1949.
5. Bazilevsky S.A. Theory of Errors in Ship Design. L., 'Sudostroe-niye', 1964.
6. Muru N.T. On the Accuracy of Results of Ship Heeling Experiments. In: USSR Register's 'Theoretical and Practical Problems of Transitional Properties of Ships'. L., 'Transport', 1967.
7. Salov V.Y., Habur V.B. The analysis of operational heeling results. Tr. CNIIMF, L. 'Transport', 1989, p.49-54.

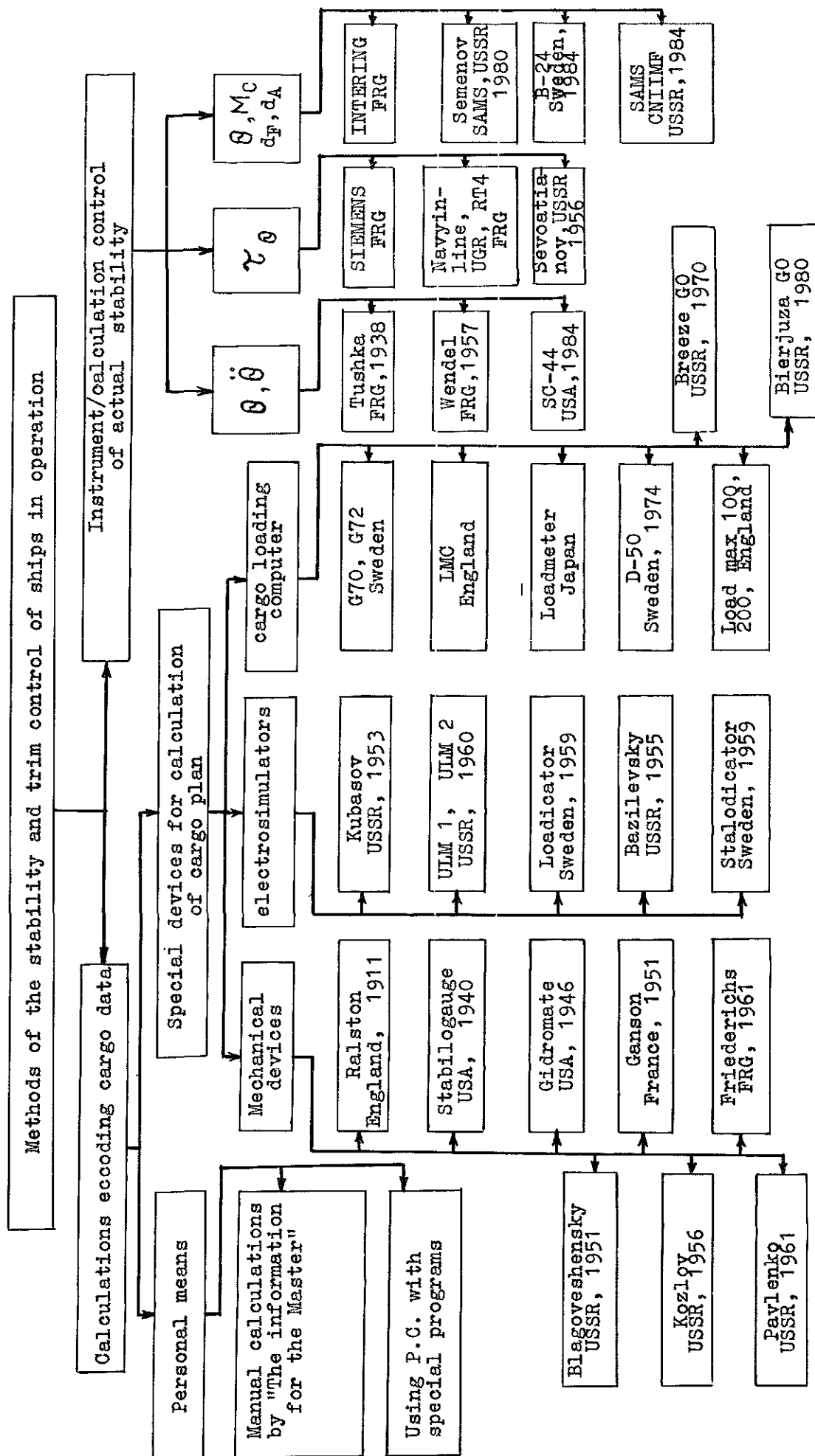


Fig.1. Systematical scheme of the stability control in operation

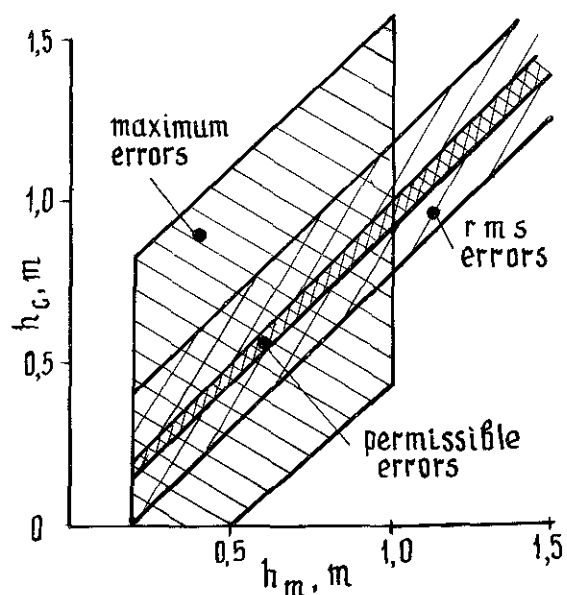


Fig. 2. Comparison of means and calculated values of n

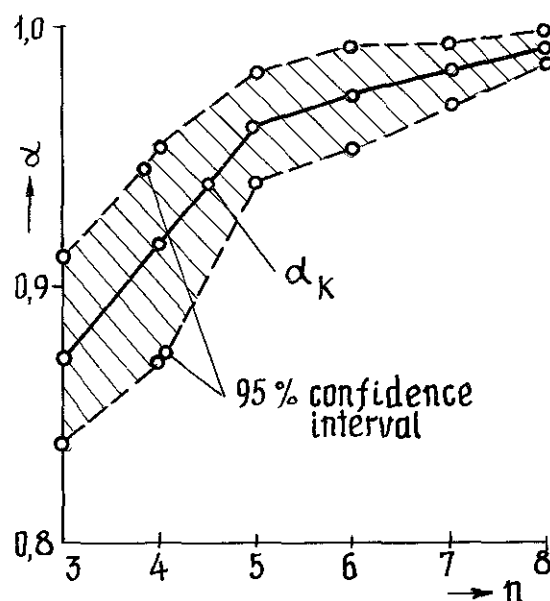


Fig. 4. Experimental value of α .

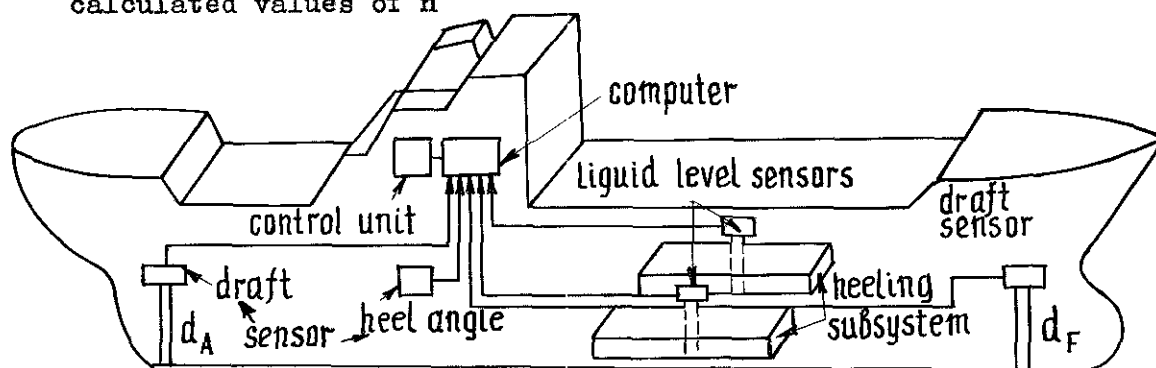


Fig. 3. Scheme of system for automated monitoring of stability and trim

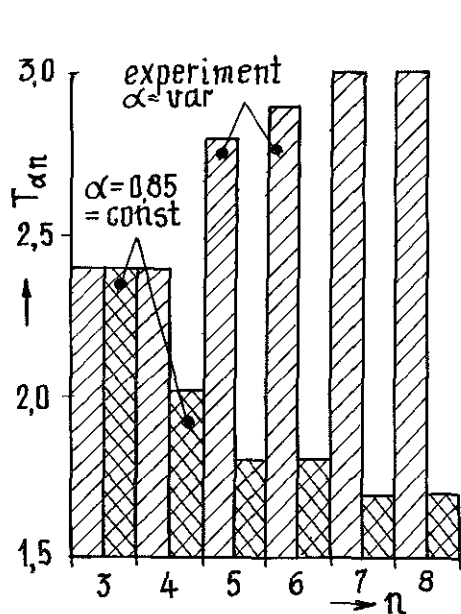


Fig. 5. Safety factor for various reliability

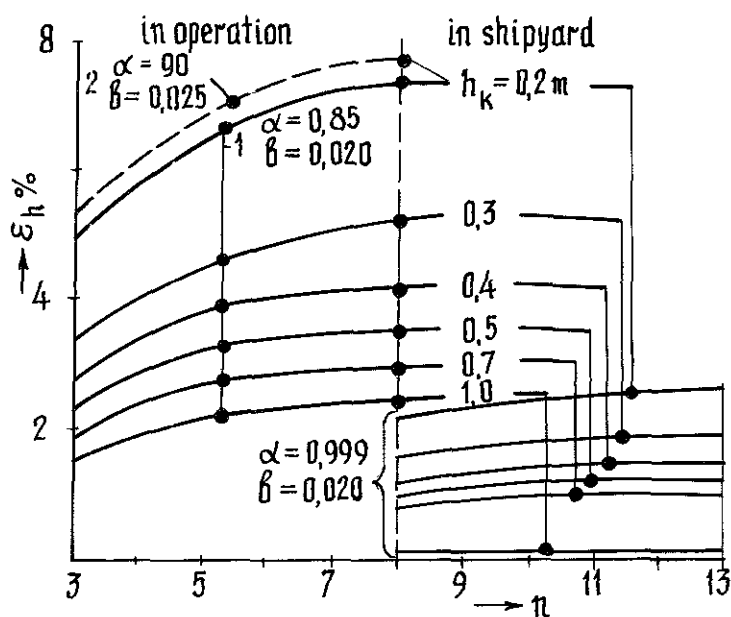


Fig. 6. Standard error of h for heeling experiment

STABILITY OF SHIP'S ROLLING IN WAVES

V.A.Nekrasov

This paper is devoted to a determination of the characteristics of nonlinear large amplitude ship motions in a regular wave by the method of moments. It is shown that the autocorrelation moments represent amplitude characteristics of the motions and the joint moments represent phase correlations between displacements and velocities of a ship and analogous characteristics of a wave surface. Therefore, a sufficiently complete description of the nonlinear interaction between the ship and the progressive wave was obtained by this method. The equations of moments were formed on the basis of nonlinear motion equations and the solution of moment equations for the stationary state ship motion was obtained by methods of nonlinear programming. A stability investigation of this solution has been carried out by the method of small additional perturbations. The proposed method of moment stability investigation gives a possibility to find the mechanism of a ship motion stochasticity which is formed due to instability of joint moments. Such type of instability breaks the phase synchronism between oscillations of the ship and oscillations of the wave surface which results in capsizing or in irregular motion of the ship.

INTRODUCTION

A method of statistical moments [Ref.1] is the most widespread investigation method of a nonlinear lateral ship motion in rough seas.

Applying assumptions of a theory of multicomponent Markovian processes to this method allows not only to determine the probability characteristics of essentially nonlinear ship motion but to carry out the eventual stability investigation which is a useful instrument for predicting ship's capsizing in irregular waves.

When breadths of spectra disturbances acting on the ship tend

to zero, the method of statistical moments transforms into the method of deterministic moments and results in the phenomena which are observed under a nonlinear motion of ship in regular wave.

The paper comprises composition of the mentioned above limit case and its application to the investigation of a ship motion and stability of motion in regular wave.

EQUATIONS OF MOTION

Let's consider a ship exposed to action of a constant wind and regular wave. The acting disturbances are denoted by $X_j(t)$ and by $Y_k(t)$ - displacements and velocities of induced ship motion.

Professor, Shipbuilding Department,
Nikolayev Shipbuilding Institute,
Nikolayev, U.S.S.R.

Let's assume that such motion describes a solution of the nonlinear differential equations

$$\frac{d\vec{Y}}{dt} = \vec{Q}(t, \vec{X}, \vec{Y}), \quad (1)$$

where $\vec{X}(t)$ is the acting disturbances vector and $\vec{Y}(t)$ is the vector of ship motion processes. We also assume that right hand sides of the system of equations (1) are formed by polynomials of variables X_j and Y_k and that these variables are presented as follows

$$\begin{aligned} X_j(t) &= \bar{X}_j(t) + \tilde{X}_j(t); \\ Y_k(t) &= \bar{Y}_k(t) + \tilde{Y}_k(t), \end{aligned} \quad (2)$$

where \bar{X}_j and \bar{Y}_k are average values of acting disturbances and ship motions processes accordingly, \tilde{X}_j and \tilde{Y}_k are their pulsatory components which will be considered as the periodical functions of a time.

EQUATIONS OF MOTION CHARACTERISTICS

Taking into account a periodicity of the considered processes we introduce a well-known operator of averaging [Ref.2]

$$M_t[\dots] = \frac{1}{2\pi} \int_0^{2\pi} [\dots] d\psi. \quad (3)$$

This operator is used in determination of the initial first order moments

$$\alpha_{i_j}^{(x)} = M_t[X_i(t)]; \quad \alpha_{i_k}^{(y)} = M_t[Y_k(t)]$$

the initial second order moments

$$\alpha_{2_j}^{(x)} = M_t[X_j^2(t)];$$

$$\alpha_{2_k}^{(y)} = M_t[Y_k^2(t)];$$

$$\alpha_{i_j i_k}^{(xy)} = M_t[X_j(t) Y_k(t)],$$

etc.

The central moments of second and higher orders are determined as

$$\mu_{2_j}^{(x)} = \alpha_{2_j}^{(x)} - [\alpha_{i_j}^{(x)}]^2;$$

$$\mu_{i_j i_k}^{(xy)} = \alpha_{i_j i_k}^{(xy)} - \alpha_{i_j}^{(x)} \alpha_{i_k}^{(y)};$$

.....

We shall further assume that a noticeable change of the moment can occur in time intervals which are longer than the period of averaging. We shall also consider a system of equations of the first and second moments only. The system of the first moment equations is composed by applying the operator (3) to the equations of a ship motion (1). The determination of the second moment equations can be carried out in a usual way. It is necessary to multiply equation (1) by $Y_k(t)$ in succession and then to use the operation of averaging (3).

The equations of ship motion (1) are nonlinear equations. Therefore, obtained equations of moments comprise not only moments of first and second orders. Thus, the system of equations of moments is not closed. For closing it or for establishing an agreement between the number of the moments to search and the number of equations of a system, the moments of higher orders are expressed through moments of the first and second orders with help correlations existing for the periodical functions. In general the solution of this problem is a bulky task. However, the forces acting on the ship due to the incident regular wave are almost harmonical functions of the time and the processes of a ship motion are almost harmonical functions also. Therefore, defining them in the first approach can be executed as follows

$$\tilde{X}_j(t) \approx A_j^{(x)} \cos(\omega t + \varphi_j^{(x)});$$

$$\tilde{Y}_K(t) \approx A_K^{(Y)} \cos(\sigma t + \varphi_K^{(Y)}).$$

This simplified solution allows to use the formulas

$$M_t[z^3] = \alpha_1^3 + 3\mu_2\alpha_1;$$

$$M_t[z^4] = \alpha_1^4 + 6\alpha_1^2\mu_2 + \frac{3}{2}\mu_2^2;$$

Thus, it gives us the possibility to close the system of equations for the moments of the first and second orders. After the closure, the system of equations for characteristics of the processes of external disturbances and the ship motion is written as

$$\begin{aligned} \frac{d\vec{\alpha}_1}{dt} &= \vec{Q}_1(\vec{\alpha}_1, \vec{\mu}_2, t); \\ \frac{d\vec{\mu}_2}{dt} &= \vec{Q}_2(\vec{\alpha}_1, \vec{\mu}_2, t). \end{aligned} \quad (4)$$

An investigation of the stationary state of a ship motion is a problem of practical importance. For the stationary motion of a ship the left hand sides of the system of equations (4) are equal to nought and this system of nonlinear differential equations is transformed into the following system of nonlinear algebraic equations

$$\begin{aligned} \vec{Q}_1(\vec{\alpha}_1, \vec{\mu}_2) &= 0; \\ \vec{Q}_2(\vec{\alpha}_1, \vec{\mu}_2) &= 0. \end{aligned} \quad (5)$$

A solution of the system of nonlinear algebraic equations of moments (5) is obtained by the methods of nonlinear programming most efficiently [Ref.3].

INVESTIGATION OF STABILITY

Let's assume that an equilibrium position of the ship in a calm water appeared to be a stable equilibrium position and the ship had

some dynamic stability which was defined by an area of the righting moment curve. Let's also assume that the weak wind-wave forces were acting on the ship and that after some time the unsteady characteristics of a ship motion were becoming steady-state characteristics.

Therefore, vectors $\vec{\alpha}_1^{(0)}$ and $\vec{\mu}_2^{(0)}$ define the set of real roots (solutions) of the equations (5) which were composed for the moments of the considered weak conditions of the wind-wave action and the ship motion. Let's introduce the additional perturbations into these conditions making the increments $\Delta\vec{\alpha}_1$ and $\Delta\vec{\mu}_2$ to the moments $\vec{\alpha}_1^{(0)}$ and $\vec{\mu}_2^{(0)}$. A system of equations for the additional perturbations is represented as

$$\frac{d\Delta\vec{\alpha}_1}{dt} = \left. \frac{\partial \vec{Q}_1}{\partial \alpha_1} \right|_{(0)} \cdot \Delta\vec{\alpha}_1 + \left. \frac{\partial \vec{Q}_1}{\partial \mu_2} \right|_{(0)} \cdot \Delta\vec{\mu}_2; \quad (6)$$

$$\frac{d\Delta\vec{\mu}_2}{dt} = \left. \frac{\partial \vec{Q}_2}{\partial \alpha_1} \right|_{(0)} \cdot \Delta\vec{\alpha}_1 + \left. \frac{\partial \vec{Q}_2}{\partial \mu_2} \right|_{(0)} \cdot \Delta\vec{\mu}_2.$$

According to the theory of A.M.Lyapunov [Ref.4] there are the following theorems:

1. The steady-state ship motion defined by a set of real roots $\vec{\alpha}_1^{(0)}$ and $\vec{\mu}_2^{(0)}$ of the equations (5) is asymptotic stable if the roots of characteristic equation corresponding to the system of equations for the additional perturbations (6) have the negative real parts.

2. The steady-state ship's motion will be unstable if a root with positive real part will be found among the roots of the characteristic equation.

The criteria of Routh-Hurwitz are the criteria of negativity of the real parts of characteristic roots. For finding them let's consider a square matrix of the first partial derivatives with respect to $\vec{\alpha}_1$ and $\vec{\mu}_2$ of the right hand sides of the

equations for moments (5), i.e. - a square matrix of the coefficients of the system (6)

$$A = \left\| \frac{\partial Q_{i_l}}{\partial \alpha_{i_m}} \right\|, \quad (7)$$

$$i = 1, 2; \quad l, m = 1, 2, \dots, N,$$

where N is a summarized number of the equations of moments of the first and second orders. A characteristic matrix B corresponding the square matrix A is written as

$$B = A - \lambda E,$$

where E is unit matrix. The determinant of characteristics matrix B is a well-known characteristic polynomial

$$f(\lambda) = |A - \lambda E| = (-1)^N \lambda^N + a_1 \lambda^{N-1} + \dots + a_N,$$

in which the coefficients a_k are expressed by the elements of the A matrix as

$$a_k = (-1)^{N-k} S_k,$$

where S_k is a sum of the principal minors of the k -th order of the A matrix. In particular

$$a_N = |A| = \lambda_1 \cdot \lambda_2 \cdot \dots \cdot \lambda_N, \quad (8)$$

where λ_i , $i=1, 2, 3, \dots, N$, are roots of the characteristic equation

$$f(\lambda) = 0.$$

Hurwitz matrix is defined on the basis of the characteristic polynomial [Ref.7] then we make the principal minors

$$\Delta_1 = a_1; \dots; \quad \Delta_N = a_N \cdot \Delta_{N-1},$$

and Hurwitz criteria are written in the terms

$$\Delta_j > 0, \quad j = 1, 2, \dots, N. \quad (9)$$

The right hand side of the equations for the moments (4) are

nonlinear functions of $\vec{\alpha}_1$ and $\vec{\mu}_2$. Therefore, a gradual increase of the external constantly-acting disturbances (wind and waves) results in the transformation of the A matrix and this matrix is becoming a function of the variables $\vec{\alpha}_1$ and $\vec{\mu}_2$. This is resulted in a change of the characteristic roots. Let's assume that all roots of characteristic equation for the equilibrium position of a ship had negative real parts. Then, after the slow intensification of the wind and wave, we can expect that real part of any root is made positive. Thus, boundary of stability domain for dynamical systems with full dissipation, i.e. for the floating body, is determined by following conditions

$$\Delta_1 > 0; \Delta_2 > 0; \dots; \Delta_{N-1} > 0; \Delta_N = 0. \quad (10)$$

According to the equality (8) we have

$$|A| = 0 \quad (11)$$

on the boundary of stability.

An addition of the equation (1) to the system of equations for moments (5) and the solution of them determine the boundary of stability in a space of ship's motion characteristics and the corresponding boundary of wind-wave actions endured by the ship in the space of the parameters of the constantly-acting disturbances.

Is a very slow transition of obtained boundary of stability connected with capsizing of ship always? A loss of stability in this case occurs in result of an occurrence of small declination of the characteristics of external forces and a ship motion from their finite values determined by the stability boundary. Therefore, the following course of the events is defined by the tendency of the induced unsteady

process:

- if in the domain of admissible dynamic states of a ship the attractive centre exists, the ship goes over to the oscillations about this centre;

- if attractive centre is the overkeel equilibrium position, the ship capsizes;

These types of instability accompany a change of the energetic level of the ship position and usually are connected with the loss of stability of the autocorrelation moments by means of which are expressed the energetic characteristics of a ship motion.

A loss of the joint moments stability, especially the moments of a tie between the oscillations of the ship and the oscillations of the water surface, results in the breach of the joint dependence of the considered processes, i.e. to the breach of the phase synchronism established between them, and during the initial time periods is accompanied with stochasticity of the ship motion. This phenomenon can be continued infinitely long if in the worst case in which the ship and the wave encounter with opposite phases, an energetical level of the induced unsteady-state process will be below the critical level.

The main role in the theoretical discovery and description of the pointed out phenomena belongs to the mathematical models of the nonlinear ship motion.

STABILITY OF SHIP'S ROLLING IN THE LONG REGULAR WAVE

In making the equations of the ship's motion we use the principle of the acting forces representation by the Taylor series expansion in powers of the displacements, veloci-

ties and accelerations of the water surface and the ship in the neighbourhood of equilibrium position in still water. Let's introduce additionally an assumption about long periodicity of the ship rolling, i.e. consider the ship motions in the long waves into the domain of the low-frequency main resonance. Let us also note that in such domain of frequencies sway and heave motions have weak influence on the roll motion.

Retaining the small quantities of the first and second orders, we shall have

$$\begin{aligned} & (\bar{J}_x + \mu_{44}) \ddot{\vartheta} + \lambda_{44}^{\text{II}} \dot{\vartheta} |\dot{\vartheta}| + \\ & + D\ell(\vartheta) = \bar{M}_0 - \bar{J}_x \alpha_{\theta} k \ddot{\eta}_B(t) - \\ & - m \alpha_{\theta} \ell(\vartheta) \ddot{\eta}_B(t) k \ddot{\eta}_B(t) + \\ & + m \alpha_z \ell(\vartheta) \ddot{\xi}_B(t) + \\ & + \frac{G}{g} \lambda_{44}^{\text{I}} \alpha \dot{\vartheta}^2 \alpha_{\eta}^2, \end{aligned} \quad (12)$$

where

$$\vartheta = \theta - k \eta_B \alpha_{\theta}, \quad k = G^2/g.$$

In the equation (12) the first summand of the exciting moment represents the constant component of a heeling moment, the second member is formed by the usual transition to the relative variables, the third member due to the additional changeability of the wet surface of a ship hull, the fourth member due to the vertical component of a wave current and the fifth member is the estimation of the moment of a wave drift.

For the presentation of the restoring moment, we have used the simplest approximation

$$D\ell(\vartheta) = D[h\vartheta + h_1\vartheta^3],$$

for the processes of acting excitations we have

$$\begin{aligned}\bar{X}_1 &= \bar{M}_0; \\ \tilde{X}_2(t) &= \eta_B(t) = r \sin \sigma t; \\ \tilde{X}_3(t) &= z_B(t) = r \cos \sigma t; \\ \tilde{X}_1(t) &= \bar{X}_2 = \bar{X}_3 = 0,\end{aligned}$$

and for the processes of a ship motion

$$\begin{aligned}Y_1(t) &= \vartheta(t); \\ Y_2(t) &= \dot{\vartheta}(t).\end{aligned}$$

Taking into account the proximity of this periodical functions to the harmonic functions, assume

$$\begin{aligned}Y_1(t) &\approx A_\vartheta \sin(\sigma t + \varphi_\vartheta) + m_\vartheta; \\ Y_2(t) &\approx \sigma A_\vartheta \cos(\sigma t + \varphi_\vartheta).\end{aligned}$$

The application of the operator (3) to the functions representing acting excitations we can receive the moments of the first order

$$m_0 = \bar{M}_0; \quad m_{\eta_B} = m_{z_B} = 0.$$

and the central moments of the second order

$$\begin{aligned}D_{\eta_B \eta_B} &= D_{z_B z_B} = D_z; \\ D_{\eta_B \dot{z}_B} &= -D_{\dot{\eta}_B z_B} = -\sigma D_z; \\ D_{\dot{\eta}_B \dot{z}_B} &= D_{\eta_B z_B} = 0; \\ D_z &= r^2/2.\end{aligned}$$

For the undetermined moments of a ship motion we define respectively

$$\begin{aligned}m_\vartheta &= M_t[\vartheta]; \\ m_{\dot{\vartheta}} &= 0;\end{aligned}$$

$$D_{\dot{\vartheta} \eta_B} = -\frac{1}{\sigma} D_{\vartheta z_B} = \frac{1}{\sigma^2} D_{\dot{\vartheta} \dot{\eta}_B} =$$

$$= \frac{1}{\sigma} D_{\dot{\vartheta} z_B} = \frac{1}{2} A_\vartheta r \cos \varphi_\vartheta;$$

$$\begin{aligned}D_{\vartheta z_B} &= \frac{1}{\sigma} D_{\vartheta \dot{\eta}_B} = -\frac{1}{\sigma} D_{\dot{\vartheta} \eta_B} = \\ &= \frac{1}{\sigma^2} D_{\dot{\vartheta} \dot{z}_B} = \frac{1}{\sigma} A_\vartheta r \sin \varphi_\vartheta;\end{aligned}$$

$$D_{\vartheta \vartheta} = \frac{1}{\sigma^2} D_{\dot{\vartheta} \dot{\vartheta}} = \frac{1}{2} A_\vartheta^2;$$

$$D_{\vartheta \dot{\vartheta}} = M_t[\dot{\vartheta} \vartheta] = 0.$$

These thirteen characteristics of a ship motion are unknown in the general case. Together with the known characteristics of the acting excitations they were used for forming the system of equations for moments. The consequent analysis of this system confirms that there are four independent variables in the approach considered. They are m_ϑ , $D_{\vartheta \vartheta}$, $D_{\vartheta \eta_B}$ and $D_{\vartheta z_B}$.

For the obtained system of nonlinear algebraic equations we make an algorithm and corresponding programme of computing the moments by the methods of nonlinear programming. The programme includes subroutine of computing the matrix of partial derivatives of the equations for moments and subroutine computing the characteristic numbers determined by the term (8).

The computation of the moment- and then amplitude- and phase frequency characteristics of the nonlinear roll motion of the ship model, which was tested by Wright and Marshfield [Ref.8], has been carry out. The corresponding characteristic numbers were also computed and on this basis the domains of instability are defined. The results of this computations are presented in Fig. 1-2.

An analysis of the obtained results points out that the main role in forming the instability domain, when the initial bias of a model equals 6° towards incident wave, is played by the moment of wave drift forces. This analysis also points out that the stability loss of the joint moment D_{η_B} , breaking the phase synchronism between oscillations of a wave surface and roll motions of a ship model, takes place together with the stability loss of the autocorrelation moment (of the amplitude). When the model has not initial bias or has 6° bias away from the wave influence, a stability loss of the obtained solutions are not observed.

NOMENCLATURE

A - roll motion amplitude
 a - vertical distance between center of gravity and center of buoyancy
 D - magnitude of buoyancy force
 D_ξ - central autocorrelation moment of wave surface oscillations
 $D_{\xi\xi}$ - central autocorrelation moment of roll motion
 $D_{\xi\eta_B}$ - central joint moment of second order
 $h(\vartheta)$ - metacentric height
 J_x - mass moment inertia about longitudinal axis
 $l(\vartheta)$ - righting arm
 M_0 - constant heeling moment
 $m_{\dot{\vartheta}}$ - average of roll motion
 m - mass of ship
 r - wave amplitude
 z_B - vertical displacement of wave surface
 η_B - horizontal displacement of wave surface
 θ - absolute angle of roll motion
 ϑ - relative angle of roll motion

$\left. \begin{matrix} x_\theta \\ x_\xi \\ x_\eta \end{matrix} \right\}$ - reduction coefficients of wave-exciting forces

λ_{44}^I - linear damping coefficient
 λ_{44}^{II} - nonlinear damping coefficient
 μ_{44} - added mass moment of inertia
 ω - wave frequency
 φ - phase lag between roll motion and horizontal displacement of wave surface

REFERENCES

1. Nekrasov V. A., "Probabilistic Problems of Seakeeping", Sudostrojenije, Leningrad, 1978.
2. Bogoliubov N.N., Mitropolsky Yu. A., "Asymptotic Methods in Nonlinear Theory of Oscillations", Fizmatgiz, Moscow, 1963.
3. Himmelblau D.M., "Applied Nonlinear Programming, Mir, Moscow, 1975
4. Lyapunov A.M., "General Problem of Motion Stability", GIITL, Moscow 1950.
5. Hayashi C. "Nonlinear Oscillations in Physical Systems", Mir, Moscow, 1968.
6. Mishina A.P., Proskurjakov I V. "Higher Algebra", Nauka, Moscow, 1965.
7. Merkin D.R. "Introduction in Theory of Motion Stability", Nauka, Moscow, 1971.
8. Wright I.H.G., Marshfield W.B. "Ship Roll Response and Capsize Behaviour in Beam Seas". -Trans. RINA, 1979, vol. 121, pp. 129-150.

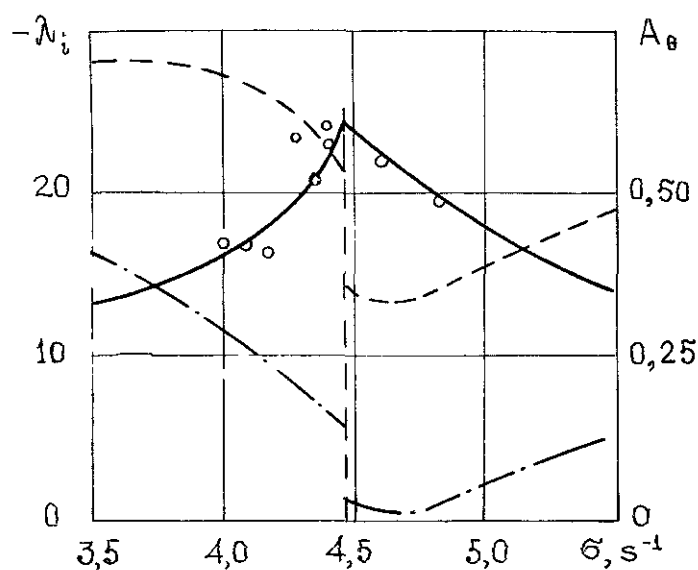


Fig. 1 Amplitude-frequency characteristic of the model tested by Wright and Marshfield. 6° bias away from the wave influence

$\circ \circ \circ$ - experiment; — - computed amplitudes;
 ----- - computed characteristic numbers of $D_{\theta\theta}$;
 -.-.- - computed characteristic numbers of $D_{\theta\eta_B}$.

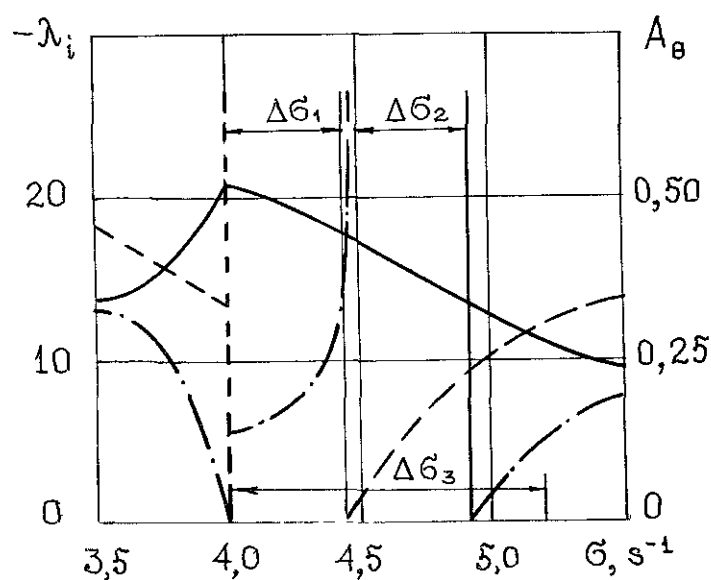


Fig. 2 6° bias towards wave

$\Delta\sigma_1$ - instability domain of $D_{\theta\theta}(A_\theta)$;
 $\Delta\sigma_2$ - instability domain of $D_{\theta\eta_B}(\eta_B)$;
 $\Delta\sigma_3$ - experimental domain of instability.

EXPERIMENTS INTO THE CAPSIZE OF SHIPS IN HEAD SEAS

R.K. BURCHER¹ BSc(Eng), PhD, FEng, FRINA, RCNC

Abstract:

Following the loss of ships apparently due to unexpected capsize, experiments have been conducted at UCL to try to reproduce the capsize of a statically stable ship model. For a model heading into waves, repeatable capsizes have been produced for a particular loading of the model and length of wave. This paper reports the observations of these experiments and discusses the possible causes.

1. INTRODUCTION

Though there are a considerable number of theoretical analyses of the problem of ships rolling in waves, there are relatively few model experiments from which to draw evidence for the extreme rolling behaviour of ships in waves. Perhaps the best known are the San Francisco Bay experiments by Paulling (1) which did result in capsizing and the investigations by Morell (2) into the loss of the GAUL. In both of these the ship model was subjected to a scaled representation of a rough sea. One of the problems with this approach is that even if capsizes do occur it is difficult to reproduce the same circumstances in order to investigate the parameters involved or check the effect of a change in parameters.

The facilities available limited the choice of experiment in that the width of the tank

constrained investigations on reasonable size models to ahead or astern wave encounters. It is recognised that following and quartering seas have their dangers. Paulling's experiments showed that as well as broaching, the passage of a wave along the ship could result in the complete loss of roll righting moment or the oscillatory variation of righting moment due to wave passage could result in parametric resonance conditions leading to capsize. It was reasoned that for reasonably stiff ships the encounter frequencies which would result in parametric resonance could occur with the vessel moving ahead into waves. It was therefore decided to explore this set of circumstances as an initial search for capsize.

2. EXPERIMENT ARRANGEMENTS

The experiments were conducted in the small towing tank installed at UCL. This tank is 22m long, 1.4m wide and a depth of water of 1.0m.

¹VSEL Professor of Submarine Design
University College London

The tank is equipped with an overhead towing carriage and a flap type wavemaker at one end. A regular sine wave is produced with quite small surface variations.

The models used were of about 1 metre length. The main model used was of boat shaped form $\frac{L}{B}$ 5.9; which approximated to the small ship/trawler forms which seem most at risk. The other model was of a larger fast form which produced some opportunity to compare overall parameters. In its original form this hull was vertical sided amidships above the water-line. For a series of tests this shape was modified by the addition of a 15° outward flare. Both models were completely unappended and unpropelled.

It was necessary to constrain the model. A single line forward from the bow at the waterline and a stern line resulted in the model being constrained in heading and surge. These constraints were of some concern as they could have a significant influence on the results. However tests on several variations led to the conclusion that this constraint had little influence on the outcome and eventually a double line system was adopted at either end, the lines being taken out at 45° to provide greater yaw and sway constraint.

Initially motions were measured with a video camera set up in line with the axis of the model and with reference axis mounted in the model and on the far mooring post. Later a roll rate gyro was installed which provided information on the roll behaviour only. Finally

a set of four rotary potentiometers were set up on the carried with light lines to the bow, stern and beam amidships.

3. TEST DESCRIPTIONS

An extensive series of tests were conducted with the model in four ballast conditions. The GM roll period for each was carefully measured and cross checked. It was found that rolling was induced in only a few of the conditions.

With the model at rest, moored by the fore and aft wires. The wave maker was started at a low frequency which generated waves of small amplitude. The model responded by heaving and pitching as it followed the waves with no evidence of roll. The frequency of wave maker was slowly increased. At first the model continued to respond only in heave and pitch but as the waves shortened, rolling of small magnitude started to occur. This appeared to be accompanied by some yawing motion so that a corkscrew motion was evident on the model. As a wavelength near to the model length was approached some conditions gave rise to more pronounced rolling with successive rolls of larger amplitude. Observation at the bow showed a phase relationship in that the bow was pitching down into the front of the wave crest at the point of maximum roll. This appeared to generate a strong restoring moment bringing the model upright and across to the other side by which time the model was again pitching down into the front of next wave crest. This process was repeated over a few cycles by which time the amplitude of roll was quite large. The model at this stage appeared to lose all of its roll stiffness and rolled over. On some occasions the

model had started to recover from a large roll angle when it capsized. This situation appeared to coincide with the stern lifting clear of the water as the model crested a wave i.e. the wave crest was about three-quarters of the way back along the ship.

For each of the four displacements rolling was seen to occur when the natural roll period was equal to the period of a wave about the length of the ship, however, the rolling did not develop to large angles. Similarly, conditions were found where some rolling occurred at a roll period equal to the period of a wave slightly longer than the ship. The most pronounced rolling and capsizes occurred when the ship was ballasted to a roll period twice the period of a wave the length of the ship.

In the most interesting experiment a capsize resulted after only 3 cycles. This is shown in Figure 1.

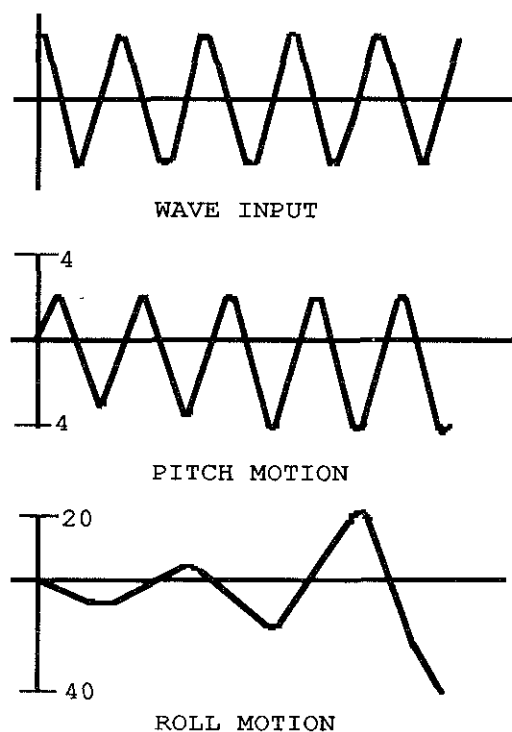


FIGURE 1

It can be seen that the pitch motion is regular and of the same frequency as the waves. Heaving motion is similar. The roll angle increases on each successive swing until capsize, and is at half the wave frequency. The sway and yaw motions were very small and irregular.

A study of the effects of initial heel was conducted. In the previous experiments the model had been ballasted so that it was upright within reasonable accuracy in calm water prior to being subjected to waves. The possibility exists that the model required some initial heel, introducing asymmetry, in order to trigger the unstable rolling that had been observed.

The model was ballasted in the upright condition so that it had a roll period of 1.82 seconds. Waves were run past the model and it was found that when the wave period was 0.96 seconds violent rolling occurred resulting in capsize after 4 rolls. A small weight, 250 gms, was moved across in the ballast box to give a heel of 5° port and the same waves passed the model. The model was observed to oscillate slightly about the 5° heel angle and then rapidly developed large rolling to both sides resulting in a capsize to port. The same result was obtained with an initial heel to starboard. A further shift of the weight was made to give 10° port heel. When the waves passed the model, the hull was observed to oscillate about 5° either side of the 10° static condition. On some occasions no further build up of rolling took place. On others the model appeared to initiate the unstable condition itself. It was observed that for capsize to occur

the model had to pass through the upright condition and develop rolling to both Port and Starboard.

In a second series, the capsize tests were repeated with a narrow beam hull. The model was quite positively stable in calm water and had an angle of vanishing stability of about $75-80^\circ$. The natural roll period and wave period were varied about the 2:1 ratio. It was found that rolling occurred when the 2:1 ratio was achieved over a narrow band of wave lengths with the most violent occurring when the wave length was $1.16 \times \text{Ship Length}$. In this condition the roll motion had an amplitude of 70° approaching the vanishing angle of stability. On either side of this frequency, rolling was observed of smaller amplitudes and with a beat characteristic, roll building up as though about to capsize and then subsiding.

Following the ideas presented in an earlier paper (3), the hull form was modified by the addition of 15° to flare above the design water line. Calculations of this form showed that the variation of GM in waves was altered. For the original model a wave crest amidships lowered the calm water GM whereas a trough amidship increased it. For the modified model both crest and trough positions slightly raised the calm water GM. This time there was still some induced rolling; in the condition which had previously resulted in violent rolling near to capsize, the model exhibited the largest rolling but it was limited to a maximum of 20° . This appears to confirm that a hull form which reduces variation of GM in waves is less subject to this form of induced rolling.

The double wire mooring system was adapted for a carriage system with lines out at 45° both port and starboard. Using this system repeat tests were carried out with the carriage stationary and similar capsizes occurred at the critical conditions. Usually they took place without any external disturbance but on some occasions the model showed no tendency to develop rolling. A slight touch to start the boat rolling was all that was necessary to start violent rolling and capsize in a very few cycles. This illustrates a very clear instability in the system and suggests that it is possible for a ship to be moving quietly in waves but a slight disturbance (yaw or gust) may be sufficient to trigger the instability and result in capsize.

The model was tested with a slightly higher GM value than the stationary critical value. It was then found that with waves the length of the ship capsize could be produced by slowly towing the model into the waves. The critical condition was then of rolling frequency half the encountered frequency. In some tests in which capsize was expected, it did not occur during the steady run but occurred as the carriage was decelerated. This behaviour was consistent with some of the stationary tests where it was found that the model more readily responded to reducing wave frequency to the critical condition rather than an approach increasing frequency.

The rate gyro revealed a distinct second harmonic content in the velocity record. Consideration of the solution of a Mathieu equation of the form

$$\ddot{\phi} = -a(1 - \delta \sin \omega_e t) \phi$$

indicates that the roll acceleration can have a significant harmonic content the higher terms of which are attenuated in the velocity and heavily suppressed in the displacement. It was observed that in bringing the model to the critical condition the roll rate trace showed a small roll velocity with a shifted phase harmonic but at critical condition not only did the amplitude increase but the harmonic shifted to a symmetric phase pattern Figure 2.

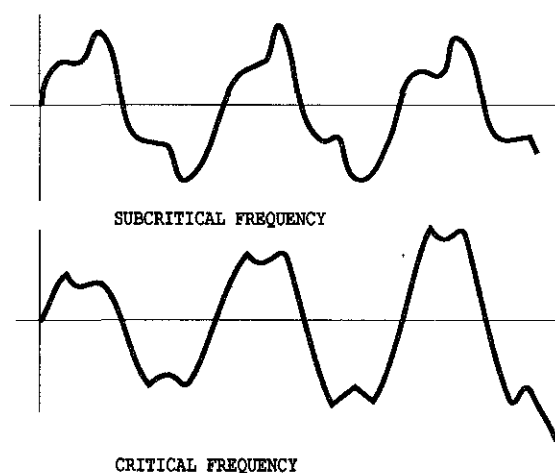


FIGURE 2

Tests were conducted in which the amplitude of the waves were changed. It was found that severe rolling and capsize centred on the frequency ratio $\frac{\omega\phi}{\omega_e} = \frac{1}{2}$ with heavy rolling or capsize occurring at each of the wave heights tested. However with the higher waves, rolling and capsize occurred over a range of frequency $.94 < \left(\frac{2\omega\phi}{\omega_e}\right)^2 < 1.15$. From the spot tests conducted it would appear that as the wave amplitude is increased so the frequency band width widens within which violent rolling or capsize can occur. This accords with the widening of the unstable zone obtained by the solution of Mathieu's equation.

As a further investigation into the physical nature of the behaviour, a simple set of tests were conducted to measure the roll righting moment of the model in waves. A calm water "inclining" experiment was conducted, for two initial fixed angles of heel; waves were run past the model gradually increasing the frequency towards the critical condition. It was found that the heel moment showed fluctuations in load above and below the static condition and that as the frequency increased the amplitude of the fluctuation increased. Close to critical frequency the model started to behave violently in roll and readings could not be taken.

The variations were oscillatory but did not appear to be sinusoidal. Rather, there was a very rapid increase to peak +ve value associated with the instant that the bow pitched into the oncoming wave slope followed by a longer slower half cycle of reduced force as the wave crest moved along the hull. There was a suggestion of a double hump in the negative part of the cycle. This indicates that the forcing function has a more complex source than simply that of wave profile on the buoyancy distribution.

4. CONCLUSIONS

The original intention of these experiments, which was to obtain a repeatable controlled capsize mechanism, has been successful. The experiments were repeated many times by a number of student experimenters.

The conditions under which the models capsized or developed very large rolling were very finely tuned

though in larger waves the band width of frequency widened. For capsizing to occur the model has to be in regular waves about the length of the hull and with an encounter frequency of twice the natural roll frequency. This can occur either with the hull stationary, when the natural roll frequency must be twice the frequency of waves the length of the hull, or for a higher roll frequency i.e. stiffer ship with the hull moving forwards at a speed to bring encounter frequency into the 2:1 ratio with roll frequency.

At first sight the mechanism observed could be readily explained by the method suggested by Paulling. The wave profile causes a change in righting moment and this gives rise to a parametric resonance as characterised by a Mathieu equation. A wave about the length of the hull would cause the greatest variation and hence the most critical condition. In Figure 3 the inferred trajectory of the model is plotted for roll angle against computed righting moment for each wave position.

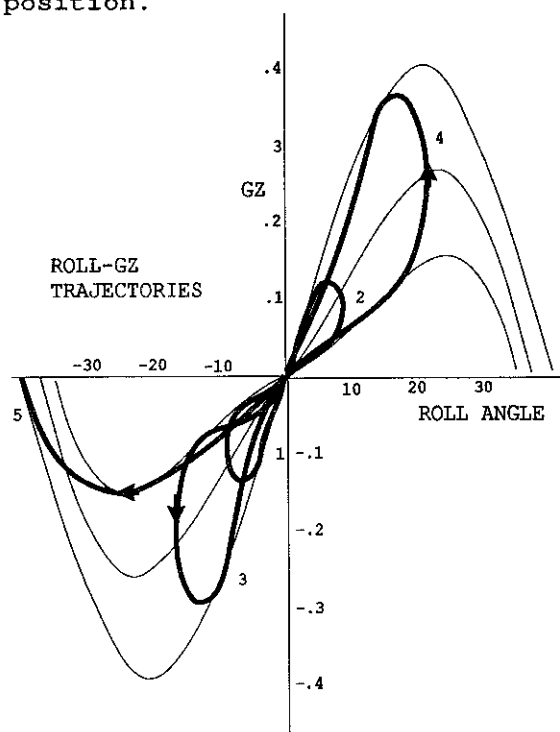


FIGURE 3

This shows a figure of eight pattern with the model rolling outwards on the low GZ curve and returning on the high GZ curve. Thus each loop represents the enclosure of a positive roll energy which, unless dissipated, contributes to a larger roll to the opposite side so that eventually the hull reaches the lower limit of stability and capsizes. Note also that this trajectory also requires a phase synchronism of roll and waves which was observed in the roll rate traces. The simple heeling force tests also support this reasoning in that the measured fluctuations agree quite well with the calculated righting moments variations in waves.

However, observations suggest that the physical process is not quite as simple as the above, though that is probably part of the action. It was noted that capsizing occurred when the pitching was synchronous with the waves so that the bow pitched down into the slope of the oncoming wave at the instant of maximum roll. Dynamic effects may be considered, the most obvious being the impact of the flared bow at an angle of heel into the face of the wave giving rise to an impulsive righting moment.

The pitch response of the ship is usually greatest in waves about the length of the ship and this is consistent with the experiments. The observed characteristic of the roll moment measurements is also consistent with the impulsive moment due to the bow plunging.

A reason for doubting that GM variation due to wave profile is solely responsible for the rolling motion is given in the different

forms tested. The wide beam model showed a significant variation of GZ in waves. This could largely account for the behaviour of this model and its rapid capsize. The narrow beam model however showed much less GZ variation in waves nevertheless it built up very large roll angles with only its much larger angle of vanishing stability saving it from capsize. The modified narrow beam model with flare had very little variation in calculated GZ in waves but it still developed 20° of roll over which angle the difference in GZ was barely discernible. This suggests that there are actions at work other than the direct "static" effect of waves on the righting moment.

Another factor to be considered is the triggering of the motion in some experiments either by a small external disturbance or by decelerating the model to the critical encounter frequency.

The experiments conducted on the models are not fully representative of a ship at sea. Nevertheless it is considered that the experiments reveal a possible circumstance in which an intact ship could rapidly develop severe rolling and capsize.

A number of physical parameters were varied during the experiments and some conclusions can be drawn.

(a) Both a short beamy hull and a long narrow hull revealed the same induced roll characteristics. This encompasses a wide range of practical monohull displacement forms with the possible exception of very high block coefficient forms. It is therefore reasoned that this behaviour could occur on any

conventional ship form.

(b) The modification to the model by addition of above water flare gave a significant reduction in roll angle.

(c) Additional damping increased the number of cycles of roll necessary to reach capsize angle. Thus roll damping can reduce risk because the probability of ship encountering a long sequence of critical frequency waves is considerably less than a short sequence.

(d) A high angle of vanishing stability also increases the number of cycles to capsize and therefore for similar reasons to (c) would reduce the risk of this happening.

(e) The occurrence requires the combination of a natural roll period related to a wave encounter frequency and a wave length about ship length. It also requires a short continuous sequence of encounters. Whilst the probability of all these factors coming together should be low the possibility exists of some losses by this mechanism. It is consistent with a ship being in no apparent trouble and very rapidly capsizing.

Some further actions could be taken to reduce the risk. If the designed GM or loading condition ensures a high frequency of natural roll the ship would need to travel at high speed into the waves. This condition could be set so that either the ship does not have the power capability to proceed at this speed or it would not be driven into waves this fast.

The critical speed can be determined from length and roll period and captains could then avoid this speed. Also from the experiments it appears advisable that if a ship is caught in these circumstances and developing large roll angles then acceleration is the best first course of action. Slowing down appears more dangerous and use of the rudder to change heading could compound the problem due to the induced heel.

Acknowledgements

The author would like to draw attention to the efforts of the students who have enthusiastically contributed to the experiments reported.

He would also like to express his thanks to the UCL Laboratory Staff who have provided models, equipment and assistance.

References

1. Paulling, J.R., Oakley, and Wood, P.A. "Ship Capsizing in Heavy Seas: The Correlation of theory and Experiments". International Conference on Stability of Ships and Ocean Vehicles. University of Strathclyde, 1975.
2. Morrall, A. "The GAUL disaster: An investigation into the Loss of a Large Trawler". RINA Spring Meeting Paper No. 2, 1980.
3. Burcher, R.K. "Influence of Hull Shape on Transverse Stability". Naval Architecture, Vol. 3, 1980.
4. Price, W.G. "A Stability analysis of the Roll Motion of a Ship in an Irregular Seaway". International Shipbuilding Progress, Vol. 27, February 1980.
5. Blocki, W. Ship Safety in connection with Parametric Resonances of the Roll. International Shipbuilding Progress. Vol. 27, February 1980.
6. Mook, D., Marshall, L., Nayfeh, A. "Subharmonic and Superharmonic Resonances in the Pitch and Roll Modes of Ship Motions". J. Hydraulics, Vol. 8, No. 1, January 1974.

A GUIDELINE TO AVOID THE DANGEROUS SURF-RIDING

Makoto KAN

The surf-riding of a ship is examined by means of the free-running model tests, as well as the numerical simulations and phase plane analyses of the nonlinear equation of surging motion. It is clarified that the surf-riding occurs when the ship speed including the oscillatory surging component, after the decay of the transitional motion, reaches the phase velocity of the wave. The speed range of the ship is divided into the three parts concerning the occurrence of the surf-riding. Below the first critical speed the ship never makes the surf-riding but makes always the periodic surging motion. Over the second critical speed, the ship inevitably falls into the surf-riding condition. Between the two critical speed, the ship makes either periodic surging or surf-riding motion depending on the initial conditions. As a practical guideline to avoid the dangerous surf-riding, a simple method to obtain the critical ship speed and the critical wave height is proposed. By the analogy with other phenomenon such as Josephson effect in the superconductivity, the surf-riding is suggested to be one of the fundamental nonlinear phenomenon in the physical science.

INTRODUCTION

The surf-riding of a ship is considered as a cause of the occurrence of a broaching-to phenomenon which may lead to capsizing of the ship [1],[2]. The phenomenon of the surf-riding was first observed experimentally by Du Cane & Goodrich [3] and discussed earlier by Grim [4], later by Boese [5], and recently again by Grim [6]. However, the mechanism of such phenomenon does not seem to be clarified in a complete manner. The author conducted a series of experiments using the free-running model of a stern trawler in the regular following waves [7],[8] and discussed about the mechanism by the numerical simulations [9] and the phase plane analyses [10]. An analogy with the Josephson effect was also discussed in some detail [11]. The present report is the revised collection of the

author's previous papers and contains some extensions.

EXPERIMENTAL TESTS

Model tests were carried out in the 80m square tank of Ship Research Institute by using the radio-controlled free-running model of the stern trawler. The body plan and principal particulars of the model are shown in Fig.1 and Table 1. The model was driven with the preset number of propeller revolution and was controlled by the manual steering to run straight in the following regular waves with the various wave length and wave height as shown in Table 2. The surging acceleration was measured by the gyro-accelerometer and the position of the model was measured every one second by the underwater supersonic device, from which the surging velocity was obtained.

Examples of the variation of the model speed is shown in Fig.2. A sudden

Ship Research Institute,
Ministry of Transport
6-38-1 Shinkawa, Mitaka, Tokyo 181, JAPAN

change occurs at 18rps, below which the large surging motions are observed. This shows that the motion changes from the large surging to the surf-riding at that point. In surf-riding condition the model speed agrees with the wave velocity referred as nonlinear, which is modified by the amplitude dispersion effect. This figure also suggests that the surf-riding occurs when the ship speed including the oscillatory surging component reaches the phase velocity of the wave. The model sometimes makes another kind of periodic surging motion even in the surf-riding condition. The surging amplitude and period are shown in Fig.3 and Fig.4. Calculations are carried out by the ordinary linear theory. Figures such as Fig.2 to Fig.4 for all tested cases in Table 2 are published in the paper [8].

THEORETICAL APPROACHES

Equation of surging motion

Using the coordinate system o-xyz fixed in the space, the wave elevation ζ is defined as

$$\zeta = -\zeta_a \cos(kx - \omega t) \quad (1)$$

where ζ_a is a wave amplitude, k is a wave number ($=2\pi/\lambda$, λ is a wave length), and ω is an angular frequency of wave. If the surging displacement of a symmetric ship is denoted by ξ in the coordinate system o'- $\xi\eta\zeta$ traveling with the ship speed in still water V , the Froude-Krilov's exciting force F and the equation of motion for the surging are represented by

$$F = F_a \sin(\omega_0 t - k\xi) \quad (2)$$

$$d^2\xi/dt^2 + A d\xi/dt = E \sin(\omega_0 t - k\xi) \quad (3)$$

where $A = \{dR(v_0)/dv - (1-\tau)dT(v_0)/dv\}/M$, $E = F_a/M$, $\omega_0 = \omega(1-V/C)$, T is the thrust, R is the resistance, τ is the thrust deduction factor, M is the mass of a ship, and v_0 may be taken as the still water speed V under consideration or the wave velocity C [9]. Further, if the surging displacement is denoted by ξ' in the third coordinate

system o''- $\xi'\eta'\zeta'$ traveling with the wave velocity C , then the following relation is obvious from Fig.5

$$\xi = \xi' + (C-V)t \quad (4)$$

Substituting eq. (4) into eqs. (2) and (3), the following expressions are obtained

$$F = -F_a \sin k\xi' \quad (5)$$

$$d^2\xi'/dt^2 + A d\xi'/dt + E \sin k\xi' = A(V-C) \quad (6)$$

An autonomous form of eq. (6) is preferable for dealing with the surf-riding motion.

There exist two static equilibrium positions satisfying the relation $E \sin k\xi' = A(V-C)$. One is the position of stable surf-riding, which exists only in the region between $-\lambda/4$ and $\lambda/4$ from the wave trough. Another is the unstable position outside this region [9].

Numerical simulation

Some examples of the numerical simulation are shown in Fig.6 (a) and (b). The only slight difference of the initial condition leads to the different final motion, namely surf-riding or periodic surging. Fig.7 is the result of the numerical search on the range of the initial position of the model which leads to the surf-riding. More examples of the simulation are published in the paper [9]. The validity of the simulation is confirmed by means of the comparison with the experiment as shown in Fig.8, which shows the typical process of the translation to the surf-riding from the periodic motion.

Phase plane analysis

In order to clarify the total situation of the nonlinear phenomenon such as the surf-riding, it is not sufficient to repeat the numerical simulations for the various initial conditions. It is necessary to use the common method of phase plane analysis for the nonlinear ordinary differential equation which expresses the surf-riding motion. Three examples of the phase plane analysis are shown in Fig.9 (a) to (c). In case of the low advance speed, Fig.9(a) shows that any initial condition leads to the periodic surging passed by the wave,

because every trajectory is attracted to the dense wavy line, which is termed a periodic attractor. In case of the medium advance speed, Fig.9(b) shows that the phase plane is divided into two domains of attraction, which means two stable solutions. The initial condition in the domain surrounded by the dotted line, which is termed a separatrix, leads to the surf-riding, because every trajectory in that domain concentrates on a stable equilibrium position, which is termed a point attractor. On the other hand, the initial condition in the outside of that domain leads to the periodic surging. This is the explanation of the different behavior due to the slight difference of the initial condition as exemplified in Fig.6. The separatrix can be drawn as the trajectories starting from the point very close to the unstable equilibrium position, which is termed a saddle point, by the time reversing simulation. In case of the higher advance speed, Fig.9(c) shows that any initial condition leads to the surf-riding. The separatrix in this case does not mean the separating line between two domains of attraction, but the separating line between the waves on which the ship falls into the surf-riding condition.

Critical speed

As presumed from the above results, the advance speed of the ship in still water is divided into three regions corresponding to the occurrence of surf-riding. The first critical speed V_{lcr} is defined as $C-E/A$. Below the speed V_{lcr} (region I), the surf-riding never occurs, because the statical equilibrium condition can not be satisfied in the equation of surging motion (6). The second critical speed V_1 is defined such that the ship inevitably falls into the surf-riding for any initial conditions beyond that speed (region III). At the speed range between the two critical speed V_{lcr} and V_1 (region II), the ship makes the periodic surging motion or surf-riding, depending on the initial condition.

The critical speed V_1 can be obtained only by the numerical trial and error method. Fig.10 (a) and (b) show such examples of the critical speed versus wave height. Though the region II seems to disappear in case of the long wave length as shown in Fig.10(b), it will appear in an unrealistic high wave. A rather simple method to obtain the second critical speed V_1 is presented as follows. The equation of surging motion (6) is converted to

$$d^2\eta/ds^2 + \beta d\eta/ds + \sin\eta = \alpha \quad (7)$$

where $\eta = k\xi$, $t = s/\sqrt{Ek}$, $\alpha = A(V-C)/E$ and $\beta = A/\sqrt{Ek}$. Once the critical value α_1 , for a given value of β in eq. (7), is obtained by the numerical trial and error, V_1 for any case can be obtained easily. Fig.11 is the result. For $\beta > 1.2$ the region II disappears, which corresponds to the case of Fig.10(b). The condition to determine α_1 is that the periodic attractor of eq. (7) coincides with the separatrix loop. Using this condition for small value of β , α_1 is expressed as $\alpha_1 = (-4/\pi)/\beta$. This expression is valid only for $\beta < 0.2$. Another expression, $\alpha_1 = (-4/\pi)/\tanh\beta$, which is obtained only by fitting, is valid in the wide range of β as shown in Fig.11.

Pull out speed

Surf-riding has two contrasting phases. One is the dangerous phase as a trigger of broaching-to phenomenon, and another is an advantageous phase as a possibility to keep the ship speed higher than the still water speed. For both cases it is desirable to know the critical speed, at which the ship can escape from the surf-riding or the ship can keep the surf-riding. Escape from the surf-riding can be realized either by decreasing the ship speed lower than V_{lcr} ($=C-E/A$) or increasing the ship speed higher than V_{ucr} ($=C+E/A$). However, if the ship speed is changed not gradually but suddenly, the critical speed V_{lp} is in general higher than V_{lcr} , and the upper critical speed V_{up} is lower than V_{ucr} . These critical escape speed is termed here a pull out speed following the analogy with

a pull out torque in the synchronous motor referred later. V_{lp} and V_{up} can be obtained again by means of the numerical trial and error method, using the corresponding initial condition. Fig.12 is an example. More general chart is also obtained as Fig.13, where $\alpha_p = A(V_p - C)/E$, with $V_p = V_{lp}$ or V_{up} . The ship speed here should be read as that in still water.

Analogy with other physical phenomena

There are several analogous phenomena in other physical problems such as a driven damped pendulum, a synchronous motor and Josephson effect in the superconductivity as illustrated in Fig.14. All these problems can be formulated by the same equation as eq. (7). The surf-riding corresponds to the equilibrium condition of the pendulum, the synchronous motion of the synchronous motor and the dc-effect of the Josephson junction, while the periodic surging motion corresponds to the rotating motion of the pendulum, the non-synchronous motion of the synchronous motor and the ac-effect of the Josephson junction. These suggest that the surf-riding is one of the fundamental nonlinear phenomena in the physical science [10],[11].

Guideline to avoid surf-riding

It has been clarified experimentally and analytically that the surf-riding occurs when the ship speed reaches the wave speed. From the practical point of view, this condition can be used to obtain the guideline to avoid the surf-riding.

Critical wave height: If an amplitude response of surging motion, in an ordinary sense of the linear equation, is denoted by ξ_1 ($=x_1/\zeta_a$, x_1 is an amplitude of surging), the above condition is written as

$$C = V + \omega_o x_1 = V + \omega_o \xi_1 \zeta_a \quad (8)$$

Using eq. (8), the relation $\omega_o = \omega(1 - V/C)$ and $C = \omega\lambda/(2\pi)$, the following expression for the critical wave height h_c is obtained

$$h_c/\lambda = 1/(\pi\xi_1) \quad (9)$$

This expression is valid for both deep and shallow water. In case of the quartering wave with an encounter angle χ , this expression becomes

$$h_c/\lambda = 1/(\pi\xi_1 \cos\chi) \quad (10)$$

Fig.15 is an example of the critical wave height calculated by eq. (9), neglecting added mass and damping, and assuming the Froude-Krilov's hypothesis in an ordinary linear equation of surging motion.

Critical speed: Amplitude response ξ_1 is expressed as

$$\xi_1 = F_a / (M\omega_o^2 \zeta_a) \quad (11)$$

By using eqs. (9) and (11), and the relation $\omega_o = \omega(1 - V/C)$, the critical speed V_c is obtained as

$$V_c = C[1 - \{F_a/(Mg)\}^{1/2}] \quad (12)$$

In case of the quartering wave, this relation becomes

$$V_c \cos\chi = C[1 - \{F_a \cos\chi/(Mg)\}^{1/2}] \quad (13)$$

Fig.16 is examples of the critical speed V_c , where experimental results is also plotted. Since the estimation is in safer side about 10% than experiments, it can be used as a guideline for the safe operation. In case of the shallow water of depth H , eq. (13) is written as

$$V_c \cos\chi = C[1 - \{F_a \cos\chi/(Mg \tanh kH)\}^{1/2}] \quad (14)$$

Examples are shown in Fig.17, which indicate that the surf-riding is easier to occur in shallow water, even at the lower advance speed as pointed out by Grim [4].

CONCLUSIONS

The phenomenon of surf-riding of a ship running in a following regular wave is clarified by means of the model experiments as well as the analytical considerations and also the numerical time simulation and phase plane analysis. Applying the confirmed condition for the occurrence of the surf-riding, a practical guideline to avoid the surf-riding is proposed.

REFERENCES

1. Motora, S., Fujino, M. and Fuwa, T., On the Mechanism of Broaching-to Phenomena. Second International Conference on Stability of Ships and Ocean Vehicles, 1982, pp.535-550.
2. Renilson, M.R., An investigation into the factors affecting the likelihood of broaching-to in following seas. Second International Conference on Stability of Ships and Ocean Vehicles, 1982, pp.551-564.
3. Du Cane, P. and Goodrich, G.J., The following seas, broaching and surging. RINA, Vol.104, No.2, 1962, pp.109-140.
4. Grim, O., Das Schiff in von achtern anlaufender See. JSTG, Vol.45, 1951, pp.264-287.
5. Boese, P., Steuern eines Schiffes im schweren achterlichen Seegang. JSTG, Vol.63, 1969, pp.337-355.
6. Grim, O., Das Schiff in von achtern kommendem Seegang. Schiffstechnik, Vol.30, 1983, pp.84-94.
7. Kan, M., Saruta, T., Yasuno, M., Yamakoshi, Y., and Suzuki, S., Surging of large amplitude and surf-riding of ships in following seas. Journal of the Naval Architects of Japan, Vol.162, 1987, pp.161-171.
8. Kan, M., Saruta, T., Yasuno, M., Yamakoshi, Y., and Suzuki, S., Model experiments on surf-riding of a fishing boat in following waves. Report of Ship Research Institute, Vol.25, No.3, 1988, pp.25-54.
9. Kan, M., Saruta, T., Yasuno, M., Surging of large amplitude and surf-riding of ships in following seas (Part 2, Numerical simulation). Journal of the Naval Architects of Japan, Vol.165, 1989, pp.111-121.
10. Kan, M., Surging of large amplitude and surf-riding of ships in following seas (Part 3, Phase plane analysis). Journal of the Naval Architects of Japan, Vol.166, 1989, pp.267-276.
11. Kan, M., On the analogy between surf-riding of a ship and Josephson effects in superconductivity. 54th Lecture Meeting of Ship Research Institute, 1989, pp.126-131.

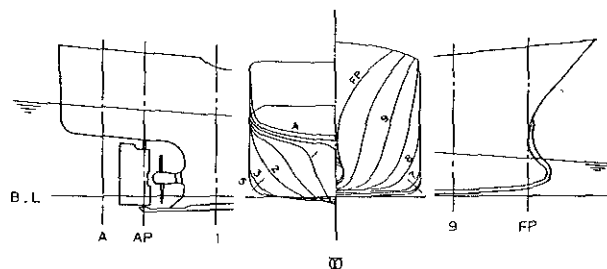


Fig.1 Body plan and side view

Table 1 Principal Particulars

Item	1/12 Model
Displacement Δ	266.0 kg
Length L_{pp}	2.548 m
Breadth B	0.615 m
Mean draft d_m	0.218 m
Trim by stern	0.187 m
Propeller dia.	0.186 m
Pitch Ratio	1.055

Table 2 Parameter of experiment

λ/L_{pp}	h/λ	n (rps)	N
0.500	1/40	5-20	14
0.625	1/20	5-21	24
	1/10	10-15	17
0.750	1/20	5-21	16
1.000	1/40	5-21	30
	1/20	5-21.5	29
1.250	1/40	5-21.5	15
	1/20	5-21	15
1.500	1/40	5-21.5	28
	1/20	5-21.5	25
	1/10	13-21	9
1.750	1/40	5-21.5	11
2.000	1/40	5-21	11
	1/20	5-21.5	21
2.500	1/40	5-21	9
3.000	1/40	5-21	9

n : number of prop. revolution
 N : number of runs

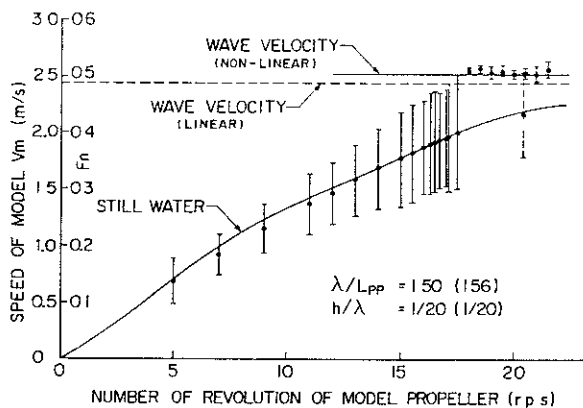


Fig.2 Variation of model speed ($\lambda/L=1.5$)

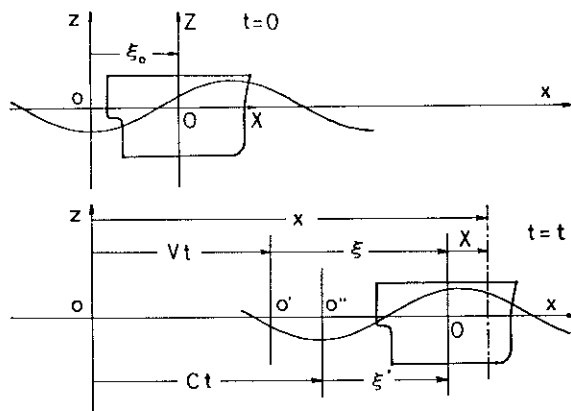


Fig.5 Coordinate system

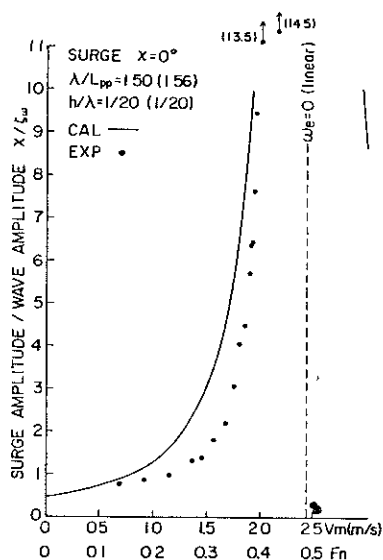


Fig.3 Surging amplitude ($\lambda/L=1.5$)

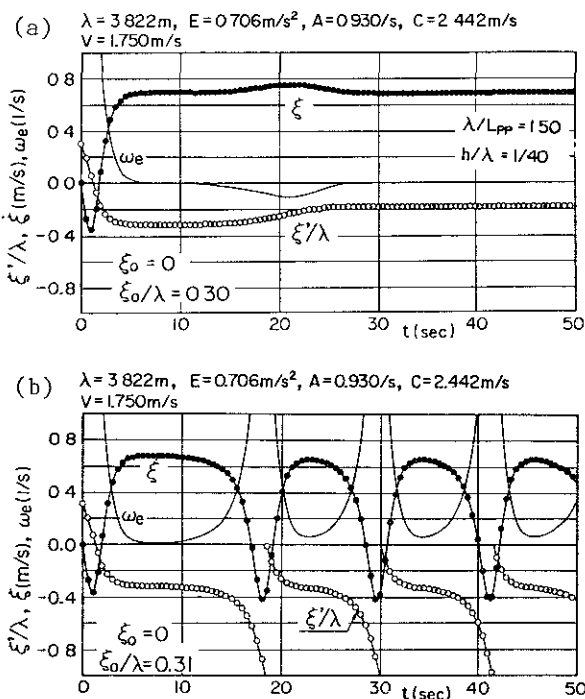


Fig.6 Examples of simulation, (a) surf-riding and (b) periodic surging

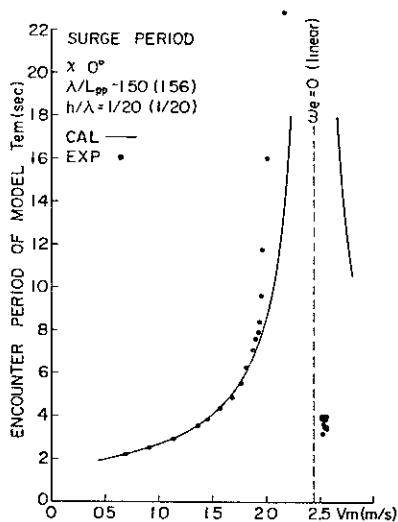


Fig.4 Surging period ($\lambda/L=1.5$)

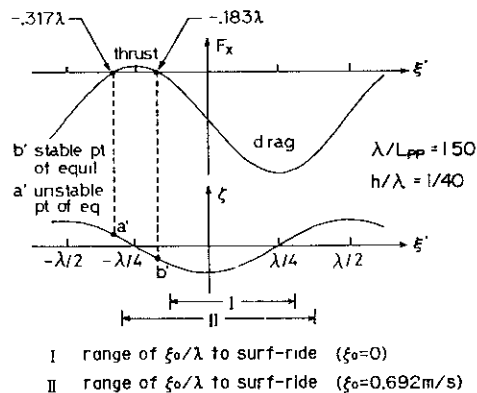


Fig.7 Initial condition to surf-riding

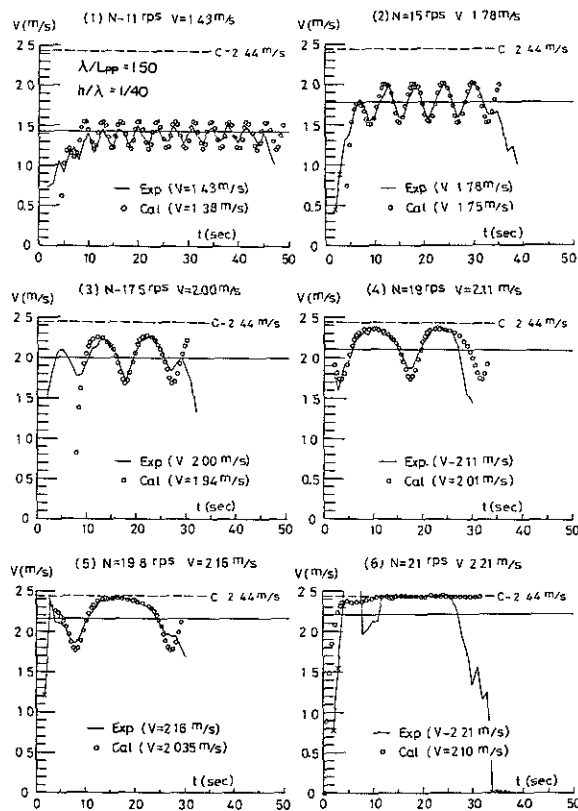


Fig.8 Comparison of simulation and experiment

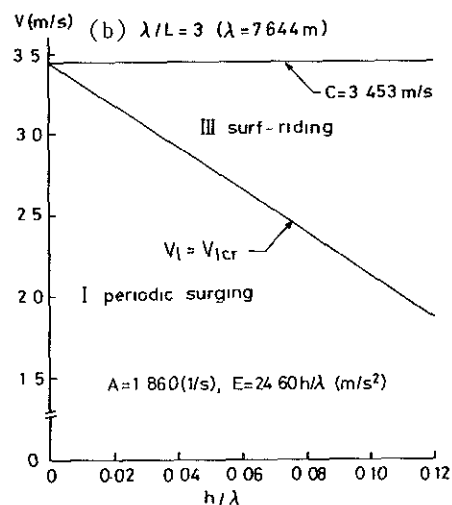
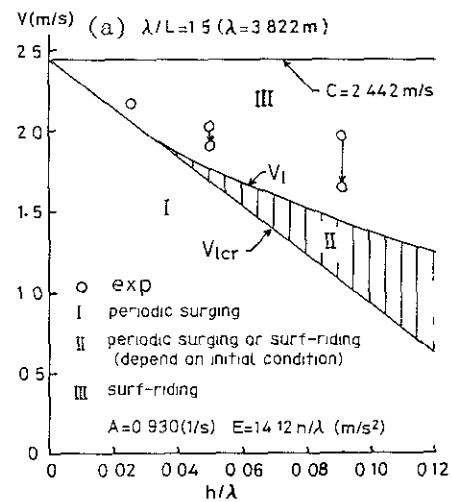


Fig.10 Critical speed, (a) $\lambda/L=1.5$ and (b) $\lambda/L=3$

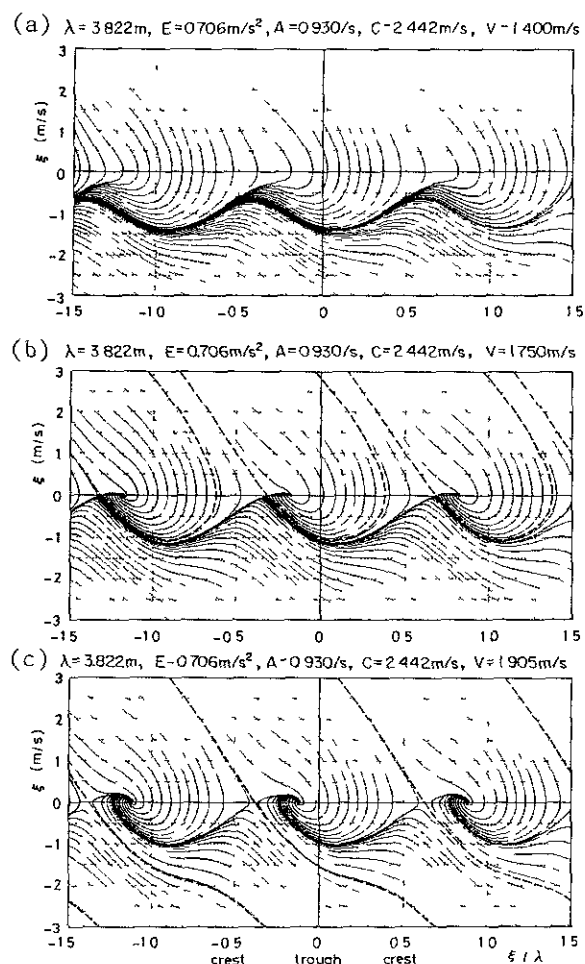


Fig.9 Phase plane portraits, (a) $V < V_{Icr}$
(b) $V_{Icr} < V < V_I$ and (c) $V_I < V$

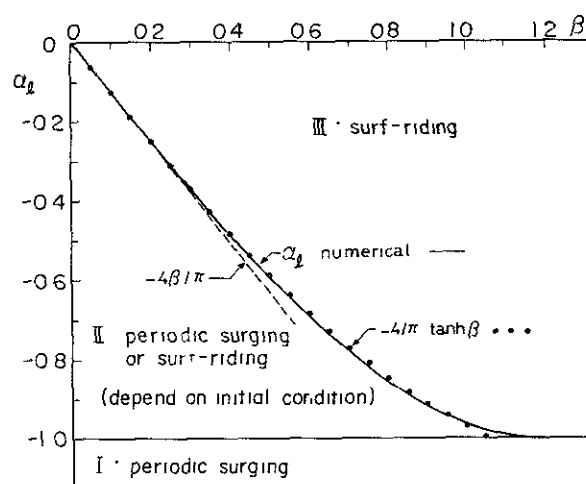


Fig.11 Chart of $\alpha_1 - \beta$

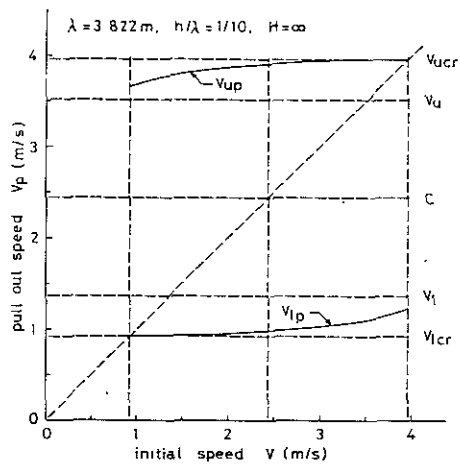


Fig.12 Pull out speed ($\lambda/L=1.5$, $h/\lambda=1/10$)

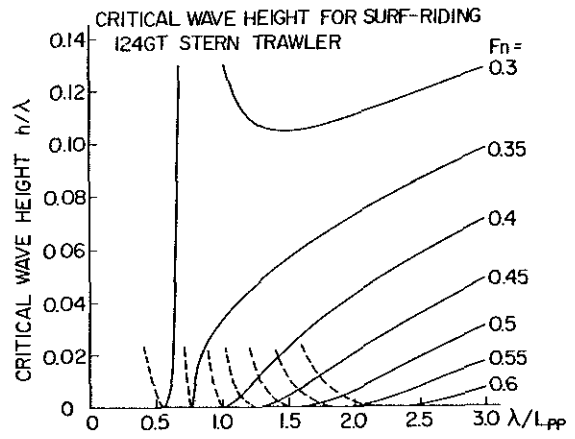


Fig.15 Guideline of critical wave height

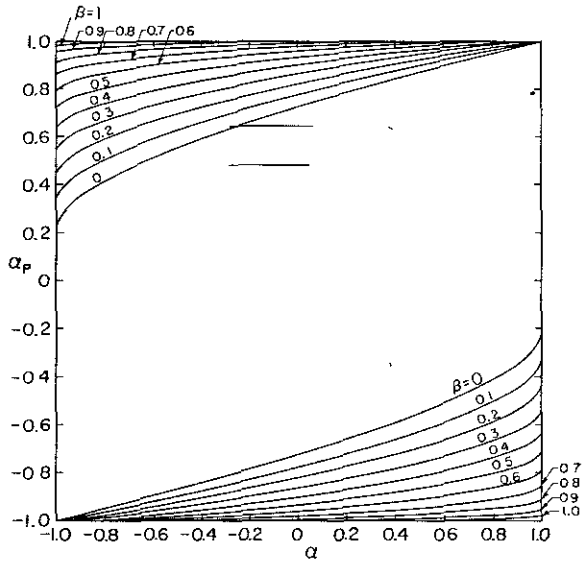


Fig.13 Chart of $\alpha_p - \alpha$ with parameter β

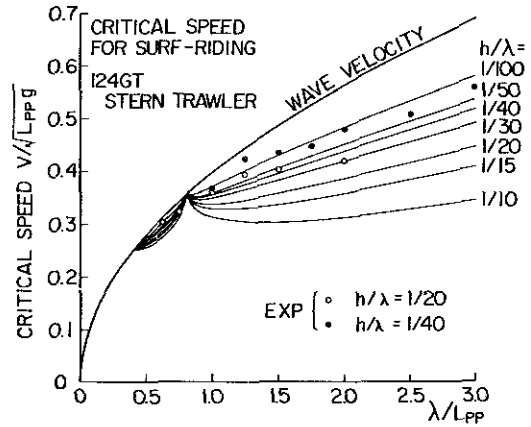


Fig.16 Guideline of critical speed

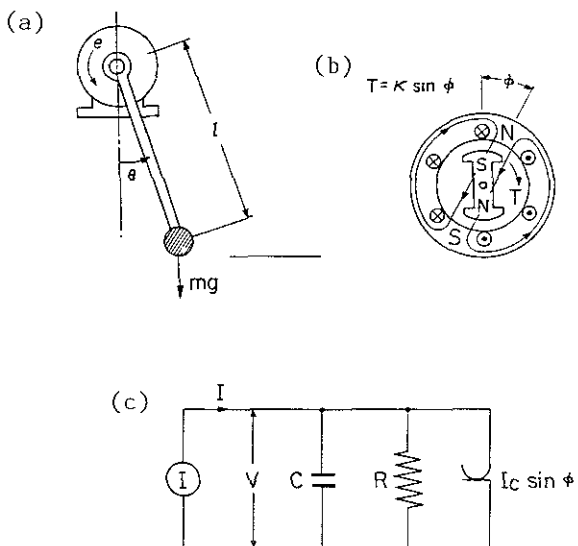


Fig.14 Analogous phenomena, (a) driven damped pendulum, (b) synchronous motor and (c) Josephson junction

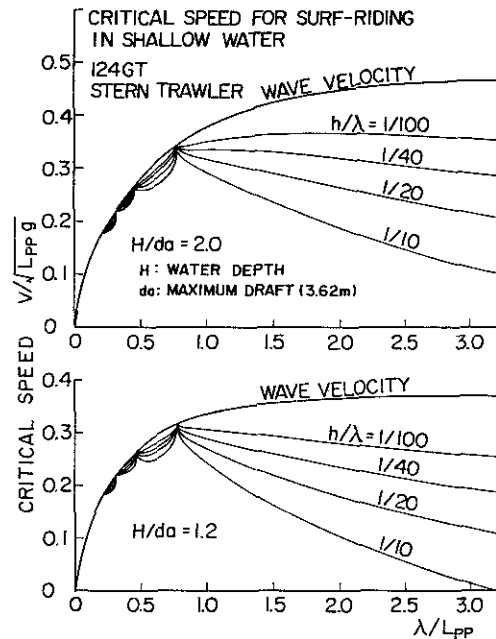


Fig.17 Critical speed in shallow water

STABILITY AND ROLLING OF A SHIP WITH SHIFTING CARGO

1) 1)
By Remez Yu. and Shestopal V.

Abstract

Investigation of stability and rolling of a ship with bulk cargo has been accomplished under the supposition that the internal friction angle of bulk media is a random value submitted to normal distribution law.

At calculation of additional heeling moment due to displacement of cargo one uses the hypothesis that the surface of cargo remains flat and the angle of its inclination to the horizon does not exceed of angle of internal friction (angle of repose).

Characteristics of rolling in rough seas have been found by methods of statistic linearization and multidimensional Markovian processes taking into account action of wind and additional moment due to cargo displacement.

Estimation of probability of heavy loose bulk cargo caving has been accomplished by methods of the theory of random processes overshoots.

to investigate the stability and motions of a ship with shifting cargo one can apply the methods of statics and dynamics of systems with the random parameters.

1. Introduction

The seaborne bulk cargoes may be divided into two categories in the dependence of the degree of mobility and character of displacement. The first category includes a dry bulk cargo with small particles (grain, sand, fine gravel) displacing gradually after the ship inclinations. While the heavy loose bulk cargo (coal, ore, broken stone) relates to the second category. Its displacement occurs suddenly as a caving of a mountain-mass in the hold.

Shifting or caving of cargo begins when the heel angle of the ship becomes approximately equal to that of an internal friction.

The seaborne cargo is under action of many random factors (waves impacts on the ship hull, motions, vibration, variations of humidity and temperature). Therefore the angle of repose is a stochastic quantity.

As it follows from systematic experiment on a free-hanged stand-pendulum [1], for such cargoes as wheat, maize, founding sand the repose angle submits to normal (Gaussian) distribution law. Thus,

2. The Curve of stability of a ship with bulk cargo

To build such a curve one must subtract the heel-moment due to cargo displacement from the ordinates of ordinary curve of stability. When the heel-angle θ exceeds the cargo repose-angle α , the additional moment due to displacement is determined by angle of shifting. Thus in any moment the equation $\theta = \beta \pm \alpha$ is true. Because α is a stochastic quantity, it may be characterized by numerical parameters: expectation m_α and variance D_α . Therefore, the moment δM due to displacement of cargo is a function on angle of shifting and random parameter α . For the estimation of expectation and variance of moment due to cargo shifting the following relations are obtained

$$M[\delta M] = M_0 \cos m_\alpha \mp \bar{M}_0 \sin m_\alpha, \quad (1)$$

$$D[\delta M] = (M_0 \sin m_\alpha \pm \bar{M}_0 \cos m_\alpha)^2 D_\alpha \quad (2)$$

Here M_0 depends on the shifting angle β

$$M_0 = p(y_\beta \cos \beta + z_\beta \sin \beta),$$

1) Professor,
Nikolaev Shipbuilding Institute,
9, av. Geroev Stalingrada,
Nikolaev, 327025, USSR

and \bar{M}_θ represents the integral with the variable upper limit

$$\bar{M}_\theta = \int_0^\theta M_\theta d\varphi.$$

The coordinates y_θ and z_θ of the cargo centre of gravity are determined by the geometry of the hold and are found using the ship lines drawing. There are analytical dependences of holds having rectangular and trapezoidal cross-sections [2].

As it is known ordinary (determinate) curve of stability calculated taking into account the displacement of cargo comprises the stable branches conforming to the rest of cargo and transient sections conforming to modes of cargo shifting.

The probabilistic curve of stability differs from ordinary one and contains families, each including three curves. One of them is a curve of expectation of moments. The latter takes into account the influence of cargo shifting similar to the determinate diagram. But the curves of standard deviation represent the values of moments which are not taken into consideration under deterministic approach while probability of their appearance may be significant.

3. Rolling of a ship with shifting cargo

The investigation is based on the nonlinear differential equation of rolling, offered by Lougovsky [3]. In this equation the moment $M_1(\theta, \alpha)$ due to cargo displacement is included as well:

$$\begin{aligned} \ddot{\theta} + 2\gamma_\theta \dot{\theta} + \omega_\theta^2 F(\theta) + M_1(\theta, \alpha) = \\ = \alpha_0 (\alpha_\theta^{(1)} + \alpha_\theta^{(2)} \theta^2) \sin \sigma t + \\ + \alpha_0 (\alpha_\theta^{(3)} + \alpha_\theta^{(5)} \theta^2) \cos \sigma t \end{aligned} \quad (3)$$

While statistic linearization of curve of stability, the nonlinear function $\omega_\theta^2 F(\theta)$ is substituted for function $\omega_\theta^2 \theta$, equivalent to nonlinear one in a statistic sense. Linearization coefficient is obtained from the condition of minimum of average square of difference between values of random functions on the outputs of nonlinear element and equivalent linear one. For the coefficient mentioned, the following formula has been obtained

$$\omega_\theta^2 = \omega_\theta^2 (a_1 + 3a_3 D_\theta + 15a_5 D_\theta^2) \quad (4)$$

where α_i are polynomial coefficients in approximation of the curve of stability.

Linearized relationship which is equivalent to the function $M_1(\theta, \alpha)$ has been obtained in the form of

$$u(\theta) = \varphi_0(\theta_1, \theta_2, \theta_3) + \sum_{i=1}^3 k_i \theta_i^0, \quad (5)$$

where φ_0 determinate function being the static characteristic of nonlinearity, k_i - static amplification factors, θ_i^0 - centred components of values θ , θ , α .

Calculation of φ_0 and k_i has been accomplished by the expansion of nonlinearity into a series on Tschebyshev Hermit polynomials

$$\begin{aligned} M_1(\theta, \alpha) = \varphi(\theta_1, \theta_2, \theta_3) = \\ = \sum \alpha_{k_1, k_2, k_3} H_{k_1}(\theta_1^0/\sigma_1) \times \\ \times H_{k_2}(\theta_2^0/\sigma_2) H_{k_3}(\theta_3^0/\sigma_3). \end{aligned} \quad (6)$$

Replacing nonlinear functions by linearized relationships into equation (3), performing Laplas transform for centred components of random functions, assuming $p = i\sigma$, where p - differentiation operator, separating the real part of the expression from the imaginary one, we obtain the amplitude frequency $\Phi^0(\sigma)$ and phase frequency characteristics of the system. Then using Khinchin-theorem one can find the variance of rolling angle of a ship with shifting cargo:

$$\begin{aligned} D_\theta = \int_0^\infty |\Phi^0(\sigma)|^2 S_\zeta(\sigma) d\sigma + \\ + M\{[k_3 \alpha^0 / (\omega_\theta^2 + k_1)]^2\} = \\ = \int_0^\infty (\alpha_{\sigma_1}^2 + \alpha_{\sigma_2}^2) 4D_\zeta \tilde{\alpha}^2 \sigma^4 (\sigma^2 + \tilde{\alpha}^2) \times \\ \times \{[(\omega_\theta^2 - \sigma^2 + k_1)^2 + (2\gamma_\theta + k_2)^2 \sigma^2] \times \\ \times \pi q^2 (\sigma^4 + 2a^2 \sigma^2 + b^4)\}^{-1} d\sigma + \\ + [k_3 / (\omega_\theta^2 + k_1)]^2 D_\alpha \end{aligned} \quad (7)$$

The second term in expression (7) takes into consideration the influence of probabilistic of repose angle on the amplitude of rolling.

One can represent the wind action by introduction of the function

$$F(t) = F_0 (1 - e^{-\lambda t}) \quad (8)$$

into equation of sway and the function

$$M(t) = F(t)(z_p - z_g) \quad (9)$$

into equation of roll.

Although such model does not take into account pulsation of the wind it is convenient for finding the remaining heel angle being an important parameter for the safety of navigation of a ship with shifting cargo.

The average value of heel angle after squall discontinuance has been found in the form of

$$m_\theta(t) = \exp(-\gamma_\theta t) [C_3 \cos \omega t + C_4 \sin \omega t] + \frac{m \exp(-\gamma_\eta t)}{\gamma_\eta^2 - 2\gamma_\eta \gamma_\theta + \omega_\epsilon^2} + \varphi_0(\theta, \dot{\theta}, \alpha) / F(p), \quad (10)$$

where C_3 and C_4 - constants of integration, $F(p)$ - polynomial operator corresponding to the left part of rolling equation.

4. Probability of loose bulk cargo caving due to lateral inclinations of a ship

The problem is solved in two stages. The first of them is dedicated to the investigation of stability of cargo mountain mass in a compartment inclined on the angle θ . While the form of cargo free surface is determined by the equation $Z=f(y)$, the equation of caving line $Z=f_0(y)$ is unknown beforehand. This line passes through the points $A(y_0, z_0)$ and $B(y_n, z_n)$, the position of which is unknown beforehand as well.

Let us estimate the degree of stability of some volume of cargo by the stability margin coefficient κ , which could be represented in the form of

$$k = \int_{y_0}^y F dy / \int_{y_0}^y \Phi dy, \quad (11)$$

where $F dy$ - retaining force acting along the caving line $Z=f_0(y)$ in limits of elementary compartment with base dS , Φdy - elementary shearing force. Coefficient κ is a functional of the form of caving line; thus the problem is reduced to finding the curve implementing the minimum of the functional mentioned.

In variational problem with immovable boundaries $A(y_0, z_0)$ and $B(y_n, z_n)$ to determine the caving line form one must find the integral of equation

$$(F - t\Phi)_z - \frac{d}{dy} (F - t\Phi)_z' = 0, \quad (12)$$

where t -parameter having the sense of κ .

Since the position of the points A and B is unknown two conditions of transversality for points $y=y_0$ and $y=y_n$ are added to ordinary boundary conditions $z(y_0)=z_0$ and $z(y_n)=z_n$:

$$[(F - t\Phi) + (\psi' - z')(F - t\Phi)_z']_{y=y_0} = 0 \quad (13)$$

$$[(F - t\Phi) + (\varphi' - z')(F - t\Phi)_z']_{y=y_n} = 0 \quad (14)$$

where $\varphi(y)$ and $\psi(y)$ - equations of the curves on which the ends of caving line $Z=f_0(y)$ are. We obtain the form of caving line and coefficient of stability margin as a result of integration.

At the second stage one determines the probability of caving of cargo mountain mass. This is determined as a probability of occurrence of rolling process ordinate which is equal to the utmost heel angle θ^* corresponding to $\kappa=1$. It means that cargo is in the state of the utmost equilibrium. The probability mentioned can be interpreted as a probability of function $\theta(t)$ overshoot over the given level θ^* . The approximate solution of the problem may be obtained proceeding on the assumption that the appearance of overshoot is a seldom event and its number during time T is submitted to the Poisson law of distribution.

Under these conditions we have obtained the probability that during time T , one overshoot (i.e. cargo caving) occurs in the form of

$$p = n e^{-n}, \quad (15)$$

where

$$n = T/2\pi \left\{ \ddot{K}_\theta(\tau) / K_\theta(\tau) \right\}_{\tau=\theta}^{1/2} \times \exp[(\theta^* - \bar{\theta}) / 2D_\theta].$$

The more exact evaluation may be given by the methods of Markovian processes theory.

It is possible to show that rolling of a ship with shifting cargo represents a component of six dimensional Markovian process. The probability of cargo caving is determined by integral

$$p(\tau) = \int_{-\infty}^{\infty} \dots \int_{-\theta^*}^{\theta^*} f(\tau, \theta_1, \dots, \theta_6) d\theta_1 \dots d\theta_6, \quad (16)$$

where restrictions are imposed only on one component of the process $\theta = \theta_1$.

The probability density f must satisfy the Fokker-Planck-Kolmogorov equation

$$\frac{\partial f(\vec{\theta}, t)}{\partial t} + \sum_{i=1}^6 \frac{\partial}{\partial \theta_i} \{ A_i \times f(\vec{\theta}, t) \} = \\ = \frac{1}{2} \sum_{i,j=1}^6 \frac{\partial^2}{\partial \theta_i \partial \theta_j} \{ B_{ij} f(\vec{\theta}, t) \} \quad (17)$$

where the values of functions A_i and B_{ij} are determined by the coefficients of the initial system of differential equations of motion.

The solution for $f(\vec{\theta}, t)$ has been found with the help of a characteristic function [4].

Assuming motions process to be a normal one and distribution of amplitudes submitting to the Rayleigh law, one can obtain the following expression for probability of event that rolling amplitude $\theta_{\text{м}}$ will exceed the angle θ^* of the cargo utmost equilibrium:

$$P(\theta_{\text{м}} > \theta^*) = \exp \left[-\frac{1}{2} \theta^{*2} / D_{\theta} \right].$$

5 - Nomenclature

- θ - heel angle;
- $\bar{\theta}$ - average rolling amplitude;
- $D_{\theta}, K_{\theta}(\tau)$ - variance and correlation function of rolling;
- α - angle of cargo repose;
- β - angle of shifting;
- m_{α}, D_{α} - expectation and variance of repose angle;
- P - weight of cargo and
- $\gamma_{\beta}, z_{\beta}$ coordinates of its centre of gravity;
- $\omega_{\theta}, \nu_{\theta}$ - natural frequency and damping coefficient of rolling;
- ν_{η} - damping coefficient of swaing;
- α_0 - angle of wave slope;
- \mathcal{X}_0^{ω} - characteristics of exciting moment;
- a, b - parameters of wave spectrum;
- z_p - z-coordinate of centre of sails;
- z_g - z-coordinate of centre of gravity;
- H_{k_i} - Tshebyshev-Hermit polynomials;
- k - coefficient of cargo stability margin.

6 - References

1. Koticov I. V. and Riabtshenko V. K. Experimental determination of stability of bulk cargoes under motions of a ship. J. Sudstroenie, 1974, 2, pp. 22-3 (in Russian).
2. Semenov-Tian-Shansky V.V., Statics and Dynamics of a ship. Sudstroenie, Leningrad 1973, pp. 139-52 (in-Russian).
3. Jougovsky V.V., Nonlinear problems of seakeeping of a ship. Sudstroenie, Leningrad, 1966, pp. 135-41 (in-Russian).
4. Sveshnikov A.A., Applied methods of theory of random functions. Nauka, Moscow, 1968, pp. 267-94 (in-Russian).

A STUDY OF STABILITY CRITERION FOR SHIPS IN IRREGULAR FOLLOWING SEAWAY

by D. L. Huang

ABSTRACT

Analytical study of the problem of stability of a ship in irregular following waves has been conducted by using the concept of motion stability theory and the approach of random differential equation. By assuming that the wave is a Gaussian stationary normal process, a formula for criterion of initial stability of a ship in irregular following waves has been derived from the rolling motion equation of ship in such environment. A numerical method for calculating the variance of the time dependent part of metacentric height of ship in waves is also presented. Two numerical examples as well as the comparison with published data are given.

1. INTRODUCTION

To ensure stability and safety of ships, especially for small ships, in several heavy sea condition is an important problem for designers. It is well known that small ships often lose their stability in following waves. For this reason, it is worthwhile to study the problem of ship stability in following sea. Linearized theory is considered to be not enough to obtain usable solution for the problem. However, it has been proved that for the study of loss of initial stability of a ship in following waves, linearized theory may be used to obtain a fundamental guidance. The purpose of present study is to establish criterion formula of ship stability in irregular following waves based on the linearized analyses.

The problem of ship stability in regular following waves has been studied intensively during the past 40 years by many authors with analytical and model experimental methods. The results of these research may be summarized as follows:

If the ratio of frequency of encounter

to the natural frequency of rolling motion of ship fall in certain value region, the ship will lose its stability and "parameter resonance" will appear. The rolling angle in such situation increases rapidly, and generally, the ship will finally capsize. [1]-[7]

During the same period, the study of ship stability in irregular following waves was considerably less than that in case of regular wave. In 1976, Vinjie, [8] had derived stability formulae for ships with weak rolling damping in irregular following waves. Numerical and experimental studies have been carried out by some authors later in order to extend the subject into irregular following sea. [9]-[10]

The main object of present study is the problem of rolling motion of ships in irregular following waves. It is assumed that the rolling motion of ship in such case can be described by a differential equation of second order with a random coefficient. A necessary condition for ensuring a stable solution of this equation is established and then can be considered as the formula of stability criterion for a

ship in irregular following sea. In addition, two numerical examples as well as the comparison with published data are provided.

2. THEORETICAL DERIVATIONS

The study of stability of a ship in following waves is essentially equivalent to that of stability of rolling motion of a ship in the same environment. Due to the random property of ships motion in irregular waves, the definition, as well as formula of stability of ship in irregular following waves is distinct from that in regular waves.

I. A brief review of problem of stability of ships in regular following waves.

A ship will be periodically located in hump and in trough when it is running in regular following waves. In such a case, the metacentric height can be expressed in the form of

$$\begin{aligned} h &= \bar{h}[1 + \beta \cos(\omega_e t)] \\ \bar{h} &= 1/2(h_h + h_t) \\ \beta &= \delta h / \bar{h}, \quad \delta h = 1/2(h_h - h_t) \end{aligned} \quad (1)$$

The rolling motion of the ship can be described with equation

$$\frac{d^2\theta}{dt^2} + 2k\omega_0 \frac{d\theta}{dt} + \omega_0^2[(1 - \beta \cos \omega_e t)] = 0 \quad (2)$$

The initial condition of motion is

$$\theta(t) = 0 \quad \text{if} \quad t = t_0$$

The stability of the ship in such case can be defined as:

The initial equilibrium position of a ship at $t = t_0$ is $\theta(t) = 0$, if the ship experienced a certain disturbance and heeled to an angle θ_0 , when $t > t_0$, the disturbance disappeared and then the rolling motion of the ship is the solution of equation (2). If $\theta(t)$ satisfies the condition

$$\lim_{t \rightarrow \infty} \theta(t) = 0$$

then the ship is considered to be stable in following waves, otherwise, it will be unstable.

Equation (2) can be rewritten into the form of a standard Mathieu equation by some variable transformation. Many authors have utilized this equation in the investigation of stability of ship in regular following waves. The results of their studies pointed out that variation of metacentric height δh and the ratio ω_0/ω_e are two important factors which affect ship stability. But ratio ω_0/ω_e is especially more important for problem. In some cases, the ship will be inherently unstable once the ω_0/ω_e falls into certain regions even if the magnitude of δh is small.

II. Stability of a ship in irregular following waves.

It is well known that a wave record measured at a certain point on sea surface, $\zeta(t)$, is a standard Gaussian random function and can be considered as a compound of a series of elemental sinusoidal waves possessing different amplitudes, frequencies and phases

$$\zeta(t) = \sum_{n=1}^{\infty} a_n \cos(\omega_n t + \varepsilon_n) \quad (3)$$

The variation of metacentric height of a ship in irregular following waves, $h(t)$, can be considered as the superposition of metacentric height of the ship running in these elemental waves. According to the central limit theorem, function $h(t)$ will also be a stationary Gaussian random function and can be represented as

$$\begin{aligned} h(t) &= \bar{h} + f(t) \\ E[h(t)] &= \bar{h}, \quad E[f(t)] = 0 \end{aligned} \quad (4)$$

Analogous to equ.(2), the equation of rolling motion of a ship in irregular following waves can be written

$$\frac{d^2\theta}{dt^2} + 2k\omega_0 \frac{d\theta}{dt} + [\omega_0^2 + \alpha(t)]\theta = 0 \quad (5)$$

$$\alpha(t) = \frac{M}{I_4 + \Delta I_4} f(t)$$

with initial condition

$$\theta(t) = 0 \quad \text{if } t = 0$$

The definition of stability of a ship in such case can be described as: The original position of equilibrium is $\theta=0$, if the ship inclined to θ_0 by a certain disturbance at t_0 , and when $t > t_0$ the disturbance disappeared, the rolling motion of the ship, $\theta(t)$, is the solution of equ.(5) and is also a random function. If $\theta(t)$ satisfies the condition

$$\lim_{t \rightarrow \infty} E[\theta(t)^2] = 0$$

then the initial position of equilibrium is asymptotically mean square stable.

In order to simplify the study, it is helpful to introduce a differential operator defined as

$$L_0(t) = \frac{d^2}{dt^2} + 2k\omega_0 \frac{d}{dt} + \omega_0^2 \quad (6)$$

Therefore, equ.(5) can be reformed to

$$L_0(t)\theta(t) + a(t)\theta(t) = 0 \quad (7)$$

and the solution of it can be written in the form

$$\theta(t) = -L_0^{-1}(t)a(t)\theta(t) + c_1\phi_1(t) + c_2\phi_2(t) \quad (8)$$

where, $L_0^{-1}(t)$ is the inverse of $L_0(t)$, $\phi_1(t)$ and $\phi_2(t)$ are two independent solutions of homongeneous equation $L_0(t)\theta(t)=0$, Coefficient C_1 and C_2 are constants which depend on initial condition of equ.(6). In present study we have

$$\phi_1(t) = e^{-\lambda_1 t}, \quad \phi_2(t) = e^{-\lambda_2 t}$$

$$\lambda_{1,2} = -i(k\omega_0 \pm i\omega_0 \sqrt{1 - k^2}) \quad (9)$$

From formula (8), the auto-correlation function of $\theta(t)$ will be

$$E[\theta(t_1)\theta(t_2)] = E[\phi(t_1)\phi(t_2)] - L_0^{-1}(t_2)E[a(t_2)\theta(t_2)\phi(t_1)]$$

$$\begin{aligned} & -L_0^{-1}(t_1)E[a(t_1)\theta(t_1)\phi(t_2)] \\ & + L_0^{-1}(t_1)L_0^{-1}(t_2)E[a(t_1)a(t_2)\theta(t_1)\theta(t_2)] \end{aligned} \quad (10)$$

By making use of following approximations [11]

$$\begin{aligned} E[a(t_1)\theta(t_1)\phi(t_2)] & \cong F[a(t_1)] \cdot E[\theta(t_1)\phi(t_2)] \\ F[a(t_2)\theta(t_2)\phi(t_1)] & \cong E[a(t_2)] \cdot E[\theta(t_2)\phi(t_1)] \\ E[a(t_1)a(t_2)\theta(t_1)\theta(t_2)] & \cong E[a(t_1)a(t_2)] \cdot E[\theta(t_1)\theta(t_2)] \end{aligned}$$

and the equalities

$$\begin{aligned} E[\phi(t_1)\phi(t_2)] & = 0 \\ E[a(t_1)] & = E[a(t_2)] = F[a(t)] = 0 \end{aligned}$$

the formula (10) can then be simplified into

$$\begin{aligned} E[\theta(t_1)\theta(t_2)] & = L_0^{-1}(t_1)L_0^{-1}(t_2) \cdot \\ & E[a(t_1)a(t_2)]E[\theta(t_1)\theta(t_2)] \end{aligned} \quad (11)$$

According to the definition of $L_0(t)$, equ.(11) will have the form

$$\begin{aligned} E[\theta(t_1)\theta(t_2)] & = \int_{-\infty}^{\infty} \int_{-\infty}^{\infty} E[a(s_1)a(s_2)] \cdot \\ & H(t_1-s_1)H(t_2-s_2)E[\theta(s_1)\theta(s_2)]ds_1ds_2 \end{aligned} \quad (12)$$

where, $H(t)$ is a weight function associated with $L_0(t)$ and can be represented in

$$H(t) = i(\lambda_1 - \lambda_2)^{-1}(e^{-\lambda_1 t} - e^{-\lambda_2 t}) \quad (13)$$

Due to that $a(t)$ is a stationary random function, the auto-correlation function of it is equal to its mean square deviation, i.e.

$$E[a(t_1)a(t_2)] = R_{aa}(t_2 - t_1)$$

Taking $t_1 = t_2 = t$, equ.(12) will be reduced into

$$E[\theta(t)^2] = R_{aa}(0) \int_{-\infty}^{\infty} H^2(t-s)E[\theta(s)^2]ds \quad (14)$$

Equation (14) can be solved by Fourier

transformation

$$E[\theta(t)^2] = \oint \frac{g(s)e^{-1st}ds}{1-R_{aa}(0)F[H(t)^2]} \quad (15)$$

where, $F[H(t)^2]$ is the Fourier-transform defined as

$$F[H(t)^2] = \int_{-\infty}^{\infty} H(t)^2 e^{ist} dt$$

and $g(s)$ is an analytic function in the analytic region of $F[H(t)^2]$.

It is obvious that the condition of convergence of $E[\theta(t)^2]$ to zero when $t \rightarrow \infty$ is that the roots of equation (16) must have negative real parts

$$1 - R_{aa}(0)F[H(t)^2] = 0 \quad (16)$$

Because the Fourier-Transformation of $H(t)^2$ has the form

$$F[H(t)^2] = \frac{-1}{\lambda_1 - \lambda_2} \left[\frac{1}{s + 2i\lambda_1} - \frac{2}{s + i(\lambda_1 + \lambda_2)} + \frac{1}{s + 2i\lambda_2} \right]$$

by substituting λ_1 and λ_2 into it, then equ.(16) can be reduced into

$$s^3 + 16k\omega_0 s^2 + 4(\omega_0^2 + 2k^2\omega_0^2)s + 8k^3\omega_0 - 2R_{aa}(0) = 0 \quad (17)$$

According to Criterion of Routh-Hurwitz, in order to obtain the negative real parts of the roots of (17), the coefficients of (17) must satisfy following inequalities:

$$8k\omega_0^3 - 2R_{aa}(0) > 0 \quad (18-1)$$

$$16k\omega_0 \cdot 4(\omega_0^2 + 2k^2\omega_0^2) > 8k\omega_0^3 - 2R_{aa}(0) \quad (18-2)$$

It can be found that if value of k and ω_0 satisfy (18-1), they will certainly also satisfy (18-2). Inequality (18-1) can be reformed into a more suitable form

$$k > \frac{R_{aa}(0)}{4\omega_0^3} \quad (19)$$

Inequality (19) is the condition to

ensure the initial position of equilibrium of the ship is asymptotically mean square stable. It means that, for given hull form and wave environment, the damping coefficient of the ship must be larger than a certain value in order to ensure the ship be stable in an irregular following seaway.

By the way, if the spectral density function of $a(t)$ is known and noted by $S_{aa}(\omega)$, then variance of $a(t)$ will be

$$R_{aa}(0) = \int_0^{\infty} S_{aa}(\omega) d\omega \quad (20)$$

III. Calculation of variation of metacentric height

A coordinate system moving with ship is adopted, x-axis is in the direction of moving of ship, z-axis is directed upward and across the center of gravity.

In order to simplify the numerical process, two hypotheses are applied here. The first is that the existence of ship hull don't change the pressure field of wave flow. It means that the diffraction effect of ship hull on incident wave is not taken into account in our study and therefore, only the Krylov-Froude force is calculated. The second is that the pitching motion of ship will not be considered. Based on these hypotheses it is only necessary to calculate the metacentric height of ship located in hump and trough.

For these reason, the sinusoidal wave surface can be represented by

$$\zeta(x) = A \cos(Kx + \varepsilon) \quad (21)$$

where $\varepsilon = 0^\circ$ or 180° for the ship located in hump and trough, respectively. The pressure of water can be calculated by

$$p = -\rho g z + \rho g A e^{Kz} \cos(Kx + \varepsilon) \quad (22)$$

It is assumed that the pressure at the depth of half draught, $T(x)/2$, of the section at x can be considered as the average pressure, \bar{p} , and be equal the product

$$p = \gamma_r(x) \cdot l(x)/2$$

$$\gamma_r(x) = \left[-\frac{2\lambda}{l(x)} e^{-K \cdot \gamma_r(x)/2} \cos(Kx + \varepsilon) + 1 \right] \gamma_0 \quad (23)$$

Let A_x and m_x is the area and moment respect to base line of section at x , respectively, then within the small length interval dx , the metacentric height of the section above base line can be evaluated by

$$Z_{mx} = \frac{1}{A_x} (m_x + \frac{2}{3} - y^2) \gamma_r(x)$$

The metacentric height of whole ship above base line is then

$$Z_m = \frac{1}{\nabla} \int_0^L (m_x + \frac{2}{3} - y^2) \gamma_r(x) dx \quad (24)$$

Therefore, the metacentric height of the ship will be

$$h = m - Z_m \quad (25)$$

It should be pointed out that the mean draught, as well as the relative position between ship and wave should be regulated in computation. A lot of computations had proved that there existed a linear relation between δh and $2A$, if $\sqrt{\lambda} < 0.08$, i. e.

$$\delta h(\lambda) = \beta(\lambda) \cdot 2A \quad \text{or} \quad \delta h(\omega) = \beta(\omega) \cdot 2A \quad (26)$$

In the case of irregular waves, the variation of metacentric height, $f(t)$, defined in equ.(5) can be represented in the form

$$f(t) = \sum_{n=1}^{\infty} \delta h(\omega_n) \cdot \cos(\omega_n t + \varepsilon_n) \\ = \sum_{n=1}^{\infty} 2a_n \cdot \beta(\omega_n) \cdot \cos(\omega_n t + \varepsilon_n) \quad (27)$$

where, $\delta h(\omega_n)$ is the variation of metacentric height in elemental wave of frequency ω_n and amplitude a_n . According to definition of wave spectrum of irregular wave, wave height $2a_n$ can be calculated by

$$2a_n = 2\sqrt{2 S_{\xi\xi}(\omega) \delta\omega}$$

where $S_{\xi\xi}(\omega)$ is wave spectrum. Then function $f(t)$ will have the form of

$$f(t) = \sum_{n=1}^{\infty} \sqrt{2 S_{\xi\xi}(\omega)} \delta\omega \beta(\omega_n) \cos(\omega_n t + \varepsilon_n)$$

The coefficient $a(t)$ in equ.(5) then can be represented as

$$a(t) = \sum_{n=1}^{\infty} \frac{2\beta(\omega_n)\omega_n^2}{h} \sqrt{2 S_{\xi\xi}(\omega) \delta\omega} \cos(\omega_n t + \varepsilon_n) \quad (28)$$

and the spectrum of it will be

$$S_{aa}(\omega) = 4 \left[\frac{\beta(\omega)\omega^2}{h} \right]^2 S_{\xi\xi}(\omega) \quad (29)$$

A computer program "STFW" for above process has been developed by the author.

3. NUMERICAL EXAMPLES

Numerical calculations for two ships, a cargo ship "American Challenger" and a fishing boat "L185-3", are carried out. The particulars of these ships are listed in following table

ship	American Challenger	L185-3
L (m)	161.23	26.00
B (m)	22.86	5.32
T (m)	9.07	1.84
h (m)	0.170	0.464
Z_m (m)	9.028	1.990
Δ (t)	19966.0	131.3
v (kn)	16.4	10.0

The variation of β of these ships with ratio of wave length to ship length are given in Fig.1

Due to lack of reliable experimental data in following sea for "American Challenger", A wave system, which has been applied in numerical simulation of the ship in following waves [9], is used as an in-

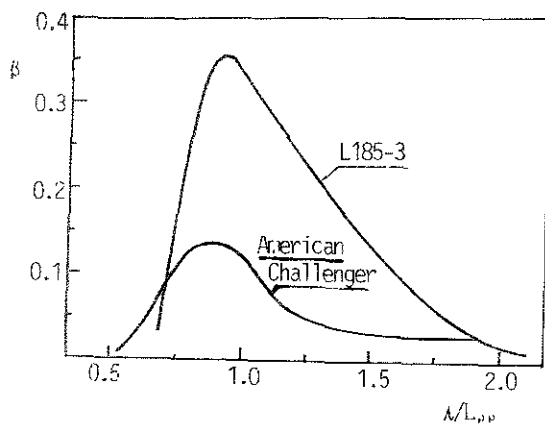


Fig.1 Variation of β with λ/L_{D0}

terim measure here

$$\zeta(t) = 1.5239(\cos 0.433t + \cos 0.601t) \quad (30)$$

The energy density of wave (30) is

$$S_{\zeta}(\omega) = 1.1611[\delta(0.601) + \delta(0.433)] \quad (31)$$

where $\delta(\omega)$ is Dirac-delta function.

In such waves, "American Challenger" has the variance of varying part of metacentric height $R_{aa}(0) = 0.001271$. The results of evaluation of natural frequency and linearized damping Coefficient of rolling motion are $\omega_0 = 0.1383 \text{ sec}^{-1}$ and $k_0 = 0.086$, respectively. Therefore, the ship is unstable. The numerical simulation study [9] (Fig.22, p.339) proved our conclusion.

In addition, computation of stability for "American Challenger" in irregular following waves has been carried out by using ITTC wave spectrum. If the significant wave height is taken to be 4.0m, it will have $R_{aa}(0)/4\omega_0^2 = 0.0369$. So the ship will be stable in such sea state.

Fishing boat L185-3 is a widely applied ship type in China in Bohai Bay and North Yellow Sea. According to crews opinion, the boats of this type occasionally show unstable phenomena in following sea. Stability computation for these boats in irregular following sea has been made for the case of significant wave height 2.0m by using ITTC wave spectrum. Computation result of $R_{aa}(0)/4\omega_0^2$ is 0.0211. The linearized damping coefficient of rolling motion

for these boats is 0.0684. So that it can be pointed out that L185-3 is stable in moderate following waves. The author would like to explain that it is easy to meet a group of wave with frequency of encounter equal to one-half of the natural frequency for small vessels in following sea, so the vessels will fall in the state of "parameter resonance" for a short period.

4. CONCLUSIONS

Based on the above analyses, the author would like to point out that:

1). Ships possessing normal damping value of rolling motion will generally not lose stability in irregular following sea of moderate wave height. However, they will easily lose their stability in regular following waves of equivalent wave height.

2). In order to ensure the stability of ship in following sea, it is necessary to arrange bilge keels of adequate area, which can provide the ships with satisfactory damping value of rolling motion.

3). The present study and relative results may be considered as a tool for stability inspection for ships, especially for small ships. It is expected that the problem of stability and rolling motion of large amplitude in irregular following sea should be attractive subjects in future study.

5. NOMENCLATURE

- A = wave amplitude
- a_n = amplitude of elemental wave
- $E[\dots]$ = mathematic expect, mean square, auto correlation function.
- $f(t)$ = time dependent part of metacentric height
- g = acceleration of gravity
- h = metacentric height
- h_n = metacentric height of ship in hump
- h_t = metacentric height of ship in trough
- I_{A+AA} = total inertia moment of rolling of ship

k = non-dimensional linearized damping coefficient of roll-motion
 K = wave number
 M = mass of ship
 p = water pressure
 $R_{aa}(t_2-t_1)$ = mean square deviation of $a(t)$
 $R_{aa}(0)$ = variance of $a(t)$
 $S_{aa}(\omega)$ = energy density spectrum of $a(t)$
 T = draught of ship
 V = ship speed
 y = half width of water line
 z_g = height of center of gravity
 γ_g = equivalent specific gravity of water
 λ = wave length
 ε = wave phase angle
 ρ = mass density of water
 ω_0 = natural frequency of rolling
 ω_e = frequency of encounter
 ω_n = frequency of elemental wave
 $\zeta(t)$ = irregular wave surface
 $\theta(t)$ = rolling angle

8. Vinje, Tor, On the stability of ships in irregular following sea. Norwegian Maritime Research, 1976, 2, 15-19.
9. Oakley, O.H., Pauling, J.R. and Wood, P.D., Ship motion and capsizing in astern sea. Tenth Symposium on Naval Hydrodynamics, 1974, 297-350.
10. Allivei, A.G., Motion and stability of a fishing vessel in transverse and longitudinal seaways, Proceedings of 11th Technology and Research Symposium (STAR), 1986, 13-31.
11. Soong, T.T., Random Differential Equations in Science and Technology. Academic Press, 1972, New York, 256-262.

(Author: D.L. Huang Associate Professor of Department of Naval Architecture. Dalian University of Technology Dalian, 116024, China)

6. REFERENCES

1. Grim, O., Betrag zum Problem der Sicherheit des Schiffes im Seegang, Schiff und Hafen. 1961, 6, 490-497.
2. Pauling, J.R., The transverse stability of a ship in a longitudinal seaway. J.S.R., vol.4, 1961, 4, 37-49.
3. Kerwin, J.E., Notes on the roll in longitudinal waves. I.S.P., vol.2, 16, 1955, 597-614.
4. Nechayev, Yu.I., Stability evaluation of ships in the following waves. (in Russian) Sudostroyenie, 1972, 7, 15-18.
5. Nechayev, Yu.I., Rating of ship stability in the following waves. (in Russian) Sudostroyenie, 1973, 1, 11-14.
6. Wellicome, J.F., An analytical study of the mechanism of capsizing. Proceedings of STARB'75, paper No.3.1.
7. Hamamoto, M. and Akiyoshi, T., Study on ship motion and capsizing in following seas. Journal of Society of Naval Architects of Japan, 1988, 161, 173-180.

MODEL TESTS ON CAPSIZING OF A SHIP IN QUARTERING WAVES

Makoto KAN, Toshihiko SARUTA, Harukuni TAGUCHI, Mikio YASUNO, Yoshifumi TAKAISHI

Model tests on capsizing of a container ship were performed in quartering waves. The encounter angle was varied precisely every 10 degrees by using an autopilot device. Among 763 runs in the irregular and regular waves, 225 capsizings were observed. Most capsizings occurred at the encounter angle 20 to 40 deg. Below some critical advance speed the capsizing never occurred. The direction of capsizing was always to the leeward. Such capsizing may be explained fundamentally as a simple static one which occurs when the capsizing moment of the wave exceeds statically the restoring moment decreased in the quartering waves at the above dangerous range of encounter angle. The reason why the capsizing occurs only in high speed and only to the leeward is also explained in connection with the surf-riding or asymmetric nonlinear surging motion. The capsizing due to the parametric oscillation which had been considered as one of the typical mode of the dynamical capsizing was not observed. Instead, a new mode of dynamical capsizing accompanied with the period bifurcations which was regarded as a precursor of chaos was observed.

INTRODUCTION

It has been said that the capsizing is likely to occur when the ship is running high speed in the following or quartering waves [1],[2]. However, the mechanism of such capsizing is not clarified. The authors performed a series of capsizing experiments using a radio controlled self running model of a container ship in regular and irregular quartering waves including pure following and beam waves. From the results, it has been clarified that most capsizing occurs at the encounter angle of 20 to 40 deg and at the high speed running, and that the capsizing occurs always to the leeward. The present paper describes these characteristic features obtained by the experiments and attempts to explain theoretically about such capsizing.

Ship Research Institute,
Ministry of Transport
6-38-1 Shinkawa, Mitaka, Tokyo 181, JAPAN

EXPERIMENTAL TESTS

Model

The model used in the experiments is a 1/38.57 scale model of container ship "G" designed at HSVA. Body plan and principal particulars are shown in Fig.1 and Table 1. The stability curves in the test condition are shown in Fig.2. The hatches and superstructures are not included in the stability calculations. The C value for GM=1.98cm in still water is 2.2, which satisfies the stability requirement of Japanese Government. The model has no bulwark so that the shipping water on the deck is not trapped.

Experiments

In order to clarify the critical condition for capsizing, the experiment was carried out by varying the encounter angle χ , from 0 deg (pure following) to 90 deg (beam), precisely at every 10 deg by using an autopilot device. The gain of the autopilot was determined such that the rudder

responds by 1.25 deg to 1 deg of the deviation of heading; but does not respond to the yawing velocity. The number of propeller revolution was varied every 1 rps and kept constant by the motor controller. The items of the measurement are roll angle, pitch angle, yaw angle, yaw rate, rudder angle, number of propeller revolution and trajectory of model (speed and course).

In case of irregular waves, runs were repeated 20 times at most under the same condition to get the capsizing rate. However, the timing to encounter the wave is not random, but is handled to meet the almost same wave group. The P-M type wave spectrum used in the test is shown in Fig.3. In order to catch the critical value of GM for this wave, the height of center of gravity was also varied.

In case of regular waves, runs were limited to once for the same condition in principle. However, sometimes runs were repeated twice in the delicate cases close to the critical border for capsizing. The value of GM was fixed to 1.98cm through the test. The wave length to ship length ratio λ/L was varied from 0.5 to 2.25 at an interval of 0.25, and the wave height to wave length ratio h/λ was selected from 1/20, 1/15, 1/12 and 1/10.

Results in irregular waves

Fig.4 shows the total capsizing rate for the all experiments in irregular waves. The occurrence of the capsize is confined to $\chi=10$ to 50 deg, and especially $\chi=20$ to 40 deg is suggested to be most dangerous. The capsizing never occurs at $\chi \geq 60$ deg and at $\chi=0$ deg. The number of runs for $\chi \geq 70$ deg might not seem to be large enough, but it is due to the conviction obtained by the observation that the model would never capsize under these conditions. Fig.5 shows the effects of the advance speed on the capsizing. Besides the fact that the encounter angle $\chi=20$ to 40 deg is hazardous, it can be observed that in the higher speed range the dangerous range

extends to $\chi=10$ to 50 deg. It seems also that the capsize never occurs for the low advance speed, namely for the Froude number $Fn \leq 0.26$. Fig.6 shows the effects of GM. The critical GM for this wave is estimated about 2.7cm. Out of the total 418 runs, 126 capsizings were observed, and all the capsizings occurred to the direction of leeward. The capsizing to the weather side was not observed at all. By performing the experiment for $\chi=-20$ deg, it was confirmed that there was no difference from $\chi=20$ deg.

Results in regular waves

Table 2 to 9 show the results in regular waves. In case of the short wave such as $\lambda/L=0.5$ (Table 2), the capsizing did not occur even for the high wave. However, a large roll to the leeward with the period 5.0 sec was observed in $\chi=40$ deg. This is not considered as a roll resonance, because the natural period is 3.4 sec. Otherwise, $\chi=40$ deg can be considered dangerous even for shorter waves due to the same reason as mentioned later for longer waves. In case of $\lambda/L=0.75$ (Table 3), $\chi=30$ to 40 deg is dangerous, but the dangerous range does not extend in higher wave. Though the capsize does not occur in lower speed, the dangerous range of the encounter angle does not seem to spread even in higher speed range. For $\lambda/L=1$ (Table 4), $\chi=20$ to 40 deg is again dangerous. As the wave height increases, the dangerous encounter angle seems to shift to the lower value. Moreover, in the higher speed and higher wave, the capsizing at $\chi=0$ deg happened, which was never observed in irregular waves. This capsizing of $\chi=0$ deg can be considered as the consequence of running obliquely due to the uncontrollable steering, accompanied with the broaching-to phenomenon. In this case the direction of capsizing was also to the leeward. Similarly with $\lambda/L=0.75$, there is a critical advance speed, below which the capsize does not occur. It is also recognized in higher wave condition ($h/\lambda=1/12$) that the dangerous range of

encounter angle tends to extend as the advance speed increases. In case of $\lambda/L=1.25$ (Table 5), the occurrence of the capsizing is comparable with the case of $\lambda/L=1$, which has been considered as the most dangerous wave length. In comparison with $\lambda/L=0.75$ and 1.0 , the capsizing of $\chi=40$ deg decreased, and the dangerous range of the encounter angle seems to be shifted by about 10 deg, namely $\chi=10$ to 30 deg.

For $\lambda/L=1.5$ (Table 6), the comparable capsizings with $\lambda/L=1.0$ are also observed. The dangerous range seems to return to $\chi=20$ to 40 deg. The capsizing of $h/\lambda=1/20$ scatters somewhat. This may be caused by the slight difference of the initial condition in the delicate case close to the critical condition for capsizing. Although the occurrence of capsizing does not seem to decrease in case of $\lambda/L=1.75$ (Table 7) and $\lambda/L=2.0$ (Table 8), it seems to decrease in case of $\lambda/L=2.25$ (Table 9). This may be considered as a sign of decrease of capsizing in longer waves.

The capsizing in following waves is usually classified into the following three categories, that is, pure loss of intact stability, parametric oscillation and broaching-to. As far as judging from the observation of present experiments, most capsizings were caused by the pure loss of intact stability. This kind of capsizing happened easily in an early stage after the model reached the prescribed speed and encountered the wave with the prescribed heading. A typical record of data is shown in Fig.7. The capsizings due to the broaching-to were observed at $\chi=0$ to 20 deg. Fig.8 shows an example of such capsizing. The capsizing due to the parametric oscillation was not observed at all. Instead, not a few capsizings as shown in Fig.9 were observed. This can be regarded as a period doubling bifurcation which appears as a precursor of the chaos. In Table 2 to Table 9, the classification of capsizing is expressed with the following abbreviations. L (pure loss of intact stability), P (period bifurcation),

B (broaching-to) and BT (tendency of broaching-to). P, B and BT are also shown even in case of non-capsizing if these phenomena are recognized. In regular waves, out of 345 runs, 99 capsizings were observed. Fig.10 shows the total capsizing rate and the classification. 64% is due to the pure loss of intact stability, 26% is due to the period bifurcation, and 10% is due to the broaching-to. The direction of capsizing is to the leeside too, except only one case ($\lambda/L=2.25$, $\chi=30$ deg, $Fn=0.37$).

THEORETICAL APPROACHES

Effects of encounter angle

Using the coordinate system of Fig.11, the capsizing moment by wave is expressed as

$$M_r = M_r \cos(k\xi' + \epsilon) \quad (1)$$

where M_r is an amplitude of the exciting roll moment in an ordinary sense. M_r by the Froude-Krilov's hypothesis is shown in Fig.12. If, besides the F-K hypothesis, the fore and aft symmetry of hull is assumed, then eq (1) becomes

$$M_r = -M_{rs} \sin k\xi' \quad (2)$$

Fig.13 shows this relation, where M_r is defined as positive for portside down. The restoring moment in quartering waves is calculated by Hamamoto's program [3]. Fig.14 is a comparison between the capsizing moment and restoring moment. In the range of $20 \text{ deg} < \chi < 50 \text{ deg}$, the capsizing moment exceeds the restoring moment. Here, the capsizing moment is a value at $\xi'/\lambda = -0.25$, position of the maximum wave slope. While, the restoring moment is calculated at crest amidship because the calculation is not completed for an arbitrary position of wave slope. Therefore such comparison does not make a strict sense, but it can be regarded as a qualitative explanation for the dangerous range of encounter angle.

Effects of advance speed

Above explanation itself is valid also to the oblique bow sea. However, the capsizing

occurs only in oblique stern sea when the ship runs at higher speed than some critical one. The reason for such capsizing is that the dangerous condition of Fig.14 continues for a longer duration in an asymmetric large surging or nearly surf-riding motion, as exemplified in Fig.15, which occurs when the ship speed approaches to the wave speed. If we can define some quantity such as a time constant for capsizing, the critical speed for capsizing may be determined by solving the nonlinear equation of surging motion and by obtaining the continuing time of the risky condition.

Direction of capsize

In asymmetric large surging or surf-riding motion, the ship remains for longer period at the downslope of wave, $-0.5 < \xi'/\lambda < 0$, as shown in Fig.15. Therefore, from eq (2), the sign of M_r is positive, that is, the capsizing moment acts to the leeside down. This is the reason why the capsizing occurs always to the leeside direction.

Period bifurcation and chaos

Nonlinear equation of motion for roll is expressed by the following simple form,

$$I d^2\phi/dt^2 + Nd\phi/dt + WGM\phi\{1-(\phi/\phi_v)^2\} = \overline{M}r\cos\omega t \quad (3)$$

where, ϕ is roll angle, ϕ_v is vanishing angle of stability, I is moment of inertia for roll, N is damping coefficient, W is displacement, ω is angular frequency of encounter and t is time.

Using the transformation of variables, $\psi = \phi/\phi_v$ and $s = \omega_0 t$ ($\omega_0 = \sqrt{WGM/I}$; natural frequency), eq (3) is transformed into

$$d^2\psi/ds^2 + \kappa d\psi/ds + \psi - \psi^3 = B\cos\Omega s \quad (4)$$

where, $\kappa = N/I\omega_0$, $B = \overline{M}r/I\omega_0^2\phi_v$, $\Omega = \omega/\omega_0$.

Eq (4) is a forced Duffing's equation with softened spring and is considered as a typical differential equation of which solution has a cascade of period multiplying bifurcations and chaotic motion under some condition of κ , B and Ω . Comprehensive studies on a similar escape equation with ψ^2 in place of ψ^3 , were carried out by Thompson and Ueda [4],[5].

Systematic examination for eq (4) with wide variety of parameters should be performed to clarify the characteristics of dynamical capsizing phenomenon. Fig.16 is examples of fractal basin boundary metamorphoses for eq (4), where the black part means the non-capsizing region of initial condition. In this case the engineering integrity diagram proposed by Thompson seems to have a feature of devil's staircase as shown in Fig.17. Further study is in progress.

CONCLUSIONS

The capsizing of the intact ship running in waves was examined by means of the self running model test. The characteristic features such as an existence of dangerous encounter angle 20 to 40 deg, its extension to 0 to 50 deg in higher advance speed, an existence of critical speed for occurrence of capsizing, inevitable leeside capsizing and so on, were clarified. Theoretical explanation for such capsizing was attempted. A new mode of dynamical capsizing accompanied with period bifurcations was proposed. Further study on capsizing with respect to the chaotic rolling should be continued.

ACKNOWLEDGEMENTS

Present research was carried out in cooperation with Hamburg Ship Model Basin. The authors would like to express their deep appreciation to Prof. O. Krappinger and Dr. P. Blume for their valuable cooperations.

REFERENCES

1. Paulling, J.R., Oakley, O.H. and Wood, P.D.; Ship Capsizing in Heavy Seas, Proceedings

of the International Conference on Stability of Ships and Ocean Vehicles, Glasgow, 1975.3.

2. Yamakoshi,Y.,Takaishi,Y.,Kan,M., Yoshino,T. and Tsuchiya,T.; Model Experiments on Capsize of Fishing Boats in Waves, Proceedings of the Second International Conference on Stability of Ships and Ocean Vehicles, Tokyo,1982.10, pp.199-214.

3. Hamamoto,M.; Transverse Stability of Ships in a Quartering Sea, Proceedings of the Third International Conference on Stability of Ships and Ocean Vehicles, Gdansk,1986.9, Vol.1, pp.7-13.

4. Thompson,J.M.T.; Chaotic phenomena triggering the escape from a potential well, Proc.R.Soc.Lond. A 421, 1989, pp.195-225.

5. Thompson,J.M.T. and Ueda,Y.; Basin boundary metamorphoses in the canonical escape equation, Dynamics and Stability of Systems, Vol.4, No.3, 1989, pp.285-294.

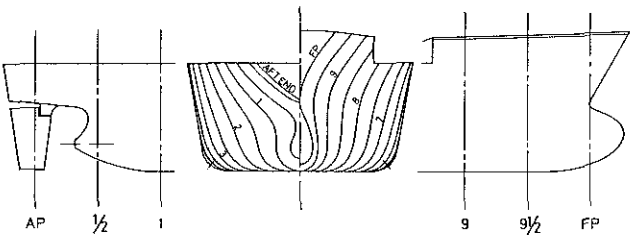


Fig.1 Body plan and side view

Table 1 Principal particulars

Item	Ship	Model
Length Lpp(m)	135.0	3.50
Breadth B (m)	24.3	0.630
Depth D (m)	11.5	0.298
Draft dm(m)	8.37	0.217
Block Coefft. C _B	0.570	0.570
Disp. Vol. ∇ (m ³)	15652	0.273

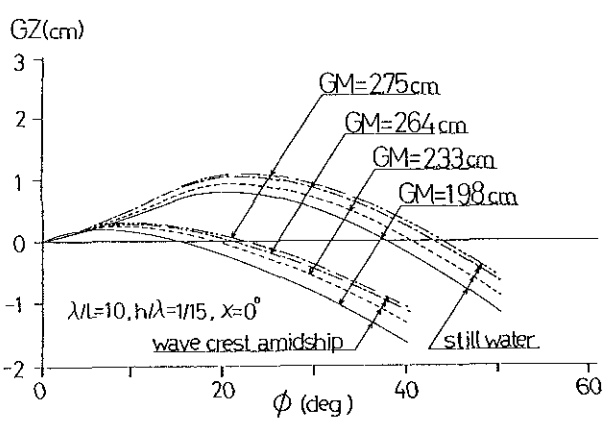


Fig.2 Stability curves

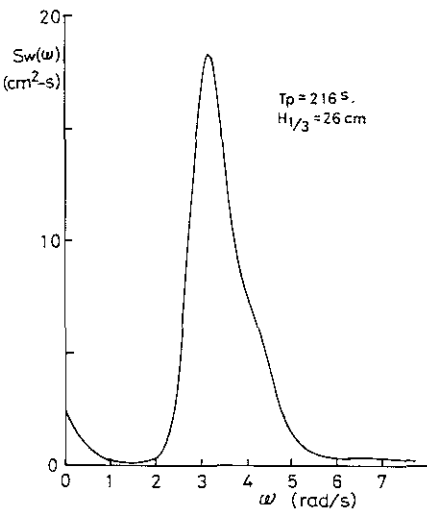


Fig.3 Spectrum of irregular wave

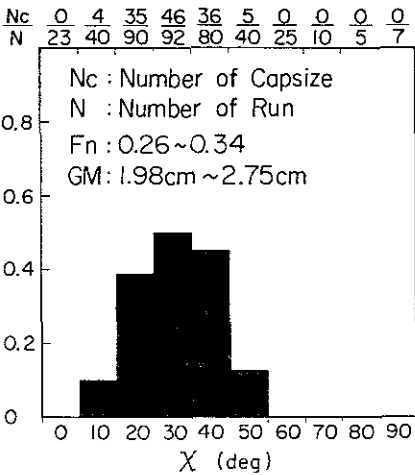


Fig.4 Total rate of capsizing in irregular wave

GM = 1.98cm

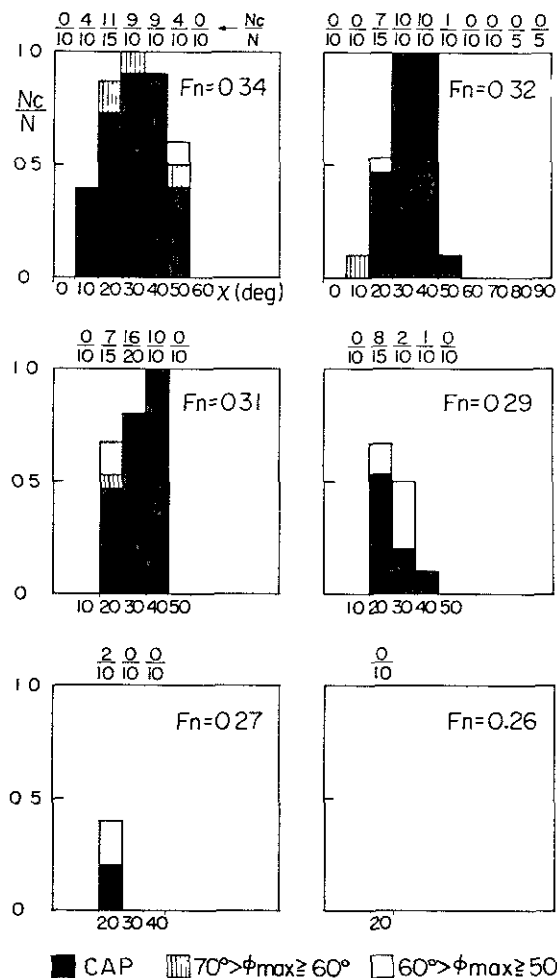


Fig.5 Effect of speed on capsizing rate

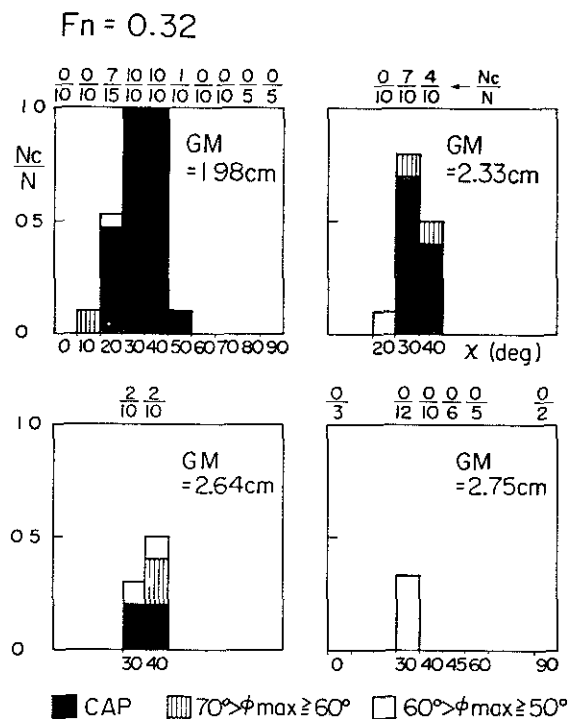


Fig.6 Effect of GM on capsizing rate

Table 2 Results in regular wave ($\lambda/L=0.5$)

λ/L	h/λ	F_n	χ (deg)									
			0	10	20	30	40	50	60	70	80	90
0.5	$1/10$	0.31										
		0.32										
		0.34					ΔP		OP			
		0.36	\circ	\circ	\circ	\circ	ΔP	\circ	\circ	\circ	\circ	\circ
		0.37					OP		OP			

GM=1.98cm

\circ Non Capsizing
 Δ $\phi_{max} > 40^\circ$
 χ Capsizing
 L Pure Loss
 P Period Breach
 B Broaching
 BT Broaching Tendency

Table 3 Results in regular wave ($\lambda/L=0.75$)

λ/L	h/λ	F_n	χ (deg)									
			0	10	20	30	40	50	60	70	80	90
0.75	$1/20$	0.36			\circ	\circ	ΔP	\circ				
		0.37			\circ	\circ	XL	\circ				
		0.31			\circ	ΔP	\circ					
		0.32			\circ	XL	OP	\circ				
		0.34			\circ	XL	XL	\circ				
	$1/15$	0.36	\circ	\circ	\circ	XL	XL	Δ	\circ			
		0.37	\circ	OB	OB	XL	XL	\circ				
		0.31		\circ	\circ	\circ	\circ	\circ				
		0.32		\circ	\circ	XP	\circ	\circ				
		0.34	\circ	\circ	\circ	XP	XP	\circ				
	$1/12$	0.36	\circ	OB	\circ	XL	XL	\circ	\circ			
		0.37	\circ	OB	OB	XL	XL	\circ	\circ			
		0.29				OP	OP					
		0.36		\circ	\circ	XP	XP	OP				
	$1/10$	0.36		\circ	\circ	XP	XP	OP				

GM=1.98cm

Table 4 Results in regular wave ($\lambda/L=1.0$)

λ/L	h/λ	F_n	χ (deg)									
			0	10	20	30	40	50	60	70	80	90
1.0	$1/20$	0.32										
		0.34										
		0.36			\circ	\circ	ΔP	\circ				
		0.37			\circ	\circ	XL	\circ				
		0.38			OB	Δ	XL	\circ				
	$1/15$	0.31		\circ	ΔP	\circ	\circ					
		0.32		\circ	\circ	XP	\circ	\circ				
		0.34		\circ	XL	XL	XP	\circ				
		0.36		OB	XBT	XP	XP	ΔP	\circ			
		0.37		OB	XBT	XL	XL	\circ				
	$1/12$	0.31	\circ	\circ	\circ	\circ	OP	\circ				
		0.32	\circ	Δ	XP	OP	Δ	\circ				
		0.34	\circ	\circ	XL	XL	Δ	\circ				
		0.36	\circ	XB	XL	XP	Δ	\circ	\circ	\circ	\circ	\circ
		0.37	XB, XB	XB	XL	XP	XP	ΔP				

GM=1.98cm

Table 5 Results in regular wave ($\lambda/L=1.25$)

λ/L	h/λ	F_n	χ (deg)									
			0	10	20	30	40	50	60	70	80	90
1.25	$1/20$	0.31			\circ	ΔP	\circ					
		0.32			ΔP	XP	OP					
		0.34			ΔP	XP	OP					
		0.36	\circ	\circ	XL	OP						
		0.37	\circ	XL	XL	Δ	OP					
	$1/15$	0.31	\circ	\circ	Δ	\circ	\circ	\circ				
		0.32	\circ	\circ	XL	ΔP	OP	\circ				
		0.34	\circ	XBT	XP	XP	ΔP	\circ				
		0.36	\circ	XBT	XBT	XL	Δ	\circ				
		0.37	OB	XB	XL	XL	XL	\circ				
	$1/12$	0.31	\circ	OP	\circ	\circ						
		0.32	\circ	\circ	XL	XL	\circ					
		0.34	\circ	ΔP	XP	XP	\circ					
		0.36	XB	XL	XL	XL	XP	ΔP				
		0.37	XB	XL	XL	XL	XP	ΔP	\circ	\circ	\circ	\circ

GM=1.98cm

Table 6 Results in regular wave ($\lambda/L=1.5$)

λ/L	h/λ	F_n	X (deg)									
			0	10	20	30	40	50	60	70	80	90
150	1/20	0.31										GM=1.98 cm
		0.32				OP	AP					
		0.34			XL	AP	OP					
		0.36				OP	AP	XP				
		0.37				XL, AP	OP					
150	1/15	0.31										
		0.32				AP	OP					
		0.34				XL	AP, XL	XP	OP			
		0.36				XL	XL	XP, AP	OP			
		0.37				XL, XL	XL	XL	XL			

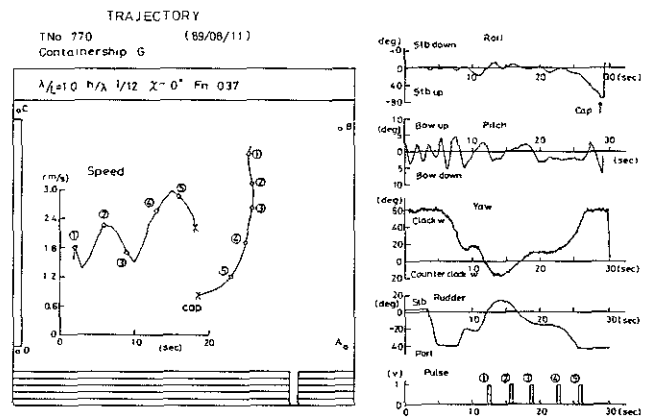


Fig.8 Example of record (broaching-to)

Table 7 Results in regular wave ($\lambda/L=1.75$)

λ/L	h/λ	F_n	X (deg)									
			0	10	20	30	40	50	60	70	80	90
175	1/20	0.31										GM=1.98 cm
		0.32				AP						
		0.34				OP, XP	XP					
		0.36				OP	AP	XP				
		0.37				AP, XL	XL					

Table 8 Results in regular wave ($\lambda/L=2.0$)

λ/L	h/λ	F_n	X (deg)									
			0	10	20	30	40	50	60	70	80	90
20	1/20	0.31										GM=1.98 cm
		0.32				OP						
		0.34					AP					
		0.36				XL	XL					
		0.37				XL	XP					

Table 9 Results in regular wave ($\lambda/L=2.25$)

λ/L	h/λ	F_n	X (deg)									
			0	10	20	30	40	50	60	70	80	90
225	1/20	0.31										GM=1.98 cm
		0.32										
		0.34										
		0.36				XL						
		0.37				XL, AP						

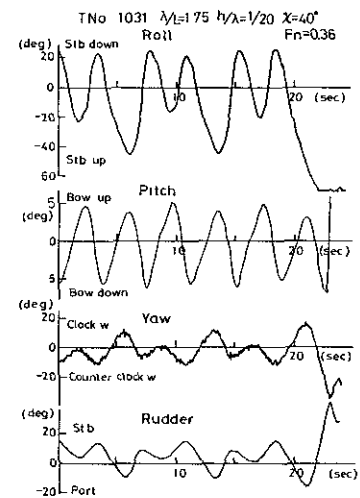


Fig.9 Example of record (period bifurcation)

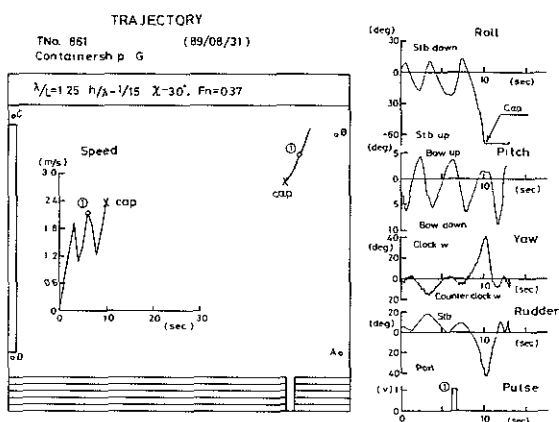


Fig.7 Example of record (pure loss of intact stability)

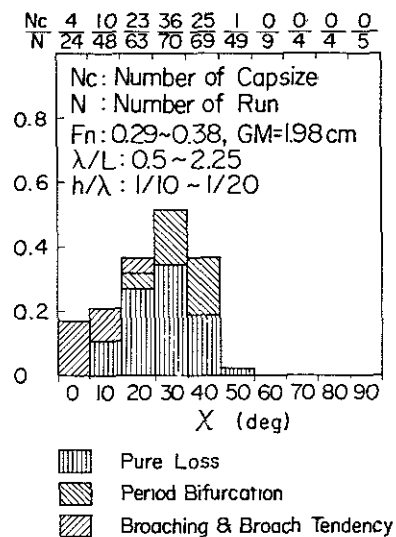


Fig.10 Total rate of capsizing in regular wave

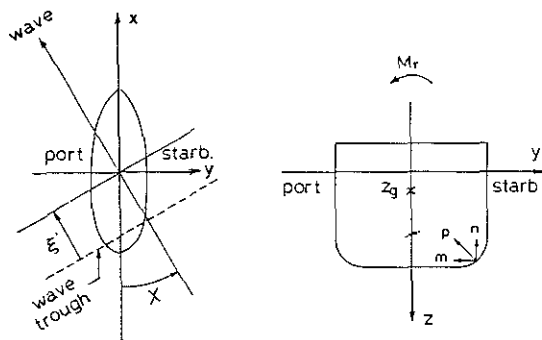


Fig.11 Coordinate system

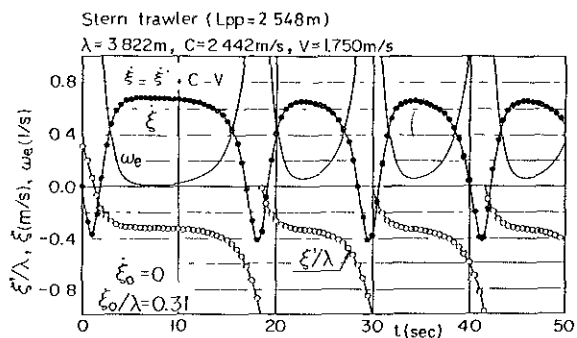


Fig.15 Example of asymmetric surge motion in following wave

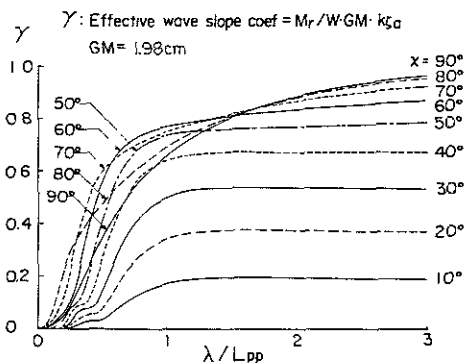


Fig.12 Amplitude of capsizing moment by wave

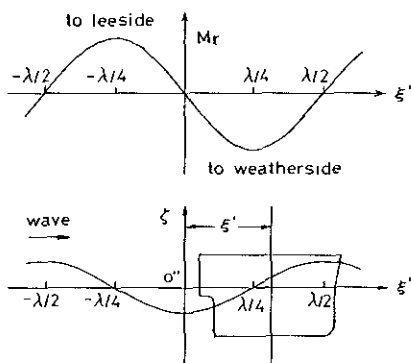


Fig.13 Relation between capsizing moment by wave and ship position

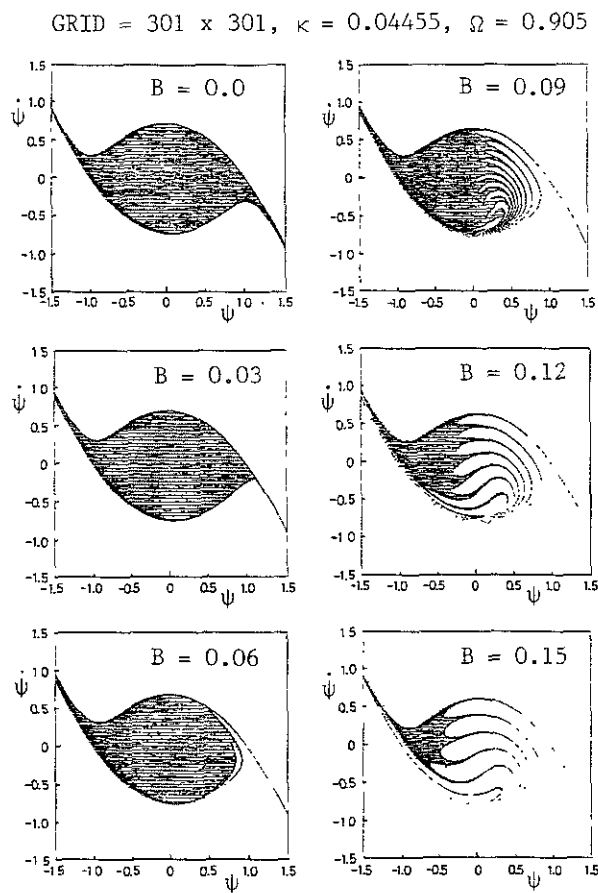


Fig.16 Basin boundary metamorphoses

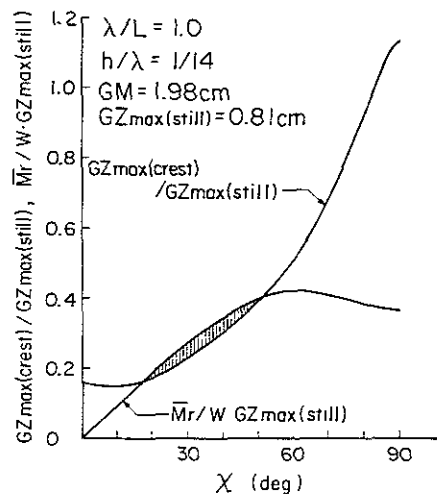


Fig.14 Comparison of capsizing moment and restoring moment

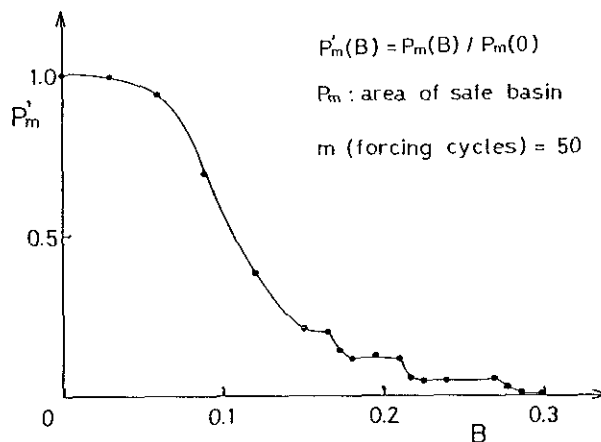


Fig.17 Engineering integrity diagram

THE PROBABILITY OF COMPARTMENT AND WING COMPARTMENT FLOODING IN THE CASE OF SIDE DAMAGE - NEW FORMULAS FOR PRACTICAL APPLICATION

WALTER ABICHT*

A new mathematical model for the distribution of side damages with respect to damage location, damage length, and damage penetration is presented. Its correspondence with the results of damage statistics is shown. For the probability that a compartment or wing compartment will be flooded, formulas are set up which are strictly based on the assumed distribution functions. It is recommended to introduce these formulas in a revised subdivision regulation applicable to all types of sea-going merchant ships. The importance of such a revision is demonstrated by a presentation of inaccuracies and shortcomings resulting from the calculation methods prescribed in the actual probabilistic subdivision rules for passenger and dry cargo vessels.

INTRODUCTION

Thirty years after Wendel [1] introduced the survival probability as a criterion for the effectiveness of watertight subdivision, two international subdivision rules based on the probabilistic concept exist: Equivalent Regulations on Subdivision and Stability of Passenger Ships (IMO-Resolution A.265) and the Regulations on Subdivision and Damage Stability of Dry Cargo Ships (IMO-MS-C.80/2.1). Both regulations are based on the assumption of the occurrence of a side damage. On account of the randomness of location and dimensions of the side damage, these quantities are presented by their distribution functions. Bottom damages and stem damages are not considered because of the rather high effectiveness of the double bottom in the case of grounding and of the collision bulkhead in the case of ramming.

The method of subdividing ships by aiming at a certain minimum survival probability is less rigid than the conventional method of arranging transverse bulkheads in accordance with a given factor of subdivision. This is a big advantage especially for dry cargo ships. By a proper arrangement of transverse and longitudinal bulkheads — if necessary, in combination with a horizontal subdivision — comparatively spacious cargo holds are possible without reducing the degree of survivability.

It is to be expected that in the near future the aforementioned probabilistic subdivision rules for passenger ships and dry cargo ships will be revised and integrated in one regulation. Furthermore, this regulation will presumably replace the antiquated subdivision requirements of SOLAS 1974 and other damage stability rules which are still based on the concept of a one-, two- or three-compartment standard. On this occasion, the errors and

shortcomings which are to be found in both existing probabilistic regulations should be eliminated. This especially applies to the formulas for the calculation of the probability of compartment and wing compartment floodings. After a short demonstration of their weak points new formulas without such flaws and suited for practical application in a revised subdivision rule will be presented.

DETERMINATION OF THE PROBABILITY OF FLOODING IN THE ACTUAL RULES

The equations by which the probability of flooding must be calculated for passenger and dry cargo vessels are based on the same damage statistics. Nevertheless, the formulas to be applied are different.

In the equivalent subdivision rules for passenger ships [2], the product $a \cdot p$ represents the probability that a compartment (and only the compartment under consideration) will be flooded. Factor a accounts for the location of the compartment within the ship's length, factor p is a basic probability of flooding for a compartment of given length. The probabilities a and p must be calculated by the formulas given in the rules.

Unfortunately, these formulas are not quite correct. This can be easily demonstrated by an example: For a compartment extending over the entire ship length, the flooding probability necessarily is exactly $a \cdot p = 1$. But the result obtained from the formulas is only $a \cdot p = 0.986$ (for $L_S \leq 200\text{m}$).

In case of a wing compartment, the flooding probability must be calculated by multiplying the product $a \cdot p$ by a third factor r . The formula for r is even more unacceptable. This becomes evident if, for instance, the distance b of the longitudinal bulkhead from the shell is very short. For $b \rightarrow 0$ the reduction factor r should converge to $r \rightarrow 0$. The values we get, however, are — depending on the length of the wing compartment — between

*Professor of Design and Safety of Ships,
Hamburg University

$r = 0.016$ and $r = 0.800$ (for revised version of the r -formula as published in the IMO-paper STAB XII/8, Annex II).

The aforementioned inaccuracies may lead to results which are completely wrong. This mainly applies to ships being able to survive floodings of two or more adjacent spaces. Here, contributions to the survival probability must be determined by subtracting relatively high probability values. It is a well known fact that the difference between two big numbers can only be correctly calculated if these numbers are absolutely exact. For this reason, the formulas for the probability calculations must strictly correspond with the distribution functions assumed for location and extent of damage. The distribution functions themselves must be in accordance with the results of damage statistics; here, and only here, approximations are unavoidable and can — because the survival probability must be seen as a criterion — be accepted. But after these functions are settled, no further approximations should be made and all calculations must follow with absolute accuracy the assumed distribution law. This principle, too much neglected in both of the existing rules, should be consequently observed in a revised regulation.

Being aware of some of the weak points of the passenger ship rules, it was tried to improve the formulas for the probability calculation when the probabilistic subdivision rules for dry cargo ships were formulated [3]. For the probability of compartment flooding new formulas were established. Factor a , evaluating the influence of the location of a compartment on the flooding probability, is now included in the formula for p_1 . For a compartment length being equal to ship's length, the correct result $p_1 = 1$ is obtained. On closer examination, however, the revised p_1 -formulas are found to have new and even more severe shortcomings. As a result of discontinuities of the probability density function, on which the p_1 -formulas are based, we get completely different flooding probabilities p_1 for a compartment located at the after or fore end of the ship and the same compartment moved a little bit in the midship direction [4].

Example:

A compartment of 0.12 L in length is shifted from the outmost forward end a little towards the midship section. According to the formulas to be applied the probability of flooding decreases from $p_1 = 0.102$ to $p_1 = 0.060$. It is obvious that such a big difference is unrealistic and that there is a need for a correction.

The method of determining the flooding probability of wing spaces is for dry cargo ships the same as for passenger ships: the flooding probability p_1 of a compartment of the same location and the same length must be multiplied by a reduction factor r . The formulas for r were partly, but not substantially revised. Generally, the critical comments on the r -formulas are also

applicable to the rules for dry cargo ships. As an example, for $b = 0$ we get $r = 0.1$ instead $r = 0$.

DISTRIBUTION DENSITIES AND DISTRIBUTION FUNCTIONS

In order to eliminate the shortcomings of the formulas in the actual rules, it is advisable to start from the foundations, namely the results of damage statistics and their mathematical presentation by distribution densities and distribution functions.

For side damages, the most important results of an analysis of the IMO damage cards are [5], [6], [7]:

- damage locations are distributed over the total ship's length. They are a little more frequent in the forward half of the ship than in the aft part.
- the distribution density curve for the ratio damage length to ship's length (= non-dimensional damage length) starts with a steep upward slope. After having reached its peak, the curve descends gradually. Damage lengths of more than 0.25 of ship's length are extremely seldom and may be neglected. The median of the damage length is somewhere between 5.55 percent and 6.68 percent of ship's length [5], [6].
- the distribution density of the ratio damage penetration to ship's breadth (= non-dimensional damage penetration) strongly depends on the dimensionless damage length. The peak of the curve is located at a penetration depth just above zero for the shortest damage lengths and moves to a penetration depth of about 0.4 of ship's breadth for the longest damage lengths. The median of the damage penetration is — growing with damage length — between a little above zero and 37.5 percent of ship's breadth.

For the damage data, the following symbols are used:

- x : damage location (= distance between forward end of damage and the aft end of the ship)
- y : damage length (= longitudinal extent of damage)
- t : damage penetration (= transverse extent of damage)

or in dimensionless writing:

$$\xi \equiv x/L \quad \eta \equiv y/L \quad \tau \equiv t/B$$

In a system of ξ - η -coordinates each side damage which may occur is represented by a point within an triangular area. This triangle is right-angled [4]. It would be an isosceles triangle if — as in the existing subdivision rules — the center of damage is taken as damage location. The latter definition, however, would complicate some of the

following calculations, and it would be a definition of damage location being different from that for bottom and stem damages [8]. So in this paper, ξ or ξ respectively is defined as written above.

For a graphic representation of the distribution of a three-dimensional random quantity like the side damage with the parameters ξ , η , and τ , at least two diagrams are needed.

In Fig. 1, a curved surface is plotted, the run of which corresponds with the statistical findings on the distributions of damage locations and damage lengths. It represents the distribution or probability density of side damages if the third parameter, the damage penetration τ , is ignored. In order to get a simple analytic expression for the density function $p(\xi, \eta)$, the curved surface is replaced by an inclined plane. According to what is said in the preceding chapter, such an approximation is acceptable.

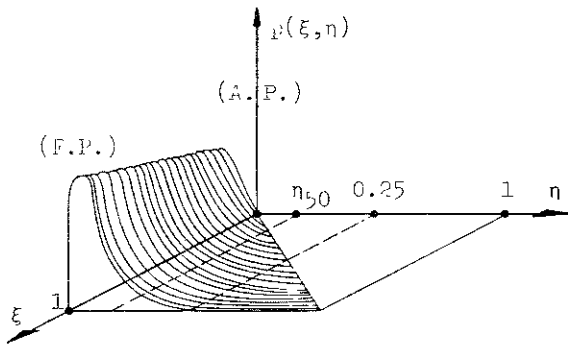


Fig. 1. Distribution density $p(\xi, \eta)$ of the two-dimensional side damage according to damage statistics

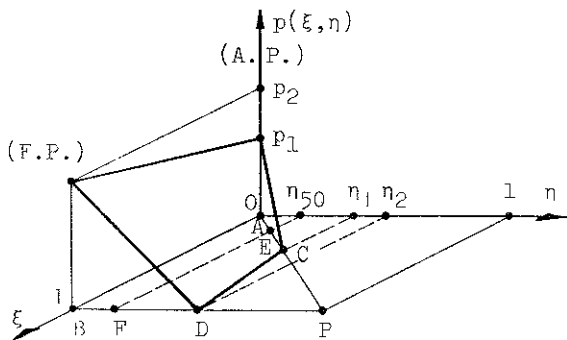


Fig. 2. Linearized distribution density $p(\xi, \eta)$ for practical probability calculations

From Fig. 2, showing this plane, follows:

$$p(\xi, \eta) = p_2 \left[\left(1 - \frac{p_1}{p_2}\right) \xi - \frac{\eta}{\eta_2} + \frac{p_1}{p_2} \right] \quad (1)$$

The constants η_1 , η_2 , p_1 , and p_2 are defined in Fig. 2. The function is only applicable to pairs of ξ - η -values located within the area

ABCD of the ξ - η -plane; beyond this range, the probability density is equal to zero.

According to the statistical results, realistic values for the p_1/p_2 - ratio and for η_2 are [4]:

$$p_1/p_2 = 0.75 \quad \eta_2 = 0.25$$

With these values we obtain $\eta_1 = 0.20$. The absolute values for p_1 and p_2 , and the median damage length η_{50} follow from two definite double integrals:

$$\iint_{ABCD} p(\xi, \eta) d\xi d\eta = 1 \quad (2)$$

and

$$\iint_{ABEF} p(\xi, \eta) d\xi d\eta = 0.5 \quad (3)$$

The probabilities 1 or 0.5 respectively, as a result of the double integration of the probability density $p(\xi, \eta)$, must be attained for the following reasons:

1. Location ξ and length η of the assumed side damage cannot be predicted. The probability, however, that a side damage will occur and that its parameters ξ and η lie within the area ABCD, is known: it is exactly 1.
2. By definition, half of the side damages are less than η_{50} in length. Accordingly, the probability of the occurrence of such a damage, the ξ - η -values of which are located within the area ABEF, is 0.5.

After having solved the integrals, we get:

$$p_1 = \frac{90}{11} \quad p_2 = \frac{120}{11} \quad \eta_{50} = 0.06268$$

A median damage length of $\eta_{50} = 0.06268$ is between the values published in [5] and [6]. The present versions of the probabilistic subdivision rules are based on a median of 0.06683. This value was taken in 1973, just before the first oil crisis. At that time, there was a clear tendency of growing speed of ships, and consequently, a growing average extent of damage was expected for the future. In the opinion of the author, this effect was overestimated. A median of $\eta_{50} = 0.06268$ seems to be more realistic. So, there is no need for revising the above numerical values for p_1 , p_2 , η_1 , and η_2 . With these values, the final function for the two-dimensional probability density $p(\xi, \eta)$ is:

$$p(\xi, \eta) = \frac{30}{11} (\xi - 16\eta + 3) \quad (4)$$

In order to give a further proof of the quality of this function, its marginal densities $p(\xi)$ and $p(\eta)$ are compared with the distribution densities $p(\xi)$ and $p(\eta)$ resulting from the statistics [4], [7]. As can be seen in Fig. 3 and Fig. 4, the curves representing the marginal densities are in good accordance with the histograms of the statistical analysis.

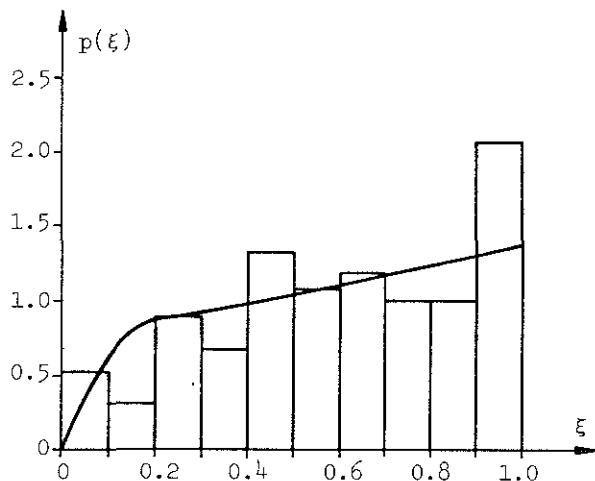


Fig. 3. Marginal density $p(\xi)$ of the linear distribution density $p(\xi, \eta)$ and histogram of damage locations according to statistical analysis

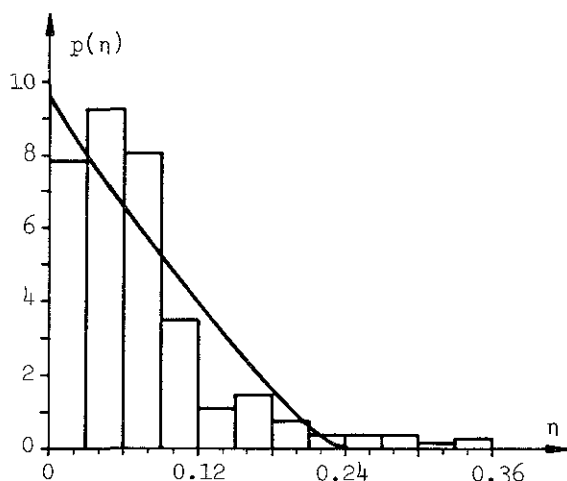


Fig. 4. Marginal density $p(\eta)$ of the linear distribution density $p(\xi, \eta)$ and histogram of damage lengths according to statistical analysis

A diagram showing the distribution of the penetration depths of side damages is given in [7]. It is presented in Fig. 5 and demonstrates the influence of the damage length: the smaller η is, the higher the probability P_τ that a given penetration τ will not be exceeded.

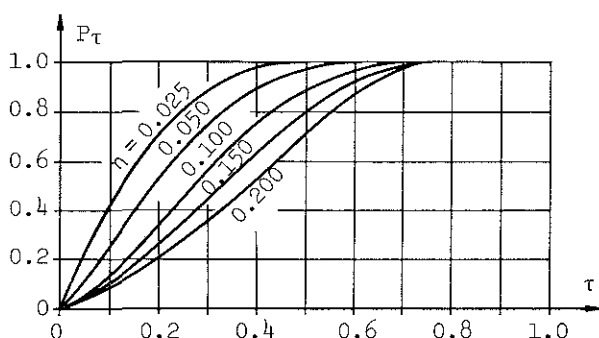


Fig. 5. Distribution functions of damage penetration τ according to damage statistics

The curves in Fig. 5 are directly elaborated from the IMO damage cards. For a translation into a mathematical formula, a function must be found, the graph of which is a family of curves running in the same way as in Fig. 5.

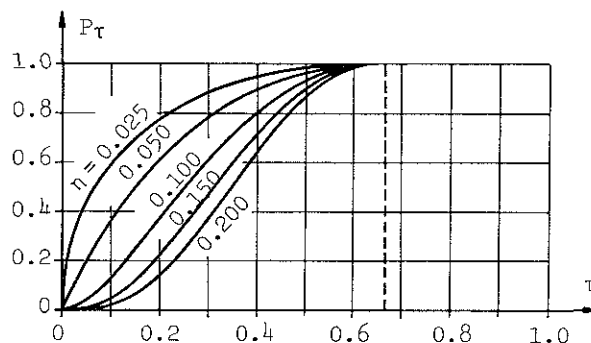


Fig. 6. Distribution functions of damage penetration τ for practical probability calculations

A function meeting this requirement quite well, is

$$P_\tau(\eta, \tau) = (1.5\tau)^{20\eta} \cdot e^{20\eta(1-1.5\tau)} \quad (5)$$

Its family of curves is plotted in Fig. 6. For damage lengths $\eta < 0.25$ and damage penetrations $\tau \leq 2/3$, the differences between the distribution functions in Fig. 5 and Fig. 6 are rather small. Beyond these limits, the formula is not applicable. According to the assumption that a damage penetration of $\tau = 2/3$ will not be exceeded, the probability P_τ of the event of a penetration depth being smaller than a given numerical value τ_1 , is for $2/3 \leq \tau_1 \leq 1$ always exactly $P_\tau = 1$. A further formula, namely for $\eta > 0.25$, is not needed because $\eta = 0.25$ is assumed to be the upper limit of the longitudinal damage extent (Fig. 2).

The statistical informations given by the presented functions $p(\xi, \eta)$ and $P_\tau(\eta, \tau)$, are sufficient to derive formulas for the probability of flooding for compartments and wing compartments. Using a model for the reality, the above functions are considered to be the true functions. In order to avoid the errors of the actual probabilistic subdivision rules, the following calculations are strictly based on these functions. They are carried out correctly without applying approximate terms.

NEW FORMULAS FOR THE SPACE FLOODING PROBABILITY

A general calculation of the flooding probability p_f for side spaces includes the special case of a breadth being equal to ship's breadth ($b = B$). Therefore, in principle, separate formulas for compartments and wing compartments are not necessary.

Before dealing with the side space, we first will have a look at a compartment. Its forward end may be located at $\xi = \xi_L$, its length may be $\Delta\xi$. In Fig. 7, showing the graph of the assumed density function $p(\xi, \eta)$,

those side damages causing a flooding of this compartment – and only of this compartment –, are represented by pairs of ξ - η -values falling into the triangular area MNO. We must differentiate between two cases:

- compartment length $\Delta\xi \leq \zeta/16$ (point O of the triangle MNO below line CD)
- compartment length $\Delta\xi \geq \zeta/16$ (point O of the triangle MNO above line CD)

where $\zeta \approx 3 + \xi_L$.

b) WING COMPARTMENTS OF $\Delta\xi \leq \zeta/16$ IN LENGTH

The flooding probability p_1 of a wing compartment depends on a further parameter, namely on its dimensionless breadth b/B . The knowledge of the distribution function $P_\tau(\eta, \tau)$ enables us to derive a formula for p_1 for side spaces being smaller than $b/B = 2/3$. The flooding probability of side spaces of $b/B > 2/3$ is – because damage penetrations of $\tau > 2/3$ are excluded – the same like that of a compartment with $b/B = 1$.

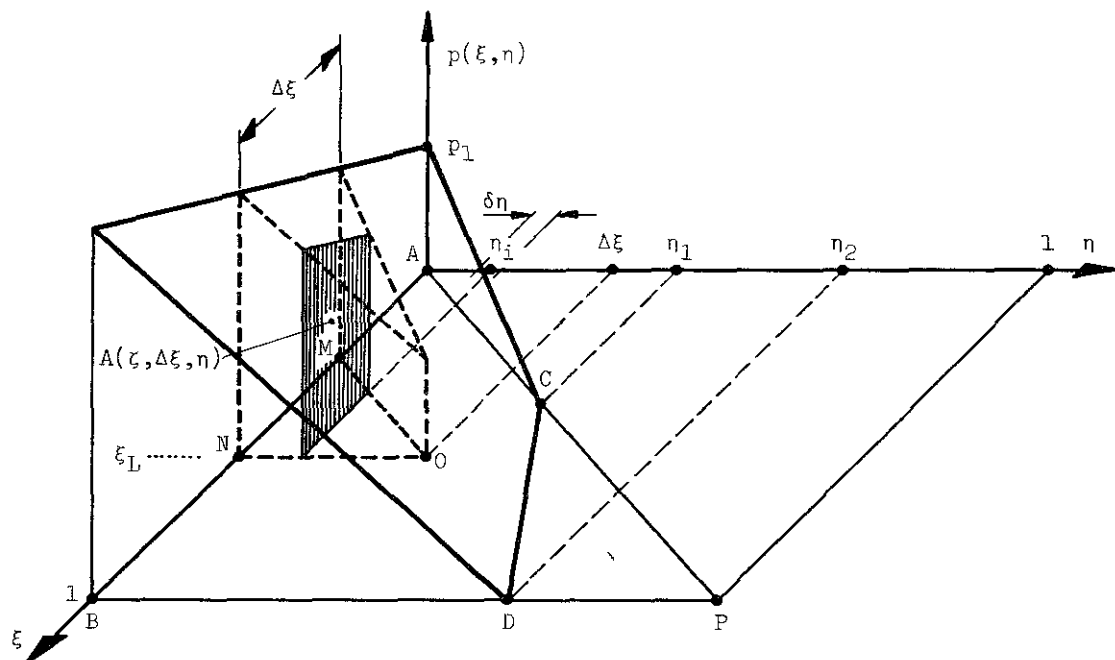


Fig. 7. Probability of flooding to a compartment of $\Delta\xi \leq \zeta/16$ by a side damage of given length η_1

a) COMPARTMENTS OF $\Delta\xi \leq \zeta/16$ IN LENGTH

The example given in Fig. 7 is a compartment of this type. The flooding probability p_1 for this compartment is obtained by an integration of the probability density $p(\xi, \eta)$ within the limits of the triangle MNO. This can be done in two steps: determination of the sectional areas $A(\zeta, \Delta\xi, \eta)$ of the prism in direction parallel to the p - ξ -plane, and integration of $A(\zeta, \Delta\xi, \eta)$ with respect to η .

For $A(\zeta, \Delta\xi, \eta)$ we get

$$A(\zeta, \Delta\xi, \eta) = \frac{30}{11} \zeta \Delta\xi - \frac{15}{11} \Delta\xi^2 - \frac{30}{11} (\zeta + 15 \Delta\xi) \eta + \frac{465}{11} \eta^2 \quad (6)$$

Its definite integral with respect to η from 0 to $\Delta\xi$ is

$$p_1 = \int_0^{\Delta\xi} A(\zeta, \Delta\xi, \eta) d\eta = \frac{5}{11} \Delta\xi^2 (3\zeta - 17\Delta\xi) \quad (7)$$

From Fig. 7 it is easy to see: the probability δp_1 that the compartment under consideration will be flooded by a side damage of given length η_1 (exactly: $\eta_1 - \delta\eta/2 < \eta < \eta_1 + \delta\eta/2$), equals the volume of a "slice" located parallel to the p - ξ -plane at $\eta = \eta_1$ and having a thickness of $\delta\eta$:

$$\delta p_1 = A(\zeta, \Delta\xi, \eta_1) \cdot \delta\eta$$

The individual distribution function P_τ to be applied if $\eta = \eta_1$, is:

$$P_\tau = (1.5 \tau)^{20\eta_1} \cdot e^{20\eta_1(1 - 1.5 \tau)}$$

By substituting b/B for τ , we get the probability that in the case of a damage length $\eta \approx \eta_1$, the damage penetration τ will be smaller than b/B :

$$P_\tau = (1.5 b/B)^{20\eta_1} \cdot e^{20\eta_1(1 - 1.5 b/B)}$$

The product of the above probabilities, $\delta p_1 \cdot P_\tau$, represents the probability that the flooding will be caused by a side damage with a longitudinal extent of $\eta \approx \eta_1$ and a transverse extent of $\tau < b/B$. If these products are evaluated for all damage lengths

— from the smallest just above zero up to a length being equal to the compartment length $\Delta\xi$ — and then summed up, the result is just the probability p_1 we are looking for: the probability of a flooding to the compartment under consideration — and only to this compartment — by a side damage with a penetration depth not exceeding a given numerical value. This probability is identical with the flooding probability p_1 of a wing compartment with a dimensionless breadth b/B . From

$$p_1 = \int_0^{\Delta\xi} A(\eta_1) \cdot P_T(\eta_1) \cdot d\eta_1$$

follows, after substitution of the analytical expressions for A and P_T , the final formula for practical application:

$$p_1 = \frac{15 \Delta\xi (2\zeta - \Delta\xi)}{11c} - \frac{30 (\zeta + 15 \Delta\xi)}{11c^2} + \frac{930 - 930e^{-c\Delta\xi} + 30c(\zeta - 16\Delta\xi)e^{-c\Delta\xi}}{11c^3} \quad (8)$$

where $c \equiv 30 b/B - 20 \ln(1.5 b/B) - 20$.

As mentioned at the beginning, the limits to be observed are:

$$\Delta\xi \leq \zeta/16 \quad \text{and} \quad b/B \leq 2/3.$$

If $b/B = 2/3$, the above formula gives us the flooding probability for a compartment of $\Delta\xi \leq \zeta/16$. In order to demonstrate this, we must write — to avoid a negative denominator (for $b/B = 2/3$ we get $c = 0$) —

$$e^{-c\Delta\xi} = 1 - c\Delta\xi + 1/2 c^2 \Delta\xi^2 - 1/6 c^3 \Delta\xi^3 + \dots$$

By introducing this series for the exponential function $\exp(-c\Delta\xi)$, we get for p_1 the same

result as presented in subparagraph a) for compartments of $\Delta\xi \leq \zeta/16$.

c) COMPARTMENTS OF $\Delta\xi \geq \zeta/16$ IN LENGTH

For compartments being more than $\zeta/16$ in length, the triangular area MNO in the ξ - η -plane extends beyond the ABCD-region where side damages are assumed to occur. As demonstrated in Fig. 8, the prism with the base MNCR, the volume of which equals the flooding probability p_1 of the compartment considered, has sectional areas of different shape. For damage lengths $\eta \leq \eta_G$, we get a trapezoidal cut surface; its area A_1 is:

$$A_1(\zeta, \Delta\xi, \eta) = \frac{30}{11} \zeta \Delta\xi - \frac{15}{11} \Delta\xi^2 - \frac{30}{11} (\zeta + 15 \Delta\xi) \eta + \frac{465}{11} \eta^2 \quad (9)$$

For damage lengths $\eta_G \leq \eta \leq \eta_R$, the cut surface becomes triangular, and its area A_2 is:

$$A_2(\zeta, \eta) = \frac{15}{11} \zeta^2 - \frac{480}{11} \zeta \eta + \frac{3840}{11} \eta^2 \quad (10)$$

From the sum of the two definite integrals

$$\int_0^{\eta_G} A_1(\zeta, \Delta\xi, \eta) d\eta \quad \text{and} \quad \int_{\eta_G}^{\eta_R} A_2(\zeta, \eta) d\eta$$

follows the formula for the flooding probability p_1 for compartments exceeding a length of $\zeta/16$:

$$p_1 = \frac{\Delta\xi \cdot \zeta (\zeta - \Delta\xi)}{11} + \frac{\Delta\xi^3}{33} - \frac{\zeta^3}{528} \quad (11)$$

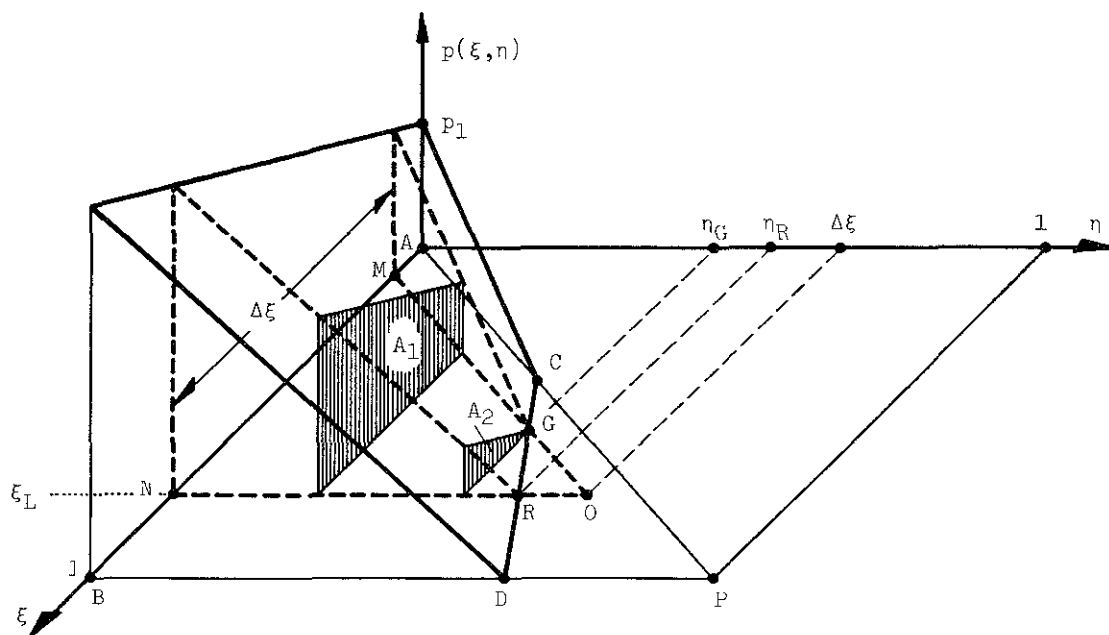


Fig. 8. Probability of flooding to a compartment of $\Delta\xi \geq \zeta/16$ by a side damage with $\eta_1 \leq \eta_G$ and with $\eta_G \leq \eta_1 \leq \eta_R$

d) WING COMPARTMENTS OF $\Delta\xi \geq \zeta/16$ IN LENGTH

The flooding probability p_1 can be calculated in the same way as described in subparagraph b). The only difference is that it must be observed whether the damage length under consideration does or does not exceed η_G (Fig. 8). According to the assumed limitation of the damage penetration to $\tau = 2/3$, the resultant formula for p_1 is only applicable to wing compartments which are smaller than $b/B = 2/3$. For side spaces of a depth of more than $2/3$ of the ship's breadth, the formula for compartments of $\Delta\xi \geq \zeta/16$ must be applied for the calculation of the flooding probability p_1 (subparagraph c). If $b/B \leq 2/3$, the steps of determining p_1 are:

Probability of flooding by a side damage of $\eta \approx \eta_1$ and any depth τ :

$$0 < \eta_1 \leq \eta_G: \quad \delta p_1 = A_1(\zeta, \Delta\xi, \eta_1) \cdot \delta\eta$$

$$\eta_G \leq \eta_1 \leq \eta_R: \quad \delta p_1 = A_2(\zeta, \eta_1) \cdot \delta\eta$$

Probability of flooding by a side damage of $\eta \approx \eta_1$ and $\tau < b/B$:

The above probabilities δp_1 must be multiplied by $P_\tau(\eta_1)$, where

$$P_\tau(\eta_1) = \left(1.5 \frac{b}{B}\right)^{20\eta_1} \cdot e^{-20\eta_1(1-1.5 \frac{b}{B})} \\ = e^{-c\eta_1}$$

Probability of flooding by a side damage of $\tau < b/B$ and any length:

$$p_1 = \int_0^{\eta_G} A_1(\eta_1) \cdot P_\tau(\eta_1) \cdot d\eta_1 + \int_{\eta_G}^{\eta_R} A_2(\eta_1) \cdot P_\tau(\eta_1) \cdot d\eta_1$$

The result of the integrations represents the flooding probability p_1 for a wing compartment of $\Delta\xi \geq \zeta/16$ and $b/B \leq 2/3$:

$$p_1 = \frac{15 \Delta\xi (2\zeta - \Delta\xi)}{11 c} - \frac{30 (\zeta + 15 \Delta\xi)}{11 c^2} + \\ + \frac{930 + 6750 e^{-\frac{c}{15}(\zeta - \Delta\xi)}}{11 c^3} - 7680 e^{-\frac{c\zeta}{16}} \quad (12)$$

From the definition

$$c \equiv 30 \frac{b}{B} - 20 \ln(1.5 \frac{b}{B}) - 20$$

follows $c = 0$ if $b/B = 2/3$. If we develop the exponential expressions into series, we get for $c = 0$ the same p_1 -formula as presented in subparagraph c) for compartments of $\Delta\xi \geq \zeta/16$.

DISCUSSION AND CONCLUDING REMARKS

The formulas derived in the preceding section for the probabilities of compartment and wing compartment floodings offer several advantages. They are applicable in practical subdivision rules and fulfil fundamental requirements such as:

- no discontinuities in the results
- the p_1 -formulas for compartments follow from the more general p_1 -formulas for wing compartments. According to the assumption that damage penetrations $\tau > 2/3$ do not occur, they are identical with the p_1 -formulas achieved for $b/B = 2/3$. This applies to compartment lengths $\Delta\xi \leq \zeta/16$ as well as $\Delta\xi \geq \zeta/16$.
- for a compartment of $\Delta\xi = 1$ the correct result $p_1 = 1$ is obtained
- the correct flooding probability $p_1 = 0$ is attained for $\Delta\xi = 0$ as well as for $b/B = 0$
- application of the p_1 -formulas for $\Delta\xi \leq \zeta/16$ and $\Delta\xi \geq \zeta/16$ results in identical formulas for $\Delta\xi = \zeta/16$

For the future, an universal probabilistic subdivision regulation, to be applied to all types of seagoing ships, is desirable. In this context, it is recommended to introduce the presented formulas into the new regulation. By such a decision the judgement of the safety of ships could be clearly improved.

Though not subject of this paper, it may be mentioned that another requirement in the present subdivision rules calls for an amendment. The assumption of a damage stability based on a vertical center of gravity which equals the allowable upper limit, is against the probability concept. Efforts, for instance, of attaining a high survivability by giving the ship a great deal of damage stability, do not find expression in the survival probability criterion called "Attained Subdivision Index" because not the actual but unrealistic small minimum stability values must be assumed to exist. Here, a replacement of the highest permissible \overline{KG} -value by a mean value or by a distribution of \overline{KG} -values should be considered.

Coming back to the flooding probability p_1 , it still remains to point out that the method of defining the side damage location by the distance of its forward end from the aft end of the ship, leads to a graphic representation of the survivable side damages which differs from the conventional graph. This is demonstrated by an example in Fig. 9. It shows a ship subdivided by five transverse bulkheads. The following floodings are assumed to be survivable: flooding of the after two adjacent compartments, of the forward two adjacent compartments, or of any of the two inner compartments.

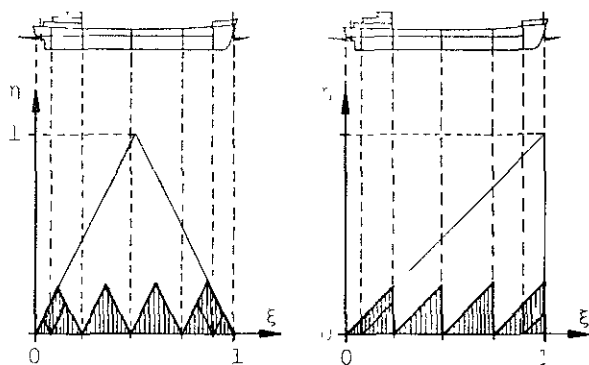


Fig. 9. Triangular hatched areas representing the survivable pairs of ξ - η values for a transversely subdivided ship. In the left graph ξ indicates the location of the center, in the right graph the location of the forward end of the side damage as well as of the floodable compartment

If the location of a side damage or a compartment is defined by the location of its center, the areas of the survivable pairs of ξ - η -values look like illustrated in the left diagram of Fig. 9. The limiting isosceles triangles change into right-angled triangles if the forward end of damage and watertight space respectively is taken to indicate the position within ship's length. We then get the diagram on the right side of Fig. 9.

In the author's opinion, it should be unproblematic to introduce the new kind of graphic representation. This view is confirmed by practical experience gained from survival probability calculations in the cases of bottom and stem damages. For these types of damages, the proposed definition of location is in use from the beginning.

ACKNOWLEDGEMENTS

The valuable assistance of Mr. U. Schilling in preparing the cameraready manuscript and of Mrs. I. Jurschek in producing the graphs is gratefully acknowledged.

REFERENCES

- [1] Wendel, K., Die Wahrscheinlichkeit des Überstehens von Verletzungen, Schiffstechnik, 1960, Vol.7, No.36, pp.47-61.
- [2] Regulations on Subdivision and Stability of Passenger Ships as an Equivalent to Part B of Chapter II of the International Convention for the Safety of Life at Sea, 1960, IMO Resolution A.265 (Correction of r-formula in Stab XII/8, Annex II).
- [3] Regulations on Subdivision and Damage Stability of Dry Cargo Ships, Including RO-RO Ships, IMO-Paper MSC 57/WP 13, April 1989.
- [4] Abicht, W., New Formulas for Calculating the Probability of Compartment Flooding in the Case of Side Damage, Ship Technology Research, 1989, Vol.36, No.4, pp.51-56.
- [5] Riepe, W., Statistische Untersuchungen über Leckgrößen bei Schiffsunfällen, Hansa, 1966, Vol.103, No.18, pp.1537-1547.
- [6] Krappinger, O., Physikalisch - statistische Grundlagen der neuen Unterteilungsvorschriften und ihre praktische Anwendung, Fifth Postgraduate Seminar, Institut für Schiffbau, Hamburg, 1974.
- [7] Sulkiewicz, H., Wahrscheinlichkeit des Ölaustritts bei Großtankern, Diploma thesis, Institut für Schiffbau, Hamburg, 1973.
- [8] Abicht, W., Damage Stability and Subdivision, Handbuch der Werften, Vol.XIX, Schiffahrtsverlag HANSA, Hamburg, 1988, pp.13-90.

THEORETICAL ANALYSIS OF MOTION AND STABILITY OF NONLINEAR SHIP ROLLING IN RANDOM BEAM SEAS

Paul Kaplan

A description is given of an analytical method for determining nonlinear roll response and stability requirements for a ship in random beam seas. The nonlinearities considered are present in both the static restoring moment and the damping moment for roll motion, when considering only that mode of uncoupled motion. The forced motion response, as well as possible system limit cycle behavior, are determined by methods used in automatic control theory analyses (viz. describing function techniques). These limit cycle characteristics are established in terms of the random forced response rms amplitude, so that there is coupling between the forced response characteristics (hence the incident wave significant height) and the vessel inherent system dynamic properties. Conditions for stability of these possible limit cycle responses are also determined, leading to establishment of criteria for capsizing in terms of the basic ship linear and nonlinear dynamic properties as well as the incident random wave properties.

INTRODUCTION

The analytical treatment of ship stability problems, as considered in the present Conference, is primarily concerned with the roll mode of motion. Over a period of many years there has been an increasing emphasis on computational methods that have been aimed at predicting ship roll responses to various types of environmental disturbances, such as those due to wind and waves. The mathematical models have increased in complexity and include nonlinearities in the basic vessel dynamic representation, time-varying properties of important basic parameters, and representation of the stochastic (i.e. random) nature of wave excitation. The methods of analysis include frequency domain techniques and time domain simulation, as well as

fundamental determination of nonlinear system dynamic properties. Representative publications illustrating such approaches are included in the Proceedings of the earlier Stability Conferences [1], as well as in particular specific papers to be cited here in the present paper.

The mathematical analyses applied in this general subject area are usually related to two different problem areas; viz. the prediction of roll motion properties and also the simulation of capsize occurrence, with both areas considering wave disturbances. While both of these problem areas are important items, the results of such studies have their major applicability toward assessment of vessel seaworthiness but they do not directly lead to the establishment of stability criteria that can be used by designers and/or regulatory agencies.

In view of the major concern with ship stability and capsize phenomena, the present paper is aimed at presenting a theoretical analysis of nonlinear roll motion responses as well as stability requirements for a ship in a random beam sea. This analysis is a initial step, using certain approximate methods and/or approaches, for this particular illustrative case. The initial results indicate the prospect of utility of the approach, with a view toward further improvements in the procedures (as well as extension to other important practical cases) as a continuation of the basic methodology.

President, Hydromechanics, Inc.
State College, PA 16803, USA

ANALYSIS OF NONLINEAR ROLL RESPONSE

The particular case analyzed here is a ship at zero speed in random beam seas with a specified wave spectrum. It is assumed that only the roll mode of motion is considered, with that motion having nonlinear properties due to both nonlinear damping and restoring moment terms. The nonlinear damping is quadratic in form (actually proportional to the sign of the roll angular velocity), and the restoring moment is cubic in roll angle. The vessel also retains the conventional linear terms in both damping and restoration (i.e. roll "stiffness"). It is also assumed that the roll excitation due to waves is not dependent on the roll angle, and that it retains the conventional form proportional to wave slope. Since roll motion is lightly damped, the response is generally expected to be sharply tuned and narrow band in nature.

The roll equation of motion is then represented by

$$\ddot{\phi} + 2\zeta\omega_0\dot{\phi} + \beta\dot{\phi}|\dot{\phi}| + \omega_0^2\phi + \gamma\phi^3 = \omega_0^2 f(t) \quad (1)$$

where ω_0 is the linear roll natural frequency and the quantity $f(t)$ is a random function equivalent to the effective wave slope. This model is similar to other roll models studied previously (e.g. [2], [3]). The wave spectrum is represented by $S_\eta(\omega)$, and the spectrum of $f(t)$ is represented by

$$S_f(\omega) = \left[\frac{\omega^2}{g} e^{-\omega^2 T/2g} \right]^2 S_\eta(\omega) = \frac{\omega^4}{g^2} e^{-\omega^2 T/g} S_\eta(\omega) \quad (2)$$

where T is the average draft of the ship (the exponential term is included here to insure adequate attenuation of the effective wave slope for high frequencies).

The procedure to be used for determination of roll responses, as measured by the rms roll angle here, is by means of quasi-linearization using the concept of describing functions [4]. Approximating a nonlinear operation by a linear one, which depends on properties of the input, is defined here as quasi-linearization, and the approximating function is referred to as a describing function. When the input signal form to the nonlinearity is a random process, the procedure is termed "stochastic linearization". The basis for applying this method is the tendency of the random process to approach a Gaussian form

after passing through low pass linear filters (when viewing the roll motion model as a dynamic system, employing control system analysis terminology). Applying the method for sinusoidal periodic input signals results in what is called "harmonic linearization".

For the present case of a random sea input to the system, the motion equation is then represented by

$$\phi + (2\zeta\omega_0 + \beta N_1)\dot{\phi} + (\omega_0^2 + \gamma N_2)\phi = \omega_0^2 f(t) \quad (3)$$

where $N_1 = N_1(\sigma_\phi)$ and $N_2 = N_2(\sigma_\phi)$ are functions of the respective rms values of their input. This equation can be placed into "operator" form, using the Laplace transform operator variable s , and also represented in block diagram form as shown in Figure 1. Referring the system input (right hand side of Eq.(3)) as ϕ_i , the transfer function relationship is given by

$$\frac{\phi}{\phi_i} = \frac{G_1(s)}{1 + (\beta s N_1 + \gamma N_2) G_1(s)} \quad (4)$$

where

$$G_1(s) = \frac{1}{s^2 + 2\zeta\omega_0 s + \omega_0^2} \quad (5)$$

This transfer function relationship can be used for frequency response evaluations by the conventional replacement $s = i\omega$.

Expressions for describing functions for many common nonlinearities in control systems, as well as general functional forms, are given in [4]. For the present case of random inputs the describing function values are given by

$$N_1 = 2 \sqrt{\frac{2}{\pi}} \sigma_\phi, \quad N_2 = 3\sigma_\phi^2 \quad (6)$$

As a consequence of the narrow band nature of roll it can be shown that $\sigma_\phi = \omega_0 \sigma_\eta$. In a similar manner, the narrow band behavior allows interpretation of the system excitation (i.e. effective wave slope) spectrum to have a constant value corresponding to the value at the roll natural frequency, i.e. $\omega = \omega_0$. This is effectively equivalent to a white noise constant spectrum at the level corresponding to that frequency (see discussions in [2] and [3] covering this same procedure). Thus

$$S_{\eta}(\omega) \approx S_{\eta}(\omega_0) = \frac{\omega_0^4}{g^2} e^{-\omega_0^2 T/g} S_{\eta}(\omega_0) \quad (7)$$

for use in further evaluations in this paper.

From the governing equations above, it can be shown that the roll motion spectrum is given by

$$S_{\phi}(\omega) = \left| \frac{1}{(\omega_0^2 + 3\gamma\sigma_{\phi}^2) - \omega^2 + i(2\zeta\omega_0 + 2\sqrt{2/\pi} \beta\omega_0\sigma_{\phi})\omega} \right|^2 \cdot \omega_0^4 S_{\eta}(\omega_0) \quad (8)$$

which is dependent on σ_{ϕ} , the rms roll angle. The rms roll angle is found from the relation

$$\begin{aligned} \sigma_{\phi}^2 &= \int_0^{\infty} S_{\phi}(\omega) d\omega \\ &= \omega_0^4 S_{\eta}(\omega_0) \int_0^{\infty} \left| \frac{1}{(\omega_0^2 + 3\gamma\sigma_{\phi}^2) - \omega^2 + i(2\zeta\omega_0 + 2\sqrt{2/\pi} \beta\omega_0\sigma_{\phi})\omega} \right|^2 d\omega \\ &= \frac{\pi\omega_0^4 S_{\eta}(\omega_0)}{8\omega_0(\omega_0^2 + 3\gamma\sigma_{\phi}^2)(\zeta + \sqrt{2/\pi} \beta\sigma_{\phi})} \end{aligned} \quad (9)$$

from which the value of σ_{ϕ} is determined by numerical iteration.

In a number of studies involving nonlinear damping phenomena, the absolute square form of nonlinear damping used here has been found to be analytically difficult to use in some of the analyses (in the frequency domain) since that functional form was discontinuous (see [5]-[7]). That form was replaced by a fitted combination of a linear and cubic term, with the coefficients of the fit being functions of the particular motion variable rms (see [7] and [8]), given by

$$\dot{\phi} \left| \dot{\phi} \right| \approx \sqrt{\frac{2}{\pi}} \sigma_{\phi} \dot{\phi} + \sqrt{\frac{2}{\pi}} \dot{\phi}^3 / 3\sigma_{\phi} \quad (10)$$

The describing function for this representation is then

$$\begin{aligned} N_1 &= \sqrt{\frac{2}{\pi}} \sigma_{\phi} + \sqrt{\frac{2}{\pi}} \cdot \frac{3\sigma_{\phi}^2}{3\sigma_{\phi}} = 2\sqrt{\frac{2}{\pi}} \sigma_{\phi} \\ &= 2\sqrt{\frac{2}{\pi}} \omega_{\phi} \sigma_{\phi} \end{aligned} \quad (11)$$

which is exactly the same as the value found directly for the absolute square model. Thus, within this level of approximation, the replacement of the quadratic damping model by a cubic model (with the appropriate change in the linear term coefficient) leads to the same result for the system transfer function, spectrum and rms value. This result

applies in the case of finding the random response rms value by use of describing function or stochastic linearization techniques.

As an illustration of an actual calculation, a case similar to that treated in [2] is evaluated numerically. The parameter values applied here are $2\gamma=0.0675$, $\beta=0.08$, $\omega_0=4$ rad/sec., $S_{\eta}(\omega_0)=9$ cm.²-sec. The quantity $\gamma=-6.4$ rad.²/sec.² is negative, corresponding to a concave downward "softening" curve for the restoring moment (which is close to the actual form of roll restoring moment for larger angles). For these conditions the rms roll angle is found to be 0.285 rad.

STABILITY ANALYSIS

One of the properties of a nonlinear system is the possible existence of steady oscillations that can occur when there is no input excitation, with such oscillations also being independent of system initial conditions. These oscillations, which can occur in nonlinear systems that are dissipative and nonconservative (i.e. they contain damping terms) are denoted as limit cycles. The limit cycles have discrete values of amplitude and frequency that are possible for any nonlinear system, with such quantities being functions of the basic system parameters.

The existence, as well as the properties of a limit cycle oscillation are determined from analytical and/or graphical procedures applied to the basic system dynamic model. The issue of stability of limit cycle oscillations relates to the behavior of such motion following perturbations in the amplitude and/or frequency. The nature of such transient oscillations is the defining issue of the stability of the limit cycle, with an indication of unstable motion being considered (in the present ship context) as the initiation of capsizing.

The determination of a limit cycle is made using the linearized system dynamic representation in terms of describing functions, for the case with no external excitation. The describing functions are determined on the basis of assuming the presence of a periodic sinusoidal signal in the system, with that signal being of the form $A \sin(\omega t + \theta)$. The quantity A is the assumed limit cycle amplitude, and ω is the associated frequency.

The equation defining undamped oscillation is the system characteristic (operator form) equation. This is the equation resulting from setting the denominator of the transfer function in Eq. (4) equal to zero, which is

$$1 + (\beta s N_1 + \gamma N_2) G_1(s) = 0 \quad (12)$$

or

$$s^2 + (2\delta\omega_0 + \beta N_1)s + \omega_0^2 + \gamma N_2 = 0 \quad (13)$$

The describing functions N_1 and N_2 are functions of A and ω_i generally, but for the present type of nonlinearities they can be shown to be only amplitude dependent. Since a natural frequency is required to exist in this system, this is found to be

$$\begin{aligned} \omega_i^2 &= \omega_0^2 + \gamma N_2(A) \\ &= \omega_0^2 + \frac{3}{4} \gamma A^2 \end{aligned} \quad (14)$$

using the sinusoidal input describing function for a cubic nonlinearity given in [4].

Leaving aside the determination of the amplitude A in the above case, it is necessary to consider the important practical case where the system is forced by a random input and there is also the possibility of a limit cycle oscillation being present. In that case there are multiple input signals entering each nonlinear element, and the describing functions are then functions of such combined inputs, viz. the sum of a random signal and a sinusoidal signal. There are different describing functions in accordance with the nature of the analytical procedure being applied, i.e. whether the limit cycle conditions are being satisfied or the forced random response rms is being determined. In each case the separate describing function gain values are determined for the different type signal component of the total input. For the case of both a random signal and a sinusoid as the input, the describing function gain for the random component is denoted as N_R and that for the sinusoid as N_A . In each case these describing functions are functions of both the random input rms and the amplitude of the assumed sinusoidal signal.

$$s^2 + (2\gamma\omega_0 + \beta N_{1A})s + (\omega_0^2 + \gamma N_{2A}) = 0 \quad (15)$$

$$\sigma_\phi^2 = \omega_0^4 S_\phi(\omega_0) \int_0^\infty \frac{1}{(\omega_0^2 + \gamma N_{2R}) - \omega^2 + i(2\zeta\omega_0 + \beta N_{1R})\omega} d\omega \quad (16)$$

Values of the describing functions for N_2 are given in [4] as

$$N_{2A} = 3\sigma_\phi^2 + \frac{3}{4} A^2 \quad (17)$$

$$N_{2R} = 3\sigma_\phi^2 + \frac{3}{2} A^2 \quad (18)$$

The determination of the describing functions for the nonlinear damping is more complex, as discussed below.

The required describing functions, for an input to a nonlinearity that is the sum of a random function and a sinusoid, are defined by double integral operations in [4]. For the case of only a random function alone, the describing function for the quadratic damping form is relatively simple in form (and also to determine analytically) as shown by the result in Eq. (6). However, for the present multiple input case, the describing functions cannot be determined in closed analytic form for the quadratic damping nonlinearity. They must be found by involved numerical procedures, in terms of the normal probability integral function and associated integration operations, etc. For the purposes of illustration of overall methodology in the present paper, the approximate representation as a sum of a linear and a cubic function, as shown in Eq. (10), is used. That expression, which is a valid approximation for the case of a purely random function input, is applied to the present case of a multiple input operation. The describing functions for such a simple polynomial form are derived in [4], and are listed for use here by representing N_1 as

$$N_1 = \sqrt{\frac{2}{\pi}} \sigma_\phi + N'_1(\sigma_\phi, \omega_i A) \quad (19)$$

where

$$N'_{1A} = 3\sigma_\phi^2 + \frac{3}{4} (\omega_i A)^2 \quad (20)$$

$$N'_{1R} = 3\sigma_\phi^2 + \frac{3}{2} (\omega_i A)^2 \quad (21)$$

In the above expressions the arguments of the functions for N_1 are the representative amplitudes of velocity terms, which for the random function is σ_ϕ and for the sinusoid is $\omega_i A$. The further relations to be used are $\sigma_\phi = \omega_0 \sigma_\phi$, and the value of ω_i defined in Eq. (14).

Inserting the values of the describing functions N_{2A} , N_{2R} , N'_{1A} and N'_{1R} given above into Eq. (15) and (16) provides the relationships allowing determination of the random response as well as the limit cycle parameters. The solution is carried out in the present case by assuming the same value for σ_ϕ as was found for the pure random signal case, which then allows determination of the value of A , the limit cycle amplitude (as well as the frequency ω_c).

The characteristic equation defining the limit cycle properties, Eq. (15), can be separated into real and imaginary parts (denoted as U and V) when the substitution $s=i\omega$ is made. The stability of the limit cycle oscillation is determined by a quasi-static analysis that ignores terms related to the time rate of change of frequency and amplitude variations following the assumption of small perturbations in the limit cycle equilibrium state. The stability requirement by this type of quasi-static analysis (see [4]) is given by

$$\frac{\partial U}{\partial A} \frac{\partial V}{\partial \omega} - \frac{\partial U}{\partial \omega} \frac{\partial V}{\partial A} > 0 \quad (22)$$

where each of the derivative terms is evaluated at the equilibrium state value of $A=A_0$, $\omega=\omega_0$. For the present case of ship roll motion that reduces to

$$\begin{aligned} & \frac{3}{2} \gamma [2\zeta\omega_0^2\sigma_\phi + \beta\sqrt{\frac{2}{\pi}}(2\omega_0^2\sigma_\phi^2 + \frac{1}{4}\omega_0^2A_0^2)] \\ & + \beta\sqrt{\frac{2}{\pi}}\omega_0^4 > 0 \end{aligned} \quad (23)$$

Computations were carried out for the case described previously, where the value of $\sigma_\phi=0.285$ rad. was found using the parameters cited there with the spectral value $S_\eta(\omega_0)=9$ cm²-sec. This condition was found to be stable, and similarly for the case with $S_\eta(\omega_0)=18$ cm²-sec. and $\sigma_\phi=0.4$ rad. With the wave spectrum ordinate $S_\eta(\omega_0)=27$ cm²-sec., where the value of $\sigma_\phi=0.5$ rad., it was found that the system was unstable (the value of $A_0 \approx 0.1$ rad. was found for this case).

DISCUSSION OF RESULTS

The preceding analysis illustrates the presence of an unstable motion, arising from limit cycle behavior, for a condition wherein a random continuous response was also present. This unstable condition occurred for the system when the level of the

external excitation, and the resultant random response properties (represented by the rms value σ_ϕ), became large enough to result in an unstable condition. This unstable condition can be viewed as indicating capsizing occurrence under these conditions. While this condition ($\sigma_\phi=0.5$ rad.) is relatively large, the analysis did not exhibit an instability for $\sigma_\phi=0.4$ rad., which is also a relatively large rolling motion condition.

The method used here to predict rms roll motion in the case of random waves, by the use of describing functions in a stochastic linearization method, is a generally accepted approach (within that level of approximation) which yields results consistent with other investigations (e.g. [2], [3]). However the stability analysis represents a further extension of such methods, with a general question as to the extent of its validity and/or the limits of such an analytical procedure. The quasi-static method of limit cycle stability analysis used here is an approximate method that ignores the presence of terms involving the time rate of change of frequency and amplitude in the analysis of perturbation response.

An extended analysis can be made with consideration of such terms in order to check that the stability limits determined by the quasi-static method are valid, but that is beyond the scope of the present paper. In addition a more precise assessment could possibly be made by use of the direct describing functions for N_{1A} and N_{1R} , which would have to be found by more extensive numerical evaluation for the case where the actual quadratic (with sign) damping functional form was used rather than the representation by a combined linear and cubic model used here.

The conditions for stability outlined here show that the system would only indicate instability for negative values of the parameter γ , which is the coefficient of the cubic term in the restoring moment. The use of such an expression for the restoring moment is an approximation of the total restoring moment of a ship (up to 90° inclination), with its specific form alone resulting in a model of the vessel dynamics which is similar to the classic nonlinear Duffing equation with damping (see [9]).

For the particular case studied here, the frequency response amplitude function for the roll response is expected to be similar to that in Figure 2. This is a condition for a soft spring response, which can exhibit unstable motion, "jump" phenomena, etc. [9].

A more complete representation of the restoring moment using higher order odd-power polynomial terms (ϕ^5 , ϕ^7 , etc.) could also be treated by the present method, with the stability conditions determined in terms of all of the parameters needed for the restoring moment model. Another possible extension of the present analysis would be the inclusion of a steady wind disturbance, which would require consideration of an additional signal to be present that would correspond to a steady bias value. The analysis in [4] considers the possibility of such a signal, in addition to the random signal and (limit cycle) sinusoid considered previously. The analysis can proceed by replacing the original nonlinear system by three quasi-linear systems, with each one processing each signal form. There are then three different describing functions, which are dependent on the magnitude of the bias, the amplitude of the sinusoid, and the rms of the random signal, with interdependent relations between the different describing functions and the major input signal variables. Simultaneous solution of the three equation relations that result will provide the representative system response measures, as well as the stability conditions.

Further applications of the present approach can be made for the case where the wind disturbance also includes gust effects, with a given wind velocity spectrum, which can be combined with the wave-induced disturbance. The basic procedure can also be applied to a ship at some forward speed, at an arbitrary heading angle (assumed to be relatively constant), as long as the roll motion equation can be established as a separate single degree of freedom equation without explicit coupling (but assuming any coupling effects are incorporated into the resulting roll equation of motion). Another item to be considered is a higher approximation to the describing function representations used here, as illustrated in [10]. This could be considered as an analogous extension to the random sea case as was the second order expansion technique given in [11] for the case of sinusoidal wave excitation.

On the basis of the above, there appears to be a number of useful extensions and/or applications of the present technique that can be useful for ship stability investigations. The results that are obtained from such procedures are in a more explicit form that can be used to establish stability criteria in terms of simple parameters representing the basic ship static and dynamic properties, as well as those due to the disturbing environments of wind and waves. This is a distinct advantage of the present analysis, in contrast to complex time domain simulation studies. That type of investigation can still be useful in order to check the validity of the present simpler predictions of response magnitudes and stability, resulting in a cohesive approach for this problem area that uses all of the available techniques developed for this field.

CONCLUSIONS

The describing function technique exhibited here has the capability of providing a useful statistical measure of roll response to seaway disturbances, as well as for determining stability characteristics defining the onset of capsize for beam sea operation. The response determination, as well as the stability conditions, are expressed in a form that allows establishment of stability criteria in a simplified form in terms of the vessel properties and the seaway characteristics. A number of further extension to more realistic operating conditions, as well as more practical representations of ship properties, and also more refined approximations and computational procedures are outlined in the paper for use of the methods described herein.

REFERENCES

1. Proc. 1st, 2nd and 3rd Int. Conf. on Stability of Ships and Ocean Vehicles, 1975, 1982, 1986.
2. Kaplan, P.: "Lecture Notes on Nonlinear Theory of Ship Roll Motion in a Random Seaway," Proc. 11th ITTC, Tokyo, 1966.
3. Vassilopoulos, L.: "Ship Rolling at Zero Speed in Random Beam Seas with Nonlinear Damping and Restoration," *Jnl. of Ship Research*, Dec. 1971.

4. Gelb, A. and Vander Velde, W.E.: Multiple-Input Describing Functions and Nonlinear System Design, McGraw-Hill Book Co., 1968.
5. Vassilopoulos, L.: "The Application of Statistical Theory of Nonlinear Systems to Ship Motion Performance in Random Seas," Int. Shipbuilding Progress, Feb. 1967.
6. Dalzell, J.F.: "Note on the Form of Ship Roll Damping," Jnl. of Ship Research, Sept. 1978.
7. Dunwoody, A.b. and Vandiver, J.K.: "The Influence of Separated Flow Drag on the Dynamic Response of Offshore Structures to Random Waves," Proc. Int. Symp. on Hydrodynamics in Ocean Eng., Trondheim, Norway, August 1981.
8. Bendat, J.S.: "Nonlinear System Dynamic Analysis Using Random Data," U.S. Naval Civil Eng. Lab. Rpt. CR-85.006, March 1985.
9. Minorsky, N.: Nonlinear Oscillations, D. Van Nostrand Co., Inc., 1962.
10. Graham, D. and McRuer, D.: Analysis of Nonlinear Control Systems, John Wiley & Sons, Inc., 1961.
11. Nayfeh, A.H. and Khdeir, A.A.: "Nonlinear Rolling of Ships in Regular Beam Seas," Int. Shipbuilding Progress, Feb. 1986.

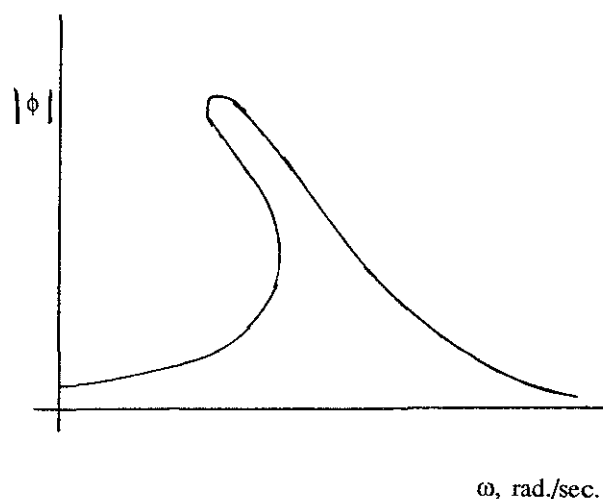


Fig. 2 Response amplitude of softening system as a function of excitation frequency

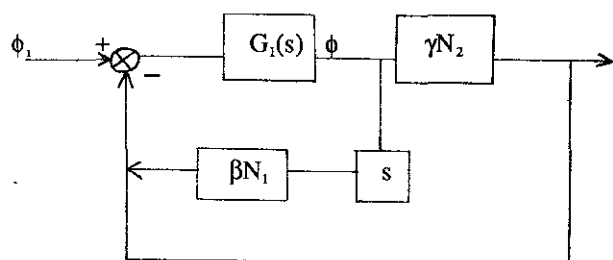


Fig. 1 Equivalent block diagram for roll motion closed loop system

STABILITY OF DAMAGED SHIP DURING SHIP MOTIONS IN WAVES

by N.N. Rakhmanin *

ABSTRACT

The paper describes the results obtained from the analysis of the problem of variation in the draft, heel, and stability of damaged ship during its motions in waves. By a damaged ship is meant one not only with flooded compartments but also with shifting of cargo. Consideration is given to a widespread case when the damaged ship has no way and is beam to the sea. The analysis is based on the study of cross-coupled equations of ship motions in transverse plane where account is taken of the asymmetry of stability curve in the presence of static heel and of the consequences of systematic shipping of green water on deck of a damaged ship with a low freeboard. By studying her rolling stability, the relationship between the safe level of damaged static stability and the sea state was established. It is believed that the wind action is not the decisive factor in decreasing the reserve of damaged stability and that the account of the wind effect may be taken, if necessary, by analogy with the intact ship.

INTRODUCTION

By tradition the term "damaged ship" is associated with the flooding of one or several compartments. Survival of ship in this state depends on a rational solution of the subdivision problem. The latter contains two key issues. One consists in the assessment of draft, list, trim and stability of the ship when flooded. The other consists in the assessment of the degree of safety of a damaged ship with the given residual buoyancy and damage stability.

So far the first problem has been solved by the statics of the ship methods proceeding from the assumption that the damaged ship is afloat in calm water. The second issue is treated with various degrees of detailing in accordance with the accepted approach to solution of the subdivision problem.

According to the widespread deterministic approach the degree of safety of a damaged ship is specified on the basis of common sense. The main idea in this case consists in that the damage stability should retain positive values within a range of heeling angles. This serves as a guarantee of

* Krylov Ship Research Institute, Leningrad, USSR.

safety for a damaged ship in calm water but at the same time it involves arbitrary decisions when damage stability requirements are worked out. At the same time the question of which state of the sea surface is to be taken as calm water remains open.

The probabilistic approach to this problem requires more clarity in so far as the assessment of the safety of ship after flooding is concerned [1]. Among other things, there is a need for establishing the relationship between the state of the sea surface (sea severity) and the minimum value of the generalized damage stability characteristic which allows the ship to avoid capsizing in the given environmental conditions. This relationship makes it possible to define the probability of the ship's survival under specified flooding conditions as the probability of the ship's finding itself in the waves whose energy level is lower than the minimum energy level of the waves capable of capsizing the damaged ship under consideration.

Finding the relationship in question is a difficult problem. Capsizing is a particularly nonlinear phenomenon and has a variety of modes. The mechanism of this hazardous phenomenon is as yet imperfectly understood in all cases. Besides, capsizing is an extraordinary event that rarely occurs. Consequently, it is unlikely that proper damage stability statistics can be made on the basis of full-scale data. For these reasons the well-known attempts to estimate the above-mentioned relationship between the sea state, ship stability and residual buoyancy in case of flooding were associated with

the model experiment performed for studying the minimum damage stability which is essential for the survival of a damaged ship in waves [3], [4].

In the present paper the interpretation of the term "damaged ship" is extended. It is suggested that in addition to ships with flooded compartments this term should include ships with shifted cargoes. The displacement of such a vessel will remain unchanged, but having a larger static heel it is subjected to a more intensive rolling, it may prove disabled and find itself in a situation as dangerous as that of a ship with flooded compartments.

The main safety problems of the damaged ship understood in this way are investigated in terms of its dynamics in waves on the basis of the nonlinear cross-coupled equations of ship motions set up to fit the approximate hydrodynamic theory of finite amplitude roll. In doing so it is shown that (a) the draft, heel and damage stability values of a ship rolling in waves may differ from those in calm water and that (b) the solution of the second problem (i.e. the assessment of the ship's safety in waves) requires an investigation into the rolling stability affected by the finite value disturbances.

MAIN GROUNDS FOR THE ANALYSIS

In order to study the damaged ship survival problem theoretically it is necessary to use a representative mathematical model of its behaviour in waves. The model should represent: (a) the typical features of the static stability curve for a damaged ship, (b) a hazardous situation in respect of the interaction

with incident waves, (c) typical reasons for a change in average parameters of the draft, heel and damage stability during ship motions in waves.

An important distinguishing feature of the damage stability curve is the asymmetry of its port and starboard branches in the presence of static heel. In the most serious cases of damage the angles of heel may be as large as 20° - 30° .

In respect of the hazardous situation, a damaged ship is supposed to have no way. In this case, following the accident, it turns around rapidly and drifts beam-on to the waves. Drifting in the absence of trim proves to be the most vulnerable from the point of view of safety. The situation was adequately substantiated with experimental data [3], [4].

As regards the reasons of change in the mean draft, static heel and stability of the damaged ship which are assumed to be known from calculation of statics for calm water conditions, there are just a few of them. Among these are, firstly, ship motions, secondly, asymmetric distribution of the damage stability reserve when the ship is inclined to port or starboard, and thirdly, accumulation of a large amount of green water on the upper deck due to systematic shipping of same. The latter circumstance is characteristic for ships with a minimum of freeboard or close to that. Many types of passenger or cargo vessels may find themselves in such conditions, being symmetrically flooded.

In conclusion let us direct our attention to the fact that no special consideration is given in

this paper to taking into account the fluid dynamics in the flooded compartments. This does not mean, however, that the liquid cargo effects should be ignored. Quite the reverse-special studies [9] show that in the presence of free surface the liquid cargoes in compartments exert influence on all the dynamic characteristics of the ship, such as inertia, resistance to motions, stability and exciting forces. These effects can be taken into account by using a number of corrections to relevant coefficients in the equations. As a result, in treating the dynamics of ship both with or without flooded compartments, provided the damage is due to shifting of cargo, the equations of ship motions can be taken to be equal in form (structure) without detriment to the quality of analysis.

EQUATIONS OF MOTIONS

For the analysis of dynamic behaviour of a damaged ship in waves differential equations of motions are suggested which are developed within the framework of an approximate hydrodynamic theory of motions with a finite amplitude 6. This theory is based on a number of assumptions which make it possible to benefit from the principal advantage of the linear hydrodynamic theory which consists in a breakdown of forces into categories. Most of the forces including inertial/damping forces and all components of exciting forces are determined using the rules of the linear theory. The restoring forces are an exception. When these forces are calculated, excessive hydromechanical pressures should be integrated over an instantaneous wetted surface with allowance for the fact that the

angles of damaged ship inclinations are finite.

An additional feature of the nonlinear interaction of an oscillating ship and green water is that time-independent exciting forces and moments can arise in principle. When oscillations of a low-freeboard ship or a damaged ship of low residual buoyancy are considered the forces of this category have the first order of small value. For a ship drifting in beam seas the main reason giving rise to these forces is accumulation of sea water when the deck is regularly washed over by waves and entrapped water does not drain away in time between two

successive wave encounters [7]. A constant heeling moment of a finite magnitude is also generated due to shifting of cargo in holds. Thus a general representation of the structure of exciting forces for the damaged ship case is more complex than that for the intact ship case.

The sway and heave of a damaged ship drifting in beam seas are described by linear differential equations with sufficient accuracy required for practical calculations [8]. Therefore, only the nonlinear roll equation is given below, which reflects all principal features of the dynamic behaviour exhibited by such ships in waves

$$\begin{aligned} (A_x + A_{44})\ddot{\tilde{\theta}} + B_{44}\dot{\tilde{\theta}} + F_4^{yz} + \int V_o \cdot GZ(\tilde{\theta}, \tilde{z}, \theta_s) = \\ = F_4^{cw} + F_4^w(t) - \int S_{w0}^E \left[(y_f^E - y_p) \cos \theta_s - (z_f^E - z_p) \sin \theta_s \right] \tilde{z}(t); \end{aligned} \quad (1)$$

$$F_4^{yz} = A_{42} \ddot{\tilde{y}} + B_{42} \dot{\tilde{y}} + A_{43} \ddot{\tilde{z}} + B_{43} \dot{\tilde{z}}; \quad (2)$$

$$\begin{aligned} F_4^R = \int V_o \cdot GZ[\tilde{\theta}(t), \tilde{z}(t), \theta_s] = \\ = \int V_o \left\{ \left[G M_o + y_p \sin \theta_s + \tilde{z}(t) \frac{S_{w0}^E}{V_o} (\tilde{p}_s + z_p - z_f^E) \cos \theta_s \right] \tilde{\theta} + \right. \\ \left. + h_o \tilde{\theta}^2 + \sum_{n=1}^{\infty} (-1)^n \left[h_n + \frac{y_p \sin \theta_s}{(2n+1)!} \right] \tilde{\theta}^{2n+1} - y_p \cos \theta_s \cos \tilde{\theta} \right\}; \end{aligned} \quad (3)$$

$$F_4^{cw} = p_w \cdot \lambda_w = \left[(y_w - y_f^E) \cos \theta_s - (z_w - z_f^E) \sin \theta_s \right] p_w; \quad (4)$$

$$F_4^w = (F_{14}^{00} \pm F_{14}^{0B}) \cos 6t - (F_{24}^{00} \pm F_{24}^{0B}) \sin 6t. \quad (5)$$

Two fixed coordinate systems are used in the relations given above. The first system, $O\tilde{x}\tilde{y}\tilde{z}$ is tied to the painted waterline of the ship at a static heeling angle θ_{st} ($O\tilde{x}$ - axis is directed to the bow, $O\tilde{y}$ - axis - to the starboard, $O\tilde{z}$ - axis is positive downwards normal to undisturbed free surface). The second moving coordinate system $Oxyz$ is tied to the waterline of the upright ship.

The guidances for calculating the weight of water entrapped on deck P_w , its coordinates (y_w, z_w) given in formula (4) and components of exciting forces from (5) can be found in Ref. [7], [5], [6], respectively.

It is seen that roll equation (1) coupled with other types of motions (2) by cross terms has to retain at least the terms accounting for nonlinearities in the restoring moment and damping moment. Investigations show that these factors are of fundamental importance for the prediction of roll stability and capsizing risks.

From (1) and (3) it follows that the relative heave has a considerable effect on the roll of the damaged ship. Firstly, this effect shows itself in a high variability (1-st order of small value) of the restoring moment (3), secondly, it gives rise to an additional exciting moment described by the last term in the right-hand part of (1).

On the whole the conditions mentioned above lead to a subharmonic build-up of ship oscillations in the frequency range corresponding to severe heaving. At a static heeling angle θ_{st} the threshold of parametric resonance is significantly lower because the depth of amplitude modulation of the re-

storing moment is increased (in this case $\tilde{p}_s \neq 0$). The severity of subharmonic oscillations experienced by the heeled models can be significantly higher than that of the upright models [8].

The validity of the mathematical model of the damaged ship motions in transverse plane is proved by satisfactory agreement between the results of motions calculations and the data obtained by experiments conducted to study complex subharmonic oscillations of a ship model in the presence of a pseudo-static heel [8].

Finally, it should be noted that the suggested roll equation also reflects the fact that the ship having some static heel is subjected to different exciting forces when the sea direction is reversed. This is treated in more detail in [5], [6].

ROLLING STABILITY OF A HEELED SHIP

If a heeled ship is not subject to shipping of green water then the risk of capsizing is attributed to the fact that the damaged stability curve is unsymmetrical and has the form given in fig.1.

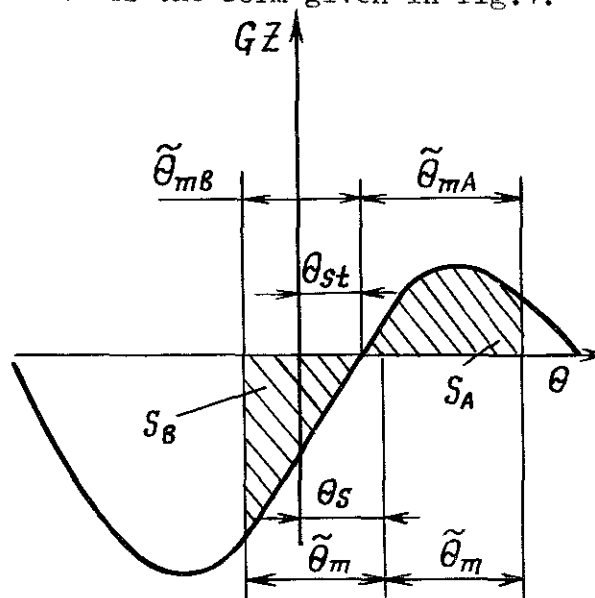


Fig.1. Unsymmetrical damaged stability curve

In the cases when the maximum kinetic energy of roll

$$T_{\max} \sim \frac{1}{2} (A_x + A_{44}) \cdot D_{\dot{\theta}} \quad (6)$$

is less than the minimum reserve of damaged ship dynamic stability

$$U_{\max}^A \sim \gamma V_0 GZ_m^A \theta_{\max}^A \sim S_A \quad (7)$$

the roll behaviour of the ship satisfies the condition of dynamic equilibrium (fig.1) when

$$S_A = S_B.$$

In this case an effect of pseudo-static inclination arises due to which the mean heeling angle in motions is different from the static heeling angle θ_{st} in calm water

$$\theta_s = \theta_{st} + \theta_{mA} - \frac{2\tilde{\theta}_m}{2}. \quad (8)$$

When the kinetic energy of roll reaches the limit of the potential reserve of positive damaged ship stability

$$T_{\max} \geq U_{\max}^A \quad (9)$$

or in terms of fig.1.

$$S_B \geq S_A$$

the pseudoheel may increase indefinitely. Condition (9) means that the rolling process becomes unstable and the ship must capsize. The character of roll is not so important, more essential is the roll severity.

This dynamic mode of capsizing was checked using an analog computer and found valid on the basis of three cross-coupled equations including (1). The irregular input process at each of the three inputs of this set of equations was

simulated by one harmonic with a frequency corresponding to the peak of the irregular wave spectrum of a given severity and an amplitude equal to the amplitude of irregular process with an exceeding probability of 20 %.

The stability of the rolling mode thus prescribed was checked using the method of finite disturbances suggested by A.Tondl [10] and based on the variation of initial conditions for analog computation of the equations in time domain. The maximum limits of finite disturbances were found from the following conditions:

$$\begin{aligned} \frac{(\tilde{\theta}_m)_{t=0}}{\tilde{\theta}_m} &\leq \frac{H_{3\%}}{H_{20\%}}; \\ \frac{(\dot{\tilde{\theta}}_m)_{t=0}}{\dot{\tilde{\theta}}_m} &\leq \frac{H_{3\%}}{H_{20\%}}, \end{aligned} \quad (10)$$

where $\tilde{\theta}_m$ and $\dot{\tilde{\theta}}_m$ - amplitude values of angular displacement and its velocity in a given stationary mode of rolling.

The risk of capsizing was assessed for ships with unsymmetrical stability curves of various maximum stability arms GZ_m and vanishing points in order to obtain data of practical interest. Fig.2 shows the studied versions of stability curve. The initial metacentric height, static heeling angle and nondimensional coefficient of roll damping were assumed the same for all cases covered by the numerical experiment and equal to 0.75 m, 15°, 0.20, respectively. The part of the stability curve corresponding to the inclination on the opposite side of the ship was assumed linear

with an error to the advantage of safety.

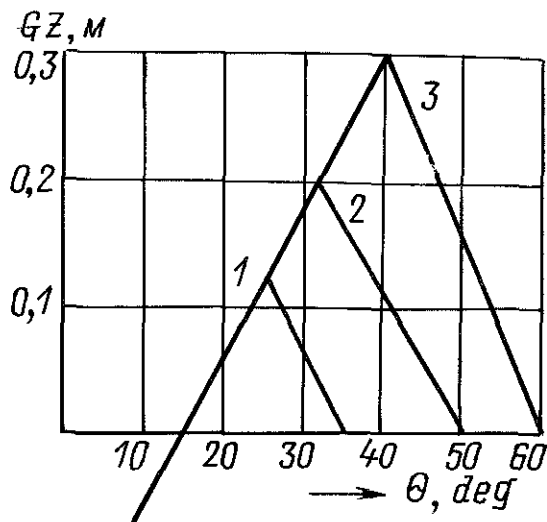


Fig. 2. The versions of the unsymmetrical damaged stability curve under study

The selected characteristics of the curve make it possible, on the one hand, to assess the USSR Register of Shipping requirements concerning the stability of damaged ships (1-st version of the curve), on the other hand, to judge the safety level of a large group of 3000-10000 m³ displacement high-freeboard ships which have relatively high values of meta-centric height and other stability characteristics corresponding to the 2-nd and 3-rd versions of the curve (fig. 2).

Based on the results of rolling stability studies obtained for various sea states an interesting plot was constructed where the safe zone of damaged stability was separated from the hazardous one (fig. 3). The maximum arm of the damaged stability curve GZ_m was taken as a generalized characteristic of stability. It is seen that the damaged stability curve complying with the requirements of

the USSR Register of Shipping ($GZ_m = 0.10$ m) ensures the safety of the damaged ship in sea states not over number 4.

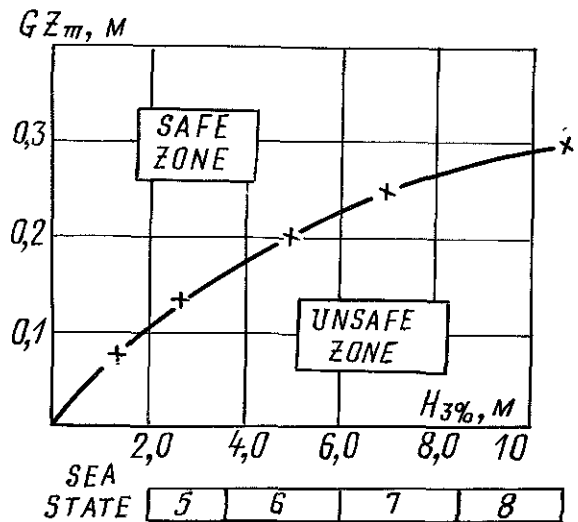


Fig. 3. Safe level of stability for a damaged high-freeboard ship

ROLLING STABILITY OF A SHIP IN UPRIGHT CONDITIONS

The mechanism of a pseudostatic inclination experienced by a damaged ship in the case discussed is mainly considered as the result of systematic shipping of green water. Accumulation of sea water on deck during ship motions in waves results in a special heeling moment (4), and the following formula is suggested to determine the arm of this moment [7]

$$\delta GZ_w = - \frac{p_w}{\delta V_0 + p_w} \left[\lambda_w(\theta) + GZ(\theta) \right], \quad (11)$$

where $GZ(\theta)$ - the righting arm of the static stability curve of the damaged ship in calm water when no water, p_w , entrapped on deck. Fig. 4 shows limiting curves of heeling arms due to water on deck

for a flush-deck ship (the lower curve) and a ship with a high bulwark in extreme conditions [8]. The curves are calculated basing on the following proportions B/d 2.1-2.3 and D/d 1.15-1.30 characteristic of the ships whose models were tested in damaged conditions in waves [3], [4].

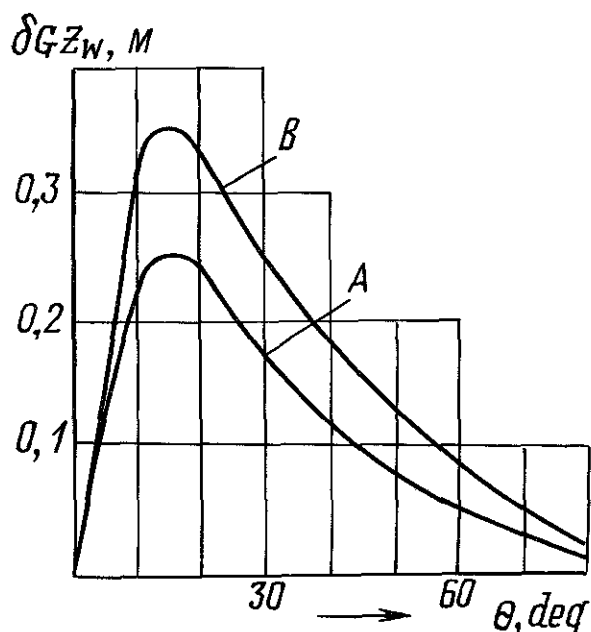


Fig.4. Limiting curves of reduced heeling arms due to water on deck (A - flush-deck ship, B - ship with a bulwark)

The graphic/analytic method suggested in [7] for finding the pseudostatic heel in the considered case can be successfully used to estimate the heel and stability of the damaged ship. The method provides good agreement with the experiment [7] and opens up a possibility for assessing the main characteristics of the minimum safe stability curve of the damaged ship which prevents capsizing in a given sea state.

The investigation into the stability of rolling of a low-freeboard ship using the method of A. Tondl [10] reveals that it is characteristic of these curves that

the pseudoheel of an oscillating ship θ_s tends to the heeling angle θ_{max} corresponding to the maximum arm of the curve. Fig.5 gives an illustration of such curves.

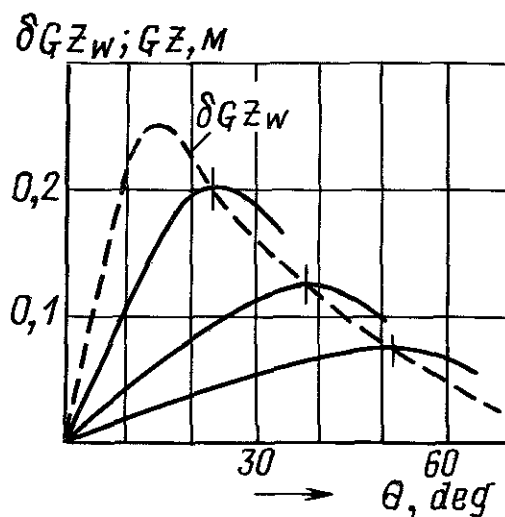


Fig.5. Definition of minimum safe stability curve for a low-freeboard ship

Considering the above definition of the minimum safe stability curve, one can indicate permissible maximum righting arms of the damaged stability curve GZ_m required to avoid capsizing of the damaged ship in high sea states when shipping of green water occur in the most intensive way. These data are determined from the curves of fig.4 and given in the table below.

Naturally, for lower sea states the requirements to the parameters of the minimum safe stability curve of the damaged ship should be less strict. It is proved by the model test data [3], [4]. Analysis of the model test data using the maximum arm GZ_m as a generalized parameter of residual buoyancy and damaged stability made it possible to arrange the results and to obtain an important plot of the safe level of damaged stability versus the sea state in irregular waves.

Table 1. Characteristics of the minimum safe stability curve of the damaged ship

At	$\theta_{\max} = 15^\circ$	$0.25 < GZ_m \leq 0.35$
At	$\theta_{\max} = 30^\circ$	$0.16 < GZ_m \leq 0.25$
At	$\theta_{\max} = 45^\circ$	$0.10 < GZ_m \leq 0.16$

The plot is given in fig.6 and corresponds to the case of a symmetrically flooded ship freely drifting with its damaged side beam-on to seas and systematically shipping green water.

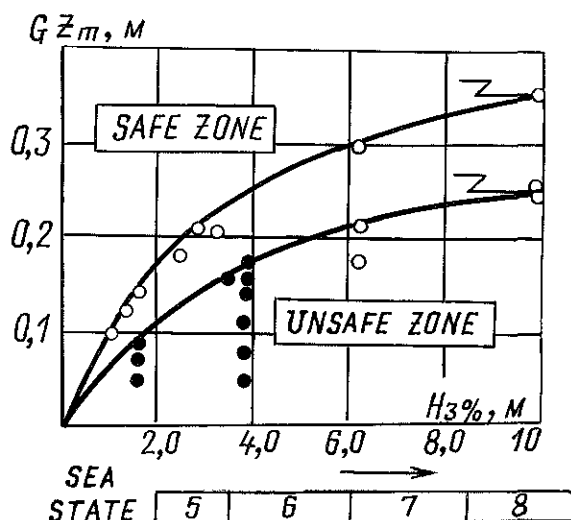


Fig.6. Safe level of stability for a damaged low-freeboard ship in waves (● - U.S. tests, ○ - U.K. tests)

Note that this plot agrees well with the data of Table 1 referring to extremely high sea states.

Table 1 gives practically the same values of the maximum arm GZ_m as those found from the experimental curves of fig.6 in sea state 8 for the case when GZ_m of the minimum safe stability curve is in the range of heeling angles from 10° to 20° which is characteristic of the models of a Mariner-type ship [3] and car ferry [4] tested on even keel. The lower curve corresponds to the conditions of the tests conducted in the USA [2] when a

flush-deck model without a bulwark was tested. The higher curve refers to a car ferry model from the U.K. tests [4]. In damaged conditions this model represents a low-freeboard ship with a bulwark of an infinite height.

CONCLUSION

The methods proposed for the calculation of pseudoheel solve the problem of predicting draft, heel and damage stability of a damaged ship during free drift in waves. These methods were used for an analysis of the materials covering the results of experimental studies on the safety of low-freeboard ships in regular waves [7] and damaged ships in irregular waves [3], [4]. Among other things, the methods gave the clue to understanding the mechanism of the damage ship capsizing, thus making it possible to obtain information needed for the assessment of the possibility of survival for such a ship with the given residual buoyancy and damage stability. It has been found that the maximum arm of the damage stability curve may be taken as a criterion of safety for a damaged ship drifting in waves.

NOMENCLATURE

a) Main particulars

B - breadth,

D - depth,

d - draft,

V_o - volume displacement in calm water,

S_{wo}^E - mean value of waterplane area at an angle of heel
 y_j^E, z_j^E - mean value of coordinates of the center of floatation in the second ship-fixed coordinate system
 $\tilde{\rho}_s$ - radius of floatation curve of a heeled ship
 θ_{st} - static heeling angle
 θ - heeling angle corresponding to the maximum of the stability curve
 GM_o - initial metacentric height
 ζ_z, ζ_m - current and maximum righting arm of static stability curve
 b) Characteristics of ship's dynamic behaviour
 A_x - transverse moment of inertia of ship mass
 y_p, z_p - coordinates of ship's gravity center in the second ship-fixed coordinate system
 A_{ij} - added-mass coefficients
 B_{ij} - damping coefficients
 F_i^w - variable exciting forces
 F_i^{cw} - constant components of exciting forces
 F_i^R - restoring forces
 c) Characteristics of waves and ship motions
 σ - wave encounter frequency
 $H_p\%$ - wave height with an exceeding probability p %
 \tilde{Y}, \tilde{Z} - instantaneous horizontal and vertical displacements of ship relative to wave surface
 θ_s - pseudostatic heeling angle
 $\tilde{\theta}$ - variation in heeling angle of ship in motions
 θ - current value of absolute heeling angle
 γ - volume weight of water
 t - time

D_ϕ - variance of angular velocity of ship motions
 T - kinetic energy
 U - potential energy

REFERENCES

1. I.B.Robertson, G.C.Nickum, R.I.Price, E.H.Middleton - The Now Equivalent International Regulations on Subdivision and Stability of Passenger Ships, Trans. SNAME, Vol.82, 1974, pp.344-381.
2. E.Numata - Tests of a Damage Stability Model in Waves, Annexed to IMCO document SDS-IV/5, delegation USA, 6 May 1965.
3. E.H.Middleton, E.Numata - Tests of a Damage Stability Model in Waves, SNAME Spring Meeting, paper N 7, April 1970.
4. H.Bird, R.P.Brown - Damage Stability Model Experiments, RINA Spring Meeting, 1973.
5. C.M.Lee, Ki-Han Kim - Prediction of Motion of Ships in Damage Condition in Waves, The 2nd Int. Conf. on Stability of Ships and Ocean Vehicles, Tokyo, 1982, pp.287-301.
6. V.V.Lugovski - Hydrodynamics of nonlinear ship motions (In Russian) Sudostroenie, M., 1980, p.255.
7. N.N.Rakhmanin - Constant Heeling Forces and their Effect upon the Stability of a Low-built Vessel in waves, The 2nd Int. Conf. on Stability of Ships and Ocean Vehicles, Tokyo, 1982, pp.15-24.
8. N.N.Rakhmanin - Rolling Motion and Stability of a Heeled Ship Freely Drifting in Waves, Scient. and Method. Seminar on Ship Hydrodynamics, 18th Session Proceedings, Vol.II, Varna, Sept.1989, pp.II.60.
9. N.N.Rakhmanin - Dynamics of Ship with a Well in a Seaway, The 4th Int. Symp. on Pract. Design of Ships and Mobile Units, Proceedings, Vol.3, Varna, Bulgaria, Oct.1989, pp.96-(1-7).
10. A.Tondl - Nonlinear oscillations of mechanical systems (In Russian) Izd-vo Mir, Moscow, 1973, p.334.

Abstract - This paper documents the application of a new method for deriving design excitations that can be used to assess the dynamic stability of ships. The method is based on the concept of mapping a weighted response of a dynamic system under study from a random domain to a deterministic domain. The key benefit of adopting the proposed approach is to include information about the dynamics of systems into the development of "design excitations". This ensures that the characteristics of both the environment and the dynamic system influence the derived excitation. The results of the study propose an empirical formulation that produces a design excitation for assessing the dynamic stability of vessels that operate in the southern North Sea. The proposed empirical formulation is compared with other "design waves" that have been developed over the years, and comparisons are drawn.

INTRODUCTION

In all branches of engineering the importance of predicting the response of dynamic systems to realistic excitations cannot be over-emphasized. With the advent of powerful computers the level of complexity of the models used to describe dynamic systems has been drastically increased. So much so, that the amount of time required to calculate representative responses can often be prohibitively long.

It has long been realised that the use of "design" excitations that represent the environment can reduce the amount of calculation required to provide representative responses.

The problem with considering design excitations based solely on environmental characteristics is that the important properties of the dynamic system are neglected, that is, their preferential response to excitations of specific frequencies. What is needed is a simple form of excitation that is equivalent to the excitation that would occur within a random environment, and also contain information of how the system would respond to the range of frequencies present.

This paper utilizes a theoretical development, and in so doing, develops an equivalent excitation to be used for assessing the dynamic stability of ships that replaces the complex wind and wave environment in which the vessels operate. The resulting excitation is dependent on fundamental vessel parameters, therefore, a number of vessels are examined in order to develop an equivalent excitation that is applicable over a range of vessel sizes.

The outcome of the research is the proposal of empirical formulae based on both vessel and environmental parameters. Finally, comparisons are drawn between this new equivalent excitation and other "design waves" that have been developed over the years.

THE NEED FOR AN IMPROVED EXCITATION

The effective modelling of complicated dynamic systems is a time consuming and expensive task. Over the years, it has been realised in many fields of engineering that any reduction in computation time while retaining the integrity of results was an important step in improving speed and therefore cost effectiveness. Hence, the concept of "design excitations" was developed.

These were specially developed excitations or loading that embodied the types of excitation a given system would be likely to experience during its operational lifetime, but in a much reduced time-scale.

Dr. Alexander : British Telecom Research Laboratories, Martlesham Heath, Ipswich IP5 7RE, U.K.

Dr. Vassalos : Department of Mechanical and Process Engineering, University of Strathclyde, Glasgow G2, U.K.

The basic problem with this type of approach is due to the fact that although much research effort had been made in the areas of deriving representative excitations, very little thought had been given to the area of incorporating the dynamic characteristics of the system under study into the analysis. Clearly, it must be obvious that if (in a simple linear example) the dynamic system is completely de-tuned from the excitation environment, then performing an analysis based on representative information from the environment is likely to prove unfruitful.

This idea is not new. Earthquake safety regulations [1] have already recognized that the relative probabilities of occurrence of earthquakes of different magnitudes should be taken into consideration. This probability variation has been observed in other fields of engineering, notably marine technology.

The earliest work in the field of vessel stability was provided by Grim [2], who developed an equivalent design wave. This wave minimised the difference between the underwater volume of a vessel calculated in a wave of $\lambda = L_{BP}$, and that obtained from an irregular wave realisation generated from a wave energy spectrum.

The other important contribution of integrating vessel characteristics and environmental parameters was provided by Lewis [3]. Environmental weighting was incorporated in a combined probability function of bending moment. This led Lewis to conclude that the worst cumulative bending occurred, not in the most severe seastate, but in a more moderate one. This meant that the elusive "worst possible storm" may not need to be found.

For the fore-going arguments the authors decided to research the area of developing a design excitation that embodied the characteristics of not only the environment, but also the dynamics of the system that would operate in the said environment. Thus, a new methodology in developing design excitations was developed based on the concept of mapping weighted dynamic responses between domains of excitation [4].

SUMMARY OF THE WEIGHTED MAPPING CONCEPT

In brief, the concept relies on weighing a suitable measure of the response of a dynamic system with the probability of occurrence of the excitation causing the response. This expectation value is expressed thus :

$$\langle \phi \rangle = \epsilon_{\phi}(\underline{x}) \cdot F_{\phi}(\underline{x} \pm \delta \underline{x}) \quad (1)$$

where ϕ is the weighted response (in this case weighted roll response)

$\epsilon_{\phi}(\underline{x})$ is the measured roll response.

\underline{x} is the vector of environmental parameters (usually wave amplitude, period and windspeed).

$\delta \underline{x}$ is a small range in the selected environmental parameters.

Using the weighted response for different domains of excitation, a solution set may be produced by finding the intersection between the two domains, thus :-

$$SS = \langle \phi \rangle_R \cap \langle \phi \rangle_D \equiv \{a_j, T_k, U_i\} \quad (2)$$

where $\langle \phi \rangle_R$ is the weighted response from the random domain, and $\langle \phi \rangle_D$ is the weighted response from the deterministic domain. This solution set defines the excitation from different source domains that can produce an equivalent effect. This is the concept of mapping weighted responses between domains of excitation.

MODEL OF VESSEL DYNAMICS

The foregoing method does depend on the type of model used to represent the dynamic system. Therefore, the chosen representation employs a method of assessing the dynamic stability of a vessel developed in the University of Strathclyde, namely the "Energy Balance" method. This method was originally proposed by Welaya[5], and subsequent research and applications have been documented in many publications, see for example [6,7,8].

Briefly, however, the basic theory is as follows. In order for a vessel to be assessed as "safe", the net energy input to the dynamic system by the environment (ie. wind and waves) must be balanced by the restoring energy of the dynamic system. This is akin to the Weather Criteria proposed in numerous IMO documents. However, the key development of the Strathclyde method in the explicit inclusion of the wave effect. This wave effect alters the dynamic righting lever curve to produce the characteristic "butterfly loop" for roll restoring lever of a vessel in following waves (see fig. 1). The hysteresis of the roll restoring lever is the direct consequence of the wave passing along the vessel (changing the underwater volume) as the vessel rolls.

Considering the physics of the situation, it is clear that a vessel will roll from some initial angle on the windward side to a final roll angle on the leeward side determined by the nature and amount of input energy and by the restoring energy of the system. However, this method of evaluation is slow and costly in computer time. A possible alternative is to choose judiciously the initial and final angles of the roll cycle and use a more abstract quantity as a representative measure of the response of the dynamic system, for example, the net energy (ie. net area under the diagram). Clearly, if the net energy is positive, then the vessel can be assessed as "safe".

The relationship between the "true" final roll angle and the abstract net energy measure is not maintained over a range of input excitations. However, provided the deviation can be shown to be small, it is reasonable to use the more abstract measure. Fortunately, this is shown to be the case [9]. Therefore, the work illustrated in this paper is based on using the net energy of the dynamic system as a measure of the response.

It should be noted that the Energy Balance is quasi-dynamic and hence the analysis undertaken in this paper considers only the following sea case where dynamic effects are minimised.

PRACTICAL APPLICATION OF THE METHOD

In order to test the method, three representatively sized vessels were selected, and their responses were evaluated in a set of seastates representing a geographic region. The selected ocean region is the

southern North Sea, as described by data provided by BMT Ltd. [10].

Deterministic Excitation Treatment

Each of the vessels was assessed in a series of sinusoidal waves in a range of operating speeds. The wave length was selected that would result in the poorest possible assessment (response). A further variation of both wave amplitude and windspeed was performed for each vessel, all other variables being kept constant.

The results of the analysis for one of the three vessels is illustrated in figures 2 and 3. This systematic analysis creates the solution domain on to which the results from the random domain will be ultimately mapped.

Random Excitation Treatment

The ocean region under examination is comprised of 15 seastates. These were used to produce 15 sets of representative wave realisations. The realisations were generated using the technique of "shaping" white noise devised by Cuong et al. [11], using a JONSWAP energy spectrum to model each seastate.

Hogben [12] indicated that wind velocity is only weakly coupled to zero crossing period, therefore, representative wind velocities are chosen for each band of significant wave height. The representative wind velocity is taken to be the mean value for all the occurrences of wind velocity within the band of significant wave heights of interest. This data is also provided by BMT Ltd.

A series of assessments for each vessel, at each of the selected operating speeds, was performed in detrimental sections of the generated wave realisation. These sections, or wave packets (not to be confused with wave groups), were selected as being detrimental to the test vessels depending on the zero crossing period and the amplitude.

In this particular series of tests, the poorest assessment at each speed considered was selected as the measured response of the vessel in the chosen seastate.

Weighting and Solution

In accordance with the proposed method, it is necessary to weigh the responses for each vessel in

both the random and deterministic domains. An analytic model of joint probability density of wave amplitude and period in a seastate is used. This function was originally put forward by Cavanie et al [13]

The function does not include any variations due to windspeed. This is reasonable since it is assumed that the windspeed generates the seastate, and thus remains constant throughout the analysis. The effect of the magnitude of the wind velocity is included in the dynamic stability assessment.

The solution set between the weighted domains is found. Figure 4 shows the solution amplitude of the deterministic wave for one of the vessels at one of the selected speeds of operation in each seastate. The variation of vessel speed has no drastic effect on the resulting equivalent excitation and as such can be omitted from further calculations.

Regional Solution

The work carried out so far, provides equivalent excitation (wave amplitude and wind velocity) for sets of individual seastates. An additional weighting procedure is required to provide equivalent excitation that represent the long term statistics of the environment. This is achieved by weighing the equivalent excitation for each seastate with the exceedence probability (ie the probability of a seastate existing with a greater significant waveheight). If the only variable to be considered is that of significant wave height, then the exceedence probability can be written in terms of stringency. That is, the percentage likelihood of that significant wave height in the region being exceeded during the period that the long term statistics are applicable.

The results for the equivalent wave amplitudes are given graphically in figure 5 for five levels of stringency. A consistent pattern of increasing amplitude with wavelength can be clearly seen throughout the levels. It should be noted that the amplitudes appear to maintain realistic magnitudes, bearing in mind the dimensions of the test vessels.

COMPARISON WITH PUBLISHED WORK

Although the method of deriving the design excitations is new, and therefore, not directly comparable with previously published work, an "order of magnitude" comparison should be possible, even to establish whether or not the method produces realistic values.

Three empirical formulae used extensively in stability research [14,15,2] are shown in figure 6. There is clear agreement in trend between the empirical formulae and the equivalent wave amplitude, in particular, at the smaller wavelengths where spread in equivalent excitation values is compressed (see fig. 5). Taking one of the empirical formula as an example, if we compare Grim's wave [2] with the weighted solution wave over the range of lengths presented, then some insight into the agreement may be gained. At short wavelengths, Grim's wave appears to agree in magnitude with the weighted solution at a stringency level of about 1%. However, for mid-range wavelengths (40m), the agreement between the Grim wave and the weighted solution wave occurs at a stringency level of about 12%. Similarly, at the longest wavelengths in the range, the agreement again occurs when the stringency level is 12%. This indicates that either all the empirical formulae possess variability with level of stringency, or that incomplete information regarding the likelihood of "testing" excitations or vessel dynamics has been incorporated during development.

Another way of examining whether the procedure produces sensible results is to compare the equivalent wave with the maximum wave that could possibly exist in the region. Hogben [16], stated that the maximum wave amplitude expected in a given seastate would be $1.07H_{1/3}$ (at the 90% confidence level). Therefore, in the same seastate the equivalent wave must have a smaller amplitude. If we consider seastates that are only exceeded 1% of the time then the maximum wave possible will have an amplitude of 7.2 metres, whereas the equivalent wave amplitude for the same level of stringency is always less than that value (see fig. 5).

Clearly, there is not enough information to ensure that the equivalent excitation is sensible over the entire range of vessel lengths. For this reason a further series of tests were performed on vessels up to 400 metres in length.

The usage of proposed procedure is laborious. Clearly, in order to apply the results of the research in practise it is necessary to develop an empirical representation of the results.

It is necessary to determine the important parameters that represent the environment and the dynamic system of interest. In this particular application, the dynamic system is a vessel in following seas. Clearly, it is not possible to include all the parameters that influence the characteristics of both the environment and the vessel systems. Only the dominant parameters can be considered. Extensive work determining the sensitivity of such parameters and their effect on the dynamic stability assessment was carried out by Barrie [9] which helps in concluding that in the following sea case, the only vessel parameter that need be considered is length.

In the case of the environment, it becomes apparent that there is remarkably little variation in the long term statistics of expected maximum significant wave height between ocean regions. However, the mean and modal values of zero crossing period does vary significantly between regions. Due to the fact that the distribution of seastates in any given region is skewed, the actual modal zero crossing period is dependent on significant wave height, or in other words the level of stringency chosen. In the southern North Sea, however, the variation of zero crossing period is confined to within one second, and can therefore be regarded as an insignificant variation with wave height. Therefore, the modal value together with the level of stringency, were the selected parameters chosen to represent the environment.

The final non-dimensionalised equivalent wave function is shown in figure 7. The task of deriving an empirical formula is simply a matter of surface fitting. A third degree polynomial is fitted to non-dimensional wave length, and a linear function is fitted to level of stringency. The resulting function is expressed thus :

$$\begin{aligned} \zeta(s, \lambda_D) = & 0.277 - 0.349s + (0.423 - 0.772s)\lambda_D \\ & + (0.431s - 0.270)\lambda_D^2 \\ & + (0.039 - 0.055s)\lambda_D^3 \end{aligned} \quad (3)$$

in the ranges $0.22 < \lambda_D < 4.06$

$$0.01 < s < 0.30$$

where s is the stringency level expressed as a decimal fraction (ie. 1% = 0.01)

λ_D is the normalised wavelength given by :

$$\lambda_D = \frac{2\pi\lambda_c}{gT_M^2} \quad (4)$$

T_M is the modal period of the region

and the critical wavelength is selected thus :

$$\lambda_c = 0.67L_{BP}$$

The second function pertaining to the equivalent wind velocity is a more straight-forward problem and can be expressed as a simple exponential thus :

$$U_{10}(s) = 19.5e^{-2.533s} \quad (5)$$

By using the above empirical formulae, representative equivalent wave and wind excitations may be calculated for vessels operating in the southern North Sea. This excitation can be subsequently applied to the stability analysis of the said vessels using the Energy Balance method.

FURTHER CONSIDERATIONS

The work described in this paper considers the first area of application of a new method for deriving design excitations based on characteristics of the dynamic system as well as the environment in which that system operates.

In many ways, the model considered in this work is crude. The omission of "true" dynamics prevents the more subtle effects from being included in the analysis, for example, unidirectional seas and wave groups.

There appears to be no reason to prevent the technique from being applied to other areas of dynamics, for example, an equivalent excitation for longitudinal bending would appear to be an obvious contender. Likewise, other engineering disciplines could also be considered as possible areas of application.

CONCLUSIONS

On the basis of the work presented in this paper, the following conclusions may be drawn :

1. Using the concept of mapping weighted responses of dynamic systems between domains of excitation, it is possible to relate the response of a vessel in a random environment to that experienced in a deterministic environment.
2. Applying the technique to a number of representative vessels in an ocean region, empirical formulae can be developed to provide equivalent excitations for the dynamic stability assessment of vessels in that region.
3. Due to the generality of the approach, it seems likely that the technique may be suitable for application in a number of engineering fields.

ACKNOWLEDGEMENTS

The authors would to thank the Marine Directorate of the Department of Transport for the financial support this work received, and the Director of Research of the British Telecom Research Laboratories.

REFERENCES

1. Clough, R.W., Penzien, J., 26-6 Selection of Design Earthquakes, Dynamics of Structures, McGraw-Hill, 1975.
2. Grim, O., Contribution to the Problem of Safety of a Ship in a Seaway, Schiff U Hafen, Vol. 13, 1961.
3. Lewis, E.V., Predicting Long Term Distributions of Wave Induced Bending Motions on Ship Hulls, Proc. SNAME, Spring Meeting, Montreal, 1967.
4. Alexander, J.G.M., Design Excitations for Dynamic Stability Assessment Based on Mapping Weighted Responses, Ph.D. Thesis, University of Strathclyde, Glasgow, 1987.
5. Welaya, Y.M.A., Application of Time Dependent Restoring for Stability Assessment of Ships and Semi-Submersibles, Ph.D. Thesis, University of Strathclyde, 1979.
6. Martin, J., Kuo, C., Welaya, Y.M.A., Ship Stability Criteria Based on Time-Varying Roll Restoring Moments, 2nd Int. Conf. on Stability of Ships and Ocean Vehicles, Tokyo, Oct. 1982.
7. Dept. Ship and Marine Technology, SAFE-SHIP(5) : Mathematical Modelling; Stability Criteria Based on Time Varying Roll Restoring/Excitation Moments, D.O.T. Contract, 1983.
8. Kuo, C., Vassalos, D., Alexander, J.G., Barrie, D., Incorporating Theoretical Advances In Usable Ship Stability Criteria, Int. Conf. on The Safeship Project : Ship Stability and Safety, RINA, June 1986.
9. Barrie, D.A., The Influence of Ship and Environmental Parameters on Stability Assessment, Ph.D. Thesis, University of Strathclyde, 1986.
10. Andrews, K.S., Dacunha, N.M.C., Hogben, N., SAFESHIP : Environmental Aspects, Report No. 185, NMI Ltd., 1983.
11. Cuong, H.T., Troesch, A.W., Birdsall, T.G., The Generation of Digital Random Time Histories, Ocean Engineering, Vol. 9 No. 6, 1982.
12. Hogben, N., Discussion of the Report of the Seakeeping Committee, 17th International Towing Tank Conference, Gothenburg, September 1984.
13. Cavanie, A., Arhan, M., Ezraty, A., A Statistical Relationship between Individual Heights and Periods of Storm Waves, BOSS '76, Trondheim, 1976.
14. Kastner, S., Long Term and Short Term Stability Criteria in a Random Seaway, Proc. Int. Conf. on Stability of Ships and Ocean Vehicles, Glasgow, 1975.
15. Miller, E.R., et al., Evaluation of Current Towing Vessel Stability Criterion and Proposed Fishing Vessel Criteria, Dept. of Transportation United States Coast Guard, Report No. CG-D-69-75, 1975.
16. Hogben, N., Basic Data Requirements - A Review with Emphasis on Wave and Wind Data, Report No. R92, NMI Ltd., Nov. 1980.

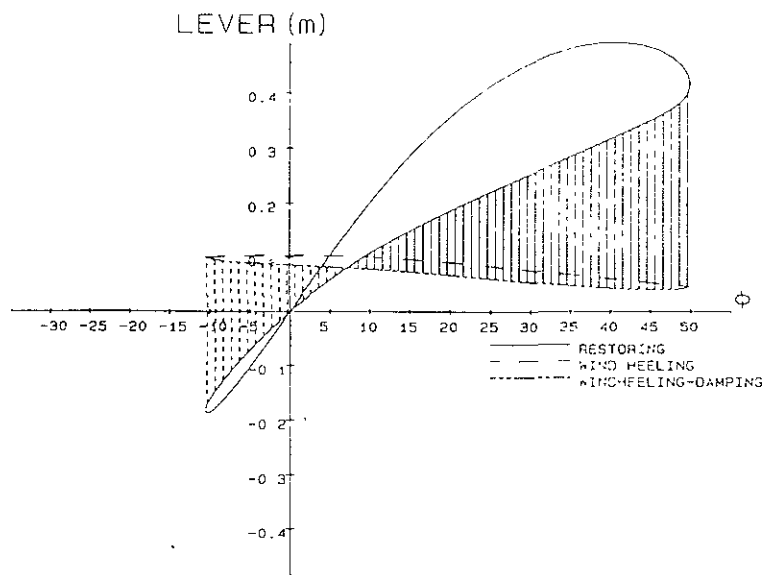


Fig 1: "Energy Balance" Butterfly Diagram

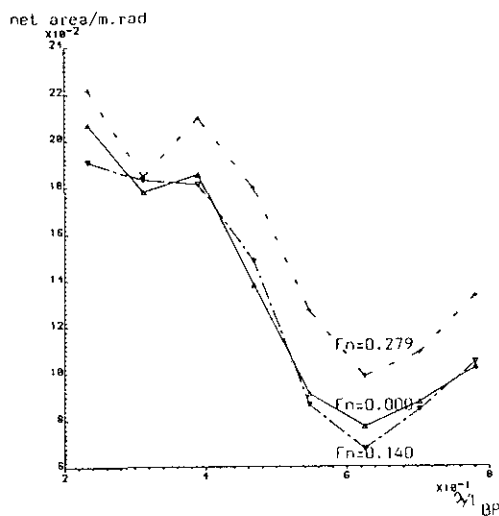


Fig 2: Net Area versus Normalised Wavelength

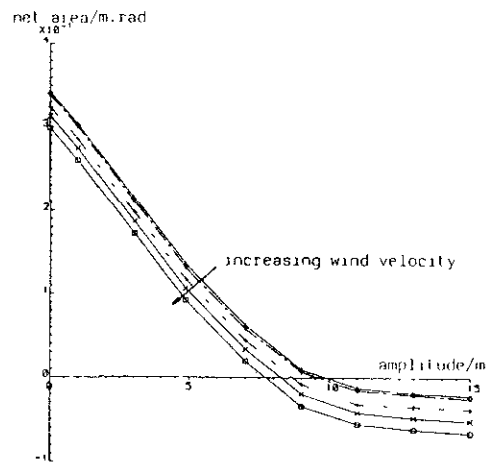


Fig 3: Net Area versus Wave Amplitude

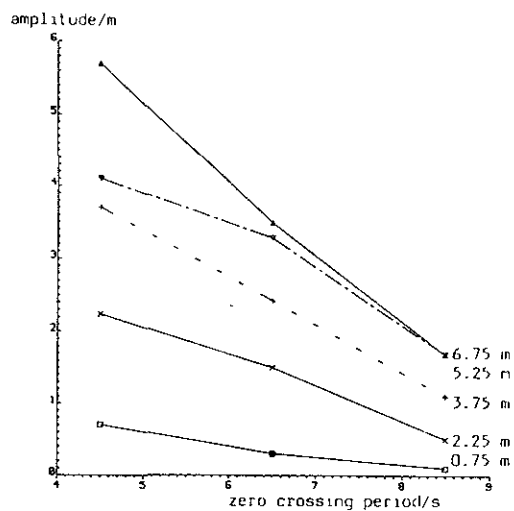
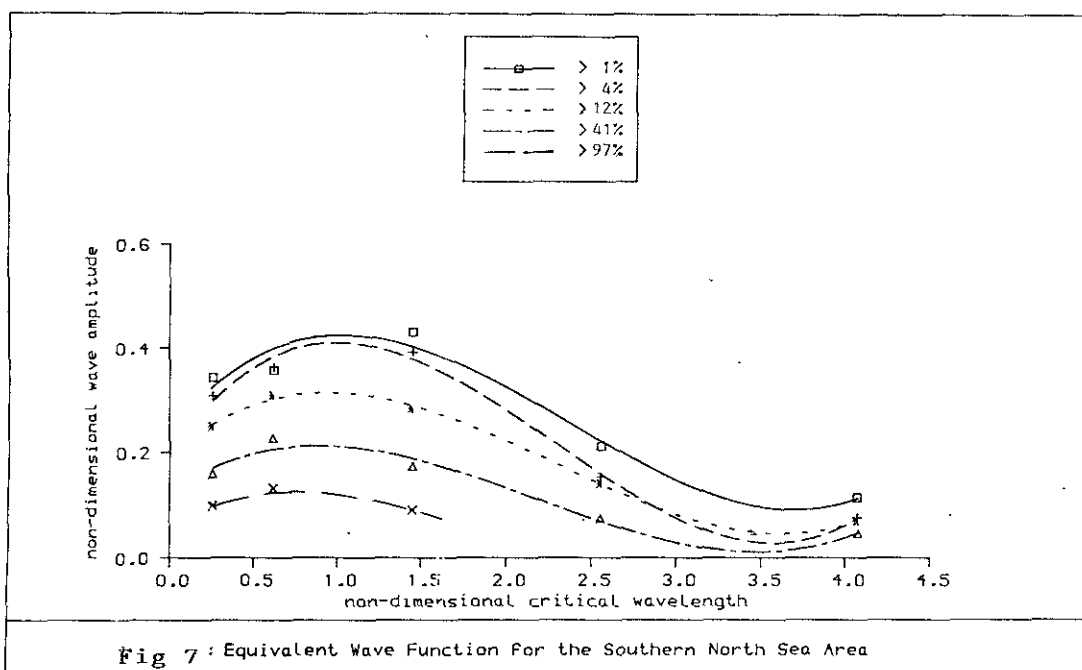
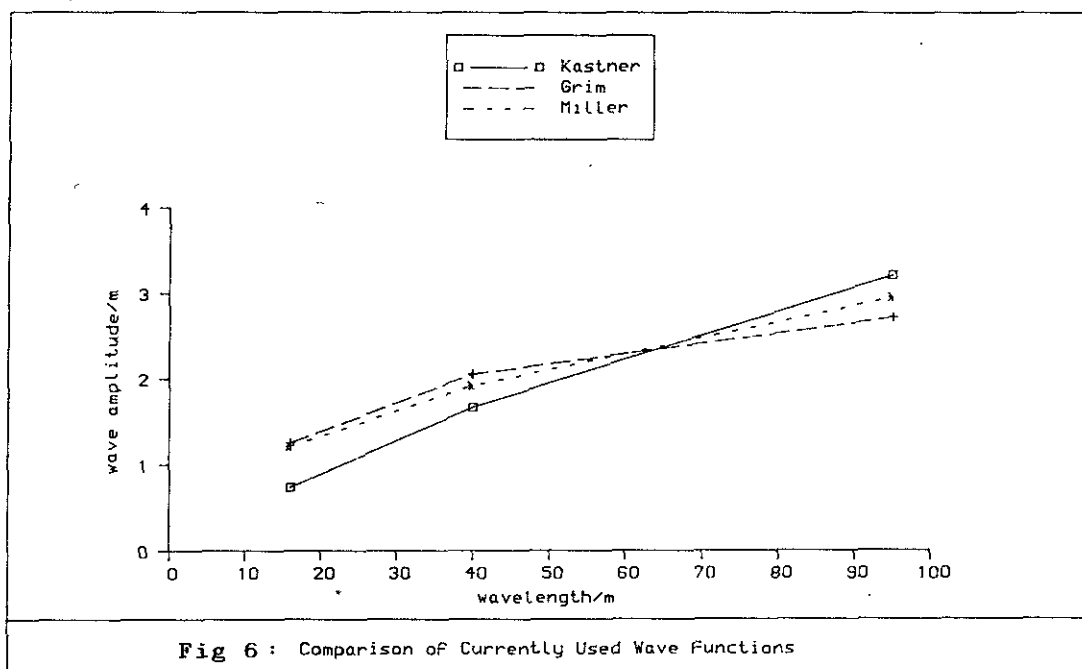
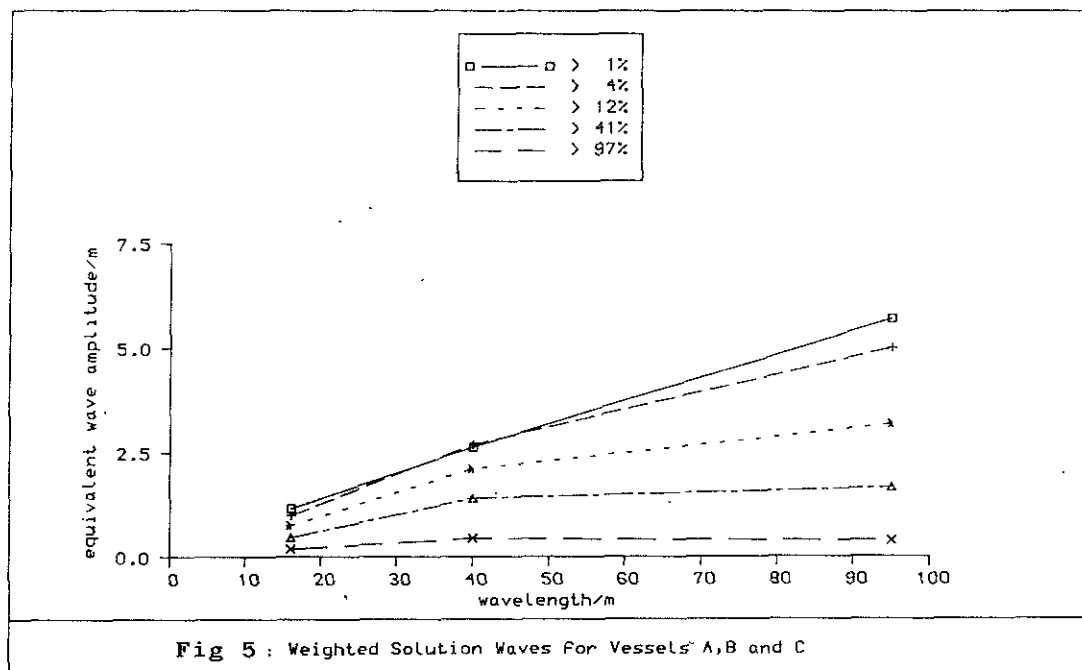


Fig 4: Equivalent Wave Amplitude for each Seastate ($f_n = 0.14$)



R.E.D. Bishop⁽¹⁾, W.G. Price^(1,3), P. Temarel⁽¹⁾ and E.H. Twizell⁽²⁾

Conventional methods of estimating dynamic stability are restricted to the roll equation governing one degree of freedom. Allowance for non-linearities when predicting large roll responses leading to capsizing does not compensate for the physical deficiency of such a rudimentary representation of the physical system.

The authors have advocated the use of a physically less restrictive mathematical model in which coupled sway, yaw and roll are admitted in the equations of motion. This approach reduces artificial constraints, justification for which is not at all clear and the effects of which are likely to be significant in the ship stability and capsizing phenomena. This more general approach has permitted a number of successful predictions and explanations to be reached and also provided greater physical insight.

In this paper the linear equations governing the antisymmetric motion of a rigid ship are developed. Fluid actions are expressed in terms of convolution integrals. The formulation of the problem includes the effects of waves and rudder deflection. The dynamic stability or instability of a ship represented by such a model is investigated.

1. INTRODUCTION

It is not possible either to build a ship with complete symmetry port and starboard or to propel it on an absolutely straight course with a fixed zero rudder angle. There will always be a slight tendency for the vessel to turn away from motion straight ahead. Superimposed on this unintentional motion, which will be ignored, there may be other antisymmetric motions due to the effect of waves, rudder deflection and directional instability. It is these, particularly the last, with which this paper is concerned.

In the past papers [1,2] a directional stability analysis of a ship allowing for time-history effects of the flow was presented. It was shown that the characteristic equation describing the directional stability of a ship may have more roots than are predicted by an 'instantaneous theory' which assumes that the motion at any instant determines the fluid forces and moments at

that instant. Unfortunately, the prediction of instability by analytical means is not easy and it is the purpose of the present paper to develop a numerical model which may be used to predict the onset of directional instability and which takes into account the history of the ship's motion.

The current work is intended to expand on and supplement earlier work where the frequency dependence of the fluid actions - represented by oscillatory coefficients [3-5] - and the effects of trim and forward speed on slow motion derivatives [6] were investigated, and their influence on the stability characteristics of a rigid ship assessed.

The equations describing the coupled linear antisymmetric motions of a ship in terms of roll, sway and yaw are formulated by expressing the fluid actions by means of convolution integrals. The characteristic equation of the motion is expressed in terms of nine functions which represent the relationships connecting sway force, rolling moment and yawing moment with sway velocity, roll angular velocity and yaw angular velocity. These nine functions, which are expressed in terms of a parameter λ , are not

(1) Department of Mechanical Engineering
(2) Department of Mathematics & Statistics
Brunel University
Uxbridge, Middlesex, UB8 3PH.
United Kingdom.

(3) Address from 1 October 1990 -
Department of Ship Science
University of Southampton
Southampton, SO9 5NH.

generally known in closed form. The parameter λ must have a negative real part to ensure dynamic stability of the ship.

An empirical formula, which models each of the nine functions in terms of the frequency of oscillation, e.g. the wave encounter frequency, is proposed.

This is achieved by adopting a discrete nonlinear least squares algorithm to obtain the corresponding optimal values of the parameters of the model formula which is a rational function of the frequency; such a numerical method is outlined in Appendix I. Inverse Fourier transform tables give the corresponding impulse response functions and Laplace transform tables then give the model forms of the nine functions of λ occurring in the characteristic equation, the roots of which are obtained numerically.

It is convenient to write the equations of motion in a dimensionless form, thus enabling the variation in the roots of the characteristic equation to be monitored as various parameters change.

2. REPRESENTATION OF THE FLUID ACTIONS

Consider a rigid ship with an orthogonal right-handed system of body axes $Cxyz$ fixed to it with origin C at the centre of gravity of the ship and the positive Cx axis lying in the plane of symmetry along the forward longitudinal axis. Cy is perpendicular to the plane of symmetry and positive to port while the Cz axis is positive vertically upwards. For such a ship moving with forward speed U , the linearized equations of anti-symmetric motion involving sway velocity $v(t)$, roll angle $\phi(t)$ or roll angular velocity $p(t) = \dot{\phi}(t) = d\phi(t)/dt$, and yaw angular velocity $r(t)$ may be written in the form [1-3]

$$\left. \begin{aligned} m(\dot{v} + rU) &= \Delta Y = (\Delta Y)_v + (\Delta Y)_p + (\Delta Y)_r + (\Delta Y)_\delta \\ I_{xx} \dot{p} - I_{xz} \dot{r} &= \Delta K = (\Delta K)_v + (\Delta K)_p + (\Delta K)_r + (\Delta K)_\delta + K_\phi \phi \\ -I_{zx} \dot{p} + I_{zz} \dot{r} &= \Delta N = (\Delta N)_v + (\Delta N)_p + (\Delta N)_r + (\Delta N)_\delta \end{aligned} \right\} (1)$$

where m is the mass of the ship, I_{xx} and I_{zz} are moments of inertia and I_{xz} is a product of inertia. The components ΔY , ΔK and ΔN are small perturbations of sway force,

roll moment and yaw moment, respectively, applied by the surrounding fluid. The indices refer to the corresponding contribution, e.g. $(\Delta Y)_v$ denotes the sway force component due to sway velocity $v(t)$, while $(\Delta Y)_\delta$ represents the sway force due to the rudder deflection $\delta(t)$. $K_\phi = -\rho g \nabla \overline{GM}$.

The most general linear expressions available for these fluid loading components were originally proposed by Cummins [7] and generalized later [8,9]. These expressions are derived from convolution integrals and, unlike "slow motion derivatives" which are constant for a given U , they make allowance for the time history of the ship's motion. For example, in still water

$$(\Delta Y)_v = \int_{-\infty}^{\infty} y_v(s) v(t-s) ds \quad (2)$$

in which $y_v(s)$ is an impulse response function. This is, in fact, a first approximation to a complete nonlinear representation using a Volterra series [9]. Suppose, now, that the ship is moving in long-crested waves. The fluid actions depend on the relative motions of the water; thus

$$(\Delta Y)_v = \int_{-\infty}^{\infty} y_v(s) [v(t-s) - v_w(t-s)] ds \quad (3)$$

where $v_w(t)$ is the lateral velocity of the wave.

This representation can only be an approximate one resting as it does on the Froude-Kryloff hypothesis that the wave pressure is not upset by the presence of the ship. Moreover, $v_w(t)$ is assumed either to be constant along the hull, which cannot be so in oblique long-crested waves, or to be an average value taken along the length of the hull. For present purposes it is unnecessary to examine the question of how an expression for $v_w(t)$ might be found.

Turning now to a typical rudder term in (1), it can be expressed as

$$(\Delta Y)_\delta = \int_{-\infty}^{\infty} y_\delta(s) \delta(t-s) ds. \quad (4)$$

Extending this approach to all components of the fluid actions, the equation of motion (1) become

$$\begin{aligned}
m(\ddot{v} + rU) = & \int_{-\infty}^{\infty} y_v(s) [v(t-s) - v_w(t-s)] ds \\
& + \int_{-\infty}^{\infty} y_p(s) [p(t-s) - p_w(t-s)] ds \\
& + \int_{-\infty}^{\infty} y_r(s) [r(t-s) - r_w(t-s)] ds \\
& + \int_{-\infty}^{\infty} y_\delta(s) \delta(t-s) ds
\end{aligned} \quad (5)$$

$$\begin{aligned}
I_{xx} \ddot{\phi} - I_{xz} \ddot{r} = & -\rho g \nabla \overline{GM} \phi \\
& + \int_{-\infty}^{\infty} k_v(s) [v(t-s) - v_w(t-s)] ds \\
& + \int_{-\infty}^{\infty} k_p(s) [p(t-s) - p_w(t-s)] ds \\
& + \int_{-\infty}^{\infty} k_r(s) [r(t-s) - r_w(t-s)] ds \\
& + \int_{-\infty}^{\infty} k_\delta(s) \delta(t-s) ds
\end{aligned} \quad (6)$$

and

$$\begin{aligned}
-I_{zx} \ddot{\phi} + I_{zz} \ddot{r} = & \int_{-\infty}^{\infty} n_v(s) [v(t-s) - v_w(t-s)] ds \\
& + \int_{-\infty}^{\infty} n_p(s) [p(t-s) - p_w(t-s)] ds \\
& + \int_{-\infty}^{\infty} n_r(s) [r(t-s) - r_w(t-s)] ds \\
& + \int_{-\infty}^{\infty} n_\delta(s) \delta(t-s) ds
\end{aligned} \quad (7)$$

where $y_v(s)$, $y_p(s)$, $y_r(s)$, $y_\delta(s)$, $k_v(s)$, $k_p(s)$, $k_r(s)$, $k_\delta(s)$, $n_v(s)$, $n_p(s)$, $n_r(s)$ and $n_\delta(s)$ are impulse response functions, ρ is the density of water, g is the acceleration due to gravity, ∇ is the displacement volume and \overline{GM} is the metacentric height.

Suppose that the motions $v(t)$, $p(t)$ and $r(t)$ are all proportional to $e^{\lambda t}$, where λ is a parameter, and define column vectors $q(t) = [v(t), p(t), r(t)]^T$ and $q_0 = [v_0, p_0, r_0]^T$, T denoting transpose, such that

$$q(t) = q_0 e^{\lambda t} = [v_0, \lambda p_0, r_0]^T e^{\lambda t} \quad (8)$$

Similarly, a vector $q_w(t) = [v_w(t), p_w(t), r_w(t)]^T$ can be identified which represents the wave motions. Assume that the waves are sinusoidal with encounter frequency ω_e , then

$$q_w(t) = [v_w^*, p_w^*, r_w^*]^T \exp(i\omega_e t) = q_w^* \exp(i\omega_e t) \quad (9)$$

where v_w^* , p_w^* and r_w^* are constants and $i = \sqrt{-1}$.

With these assumptions in mind, consider a typical integral in the equations (5-7), for instance, the first integral in equation (5) may be split in two parts, namely

$$\begin{aligned}
(\Delta Y)_v &= v_0 e^{\lambda t} \int_{-\infty}^{\infty} y_v(s) e^{-\lambda s} ds \\
&- v_w^* \exp(i\omega_e t) \int_{-\infty}^{\infty} y_v(s) \exp(-i\omega_e s) ds
\end{aligned} \quad (10)$$

or

$$(\Delta Y)_v = Y_v(\lambda) v_0 e^{\lambda t} - y_v(\omega_e) v_w^* \exp(i\omega_e t)$$

in which $y_v(\omega_e)$ is the Fourier transform of $y_v(s)$ and $Y_v(\lambda)$ is the Laplace transform of the same impulse response function.

Finally, assuming that $\delta(t) = \delta_0 e^{\lambda t}$ then a typical rudder term given by equation (4) becomes

$$(\Delta Y)_\delta = \delta_0 e^{\lambda t} \int_{-\infty}^{\infty} y_\delta(s) e^{-\lambda s} ds = Y_\delta \delta_0 e^{\lambda t} \quad (11)$$

as it is unlikely that a rudder will have a significant memory effect and so $y_\delta(s)$ will approximate to a delta function.

Equations (5-7) can then be written in matrix form, as follows

$$D(\lambda) q_0 e^{\lambda t} = M(\omega_e) q_w^* \exp(i\omega_e t) + u \delta_0 e^{\lambda t} \quad (12)$$

where

$$u = [Y_\delta, K_\delta, N_\delta]^T$$

with Y_δ , K_δ and N_δ constants,

$$D(\lambda) = \begin{bmatrix} m\lambda - Y_v(\lambda) & -\lambda Y_p(\lambda) & mU - Y_r(\lambda) \\ -K_v(\lambda) & \lambda^2 I_{xx} - \lambda K_p(\lambda) & -\lambda I_{xz} - K_r(\lambda) \\ -N_v(\lambda) & -\lambda^2 I_{zx} - \lambda N_p(\lambda) & \lambda I_{zz} - N_r(\lambda) \end{bmatrix} + \rho g \nabla \overline{GM} \quad (13)$$

and

$$M(\omega_e) = \begin{bmatrix} y_v(\omega_e) & y_p(\omega_e) & y_r(\omega_e) \\ k_v(\omega_e) & k_p(\omega_e) & k_r(\omega_e) \\ n_v(\omega_e) & n_p(\omega_e) & n_r(\omega_e) \end{bmatrix} \quad (14)$$

The complementary function of the equation of motion (12) satisfies the equation

$$\tilde{D}(\lambda) \tilde{q}(t) = 0.$$

If $\tilde{q}(t)$ is not to have a trivial form, that is if $\tilde{q}_0 \neq 0$, then the determinant of $\tilde{D}(\lambda)$ must vanish, giving

$$|\tilde{D}(\lambda)| = 0. \quad (15)$$

This is the characteristic equation of the motion. It has roots $\lambda_1, \lambda_2, \dots$ and the ship suffers dynamic instability if any of these roots has a positive real part, for then $\tilde{q}(t)$ will grow with time. In other words the ship cannot perform its intended function of moving straight ahead when the rudder is undeflected. A real positive root will relate to a spontaneous unidirectional and growing departure from motion ahead, while a complex root with a positive real part will correspond to a growing oscillatory departure from the reference motion. In either of these events the ship is *directionally unstable* or *dynamically unstable*. In the event that directional instability did occur, it would quickly become of overriding importance. Its severity would be such that the ship would cease to be controllable by means of its rudder and could very well roll onto its beam end.

It will be convenient to write the equations of motion (5-7) in dimensionless forms. This is achieved by dividing equation (5) by $\rho U^2 L^2$, where L is the length of the ship, and equations (6) and (7) by $\rho U^3 L^3$. The dimensionless characteristic equation becomes

$$|\tilde{D}(\lambda)| = 0 \quad (16)$$

where

$$\tilde{D}(\lambda) = \begin{bmatrix} \tilde{m} - \tilde{Y}_v(\lambda) & -\lambda \tilde{Y}_p(\lambda) & \tilde{m} - \tilde{Y}_r(\lambda) \\ -\tilde{K}_v(\lambda) & \lambda \tilde{I}_{xx} - \tilde{K}_p(\lambda) & -\lambda \tilde{I}_{xz} - \tilde{K}_r(\lambda) \\ -\tilde{N}_v(\lambda) & -\lambda^2 \tilde{I}_{zx} - \lambda \tilde{N}_p(\lambda) & \lambda \tilde{I}_{zz} - \tilde{N}_r(\lambda) \end{bmatrix} + \frac{\tilde{VGM}}{(\tilde{LF}_n^2)} \quad (17)$$

where $F_n (=U/\sqrt{Lg})$ is the Froude number. The parameter λ and all other constants and functions are now in dimensionless form such that, for example, $\lambda = \lambda L/U$, $\tilde{m} = m/(\rho L^3)$, $\tilde{Y}_v(\lambda) = Y_v(\lambda)/(\rho U L)$, etc. [2].

The variation of the roots $\lambda_1, \lambda_2, \dots$ may now be assessed as the values of the other dimensionless quantities change. Equation (16) will, therefore, be used in studying the variation of the zeros of $\tilde{D}(\lambda)$ as $\tilde{GM}/(\tilde{LF}_n^2)$ changes for a fixed Froude number; there is experimental evidence that the dimensionless roots vary with Froude number [10].

3. NUMERICAL MODEL

It is particularly unfortunate that the prediction of instability by analytical means is very difficult indeed. To date, the best that has been achieved has relied on highly simplified formulation of the matrix $\tilde{D}(\lambda)$ given in equation (17). The nine functions $\tilde{Y}_v(\lambda)$, $\tilde{Y}_p(\lambda)$, $\tilde{Y}_r(\lambda)$, $\tilde{K}_v(\lambda)$, $\tilde{K}_p(\lambda)$, $\tilde{K}_r(\lambda)$, $\tilde{N}_v(\lambda)$, $\tilde{N}_p(\lambda)$ and $\tilde{N}_r(\lambda)$ in $\tilde{D}(\lambda)$ are not known in closed form and in the existing literature they have been given constant values [6]. Resorting to approximations of these functions by constants ignores the history of the ship's motion. Such historical data can be measured and used to compile a more sophisticated numerical model, as is done in the following section

Data are, however, available describing the variation of the fluid actions with the frequency of oscillation ω in the form of (dimensionless) velocity and acceleration oscillatory coefficients, namely $\tilde{Y}_v(\omega)$, $\tilde{Y}_p(\omega)$ etc. such that

$$\begin{aligned} \tilde{y}_v(\omega) &= \int_{-\infty}^{\infty} \tilde{y}_v(s) \exp(-i\omega s) ds \\ &= \tilde{Y}_v(\omega) + 1 + \tilde{Y}_v(\omega). \end{aligned} \quad (18)$$

These data may be used to find empirical numerical models which approximate the nine functions. Inverse Fourier transform tables then give approximations to the nine impulse response functions $\tilde{y}_v(s), \tilde{y}_p(s), \dots$, following which Laplace transform tables give

numerical models which approximate the nine functions. Clearly, empirical formulae must be chosen which fit the experimental data as closely as possible and have inverse Fourier transforms. Then, these inverse Fourier transforms must have Laplace transforms which are used in equation (16) to determine the roots $\tilde{\lambda}_1, \tilde{\lambda}_2, \dots$.

Visual inspection of the data reveals that $Y_V(\omega)$, for instance, may be modelled by the equation

$$\tilde{Y}_V(\omega) = \frac{ca}{2\pi} \left[\frac{1}{a^2 + (b+\omega)^2} + \frac{1}{a^2 + (b-\omega)^2} \right] \quad (19)$$

in the interval $0.05 < \omega < 2.1$ (see Figures 1,2), with similar models for the other eight functions.

Optimal values of the parameters a , b and c in equation (19) may be computed, using the nonlinear least squares algorithm outlined in Appendix I.

The inverse Fourier transform of $Y_V(\omega)$, as given by (19), is

$$\tilde{Y}_V(s) = \begin{cases} ce^{as} \cos bs, & s < 0 \\ ce^{-as} \cos bs, & s > 0 \end{cases} \quad (20)$$

and Laplace transform tables then give

$$Y_V(\tilde{\lambda}) = \frac{c(a+\tilde{\lambda})}{b^2 + (a+\tilde{\lambda})^2}, \quad \tilde{\lambda} > -a. \quad (21)$$

Using expressions similar to equation (19) for other elements of $\tilde{D}(\tilde{\lambda})$ in equation (17) it is now possible to obtain the roots $\tilde{\lambda}_1, \tilde{\lambda}_2, \dots$ of equation (16). These roots can be obtained iteratively using the Newton-Raphson method, however, this is a cumbersome process and the derivation of all the roots cannot be guaranteed. On the other hand, it is possible to expand equation (16) into a polynomial

$$|\tilde{D}(\tilde{\lambda})| = \tilde{\lambda}^{22} + d_{21}\tilde{\lambda}^{21} + \dots + d_1\tilde{\lambda} + d_0 \quad (22)$$

from which all the roots can be obtained.

4. DISCUSSION OF NUMERICAL RESULTS

The data used to illustrate the numerical model developed are for the vessel EDITH TERKOL [4-6]. In the absence of any relevant experimental results the frequency dependent derivatives (i.e. oscillatory coefficients) are calculated from the

corresponding hydrodynamic coefficients using three-dimensional potential flow analysis [11,12]. The velocity oscillatory coefficients $\tilde{Y}_V(\omega)$, $\tilde{N}_V(\omega)$, $\tilde{Y}_R(\omega)$, $\tilde{N}_R(\omega)$ are corrected so that their zero frequency values are comparable to existing experimental results [10,13]. This correction, as can be seen, from Figures 1(a,c) is applied throughout the frequency range. All calculations refer to a Froude number $F_n = 0.2$ and level trim.

Although the numerical model of section 3 does not make explicit use of the inverse Fourier transform of equation (20), tests were carried out to examine the suitability of the Fourier transform pair given by equation (18). Some examples are shown in Figure 1 where \square indicates the frequency dependent input data while the solid line indicates the values derived using the velocity impulse response function obtained from the relevant velocity oscillatory coefficients. The agreement is reasonably good despite the relatively small frequency range $0.05 < \omega \leq 2.1$ (r/s) taken.

The results of modelling the velocity oscillatory coefficients according to equation (19) are illustrated in Table 1 in terms of the optimum values of the parameters a , b and c . Examples of these least-squares fits are shown in Figure 2 where \square indicates the input data and the solid lines represent equation (19). As can be seen, although the overall fit is good, it is particularly lacking in the low frequency region. This is significant as it changes the slow motion derivatives, and thus the corresponding behaviour of the vessel in question.

The dimensionless roots of the characteristic equation were calculated from equation (22) using the parameter values shown in Table 1 and $\tilde{m} = V = 0.00577$, $\tilde{I}_{xx} = 0.0000213$, $\tilde{I}_{xz} = 0 = \tilde{I}_{zx}$, $\tilde{I}_{zz} = 0.000265$, $L = 58.6_m$ and $g = 9.81 \text{ m/s}^2$. The resultant dimensionless roots are shown in Table 2 for $GM/L F_n^2 = 0.1$. The accuracy of the solutions were verified using the Newton-Raphson iteration.

It must be noted, however, that equation (21) imposes a restriction, namely $\lambda_1 > -a$. By inspection of Table 1, this implies that $\text{Real}(\tilde{\lambda}_1) > -0.1347$, however, this detail can often be ignored [14].

It is interesting to examine the differences in the roots of the characteristic equation when different models of fluid action representation are used. Values of the slow motion derivatives are shown in Table 3 where Case 1 corresponds to the input data [6] while Case 2 corresponds to values determined by the numerical model of equation (19) and employing equation (18) for $0.05 < \omega \leq 2.1$ (r/s). The corresponding roots of the characteristic equation are shown in Table 4.

Direct comparison of the roots shown in Tables 2 and 4 is not valid as they represent different fluid action models. However, it is possible to compare the overall stability characteristics. The calculations were repeated for a range of values $0 \leq \text{GM/L} F_n^2 \leq 1.0$. Case 2 - with slow motion derivatives relevant to the numerical model introduced - indicates stability - directional as well as dynamic - for all the range of $\text{GM/L} F_n^2$ values. On the other hand, the roots of Table 2 reveal a dynamic instability for $\text{GM/L} F_n^2 < 0.8$.

5. CONCLUSIONS

Analytical prediction of the phenomenon of directional instability of a ship is a matter of some difficulty if the history of the ship's motion is to be taken into account. The task is made easier by an 'instantaneous theory' employing slow motion derivatives in which fluid actions are assumed to correspond to prevailing motions. Such a theory, however, predicts that the characteristic equation of the motion has fewer roots than is the case when memory is admitted.

It has been the authors' purpose to present a physically more realistic numerical model which, incidentally, locates more of the roots $\tilde{\lambda}_1, \tilde{\lambda}_2, \dots$ of the characteristic equation (16). This is achieved by expressing, first of all, the nine

functions of $\tilde{\lambda}$ which appear in the characteristic equation as rational functions of ω , the frequency of oscillation.

Optimal values of the parameters of these model functions are found by using a discrete nonlinear least squares routine to analyse observed data. Tables of inverse Fourier transforms and Laplace transforms then yield the constituent functions of the characteristic equation, the roots of which are determined.

Numerical experiments were carried out using dimensionless data relating to the EDITH TERKOL, a coastal tanker. The numerical results obtained for a fixed Froude number predicted that the real part of one of the roots of the characteristic equation associated with the data sets remains positive for a large metacentric height (i.e. $\text{GM/L} = 0.8 F_n^2$) which is not predicted by the instantaneous theory. The consequence predicted by the present numerical model is that the vessel is dynamically unstable for a larger metacentric height contrary to the predictions of simpler models which fail to locate crucial roots of the characteristic equation.

REFERENCES

1. Bishop, R.E.D., Burcher, R.K., Price, W.G. Directional stability analysis of a ship allowing for time history effects of the flow. Proc. Royal Soc. London, 1973, A335, 341-354.
2. Bishop, R.E.D., Price, W.G., Temarel, P. General linear antisymmetric motions of a rigid ship. Int. Conf. The Safeship Project. Ship Stability and Safety, 1986, paper 5.
3. Bishop, R.E.D., Neves, M. De A.S., Price, W.G. On the dynamics of ship stability. Trans RINA, 1982, 124, 285-302.
4. Bishop, R.E.D., Price, W.G., Temarel, P. On the role of the encounter frequency in the capsizing of ships. 2nd Int. Conf. Stability of Ships and Ocean Vehicles, 1982, 103-112.
5. Bishop, R.E.D., Price, W.G., Temarel, P. The influence of load conditions in the capsizing of ships. 3rd Int. Conf. Stability of Ships and Ocean Vehicles, 1986, 3, 37-41.
6. Bishop, R.E.D., Price, W.G., Temarel, P. On the dangers of trim by the bow. Trans RINA, 1989, 131, 281-304.

7. Cummins, W.E. The impulse response function of ship motions. Schiffstechnik, 1962, 7, 101-109.
8. Bishop, R.E.D., Burcher, R.K., Price, W.G. The uses of functional analysis in ship dynamics. Proc. Royal Soc. London, 1973, A332, 23-35.
9. Bishop, R.E.D., Price, W.G., Temarel, P. A functional representation of fluid actions on ships, Int. Shipbuilding Prog., 1984, 31, 239-250.
10. Gerritsma, J. Hydrodynamic derivatives as a function of draught and ship speed. Delft Un. Tech., 1979, Rep 477.
11. Bishop, R.E.D., Price, W.G. On the use of equilibrium axes and body axes in the dynamics of a rigid ship. J. Mech. Eng. Science, 1981, 23, 243-256.
12. Inglis, R.B.I., Price, W.G. A three dimensional ship motion theory - The hydrodynamic coefficients with forward speed. Trans RINA, 1982, 124, 141-157.
13. Leeuwen, G. Van. The lateral damping and added mass of a horizontally oscillating ship model. Neth Res Centre TNO, 1964, Rep 65S.
14. Kaplan, W. Advanced Mathematics for Engineers. Addison-Wesley Publishing Company, 1981, Chapter 4.2.
15. Levenberg, K. A method for the solution of certain nonlinear problems in least squares. Q. Appl. Math. 1944, 2 164-168.
16. Marquardt, D.W. An algorithm for least squares estimation of nonlinear parameters. SIAM J. 1963, 11(2), 431-441.
17. Twizell, E.H. Numerical methods, with applications in the biomedical sciences Ellis Horwood and John Wiley & Sons, 1988.

TABLE 1

Values of the parameters a, b and c used in equations (19) and (21)

Function	a	b	c
$\tilde{Y}_v(\lambda)$	0.5120	1.929	-0.2054
$\tilde{Y}_p(\lambda)$	0.4561	1.850	-0.0118
$\tilde{Y}_r(\lambda)$	0.2860	2.004	0.0112
$\tilde{K}_v(\lambda)$	0.4545	1.849	-0.0115
$\tilde{K}_p(\lambda)$	0.4614	1.791	-0.0009
$\tilde{K}_r(\lambda)$	0.2268	1.988	0.0002
$\tilde{N}_v(\lambda)$	0.1347	2.016	0.0054
$\tilde{N}_p(\lambda)$	0.5811	0.841	-0.0009
$\tilde{N}_r(\lambda)$	0.5432	2.128	-0.0205

TABLE 3

Values of slow motion derivatives $\times 10^4$

	Case 1	Case 2		Case 1	Case 2
\tilde{Y}_v	-56.8	-84.2	\tilde{Y}_v	-24.7	-23.7
\tilde{Y}_p	0	-4.73	\tilde{Y}_p	-1.97	-1.44
\tilde{Y}_r	4.70	2.50	\tilde{Y}_r	1.64	1.99
\tilde{K}_v	0	-4.62	\tilde{K}_v	-1.95	-1.41
\tilde{K}_p	0	-0.39	\tilde{K}_p	-0.219	-0.108
\tilde{K}_r	0	0.043	\tilde{K}_r	0.047	0.048
\tilde{N}_v	-14.3	0.567	\tilde{N}_v	1.61	1.65
\tilde{N}_p	0	-1.61	\tilde{N}_p	0.041	-0.089
\tilde{N}_r	-9.70	-7.37	\tilde{N}_r	-1.15	-2.10

TABLE 2

Dimensionless roots $\tilde{\lambda}_i$ of the characteristic equation (22) for $GM/L F_n^2 = 0.1$.

0.473 ± i 8.827
-0.104 ± i 2.006
-0.215 ± i 1.984
-0.253 ± i 1.879
-0.302 ± i 2.011
-0.396
-0.404 ± i 1.394
-0.471 ± i 3.850
-0.511 ± i 1.813
-0.613
-0.663 ± i 0.775
-0.701 ± i 9.666

TABLE 4

Roots of the characteristic equation using slow motion derivatives for $GM/LF_n^2 = 0.1$.

Case 1	Case 2
0.176	-0.457 ± i 4.484
-0.016 ± i 3.845	-0.778
-3.840	-2.091

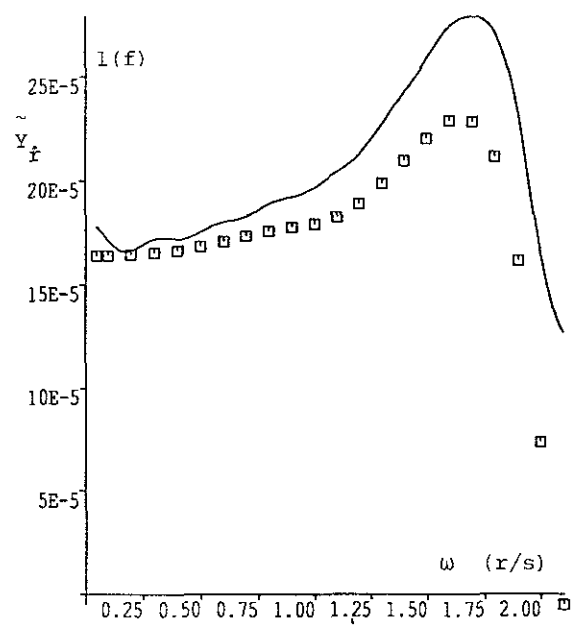
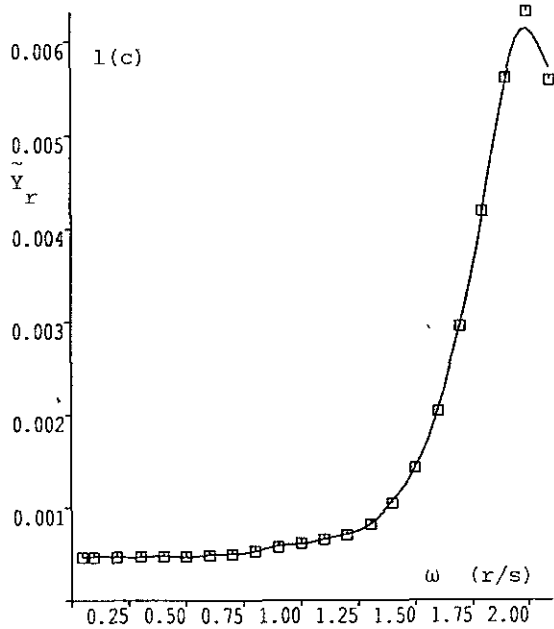
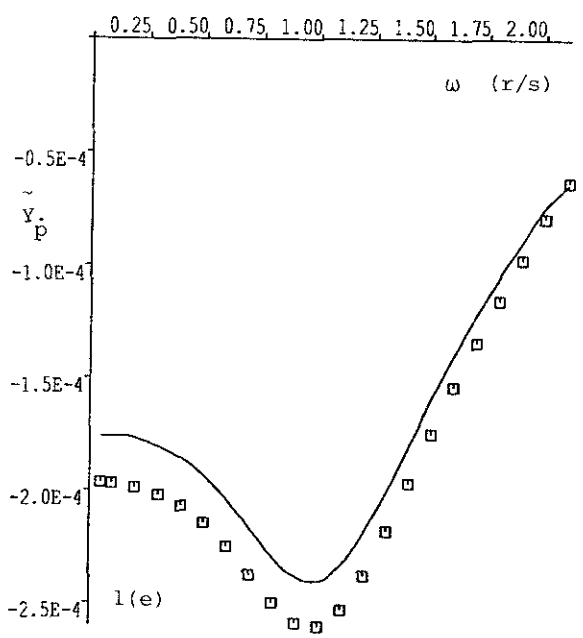
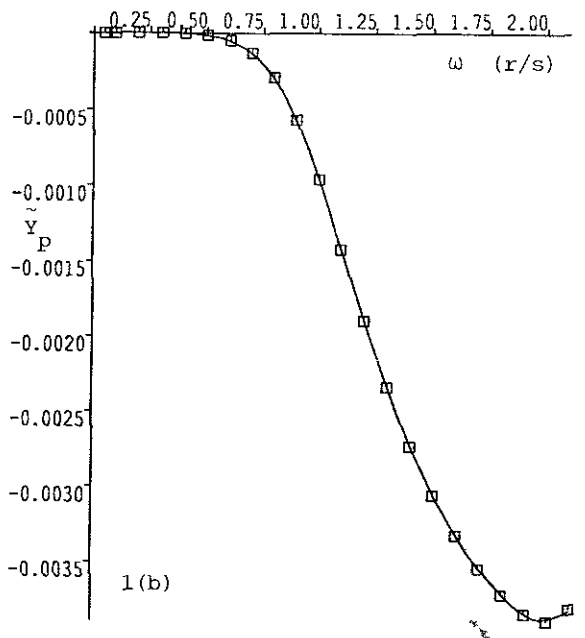
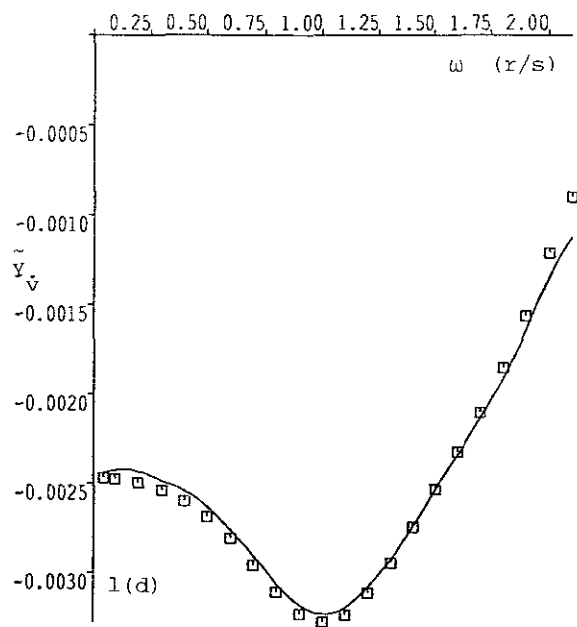
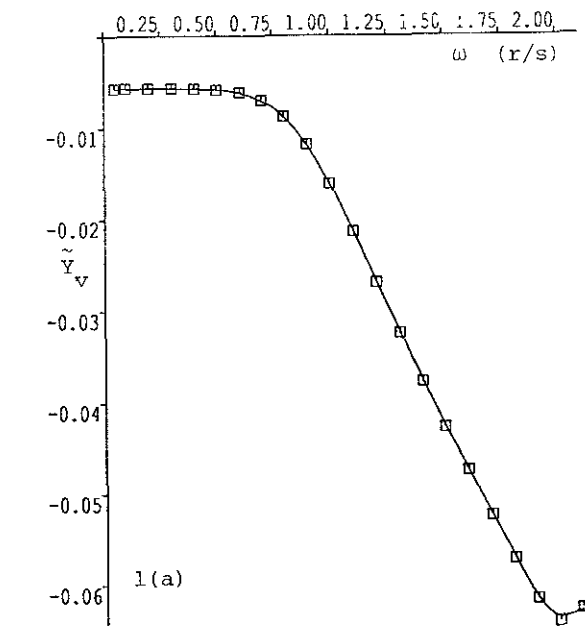


Figure 1. Examples of the Fourier transform pair described by equation (18). a) $\tilde{Y}_v(\omega)$, b) $\tilde{Y}_p(\omega)$, c) $\tilde{Y}_r(\omega)$, d) $\tilde{Y}_v(\omega)$, e) $\tilde{Y}_p(\omega)$ and f) $\tilde{Y}_r(\omega)$; \square indicates original data.

APPENDIX I

Consider the set of N data points (ϵ_m, σ_m) , $m=1,2,\dots,N$, where ϵ_m represents a value of ω and σ_m is the observed value of $\tilde{Y}(\epsilon_m)$.

The nonlinear least square criterion requires that the sum of squares

$$S(a,b,c) = \sum_{m=1}^N f_m^2 = \left[\sigma_m - \frac{ca}{2\pi} A \right]^2 \quad (23)$$

$$\left(A = \frac{1}{a^2 + (b+\epsilon_m)^2} + \frac{1}{a^2 + (b-\epsilon_m)^2} \right)$$

be minimized, this minimum of S being reached by computing optimal values of the parameters a , b and c .

Let $\tilde{x} = [x_1, x_2, x_3]^T \equiv [a, b, c]^T$ and let $\tilde{f} = \tilde{f}(\tilde{x}) = [f_1, f_2, \dots, f_N]^T$ with $f_m = f_m(\tilde{x})$ for $m = 1, 2, \dots, N$ (see equation (23)). Define a matrix $\tilde{P} = [p_{mn}]$ of order $N \times 3$ in which the element

$$p_{mn} = \partial f_m / \partial x_n$$

so that, for equation (23),

$$p_{m1} = -\frac{c}{2\pi} (e_m + g_m) + \frac{ca^2}{\pi} (e_m^2 + g_m^2),$$

$$p_{m2} = \frac{ca}{\pi} [(b+\epsilon_m)e_m^2 + (b-\epsilon_m)g_m^2],$$

and

$$p_{m3} = -\frac{a}{2\pi} (e_m + g_m),$$

where

$$e_m = 1/[a^2 + (b+\epsilon_m)^2] \text{ and } g_m = 1/[a^2 + (b-\epsilon_m)^2]$$

and $m = 1, 2, \dots, N$.

Construct, now, the square matrix $\tilde{Q} = 2\tilde{P}^T \tilde{P}$ of order 3. Then the algorithm

$$\begin{aligned} \tilde{x}^{(k+1)} &= \tilde{x}^{(k)} \\ &- 2[\tilde{Q}^{(k)} + \gamma^{(k)} \tilde{I}]^{-1} \times (\tilde{P}^{(k)})^T \tilde{f}(\tilde{x}^{(k)}); \end{aligned} \quad (24)$$

$k=0, 1, 2, \dots,$

in which $\gamma^{(k)}$ is a parameter and the superscript k denotes iteration number, may be used to obtain the optimal values of a , b and c which minimize S in (23) from some starting vector $\tilde{x}^{(0)} = [a^{(0)}, b^{(0)}, c^{(0)}]^T$. In (24) \tilde{I} is the identity matrix of order 3.

Equation (24) is known as the Levenberg-Marquardt algorithm for minimizing S [15,16]. Criteria for choosing $\gamma^{(k)}$ ($k = 0, 1, 2, \dots$) and convergence criteria are given in many numerical analysis texts ([17] for example).

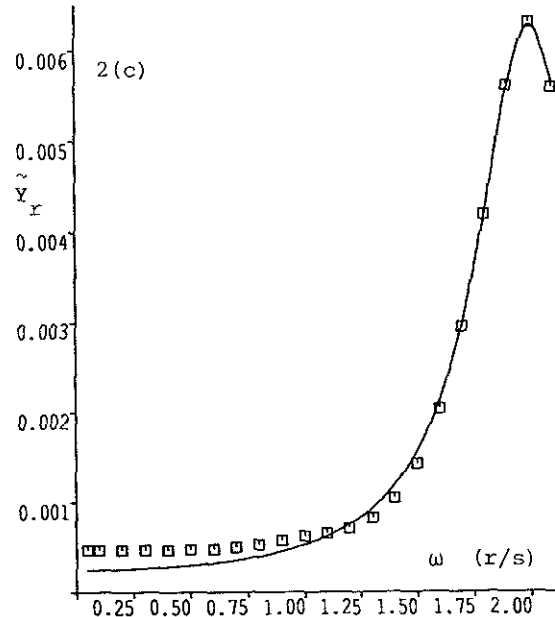
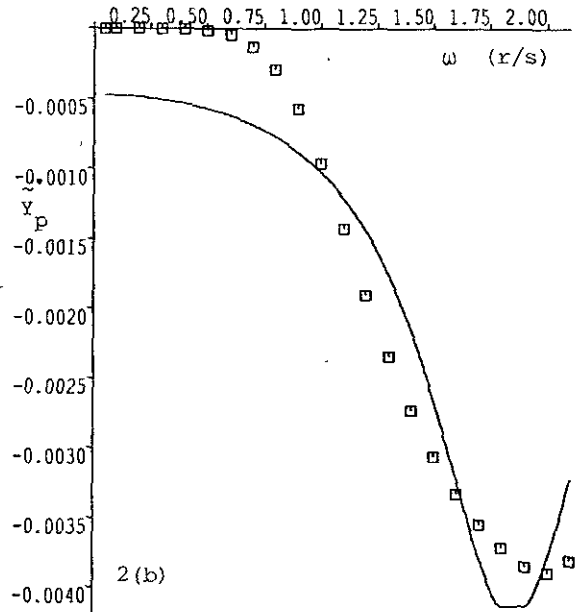
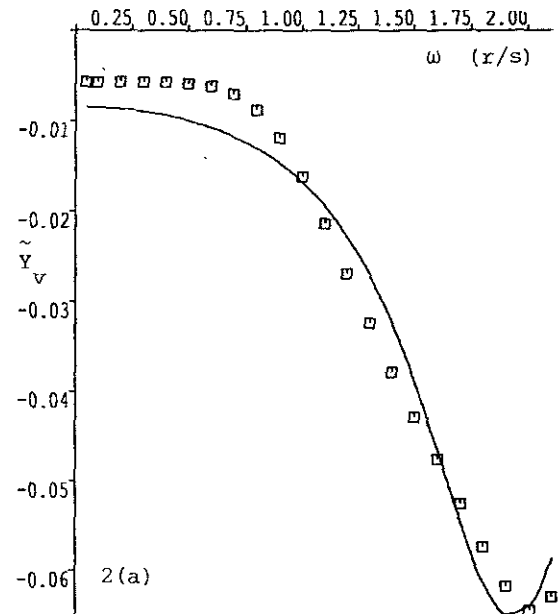


Figure 2. Examples of the numerical model described by equation (19). a) $Y_v(\omega)$, b) $Y_p(\omega)$ and c) $Y_r(\omega)$; \square indicates original data. P

EXPERIMENTAL INVESTIGATION OF ROLL DAMPING

CHARACTERISTICS OF A DESTROYER MODEL

D. CUMMING¹, M.R. HADDARA² and ROSS GRAHAM³

ABSTRACT

An extensive experimental program was carried out in the towing tank of the Institute for Marine Dynamics, in St. John's, Newfoundland, Canada to investigate the roll damping characteristics of a nine meter long destroyer hull model. Roll decay records were obtained for the model fitted with and without bilge keels at a wide range of forwards speeds. Tests were also carried out at zero forward speed, for the model free to sway and restrained against sway.

The energy approach was used to analyze these roll decay curves. The damping was divided into viscous and nonviscous components, and the dependence of these components on roll angle was investigated.

INTRODUCTION

The past two decades have witnessed a significant increase in the number of studies dealing with rolling motion prediction. This is mainly because of the increasing interest in the formulation of improved criteria for the margin of safety against capsizing. An accurate quantitative estimate of the roll damping is a prerequisite for good rolling motion prediction. In addition, the use of a realistic damping moment form is important when large rolling motion is considered. In the absence of a concrete theory, estimation of roll damping is still based on empirical formulae. Experimental studies of roll damping are not only important as a tool for the understanding of the physics of the problem, but also necessary for the verification of the empirical methods.

The purpose of this present work is twofold. First, to provide a data base for

the damping data for a destroyer hull model. Second, to investigate the form of the damping moment at large angles and try to understand the physics behind it. The damping coefficient estimates were obtained using a recently developed energy approach [1]*. One of the main advantages of this method, is the ability to analyze very short roll decay curves. In fact, a single roll cycle can be analyzed to obtain a reasonably accurate estimate for linear and nonlinear damping coefficients. This is a major benefit when dealing with highly damped models e.g. a model fitted out with bilge keels and moving with high forward velocity. Another advantage, is the ability to relate the damping coefficient to the roll angle directly, thus yielding a natural division of damping into viscous and non-viscous components. In addition, the behaviour of damping at large roll angles can be investigated.

MODEL SETUP DESCRIPTION

The roll decay experiments were carried out in the Institute for Marine Dynamics 200 m * 12 m Towing Tank on a 9 m long, 13.46 scale model. A body plan of the model is provided in Figure 1. The model was

1. National Research Council Canada, Institute for Marine Dynamics, St. John's, Newfoundland, Canada.
2. Memorial University of Newfoundland, Faculty of Engineering and Applied Science, St. John's Newfoundland, Canada, A1B 3X5.
3. Department of National Defence, Defence Research Establishment Atlantic, Canada.

* Numbers between brackets indicate references at the end of the paper.

not fitted with a rudder, but was fitted with shaft brackets; however, no propellers were used for these tests. Experiments were carried out with and without bilge keels. Bilge keel particulars are given in Table 1.

An apparatus was designed and fitted to the tow tank carriage permitting the model sufficient scope to pitch, heave and roll while being rigidly constrained in sway and yaw. The arrangement eliminated the sway-roll and yaw-roll coupling terms from the model damping equation while allowing the relevant motions with a minimum of mechanical friction. Also enough surge displacement was permitted such that the model trimmed correctly while being towed. The vertical position of the roll axis, 0, was fixed for all tests. Rolling was induced by the release of a moment applied to a 2.5 m long mast located at the model center of floatation.

Model motions were assessed using a ring laser gyro based sensor package located at the center of gravity, G, of the model capable of measuring the six degrees-of-freedom motions of the rigid body very accurately. This package consisted of a triad of ring laser gyros and accelerometers feeding signals to a microprocessor that employed an inertial navigation algorithm to calculate and output the correct motions. Analog signals were digitized at 20 Hz and recorded on a microVax II computer. Additional information on the theory behind the operation of ring laser gyros can be found in [2].

EXPERIMENT DESCRIPTION

Roll decay data were recorded for three model conditions, nine forward speeds, and eight initial heel angles. Three metacentric heights were chosen ranging from 6% to 10% of the model beam. The roll period was adjusted for each condition to preserve a constant roll moment of inertia. The nine model forward speeds varied from $F_n = 0.0$ to 0.4 while the eight initial heel angles ranged from 4 to 25 degrees.

A number of zero-speed runs were also carried out in each condition without

laterally constraining the model to assess the influence of the sway-roll and yaw-roll coupling terms. One set of runs was carried out with the unconstrained model arranged across the tank to ascertain the influence of tank wall reflection. Two more conditions of the model were also tested at zero forward speed. These conditions correspond to metacentric heights of 4% and 12% of the model beam. The model GZ-curve for each of the five cases tested is essentially linear up to a heel angle of 30°, see [3]. A total of 424 runs were executed on the model fitted with and without bilge keels.

LINEAR ANALYSIS

The motion of a ship rolling freely about a longitudinal axis through the point 0, as shown in Figure 1, can be expressed as

$$\ddot{\phi} + N(\phi, \dot{\phi}) + D(\dot{\phi}) = 0 \quad (1)$$

where ϕ is the roll angle, N and D are the nonlinear damping and the restoring moments per unit virtual moment of inertia of the ship, respectively. In the linear analysis, the damping moment is replaced by an equivalent linear function of the roll velocity. The equivalent linear damping coefficient can be determined from an experimentally measured free roll decay curve. In this paper, we use the energy approach introduced in [1]. The first cycle of the roll decay curve is digitized and the magnitudes of the roll angle ϕ_i , $i=1, \dots, n$ are measured. The equivalent linear damping coefficient N_e , is determined from the relation

$$N_e = \sum u_i h(t_i) / \sum u_i^2 \quad (2)$$

where

$$u_i = - \int_{t_i}^{t_{i+1}} \dot{\phi}_i^2 dt$$

$$h(t_i) = V(t_{i+1}) - V(t_i)$$

$$V(t) = \frac{1}{2} \dot{\phi}^2(t) + \int_0^\phi D(x) dx$$

The nondimensional equivalent linear damping coefficient ζ_e , can be obtained by dividing

N_e by twice the natural roll frequency, ω . To investigate the reliability of the results obtained using this method, a complete roll decay curve was reconstructed using damping estimates obtained from the analysis of the first cycle of the curve. Comparison of the predicted amplitudes with the experimental ones showed that damping coefficients obtained using the energy method can be reliably used outside the range of the experimental data, see [3].

Because only one cycle is used to obtain a value for the equivalent nondimensional linear damping coefficient ζ_e , it is possible to relate this value to the motion amplitude. The damping coefficient ζ_e for a certain forward speed can thus be expressed as

$$\zeta_e = \zeta_e(\phi_0) \quad (3)$$

where ϕ_0 is the roll amplitude at the beginning of the cycle. This roll amplitude will be called the initial amplitude. The procedure was carried out for the roll decay records obtained experimentally from the six sets of tests described in the previous section. These six sets refer to the tests obtained for three values of the metacentric heights 6%, 8% and 10% of the model beam (conditions L, M and H, respectively) for the model fitted with and without bilge keels. The values for the nondimensional equivalent linear damping coefficient were determined. Because of the space limitation, we show only the damping coefficients for condition M in Figures 2 and 3. Model damping coefficients for the other conditions are given in [3]. The results were also used to investigate the form of the functional relationship in equation (3). It seems that the relationship between the equivalent linear damping coefficient ζ_e and the initial amplitude ϕ_0 , for a constant forward velocity, can be described fairly accurately by the linear relationship

$$\zeta_e = m \phi_0 + c \quad (4)$$

This can be seen from the small deviation of the data points about the regression lines shown in Figures 2 and 3. The slope m and the intercept c are both functions of

the forward speed and the distance between the center of roll and the center of gravity of the model OG. Using this formulation, one can then consider the slope m to be indicative of the viscous damping component, while c can be considered as a measure of the inviscid damping component. The values of the slope m and the intercept c were evaluated using regression analysis.

In comparing results obtained for the three different GM cases (L, M and H), the dimensional damping coefficient N_e will be used. The intercept and slope of this damping coefficient were obtained for the six sets of experiments referred to earlier. The intercept has been plotted as a function of forward speed in Figure 4. The points have been fitted to a quadratic polynomial in the forward speed. It can be seen that the values for the low GM case (condition L) increase at a much faster rate than in the other two cases. For the model fitted with bilge keels, the nonviscous damping component increases with the metacentric height up to a speed of 1.4 m/sec ($F_n < 0.14$). Above this speed range, the damping coefficient seems to have a minimum value for the medium metacentric height case (condition M). The same trend is exhibited by the curves for the model without bilge keels, except that the threshold velocity is increased to about 3.0 m/sec (about $F_n = 0.3$). This may be caused by the bilge keels and the sway-roll coupling as will be discussed later. Two comments seem to be in order here. First, the nonviscous component appears to be a nonlinear function of the forward velocity, generally quadratic in nature. Second, the damping curve shows only minor evidence of the hump-hollow phenomenon observed by Ikeda et al [6], and attributed to the wave damping component.

The behaviour of the slope as a function of forward velocity is much more complicated as seen from Figure 5. The analysis is further complicated by the presence of scatter in the results. The best fit for the data points in Figure 5 seems to be a cubic polynomial. One can identify

three regions in the three cases where the model was fitted with bilge keels. In the first region, for which $v < 1.0$ m/sec ($F_n < 0.1$), the slope decreases with increasing velocity. In the second region, $1.0 < v < 2.5$ m/sec ($0.1 < F_n < 0.25$), the slope is increasing slightly. In the third region, 2.5 m/sec $< v$ ($0.25 < F_n$), the slope decreases rapidly as the velocity increases. The behaviour depicted in Figure 5 can be explained in light of the fact that the major contributors to the viscous damping component are the bilge keels. Cox and Lloyd [4] cite experiments performed independently by Bolton and Lofft in which the bilge keel damping coefficient for speeds corresponding to $F_n < 0.1$ was observed to be smaller than the value at zero speed. They hypothesized that a vortex cancellation mechanism is involved. According to this hypothesis, the minimum roll damping moment occurs when the ship travels a distance equal to the bilge keel length in a time equal to the natural roll period. Using this rule, the minimum damping moment for our model should occur at a speed between 0.85 m/sec and 1.07 m/sec. This is in agreement with the data shown in Figure 5. The fact that the analysis in the present work shows that this phenomenon is associated with the viscous component of the damping supports this hypothesis. The weak dependence of the viscous component on forward speed, apparent in the second region, has also been observed before [6]. This observation led some researchers to conclude that bilge keel damping is essentially independent of forward speed [4]. In the third region, the sharp decline in the damping coefficient may be due to the decline in the eddy making component of the bilge keels.

The values for the equivalent linear damping coefficient N_e are shown in Figure 6 as functions of forward velocity, for the case $\phi_0 = 0.3$ rad. Also shown are quadratic fits to the data obtained using regression analysis. The fits are generally good except around a speed of 1.0 m/sec, for the model with bilge keels. This is due to the minimum in the viscous component of the damping that

occurs at this speed. It is clear that the viscous component has a greater effect on the magnitude of the damping coefficient at the lower forward speed values. The effect of the nonviscous component becomes more predominant as the forward speed increases.

SWAY COUPLING

To obtain the free roll decay curves for the model moving with a constant forward velocity, it was necessary to attach the model to the towing carriage as explained in the description of the experimental set up. This resulted in forcing the model to roll about a fixed roll center. Since the model was free to heave and pitch but restrained against sway, it is necessary to examine the effect of this constraint on the measured values of the damping coefficient. For a model with a fixed center of roll, see Figure 1, the measured damping coefficient B_{44}^0 can be related to the damping coefficient caused by pure rolling of the model using the following equation [5]:

$$B_{44}^0 = B_{44}^G + [B_{24} + B_{42}]l \quad (5)$$

where B_{44}^G denotes the pure roll damping moment, B_{24} denotes the sway force coefficient caused by roll velocity ($\dot{\phi}$), B_{42} is the roll damping moment coefficient caused by the sway velocity ($l\dot{\phi}$) and l is the distance between the point of action of the sway force and the axis about which the model rolls. The damping coefficient in equation (5) can be obtained from that given in equation (2) by multiplying the latter by the virtual moment of inertia of the model about a longitudinal axis through point O. To separate the different quantities in equation (5), the model was tested at zero forward speed without attaching it to the carriage. Thus, in these tests the model was free to move in six degrees of freedom.

The regression results representing the nondimensional equivalent linear damping coefficients obtained for the model with and without sway constraint, for $\phi_0 = 0.5$ rad, are shown in Figure 7. It is clear from these plots that restraining the model against sway motion does not have any significant effect on the measured damping

coefficient when the model was tested without bilge keels. The same conclusion applies for the model fitted with bilge keels in the case of medium GM. If this can be taken as an indication to what happens in the case when the model moves with forward speed, then the results presented for the medium GM case in the previous section are valid representations of the damping caused by pure roll; however, this needs to be investigated further. A series of free running model tests is planned in the near future. In the two cases of the high and low GM, there is a difference of about 9.5% and - 12% in the damping coefficient respectively. This difference is caused by the sway force produced by the induced sway velocity. The damping coefficient of the restrained model, for low GM, is smaller than that for the free to sway model, while it is larger for the high GM case. This suggests that the distance l in equation (5) has a negative sign for the low GM case and a positive sign for the high GM case. This was expected since the model was forced to roll about an axis considered to be suitable for the medium GM case.

BILGE KEEL DAMPING

The contribution of the bilge keels to the total damping of the model was estimated by subtracting the damping coefficient of the model without bilge keels from its value for the model fitted with bilge keels. This contribution includes both the damping caused by the bilge keels alone and the increase in the hull damping caused by the presence of the bilge keels. The bilge keel part of the dimensional equivalent linear damping was calculated as a function of the forward velocity, as well as the slope and intercept of this component, see [3]. The curve for the slope exhibits the three regions previously observed in the slope of the total damping coefficient of the model. The intercept varies as a smooth quadratic function of the velocity. It is clear from these results that most of the model damping is caused by the bilge keels. The damping coefficient is a strong function of the roll

amplitude. When the roll amplitude is small the nonviscous part of the damping has an overriding effect and the total damping coefficient appears to be behaving like a quadratic polynomial in forward speed. For large roll amplitudes the effect of the viscous component is predominant and the total damping coefficient appears to be behaving like a cubic polynomial in forward speed. It is interesting to note that the total damping due to the bilge keels has a weaker dependence on forward speed than either the viscous or the nonviscous components individually.

The effect of the natural frequency on the bilge keel damping has also been studied, for the case of zero forward speed. Interpretation of these results is complicated by the fact that the roll axis changes with loading condition, and the resulting change in the roll moment arm may have a larger influence than the change in the natural frequency. In order to look at the effect of frequency on the bilge keel damping component, it is necessary to first remove the effects of the roll moment arm. This can be done approximately by assuming that the viscous and nonviscous components of the bilge keel damping are proportional to r_0^3 and r_0^2 , respectively, where r_0 is the distance from the CG to the bilge keel root. Figure 8 shows a plot of the slope and intercept components normalized by r_0^3 and r_0^2 , respectively. It can be seen that the normalized slope component is an increasing function of frequency, while the normalized intercept component is almost independent of the frequency.

COMPARISON WITH THEORY

Theoretical predictions made using the DREA ship motion computer program SHIPMO [7] were compared with the experimental results. Figure 9 compares zero-speed results. It can be seen that the agreement is good in this case. The trend with forward speed was not as well predicted. This seems to be mainly due to the linear theory used for predicting the nonviscous component of the damping coefficient. Analysis of the experimental

results indicates that this component has a nonlinear dependence on forward speed. For the model fitted with bilge keels, SHIPMO was found to overpredict the damping at low speeds and underpredict it at high speeds. The theoretical and experimental curves cross at an intermediate speed which, for the medium GM case, was found to be about 1.9 m/sec. The dependence of the nonviscous component of damping on forward speed requires further investigation.

It should be noted that the rudder is an important source of dynamic lift damping for warship hulls. The absence of a rudder for these tests resulted in a reduction in the relative importance of this component. It is expected that the rudder dynamic lift damping would be well predicted by SHIPMO, and therefore that the relative error in the total roll damping at forward speed would be significantly reduced by the presence of a rudder.

CONCLUSIONS

In this work, we have presented the results of the analysis of a series of experimentally obtained free roll decay curves for a destroyer model. We hope that these results will provide a data base for the damping coefficients of such a hull form. The method of analysis used allows the study of the form of the damping moment as a function of the roll amplitude. This should be useful in large amplitude investigations of the motion. The technique presented was shown to be successful in identifying the viscous and nonviscous components of the damping. It also helped in studying the effect of forward speed on the damping, especially for the case of the model fitted with bilge keels since the damping coefficients could be obtained by analyzing single roll cycles. Theoretical predictions for the damping coefficient, obtained using SHIPMO4, are in good agreement with the experimental results, for the case of zero forward speed; however, the agreement was less good for the case with forward speed. This is a point that requires further investigation. It is

evident from the experimental results that the measured roll damping coefficient is sensitive to the location of the center of roll and to the resulting sway coupling. It is planned to investigate this further by conducting experiments with a free running model.

There are a number of qualitative conclusions that may be deduced from this study :

- 1- The roll damping coefficient for this hull form increases linearly with the roll amplitude.
- 2- The nonviscous part of the damping moment can be represented by a quadratic polynomial in the forward velocity, while the viscous component is best represented by a cubic polynomial in forward speed. The final form of the total damping moment depends on the magnitude of the motion.

ACKNOWLEDGEMENT

The authors would like to express their gratitude to the Defence Research Establishment Atlantic and the Natural Sciences and Engineering Research Council of Canada for supporting this project financially.

REFERENCES

1. Bass, D.W., Haddara, M.R. "Nonlinear models of ship roll damping", International Shipbuilding Progress, vol. 35, no. 401 (1988), pp. 5-24.
2. Sargent III, M. "Basic ring laser gyro theory", SPIE vol. 487, Physics Of Optical Ring Gyros (1984).
3. Cumming, D., Haddara, M.R. "On the roll damping characteristics of a destroyer model", Institute of Marine Dynamics Report, National Research Council, St. John's, Newfoundland, Canada, in Press.
4. Cox, G.G., Lloyd, A.R. "Hydrodynamic design basis for navy ship roll stabilization", SNAME Transactions, vol. 85, 1977, pp. 51-93.
5. Bass, D.W., Haddara, M.R. "Roll damping for small fishing vessels", Twenty Second American Towing Tank

Conference St John's, N F , August 1989

- 6 Hareno, Y "Prediction of ship roll damping - State of the art", University of Michigan report no 239, (1981)
- 7 Graham R , Trudelle,C "SHIPMO4 An updated user's manual for the SHIPMO computer program incorporating an extended hydrostatics capability and an improved viscous roll damping model", Defence Research Establishment Atlantic Technical Communication 87/304, March 1984

Table (1) Bilge Keel Details

STATION	DISTANCE FROM CLINELINE(M)	DISTANCE FROM BASELINE (M)
12	0 465	0 138
11	0 483	0 120
10	0 495	0 115
9	0 500	0 117
8	0 497	0 121
7	0 482	0 124
6	0 458	0 132

Length 3 093 m
Spm = 0 045 m

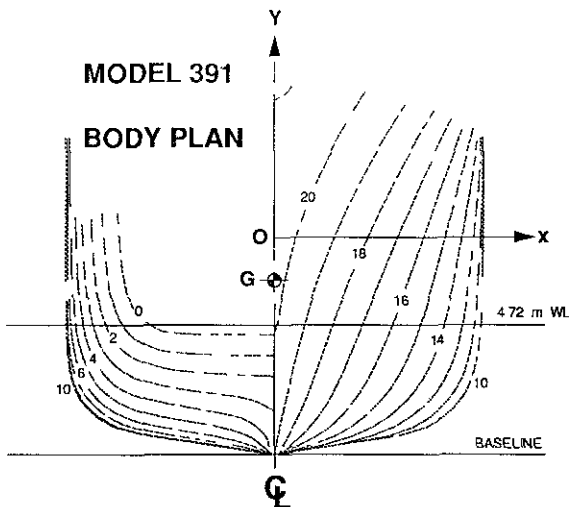


Figure 1. Model body plan and coordinate axes.

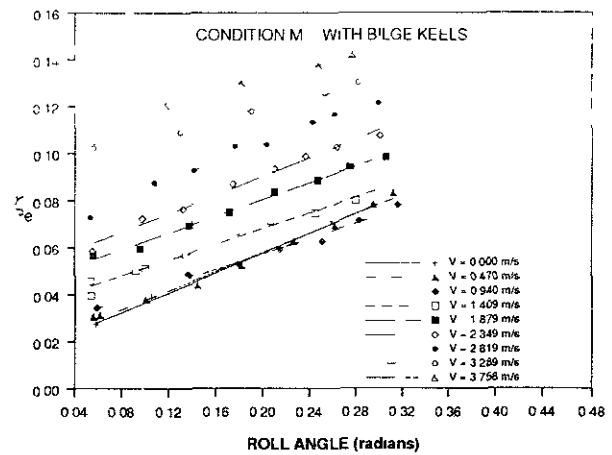


Figure 2. Nondimensional equivalent linear damping coefficient.

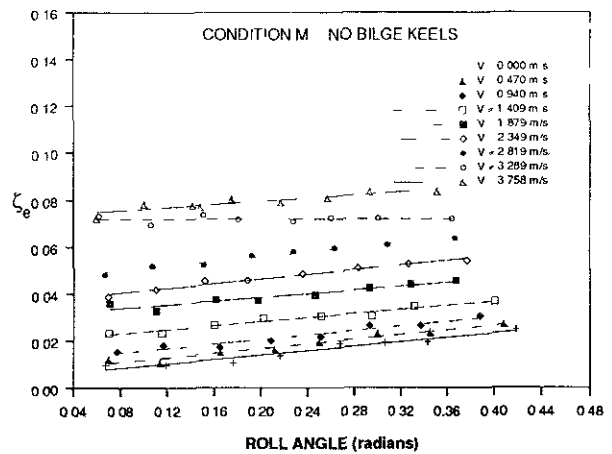


Figure 3. Nondimensional equivalent linear damping coefficient.

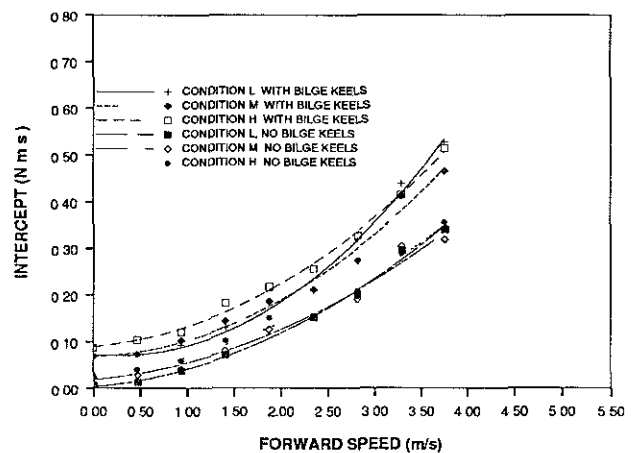


Figure 4 Intercept of the equivalent dimensional linear damping coef.

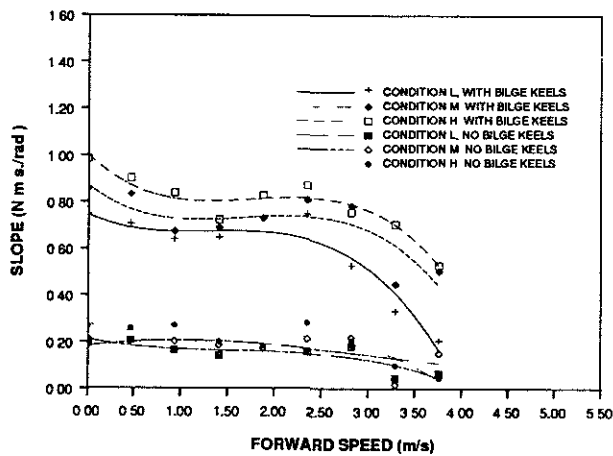


Figure 5 Slope of the equivalent dimensional linear damping coef.

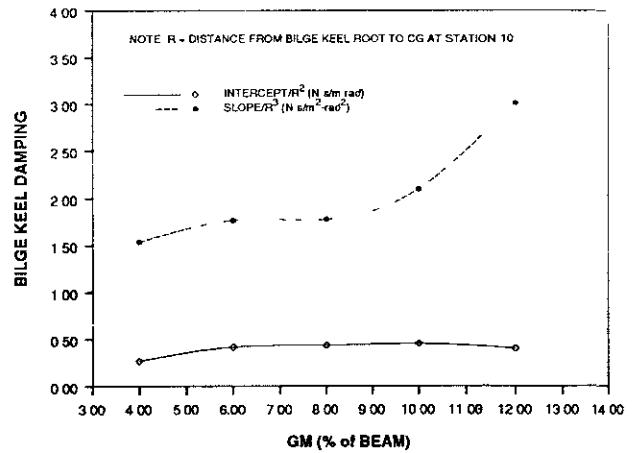


Figure 8 Normalized slope and intercept of the dimensional damping coefficient of the B.K.

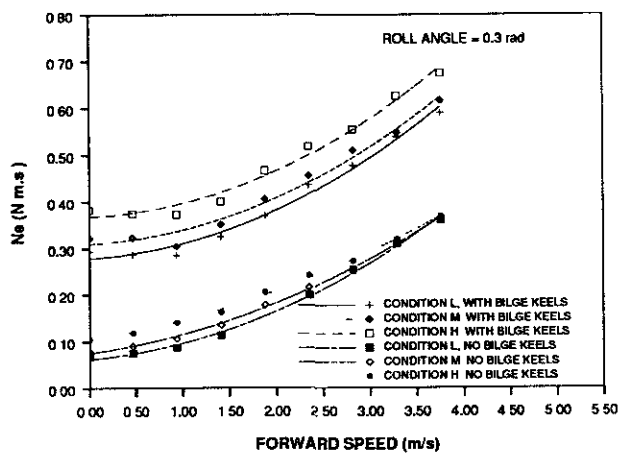


Figure 6 Dimensional equivalent linear damping coefficient.

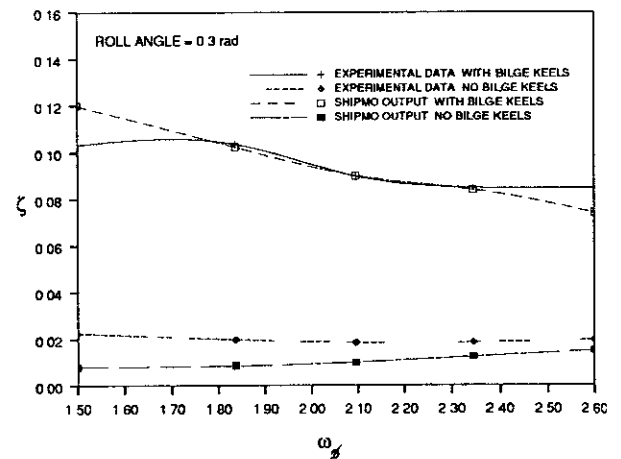


Figure 9 Nondimensional equivalent linear damping coef. vs. GM.

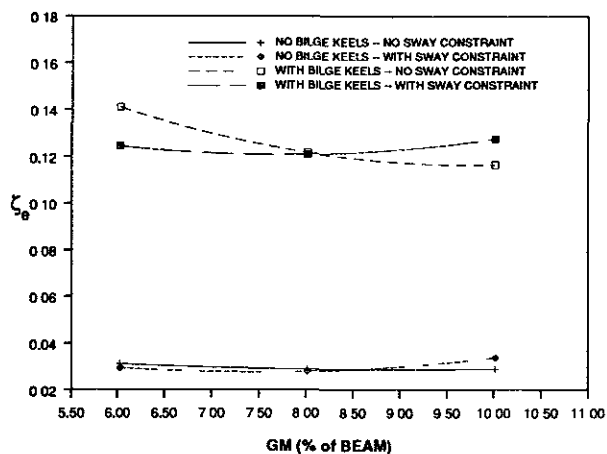


Figure 7 Nondimensional equivalent linear damping coef. vs GM.

THE TRANSVERSE STABILITY OF A PATROL BOAT TRAVELLING IN FOLLOWING WAVES

Zhenhai Cao

ABSTRACT

The present paper describes an investigation of the transverse stability of a patrol boat travelling in following waves. A series of partially captive model tests and calculations of the righting moment in various ship-wave relative positions are included. The model was towed in following regular waves at a speed slightly less than the wave celerity. The righting moment, trim angle and sinkage were recorded by means of strain gage and potentiometers respectively. An analytical method which was developed by M. Hamamoto et al in the previous conference was adopted in this investigation for calculating the righting moment. But the formulae of the method have been modified to enable them to be extended to the calculation of righting moment for various relative ship-wave positions up to angles of vanishing stability. A comparison between the results of the model test and the calculation is provided. Finally, some comments about this investigation are made.

INTRODUCTION

There are two factors which determine the stability of a ship. The first one is extrinsic. It may be called the environmental factor, such as influence of wind and waves. The second one is intrinsic. That is the anticapsizing ability or stability characteristics of the ship itself. If a ship travels in following waves, the ship-wave encounter period may become very long. So the stability characteristics would be affected by the wave profile remarkably. When a ship is positioned on a wave crest and travelling with a velocity nearly equal to the phase velocity of the wave, its stability would be decreased drastically. However, up to the present, most maritime countries still use restoring moment curves calculated in calm water conditions as the basis for judgement of ship stability. Along with increase in statistics of navigation accidents and deepening in understanding on ship stability in waves, the loss of stability of a ship in following waves has progressively attracted more attention, especially, for high speed vessels such as destroyers, escort vessels and patrol boats. This is due to the fact

that for high speed vessels even if they have sufficient stability in calm water, capsizing accidents or large angles of roll may frequently occur when they are operated in following waves. Because the block coefficients of these vessels are small, so loss of stability in following waves would be more serious for them. Some authors suggested that the stability characteristic of a ship in following waves may be adopted as a criterion for ship stability [1] [2]. However, in order to obtain stability characteristics in the following waves a convenient and well-validated calculation method is badly needed. It is well known that if a ship sails in following waves at the same speed as the wave celerity, the ship's heel is usually accompanied by definite trim and sinkage relations in order to satisfy the equilibrium of force and moment acting generally on the ship. Therefore, it is necessary to obtain an exact method of calculating the attitude of floatation in any ship-wave position. As asymmetry between the forebody and aftbody of a modern ship becomes more and more marked, trim would almost always occur even if the ship were heeled in calm water. Therefore, if influence of trim were neglected, not insignificant errors may be introduced in stability calculations.

The author has undertaken a research project to study the transverse stability of certain high speed vessels travelling in following waves. The contents of this project are divided into three parts. 1. the calculation method of ship stability in following waves. 2. a partially captive model test in following waves and the comparison between the results of model test and theoretical calculation. 3. a suggestion on stability criterion of high speed vessels in following waves. A brief account of the first two parts of the project is described in the present paper. The analytical method developed by Hamamoto and Namoto [3] in the previous stability conference and the author's own work as a modification and a complement of their method has been applied, wherein stability characteristics for any given relative ship-wave position may be calculated. Partially captive model tests on the model of a patrol boat had been carried out in the seakeeping basin of CSSRC. Through comparison between results of calculation and that of model tests, the validity of the method and of the formulae have been established. It seems that the method may be a useful device for calculating ship stability

Senior Engineer, China Ship Scientific
Research Center
Wuxi, Jiangsu, China

characteristics either in calm water or in following waves.

THE CALCULATION FORMULAE

According to Froude-Krylov Hypothesis, the existence of the ship does not change the structure and pressure distribution of the wave. So long as the exact relative ship-wave attitude at various angles of heel are known and orbital motions of water particles are taken into account, the exciting moment produced by the wave profile on each section of the ship may be obtained. By integrating these static moments along the ship length, the total righting moment of the ship in wave can be easily obtained. There are two coordinate systems adopted in this paper, one is fixed on earth and the other on ship. The earth-bound coordinates $O_1\xi\eta\zeta$ and the ship-bound coordinates $OXYZ$ are right hand coordinates systems. The horizontal plane $O_1\xi\eta$ coincides with the calm water surface and the origin O_1 is located in the wave trough. The positive direction of $O_1\zeta$ is downward. The plane OXY coincides with design water line of the ship in calm water and the origin O is located on the same vertical line as the L.C.G. of the ship in upright condition. The positive direction of OZ is toward the keel and that of OX is toward the bow. Because the ship and wave traveled at same velocity, the wave elevation ζ_w at a certain time and a certain place may be represented by the following equation:

$$\zeta_w = a \cos k(\xi_0 + x) \quad (1)$$

wave pressure p can then be calculated as:

$$p = \rho g \zeta - \rho g a e^{-k\zeta} \cos k(\xi_0 + x) \quad (2)$$

The vertical pressure gradient at a cross section of the ship is then

$$\left(\frac{dp}{dx}\right)_{\Lambda(x)} = \rho g [1 + a k e^{-k\zeta} \cos k(\xi_0 + x)] \quad (3)$$

Fig.1 is a schematic explanation of the relationship between the ship and wave coordinates. Formula (3) implies that the effect of the orbital motion on the vertical pressure gradient may virtually be expressed as a change of the water density, with apparent high density at troughs and low density at crests. Such an apparent density at a cross section $\Lambda(x)$ may be written as:

$$\rho^* = \rho [1 + a k e^{-k\zeta} \cos k(\xi_0 + x)] \quad (4)$$

In ship-bound coordinates $OXYZ$, the righting moment M_r for a heeled ship in a longitudinal wave may be written as:

$$M_r = \int_{XA}^{XF} \left(\frac{dK_n}{dx}\right) dx - W \overline{OG} \sin \phi \quad (5)$$

$$n = 1, 2 \text{ or } 3$$

where $\frac{dK_n}{dx}$ denotes the restoring moment, about axis OX , generated by the buoyant force acting on the section which is located at x . n is chosen to be 1, 2 or 3 according

to the locations of the two points of intersection between the wave profile and the contour of the cross section. The two points where the section contour intersect the wave profile is named P for left and S for right. Four different situations may be distinguished as follows assuming that the ship is heeled in the positive direction.

1. P lies on the Ship Side Contour at Port and S lies on the Ship Side or Deck Contour at Starboard

This situation denotes that the keel point K of the section lies below the water surface and the crown point T of section contour lies above the water surface. This is the situation for most sections of the heeling ship in the beginning stage, as shown in Fig.2. According to Fig.2, $\frac{dK_1}{dx}$ may be obtained by the following formula:

$$\begin{aligned} \frac{dK_1}{dx} = & -\rho g [1 + a k e^{-k\zeta} \cos k(\xi_0 + x)] \quad (6) \\ & \{ \cos \phi \int_{Z_S}^{Z_P} b^2(Z) dZ - \sin \phi [\int_{Z_S}^0 Z b(Z) dZ + \\ & \int_0^{Z_P} Z b(Z) dZ + \int_{Z_P}^0 2Z b(Z) dZ] - \\ & \frac{(1 - \tan^2 \phi) \sin \phi}{6} [b^3(Z_P) + b^3(Z_S)] - \\ & \frac{\tan \phi \sin \phi}{2} [Z_P b^2(Z_P) - Z_S b^2(Z_S)] \} \end{aligned}$$

when the Z_P and Z_S for each section are found, M_r may be easily calculated by formulae (5) and (6). But the Z_P and Z_S are still unknown at this stage. Let O' be the point where axis OX penetrates the section. Owing to the sinkage and trim of the ship, the perpendicular distance between O' and the wave profile becomes:

$$O'E = -(\zeta - x\theta) + a \cos k(\xi_0 + x) \quad (7)$$

It is found from Fig.2 that Z_P , Z_S and $O'E$ satisfy the following relations:

$$O'E = Z_P \cos \phi - b(x, Z_P) \sin \phi \quad (8)$$

$$O'E = Z_S \cos \phi + b(x, Z_S) \sin \phi$$

By comparing (7) and (8), the expressions for Z_P and Z_S may be obtained as follows:

$$Z_P = - \frac{\zeta - x\theta - b(x, Z_P) \sin \phi - a \cos k(\xi_0 + x)}{\cos \phi} \quad (9)$$

$$Z_S = - \frac{\zeta - x\theta + b(x, Z_S) \sin \phi - a \cos k(\xi_0 + x)}{\cos \phi} \quad (10)$$

The increments of Z_P and Z_S , namely ΔZ_P and ΔZ_S , caused by increment $\Delta \phi$ in heel angle are:

$$\Delta Z_P = - \frac{\Delta \zeta - x \Delta \theta - \Delta \phi [b(Z_P) \cos \phi + Z_P \sin \phi]}{\cos \phi - b'(Z_P) \sin \phi} \quad (11)$$

$$\Delta Z_S = - \frac{\Delta \zeta - x \Delta \theta + \Delta \phi [b(Z_S) \cos \phi - Z_S \sin \phi]}{\cos \phi + b'(Z_S) \sin \phi} \quad (12)$$

where $b'(Z) = \frac{db}{dZ}$

The variables ϕ , $\Delta \phi$, x , $b(Z_P)$, $b(Z_S)$, $b'(Z_P)$, $b'(Z_S)$, Z_P and Z_S in formulae (11) and (12) are all known. The increment of sinkage and trim, $\Delta \zeta$ and $\Delta \theta$, caused by $\Delta \phi$ may be obtained by solving the following simultaneous equations:

$$\Delta \zeta \int_{XA}^{XF} [b(Z_p) + b(Z_s)] dx - \Delta \theta \int_{XA}^{XF} x [b(Z_p) + b(Z_s)] dx = \Delta \phi \int_{XA}^{XF} F_1(x) dx \quad (13)$$

$$\Delta \zeta \int_{XA}^{XF} x [b(Z_p) + b(Z_s)] dx - \Delta \theta \int_{XA}^{XF} x^2 [b(Z_p) + b(Z_s)] dx = \Delta \phi \int_{XA}^{XF} x F_1(x) dx$$

where

$$F_1(x) = \frac{1}{2} [b^2(Z_p) - b^2(Z_s)] (1 - \tan^2 \phi) \cos \phi + [Z_p b(Z_p) + Z_s b(Z_s)] \sin \phi \quad (14)$$

The new floatation attitude of the ship in a certain wave profile may be obtained by considering these increments caused by $\Delta \phi$. Then the righting moment may be easily calculated. The derivation of these formulae are referred to [3].

2. Both P and S lie to the Starboard of the Central Longitudinal Plane

This situation denotes that the keel point X of the section has emerged from the water surface. Such an attitude may be taken up by sections located in a wave trough after the ship has heeled over a moderate angle, as shown in Fig. 3.

According to Fig. 3, $\frac{dK_2}{dx}$ may be obtained by the following formula:

$$\begin{aligned} \frac{dK_2}{dx} = & -\rho g [1 + a k e^{-k \zeta_s \cos(\xi_0 + x)}] \\ & \{ \cos \phi \int_{Z_s}^{Z_p} \frac{1}{2} b^2(Z) dZ - \sin \phi \left[\int_{Z_s}^0 Z b(Z) dZ + \int_0^{Z_p} Z b(Z) dZ \right] - \frac{(1 - \tan^2 \phi) \sin \phi}{6} \\ & [b^3(Z_s) - b^3(Z_p)] - \frac{\tan \phi \sin \phi}{2} [Z_p b^2(Z_p) - Z_s b^2(Z_s)] \} \end{aligned} \quad (15)$$

Because both P and S lie on the starboard side, the relations between O'E and Z_p and the between O'E and Z_s take same form as follows:

$$\begin{aligned} O'E &= Z_p \cos \phi + b(Z_p) \sin \phi \\ O'E &= Z_s \cos \phi + b(Z_s) \sin \phi \end{aligned} \quad (16)$$

By comparing (7) and (16), the following expressions may be obtained:

$$\begin{aligned} Z_p &= - \frac{\zeta - x \theta + b(Z_p) \sin \phi - a \cos k(\xi_0 + x)}{\cos \phi} \\ Z_s &= - \frac{\zeta - x \theta + b(Z_s) \sin \phi - a \cos k(\xi_0 + x)}{\cos \phi} \end{aligned} \quad (17)$$

The increments of Z_p and Z_s caused by an increment of the heel angle may be obtained from the following expressions:

$$\begin{aligned} \Delta Z_p &= - \frac{\Delta \zeta - x \Delta \theta + \Delta \phi [b(Z_p) \cos \phi - Z_p \sin \phi]}{\cos \phi + b'(Z_p) \sin \phi} \\ \Delta Z_s &= - \frac{\Delta \zeta - x \Delta \theta + \Delta \phi [b(Z_s) \cos \phi - Z_s \sin \phi]}{\cos \phi + b'(Z_s) \sin \phi} \end{aligned} \quad (18)$$

The increments of sinkage and trim, $\Delta \zeta$ and $\Delta \theta$, caused by $\Delta \phi$ may be obtained by solving the following simultaneous equations. The detailed derivation of these expressions may be seen from reference [4].

$$\begin{aligned} \Delta \zeta \int_{XA}^{XF} [b(Z_s) - b(Z_p)] dx - \\ \Delta \theta \int_{XA}^{XF} x [b(Z_s) - b(Z_p)] dx = \\ \Delta \phi \int_{XA}^{XF} F_2(x) dx \end{aligned} \quad (19)$$

$$\begin{aligned} \Delta \zeta \int_{XA}^{XF} x [b(Z_s) - b(Z_p)] dx - \\ \Delta \theta \int_{XA}^{XF} x^2 [b(Z_s) - b(Z_p)] dx = \\ \Delta \phi \int_{XA}^{XF} x F_2(x) dx \end{aligned}$$

where

$$\begin{aligned} F_2(x) = & \frac{1}{2} [b^2(Z_p) - b^2(Z_s)] \\ & (1 - \tan^2 \phi) \cos \phi - \\ & [Z_p b(Z_p) - Z_s b(Z_s)] \sin \phi \end{aligned} \quad (20)$$

3. Both P and S lie to the Port of the Center Plane

This situation denotes that the crown point T of the section contour is immersed in water. Such an attitude may be taken up on sections located in a wave crest after the ship has heeled over a moderate angle, as shown in Fig. 4. According to Fig. 4, $\frac{dK_3}{dx}$ may be obtained by the following formula:

$$\begin{aligned} \frac{dK_3}{dx} = & -\rho g [1 + a k e^{-k \zeta_s \cos(\xi_0 + x)}] \\ & \{ \cos \phi \int_{Z_p}^{Z_s} \frac{1}{2} b^2(Z) dZ - \sin \phi \left[\int_{Z_p}^0 Z b(Z) dZ + \int_0^{Z_s} Z b(Z) dZ \right] - \\ & + \int_{Z_p}^0 2b(Z) Z dZ + \int_0^{Z_s} 2b(Z) Z dZ - \frac{(1 - \tan^2 \phi) \sin \phi}{6} [b^3(Z_p) - b^3(Z_s)] - \\ & \frac{1}{2} [Z_p b^2(Z_p) - Z_s b^2(Z_s)] \tan \phi \sin \phi \} \end{aligned} \quad (21)$$

Because both P and S lie on the port side, the relations between O'E and Z_p and that between O'E and Z_s have the same form as follows:

$$\begin{aligned} O'E &= Z_p \cos \phi - b(Z_p) \sin \phi \\ O'E &= Z_s \cos \phi - b(Z_s) \sin \phi \end{aligned} \quad (22)$$

By comparing (7) and (22), the following formulae may be obtained:

$$\begin{aligned} Z_p &= - \frac{\zeta - x\theta - b(Z_p)\sin\phi - a\cos k(\xi_0 + x)}{\cos\phi} \\ Z_s &= - \frac{\zeta - x\theta - b(Z_s)\sin\phi - a\cos k(\xi_0 + x)}{\cos\phi} \end{aligned} \quad (23)$$

The increments of Z_p and Z_s caused by the increment of heel angle may be obtained from following expressions:

$$\begin{aligned} \Delta Z_p &= - \frac{\Delta\zeta - x\Delta\theta - \Delta\phi [b(Z_p)\cos\phi + Z_p\sin\phi]}{\cos\phi - b'(Z_p)\sin\phi} \\ \Delta Z_s &= - \frac{\Delta\zeta - x\Delta\theta - \Delta\phi [b(Z_s)\cos\phi + Z_s\sin\phi]}{\cos\phi - b'(Z_s)\sin\phi} \end{aligned} \quad (24)$$

The increments of sinkage and trim, $\Delta\zeta$ and $\Delta\theta$, caused by $\Delta\phi$ may be obtained by solving the following simultaneous equations. The detailed derivation of these expressions are referred to reference [4].

$$\begin{aligned} \Delta\zeta \int_{XA}^{XF} [b(Z_p) - b(Z_s)] dx - \Delta\theta \int_{XA}^{XF} x [b(Z_p) - b(Z_s)] dx &= \Delta\phi \int_{XA}^{XF} F_1(x) dx \\ \Delta\zeta \int_{XA}^{XF} x [b(Z_p) - b(Z_s)] dx - \Delta\theta \int_{XA}^{XF} x^2 [b(Z_p) - b(Z_s)] dx &= \Delta\phi \int_{XA}^{XF} x F_2(x) dx \end{aligned} \quad (25)$$

where

$$F_1(x) = \frac{1}{2} [b^2(Z_p) - b^2(Z_s)] (1 - \tan^2\phi) \cos\phi - [Z_s b(Z_s) - Z_p b(Z_p)] \sin\phi \quad (26)$$

4. The Sections Emerged from Water Surface

The three typical cases mentioned above may solve all the situations where the ship section is intersected by the wave profile. But, under certain circumstance, a section of a ship hull at initial stages of heel may be totally emerged from water surface. Namely, the sectional areas for these sections are zero under water. For example, some sections at the bow and stern may take up this position provided the midship section is positioned on a relatively high wave crest (See Fig 11). As the heel angle increases, these sections would eventually be intersected by the wave profile successively and the sectional area under the water surface would be increased progressively. The contribution of these sections on stability may not be neglected since they may decrease the restoring moment. To seek the critical moments of intersection between these sections which emerged from the water surface and the wave profile, the search method seems to be the best. According to the results of previous stage of calculation, the attitude parameters ϕ , θ , ζ are known. So that the value of $O'E$ at each section including the sections that totally emerged from water surface are known from formula (7). The intersection point at the starboard side satisfies the following relation of (28).

$$O'E = Z\cos\phi + b(x, Z)\sin\phi \quad (28)$$

In searching for the coordinates of a point of intersection on the starboard side,

substitute them in formula (28), if the value of $O'E$ so obtained satisfy (7) and (23) simultaneously, then that is the point being searched for which is the exact intersection point. In actual practice, it is difficult to match the value of $O'E$ obtained from (23) to that of $O'E$ obtained from (7) exactly. If the difference between the two values of $O'E$ is in the region of permissible error, then that point is regarded as the exact intersection point. Using (22) instead of (28), the intersection point at the port side may also be searched in a similar manner.

$$O'E = Z\cos\phi - b(x, Z)\sin\phi \quad (29)$$

According to different locations of P

and S, the functions $\left(\frac{dKn}{dx}\right)$, $F_1(x)$ and $F_2(x)$

may be calculated and the contribution of the part of the section which newly immersed into water is obtained. In the case where the section entered into water, the search method is no longer adopted.

In practical calculations, the computation must start from the upright condition ($\phi=0$) and advancing for equal intervals of heel increments $\Delta\phi$ respectively. By repeating these operations several times, the required floatation attitude defined by ϕ , ζ and θ may be reached and the restoring moment provided by the ship under this attitude may be obtained. To start the calculations, ζ and θ must first be given for the upright condition ($\phi=0$) in a required wave condition. Since the ship is upright, the immersions at port and starboard are equal, so that $Z_p=Z_s=Z_c$. Putting Z_c into formulae (9) and (10) the following relation is obtained:

$$Z_c = -\zeta + x\theta + a\cos k(\xi_0 + x) \quad (30)$$

To determine the initial values of ζ and θ for a ship placed in a wave profile in the upright condition, it is necessary to solve the following simultaneous equations [3].

$$\begin{aligned} \Delta\zeta \int_{XA}^{XF} 2b(Z_c) dx - \Delta\theta \int_{XA}^{XF} x 2b(Z_c) dx \\ = \Delta a \int_{XA}^{XF} G(x) dx \end{aligned} \quad (31)$$

$$\begin{aligned} \Delta\zeta \int_{XA}^{XF} x 2b(Z_c) dx - \Delta\theta \int_{XA}^{XF} x^2 2b(Z_c) dx \\ = \Delta a \int_{XA}^{XF} x G(x) dx \end{aligned}$$

$$G(x) = [2b(Z_c) - kA_0(x)e^{-k\zeta_s}] \cos k(\xi_0 + x) \quad (32)$$

Where $A_0(x)$ is sectional area under calm water surface.

In practical calculations, equation (31) must be solved starting from the basic case of calm water. By advancing Δa each time, the required values of ζ and θ for a

ship in a certain wave profile may be obtained after several iterations. The contour of each section of the ship may be divided into several regions. The section lines in each region may be simulated by a polynomial as follows:

$$b(x, Z) = \sum_{n=0}^N b_n Z^n \quad (33)$$

where $n=1, 2, 3$ or more.

The region number of the section contour may be divided and the order of the polynomial which simulated the section lines in a certain region depend on the form and curvature of the section. In general the region number of the section contour is about seven and the order of the polynomial is less than five.

PARTIALLY CAPTIVE MODEL TEST IN FOLLOWING WAVES

The main object of the test was to provide a comparison of the results between calculation and testing as a means of validation. The model for test was a patrol boat model. The principal characteristics of the model is as follows.

L	3.1 m
B	0.4 m
d	0.12 m
Δ	63 kg
KG	0.16 m

The test was carried out in the seakeeping basin of CSSRC. The wave length chosen for the test was 3.1 m and the wave height was 0.12 m. The wavemaker is of the pneumatic type. The model at a certain heel angle was captivated at the lower end of a dynamometer equipped with strain gages. The model and the apparatus are free to pitch and heave, but refrained from roll, sway, yaw and surge. The heel angle of the model is adjustable and may be locked after each adjustment. The model was towed under the towing carriage. Transverse force and moment act on the heeled model were measured by the strain gage while pitch (or trim angle) and heave (or sinkage) were measured by servos and potentiometers. The carriage and model were kept still in front of wave maker at the beginning of each run. When the wave front generated by the wavemaker has reached mid-length of the basin, the carriage and model was started, and made to follow the wave celerity. There is little possibility that the model speed may be made exactly equal the wave celerity, due to the fact that the carriage and wavemaker are two independently controlled systems. The model speed is made always slightly less than the wave celerity, so that the wave crest was encountered by the model only once during each run. The encounter frequency was kept about 0.04 HZ. The hydrodynamic effects acting on the model may thus be neglected under such a low model-wave encounter frequency as shown by the test results. Under these conditions, stationary values of the global forces and moments acting on the model, and values of trim and sinkage may be obtained for various ship-wave positions in a single run. For each angle of heel, the model is towed under the same wave conditions for five runs or more and the average

of them is taken to reduce random errors.

COMPARISONS OF RESULTS BETWEEN CALCULATION AND MODEL TEST

For the model tested and calculated under various ship-wave relative positions the results are shown in Fig. 5-Fig.14. (Among them: Fig A denotes the relative ship-wave position at upright condition, Fig B denotes the GZ Curve) Four typical relative positions are respectively: midship located at the wave crest ($\xi_0 + XG = \frac{1}{2}\lambda$), at the wave trough ($\xi_0 + XG = \lambda$), at the point of inflexion on the back of the wave ($\xi_0 + XG = \frac{3}{4}\lambda$) and at the point of inflexion on the front of the wave ($\xi_0 + XG = \frac{1}{4}\lambda$). The wave length chosen for calculation is 3.1 m and the wave heights are 0.12 m and 0.24 m respectively. The former is the same as the height chosen for model test. Thus, the results between calculation and model test may be compared conveniently. The model test values were plotted on Fig.5-Fig.10. It is shown from these figures that the results of calculations and of the model tests are in good agreement with one another.

CONCLUDING REMARKS

The present paper describes the stability of a patrol boat travelling in following waves. Through stability calculations of the model in following waves with two different wave height and through model tests in the same following wave the following conclusions are reached.

1. The stability characteristic of a ship in following waves may be calculated by the method provided in this paper. The relative position between ship and wave may be arbitrarily chosen and the calculations may be extended in range to the angle of vanishing stability.
2. When partially captive model tests in following waves are carried out in the seakeeping basin, the test results of various relative ship-wave positions may be obtained during a single run by using the slight difference of speed between the model and the wave.
3. The results between calculation and model test are good in agreement, thus validating the accuracy of calculation.
4. The method is also suitable for calculating stability characteristic of a ship in calm water. In this case the wave amplitude may be imputed as zero.
5. As far as the model of this patrol boat is concerned, the stability in a following wave with a 0.24m wave height is less than that with a 0.12 m wave height for any relative ship-wave position. As far as the relative ship-wave position is concerned, the stability is the worst when the midship section is located at the wave crest followed by the case when the midship section is located at the point of inflexion on the frontal slope of the wave. They are all smaller than the corresponding stability

in calm water.

NOMENCLATURE

L	Ship length
B	Ship breadth
b(Z)	Offset of cross section
d	Section draft at upright condition
Z _p	Distance between the origin and left intersection in Coordinate Z
Z _s	Distance between the origin and right intersection in coordinate Z
a	wave amplitude
Δa	Increment of wave amplitude
λ	wave length
k	wave number
ρ	water density
g	Acceleration due to gravity
ξ ₀	Distance between center of gravity of the ship and the origin of earth-bound coordinates in ξ direction
XF	Distance between center of gravity of the ship and the FP in coordinate x
XA	Distance between center of gravity of the ship and the AP in coordinate x
OG	Distance between center of gravity of the ship and the origin of ship-bound coordinates in coordinate Z
XG	Distance between center of gravity of the ship and midship section in coordinate x
θ	Trim angle
Δθ	Increment of trim
φ	Heel angle
Δφ	Increment of heel

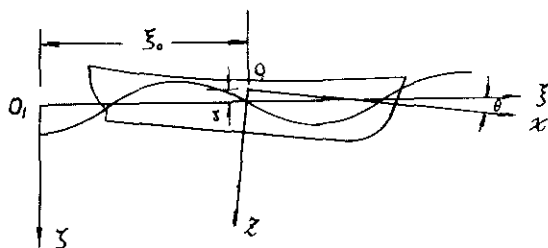


Fig. 1

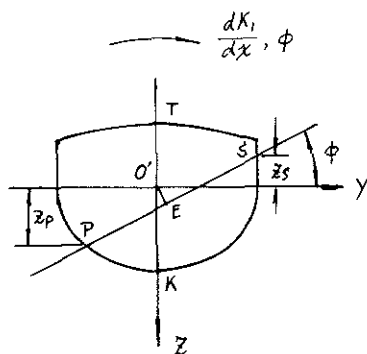


Fig. 2

Vertical sinkage or heave measured at point O, the origin of the ship-bound coordinates
 Δζ Increment of sinkage
 ζ_s Representative draft of the section, defined as the sectional area divided by the sectional breadth on design water line.

REFERENCES

- [1] C.Kuo, et al: Incorporating Theoretical Advances in Usable Ship Stability Criteria. Proceedings of International Conference on the Sateship Project: Ship Stability and Safety June 1986.
- [2] Cunler Helas: Intact Stability of Ship in Following Waves. Proceedings of STAB'82 Oct.1982.
- [3] Masami Hanamoto and Kensaku Honoto: Transverse Stability of Ship in a Following Sea. Proceedings of STAB'82 Oct.1982.
- [4] Zhenhai Cao: Theoretical Formulae and Calculation Procedure for Calculating Intact Stability of Ships in Following Waves. Technical Report of CSSRC (in Chinese) 1989.

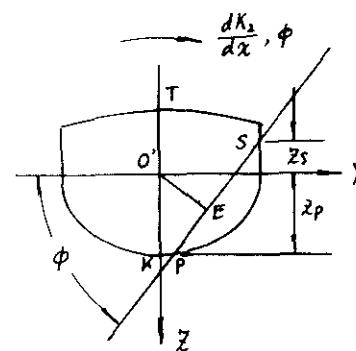


Fig. 3

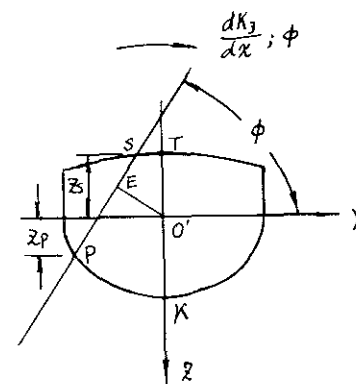


Fig. 4

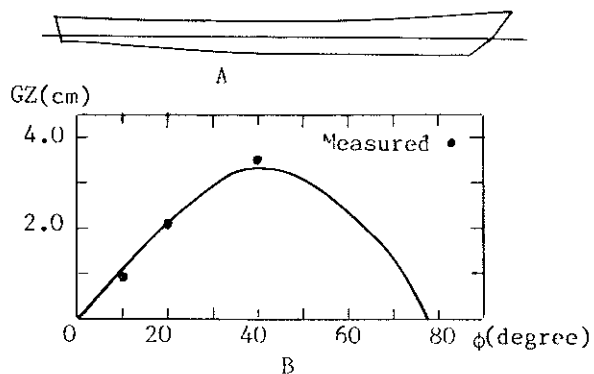


Fig.5 Calm water condition

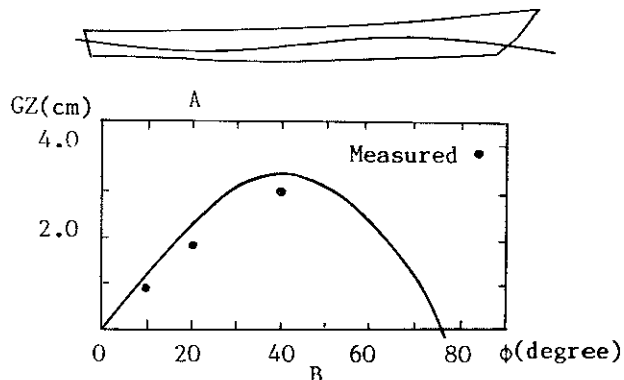


Fig.8 Midship located at the point of inflexion on the back of the wave $a=0.06m$

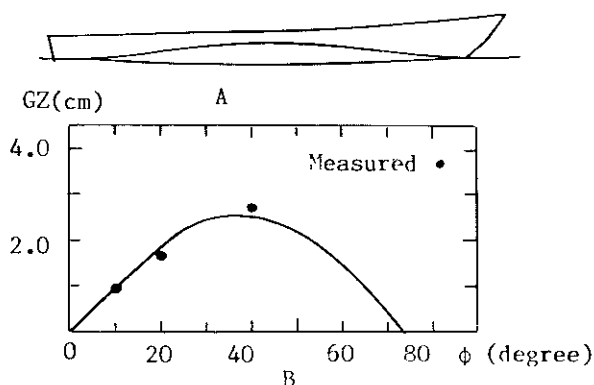


Fig.6 Midship located at the wave crest $a=0.06m$

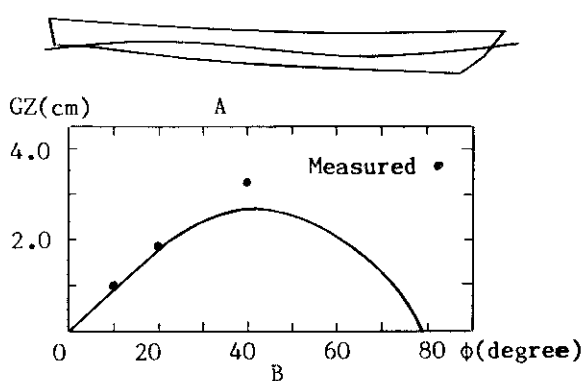


Fig.9 Midship located at the point of inflexion on the front of the wave $a=0.06m$

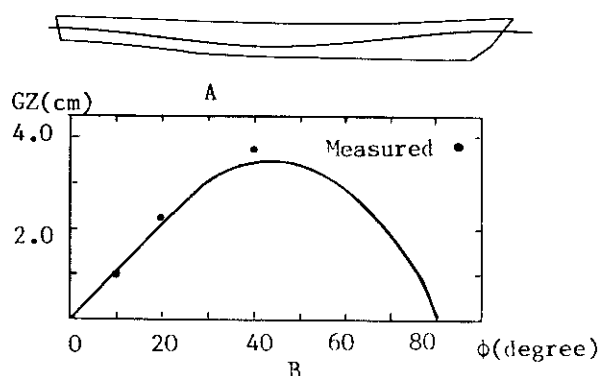


Fig.7 Midship located at the wave trough $a=0.06m$

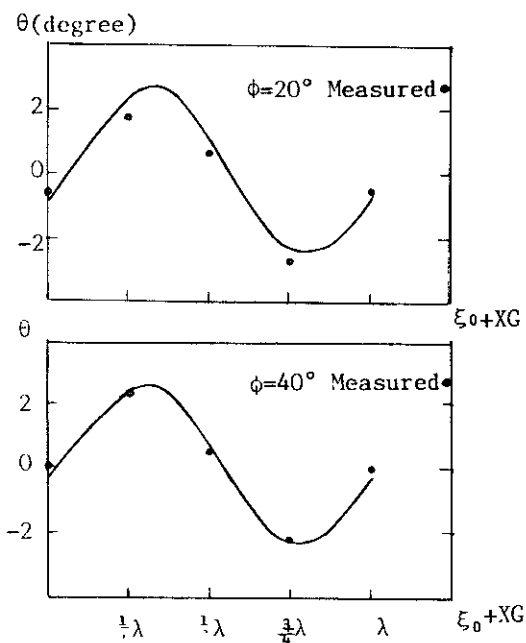


Fig.10 Change in trim with relative position of model to wave

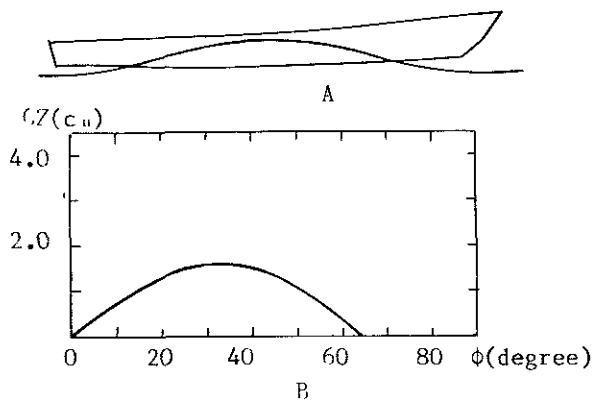


Fig.11 Midship located at the wave crest
a=0.12m

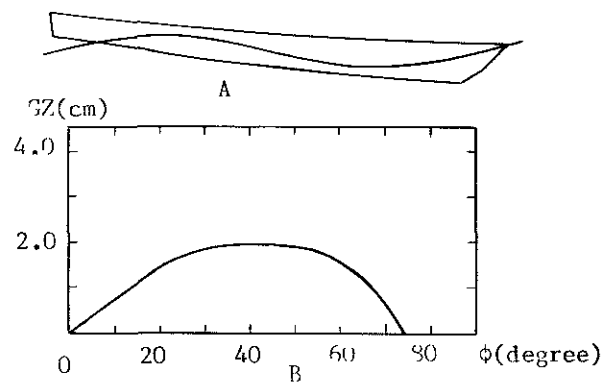


Fig.14 Midship located at the point of
inflexion on the front of the wave
a=0.12m

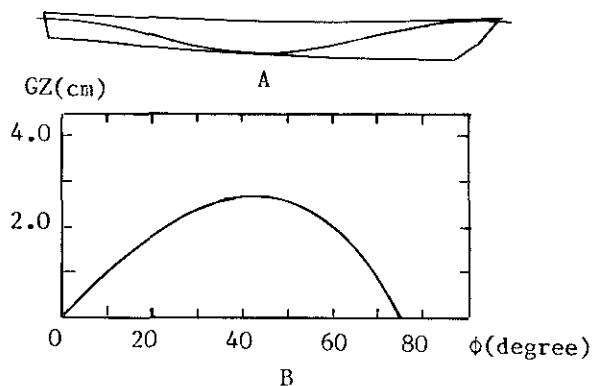


Fig.12 Midship located at the wave trough
a=0.12m

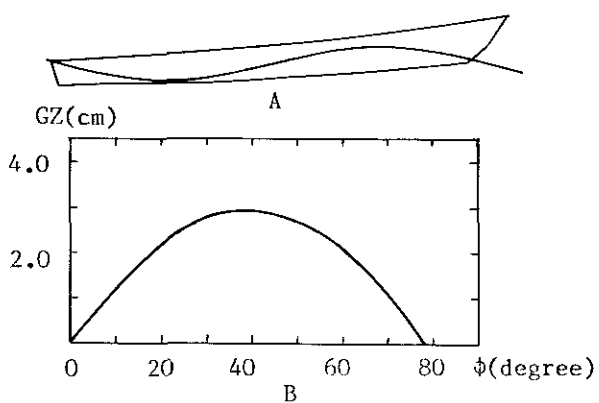


Fig.13 Midship located at the point of
inflexion on the back of the wave
a=0.12m

SAFETY LIMITS FOR SMALL FISHING VESSELS AT SEA

Kiyoshi AMAGAI and Nobuo KIMURA

In this paper sea conditions under an approaching typhoon were investigated off the coast of Hokkaido. Measurements were done on the ship's motion of small fishing vessels in danger of capsizing under these exceptional conditions.

From these data, the power spectra of wind waves and ship's motion were obtained. Rolling response functions were calculated for typical fishing vessels in Hokkaido.

From the above results, the extreme maximum rolling angles of these ships were predicted in rough seas. Work safety conditions were studied using the distribution of acceleration on deck in conjunction with the prediction of maximum ship's motion. Human balance threshold values for on deck situations were obtained using a linear discriminate function.

Analyzing the above information produced the following results.

1. The static safety range of the transverse stability in various fishing operations is in agreement with experiential wind velocity.
2. Safety dynamics for typical fishing vessels are explained in consideration of extreme maximum rolling and pitching angles.
3. The range between which the crew was unable to maintain their balance was also obtained.

Two aspects of safety limits at sea for fishing operations are explained. These two safety aspects are the crew balance threshold and the maximum rolling angles.

INTRODUCTION

Fishing vessels of less than 5 gross tons (GT) are predominant in the sea of Japan. However, additional ship's types include those with the capacity of 19 GT, 96 GT, and 124 GT. In terms of gross tonnage, the proportion of various sized fishing vessels in the sea of Japan is shown in Table 1. Stability of each fishing vessel over 20 GT is determined by the ship's stability rule, it's draught rule under loaded conditions and the vessel's performance standard. In addition, important matters of stability to small fishing vessels less than 20 GT are given by the vessel's safety standard. Through the use of these important matters of stability, the safety of Japanese fishing vessels can be secured. Every year fishing vessels capsize in the sea of Japan. Some of these accidents may occur due to limited attention given to these vessel's safety standards. Investigations are regularly conducted to determine

the cause of these incidents. In this paper, authors examined vessel's static stability under actual sea conditions for both 19 GT and 124 GT fishing vessels. These are the typical sizes for fishing vessels in Hokkaido.

Fishing vessel's movement limitations are studied by calculating the spectra of ship's motions under actual a typhoon conditions. Furthermore, the authors estimated a linear discriminate functions capable of describing when physical limitations for humans experiencing on-deck acceleration results in their inability to maintain their balance. Also investigated was the relationship between excessive vessel's movement and safe on-board working conditions. And we studied regarding the limits to movement of the fishing vessels in terms of safe working.

FISHING VESSEL'S STABILITY QUESTIONNAIRE

A questionnaire was conducted to pro-

vide additional information on the stability of various sized vessels under stormy weather conditions. The results from this questionnaire are presented in Table 2.

STABILITY OF FISHING OPERATION

Vessel's stability is significantly effected by the type of fishing gear being utilized. Since a given vessel may change gear types with each season, the stability of each small fishing vessel also can change seasonally. In addition, the deployment of gear affects stability. Therefore, even when only one type of fishing is underway, vessel's safety conditions may change from hour to hour. The transverse stability during various fishing operations of 19 GT and 124 GT fishing vessels are shown in Table 3. When 19 GT fishing vessels leave port, the position of the center of gravity is highest and the transverse metacentric height (GM) changes significantly with the type of fishing to be conducted. Conditions of the 124 GT fishing vessel refer to data obtained from the ship yard.

SAFETY DETERMINATION BASED ON A STABILITY ANALYSIS

The principal dimensions and body plans of B type ships (19 GT) and C type ships (124 GT) listed in Table 3 are shown in Fig.1. The stabilities of both ships were examined depending on their C coefficients. This study conducted stability analysis C1, C2, and C3 coefficients obtained from vessel's statical stability curves. The C2 coefficient is defined by the ship's stability rule. The C1 coefficient determines whether or not large quantities of sea water are being washed across the deck due to rough sea conditions. The C3 coefficient is used in the case where the shipping water on deck is included in a calculation. Fig.2 shows the GM-Freeboard diagram with a solid line as an example where the C2 coefficient of a B type ship every trim equals 1. The right side of a

solid line (C2=1) is the safety zone and the left side is considered unsafe. Each condition shown in Table 3 is entered in a non-safety zone for each case. However, the calculated results of ship's sides are added and presented in Fig.3. At a wind velocity of 15 meters per second (m/sec) each condition is within the ship's stability safety zone. However, when wind velocity reaches 19m/sec conditions are considered unsafe. In addition, if shipping water on deck is included, each condition is considered unsafe when wind velocity is 15m/sec. Fig.4a and 4b show the analysis of C type ships. Conditions are considered safe when wind velocity is 19m/sec provided these vessels are leaving the fishing grounds and returning to port. However, this situation is considered unsafe if the wind velocity reaches 26m/sec. These results indicate that when the wind velocity is excessive, fishermen accurately sense danger and suspend their fishing operations. The maximum wind velocity value of 22m/sec or 25m/sec is sufficient to capsize a 19 GT fishing vessel.

TYPHOON WEATHER CONDITIONS

Wind Velocity

In 1979, Typhoon 20 traversed the Japanese Islands from south to north causing serious damage to fishing fleets in northern Japanese waters. The route and transit time of Typhoon 20 are shown in Fig.5. The change of the wind velocity at each observation point is shown in Fig.6. The numerical values in parentheses describes the shortest distance from the route of the typhoon to the corresponding cities. The time is shown with an arrow. The wind velocity was at its maximum immediately after the typhoon had passed. However, the duration time of individual wind gusts decreased as the typhoon's distance increased.

Waves

Wave height was measured at ten places in the coastal waters of Hokkaido. The wave

height and period observed offshore of Tokachi port are shown in Fig.7. The maximum wave height in Tokachi was measured at two o'clock on October 20th 1979. The maximum wave height, wave period, significant wave height, and significant wave period in Tokachi were 10.5m, 12.0sec, 7.19m, and 12.3sec respectively.

Wave Spectrum

From October 19th to 20th, wave height was measured continuously by supersonic wave recorders located offshore of Tokachi. The wave spectra calculated from these data are shown in Fig.8. Characteristics of the wave spectra in Tokachi are as follows. As the typhoon approached, the spectrum peak gradually increased and the wave period became longer. The maximum peak occurred at two o'clock October 20th. The wave spectrum moment values (m_0) and the band quantity (ϵ) were calculated from each wave spectrum and are shown in Table 4. The comparisons between these m_0 and with those of the ITTC wave spectrum and the Pierson-Moskowitz wave spectrum are shown in Fig.9. The m_0 of the wave spectrum observed when the typhoon passed Hokkaido showed a larger value than the ITTC m_0 or the m_0 for the Pierson-Moskowitz wave spectrum.

LIMITS TO MOVEMENT OF THE FISHING VESSELS BY THE SPECTRUM OF SHIP'S MOTION

Ship's Motions of 19 GT Fishing Vessels in Rrough Seas

In early morning, when the wind from 8m/sec to 10m/sec did not stop blowing, fishing fleet leaders discussed whether or not they should attempt fishing. As a result, the whole fleet left for cod fishing using gillnets at 03:40. Because violent pitching occurred, the ship's speed was decreased by half speed at 04:07. The order to turn back was given to the whole fleet by fishing fleet chief leader at 04:20. The authors got on board a 19 GT M type ship whose body line is shown in Fig.10. After leaving port, the vessel's rolling and pitching motions were measured.

Fig.11 and 12 show the power spectra from these pitching and rolling measurements. The spectra from 1 through 4 occurred when an M type ship went to a fishing ground in bow-seas. The spectra 5 occurred when an M type ship returned to port in quarter-seas. Because pitching of an M type ship became violent as it approached the fishing grounds, it was determined necessary to turn back. The power of the rolling spectrum after turning back was bigger compared to the spectra when approaching the fishing grounds. This is remarkable from a safety viewpoint. Pitching amplitude became small after turning back, but rolling amplitude increased significantly. These probability density curves were confirmed from the result of a chi-square test having approximations to a Rayleigh distribution with the dangerous rate of 5 %. Statistical and spectral analyses results for the time series pitching and rolling data are shown in Table 5. The maximum conceivable pitch limit for a 19 GT M type ship occurs when the m_0 value equals 4.1.

Estimated Movement Limits for 124 GT Type Fishing Vessels

The relationship between a frequency response characteristic of ship $H_{\zeta}(\omega)$, a wave spectrum of $S_{\zeta\zeta}(\omega)$, and a spectrum of ship's motion $S_{yy}(\omega)$ is given below.

$$S_{yy}(\omega) = |H_{\zeta}(\omega)|^2 \cdot S_{\zeta\zeta}(\omega) \quad (1)$$

These quantities may be replaced by $H_{\zeta}(\omega_e)$, $S_{\zeta\zeta}(\omega_e)$, and $S_{yy}(\omega_e)$ so that the output-input relation becomes

$$S_{yy}(\omega_e) = |H_{\zeta}(\omega_e)|^2 \cdot S_{\zeta\zeta}(\omega_e) \quad (2)$$

Therefore, the spectra for pitch and roll motion can be calculated by the frequency response characteristics of rolling and pitching of a 124 GT fishing vessel (C type ship). The wave spectra for this situation in Tokachi after the typhoon passed are shown in Fig.8. The m_0 moment for these estimated spectra was calculated. The probability distribution extreme values

for pitching and rolling motions are considered approximates with the Rayleigh distribution. The maximum value, significant value, and expected value can be predicted from Table 6 by using the following relationship.

$$E = H_{rms}^2 = 16m_0 \quad (3)$$

In this paper, the band width quantity (ϵ) was calculated at route 2/3. The maximum expected value for the pitching and rolling is 1000 times every two hours and is shown in Fig.13. The rolling period of a 124 GT fishing vessel is about 7 or 8 sec. Therefore, a rolling motion happens 1000 times every two hours. Accordingly, a maximum expected value of rolling activity was estimated. Shown in black in Fig.13 is where the rolling angle was more than 20 degrees. 20 degrees is the angle that a bulwark of a C type ship would sink into the water. The rolling angle of a C type ship exceeded 20 degrees to the wave in beam-seas and quarter-seas after four hours the typhoon passed. This wave spectra's m_0 value was from 8.04 to 9.43 and the rolling spectra's m_0 value was from 7.86 to 10.29. When comparing this wave spectrum m_0 moment with the ITTC spectrum's m_0 value, the wind velocity is equal to 25 m/sec.

ONBOARD MOVEMENT AND BALANCE LIMITATIONS FOR CREWMEN

In addition to vessel safety concerns, the authors also investigated with the viewpoint for crew safety. This was done with specific regard to potential occupational accidents which may occur when the fishing vessel experiences hazardous weather conditions. It was noticed that the inability to maintain balance on board in heavy seas resulted in on-deck injuries and manoverboard situations. The ship's motion acts as a dynamic oscillatory balancing force in the work and actions of crewmen on board the vessel. Accordingly, it is necessary to clarify the relationship between vessel's motion and the maintenance

of balance of humans onboard.

Method for Evaluating Crew Balance on Deck

Individuals on board make linear responses to vessel's motion. The authors utilized an input-output model describing how a human body's center of gravity (C.G.) is accelerated by a vessel's oscillatory motion; especially with respect to the ship's acceleration on deck. The acceleration on deck is an important element when the balance condition of a crewman is evaluated. The size and frequency of acceleration have an effect on human balance. The maintenance of balance was judged on the basis of whether or not the subject could hold a posture on a FORCE-PLATE (60 X 180 cm) through the end of the measurement time. The experiments were done repeatedly under various sea conditions. One measurement time is equal to one minute. As a result, we could discriminate whether or not a crewman could maintain his balance on deck by evaluating the X, Y, and Z-directional acceleration. The primary moment (m_l) in the power spectrum for acceleration generated on deck was considered a discriminatory factor. This was determined because the maintenance of balance relied on frequency. The relationship between the m_l value and the subject's balance condition is shown in Fig.14. Each axes indicates an m_l value in each direction. Dotted marks indicate a subject's stable posture condition on deck. An X-mark indicates the subject had completely lost his balance. It is anticipated that the maintenance of balance becomes difficult when values of m_l in each direction exceeded a given range as shown in Fig.14. Therefore, the authors judged that these are proper discriminatory factors in order to evaluate human balance on deck. The linear discriminatory function through the use of m_l in each direction is defined below.

$$T = C_x \cdot M_{lx} + C_y \cdot M_{ly} + C_z \cdot M_{lz} \quad (4)$$

where C_x , C_y , and C_z are relationally estimated coefficients. On the basis of 256

data samples, these coefficients were estimated logically. If in one set $C_x=1$, then $C_y=0.1659$, $C_z=0.1133$, and a discriminatory standard of $T=0.220$ is the result. The classified results from 256 examples using equation (4) is shown in Fig.15. It is determined that $T=0.220$ is a threshold value beyond which the subject cannot maintain his balance.

The Limit to Movement of a Fishing Vessel Based on the Value of Index T

Since it is not possible to evaluate maintaining of balance with only roll and pitch information, the value of T comes into application. When a C type ship traversed the Tokachi area while returning to port with 10 knots, the T -values on deck were calculated by the O.S.M method. This example is considered as beam-sea conditions. The black area in Fig.16 indicates when the T -values on deck are greater than 0.220. With the exception of Number 7 spectrum, maintaining balance is difficult on deck near the stern of the vessel throughout the wave spectra. Occupational risk is expected to decrease if the crew is warned with sufficient time to stow fishing gear and deck machinery. The extent to which accident risk may decrease is dependent on the vessel's balance as indicated by the distribution of T -values.

CONCLUSION

Stability analysis and spectra analysis of typical Japanese fishing vessels were conducted to establish vessel safety limits aimed at preventing capsizing and reducing life-threatening situations at sea. On the whole, the authors have established that fishermen evaluate wind velocity primarily on the basis of the structural limitations of the vessel itself. However, results from this study suggest many capsizes occurred due to factors of human limits rather than vessel's limitations. The primary factors causing capsizes include the following interrelated elements:

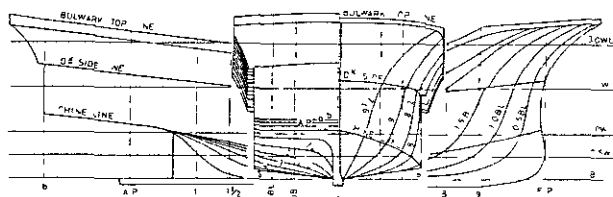
1) disregarding of weather forecasts; 2) misjudging transit time needed to reach safe refuge from an approaching storm; 3) poor preparation for oncoming stormy weather; 4) poorly stowed gear and equipment; and 5) inadequately maneuvering to waves.

In other words, capsizes occurring under conditions that are within the physical tolerance limits for the vessel, are strongly influenced by how the ship's crew maneuver the boat when attempting to compensate for the various external wind and wave forces. Accordingly, it is necessary for operators to recognize that the ship's motion in heavy seas will strongly be influenced by: 1) positioning of the vessel's load both in the hull and on deck; 2) the ship's course; and 3) vessel's speed.

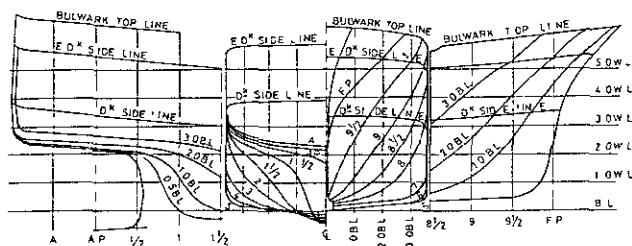
The authors have pointed out the risk of capsizing for small fishing vessels based in Hokkaido by using wave spectra m_0 values measured under typhoon conditions. Human limitations to keeping balance on deck was described by simultaneously solving linear discriminate functions. The establishment of safety limitations for crewmen moving about on small fishing vessels has also been proposed. It is strongly suggested that further examinations should be conducted toward identifying the most appropriate operation methods that encourage increased safety conditions for both fishing crew and vessel.

REFERENCES

1. N.Kimura and K.Amagai, On the relationship between the maintenance of human posture and the ship oscillatory motions, Proceedings World Symposium on Fishing Gear and Fishing Vessel Design, Canada, pp 564-568, 1988.
2. K. Amagai and N. Kimura, A proposal to prevent occupational accidents in scallop beam trawler, Safety and Working Conditions Aboard Fishing Vessels, Canada, 1989.



B ship (Lpp 15.20m x B 3.80m x D 1.48m)



C ship (Lpp 30.00m x B 7.16m x D 2.65m)

Fig.1 Principal dimensions and body plans of B and C ship

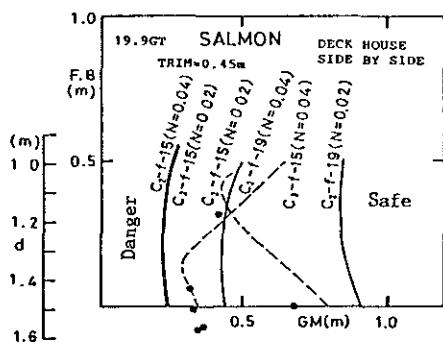


Fig.2 C2 coefficient and conditions in various fishing operations of 19 GT type B ship in Table 3

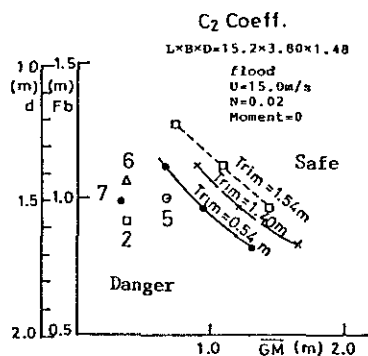


Fig.3 C2 and C3 coefficients and actual conditions in salmon fishing of B ship

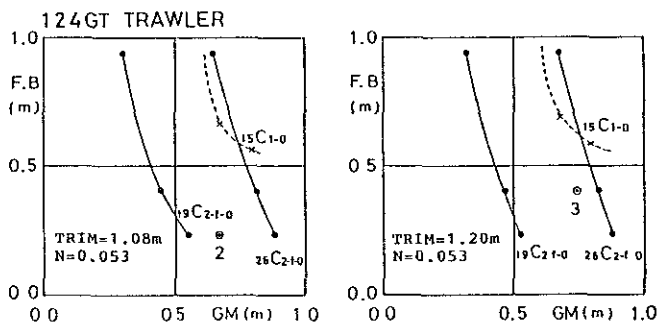


Fig. 4a

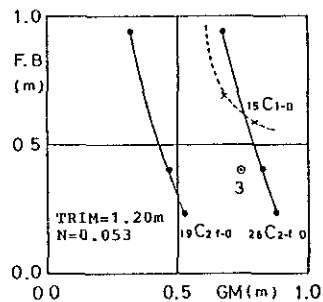


Fig. 4b

Fig.4 C2 coefficient and conditions in Table 3 of 124 GT type C ship

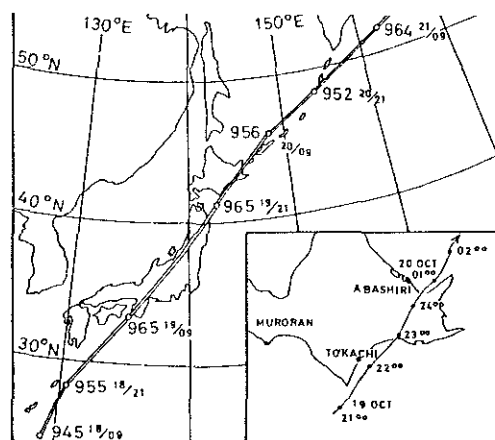


Fig.5 The route and transit time of the Typhoon 7920

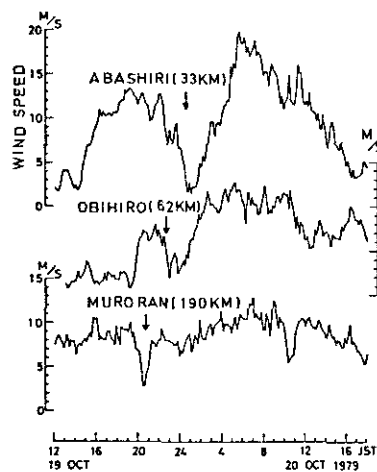


Fig.6 The change of the wind velocity when the typhoon passed

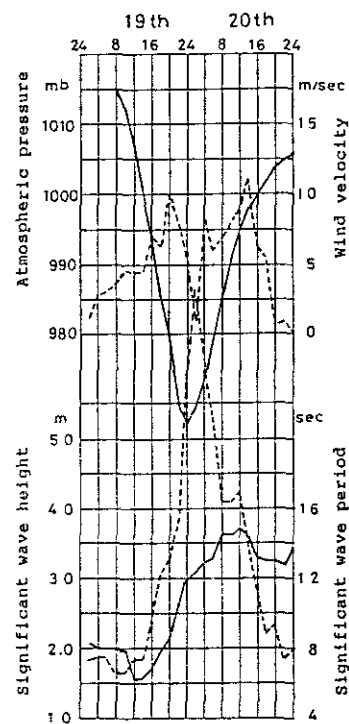


Fig.7 The atmospheric pressure, wind velocity and significant wave height and period in offshore of Tokachi

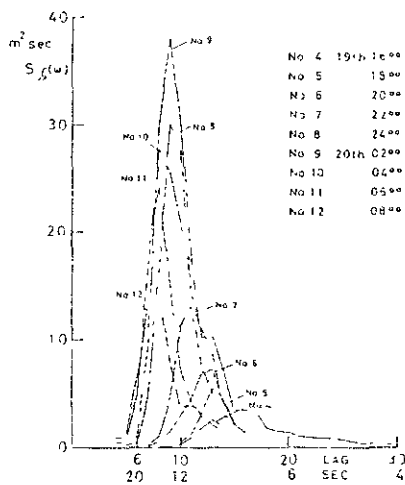


Fig.8 The wave spectra in Tokachi

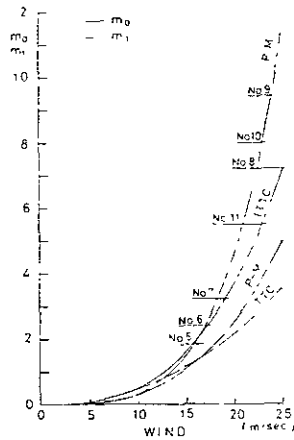


Fig.9 The comparison measured m_0 when the typhoon passed with m_0 of the ITTC and the Pierson-Moskowitz wave spectrum

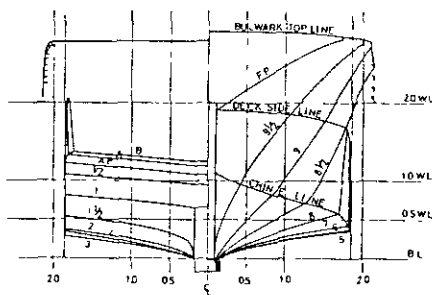


Fig.10 Body line of 19 CT type M ship

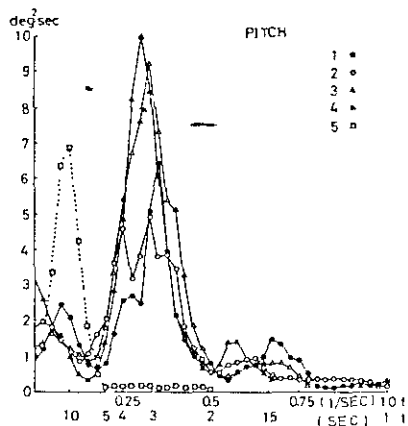


Fig.11 Power spectra of pitching of M ship

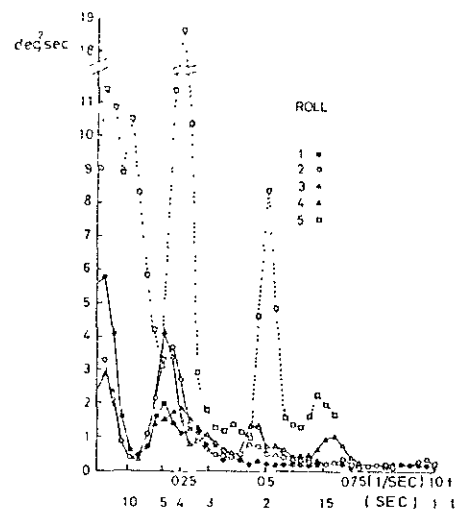


Fig.12 Power spectra of rolling of M ship

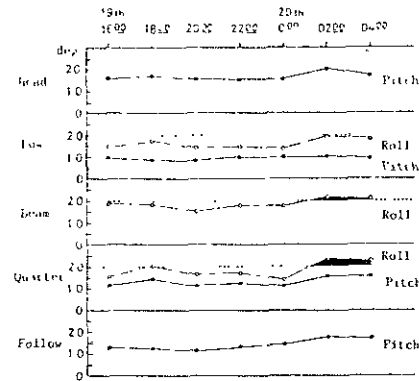


Fig.13 The expected values of maximum of pitching and rolling of C ship when the typhoon passed

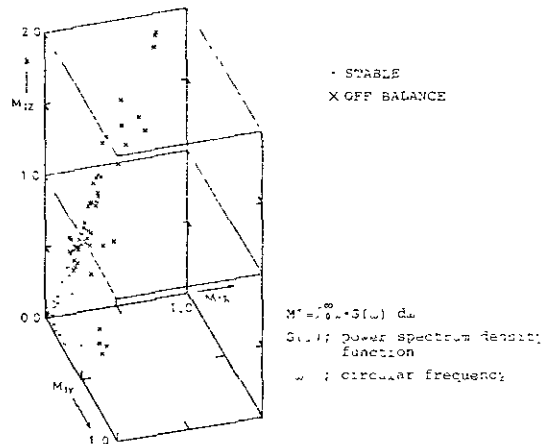


Fig.14 The relationship between human balance and distribution of first spectra moment of ship acceleration

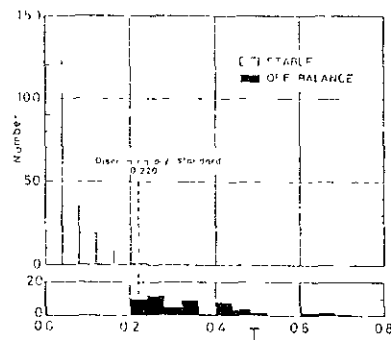


Fig.15 Discrimination of the state of human posture by the linear discrimination function

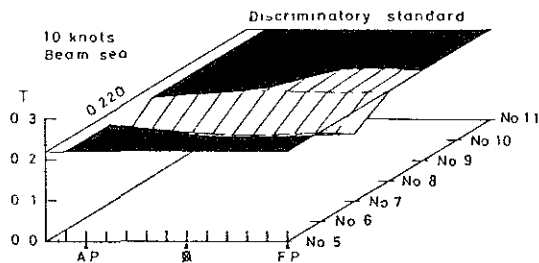


Fig.16 The distribution of the range where the crew is not able to maintain his balance

Table 1 The numbers of the powered fishing vessels in the sea

Size (G T)	Japan	Hokkaido
0- 4.9	356474	41214
5- 9	17664	2775
10- 14	5990	652
15- 19	5382	1151
20- 29	135	51
30- 49	735	80
50- 99	2153	164
100-199	1479	222
200-499	1646	206
500-999	54	
1000-	166	
Total	391878	46515

Table 2 The questionnaire with regard to safety of fishing vessels

Ship type Item	19.9 G T			124 G T	349 G T
	Ship a	Ship b	Ship c		
Wind velocity to suspend fishing operation	10m/sec			15~16m/sec	20m/sec
Wave height and direction in feeling a danger	More than 2m Beam, Quarter sea	Following sea	Beam, Quarter sea		
Experienced maximum wave height and wind velocity	5~6m, 24~25m/sec a moment 27m/sec	7~10m, 24~30m/sec	4~5m, 22~23m/sec a moment 35m/sec		
Times of experience in feeling a danger of capsizing	Gill net fishing for flounder	Stick held dip net fishing for saury	gill net fishing for salmon		

Table 3 The characteristics of transverse stability in various fishing operations

Ship type	Ship condition	dm	df	da	lrm	KM	Disp	GM	KG	lr	k
B ship (19.9GT)	1 Salmon fishing leav port	1.63	1.05	2.20	1.15	2.096	78.77	0.265	1.830	6.56	0.538
	2 arriv port	1.57	1.34	1.79	0.45	1.982	74.59	0.367	1.615	6.05	0.480
	3 unload fishing gear	1.57	1.30	1.84	0.54	1.951	75.45	0.350	1.601	6.10	0.473
	4 unload catches	1.18	0.91	1.44	0.53	2.107	50.38	0.416	1.691	6.90	0.583
	5 Squid fishing leav port	1.49	0.94	2.04	1.10	1.997	73.74	0.678	1.319	6.20	0.669
	6 Stick held dip netfishing leav port	1.43	0.66	2.20	1.54	2.068	72.78	0.310	1.758	6.30	0.460
	7 Gill net fishing leav port	1.50	0.92	2.08	1.16	2.002	74.75	0.329	1.673	6.70	0.503
C ship (124GT)	1 Light condition	1.75	0.70	2.79	2.09	4.085	299.7	0.682	3.403	7.10	
	2 leav fishing ground	2.46	1.92	3.00	1.08	3.569	369.6	0.675	2.894		
	3 arriv port	2.29	1.69	2.89	1.20	3.677	329.7	0.741	2.936		

Table 4 The values of m_0 and ϵ of the wave spectra in offshore of Tokachi

Wave spectra	m_0	ϵ
No. 5	1.8329	0.710
No. 6	2.3909	0.822
No. 7	3.2444	0.823
No. 8	7.2358	0.814
No. 9	9.4281	0.795
No. 10	8.0390	0.877
No. 11	5.5033	0.907

Table 5 The results of a statistical and spectral analysis

		Spectral Analysis				No of D Amj
Exp		ϵ	I_{acc}	m_0	σ	
1	PITCH ROLL	0.785 0.887	2.59 3.69	1.122 0.688	1.498 1.172	54 40
2	PITCH ROLL	0.808 0.856	2.71 2.91	1.703 0.740	1.554 1.216	51 47
3	PITCH ROLL	0.811 0.836	2.92 3.05	1.460 0.675	1.708 1.118	48 47
4	PITCH ROLL	0.780 0.816	2.80 3.30	1.571 0.915	1.777 1.352	47 45
5	PITCH ROLL	0.908 0.780	4.57 2.4	0.637 4.06	1.128 2.818	47 47
Statistical Analysis of Time History						
\bar{H}	H_{ms}	$H_{1/3}$	$H_{1/10}$	$H_{1/100}$	χ^2 value $\chi^2(0.05)$	
3.602 2.420	1.140 2.748	5.896 4.861	8.331 4.877	10.701 5.88	12.70 1.35	18.31 11.07
3.711 2.741	3.993 3.015	5.292 4.220	6.882 5.426	7.241 6.111	11.65 2.61	14.07 12.59
4.293 2.663	4.686 2.960	6.245 4.126	8.561 5.452	9.211 6.018	9.70 5.45	16.92 12.59
4.611 3.111	4.980 3.414	6.819 4.693	8.190 5.824	9.081 7.113	1.96 6.05	16.92 14.07
1.981 6.257	2.422 7.340	3.451 10.954	4.595 11.875	5.593 15.417	4.98 20.60	11.07 25.00

Table 6 Statistical values for the expected value of maximum

	$\epsilon=0$	$\epsilon=\sqrt{2/3}=0.816$
\bar{H}	$0.886\sqrt{E}$	$0.511\sqrt{E}$
$H_{1/3}$	$1.415\sqrt{E}$	$1.21\sqrt{E}$
$H_{1/10}$	$1.80\sqrt{E}$	$1.647\sqrt{E}$
$H_{1/100}$	$2.28\sqrt{E}$	$2.157\sqrt{E}$
$H_{1/1000}$	$2.74\sqrt{E}$	$2.636\sqrt{E}$

\bar{H} , Average roll amplitude,
 $H_{1/3}$, Significant roll amplitude,
 $H_{1/10}$, One-tenth highest roll amplitude, and so forth

MOHAMED S. SOLIMAN*

ABSTRACT

Numerical analysis of the steady state and transient motions of the semi-empirical nonlinear differential equations, which have been used to model the resonant rolling motions of two ships, are presented in this paper. Examination of the safe basin in the space of the starting conditions shows that transient capsizes can occur at a wave height that is a small fraction of that at which the final steady state motions lose their stability. It is seen that the basin is eroded quite suddenly throughout its central region by gross striations, implying that transient capsize might be a reasonably repeatable phenomenon, offering a new approach to the quantification of ship stability in waves. Such an approach has the twin advantages of being both conceptually simpler, and at the same time more relevant, than one based on the steady state rolling motions. The latter analysis can be dangerously non conservative.

1 INTRODUCTION

Although sea states are essentially random processes (but not necessarily stationary ones), a short train or *pulse* of regular waves that can excite resonant motions, can usefully be viewed as a worst-case scenario when considering capsize. For practical purposes a long train of regular waves can be considered to have a probability of zero. Despite this, most researchers in the extensive literature on ship capsize under regular forcing, focus on just the single predominant *steady state* motion, be it harmonic, subharmonic or even chaotic. In this, they follow the tradition of classical analysis, despite the fact that for a boat, with its relatively light damping, regular waves will manifestly never persist long enough for transients to decay substantially. Not only is steady state analysis inapplicable, for this reason, but we show that it is also grossly non-conservative.

In this paper we focus attention on the transient motions of a ship which we investigate against the background of the steady-state behaviour [1]. Firstly, we present a steady state bifurcation diagram, in the control space of a wave height parameter, H , against wave frequency, ω , at which distinct local bifurcational phenomena take place. These typically include a jump to resonance at a cyclic fold bifurcation (saddle-node); a build-up of subharmonic oscillations at a flip bifurcation, as well as a stability boundary of capsize conditions.

Secondly, we consider the transient motions of a ship subjected to a short pulse of regular waves: and since starting conditions of a ship at the beginning of a pulse may vary widely, and in any event are unknown, we look at *all* possible transient motions. The simplest and most direct way to do this is to take a grid in the starting conditions of roll angle, θ_0 , and angular roll velocity, $\dot{\theta}_0$. Running simulations from each grid point, we can easily map out the *safe basin* from which transient motions do not lead to capsize within the specified duration of the pulse. Now as Soliman and Thompson [2] have identified and quantified for an archetypal driven oscillator there can arise a loss of engineering integrity accompanying the rapid erosion and stratification of the safe basin as a control parameter is varied. We show here that this behaviour does indeed take place in the analytical models of two real ships giving a critical wave height, H^t , at which the ship loses the bulk of its calm water stability. We use *engineering integrity curves* and *transient capsize diagrams* to quantify this behaviour.

2 GENERAL ROLL EQUATION

We consider, in common with many authors [3,4], that the roll motion of a ship, when subjected to wave and wind moments, can be modelled by the non-linear differential equation

$$I\ddot{\theta} + B(\dot{\theta}) + C(\theta) = M(t) + W_M(\theta, t) \quad (1)$$

where I is the roll inertia (included added hydrodynamic

*Department of Civil Engineering,
University College London,
University of London, England.

velocity and acceleration respectively), $B(\theta)$ is the non-linear damping moment and $C(\theta)$ is the non-linear restoring moment; these represent the stabilizing moments. The wind moment, $W_M(\theta, t)$, and the wave moment, $M(t)$, represent the de-stabilizing moments. Both these moments occur randomly in real seas but for the sake of simplicity, and for a worst case scenario, they can be considered to be deterministic quantities.

In order to illustrate the ideas presented in this paper we have considered two different ships which have been well documented and researched following their capsize. Both have the following specific equation of motion:

$$\ddot{\theta} + b_1 \dot{\theta} + b_2 |\dot{\theta}| \dot{\theta} + c_1 \theta + c_2 |\theta| \theta + c_3 \theta^3 + c_4 |\theta| \theta^3 + c_5 \theta^5 = \frac{M(t)}{I} + \frac{W_M}{I} \quad (2)$$

The first is the *Gaul* [5], with a GZ curve and damping characteristics taken from [6]. Here $b_1 = 0.0555$, $b_2 = 0.1659$, $c_1 = 0.2227$, $c_2 = 0.0$, $c_3 = -0.0694$, $c_4 = 0.0$, $c_5 = -0.0131$ and $I = 64489$. The second is the *Edith Terkol* [7]. Here $b_1 = 0.0043$, $b_2 = 0.0225$, $c_1 = 0.385$, $c_2 = 0.1300$, $c_3 = 1.0395$, $c_4 = -4.070$, $c_5 = 2.4117$ and $I = 1174$ (taken from [8]). We have approximated from these that their linear natural frequencies, ω_n , are 0.47 and 0.62 radians per second respectively and their equivalent linear damping ratios, ζ , are 0.075 and 0.01. The latter value of damping is unrealistically low, but is adopted uncritically in this study to illustrate the effect of damping on our analyses. We have assumed in common with other authors that $M(t) = A \sin \omega_E t$ where ω_E is the wave frequency and A is the amplitude of the wave moment which in general will be a function both of the wave frequency and height [9]. We have also assumed for the sake of simplicity that the wind moment is a constant value independent of roll angle and time: it is zero unless otherwise stated. We refer to the ratio of the forcing frequency to the linear natural frequency as ω , such that $\omega = \omega_E / \omega_n$ and refer to a wave height parameter H , such that $H = A / \omega_n^2$.

3 BACKGROUND THEORY

Before summarizing the results, a brief review of the dynamics theory, mapping techniques and terms employed is appropriate [10]. Considering the single-degree-of-freedom system (1) it is well known that to completely define the motion of a ship under given environmental conditions (such as wave height, period, etc) and from certain initial conditions (roll angle and angular velocity), the three dimensional trajectory in $(\theta, \dot{\theta}, t)$ phase-space must be determined. Trajectories which do not lead to capsize, will eventually settle down to a bounded stable motion (for example periodic or

motion is called an *attractor*. All starting conditions which generate trajectories that tend towards an attractor, thus define its *basin or domain of attraction*. There may be alternative co-existing attractors, depending on the starting conditions, but we shall define the *union* of the basins of all the non-capsizing attractors as the *safe basin*.

In the case of a ship rolling in regular waves, the concept of phase space is extended by the Poincaré map, for which the continuous trajectory is replaced by a succession of points obtained by stroboscopically sampling the motion of the ship at the wave period. This sampling technique produces a sequence of points (Poincaré points) in the $(\theta, \dot{\theta})$ plane which may converge to a fixed point corresponding to a stable periodic state, converge to alternating points for subharmonic motion (a period N attractor with N points visited in sequence) or possibly to a chaotic attractor. Such sampling techniques have been employed in the field of non-linear dynamics for their obvious advantages of summarizing the motion in a relatively simple fashion.

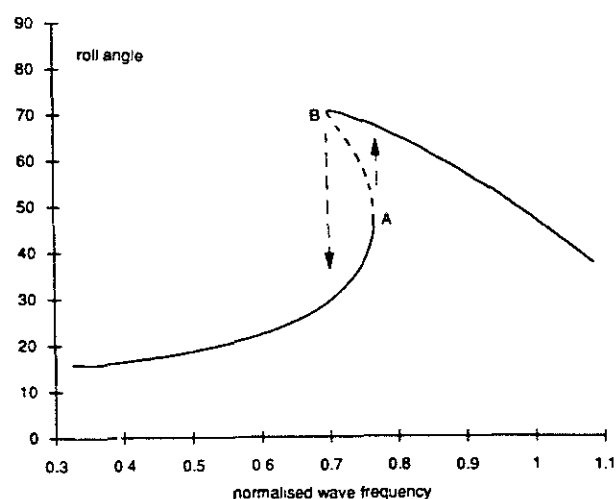


Figure 1. Typical resonance response curve for the Gaul ($H=0.24$). Here the solid lines represent stable steady state response; arrows indicate a jump to and from resonance. Dashed lines represent the unstable steady state response.

4 STEADY STATE BEHAVIOUR.

4.1 Bifurcation diagram

Excitation, corresponding to a *slowly evolving* sea state, can lead to resonance or large amplitude rolling as shown, in figure 1. As we slowly vary the frequency, so that transients have always effectively decayed, we see that the roll response is a smooth function of ω at all but two values. At $\omega=0.77$ there exists a dangerous but not fatal *jump to resonance*, in the sense that the ship restabilizes at a greater amplitude of oscillation. At

shows the *unstable* steady state solutions, and although they are not physically realizable, and indeed will not appear in the direct time domain simulations, they provide useful information about the global behaviour and for example play a key role in determining domains of attraction [11]. It is observed that due to the *overall* softening nature of the restoring moment curve the peak amplitude of oscillation occurs below the linear natural frequency. Such observations clearly illustrate that resonant frequencies should be avoided. Such resonant behaviour can also be observed by gradually increasing the wave height from the fundamental $H = \theta = \dot{\theta} = 0$ state until the ship capsizes for a fixed value of wave frequency. Complex bifurcations of the steady states were observed as, for example at $\omega=0.80$, there is a jump to resonance at $H^A=0.21$ and then a flip to an $n=2$ subharmonic at $H^C=0.44$. A further increase in H results in a period-doubling cascade and chaotic motion leading to capsize at $H^S=0.45$. It was also found that the optimal capsize condition, corresponding to capsize under a minimum H , occurs at about $\omega=0.70$.

Having outlined that steady states can undergo various complicated bifurcations including folds, flips and ultimate capsize, we show how the ship motion in a slowly evolving sea state may be summarised using a *steady state bifurcation diagram*. Such an analysis may help in predicting instabilities and capsize. Regions showing when and how the ship capsizes may be determined. Dangerous and fatal jumps to resonance, subharmonic oscillations and chaotic behaviour may be determined, all of which can add to the overall understanding of ship behaviour and capsize phenomena. Before summarising the results, we give a brief review of the analysis.

4.2 Analysis

The relationship between two consecutive Poincaré points in the Poincaré map will be governed by a complex non-linear relationship, but close to a fixed point (whether it be periodic or subharmonic) we may approximate the Poincaré map by a 2-dimensional linear map in the form

$$\begin{aligned}\theta_{i+1} &= a\theta_i + b\dot{\theta}_i \\ \dot{\theta}_{i+1} &= c\theta_i + d\dot{\theta}_i\end{aligned}\quad (3)$$

in which $\theta_{i+1}, \dot{\theta}_{i+1}$ can be evaluated numerically for any $(\theta_i, \dot{\theta}_i)$ by making a numerical time integration through one forcing period. In this variational equation it is understood that θ and $\dot{\theta}$ are measured from the fixed point. The nature of the stability of the system may be determined by calculating the eigenvalues, λ_1, λ_2 , of the

Jacobian matrix $\begin{bmatrix} a & b \\ c & d \end{bmatrix}$. For stability both of these must

be less than one in modulus. The stability can be characterized by the position of the eigenvalues in the complex plane [10].

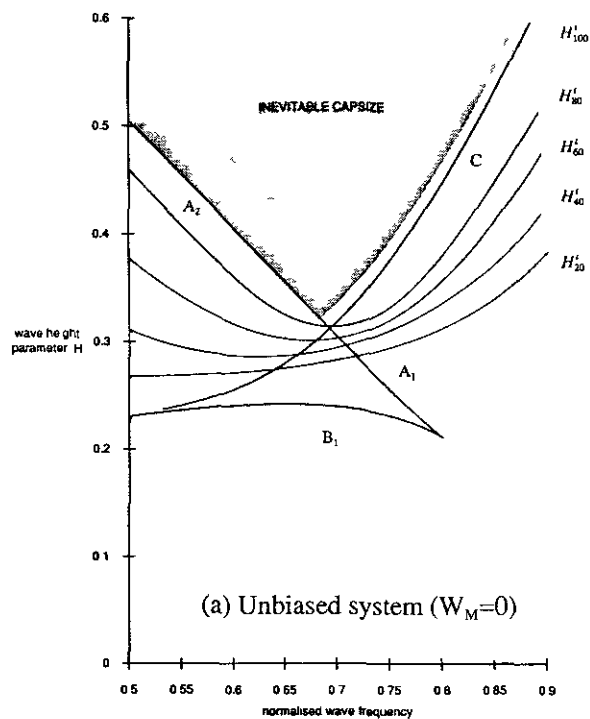
In a changing sea-state both the fixed point and the coefficients of the linear map will vary so that the eigenvalues will describe a path in the complex plane. If the eigenvalues are real one of them can cross the stability boundary at +1, a *cyclic fold* (a *saddle-node bifurcation*), or at -1 producing a *flip bifurcation* (a transition to resonance of order $n=2$). These events are clearly of interest to the naval architect [12]. The fold point (points A and B in figure 1) corresponds to a resonant hysteresis jump which may cause the ship to capsize if the resulting transients are large enough to carry the ship beyond its righting moment limit, or may cause the ship to oscillate at a different (and often a considerably larger) amplitude. The crossing at -1 results in the ship oscillating in a $n=2$ subharmonic manner. This, as has been shown, is often the precursor of chaotic oscillations and hence capsize [13].

Using such stability properties we have drawn a *steady state bifurcation diagram* which summaries the bifurcational behaviour of the ship over a whole range of frequencies and wave heights. We focus most attention just below $\omega=1$ as resonant phenomena will normally govern ship safety. Figure 2a shows the bifurcation diagram for the Gaul such that $W_M=0$. Bifurcations can easily be seen from this diagram; e.g. at $\omega=0.75$ the ship initially oscillates in a periodic manner, but as H is increased the ship makes a *dangerous but not fatal* jump to resonance at A_1 in which the ship starts to oscillate at an increased amplitude. A reduction of H at this stage would cause a jump from resonance at B_1 , giving rise to a region of resonant hysteresis as typically shown in figure 1. A further increase of H beyond A_1 results in a flip bifurcation at C and as can be seen the ship capsizes shortly afterwards at $H^S=0.38$. By keeping H constant and varying the frequency also allows us to determine the regions of resonant hysteresis in the frequency plane. Indeed in real situations *both* the wave frequency and height change simultaneously and such behaviour can be interpreted by this diagram. The *steady state stability boundary*, $H^S(\omega)$ indicates the region of inevitable capsize. Figure 2b shows the bifurcation diagram for the same ship subjected to a steady wind moment by incorporating a static bias term in eqn (1). It can be seen that this asymmetry increases the likelihood of capsize by lowering the steady state stability boundary. At $\omega=0.85$, $H^S=0.26$ for the biased system, whereas $H^S=0.54$ for the unbiased case.

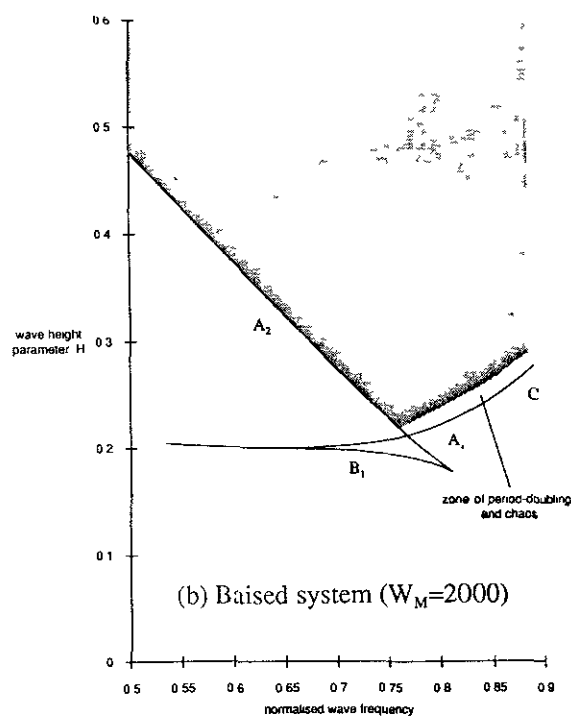
5 TRANSIENT BEHAVIOUR

5.1 Safe basins

A ship subjected to a train of regular waves can exhibit



(a) Unbiased system ($W_M=0$)



(b) Biased system ($W_M=2000$)

Figure 2. Steady state Bifurcation diagrams for the Gaul depicting: Dangerous folds (jumps to resonance (A_1); from resonance (B_1)); Fatal folds (instantaneous capsizing (A_2)); Subharmonic instabilities (period doubling (C)); Capsizing from a chaotic attractor; Regions of inevitable capsizing. Contours of transient stability, (H_p^t, ω), are also shown in figure 2a.

a multitude of modes of capsizing [14] as well as having various types of stable steady states. Indeed these steady states can undergo intricate bifurcating patterns until they reach the point of capsizing [15].

In this section we consider the *transient motions* of a ship subjected to a short pulse of waves, by making *safe basin* studies, as they are both easier to perform, and at the same time more relevant to ship capsizing than the steady state analyses. There are several reasons for this. Firstly, for a ship with its relatively light damping, regular waves will evidently never persist long enough for transients to have decayed substantially for steady state behaviour to take place. A short pulse of regular waves can thus be viewed not only as a worst-case scenario, but as a more realistic representation of a sea state than a long train of regular waves. Secondly since the starting conditions of a ship at the beginning of a pulse may vary widely, and are indeed unknown, we must look at *all* motions rather than focus obsessively on one predominant steady state.

Finally we show that by making such a transient analysis the area of the safe basin, $A(H, \omega)$, can fall dramatically at a steep cliff at H^t , which can often be at a small fraction of H^s , the wave height at which the final attracting steady state loses its stability.

By acknowledging that a ship from $\theta_0, \dot{\theta}_0$ can experience various combinations of wave height, wave frequency and wind moments, we can say that the five dimensional *phase-control space* spanned by $(\theta_0, \dot{\theta}_0, H, \omega, W_M)$ defines the ensuing motion. (Poincaré

phase space has already been defined as $\theta, \dot{\theta}$ space while control space refers to the external parameters such as H, ω or W_M). To determine a safe basin, we use fourth order Runge Kutta numerical time-integrations from a simple grid of starts, typically 100 by 100. Each integration is continued until either the roll angle *exceeds* a capsizing criterion, θ_c , at which point the ship is deemed to have capsized, or the maximum allowable number of cycles, $m(=16)$, is reached, in which case it is assumed that the ship will remain upright under these conditions [16]. In this way we can define a set of points in the five dimensional space that do not capsize in m cycles and hence define a transient safe basin [17]. In this study we have chosen $\theta_c = \pi$ for the Gaul and $\theta_c = 0.88$ for the Edith Terkol.

Specifying the controls and taking a grid in the $(\theta_0, \dot{\theta}_0)$ plane allows us to draw the conventional cross-sections in the phase-space of the starting conditions: while specifying $\theta_0, \dot{\theta}_0$ (say $(0,0)$ in the case of the ship starting originally in its equilibrium position in calm water) and taking a grid in (H, ω) plane allows us to draw the cross-section of the transient basins in the two-dimensional control space [1].

In contrast to the steady state analysis, we are making no note of the final steady state motion (attractor) of the ship to which the non-capsizing motions might settle, whether it is harmonic, subharmonic, small amplitude, large amplitude or chaotic oscillations. At many control settings there can be of course many competing attractors, as in a region of resonant hysteresis, some with exceedingly small regions of attraction.

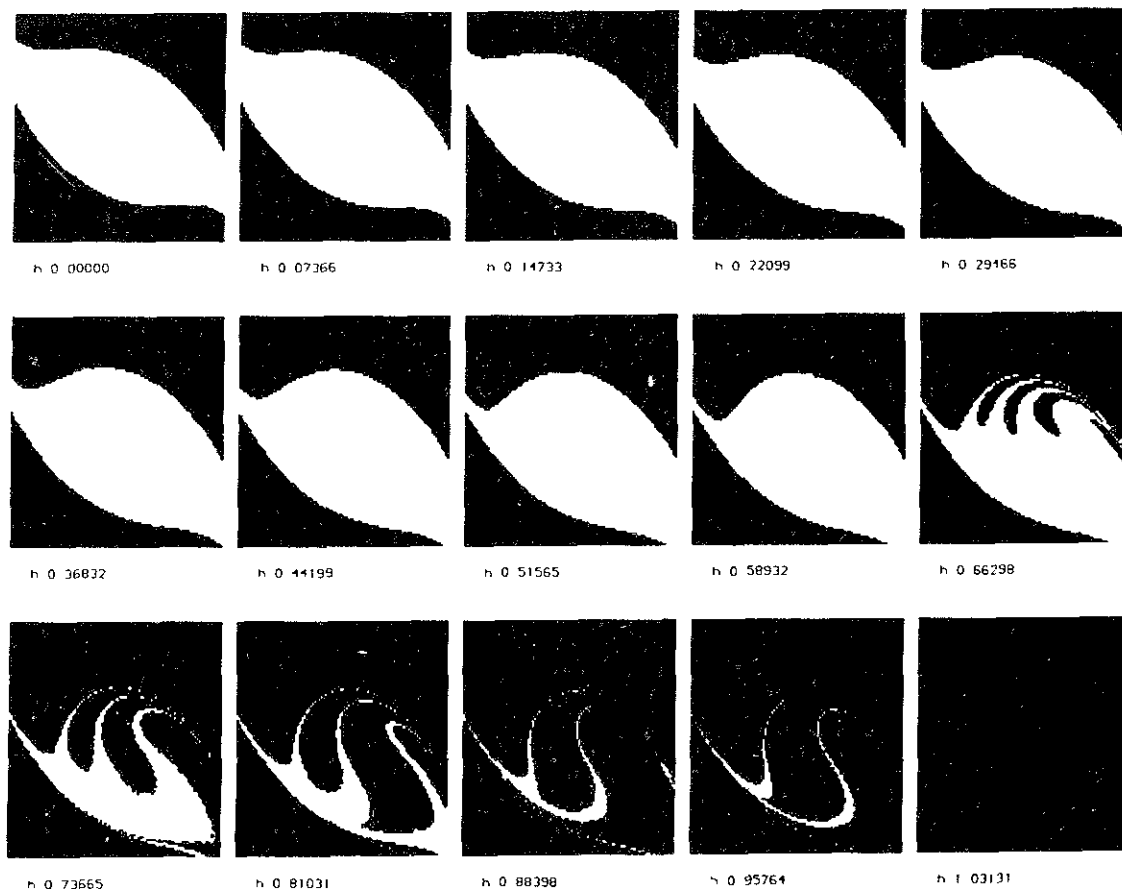


Figure 3 Safe basins in phase space for $\omega=0.85$. Here white represents initial conditions whose trajectories *do not* capsize within 16 forcing cycles and black represents initial conditions whose trajectories *do* capsize within 16 forcing cycles. For each basin the normalised wave height parameter $h=H/H^S$ is shown $W_M=0.0$ with

$$-1.74 < \theta < 1.74 \quad -1.05 < \vartheta < 1.05 \quad \theta_C = 3.142 \quad H^S \approx 0.54$$

5.2 Erosion of the basins and the transient capsize diagram

Figure 3 shows a sequence of safe basins, for fifteen equally spaced values of the normalised wave height parameter, $h=H/H^S$, for the Gaul. Here the frequency is kept fixed at $\omega=0.85$, a value of interest as it is close to the optimal capsize condition. It can be seen that there is little change in size or position of the transient basins up to $h \approx 0.60$. However after that the basin boundary becomes fractal (infinitely textured) due to a *homoclinic tangling* at H^M in the underlying dynamics [18]. Starts within this fractal zone lead to *chaotic transients* which oscillate hesitatingly for an arbitrary length of time before the ship either capsizes or settles to a safe steady state harmonic rolling. Moreover, fractal zones are particularly sensitive to initial conditions, external forces such as an impact load or random noise can often push trajectories across basin boundaries and thus cause a ship oscillating originally in a safe basin to oscillate in an unsafe basin and hence cause capsize [19,20]. This phenomena is not serious in itself, provided that the fractal zone to which it is confined remains as a thin layer around the edge of the boundary, as it does for H just above H^M . However as H is further increased the fractal boundary soon becomes incursive with thick finger like

striations penetrating into the very heart of the central zone resulting in a dramatic erosion of the safe basin. Here we can quantify the size of the basin, A , within the window represented by our grid, by recording the proportion of starts that do not capsize within m wave periods. As can be seen from the integrity curves (figure 4) the ship retains practically all of its still water stability up to a critical value H^I (≈ 0.32), and thereafter loses almost all of it. Indeed, the value of H^I in which the ship loses *most* of its calm water stability is sometimes not so well defined. It is thus more convenient to plot in the (H, ω) plane, contours of H_P^I where we define H_P^I as the value of wave height in which the ship has lost $P\%$ of its calm water stability. Indeed, the three dimensional (A, H, ω) surface completely defines the area of the safe basin for any given H and ω . By fixing ω , and taking a cross-section in the (A, H) plane gives us the typical integrity curves, whereas fixing A we may obtain a contour of transient stability H_P^I . H_{100}^I then represents the contour in which the ship has lost all of its calm water stability i.e. H just above H^S , whereas H_0^I represents the contour in which the ship retains all of its calm water stability. These two contours represent upper and lower bounds on the transient stability, H_P^I can then be chosen for the required margin of safety. Figure 2a shows

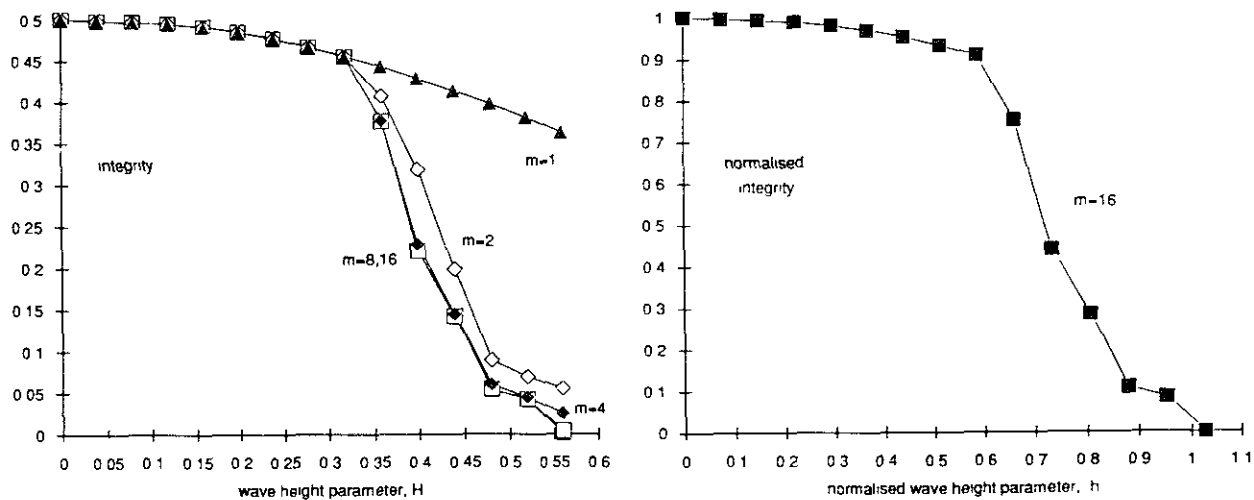


Figure 4. Integrity curves representing the erosion of the safe basin described in figure 3.

several transient contours. It can be seen that steepest *cliff* occurs at about $\omega=0.70$.

This behaviour clearly illustrates how the steady state analysis that predicts the final capsizes, say $H^S=0.54$ at $\omega=0.85$, dangerously over-estimates the overall stability of the ship. Such results clearly display, for a designer, that H^I should be adopted in preference to H^S in defining the operational locus in the (H, ω) domain.

Similar studies were made for the biased system. The effect, as expected is to reduce the value of H^I [1]. We have also made a safe basin study for the Edith Terkol (figures 5, 6). Here we observe that unlike the previous case considered, the erosion of the safe basin is both less dramatic and starts to take place at a relatively small value of H . The reasons for such behaviour are discussed in the next section.

6 THE EFFECT OF ROLL DAMPING.

As is to be expected, both the steady state and transient behaviour of the *Gaul* and the *Edith Terkol* were different. However by examining the the *normalised* integrity curves of each ship we may make a relative, if not completely justified, comparison. As can be seen the *Edith Terkol* loses its integrity at a much lower value of H/H^S than the *Gaul*. We believe, that this feature is mainly due to the fact that the *Edith Terkol* was much more lightly damped (using the model considered here), than the *Gaul*.

Indeed making numerical simulations of an archetypal capsizes model with both linear and nonlinear stiffnesses and linear damping ratios of $\zeta=0.005, 0.025, 0.05$ and 0.15 reveals that the damping level determines the process of the erosion of the safe basin (see figure 7) and hence the transient capsizes diagram. This study uses the

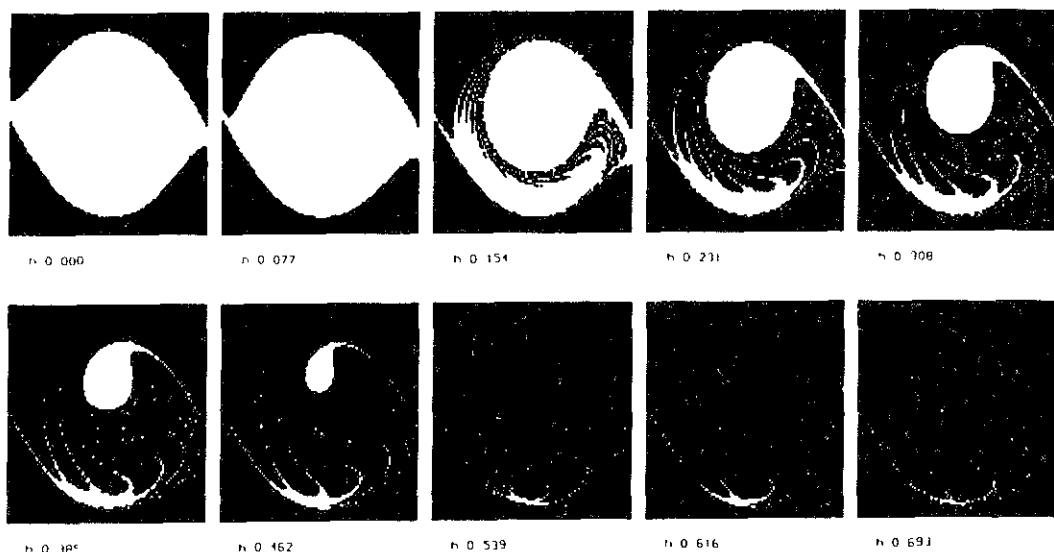


Figure 5. Similar figure to fig 3 but for the Edith Terkol, $W_{N1}=0.0$ and $-0.88 < \theta < 0.88$ $-0.52 < \phi < 0.52$ $\theta_c = -0.88$ $H^S = 0.22$

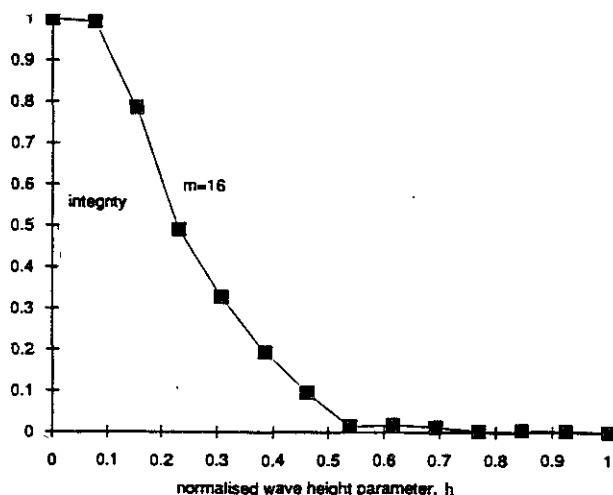


Figure 6. Integrity curves representing the erosion of the safe basin described in figure 5.

canonical escape equation of Thompson [15] both with and without the stiffness nonlinearity, the linearized system being deemed to fail if the displacement x exceeds unity: more details of this comparative analysis will be given in a forthcoming paper [21]. This type of behaviour, although difficult to analyze practically due to the nonlinear damping effects, can help the naval architect in his design. Bilge keels can be designed such that a *minimum* damping level can be achieved for a given ship.

7 CONCLUSIONS

(a) Using steady state analysis, we have drawn an (H, ω) bifurcation diagram. We have defined regions of inevitable capsizing; jumps to resonance as characterised by a fold point; and subharmonic instabilities as characterised by a flip bifurcation. The optimal capsizing wave height occurs at about 70% of the linear natural frequency and obviously that frequency should be avoided. This behaviour is obviously very important to the naval architect and such a diagram would obviously be helpful to his dynamic analyses of ship stability.

(b) We have used a simple and direct method for finding the critical wave height by analysing the transient basins and engineering integrity curves. We have shown that using this method several important deductions can be made.

Roll stability analysis using the classical methods, such as harmonic balance, which locates the main attractor, tests its stability (using a perturbation or Liapunov analysis) and then follows the evolution of daughter attractors, abandoning each in turn as it becomes unstable, is both a daunting, if not impossible prospect (strictly impossible in detail due to the inevitable appearance of subharmonics of infinitely higher order). We have used numerical path following

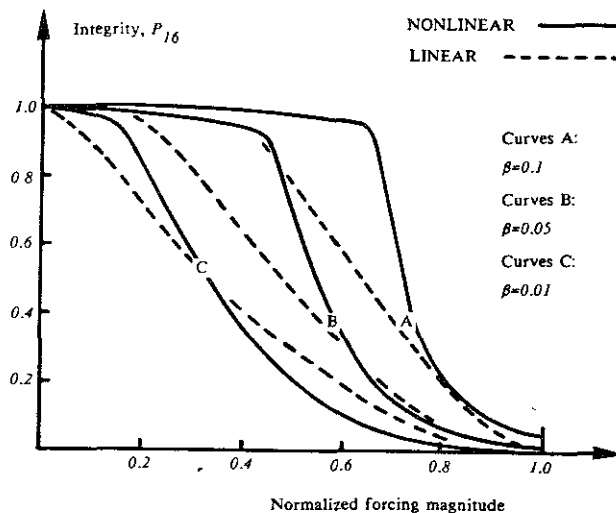


Figure 7. The effect of damping on the erosion of the safe basins for linear and nonlinear archetypal capsize models. Here the canonical escape equation and its linearization are considered with $\omega = 0.85$ and $\beta = 2\zeta$.

routes to overcome this problem. However whichever technique is used the results can be misleading in terms of ship stability. We have shown that the ship up to H^i retains all its calm water stability, and thereafter loses almost all of it, as exemplified by the integrity curves. Classical methods would find the ship stable up to H^s which is obviously, for practical purposes, grossly non-conservative. Using Liapunov functions, in estimating the domains of attraction, would also be quite impossible due to the homoclinic tangencies and hence the extremely complex shape of the safe basins.

(c) By plotting H_p^i contours we can make a critical judgement for the safe operational locus (H^i, ω) of a ship subjected to a short pulse of regular waves. The sudden loss of safe basin does moreover suggest that a transient capsizing diagram can offer a useful and repeatable index of capsizability, that might have important implications for naval architects [16].

(d) The roll damping plays a most critical part in the erosion of the safe basins. This was illustrated by making a safe basin study on both *linear* and *nonlinear* archetypal capsize models. Such behaviour demonstrates, that as well as designing a ship with a minimum criterion for certain characteristics of its righting lever arm, a *minimum damping level* should be included to ensure greater stability.

(e) The stability analysis considered by making a safe basin study can equally be applied for non-capsizing but dangerous motions. Indeed a linear safe basin study can be made (section 6). For example we have considered that the Edith Terkol loses its stability at the angle of vanishing stability ($\theta_v \approx 46^\circ$): however for practical purposes motions can become dangerous to both the passengers and the structure of the ship when the ship

executes large amplitudes. So for a more reasonable analysis the ship can be deemed dangerous once the motion exceeds a given angle of roll (say 25°) and that angle rather than the angle of vanishing stability can be chosen as a limiting criterion. Indeed by comparing a realistic approach with the extreme limiting condition gives a feel for the *margin of safety* made in this transient analysis; analogues to elastic and plastic design in the field of structural engineering can be observed here.

(f) Advances made in recent research in the field of nonlinear dynamics can help to understand dynamic ship phenomena.

REFERENCES

1. SOLIMAN, M.S., and THOMPSON, J.M.T., Transient and steady state analysis of capsize phenomena. Applied Ocean Research 1990 (to appear)
2. SOLIMAN, M.S., and THOMPSON, J.M.T., Integrity measures quantifying the erosion of smooth and fractal basins of attraction. Journal of Sound and Vibration, 1989, **135**, 453-475.
3. WRIGHT, J.H.G. and MARSHFIELD, W.B., Ship roll response and capsize behaviour in beam seas. Trans. RINA, 1980, **122**, 129-144
4. NAYFEH, A.H., On the undesirable roll characteristics of ships in regular seas. Journal of Ship Research, 1988, **32**, 92-100.
5. MORRALL, A., The Gaul disaster: An investigation into the loss of a large stern trawler. Trans. RINA, 1980, 391-416.
6. CADWELL J.B., and YANG, Y.S., Risk and reliability analysis applied to ship capsize: A preliminary study. Proc. Int. Conf. on the SAFESHIP Project: Ship stability and safety, London, RINA, 1986.
7. KURE, K., and BANG, C.J., The ultimate half roll. Proc. Int. Conf. on the Stability of Ships and Ocean Vehicles, Strathclyde, 1975.
8. ODABASSI, A.Y., Ultimate stability of ships. Trans. RINA, 1976, 237-256.
9. LLOYD, A.R.J.M., Seakeeping: Ship behaviour in rough weather. Ellis Horwood, 1989.
10. THOMPSON, J.M.T., and STEWART, H.B., Nonlinear dynamics and chaos, Wiley, Chichester, 1986.
11. ALEXANDER, N.A., Production of computational portraits of bounded invariant manifolds. Journal of Sound and Vibration, 1989, **135**, 63-77.
12. BISHOP, S.R., LEUNG, L.M. and VIRGIN, L.N., Predicting incipient jumps to resonance of compliant marine structures in an evolving sea. Proc. 5th Int. Conf. OMAE, ASME, Tokyo, 1986, 175-185.
13. VIRGIN, L.N. The nonlinear rolling response of a vessel including chaotic motions leading to capsize in regular seas. Applied ocean research, 1986, **9**, 89-95.
14. KUO, C., and ODABASSI, A.Y., Application of dynamic systems approach to ship and ocean vehicle stability. Proc. Int. Conf. on the Stability of Ships and Ocean Vehicles, 1975, Strathclyde.
15. THOMPSON, J.M.T., Chaotic phenomena triggering the escape from a potential well. Proc. Roy. Soc. Lond. 1989, **A 421**, 195-225.
16. RAINEY, R.C.T., and THOMPSON, J.M.T., The transient capsize diagram - A new method of quantifying stability in waves. Journal of Ship Research, 1990 (in press)
17. THOMPSON, J.M.T., and SOLIMAN, M.S., Fractal control boundaries of driven oscillators and their relevance to safe engineering design. Proc. Roy. Soc. Lond. 1990, **A 428**, 1-13.
18. GREBOGI, C., OTT, E. and YORKE, J.A., Basin boundary metamorphoses: changes in accessible boundary orbits. Physica 1987, **24D**, 243-262.
19. GWINN, E.G., and WESTERVELT, R.M., Fractal basin boundaries and intermittency in the driven damped pendulum. Physical Review 1986, **A**, 4143-4155.
20. SOLIMAN, M.S., and THOMPSON, J.M.T., Stochastic penetration of smooth and fractal basin boundaries under noise excitation. Dynamics and Stability of Systems, 1990 (in press).
21. THOMPSON, J.M.T., RAINEY, R.C.T., and SOLIMAN, M.S., Ship stability criteria based on chaotic transients from incursive fractals. Phil. Trans. Roy. Soc. Lond., 1990 (in press)

THE EFFECT OF WIND ON SMALL VESSELS

E. Aa. Dahle ¹⁾, D. Myrhaug ²⁾ and S.J. Dahl ³⁾

ABSTRACT

Small vessels, and in particular small fishing vessels, are subject to several environmental forces. Of these, wind forces are of particular interest because the windage area often is relatively high.

Recently, IMO has adopted a weather criterion to ensure safety in beam seas with wind. However, the wind profile near the sea surface is undefined in the criterion, and is dealt with in the paper. The calculation method is explained, and should enable a better estimation of the wind moment for steady wind. More important; wind gust near steep land formations, or fall winds, are also covered in the paper. To indicate the large angles of heel that can occur as result of wind moments, a recent, serious accident is described. The calculations indicate that angles of heel above 90 degrees are feasible for strong fall winds from the side. Practical advice on avoidance by design and operational guidance are also discussed.

INTRODUCTION

International concern for safety of ships has been concentrated on ships in international trade. The lower length limit is about 24 m.

For fishing vessels below 24 m in length, FAO/ILO/IMO issued "Guidelines for design, construction and equipment" in 1980. These guidelines are based upon the Torremolinos Convention text.

For open boats and for decked vessels below 12 m, no international design guidance exists. However, a set of

regulations called "Nordic Boat Standard" were first published in 1983, covering the safety of all types of vessels below 15 m in length. During 1989 these regulations have been extensively revised, and they are recently published as "Nordic Boat Standard 1990".

The safety of smaller vessels and their crew is nevertheless considered a matter for the owner only. In some countries, however, safety of small vessels is gradually being considered as a national matter.

A clear philosophy should be the basis for development of safety guidelines or regulations. Such a basis is risk that a vessel is exposed to.

Risk is defined as the product of frequency and consequence, and the vessel design process will include measures to reduce hazard frequency and consequences of hazards.

HAZARDS IN TRANSIT

Hazards while underway are general for all types of vessels. Those related to the intact stability of the vessel are hazards

- in following waves;
- with wind from the side;
- with waves and wind from the side;
- with water on deck;
- with ice accretion.

These hazards have been subject to extensive studies in several countries, and are still on the agenda in IMO. A criterion for simultaneous severe wind and rolling was agreed upon in IMO in 1988.

The frequency of such hazards depends upon environmental conditions and mode of operation. Operational restrictions related to vessel heading and speed, wave height, wind and operational area (including weather forecast availability and reliability) seem to be a logical approach to control the hazard frequency. This matter has been elaborated in general by Dahle and Nedrelid [1] and specifically for dangerous waves by Dahle et al. [2].

¹⁾ Governmental Fishing Vessel Accident Commission, Department of Justice, Oslo, Norway.

²⁾ Division of Marine Hydrodynamics, Norwegian Institute of Technology, Trondheim, Norway.

³⁾ Norwegian Maritime Directorate, Oslo, Norway.

Consequences of effect of environmental forces can to some extent be controlled by design measures, adjusting the capability of the vessel to withstand defined environmental forces.

In present regulations and guidelines the latter approach is prevailing. A typical example is requirements to stability of the vessel. These are given without any reference to what level of external moments and forces that the stability of the vessel is expected to withstand, and without any indication as to how to reduce or avoid such external moments.

It seems that guidelines or regulations should be supplemented by explicit identification of relevant hazards (e.g. the vessel, with its level of stability, is unsafe in weather intensity above Bf 7), with subsequent advice on how to control the hazard (e.g. seek shelter or don't leave harbour when weather above Bf 7 is expected).

INFLUENCE OF DESIGN AND CONSTRUCTION ON SAFETY

Intact stability is an important element of safety in relation to hazards imposed by the environment, and should receive due attention in the design and construction process of smaller vessels. However, proper, safe operational procedures for the intended service and environmental conditions have to be followed to maintain the hazard frequency on a low level. This is more important for small than for large vessel simply due to the relative size of the waves.

Small vessels should have relatively large GM values, a relatively wide range of stability, and strong and reliable closing appliances. There are several reasons for this:

- small vessels are operating near coasts, encountering waves of a dangerous nature due to wave refraction and reflection, shallow water effects and wave-current interaction;
- for vessels operating near steep coasts, exposure to fall winds are frequent;
- broaching is also a hazard more frequently encountered by small vessels than by large;
- shifting of cargo is considered more likely on small vessels.

THE INFLUENCE OF WIND ON SMALL VESSELS

In the following, the specific hazard of wind from the side will be discussed. Even when the weather is moderate, vessels operating near steep coasts may experience extremely strong wind gusts, or "fall winds".

Experience in Norway has shown that fall winds can reach force Bf 12 when the wind force is otherwise not above Bf 8. Furthermore, the fall wind can have a direction different from the prevailing wind direction. Waves under these circumstances are of small size as the wind is coming from land.

Fall winds attack unexpectedly, and the frequency of the fall wind hazard cannot be controlled by the vessel operator by change of course before being hit.

For small, coastal vessels, not being subjected to operational restrictions, an important part of the design basis should therefore be the ability to withstand the consequences of the following hazards:

- steady wind of force Bf 8;
- wind gust of strength Bf 12;
- moderate waves.

If the design does not meet these minimum requirements with reasonable margins, operational restrictions should be imposed, or the design should be changed.

The probability of downflooding is an important aspect regarding the ability to withstand the fall wind hazard.

CALCULATION OF WIND MOMENTS

Calculation of wind moments and the effects on a small vessel are described by Wills et al. [3]. In the report, a wind profile with height above the mean sea surface as the only variable is given.

In Appendix 1 to this paper, a more refined method for calculation of the steady wind profile is described, taking also the roughness of the sea surface into account. The roughness factor is dominated by the geometry of the waves.

Also in Appendix 1, it is stated that wind gusts do not exhibit a boundary layer as does steady wind. For small vessels this is of importance as the wind gust moment will increase considerably as compared to calculations with a wind gust profile.

TABLE 1. Environmental data at time of accident.

	Data
Vessel particulars (see Fig. A2.3)	LOA = 8.4 m B = 2.9 m
Place of accident	Fjord, Northern Norway
Description of accident	Vessel had steady wind from the side, was subject to sudden fall wind, foundered
Significant wave height	1 m
Wave length	10 m
Steady wind	19 m/sec
Gust wind	33 m/sec

To demonstrate the calculation of wind moments, a serious accident with a small vessel in strong winds in confined waters on the coast of Norway has been chosen. The vessel capsized in 1989 and the crew of 3 was lost. The accident was investigated by the Norwegian Accident Commission for the Fishing Fleet. The cause of the accident was large heel angles in very strong winds, causing by flooding of the deck and subsequent downflooding through deck openings. The external conditions for the case were as shown in Table 1 and the vessel is shown in Fig. A2.3 (Appendix 2).

Following the calculation procedure outlined in Appendix 1 the results are as given in Table 2 together with the observations. The predicted values are obtained as follows: The wave period associated with the observed wave length is $T_p = 2.5$ sec. Use of $U_{10} = 19$ m/sec and $T_p = 2.5$ sec. in Fig. A1.1 (Appendix 1) (which represents the solution of Eq. (A1.5)), gives the drag coefficient (C_D). The friction velocity (u_*) and sea surface roughness (z_0) parameters are then obtained from Eqs. (A1.3) and (A1.7), respectively. Then the mean wind velocity profile is given by Eq. (A1.2), which gives $U_{10} = 19.7$ m/sec corresponding well to the observed value. The significant wave height is determined from Eq. (A1.6) and appears to be in good agreement with the observed value. The standard deviation (σ_u) and the intensity of the wind gust (σ_u/U_{10}) are given in Eqs. (A1.10) and (A1.11), respectively. It appears that the observed maximum wind speed ($U_{10,max}$) exceeds the mean wind speed by a factor of 4.6 σ_u . It should be noted that U_{10}

TABLE 2. Observed and predicted environmental parameters at time of accident (for details, see Appendix 1).

Parameters	Results	
	Observations	Predictions
U_{10} (m/s)	19	19.7
$U_{10,max}$ (m/s)	33	-
C_D	-	0.0038
u_* (m/s)	-	1.17
z_0 (m)	-	0.012
H_s (m)	1	0.83
σ_u (m/s)	-	3.03
σ_u/U_{10}	-	0.16
$\frac{U_{10,max} - U_{10}}{U_{10}}$	0.74	-

TABLE 3. Heeling angles in steady wind and in wind gust.

	Data
Constant heeling angle in steady wind	43 degrees
Instantaneous heeling angle in wind gust	>90 degrees

is the wind speed commonly referred to in weather forecasts. The profiles for mean (steady wind) and wind gust are shown in Fig. A2.2 (Appendix 2).

HEELING ANGLE IN STEADY WIND AND GUST WIND FROM THE SIDE

With the actual stability curve of the vessel, and applying the calculation procedure described by Wills et al. [3], the heeling angles for steady wind and wind gust can be calculated. The calculations are given in Appendix 2, and the results are given in Table 3.

The sample calculation shows that the steady wind component leads to heel angles up to 40 degrees. The fall wind, however, is

extremely important due to its dynamic nature, and constant strength from the sea surface upwards, leading to an heel angle of 90 degrees or more. Such angles occur in spite of the contribution of the bulwark to the form stability of the vessel being taken into account. Such large angles will normally cause foundering due to downflooding and lack of stability beyond 90 degrees of heel.

The heel angles are calculated in a simplified manner by neglecting hydrodynamic damping and the change in drag coefficients caused by heel.

DOWNFLOODING

It has been demonstrated that water will enter the deck for the small fishing vessel discussed above. However, this should not endanger the vessel. The reason for the foundering in this case is downflooding through unprotected openings. It is an unfortunate fact that the hatches on several small, Norwegian vessels are equipped with weak covers which are not fastened. The coamings are often flush with the deck. In addition, the door to the wheel house is sometimes left open even in bad weather. This was the case for the vessel discussed above.

In general casualty statistics show that downflooding is one of the most important causes for foundering of smaller vessels.

INFORMATION TO THE SKIPPER

Even for a vessel which is properly designed, with stability margins and proper closing appliances, the skippers actions are of major importance to the safety of the vessel.

Based on accident statistics, which indicated that faulty operations were a major contributor to capsize and foundering of small vessels, the Norwegian Maritime Directorate (NMD) realized the importance of providing the skippers with some operational guidance. This comes in addition to the approval of the stability in accordance with the regulations, when applicable, and mandatory safety training for professional fishermen.

For the smaller vessels, not subject to control by NMD, the operational guidance is given on a poster in the wheelhouse. This is based on stability calculations in accordance with "Nordic Boat Standard" and shows four typical loading conditions indicating the maximum allowable loads for each condition.

In addition, simple measures to ensure stability are given in the poster:

- secure doors and hatch covers;
- secure catch and fishing gear against shifting, or move fishing gear and catch from deck to hold;
- minimum freeboard should be above 0.2 m;
- avoid excessive trim;
- avoid following seas;
- avoid excessive forces from fishing gear;
- do not go to sea when icing is expected. Remove all snow and ice from the vessel.

The posters are distributed to the vessels through the local fishery advisers along the coast of Norway and also by the surveyors of the Norwegian Ship Control.

For larger fishing vessels under NMD control, an illustrated Operational Manual has been worked out. It is still under preparation, and has not yet found its final format. The Manual covers the following topics:

- the responsibility of the skipper;
- the design process;
- the inclining test;
- the presentation of the stability particulars to the skipper.

The intention is through regulation to supply this general information together with the approval documents for all fishing vessels being newbuilt or converted to an extent requiring review and approval of stability. In addition the surveyors of the Norwegian Ship Control will distribute this information to existing vessels in connection with renewal of certificates etc.

CONCLUSIONS

In the paper it is demonstrated that the wind profile for steady wind can be accurately calculated based upon the roughness of the sea surface.

In addition, for vessels operating near steep coasts, strong gusts or "fall winds" may occur unexpectedly. Fall wind exhibit an even wind profile from the sea surface upwards.

The wind moments for steady wind and fall wind can be found separately by numerical integration by dividing the ships lateral area in suitable horizontal strips.

The sample calculation shows that the steady wind component leads to heel angles of 25-40 degrees. The fall wind, however, is extremely important due to its dynamic nature, and constant strength from the sea surface upwards, leading to an heel angle of 90 degrees or more. Such angles occur in spite of the contribution of the bulwark to the form stability of the vessel being taken into account. Such large angles will normally cause foundering due to downflooding and lack of stability beyond 90 degrees of heel.

The heel angles are calculated in a simplified manner by neglecting hydrodynamic damping and the change in drag coefficients caused by heel.

Unfortunately, small vessels often have inferior closing appliances. Therefore they are sometimes subject to downflooding as a consequence of heeling angles for which the bulwark is submerged.

In areas with fall winds, it therefore seems reasonable to design a small vessel with sufficient stability to prevent the top of the bulwark to submerge in fall winds.

Also, the closing appliances should be of good quality, and should always be closed under difficult circumstances.

REFERENCES

1. Dahle, E., Aa. and Nedrelid, T., Operational manuals for improved safety in a seaway. *Proc. 3rd Int. Conf. on Stability of Ships and Ocean Vehicles*, Gdansk, Poland, 1986.
2. Dahle, E., Aa., Myrhaug, D. and Dahl, S.J., Probability of capsizing in steep and high waves from the side in open sea and coastal waters. *Ocean Engng.*, 1988, pp. 139-151.
3. Wills, J.A.B., Cole, L. R. and Stovold, A.J., SAFESHIP: Environmental Aspects, Part II: Wind effects on vessels. NMI Ltd., Report R 186, April 1984.
4. Schlichting, H., *Boundary-Layer Theory*, McGraw-Hill, New York, 1979.
5. Toba, Y. and Koga, M., A parameter describing overall conditions of wave breaking, whitecapping, sea-spray production and wind stress. In *Ocean Whitecaps*, ed., E.C. Monahan and G. M. Niocaill, D. Reidell Publishing Company, Dordrecht, 1986, pp. 37-47.
6. Charnock, H., Wind stress on a water surface. *Quart. J. Roy. Meteor. Soc.*, 1955, 81, 639-640.
7. Wu, J., Wind-stress coefficients over sea surface near neutral conditions - A revisit. *J. Phys. Oceanogr.*, 1980, 10, 727-740.
8. Buckles, J., Hanratty, T.J. and Adrian, R.J., Turbulent flow over large-amplitude wavy surfaces. *J. Fluid Mech.*, 1984, 140, 27-44.
9. Davenport, A.G., Wind structure and wind climate. In *Safety of structures under dynamic loading*, ed., I. Holand et al., Tapir, Trondheim, 1978, pp. 209-284.
10. Forristall, G.Z., Wind spectra and gust factors over water. *Proc. 20th Offshore Tech. Conf.*, Paper No. 5735, Houston, Texas, 1988, 449-460.
11. Ochi, M. K. and Shin, Y. S., Wind turbulent spectra for design consideration of offshore structures. *Proc. 20th Offshore Tech. Conf.*, Paper No. 5736, Houston, Texas, 1988, 461-467.
12. Harris, R.I. and Deaves, D.M., The structure of strong winds, *Proc. CIRIA Conf. on Wind Engineering in The Eighties*, CIRIA, London, 1981.

APPENDIX 1

Wind modelling over the sea

The wind velocity is usually splitted in two parts, that is, as mean wind and wind gust. If the mean wind, $U(z)$, and the wind gust, $u(z,t)$, have the same direction, then the total wind is given as

$$U(z,t) = U(z) + u(z,t) \quad (A1.1)$$

where z is the elevation above the sea surface and t the time. The mean wind and wind gust will be discussed subsequently in separate sections.

Mean wind

The mean wind is commonly assumed to be given by the logarithmic velocity profile (Schlichting [4])

$$U(z) = \frac{u_*}{\kappa} \ln \left(\frac{z}{z_0} \right) \quad (A1.2)$$

where u_* is the friction velocity parameter, z_0 is the sea surface roughness parameter and $\kappa = 0.41$ is von Karman's constant. The

logarithmic boundary layer flow model is considered to be valid when the air is in neutral stability and the flow is steady.

The drag coefficient referred to the $z_{10} = 10$ m elevation wind speed U_{10} is defined as

$$C_D = \left(\frac{u_*}{U_{10}} \right)^2 \quad (\text{A1.3})$$

It should be noted that U_{10} is the wind speed commonly referred to in weather forecasts. Following Toba and Koga [5] the sea surface roughness parameter for irregular waves is given by

$$z_0 = \frac{\gamma}{2\pi} u_* T_p \quad (\text{A1.4})$$

where T_p is the peak period in the wave energy spectrum and $\gamma = 0.025$. By combining Eqs (A1.2)-(A1.4) the drag coefficient can be expressed as

$$C_D = \left[\frac{\kappa}{\ln\left(\frac{2\pi z_{10}}{\gamma T_p U_{10} C_D^{1/2}}\right)} \right]^2 \quad (\text{A1.5})$$

which determines C_D implicitly for given values of U_{10} and T_p . The results are given graphically in Fig. A1.1. The results in the figure and the meaning of c/U_{10} will be discussed subsequently. Thus the mean wind profile is determined from Eq. (A1.2) by using u_* and z_0 from Eqs. (A1.3) and (A1.4), respectively.

It should also be noted that according to Toba and Koga [5], the significant wave height is given by

$$H_s = 0.062 (g u_*)^{1/2} T_p^{3/2} \quad (\text{A1.6})$$

where g is the acceleration of gravity.

It is worth noting that the sea surface roughness parameter can be rewritten to the form

$$z_0 = \beta' \frac{u_*^2}{g} ; \beta' = \gamma \frac{c}{u_*} = \gamma \frac{c}{C_D^{1/2} U_{10}} \quad (\text{A1.7})$$

where c is the phase velocity of a sinusoidal wave in deep water with a wave period corresponding to the peak period in the wave energy spectrum, that is, given by $c = g T_p / 2\pi$. Eq. (A1.7) can be taken as a generalization of Charnock's [6] formula originally given by

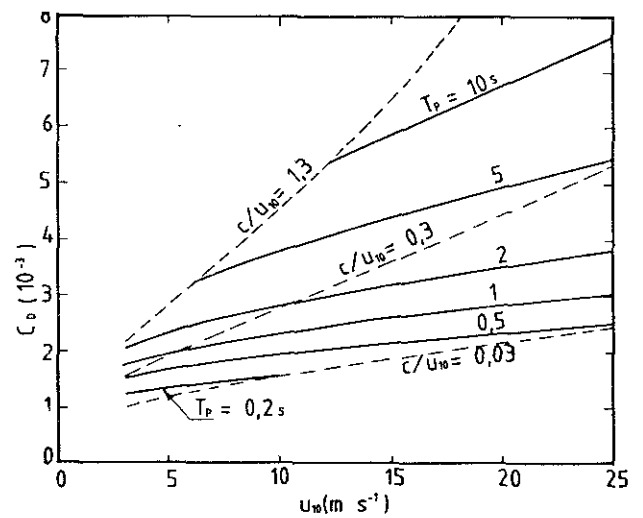


Figure A1.1 C_D versus U_{10} for given values of T_p according to Eq. (A1.5) (reproduced from Toba and Koga [5]).

$$z_0 = \beta \frac{u_*^2}{g} ; \beta = 0.012 \quad (\text{A1.8})$$

which has been widely accepted. Wu [7] proposed an optimal value of $\beta = 0.0185$. The ratio c/u_* (or c/U_{10}), which enters in Eq. (A1.7), is often referred to as the wave age.

Fig. A1.1 shows C_D as a function of U_{10} for $U_{10} > 3$ m/sec for different values of T_p (full curves). Three values of the wave age are also given (broken curves), where the value $c/U_{10} = 1.3$ gives the maximum values of C_D which correspond to the saturation condition for wind waves for the respective wind velocities and wave periods. From Fig. A1.1 it appears that C_D increases as U_{10} increases for specified T_p values; C_D increases as T_p increases for given U_{10} values; it is noted that C_D is much more sensitive to T_p than to U_{10} ; and C_D increases with wave age c/U_{10} .

It should be noted that in the present description the sea surface roughness parameter (z_0) is representative for that over a larger region of an irregular sea surface. Thus z_0 , as well as the associated shear stress at the sea surface and the mean wind profile near the surface, represent the regional average characteristics over irregular wind waves, rather than the local conditions over an individual wave in the sea-state. The local air flow circulation might be modified over an individual sinusoidal wave, where separation and re-circulation below the wave crest occur, Buckles et al. [8].

Finally, it should be noted that the waves considered herein are purely wind waves, and thus, in cases where large swells also are present, T_p and c values related to the wind waves components should be used (Toba and Koga [5]).

Wind gust

The wind gusts are reasonably well modelled as Gaussian stochastic processes and are therefore fully described by the wind gust energy spectrum, $S(f)$. Many spectral models have been proposed, but among these the Harris and Davenport wind gust spectra have been widely used and accepted (Davenport [9]). However, it is worth noting that both these formulations are based on wind information over land. It seems to be well documented that wind gust spectra obtained from measurements over sea contain significantly more energy at lower frequencies compared to those over land (Forristall [10], Ochi and Shin [11]). The implications of this are particularly important for the response of structures which are very sensitive to low-frequency excitations, but is probably not very important for the wind effect on smaller vessels. The Harris spectrum has been recommended for use over sea for $f > 0.01$ Hz, which should be relevant for the present purpose. The Harris wind gust spectrum is given as (Harris and Deaves [12])

$$\frac{fS(f)}{u_*^2} = \frac{4x}{(2+x^2)^{5/6}} \quad (A1.9)$$

$$x = \frac{l f}{U_{10}}, \quad l = 1800m$$

which gives the energy in the wind fluctuations (gusts) in the direction of the mean wind. It is noted that according to this formulation the wind gust is independent of the elevation above the surface, and only dependent on U_{10} (which is specified) and u_* given by Eqs. (A1.3) and (A1.5). Integration of the spectrum in Eq. (A1.9) gives the variance of the wind gust, i.e.

$$\sigma_u^2 = \int_0^\infty S(f) df = 6.685 u_*^2 \quad (A1.10)$$

which gives the following intensity of the wind gust referred to the 10 m elevation

$$I_u = \frac{\sigma_u}{U_{10}} = 2.586 \sqrt{C_D} \quad (A1.11)$$

where Eq. (A1.3) has been used, and C_D is given in Eq. (A1.5).

More details on other wind gust spectral formulations are given in Forristall [10] and Ochi and Shin [11].

APPENDIX 2

Heeling under the influence of wind

When heeled over under the influence of constant wind from the side, an equilibrium exists between the wind force and the hydrodynamic reaction force caused by sideways drift. The static heeling moment is made up by these forces and the distance between them.

Superimposing this moment on the stability curve of the vessel, the static angle of heel is found, see Fig. A2.1. The main difficulties in such a calculation is to determine the drag coefficient of the part of the vessel above water, and the point of attack of the opposing hydrodynamic force.

When a wind gust hits the vessel, the reaction force will act through the centre of gravity of the vessel. As sideways drift velocity increases, a hydrodynamic reaction force is set up. The resulting forces, moments and coupled roll and drift motions can be found by using computer programs. The coefficients to be used are, however, relatively uncertain. The principle for finding the dynamic heeling angle under influence of gust wind is shown in Fig. A2.1. Damping is neglected.

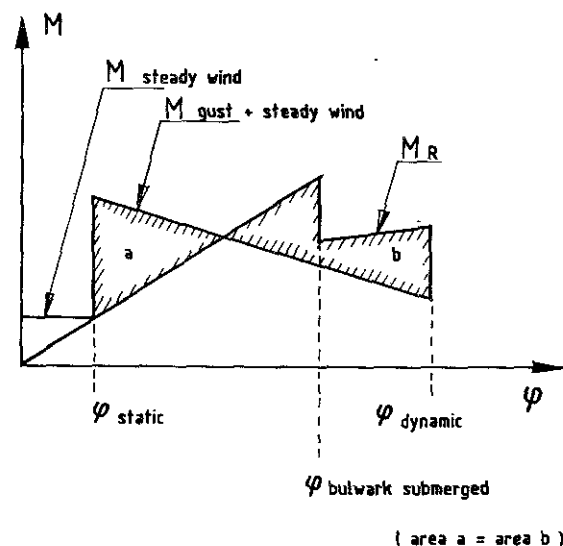


Figure A2.1 The principle of finding static and dynamic angle of heel for a vessel subject to steady wind and fall wind (gust), and with a righting moment M_R .

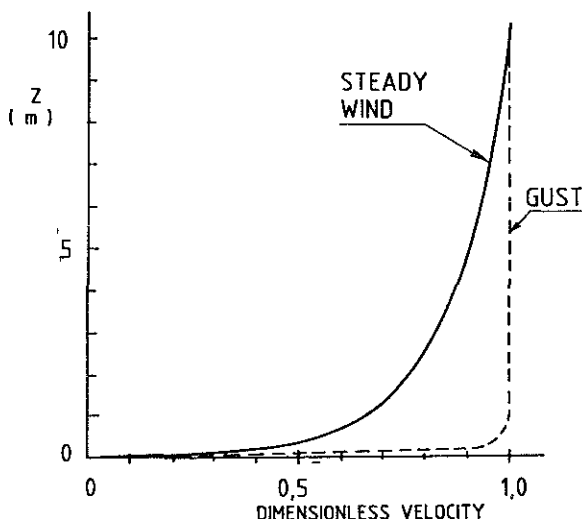


Figure A2.2 Profiles for steady wind and wind gust. As indicated the wind gust profile has to go to zero at the surface (probably with a very large gradient).

The simplified equation for determination of heeling moments from wind is then

$$M = F a - \frac{1}{2} \rho C_D A \cdot U^2 a \cdot \cos^2 \phi \text{ (Nm)} \quad (\text{A2.1})$$

where

- F = wind force (N)
- a = moment arm (m)
- ρ = density of air (1.3 kg/m^3)
- C_D = drag coefficient (-)
- A = lateral side area exposed to wind (m^2)
- U = wind speed (m/sec)
- ϕ = heeling angle

As described by Wills et al. [3], the lateral side area A should be divided into a suitable number of subareas, and the wind speed should be applied at the centroid of these subareas. This wind speed should be calculated from the wind profile.

For gust wind, which has an uniform profile as explained in the paper, it is sufficient to calculate the centroid of the total area A. The calculation of wind profiles are given in Fig. A2.2 and the calculation of wind moments are shown in detail in Table A2.1 and A2.2 for steady and gust wind, respectively.

The centre of gravity of the subject vessel, shown in Fig. A2.3, was found by an inclining experiment carried out after the sunken vessel was retrieved.

Until the bulwark becomes submerged the uprighing moment can be approximately expressed by:

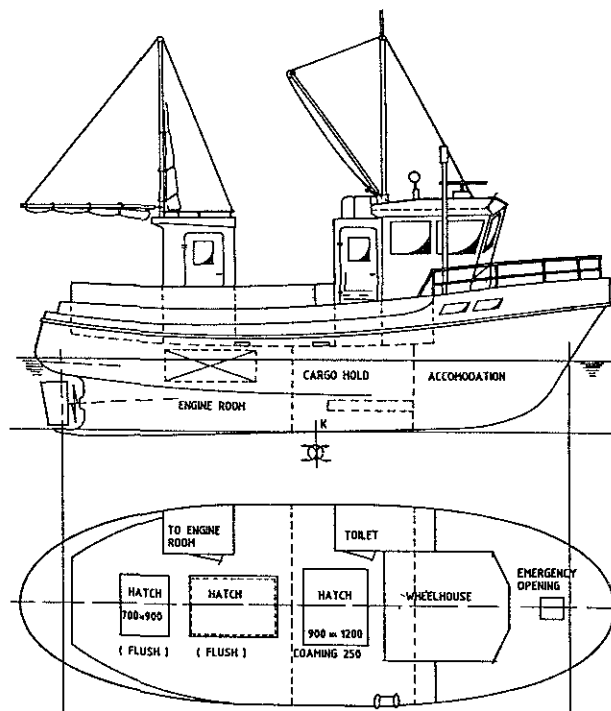


Figure A2.3 General arrangement of subject vessel.

$$M_R = \Delta \cdot GZ \approx \Delta \cdot GM \cdot \sin \phi \text{ (kNm)} \quad (\text{A2.2})$$

where

- Δ = displacement (kN)
- GZ = righting moment arm (m)
- GM = metacentric height (m)
- ϕ = heeling angle

For the subject vessel, Eq. (A2.2) gives

$$M_R = 4.43 \cdot \sin \phi \text{ (kNm)}$$

For larger heeling angles, traditional GZ-calculations must be carried out. The GM-value of the vessel is almost twice the figure recommended for larger fishing vessels (0.35 m).

The bulwark becomes submerged at an angle expressed by;

$$\phi_B = \arctg (2 \cdot F/B) \quad (\text{A2.3})$$

where

- F = freeboard to top of bulwark (m)
- B = breadth of vessel (m)

For the subject vessel, Eq. (A2.3) gives

$$\phi_B = \arctg (2 \cdot 0.65/2.9) = \underline{24^\circ}$$

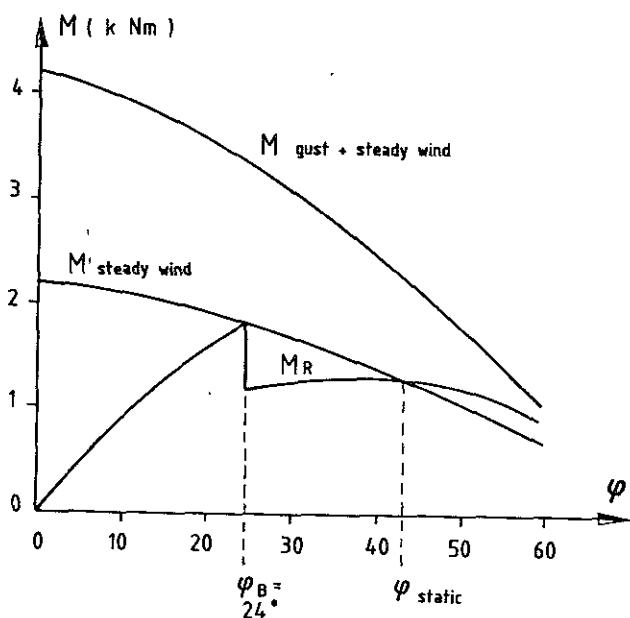


Figure A2.4 Righting moment M_R versus wind moments for the subject vessel.

The imposing of the wind moments onto the static stability curve is shown in Fig. A2.4. The heeling angle for steady wind is about 43° . For gust wind, however, an angle of equilibrium cannot be found as the wind moment is higher than the righting moment.

Consequently, the vessel was turned over to an angle of heel probably exceeding 90° . Had the vessel been properly closed, as was not the case, it could possibly returned to upright position as it was not loaded.

This case illustrates that the vessel was not designed for the fall wind hazard, and that it was also poorly operated under the circumstances.

TABLE A2.1 Wind heeling moment for steady wind ($U_{10}=19$ m/sec).

n	A_n	Z_n	$U(z)/U_{10}$	$(U(z)/U_{10})^2$	$A_n (U(z)/U_{10})^2$	$A_n (U(z)/U_{10})^2 Z_n$
1	7.5	0.60	0.55	0.30	2.25	1.35
2	1.0	1.70	0.74	0.55	0.55	0.94
3	3.5	1.60	0.72	0.52	1.82	2.91
4 ^{a)}	1.0	2.50	0.80	0.64	0.64	1.60
^{a)} mast, rigging, rail					5.26	6.80

$$M = \frac{1}{2} \rho C_D \sum A_n U(z)^2 a_n \cos^2 \phi$$

$$= \frac{1}{2} \rho C_D U_{10}^2 \sum A_n (U(z)/U_{10})^2 (Z_n + \frac{T}{2}) \cos^2 \phi$$

$$= \frac{1}{2} \rho C_D U_{10}^2 [\frac{T}{2} \sum A_n (U(z)/U_{10})^2$$

$$+ \sum A_n (U(z)/U_{10})^2 Z_n] \cos^2 \phi$$

Using $C_D = 1.0$, the result is:

$$M = \frac{1}{2} \cdot 1.3 \cdot 1.0 \cdot 19^2 \cdot (0.50 \cdot 5.26 + 6.80) \cos^2 \phi$$

$$M = 2.2 \cdot \cos^2 \phi \text{ (kNm)}$$

TABLE A2.2 Wind heeling moment for gust wind ($U_{10, \max} = 33$ m/sec).

(See Table A2.1 for geometry of vessel.

Note that gust wind speed is

$$u = U_{10, \max} - U_{10} = 14 \text{ m/sec}$$

n	A_n	Z_n	$A_n \cdot Z_n$
1	7.5	0.60	4.50
2	1.0	1.70	1.70
3	3.5	1.60	5.60
4	1.0	2.50	2.50
			14.30

$$M = \frac{1}{2} \rho C_D (\sum A_n Z_n) u^2 \cos^2 \phi$$

Using $C_D = 1.0$ the result is:

$$M = \frac{1}{2} \cdot 1.3 \cdot 1.0 \cdot 14.3 \cdot 14^2 \cos^2 \phi$$

$$M = 1.82 \cos^2 \phi \text{ (kNm)}$$

THE AMPLITUDE MOTION CALCULATIONS FOR VW-TYPE HULLS IN WAVES

1)
VOROBYOV Yu.L.

ABSTRACT

A new approach to the determination of hydrodynamic and kinematic characteristics of floating structures having hulls with vertical side walls (VW-type hulls) under the regular wave action and deep water conditions is described. The approach mentioned is based upon three-dimensional boundary value problem approximate solution. The details are illustrated in calculations for rolling motion characteristics of a pontoon with vertical walls and rectangular plan view shape.

INTRODUCTION

The determination of stability characteristics of sea-going vessels and structures under different weather conditions includes as an important element the evaluation of amplitudes of floating body motions in waves. In recent years the number of floating structures having hulls with vertical side walls (VW-type hulls) is permanently increasing. The plan view shape of such hulls widely differs from the traditional ship waterline shape. That is why the strip method usually used for ship motion calculations is not valid for those VW-type hulls which are not elongated. In this case a new approach has to be worked out taking into consideration the fact of three-dimensionality of fluid flow around the hull of floating structure. This report presents ideas of treating the problems concerning the oscillation characteristics determination for floating structures with vertical side walls and an arbitrary waterline shape in regular waves. The approach to the determination of hydrodynamic characteristics is illustrated for VW-type hull with a rectangular waterline shape. Special correction of damping forces is elaborated taking into account the flow separation phenomena for a hull with sharp edges. Obtained theoretical results are realized in a set of special computer programs. Calculated values are compared with experimental results that were received in the towing tank of Odessa Institute of Marine Engineers (OIME TT).

BACKGROUND

Two methods of determination of hydrodynamic characteristics are known to be used in conventional theory of ship oscillations. The traditional one is based on the procedure of hydrodynamic pressure integration over a ship hull surface. Being rather simple and clear the method has some shortcomings that cause difficulties in practical usage. Radiation function in the vicinity of a hull, e.g. near the singularity system has an extremely complicated form and it is necessary to solve a diffraction problem to obtain exciting forces.

The second method is free from the above mentioned disadvantages. It is based on using only asymptotic expansions of radiation functions far from the ship hull for determination of damping and exciting forces [1, 2]. But the added masses can not be expressed directly in terms of radiation potential asymptotics. In this case the Kramers-Kronig formula may be used [3]:

$$\lambda_{p,1}(\sigma) = \lambda_{p,1}(\infty) + \frac{2}{\pi} \int_0^{\infty} \frac{\mu_{p,1}(\xi) d\xi}{\xi^2 - \sigma^2} \quad (1)$$

So for evaluating the second method one needs an asymptotic expansion of radiation function far from the hull and the added mass value when frequency tends to infinity.

Theoretical approach for determination of hydrodynamic characteristics

An asymptotic expression of radiation potential is obtained using a special rather simple method. Its general concept can be demonstrated in details by following example.

Heaving of a rectangular contour

Let a rectangular contour is floating on a free surface of an ideal fluid and is heaving with the vertical velocity $\dot{\theta}(t) = \cos \sigma t$. The velocity potential $\Phi(y, z, t)$ can be taken in a form $\Phi(y, z, t) = \Phi_c(y, z) \cos \sigma t + \Phi_s(y, z) \sin \sigma t$.

1)

Professor, Head of Theory of Ship Department, Rector of Odessa Institute of Marine Engineers

Let us divide the fluid domain into two zones. internal zone $|y| < \frac{1}{2}B$, $T \leq z < \infty$, and external zone $|y| > \frac{1}{2}B$, $0 \leq z < \infty$.

The iterative procedure is offered for determination of Φ_c and Φ_s functions. According to this procedure the boundary value problems in internal and external zones are solved one after another and "matching" of the solutions obtained is done step by step. The "matching" means setting equal both potentials and their normal derivatives found in two zones on the boundaries $y = \pm \frac{1}{2}B$, $T \leq z < \infty$. As the first step we determine $\Phi_c^{(0)}$ in the inner region as a harmonic function satisfying the boundary conditions

$$\frac{\partial \Phi_c(y, T)}{\partial z} = 1, \quad \Phi_c(\pm \frac{1}{2}B, z) = 0$$

Using the Fourier expansion

$$1 = \frac{4}{\pi} \sum_{k=1}^{\infty} \frac{\sin(2k-1)\eta}{2k-1},$$

$$0 \leq \eta \leq \pi.$$

we can find $\Phi_c^{(0)}$ function in a form

$$\begin{aligned} \Phi_c^{(0)}(y, z) = & - \frac{4B}{\pi^2} \sum_{k=1}^{\infty} \frac{(-1)^{k-1}}{2k-1} * \\ & * \exp\left[-(2k-1) \frac{B}{\pi} (z-T)\right] * \\ & * \cos\left[(2k-1) \frac{B}{\pi} y\right] \\ & * \frac{1}{2k-1}. \end{aligned} \quad (2)$$

Now we get $f_c(z) = \frac{\partial}{\partial y} \Phi_c^{(0)}(\pm \frac{1}{2}B, z)$

from the formula (2)

$$f_c(z) = - \sum_{k=1}^{\infty} \frac{4}{\pi} \frac{1}{2k-1} \exp\left[-(2k-1) \frac{B}{\pi} (z-T)\right] =$$

$$= - \frac{2}{\pi} \ln \operatorname{cth} \frac{\pi}{B} (z-T),$$

$$T \leq z < \infty. \quad (3)$$

Everything is ready to make the next step and to investigate the boundary value problem in the outer zone for $\Phi_c^{(0)}$ potential function

$$\left(\frac{\partial^2}{\partial y^2} + \frac{\partial^2}{\partial z^2}\right) \Phi_c^{(0)}(y, z) = 0,$$

$$|y| > \frac{1}{2}B, \quad 0 \leq z < \infty;$$

$$\left(\frac{\partial}{\partial z} + \kappa\right) \Phi_c^{(0)}(y, 0) = 0,$$

$$|y| > \frac{1}{2}B, \quad \kappa = \frac{\sigma^2}{g}; \quad (4)$$

$$\frac{\partial}{\partial y} \Phi_c^{(0)}(\pm \frac{1}{2}B, z) = 0, \quad 0 \leq z < T;$$

$$\frac{\partial}{\partial y} \Phi_c^{(0)}(\pm \frac{1}{2}B, z) = \pm f_c(z), \quad T < z < \infty;$$

$$\lim_{z \rightarrow \infty} \operatorname{grad} \Phi_c(y, z) = 0.$$

One can notice that sine component $\Phi_s^{(0)}$ of potential function satisfies the homogeneous boundary value problem that comes from (4) by changing subindex "c" to "s" and taking $f_c(z)$ equal to zero.

The potential function $\Phi^{(0)}(y, z, t) = \Phi_c^{(0)}(y, z) \cos \sigma t + \Phi_s^{(0)}(y, z) \sin \sigma t$ ought to satisfy the radiation principle according to which the waves disturbed by contour motions run from it to the infinity. The function $\Phi_c^{(0)}$ that satisfies the boundary value problem (4) can be expanded into Fourier-Michell integral [4]:

$$\Phi_c^{(0)}(\eta, z) = \int_0^{\infty} g_c(\eta, \mu) \phi(z, \mu) \frac{\mu^2 d\mu}{\mu^2 + \mu^2} +$$

$$+ \Gamma_c(\eta) \exp(-\kappa z),$$

$$\eta = y - B/2.$$

$$g_c(\eta, \mu) \int_0^{\infty} \Phi_c^{(0)}(\eta, z) dz;$$

$$\Gamma_c(\eta) = 2\kappa \int_0^{\infty} e^{-\kappa z} \Phi_c^{(0)}(\eta, z) dz. \quad (5)$$

The system of functions $\phi(z, \mu) =$

$$= \cos \mu z + \frac{\kappa}{\mu} \sin \mu z, \quad e^{-\kappa z} \text{ is full}$$

and orthogonal on $0 \leq z < \infty$, so it comes from the first equation of (4)

$$\left(\frac{d^2}{d\eta^2} + \kappa^2\right) \Gamma_c(\eta) = 0,$$

$$\left(\frac{\partial}{\partial \eta^2} - \kappa^2\right) g_c(\eta, \mu) = 0. \quad (6)$$

The bounded at the infinity solution of the differential equations (6) are obtained in a form

$$\Gamma_c(\eta) = a_c \cos \kappa \eta + 2 \sin \kappa \eta \int_0^{\infty} e^{-\kappa z} *$$

$$* f_c(z) dz;$$

$$g_c(\eta, \mu) = - \frac{2}{\mu \pi} e^{-\mu \eta} \int_0^{\infty} \phi(z, \mu) f_c(z) dz.$$

Taking into account considerations about $\Phi_s^{(0)}$ function and "radiation principle", we have $a_c = 0$, $g_s(\mu, \eta) = 0$;

$$\Gamma_s(\eta) = - 2 \cos \kappa \eta \int_0^{\infty} e^{-\kappa z} f_c(z) dz.$$

so the functions $\Phi_c^{(n)}$, $\Phi_s^{(n)}$ have the form at the boundaries $y = \pm \frac{1}{2} B$ and $y \rightarrow \pm \infty$ of the outer zone

$$\Phi_c^{(n)}(\pm \frac{1}{2} B, z) = A_c(z) = -\frac{4}{\pi^2} \int_T^\infty \ln \operatorname{cth} \frac{\pi}{2B} (\zeta - T) * \quad (6)$$

$$* \{ \exp[-\kappa(z+\zeta)] E_1[\kappa(z+\zeta)] - \frac{1}{2} \ln \left| \frac{z+\zeta}{z-\zeta} \right| \} d\zeta, \quad T < z < \infty. \quad (7)$$

$$\Phi_s^{(n)}(\pm \frac{1}{2} B, z) = A_s(z) = -\frac{8T}{\pi} \exp[-\kappa(z+T)] * \quad (8)$$

$$* \sum_{k=1}^{\infty} \{ (2k-1) \left[\frac{\pi T}{B} + \kappa T \right] \}^{-1},$$

$$T < z < \infty.$$

$$\Phi_c(\pm \infty, z) = 2 \quad (9)$$

$$\Phi_s(\pm \infty, z) = \kappa$$

$$* \left\{ \frac{\sin \kappa(y-B/2)}{\cos \kappa(y-B/2)} \right\}, \quad 0 \leq z < \infty. \quad (8)$$

Let us now make the next step in iterative procedure and find both $\Phi_c^{(2)}$ and $\Phi_s^{(2)}$ potentials in the inner zone. Being harmonic these functions ought to satisfy the boundary conditions

$$\frac{\partial}{\partial z} \Phi^{(2)} c, s(y, T) = 0, \quad |y| < \frac{1}{2} B; \quad (9)$$

$$\Phi^{(2)} c, s(\pm \frac{1}{2} B, z) = A_c, s(z), \quad T < z < \infty.$$

We expand the unknown functions $\Phi^{(2)} c, s(y, z)$ into Fourier integral ($\zeta = z - T$):

$$\Phi^{(2)} c, s(y, \zeta) = \int_0^\infty Gc, s(\mu, y) \cos \mu \zeta d\mu; \quad (10)$$

As soon as the functions $\Phi^{(2)} c, s(y, \zeta)$ are harmonic, the functions $Gc, s(\mu, y)$ satisfy the following equation:

$$\left(\frac{\partial^2}{\partial y^2} - \mu^2 \right) Gc, s(\mu, y) = 0.$$

Taking into consideration the second condition of (9), we get

$$Gc, s(\mu, y) = -\frac{2}{\pi} \frac{\operatorname{ch} \mu y}{\operatorname{ch} \frac{1}{2} \mu B} \int_0^\infty A_c, s(\zeta) \cos \mu \zeta d\zeta. \quad (11)$$

Using formula (11), the first formula of (10) and convolution theorem, it comes

$$\Phi^{(2)} c, s(y, z) = -\frac{2}{B} \int_0^\infty A_c, s(\zeta) \cos \frac{\pi}{B} y * \quad (12)$$

Now the cosine component of velocity potential in the inner region equals to $\Phi_c^{(1)} + \Phi_c^{(2)}$ and its sine component equals to $\Phi_s^{(2)}$. The iteration can be continued by evaluating

$$\frac{\partial}{\partial y} \Phi^{(2)} c, s(\pm \frac{1}{2} B, z) = f_{c, s}^{(2)}(z),$$

investigating the boundary value problem like (4) in the outer zone and returning again into the inner zone. But we can show that it is not necessary. Really, integrating the hydrodynamic pressure obtained using the potential functions $\Phi_c^{(1)} + \Phi_c^{(2)}$ and $\Phi_s^{(2)}$ along the rectangular contour, we get added mass λ_{33} and damping coefficient μ_{33} expressions

$$\bar{\lambda}_{33} = \frac{\lambda_{33}}{\rho B T} = \bar{\lambda}_{33}^{(1)} + \bar{\lambda}_{33}^{(2)};$$

$$\bar{\lambda}_{33}^{(1)} = \frac{8\theta}{\pi} \sum_{k=1}^{\infty} (2k-1)^{-3};$$

$$\bar{\lambda}_{33}^{(2)} = -\frac{16}{\pi^3 b} \int_0^\infty \ln \operatorname{th} \frac{\pi}{2b} (\zeta-1) * \quad (13)$$

$$* \int_0^\infty \{ \exp[-\frac{\gamma_0^2}{b} (\tau + \zeta + 1)] * \quad (14)$$

$$* E_1[\frac{\gamma_0^2}{b} (\tau + \zeta + 1)] - \frac{1}{2} \ln \left| \frac{\tau + \zeta + 1}{\tau - \zeta + 1} \right| \} * \quad (15)$$

$$* \ln \operatorname{th} \frac{\pi}{2b} \tau d\tau d\zeta;$$

$$\bar{\mu}_{33} = \frac{\mu_{33}}{\rho T \sqrt{g B}} = \frac{32}{\pi^3} \Psi(\gamma_0) * \quad (16)$$

$$* \int_0^\infty \exp[-\frac{\gamma_0^2}{b} (\tau + 2)] \ln \operatorname{th} \frac{\pi}{2b} \tau d\tau;$$

$$\Psi(\nu_0) = \sum_{k=1}^{\infty} \left[(2k-1)(2k-1 + \frac{\nu_0^2}{\pi}) \right]^{-1};$$

$$\nu_0 = \sigma \sqrt{B/g}, \quad b = \frac{B}{T}. \quad (13)$$

The results of $\bar{\lambda}_{33}$ and $\bar{\mu}_{33}$ calculations are compared with Vugts' experimental data /5/ on fig.1 and fig.2.

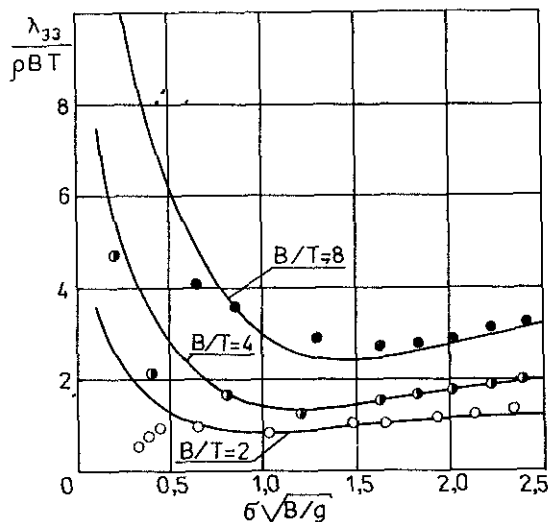


Fig.1 Added mass of heaving rectangle (solid lines - theory, dots - experiment)

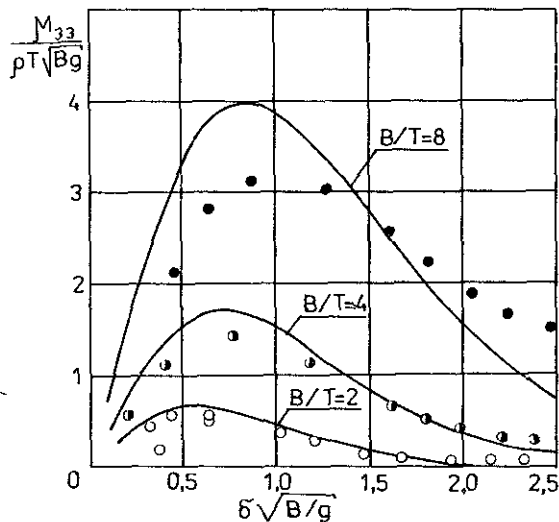


Fig.2 Damping of heaving rectangle (solid lines - theory, dots - experiment)

The correlation is good, so the approximate solution of the linear boundary value problem for a velocity potential is valid for calculating the hydrodynamic characteristics. If Has-kind approach is used /1/, the damping coefficient μ can be found on the base of asymptotic expression of $\Phi_s^{(n)}$ given in (8) when $y \rightarrow \pm \infty$:

$$\bar{\mu}_{33} = \frac{64}{\pi^4} \nu_0 b \Psi^2(\nu_0) \exp\left(-2 \frac{\nu_0^2}{b}\right) \quad (14)$$

Although formulae (13) and (14) differ one from the other, numerical calculation both of them gives absolutely equivalent results. This fact may be considered as a practical proof

of a possibility to obtain the damping coefficients and exciting forces using the first approximation of the boundary value solution in the outer zone. This conclusion was confirmed by the calculation results for a wide range of B/T values and taken as a background for solving three-dimensional hydrodynamic problem.

Rolling of VW-type hull floating structure with a rectangular waterline

Let a rectangular pontoon is rolling on a free surface of deep calm water. The angular velocity of oscillations is $\theta(t) = \cos \omega t$. The cosine $\Phi_c(x, y, z)$ and sine $\Phi_s(x, y, z)$ amplitudes of the velocity potential $\Phi(x, y, z, t) = \Phi_c(x, y, z) \cos \omega t + \Phi_s(x, y, z) \sin \omega t$ are harmonic functions in a fluid domain and satisfy the following conditions on the hull surface

$$\frac{\partial}{\partial x} \Phi_c, s\left(\pm \frac{L}{2}, y, z\right) = 0,$$

$$|y| < \frac{1}{2}B, \quad 0 \leq z < T;$$

$$\frac{\partial}{\partial y} \Phi_c(x, \pm \frac{1}{2}B, z) = -z;$$

$$\frac{\partial}{\partial y} \Phi_s(x, \pm \frac{1}{2}B, z) = 0,$$

$$|x| < \frac{1}{2}L, \quad 0 \leq z < T;$$

$$\frac{\partial}{\partial z} \Phi_c(x, y, T) = y, \quad \frac{\partial}{\partial z} \Phi_s(x, y, T) = 0,$$

$$|x| < \frac{1}{2}L; \quad |y| < \frac{1}{2}B. \quad (15)$$

The fluid domain may be divided into two zones: an internal zone

$$|x| < \frac{1}{2}L; \quad |y| < \frac{1}{2}B; \quad T \leq z < \infty,$$

and an external zone

$$|x| > \frac{1}{2}L; \quad |y| > \frac{1}{2}B; \quad 0 \leq z < \infty.$$

Following the procedure described in the previous paragraph we find the potential $\Phi_c^{(n)}$ in the inner zone from the boundary value problem

$$\left(\frac{\partial^2}{\partial x^2} + \frac{\partial^2}{\partial y^2} + \frac{\partial^2}{\partial z^2} \right) \Phi_c^{(n)}(x, y, z) = 0,$$

$$|x| < \frac{1}{2}L; \quad |y| < \frac{1}{2}B; \quad T < z < \infty;$$

$$\Phi_c^{(n)}(\pm \frac{1}{2}L, y, z) = 0, \quad |y| < \frac{1}{2}B;$$

$$\Phi_c^{(n)}(x, \pm \frac{1}{2}B, z) = 0, \quad |x| < \frac{1}{2}L, \quad T < z < \infty;$$

$$\frac{\partial}{\partial z} \Phi_c^{(n)}(x, y, T) = y, \quad |x| < \frac{1}{2}L, \quad |y| < \frac{1}{2}B,$$

$$\lim_{z \rightarrow \infty} \text{grad } \Phi_c^{(n)}(x, y, z) = 0. \quad (16)$$

tifies the same type of the boundary value problem with zero potential derivatives on a hull surface. So $\Phi_s^{(0)}(x, y, z) \equiv 0$ in the inner zone. The solution of the boundary value problem (16) can be found on the base of sine Fourier expansion of a linear function

$$u - \pi = -2 \sum_{m=1}^{\infty} \frac{\sin mn}{m}, \quad 0 < u < 2\pi.$$

So it comes

$$\Phi_c^{(0)}(x, y, z) = \frac{4B}{\pi^3} \sum_{m=1}^{\infty} \sum_{l=1}^{\infty} (-1)^{m+l} *$$

$$\frac{\sin \frac{2\pi\mu y}{B} \cos \frac{(2l-1)\pi x}{L}}{\lambda_{2l-1, 2m} \cdot m(2l-1)} *$$

$$* \exp[-\pi \lambda_{2l-1, 2m} \cdot (z-T)]; \quad (17)$$

$$\text{where } \lambda_{p,q} = \sqrt{\frac{p^2}{L^2} + \frac{q^2}{B^2}}.$$

Formula (16) gives a possibility to find the potential $\Phi_c^{(0)}$ derivatives on the boundaries between inner and outer zones

$$\frac{\partial \Phi_c^{(0)}}{\partial x} (\pm \frac{1}{2}L, y, z) = Q(y, z),$$

$$|y| < \frac{1}{2}B, \quad T < z < \infty,$$

$$\frac{\partial \Phi_c^{(0)}}{\partial y} (x, \pm \frac{1}{2}B, z) = P(x, z),$$

$$|x| < \frac{1}{2}L, \quad T < z < \infty.$$

The potential functions $\Phi_c^{(0)}$ and $\Phi_s^{(0)}$ in the outer zone satisfy the boundary value problem

$$\left(\frac{\partial^2}{\partial x^2} + \frac{\partial^2}{\partial y^2} + \frac{\partial^2}{\partial z^2} \right) \Phi_{c,s}^{(0)}(x, y, z) = 0,$$

$$|x| > \frac{1}{2}L, \quad |y| > \frac{1}{2}B, \quad 0 \leq z < \infty.$$

$$\left(\frac{\partial}{\partial z} + \kappa \right) \Phi_{c,s}^{(0)}(x, y, 0) = 0,$$

$$|x| > \frac{1}{2}L, \quad |y| > \frac{1}{2}B;$$

$$\frac{\partial}{\partial x} \Phi_c^{(0)}(\pm \frac{1}{2}L, y, z) = \begin{cases} 0, & 0 \leq z < T; \\ Q(y, z), & T < z < \infty; \end{cases}$$

$$\frac{\partial}{\partial y} \Phi_c^{(0)}(x, \pm \frac{1}{2}B, z) = \begin{cases} -2, & 0 \leq z < T; \\ P(x, z), & T < z < \infty; \end{cases}$$

$$\frac{\partial}{\partial x} \Phi_s^{(0)}(\pm \frac{1}{2}L, y, z) = 0, \quad |y| < \frac{1}{2}B; \quad (18)$$

$$\frac{\partial}{\partial y} \Phi_s^{(0)}(x, \pm \frac{1}{2}B, z) = 0, \quad |x| < \frac{1}{2}L, \quad 0 \leq z < \infty;$$

$$\lim_{z \rightarrow \infty} \text{grad } \Phi_{c,s}^{(0)}(x, y, z) = 0,$$

$$|x| > \frac{1}{2}L, \quad |y| > \frac{1}{2}B.$$

The potential function $\Phi^{(0)}(x, y, z, t) = \Phi_c^{(0)}(x, y, z) \cos \omega t + \Phi_s^{(0)}(x, y, z) \sin \omega t$ satisfies the radiation principle. The solution of the boundary value problem (18) is taken in a form of Fourier-Michell integral /4/:

$$\Phi_c^{(0)}(x, y, z) = \int_0^{\infty} G(x, y, \mu) \phi(z, \mu) \frac{\mu^2 d\mu}{\mu^2 + \kappa^2} +$$

$$+ U_c(x, y) e^{-\kappa z},$$

$$G(x, y, \mu) = \frac{2}{\pi} \int_0^{\infty} \Phi_c^{(0)}(x, y, z) \phi(z, \mu) dz;$$

$$U_c(x, y) = 2\kappa \int_0^{\infty} \Phi_c^{(0)}(x, y, z) e^{-\kappa z} dz. \quad (19)$$

The function $\Phi_c^{(0)}$ is harmonic and the set of functions $\phi(z, \mu), e^{-\kappa z}$ is orthogonal, so it comes

$$\left(\frac{\partial^2}{\partial x^2} + \frac{\partial^2}{\partial y^2} - \mu^2 \right) G(x, y, \mu) = 0;$$

$$\left(\frac{\partial^2}{\partial x^2} + \frac{\partial^2}{\partial y^2} + \kappa^2 \right) U_c(x, y) = 0,$$

$$|x| > \frac{1}{2}L, \quad |y| > \frac{1}{2}B.$$

Using the Kirhgoff formulae we can express the magnitudes of $G(x, y)$ and $U_c(x, y)$ in an arbitrary point of xy-plane outside the rectangle bounded by straight lines $x_0 = \pm \frac{1}{2}L$ and $y_0 = \pm \frac{1}{2}B$. The integral operators in these formulae include values of known derivatives and unknown functions along the sides of rectangle. The derivatives mentioned are obtained from the boundary conditions in (18) and the second formulae in (19).

The same way may be used for deriving $\Phi_s^{(0)}(x, y, z)$ function from boundary value problem (18). The final expressions can be found after satisfying the radiation principle. The far field asymptotics of the radiation potential includes

$$U_c(x, y) e^{-\kappa z} \cos \omega t \text{ and } U_s(x, y) * e^{-\kappa z} \sin \omega t.$$

Functions $U_{c,s}(x, y)$ are taken in the far field where $r = \sqrt{x^2 + y^2}$ tends to infinity. The expressions for $U_{c,s}$ include values $U_{c,s}(x, y)$ of these functions on the sides $x_0 = \pm \frac{1}{2}L, |y| < \frac{1}{2}B; |x| < \frac{1}{2}L, y_0 = \pm \frac{1}{2}B$ of the

rectangle. The values mentioned are determined as solutions of a set of simultaneous integral equations of the form

$$\begin{aligned} \begin{Bmatrix} U_c(x, y) \\ U_s(x, y) \end{Bmatrix} &= \frac{1}{4} \oint \frac{\partial}{\partial \nu} U_c(\xi, \eta) \begin{Bmatrix} N_o(\xi R) \\ J_o(\xi R) \end{Bmatrix} \pm \\ &\pm \frac{\partial}{\partial \nu} U_s(\xi, \eta) \begin{Bmatrix} J_o(\xi R) \\ N_o(\xi R) \end{Bmatrix} - \\ &- U_c(\xi, \eta) \frac{\partial}{\partial \nu} \begin{Bmatrix} N_o(\xi R) \\ J_o(\xi R) \end{Bmatrix} \mp \\ &\mp U_s(\xi, \eta) \frac{\partial}{\partial \nu} \begin{Bmatrix} J_o(\xi R) \\ N_o(\xi R) \end{Bmatrix} d\Gamma \end{aligned} \quad (20)$$

It has to be noticed that

$\frac{\partial}{\partial \nu} U_{c,s}(\xi, \eta)$ are known and that

$U_{c,s}(\xi, \eta) \equiv U_{c,s}(x_k, y_k)$ are unknown functions. A numerical iterative method for solving set of integral equations (20) was specially worked out. At the first step it is taken $U_{c,s} \equiv 0$ and at the next steps $i=1, 2, \dots$ it is taken

$(i-1)$

$U_{c,s}(\xi, \eta) = U_{c,s}^{(i-1)}(\xi, \eta)$ in the right-hand side of (20). Computational experiments confirm high effectiveness of the proposed method. The far field asymptotics of radiation potentials for another modes of oscillation can be found in the same way.

Hydrodynamic forces acting on VW-type hull structure in regular waves

Exciting forces and moments acting on a floating body in regular waves can be obtained from Haskind-Newman formula [1]. The complex exciting force amplitude $X_j = X_{cj} + iX_{sj}$ ($j=1, 2, \dots, 6$) is expressed in a form

$$X_j = i\sigma \int_0^{2\pi} \int_0^{\infty} \left(\Phi_w \frac{\partial}{\partial r} \Phi_j - \Phi_j \frac{\partial}{\partial r} \Phi_w \right) r dz d\theta, \quad (21)$$

where regular wave motion potential

$$\Phi_w(r, \theta, z) = \frac{g r_w}{\sigma} \exp[-\alpha z + i\alpha r \cos(\theta - \phi)],$$

Φ_j - j -th mode radiation potential far field asymptotics.

The integration in (21) is held for $r \rightarrow \infty$. Final formulae are complicated and not presented here. The computational results for VW-type rectangular pontoon with $L/B = 3.607$, $B/T = 9.733$ are given on figures 3 and 4. Undimensional exciting force \bar{X}_2 for swaying and exciting moment \bar{X}_4 for rolling motions are plotted versus undimensional frequency ν for three angles of wave heading.

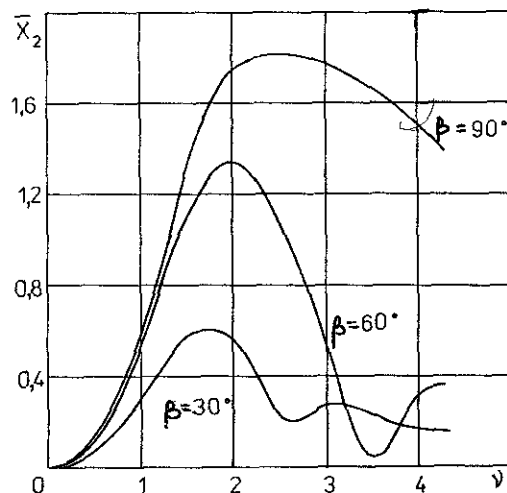


Fig.3 Sway exciting force at different heading angles β .

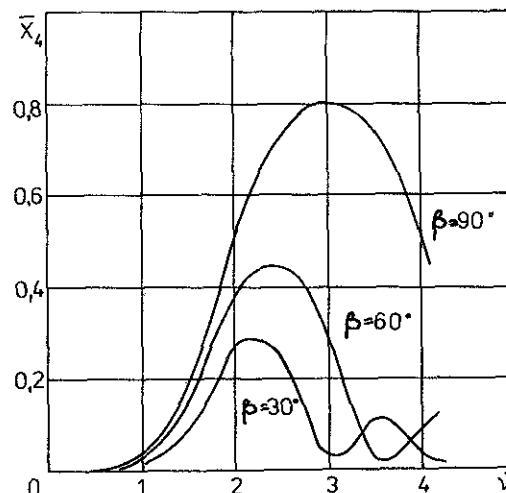


Fig.4 Roll exciting moment at different heading angles β

The formula for wave damping coefficients μ_{ij} may be found from Haskind-Newman relation [2] based on the analysis of wave flow energy from the oscillating body to the infinity. The results of the numerical calculations using these formulae are given on fig.5, where nondimensional wave damping coefficients $\bar{\mu}_{22}$ and $\bar{\mu}_{44}$ are plotted versus ν . The added mass coefficients are calculated according to (1) and a special method of principal value integral computation is used. The results are shown on figure 6 for sway added mass $\bar{\lambda}_{22}$ and roll added moment $\bar{\lambda}_{44}$ coefficients.

Rolling and swaying motion calculations

If a linear approach is taken the motion of a floating body in regular waves is described by a set of six linear differential equations. In a case of double symmetry of a body (symmetry with reference to diametral plane and midship section) the set of equations is decomposing into two independent systems (surging and pitching, rolling and swaying) and

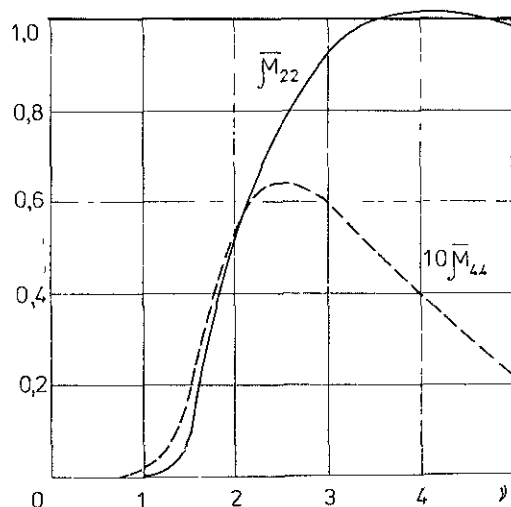


FIG. 5. SWAY AND ROLL DAMPING COEFFICIENTS

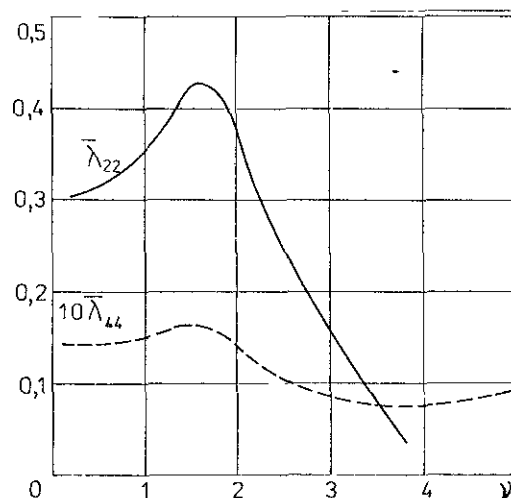


FIG. 6. SWAY AND ROLL DAMPING COEFFICIENTS

separate equations for heaving and yawing.

Treating the stability problems we investigate an ordinary set of differential equations for heaving and swaying but use two corrections in them. First of all, nonlinear restoring moment $Dl(\theta)$ is taken into consideration; secondly, approximate method of calculating the separation damping phenomena is used. So the total damping force (moment) is taken as a sum of the wave damping component and the additional damping component caused by the vortex separation on rectangular sides of a hull as on the plates translating or rotating in the uniform flow. For example, the additional damping moment due to flow separation is equal to $W_{44} [\dot{\theta}(t)]^2 \text{sign} \dot{\theta}$,

$$W_{44} = \rho L B C_x \left[\frac{L}{32B} + \frac{L}{16T} \left(\frac{T}{B} \right)^4 \right],$$

C_x being a resistance coefficient for a flat plate. For simplicity the quadratic damping is substituted by its linear analogue based on the equ-

ality of damping moment work per period of oscillations. So the equation of rolling remains linear but the total damping coefficient has two parts, one being a function of frequency of encounter. The solution of linearized differential equation of rolling can easily be found by a simple iterative process. The analysis based on the computational results shows the negligible influence of vortex separation damping to the total damping of sway. That's why the sway oscillation equation remains linear. The floating structures which performance at sea is studied have usually large dimensions and displacement. So for practical use a set of two linear differential equations of rolling and swaying has to be solved and for specific cases only the equation of rolling has to be taken nonlinear using nonlinear restoring moment $Dl(\theta)$. The computational results for rolling of a rectangular pontoon with $L/B=3.607$ and $B/T=9.733$ are given in fig. 7. There are two curves. One curve corresponds to the solution of set of equations, another one to the solution of a separate equation of rolling. The dots correspond to the experimental results obtained in OIME TT.

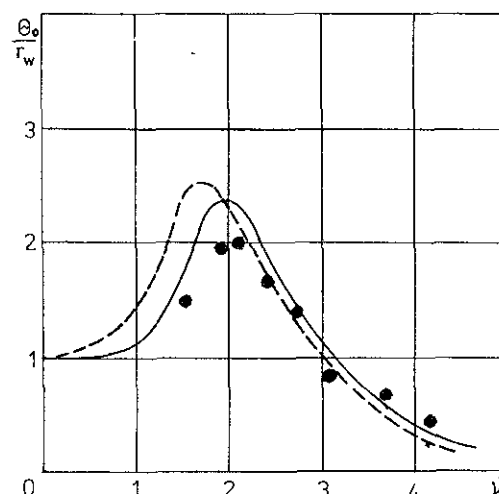


FIG. 7. ROLL MOTION AMPLITUDE θ_0/τ_w
SOLID LINE - PURE ROLLING,
DASHED - ROLLING WITH
SWAYING

CONCLUSIONS

The effective method has been worked out for calculation of hydrodynamic forces acting in waves on VW-type hull floating structures with an arbitrary waterline shape. It makes possible to determine the hydrodynamic characteristics omitting strip method assumptions. A simple idea gives a chance to take into account the damping force component due to vortex separation while hull is oscillating.

The comparison shows good enough agreement of theoretical results and experimental data.

ACKNOWLEDGEMENTS

Naval architect S. Baskakov who had his post graduate course under the author's guidance did his best in practical adoption of mathematical ideas, receiving computational results, performing model tests. This activity is greatly acknowledged by the author.

Nomenclature

$\lambda_{p,j}$ - added mass;

σ - frequency of encounter;

μ - damping coefficient;

p, j

p, j - modes of oscillation;

B - beam of a hull (contour);

T - draft of a hull (contour);

x, y, z - Cartesian coordinates;

$E_1[u]$ - the integral exponent function of the argument u ;

x_k, y_k and ξ, η - coordinates of the points belonging to a rectangular contour $\{x_0 = \pm \frac{1}{2}L, |y| < \frac{1}{2}B, |x| < \frac{1}{2}L, y_0 = \pm \frac{1}{2}B\}$;

$\frac{\partial}{\partial n}$ - differential operator along an external normal to a contour;

\oint - integral over the contour X ;

$R = \sqrt{(x_k - \xi)^2 + (y_k - \eta)^2}$ - radius;

$J_0(u), N_0(u)$ - Bessel functions of an argument u ;

$X_{cj}(X_{sj})$ - cosine (sine) amplitude of the exciting force in j -th mode;

r_w - wave amplitude;

ϕ - angle between the direction of wave front propagation and hull ceterplane;

$r = \sqrt{x^2 + y^2}$ - radius;

$\bar{X}_2 = \frac{X_2}{\rho r_w L T}$ - undimensional exciting force amplitude for swaying;

$\bar{X}_4 = \frac{X_4}{\rho r_w L B T}$ - undimensional exciting moment amplitude for rolling;

$\nu = \sigma \sqrt{L/g}$ - undimensional frequency of encounter;

$\bar{\mu}_{22} = \frac{\mu_{22}}{\rho L B T}, \bar{\mu}_{44} = \frac{\mu_{44}}{L B T}$ - nondimensional wave damping coefficients for swaying and rolling;

$\bar{\lambda}_{22} = \lambda_{22} \frac{1}{\rho L B T}, \bar{\lambda}_{44} = \lambda_{44} \frac{1}{\rho L^3 B T}$ -

nondimensional sway and roll added masses;

D - displacement of a floating body;

$l(\theta)$ - static stability arm;

η, θ - sway and roll motion amplitudes;

α_w - maximum wave slope.

REFERENCES

1. NEWMAN J.N. The damping of an oscillating ellipsoid near a free surface. Journal of Ship Research, 1961, vol. 5, No 3, pp. 44-58.
2. NEWMAN J.N. The exciting forces on fixed bodies in waves. - Journal of Ship Research, 1962, vol. 6, No 3, pp. 10-17.
3. LANDAU L., LIFSHITS E. Theoretical physics, vol. 5. Statistical physics. Moscow, Nauka, 1964. - 567 p.
4. VOROBYOV Yu. L. Linear asymptotic theory for pitching and heaving of a ship in deep water. - Prikladnaya Mekhanika, Akademija Nauk Ukrainskoy SSR, 1975, vol. XI, part II, pp. 106-112.
5. VUGTS J.N. The hydrodynamic coefficients for swaying, heaving and rolling cylinders in a free surface, Int. Shipb. Progr., July 1968, vol. 15, No 167, pp. 251-276.

**SURVIVAL TESTING, A TOOL AND TECHNIQUE TO ESTABLISH THE SAFETY LEVEL OF
MARINE FLOATING STRUCTURES; SMALLER VESSELS - TO LARGE OFFSHORE STRUCTURES.**

TERJE NEDRELID, MARINTEK A/S, TRONDHEIM, NORWAY

ABSTRACT

At Marintek, stability research has been performed for several years. This research often have implied testing of specific designs in critical wave situations. Single investigations have been performed to find the reason for an actual capsize event. More systematic testing with a number of models have been performed to establish the correlation between the ruling static stability - criteria and the probability for even "stable" vessels to experience capsizing. The last type of investigations refer to the study of the influence of dynamic motions on static stability. Smaller vessels, fishing vessels, coasters and large offshore structures such as drilling-rigs and floating production systems have been tested. This paper presents the technique and philosophy behind the survival testing methods and summarizes the unpublished results for several actual designs. The presentation of the results is made in order to show how, in addition to identifying poor designs, survival testing is a method and a tool to:

1. Increase the physical understanding of the dynamic capsizing event in various wave situations.

2. Qualify ruling stability criteria and improve existing stability procedures.

3. Define operational procedures to avoid critical situations.

Terje Nedrelid, Div. Mgr., Marintek,
P.O.Box 4125, 7002 Trondheim, Norway.

1. GENERAL PHILOSOPHY ON SURVIVAL TESTING

Following an accident, investigations are often performed to find the reason for the mishap. We are using theoretical tools as well as model tests to find the answers, which is the normal procedure adhered to by Norway through all the years we have been a sea industry nation. In modern days when the public opinion is watching more closely, investigations follow every large sea disaster. Results from these investigations form the basis of the ruling stability criteria today.

Theoretical tools for calculating dynamic motions have been improved. However, even when using supercomputers, the advanced theory does not handle the extreme motions, characterizing the capsizing event precisely enough. Modern model test techniques are, however, improved. Our knowledge of wave kinematics and the waves statistical properties enables us to accurately model the effects in a laboratory. This has provided new light into the investigation of accidents.

The symbiosis of advanced theoretical tools, advanced model test technique and improved knowledge of wave statistics has put us in a position of doing something new: Survival testing of marine structures. In effect this means that we today perform survival testing even before any accident happens. When designing any offshore structure, this has been normal procedure, but it is a new idea when it comes to the traditional shipping industry.

One should accept the general stability criteria system, even if this only counts for statical situations. Substantial research work during many years shows that a high level of experience and practical, real life statistics are built into these criteria. The new idea of survival testing of vessels can be used to adjust the criteria, to establish a safety "feeling" around a new type of vessel. If one does not accept the design resulting from these tests, it should be adjusted, in other words improved. As will be seen, operational procedures can also be defined as a result of this type of investigations.

An offshore structures design is not only ruled by stability criteria as such, it should withstand any reasonably defined weather situation defined by a given return period. This means that almost all larger offshore structures are analysed in survival situations (i.e. to withstand a 100 or 1000 year storm). As offshore constructions varies in geometry, it is often difficult to establish the same "feeling" of safety as for traditional a monohull vessel. The survival testing is a more integrated part of the design work of such constructions.

Survival testing should be used to observe the extreme motion of a floating structure when exposed to environmental forces. In principle an intact structure behaviour is analysed. We know, however, that waterfilling/flooding and shifting of cargo often are the part of the total capsizing event. Phenomena such as these have also been investigated by the Norwegian research work through the latter years.

The survival procedure will normally be as follows:

- Define critical environmental events.
- Test the floating structure in the critical event and observe the results.

- Establish the levels for the capsizing event with respect to the "size of the waves, wind and current".
- Establish the statistical base for the occurrence of the environmental situation and the capsizing events.
- Perform a parametric analysis, by theoretical tools or model tests to find the "sensitiveness" of the design or the criteria system.
- Use the results according to the given purpose:
 - to approve the design
 - to adjust stability criteria levels
 - to define operational procedures.

In the following, some results from examples of survival testing will be presented.

2. EXAMPLES OF SMALLER VESSELS

Survival testing have been performed on various examples of Norwegian ship designs. The purpose of the tests differed from one example to the next. Here we will comment on following the examples:

- 3 smaller fishing vessels
(15-30 m of length)
- a small Norwegian coaster
(43 m length)
- a traditional supply vessel
- a small monohull planing vessel
(see Fig. 1a, 1b, 1c)

For the fishing vessels and the coaster the tests were originally performed with the intention of investigating situations concerning the stability criteria. The following wave-vessel situations were defined as critical:

Waves on the beam:

- motions in large irregular waves
- motions in breaking waves
- motions in tuned combinations of wave train periods and rolling periods, including breaking waves.

In following waves:

- loss of stability on a wave top
- parametric resonance in wave trains
- broaching situations
- critical combinations of quartering seas, with tests performed in long-crested and shortcrested waves. Certain combinations with swell were also tested.

Parameters such as: Wave kinematics, wave heights, static stability of the vessel and detailed superstructure design have been varied (see Fig. 2 Stability curves) through the tests. The stability of the vessels varied around the minimum stability given by the existing stability criteria. The tests were performed in the Marintek Ocean Basin and in the Towing Tank No III. Motions, acceleration and water ingress were measured. Most of the tests were referred to the intact vessel. However, some cases of water filling in shelter deck areas were also investigated.

Results

The wave situation chosen for the testing of the fishing vessels and the coaster, were close to a gale or storm conditions and varied from 4-7m significant wave height, the breaking waves heights varied from 6-10 m. It is believed unlikely that larger waves and stormier weather give more extreme conditions and cause more capsizing situations. Rather, this is due to rolling periods and wave periods, steepness and breaking conditions of the waves. The weather situations also represent waves of a certain probability of likelihood to occur along the Norwegian coast.

The general impression when analysing the results from the fishing vessel and coaster tests is that for an intact vessel the today level of static stability provides a reasonably good safety against capsizing. Large rolling angles occur only in extreme breaking waves from the side. For general wave situations, large vertical accelerations were measured both on the fishing vessels and on the coaster, (see Fig. 3). In short-crested waves the vessel is exposed to large vertical accelerations close to $1g$ in all wave directions. This means that in a confused wave situation, ship heading changes makes no difference. This situation is critical with respect to shifting of cargo. In following waves loss of stability and broaching situations may occur, see Fig.4.

When comparing some of the results, i.e. in breaking waves from the side, one should note that "All the vessels were tested for the same scale factor and in exactly the same waves, plungers and spilling breakers".

In small breaking waves all vessels with normal stability experience the same level of rolling angle, $30 - 50^\circ$. The vessel with lowest freeboard and positive stability only up to $50 - 60^\circ$ heeling is most exposed to the capsizing event. Some examples on results are presented in Fig. 5a, 5b, 5c. If we put all results into the same diagram we will get an image of the energy of a breaking waves against the vessel total resistance against heeling, see Fig. 6a and 6b. These diagrams give a good impression of the sensitivity of any vessel to ever experience capsizing in a breaking wave. This can be used for practical purposes when planning new designs.

A supply vessel with a very high deck coaming design was investigated for survival situations. Due to the possibility of trapping large amounts of water on deck in following waves, this situation appeared to be critical. Survival tests show that even for large initial stability ($GM_0 > 3-4$ m) such a vessel will capsize. The observation is that this is caused by the long period needed to get rid of the water on deck compared to with the rolling period. Openings in the coamings were of no use (Fig. 7).

Fig. 6a and 6b showed that all kinds of small vessels can capsize in breaking waves. This is due to their low displacement or stability. Even vessels with total positive righting level arm, a "self-rightening" vessel, can be caught by such a wave and turned around 360° . During survival testing of a self-rightening, high speed planing vessel, see Fig. 8, this was experienced.

When the breaking wave hit "correctly" the vessel turned around 360° . This happens as a very rare event. For most of the tests the model behaved gently and only minor rolling angles occurred. The observations show that one should carefully examine the total design of any vessel. See Fig. 9.

3. EXAMPLE ON OFFSHORE STRUCTURES

During the investigation of the Ocean Ranger capsizing disaster, a comprehensive survival testing program was conducted. A later Norwegian research program, the MOPS-project, also performed such testing of offshore structures. Later on a large number of offshore structures have been exposed to survival conditions when referring to environmental forces. A large amount of results have been gained through this testing.

For ships we have observed that one single large breaking wave may capsize a small vessel. Physically this means that the angular momentum in roll direction transferred to the vessel by the wave, is sufficient to overturn it. A semisubmersible is fundamentally different from a small ship regarding roll and pitch characteristics. First of all the resonant periods are entirely different. More important is the question: What angular momentum can the rig absorb from the wave?

The case of a semisubmersible in intact condition and with reasonable GM value can be treated relatively accurately by present day methods for calculating wave loads and motions. At least for wave periods well below the resonant roll periods the conclusion is that only small roll angles can occur, and there is no danger of capsizing. Many model tests have confirmed this conclusion.

With such platforms in damaged condition, the situation could be different. At a larger angle of list, parts of the pontoons will get close to, or even pierce the surface. In such cases even the deck structure can be subjected to wave loads. In this situation the wave loads will be much larger than in intact condition. One can no longer exclude the possibility that single waves could transfer such angular momentum to the rig that it would capsize.

When discussing capsizing of rigs we also have to add events that involve misoperation of ballast system, damage and flooding, thus giving the semisubmersible an abnormal floating condition. At Marintek, the survival tests in waves were therefore first conducted for varying draught with large trim/ heeling angles ($5-15^\circ$). The models were opened to allow for progressive flooding through openings in the columns and deck houses.

CONCLUSIONS

The conclusions from the Marintek survival testing research is that single waves cannot capsize a rig in normal intact condition with reasonable metacentric height. In damaged condition at very large angles of list we are hardly able to calculate theoretically the wave forces and detailed effect of waves on the capsizing process. The most efficient way to study such phenomena is therefore by model tests, survival testing.

Present-day stability criteria have shown to provide a satisfactory level of safety against capsizing, as long as operational failures are avoided.

An intact rig with watertight deck structure is inherently very safe against capsizing. This is due to its typical shape of the righting arm curve, as shown compared to a ship in Fig. 10.

At MARINTEK a large number of offshore structures, e.g. floating production systems, have been tested for very extreme weather conditions; storms with return periods more than 100 years, 1000 years and so forth. These tests have very seldom showed the capsizing event as being the final happening of the disaster, not even for turret moored monohull vessels (see Fig. 11, the model of the Petrojarl I vessel). Broken mooring line systems, position systems that have too low thruster capacity leading to drift-off situations, water on deck and local damage of the structures i.e. have been observed.

These tests have, however, put us in a position to judge the total safety of the structure when placed in a given site position. The authorities' approval of such an offshore structure design is based upon this type of results.

4. ON THE UNDERSTANDING OF THE CAPSIZING EVENT

For some of the cases studied by survival testing, the understanding of the capsizing mechanism and to establish the probability of the capsizing event was the intention of the study. It often turned out to be a very complex explanation as dynamic and statical phenomena are acting. In theoretical terms, hydrodynamical potential theory effects and viscous phenomena occur.

Monohulls:

The capsizing of a monohull vessel is an extreme physical motion. Linear ship theory or other basic ship motion theories can not be extended to predict or calculate this phenomena correctly.

The tests have shown that:

- For very small vessels (eg. the planing vessel) it is an event dominated by dynamic phenomena. This means that when the wave hits correctly, the dynamic wave force easily turns the vessel around (the impulse of the wave water jet).
- For all vessels of some size (i.e. above 10-15 tonnes displacement) the dynamics related to the water jet impact is of minor importance. This means that in the cases of the breaking waves, it is the "quasi-static force" varying as with the wave profile moves (steepness of the wave) and the relative position of the vessel in the wave that counts. These effects create moments that turn the vessel into large angles of heel and capsizing.
- For low freeboard vessels, low stability and long rolling periods, wave geometry and water on deck create an even more complex situation. Water on deck do change the initial stability.

However, the mechanism can still be explained by the "quasistatic wave force" and assumption on how the wave profile moves and the relative position of the vessel in the waves.

- Wind and current does necessarily often not contribute much to the capsizing events, but will always expose the vessel into rolling motion situations.

Offshore structures

Referring to offshore structures of non-monohull geometry, we experience that the wave forces does not create large rolling moments at all. Most of these tests show that the capsizing event for such structures often are purely static, which means that such structures capsize only when they are close to sinking situations. This is discussed in more detail in Section 3.

5. STABILITY CRITERIA

To Quantify Criteria

The main purpose of survival testing technique is to quantify stability criteria. Stability criteria for floating monohull vessels have been developed through a period of many years. Different survival test-like results have been put on the table as an argument for the criteria. All this is done rather unsystematically. The laboratory facilities, the ability of making correct measurements and waves have been varied. However, as a result of statistics on accident statistics coupled with fullscale experience, reasonably good criteria have been established.

All tests performed in Norway during the last decade have shown that the existing international stability criteria do function well. It is based on practical parameters that can be used in a designing process for vessel construction, and

employed by the approving authorities as well as the ship owners when they are planning a journey. The crew onboard when operating the vessel, can also understand the parameters used in the criteria. We should bear this in mind when we discuss new approaches for a criteria system. We often mention methods of probability as a future basis. This implies new parameters not very well understood by the typical practitioner as yet.

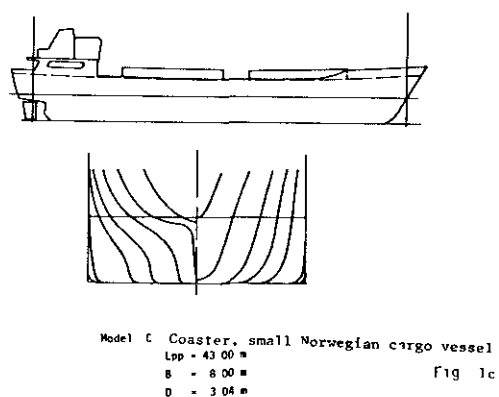
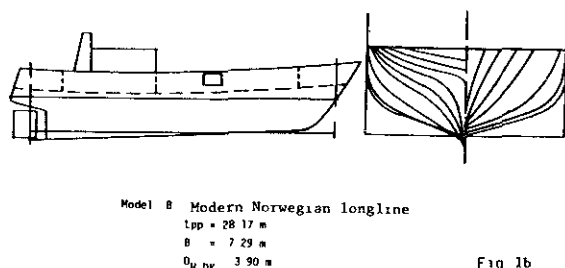
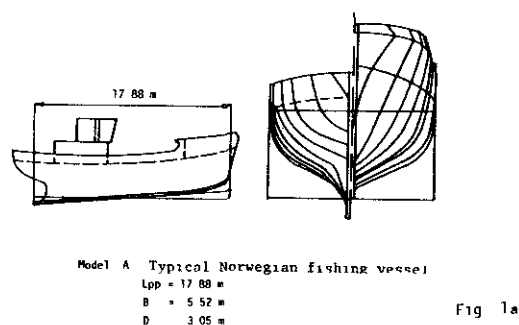
Our tests showed that vessels having at least the minimum required stability, very seldom capsizes. However, in Norway we have found, through this type of results, that by adjusting the requirement for the rightening lever arm up to above 60° - 80° heeling, the safety level of Norwegian fishing vessels against capsizing will increase. The Norwegian maritime authorities have put this adjustment of the criteria into force through the Norwegian ruling regulations for fishing vessels. this is an example on how to use the survival technique to adjust the criteria system itself.

6. A TOOL TO DEFINE OPERATIONAL PROCEDURES

In some cases during a survival testing situation, one realize that increased static stability does not necessarily lead to increased safety. The best solution for increasing safety will be more on an operational level. If one experiences a critical event, an operational change of a parameter could lead to a less critical situation. This is often the case with a monohull in following waves. By changing the heading and speed (see example Fig. 8) the situation that is close to a broaching, could be avoided. If practical operational stability work onboard a vessel also in the future will involve an operational manual, the results from survival testing in model scale might give important input to such manuals.

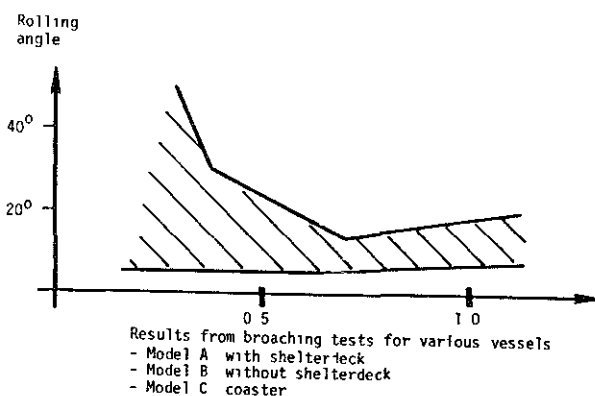
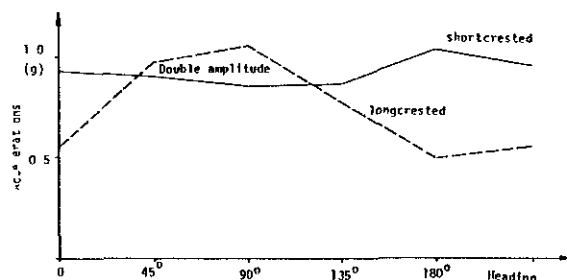
For offshore structures the survival testing results will give input to how to operate the tension in the mooring lines in critical weather situations. Results from survival testing can also give input to the control strategy to a dynamic positioning system if thrusters or thrusters in combination with mooring lines are used.

Some of the results of the survival testing of semisubmersible rigs also show that one can design for larger GM values, thus creating a situation less sensitive to operational failures. The tests have shown that within reasonable limits, the GM value does not significantly influence the pitch and roll motion of the rig in operation.



REFERENCES

- Nedreid, T., Future Stability Criteria for Vessel Survival Tests in Critical Wave Situation. Marintek (NHL) report, from the "Stability Criteria" Project (in Norwegian).
2. Huse, E. and Nedreid, T., Hydrodynamic Stability of Semisubmersibles Under Extreme Weather Conditions. OTC 1985, Paper 4987.
3. Nedreid, T. and Reitan, O.E., Stability and Safety of Small Vessels in Extreme Weather Conditions. Measurement of Changes in Righting Lever for a Vessel Running in Following Waves. Model test. Marintek (NHL) report 1984.



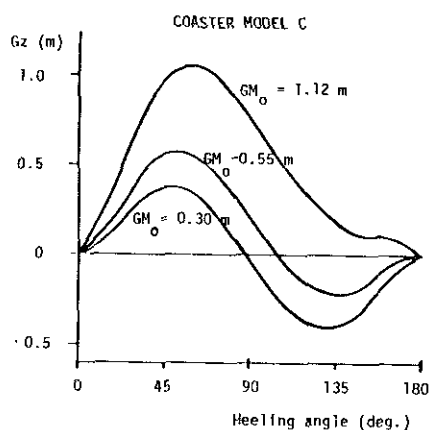
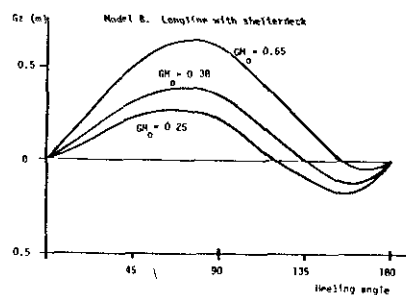
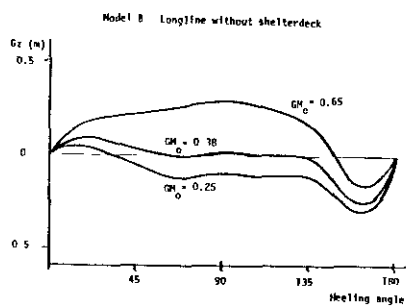
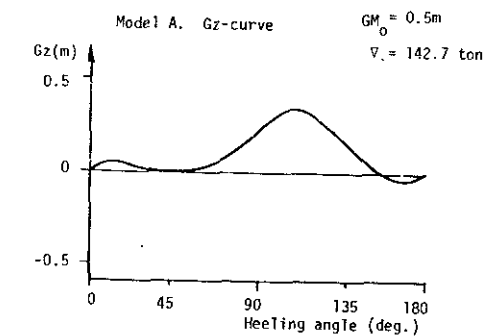


Fig. 2. Stability curves for the models a, b, c.

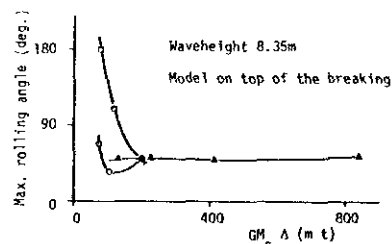
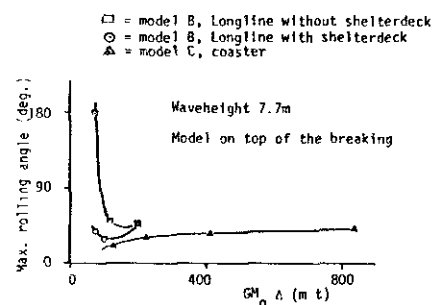


Fig. 5a Examples of measurements from capsizing tests

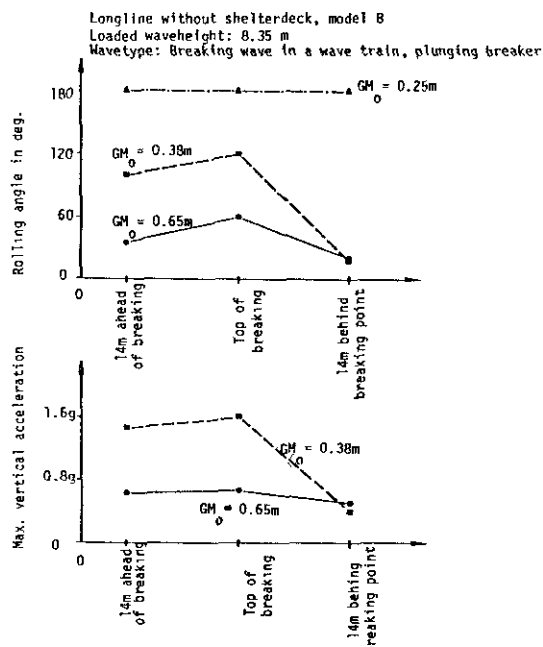


Fig. 5b. Examples of measurements from vessel capsizing tests in breaking waves.

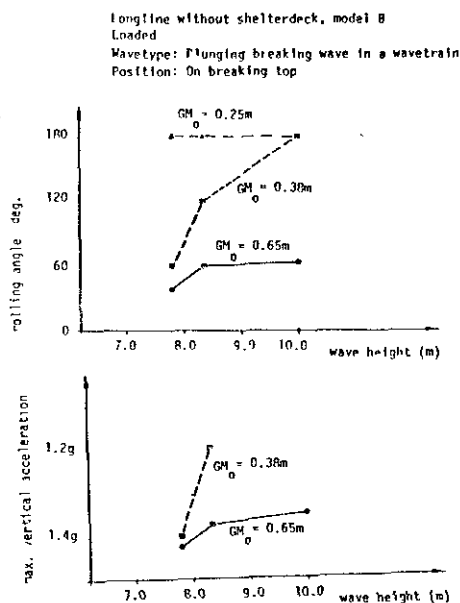


Fig. 5c. Examples of measurements from tests in breaking waves.

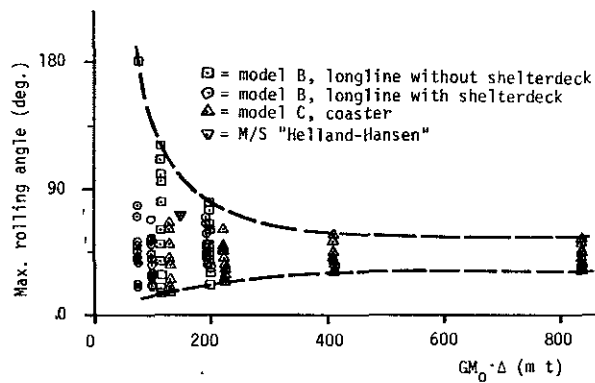


Fig. 6a. Results from a large number of capsizing tests at Marintek shown in one diagram.

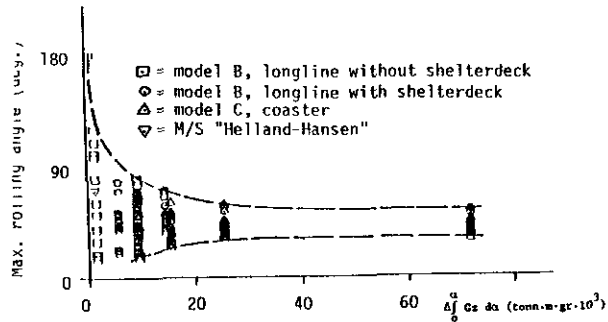


Fig. 6b. Results from a large number of capsizing tests at Marintek shown in one diagram.

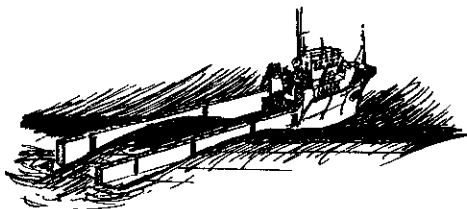


Fig. 7. Supply vessel, water on deck in critical situation



Fig. 8. The model of the Petrojarl I vessel

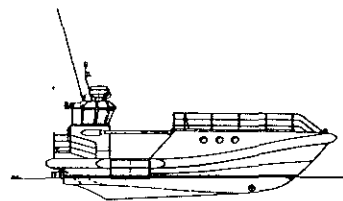


Fig. 9a. Small self-rightening vessel

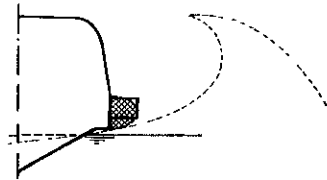


Fig. 9b. Local design elements might be important in a breaking jet.

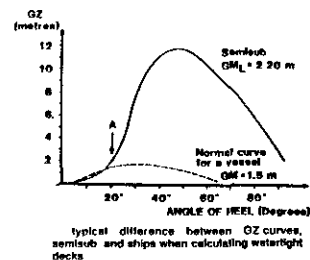
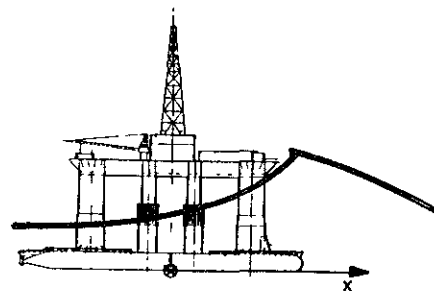
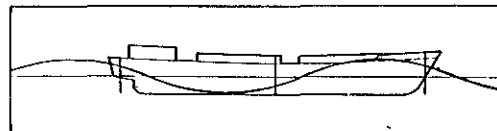
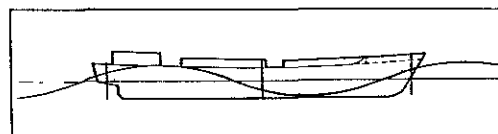


Fig. 10. Typical semisubmersible rig and stability curves.



Situation with the wave crest positioned in the foreship. The model was under control.



Situation with the wave crest positioned in the aft ship. The situation is dangerous and not under control.

Fig. 11. Situation in following seas.

AN INVESTIGATION OF VESSEL STABILITY IN WAVES
BY MEANS OF NUMERICAL MOTION SIMULATIONS

Jacek S. Pawlowski¹ and Donald W. Bass²

ABSTRACT

The paper presents an application of the notional and algorithmic framework of a novel, rational procedure for assessing stability of floating vessels to an investigation of the stability of a small fishing vessel. Within the procedure the stability properties of a vessel are represented by stability diagrams. The identification of the stability diagrams by means of either model tests or numerical simulations of vessel motion, constitutes the main technique of the stability analysis. In the paper the identification is carried out with the use of an advanced, time domain, non-linear numerical model of vessel motion. The results provide new insights into the stability of vessels in quartering seas and demonstrate the usefulness of the novel approach and technique.

INTRODUCTION

The need to rationalize the existing procedures for assessing stability of floating vessels, such as ships and semisubmersibles, has been widely recognized in the last decade. The main difficulties in implementing the required rationalization were discussed in [1]. They may be considered to follow from the inability to abandon the application of the righting arm (GZ) curve in one form or another, in the consideration of the dynamic behaviour of the vessel in waves. This leads to nominal, see [1], rather than rational stability assessment procedures, since: stability criteria defined by means of the GZ curve are not directly related to constructional features of the vessel, which determine its safety in the seaway, and there is no explicit or well defined relation between the GZ curve and the dynamics of vessel response to environmental excitations. A recent example of an otherwise rational approach in which eventually a nominal application of the GZ curve had to be used, can be found in [2].

In [3] and [1], a new rational procedure for assessing the stability of floating vessels was proposed and developed. One of the features of

the procedure is the application of stability diagrams to represent the range of stability and in this respect may be considered as rational replacements of GZ curves. One of the main advantages of the concept of stability diagram is that it provides a direct relation between the dynamics of vessel response to environmental excitations and rational stability criteria. As a result stability diagrams can be identified by means of model tests or numerical simulations of vessel motion.

Stability diagrams for semisubmersibles were investigated in relation to nominal stability criteria in [1]. In the present paper for the first time stability diagrams are identified by means of an advanced time domain, nonlinear motion simulation program, [4]. The study gives an example of how the rational stability assessment procedure developed in [3] and [1] can be implemented using an advanced numerical model of vessel motion in waves. It also demonstrates the technique, usefulness and implications of the use of stability diagrams in the investigation of the stability of a floating vessel.

THE RATIONAL ASSESSMENT OF STABILITY
AND STABILITY DIAGRAMS

A rational procedure for assessing the stability of floating vessels consists of a notional and corresponding algorithmic framework through which the knowledge of the physics of interaction between the vessel and marine environment is applied, primarily in the design process, to ensure a socially

¹ Head, Computational Hydrodynamics Laboratory, Institute for Marine Dynamics, National Research Council Canada, St. John's, Newfoundland

² Professor, Faculty of Engineering and Applied Science, Memorial University of Newfoundland, St. John's, Newfoundland

lives and property. The general outline of such a procedure was described by the first author in [3] and [1], and only its basic features need to be restated here.

A rational stability assessment procedure must as closely as possible reflect the physical relationships governing the vessel's response to environmental excitations. In addition, it should take into account that the safety of the vessel depends not only upon the response but also on the capacity of the hull and operating systems of the vessel to remain intact, operational and to protect the crew and load on board. Therefore a fully rational assessment of the stability needs to follow from an explicit examination of the dynamic response in conjunction with constructional features of the vessel (such as the vulnerability of the weather deck, efficiency of the ballast system, etc.). These requirements cannot be satisfied unless rational (as opposed to nominal, based e.g. on the GZ curve) stability criteria are formulated explicitly as bounds limiting relevant parameters of the dynamic response of the vessel.

It was demonstrated in [1] that the above requirements lead to the following key notions inherent in every rational procedure for stability assessment: the generalized instantaneous configuration of the vessel, criteria of stability, and control parameters.

The definition of the generalized configuration includes all the parameters of the absolute and relative (with respect to the water surface) motion of the vessel, which determine static and dynamic effects such as: force loads on the hull and equipment on board, wetness on deck, shipping of green water or permanent submergence of the deck and downflooding. In particular some or all of the parameters necessary to describe the absolute and relative motion of the vessel are contained in the definition, depending on the application.

The criteria of stability represent bounds imposed on the generalised configurations assumed by the vessel over its lifetime, within which the risk of the losses referred to above is reduced to an acceptable minimum. The criteria depend inherently on constructional features of the vessel and on its mission.

The control parameters are defined by parameters determining the geometry of the buoyant volume (i.e. the volume which if submerged contributes to the buoyancy force),

and the mass and mass distribution of the vessel. The control parameters are totally or partly controlled by the designer and operator of the vessel, and in any environmental conditions the values assumed by the generalized configuration of the vessel depend upon them for a given regime of the vessel's operation (defined for example by forward speed and course angle).

The procedure for assessing stability provides an algorithm for bounding, within certain risk limits, the possibility that during the lifetime of the vessel the generalized configuration assumes unacceptable values defined by the criteria of stability. Since the generalized configurations depend on control parameters (over a set of considered environmental conditions and regimes of operation) and the control parameters evolve constantly over the lifetime of the vessel, the fundamental purpose of the procedure is to ensure that the evolution of the control parameters does not lead to a violation of the stability criteria.

It follows from the definition of the procedure for assessing stability that as a result of its application a range of allowable evolutions of the control parameters must be found, which corresponds to the adopted stability criteria and to the assumed set of environmental conditions and regimes of operation. It was explained in [3] and [1] that the range of allowable control parameters can be expressed in a simple form by means of a stability atlas consisting of a number of stability diagrams. Each stability diagram applies to a given environmental condition, operational regime, geometry of the buoyant volume and displacement of the vessel.

For a chosen geometry of the buoyant volume and displacement of the vessel, an upright configuration of hydrostatic equilibrium of the vessel is defined. In the upright configuration the projection, K , of the centre of buoyancy onto a horizontal base plane, provides the origin of a system of reference fixed with the vessel. The location of the centre of gravity, CG , is considered as evolving in a plane perpendicular to the base plane. The coordinates of CG are read with respect to the axis defined by the crossing line of the plane of evolution of CG and the base plane, with the origin at K (co-ordinate GG'), and the axis through K perpendicular to the base plane and directed upwards (coordinate KG), see Fig. 2a.

In the described system of reference the stability diagram consists of a pair of diagrams, a

static diagram and a dynamic diagram. Each of the diagrams is represented in principle by two lines, defining the limiting values of GG' for a given KG . The static diagram corresponds to stability criteria imposed upon static generalized configurations of the vessel (achieved at hydrostatic equilibrium). The dynamic diagram indicates the limiting values of GG' determined by stability criteria imposed upon generalized configurations which the vessel assumes under the specified regime of operation and environmental condition. The construction of the diagram implies that for a given displacement the moments of inertia are single valued functions of the location of CG. Otherwise additional diagrams must be constructed. The difference between GG' values read off the static and dynamic diagrams on the same side of the stability diagram for a given KG , provides a measure of the influence of the regime of operation and environmental condition upon the stability of the vessel.

The concept of stability diagram is analogous to that of bifurcation set applied in catastrophe theory, see e.g. [5]. The space of control parameters used in the procedure for stability assessment and of parameters defining operational regimes and environmental conditions corresponds to the control space of catastrophe theory. As the control variables which define the control space are altered a control trajectory is traced through the stability atlas. In particular if the buoyant geometry, displacement, regime of operation, and environmental condition are kept fixed, and the location of CG is restricted to the plane of a stability diagram, then the control trajectory is contained in the plane of that stability diagram. If the control trajectory carries the vessel from one side to the other of the line of a stability diagram (static or dynamic) a qualitative change of the corresponding generalized configurations occurs (from the ones which satisfy the stability criteria to those which do not or vice versa, depending on the direction of the trajectory). In this sense the lines of the stability diagrams represent bifurcation sets in the control space. The construction of stability diagrams involves the assumption that the qualitative change of generalized configurations is restricted to the lines of stability diagrams. Such an assumption is partly justified by derivations of stability diagrams from the nominal stability criteria defined in terms of the GZ curve, see [1].

Another interpretation of stability diagrams is also possible and useful. For a fixed value of KG a shift of CG determined by a chosen GG'

corresponds to the application of an inclining moment dependent on the absolute configuration of the vessel. The moment may be considered as a testing load of the magnitude defined by the value of GG' . Adopting such a definition, for any particular set of the control parameters and for a fixed environmental condition and regime of operation, the values of allowable (i.e. limited by the stability diagram) GG' define measures of the vessel's stability, which are explicitly dependent on the chosen stability criteria. This is particularly important in considerations requiring the determination of the excess stability of a vessel, necessary to provide sufficient safety margins, as e.g. in the construction of safety regulations. The inability to define appropriate stability margins in direct reference to rational stability criteria forces a resort to a nominal stability assessment procedure, as is typified by the work presented in [2] where in spite of the initial adoption of rational criteria, the stability margins were imposed nominally with the use of the GZ curve.

The same interpretation of stability diagrams allows their direct identification by means of model tests or numerical simulations of vessel motion. Although testing loads (moments) other than those defined by GG' values can be used conveniently in the numerical simulations, the shifts of CG are the most readily applicable in model tests.

THE NUMERICAL MODEL OF VESSEL MOTION

For the identification of stability diagrams by means of numerical simulation, a sufficiently advanced numerical model of vessel interaction with the environment must be available. A model of this type was developed on the basis of the weak scatterer hypothesis [6], [7], [4]. Under the hypothesis, motions of a vessel in waves are modelled in the time domain, including nonlinear effects resulting from large amplitudes of the oncoming waves and vessel displacements. However, in comparison with those amplitudes, the disturbance of the oncoming wave flow, which is induced by the presence of the hull, is assumed to remain of a smaller order of magnitude, [6]. The simulation of the vessel's motion is obtained by the integration with respect to time of the full equations of rigid body motion.

The hydrodynamic forces exerted on the hull are evaluated in the time domain as a sum of generalized Froude-Krylov and scattering forces. The Froude-Krylov forces are obtained through a direct integration of the

undisturbed pressure of the oncoming wave over the instantaneous wetted surface of the hull. The scattering forces which are generated owing to the disturbance of the oncoming wave flow (assumed to be known in the form of a velocity potential) by the presence of the impermeable hull, are determined on the instantaneous wetted surface of the hull by means of the method of modal potentials [8], [4] [6], in conjunction with the hypothesis of weak scatterer [6], [4]. This leads to the following form of the expressions for the components of the generalized scattering forces in a system of reference fixed on the vessel:

$$F_{ji} = -\dot{\beta}_i(t) \mu_{ji} + \beta_i(t) U \mu'_{ji} + \int_{-\infty}^t d\tau [-\dot{\beta}_i(\tau) K_{ji}(t-\tau) + \beta_i(\tau) U K'_{ji}(t-\tau)] \quad (1)$$

where F_{ji} denotes the j -th generalized force component ($j=1$ for surge, $j=2$ for sway, ..., $j=6$ for yaw mode) induced by the i -th modal scattering potential (the scattering velocity potential is represented by a finite sum of modal scattering potentials), $\beta_i(t)$ is the time dependent amplitude of the i -th modal scattering potential, t denotes the time variable, and dot indicates differentiation with respect to time. μ_{ji} and μ'_{ji} signify appropriately defined infinite frequency added masses, and K_{ji} and K'_{ji} are the corresponding force memory functions, whereas U denotes the average forward speed of the vessel. In the quasi-linear expressions (1) the amplitudes of modal scattering potentials $\beta_i(t)$ are defined as functionals of the instantaneous velocity field induced by the oncoming wave and functions of the configuration of the instantaneous wetted surface of the vessel and of the linear and rotational velocity of the hull.

The expressions (1) can be simplified significantly if the oncoming wave is long-crested and monochromatic or almost monochromatic. Under such circumstances it is possible to approximate expressions (1) by:

$$F_{ji} = -[\dot{\beta}_i(t) (A_{ji} + \frac{U}{\omega^2} B'_{ji}) + \beta_i(t) (B_{ji} - UA'_{ji})] \quad (2)$$

with A_{ji} and A'_{ji} , and B_{ji} and B'_{ji} denoting (respectively) appropriately defined pairs of added mass and damping coefficients evaluated at the frequency of encounter ω which is determined by the dominant oncoming wave frequency, mean forward speed of the vessel U , and mean course angle χ of the vessel relative to the oncoming waves.

In [4] hydrodynamic forces and vessel motions computed by means of the numerical model described above, using expressions (2), were presented and compared with steady state and time history values obtained from model tests. In particular, good agreement was found between the experimental and computed results for a stern trawler operating in steep quartering seas.

AN EXAMPLE OF THE IDENTIFICATION OF A DYNAMIC STABILITY DIAGRAM BY MEANS OF NUMERICAL MOTION SIMULATIONS

The technique of investigating vessel stability through the identification of stability diagrams was applied to the stern trawler, referred to above, operating in steep quartering seas, for which a wide range of model test results is available, [9], and the applicability of the version of the numerical model used in [4] had been checked. This version was therefore adopted in the present study. In the following, all the data are given in the model scale 1:14.

The identification of stability diagrams was carried out for the volume of displacement of 0.0531 m^3 (loading condition for part of departure, [9]). In the upright configuration, the main particulars of the model are: length between perpendiculars $L=1.328 \text{ m}$, breadth at midships $B=0.435 \text{ m}$, draught at midships $d=0.198 \text{ m}$, and CG located aft of midships at $LCG=-0.009 \text{ m}$. The body lines of the model can be found in [9]. The GZ curve for $KG=0.2176 \text{ m}$ ($GM=0.0350 \text{ m}$), which includes the effect of the buoyant volume limited by the weather deck, is shown in Fig. 1. The environmental condition is defined by a long-crested wave of length $\lambda=3.18 \text{ m}$ (frequency 4.4 rad/sec) and height $H=0.33 \text{ m}$ (steepness $H/\lambda=0.10$). The regime of operation is characterized by the mean forward speed $U=0.80 \text{ m/sec}$ (Froude number $Fn=0.22$) and the mean course angle relative to the direction of wave propagation $\chi=30^\circ$ (180° corresponds to head seas). The corresponding mean frequency of encounter is $\omega=3.03 \text{ rad/sec}$.

Adopting the interpretation of stability diagrams as maps of vessel stability measured in terms of testing loads, the plane of the stability diagram to be investigated is chosen to coincide with the cross-sectional plane of the CG location in the upright configuration of the vessel. Since the investigation is not related to any specific design problem in which constructional features of the vessel would be defined in sufficient detail, the choice of static and

dynamic stability criteria remains somewhat arbitrary.

The static stability criterion is defined by the maximum angle of heel $\theta_c = 27^\circ$. For the considered volume of displacement, at this angle of heel the centre-line of the deck and top of the bulwark are submerged at midships. For any KG for which the range of positive righting arms is greater than 27° , the testing load bringing the vessel to hydrostatic equilibrium at θ_c can be determined from the relation:

$$GZ(\theta) = GG' \cos(\theta) \quad (3)$$

with $\theta = \theta_c$, and the testing load $GG' \cos(\theta)$ being defined by the value of GG' obtained from (3). The equilibrium at θ_c becomes unstable for $KG > 0.2176$ m ($GM < 0.035$ m, GM denotes initial metacentric height) and stable equilibria are obtained at $\theta < \theta_c$ (e.g. at $\theta = 25^\circ$ for $GM = 0.028$ m and at $\theta = 18^\circ$ for $GM = 0.0210$ m) for the corresponding testing loads. For the purpose of the present discussion the static stability diagram is represented by the graphs $GG' = GG'(KG; \theta_c)$, i.e. the graphs which for a given KG (or GM) give the value of GG' derived according to formula (3). The static stability diagram is shown in both Fig. 2a and 2b by the pairs of continuous, symmetric straight lines, over the range of 0.2120 m $< KG < 0.2316$ m (0.0210 m $< GM < 0.0406$ m).

The dynamic stability criterion is defined by the occurrence of extensive shipping of green water on deck. During the model tests, [9], it was observed that extensive shipping of water on deck, significantly influenced the model's motion, and usually took place when the top of the bulwark over at least half of the length of the model was submerged, [10]. In the numerical simulations such a critical event was specified by the exceedance of the top of bulwark by the water level on one side of the model, simultaneously at any 11 out of 19 stations equally spaced along the vessel (i.e. excluding the end sections), at a time step of the simulation.

In order to identify a dynamic stability diagram, numerical motion simulations were run for over 50 loading conditions at the given volume of displacement, for $KG = 0.2120$, 0.2176 , 0.2246 and 0.2316 m ($GM = 0.0406$, 0.0350 , 0.0280 and 0.0210 m respectively), thus covering a range of KG broader than that investigated by the model tests. The simulations were performed at the wave condition and regime of operation indicated above. The oncoming wave was represented by an Airy wave velocity potential in conjunction with the second order wave elevation, [11]. For any particular value of GG' the

hydrodynamic force coefficients were adjusted to their values at the corresponding stable hydrostatic equilibrium configuration of the vessel (evaluated at increments of θ of 2.5° between 0° and 20°). The adjustment included the additional hydrodynamic couplings associated with the inclined configurations. However, the viscous damping and coefficients characterizing the manoeuvring forces were not adjusted for the heeled configuration due to the lack of reliable data.

Two dynamic stability diagrams were identified, one with the hydrodynamic force coefficients (operational) evaluated at the frequency of encounter corresponding to the wave condition and regime of operation specified above, and another with the coefficients (changed) evaluated at the frequency changed arbitrarily to $\omega = 3.57$ rad/sec. In addition, motion simulations were carried out at $GM = 0.0280$ m and $GM = 0.0406$ m, with the operational hydrodynamic coefficients and with the viscous damping moment of roll increased by 50%.

The duration of each motion simulation was 22 seconds, with the first 2 seconds used for ramping in the wave amplitude and the vessel's speed from zero initial conditions to their assumed values. In this manner the influence of initial conditions upon the results of computations was controlled. A number of simulations performed with the ramping time of 4 seconds did not show a significant difference in comparison with the 2 sec ramping. The motion time histories for a typical simulation (operational hydrodynamic force coefficients and roll damping, and 2 sec ramping time) are shown in Fig. 3a-3d, where the occurrence of a critical event over a time period is indicated by the absence of the continuous line.

The results of the simulations in which the operational hydrodynamic force coefficients were used are presented in Fig. 2a. The mass distributions for which the simulations were performed (obtained by imposing shifts GG' of CG at the four GM values listed above, with the assumption that the central moments of inertia are not affected) are marked in the figure by symbols which indicate the number of occurrences of critical events during the corresponding simulations or a capsizing. The port and starboard (stbd) sides of the vessel are also indicated. Relative to the oncoming waves, starboard is on the leeside. The results obtained with the increased viscous roll damping are shown in brackets below the corresponding GM lines.

Two patterns of the dependence of the frequency of occurrence of the critical events upon GG' are observed in Fig. 2a. For $GM=0.0406$ m the frequency of occurrence decreases gradually with GG' growing from its extreme negative value to $GG'=0.0036$ m. That value of GG' may be considered as defining a point on one branch of the dynamic stability diagram (indicated by the broken line). For $0.0036 \text{ m} < GG' < 0.0150 \text{ m}$ no critical events are indicated and since critical events occur at $GG'=0.0150$ m, this value defines a point on the other branch of the dynamic stability diagram, beyond which the number of occurrences increases with growing GG' . It is clear that the location of the points which define the branches of the dynamic stability diagram would change continuously if the number of allowable critical events in the definition of the stability criterion was increased. Another, qualitatively different pattern is discerned at the lower values of GM . Taking for example $GM=0.0350$ m, a local increase of the frequency of occurrence appears in a vicinity of $GG'=0.0040$ m. Therefore if the allowable number of critical events was increased to 20 (from 0), then in addition to the continuously varying branches of the dynamic stability diagram at $GG'=0.0061$ m and at $GG'=0.0130$ m (moved from 0.0120 m) two additional branches would appear at $GG'=-0.0032$ m and $GG'=0.0045$ m. Such a structure of a dynamic stability diagram is shown at $GM=0.0280$ m by the simulations carried out with the increased roll damping (which diminishes the overall level of the frequency of occurrence of critical events without the modification of the stability criterion).

In Fig. 2b the results of the simulations in which the changed hydrodynamic force coefficients were applied are shown. A comparison between the results presented in Figs. 1a and 1b provides an indication of the sensitivity of the motion simulations to the variation of the assumed frequency of encounter, but also may serve to point out the possibility of changing the dynamic stability of the vessel by varying its underwater shape (as this would also produce a change of the hydrodynamic coefficients). The effects of the change of hydrodynamic force coefficients on the frequency patterns are similar to the ones observed in Fig. 2a, which are due to the increase of viscous roll damping. However, in contrast to the data in Fig. 2a, the regions of the higher frequency of critical events in the vicinity of $GG'=0.0040$ m at $GM=0.0280$ m and $GM=0.0350$ m are reduced to single points which produce an isolated

branch of the stability diagram (the three branches are again marked by broken lines).

On the whole, the results of the simulations of motion discussed above, are qualitatively very consistent. The strong qualitative features common to the patterns of dependence of the frequency of critical events upon GG' , in spite of the variations of the hydrodynamic coefficients and roll damping, are: the asymmetry of the frequency patterns with respect to GG' values (port versus starboard), and the appearance of the local increases of the frequency of occurrence at the GM values higher than 0.0406 m. Taking into account the interpretation of GG' value as a measure of stability, both features display qualities of the model's stability which would be difficult to quantify or discover without the use of the technique applied in the identification of the stability diagrams.

The dynamic stability diagram in Fig. 2a through its asymmetry indicates a strong susceptibility of the model to testing loads inclining the model to starboard i.e. to the leeside relative to the oncoming waves. This reduction of the model's stability as measured by the testing loads in the numerical simulation may be perceived to correspond to the vulnerability of the vessel to the submergence of bulwark on the leeside observed in the model tests at the same displacement, forward speed and heading. Although the numerical model does not represent the hydrodynamic phenomena pertinent to the bulwark submergence as one of the major mechanisms leading to capsizing (identified and described in [9]), the reduced stability may enhance both the occurrence of the bulwark submergence and its capsizing effects.

It is possible to interpret the asymmetry of the dynamic stability diagram in terms of a substantial asymmetric reduction, induced by the asymmetry of the oncoming wave pattern and measured by the testing loads, of the vessel's stability in comparison with the hydrostatic condition. Such asymmetric stability properties of vessels are not included in the usual stability assessment procedures based on nominal applications of the GZ curve. However, the results of the numerical simulations analysed by means of the stability diagram appear to indicate their practical importance.

The concept of dynamic stability diagram used in the present discussion assumes the absence of critical events within the region of GG' bounded by the two branches of the diagram for any particular KG , as shown in Fig.

2a. The appearance inside such regions of unstable configurations (according to the adopted rational dynamic criteria) shown by the isolated branch of the stability diagram in Fig. 2b, requires a modification of the meaning of the stability diagram. It also contradicts the assumption that regions of safe operation can in general be defined in the control space by a set of appropriate upper or lower bounds. However, the assumption is tacitly used in the current approaches to the assessment of stability.

CONCLUSION

The present investigation of vessel stability gives the first example of the application of the rational procedure for assessing stability developed in [3] and [1], in which an advanced numerical model of vessel motion in waves is implemented. Irrespective of its specific results the study demonstrates that the notional and algorithmic framework of the procedure can be used effectively to employ the advanced knowledge of the dynamics of floating vessels, embodied in numerical motion simulation models, in rational stability investigations and assessments.

The application of the dynamic stability diagrams and of their interpretation as maps of vessel stability measured by means of testing loads, provides an efficient tool for stability investigations. This is exemplified by the identification in the present study of the strong asymmetry of the vessel's stability in quartering seas and of the possibility of the occurrence of isolated unstable regions embedded in stable regions between the external branches of a stability diagram.

Although the specific findings of the present study require further research and confirmation before they could be routinely accepted and used, it appears that a novel potent route of stability investigation and assessment is available.

ACKNOWLEDGEMENT

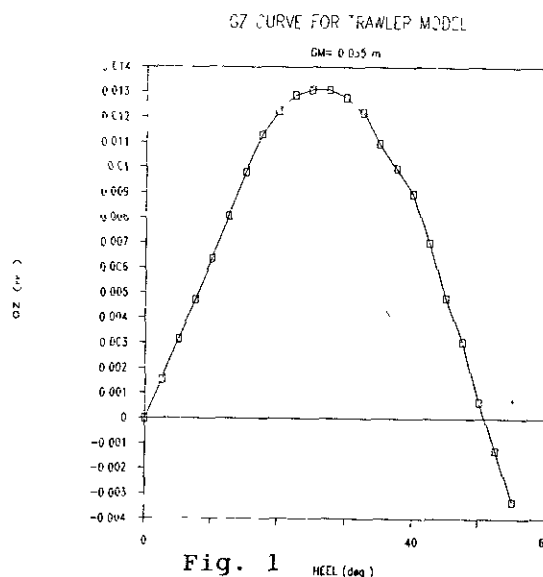
The authors would like to express their gratitude to Dr. S. Grochowalski of the National Research Council for his valuable comments on the results of the model tests.

REFERENCES

1. Pawlowski, J.S. and Deb, M.K., The Study of a New Procedure for Assessing Stability of Ships and Offshore Structures. Advances in Underwater Technology, Ocean Science and Offshore Engineering,

Vol. 9 ed. C. Kuo, Graham & Trotman 1986, pp 149-161.

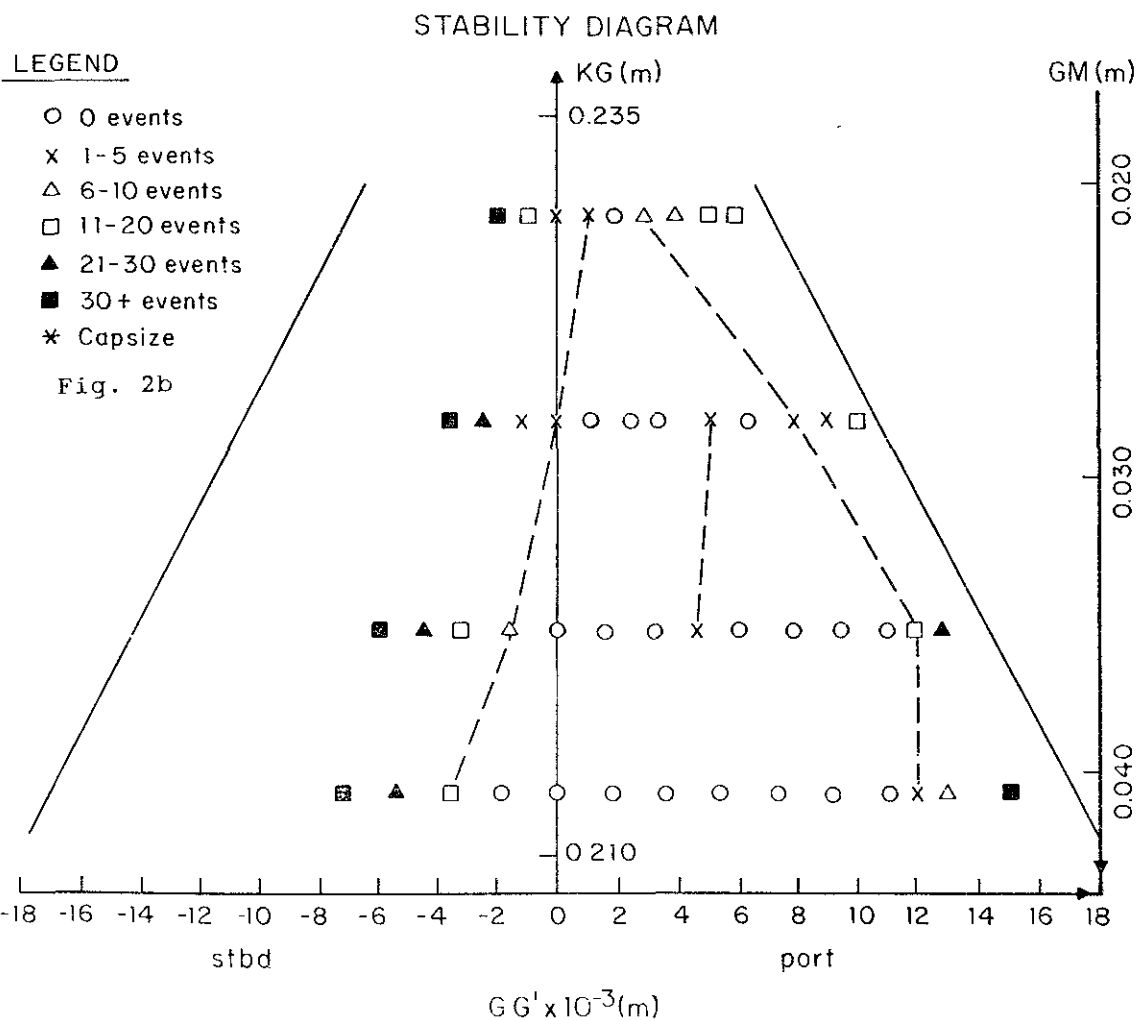
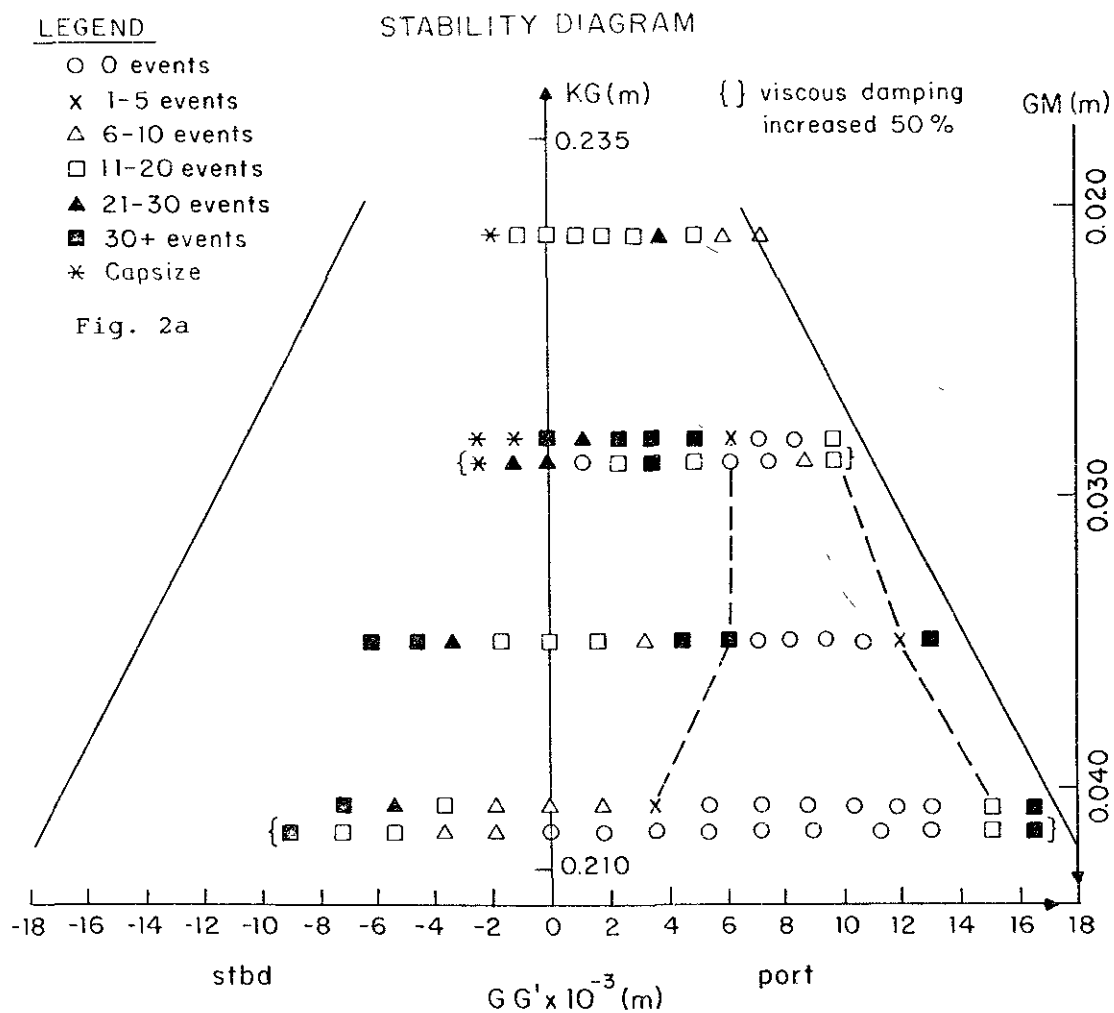
2. Shark, G., Shin, Y.S. and Spencer, J.S., Dynamic-Response-Based Intact and Residual Damage Stability Criteria for Semi-submersible Units. Annual Meeting of the Society of Naval Architects and Marine Engineers, November 15-18, 1989.
3. Pawlowski, J.S., A New Procedure for Assessing Stability of Floating Structures. Institute for Marine Dynamics, NRCC, Report No. MTB-158, January 1985.
4. Pawlowski, J.S., Bass, D.W. and Grochowalski, S., A Time Domain Simulation of Ship Motions in Waves. Seventeenth Symposium on Naval Hydrodynamics, National Academy Press, Washington, D.C. 1989, pp. 597-615.
5. Saunders, P.T., An Introduction to Catastrophe Theory, Cambridge University Press, 1980.
6. Pawlowski, J.S., Elements of a Non-linear Theory of Ship Motions in Waves, in preparation.
7. Pawlowski, J.S. and Bass, D.W., The Development of a Time Domain Simulation Method for the Prediction of Scattering Forces and Ship Motions in Waves. The Fifth International Workshop in Water Waves and Floating Bodies, Didsbury, England, 1990.
8. Pawlowski, J.S., The Estimation of Diffraction Force Components from the Equivalent Motion Concept. International Shipbuilding Progress, Vol. 29, 1982, pp. 62-73.
9. Grochowalski, S., Investigation into the Physics of Ship Capsizing by Combined Captive and Free-Running Model Tests. Annual Meeting of the Society of Naval Architects and Marine Engineers, November 15-18, 1989.
10. Grochowalski, S., private communication.
11. Newman, J.N., Marine Hydrodynamics, MIT Press, 1980.



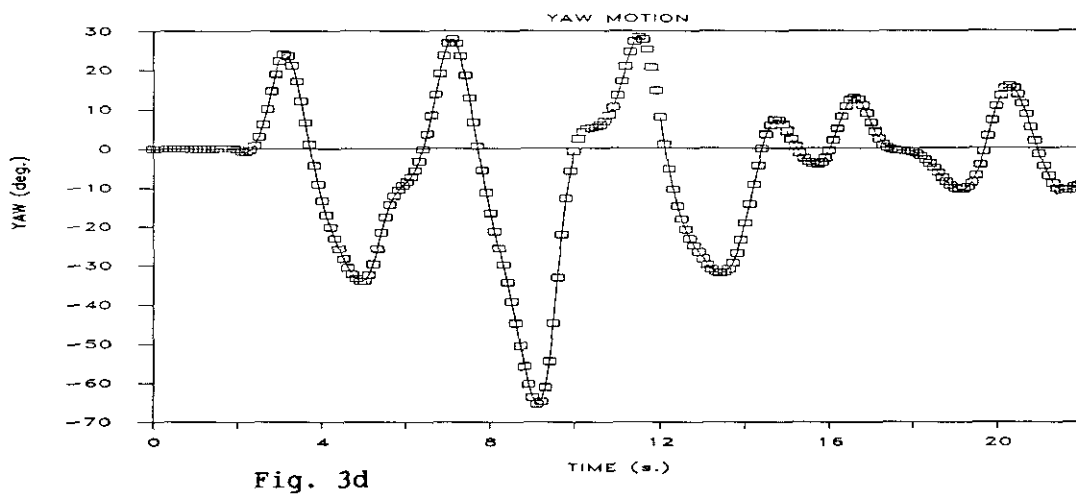
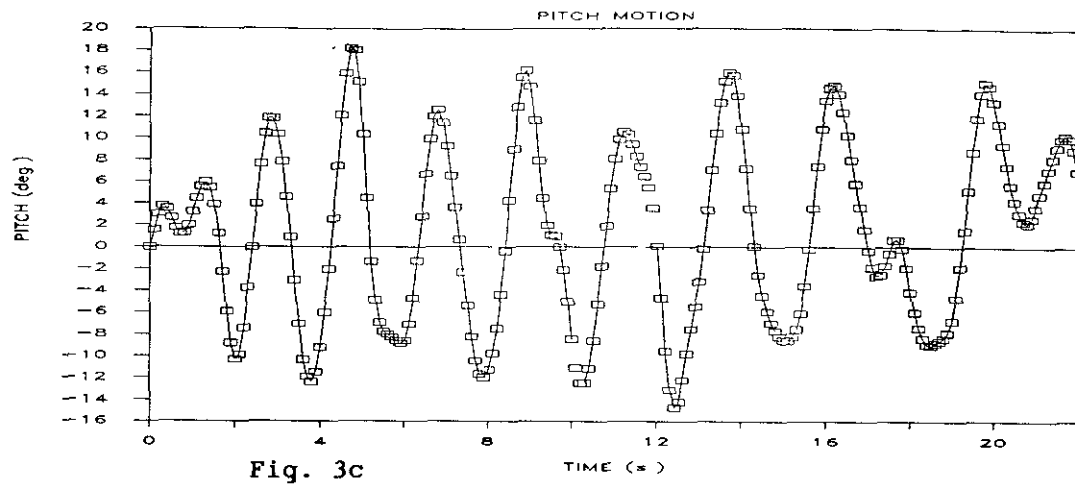
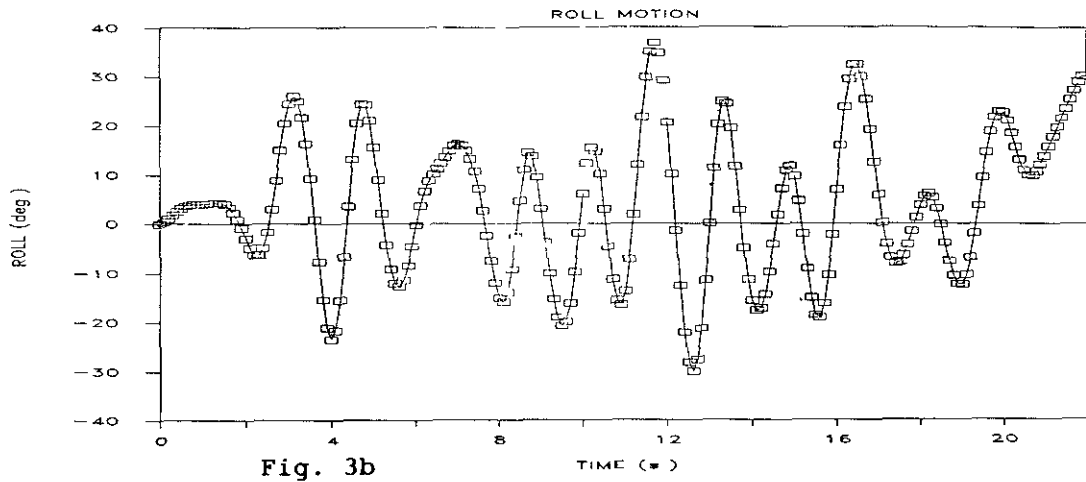
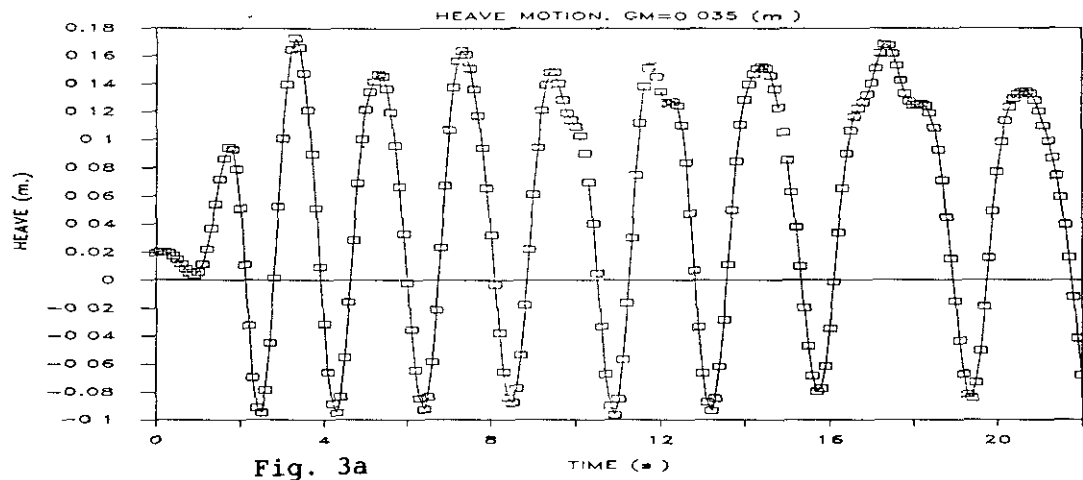
LEGEND

- 0 events
- × 1-5 events
- △ 6-10 events
- 11-20 events
- ▲ 21-30 events
- 30+ events
- * Capsize

Fig. 2a



TRAWLER MODEL.2 5 (deg) HEEL STBD



ON THE DETERMINATION OF SHIP STABILITY DURING SERVICE

Hermann Kaps¹ and Sigismund Kastner¹

ABSTRACT

The upper limit of container stowage on deck of container vessels is governed by minimum stability requirements to ensure safety from capsizing. So far there exist no general standards or rules on the control and accuracy of stability estimates for planning of container stowage. It has turned out that a number of input data are often incorrect, such as container mass and its centre of gravity.

For a ship close to the minimum stability limits, any inaccuracy in the stability estimates increases the danger from capsizing. Therefore, a research project funded by the Federal Ministry of Transport was carried out in order to study the methods of calculation and measurement of ship stability and their accuracies, in particular

- methods of carrying out the operational ship inclining experiment in port for the ship during service (OSI)
- influence of disturbances
- heeling moments
- measuring gauges required
- error propagation and accuracy of results
- inclusion of testing procedure (OSI) into ship loading process.

A number of ship inclining experiments has been carried out with container ships of different size in port.

As a result, the accuracy of the operational ship inclining experiment (OSI) exceeds the accuracy of stowage calculations considerably, while the effort is reasonably small. OSI is suggested to complement stability calculations of container vessels.

This procedure can be extended to other types of vessels with critical stability as well.

INTRODUCTION

Shipping of containers by sea has resulted in stowing between 40 and 60 p.c. of the total cargo above the main deck of the vessel. This is due to the fact that the container itself can provide sufficient weather protection for the cargo, while the handling during loading and unloading is substantially more effective. Both the upper limit for the height of container stowage, and the distribution of the container weight, are dictated by the minimum stability required.

Although digital computers are in wide use for stowage calculations, accuracy of the input data in loading and stability control calculations are doubtful, and there has been no knowledge on the inaccuracies in the procedures for stability estimates. Any inaccuracies can erode inherent safety margins in stability criteria, and the ship runs a higher and unacceptable risk of capsizing, when loaded at her limits of stability.

RESPONSIBILITY FOR STABILITY CONTROL

Three main criteria for planning of loading and cargo distribution aboard the vessel must be considered:

- (i) cost effective utilisation of the vessel, which is strongly determined by a fast container loading and unloading in port without the need to restow
- (ii) consideration of particular qualities of the cargo, such as the IMDG code (International Maritime Dangerous Goods), refrigerated containers, special containers, additional general cargo
- (iii) consideration of particular properties of the ship herself, i.e. stability, trim, structural strength, cargo

¹ Professor, Hochschule Bremen
Neustadtswall 30, F.R.G.

securing, and sea behaviour

The various agencies and specialists responsible for the shipping of cargo at sea naturally do not care equally for all these considerations on effective and safe shipping. Stability control is just one part of the responsibilities of the ship master. Quite often, the ship master is locked with his classical conflict: he is held responsible to keep the interests of the ship owner and of the charterer, as well as the interests of the agents for handling the cargo. The practical aspects of safety and survival in the sea environment cannot be allowed to suffer from a large number of tasks. The ship master needs tools and guidance on how to control ship stability during service effectively and accurately.

STATIC SHIP STABILITY CHARACTERISTICS

Here we note the basic and well known procedure to calculate static stability of ships just to make sure what we are talking about. If we look at the intact stability status of any vessel, we consider the uprighting lever GZ versus heel Φ . This GZ-curve must be able to overcome any external and internal heeling or reducing lever at sea. GZ is calculated from

$$GZ = KN - KG \sin \Phi \quad (1)$$

While the size of KN is governed by the ship hull form and dimensions, the resulting total height of the centre of gravity KG is governed by the way the ship is loaded.

KG can be estimated for any loading condition from either

- (i) static mass moment calculation
- (ii) ship inclining experiment.

In the latter, KG is calculated by the equation

$$KG = KM - GM \quad (2)$$

KM is taken from calculated hydrostatic curves due to the hull form, and the metacentric height GM is taken from measurement at the actual ship condition with the operational ship inclining experiment (OSI).

GM is evaluated according to the formula

$$GM = \frac{p \cdot e}{D \cdot \tan |\Phi_{II} - \Phi_I|} \quad (3)$$

Input data are the heeling moment $p \cdot e$, (from horizontal shift e of a mass p) the resulting heel angle Φ measured, and the displacement D via draught readings and curves.

STABILITY CALCULATION SUPPORTED BY MEASUREMENT

Fig. 1 shows a typical error ellipse in the KG-displacement plane.

This example is a result of tests with a fully loaded 700 TEU container/multi-purpose vessel. The error ellipses indicate the 95% confidence level of the data. The large random errors resulting from pure weight and mass moment calculation of KG and displacement D is demonstrated by the larger ellipse. The measurement with the inclining experiment reduces the size of the error ellipse considerably.

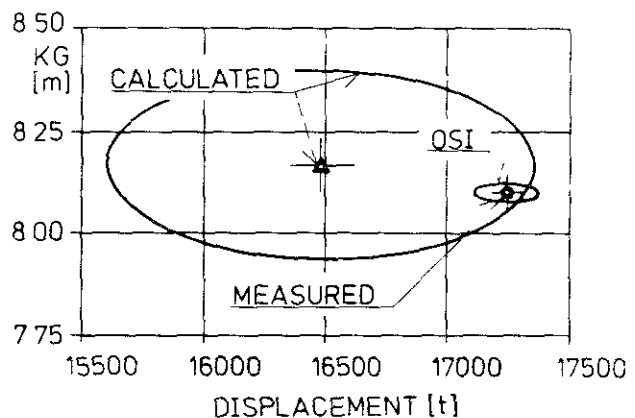


Fig. 1: Random Error Ellipses at 95% Level for KG versus Displacement

Fig. 1 demonstrates clearly the large error possible based on pure calculation. Such large discrepancies cannot be tolerated for a reliable judgement of stability and ship safety. On the contrary, the values determined by measurement show a smaller error ellipse. We can conclude that measurements are a proper tool to update actual stability estimates during service.

TIMING OF THE STABILITY CHECK BY EXPERIMENT

It has been a common misconception, that the check of stability should be carried out at the end of the cargo loading, i.e. before the ship is about to leave port. On the contrary, the experimental stability check must better be carried out during the ship loading process, in order to allow the master to take measures in time. The whole OSI procedure takes only up to 10 minutes time.

Any major error can be detected already during the loading process, when the bulk of cargo has been loaded. For a practical choice, we recommend to carry out the operational ship inclining in the order of 5 % below the maximum allowable KG-value, and with a cargo still to be loaded of about 3% of the displacement, see example in Fig. 2.

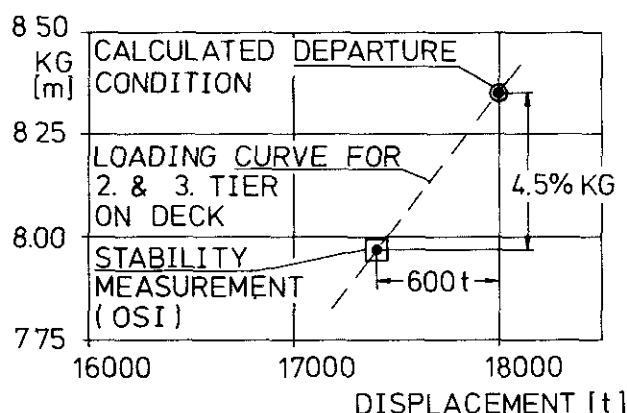


Fig. 2: Suitable Timing of Stability Measurement during Loading

THE OPERATIONAL SHIP INCLINING EXPERIMENT (OSI)

The inclining experiment for the ship in service must be

- accurate
- quick
- cheap
- easy to perform

As early as 1887, i.e. more than 100 years ago, Sir Archibald Denny was the first to suggest inclining of ships before departure at a meeting of the Institution

of Naval Architects in London /3/. Still, it is not commonly used in shipping. Due to sensors, computers and electronic circuits, a full automation of stability control at any instant seems to be possible now and will certainly come in the future. First steps have been started at a private firm in Germany, with a built-in mechanical pendulum. However, automation is not a necessary prerequisite for applying the ship inclining.

In our Bremen project /1/, we have studied the ways to put the ship inclining experiment for the control of container ship stability into practice. We have put emphasis on the most simple and reliable ways of performing the ship inclining experiment during service, while using a chord pendulum.

ACCURACY CONSIDERATIONS

Displacement

Ship displacement must be calculated from ordinary draught readings fore and aft. In order to avoid a systematic error, a lump sum correction for the usual hogging deflection should be applied. This is the proper combination of minimum reading effort with numerical correction to show good results.

Heeling Moments

For container ships, three different ways of producing the heeling moment required at the operational ship inclining experiment are available:

- if the vessel is equipped with cranes, the crane jibs should be pivoted from one ship side to the other side. This implies that the crane manufacturer has established the size of the induced heeling moment with sufficient accuracy, and with specific documentation, see /1/ on the crane moment estimation.
- water in either ballast or special heeling tanks shifted from one ship side to the other side.
- One or two large weight containers as being part of the cargo must be loaded onto the ships side stack position, or shifted sideways as much as possible in the container stacks. This method requires to weigh those containers used for heeling just before loading.

The means of applying and the size of the heeling moment should be approved by classification.

Fortunately, the moment needed for a ship inclination during service (OSI) is considerably less than for the ship yard inclining experiment before delivery (SYI). The unit heeling moment pe/D for OSI is in the order of 0.02 tm/t. Fig. 3 shows a graph of GM versus heel angle Φ for constant unit heeling moments.

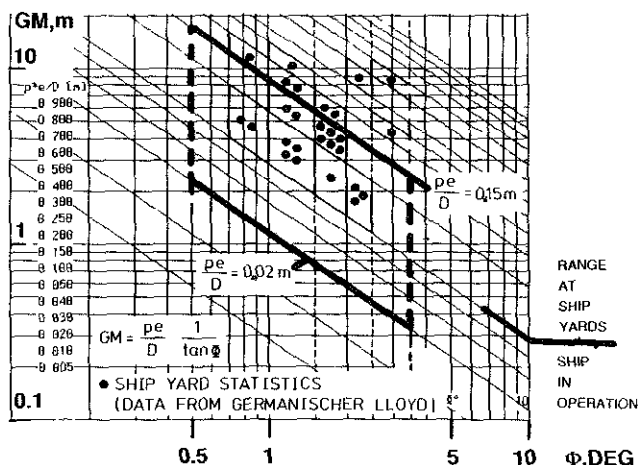


Fig. 3: Metacentric Height GM versus Inclination Angle depending on Unit Heel Moment pe/D

Record of Heel Angle

It is of advantage to record the heel or ship inclination angle during the heeling experiment versus time. Furthermore, a record allows to check the vessel's ability to roll freely, i.e. without being hampered by her moorings. Under certain conditions, even the natural roll period can be estimated from the heel angle record, which most of the time shows small oscillations.

Fig. 4 depicts an OSI record for a container multi-purpose ship, taken during a 2 month round trip. The (OSI) record in Fig. 5 shows the static heel as well as slight superimposed micro-roll oscillations.

However, it is sufficient to take careful notes on the heel measured, but the gauge used to measure heel angle should be specifically stated and approved by authorities.

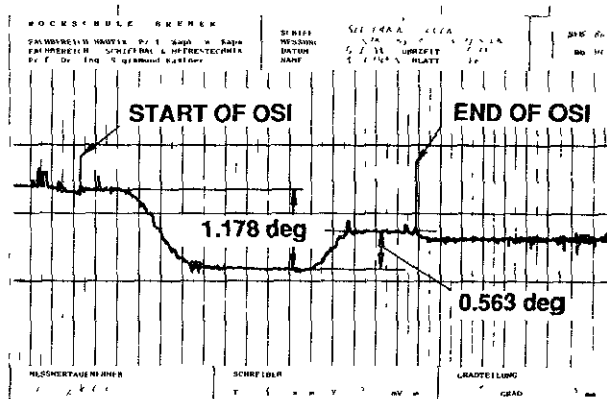


Fig. 4: Example Record of Operational Ship Inclining Experiment (OSI) for Ship during Service

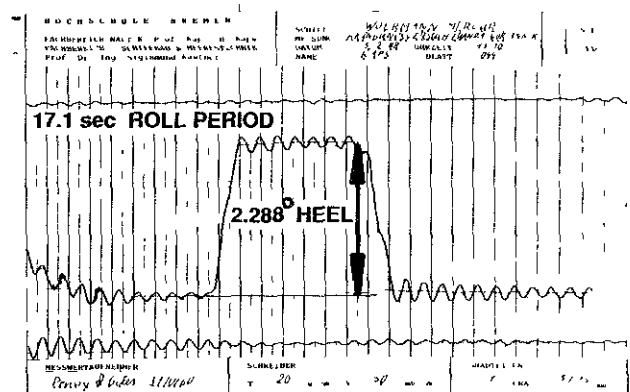


Fig. 5: OSI Record with Superimposed Micro-Roll

Heel Angle Measurement

The specific equipment required to measure heel angle can be very simple. Theoretical considerations and practical trials aboard container ships have shown, that a chord pendulum of 1.146 m length gives the best results for OSI. This length can be easily set up and read in the wheel-house or any accommodation space. Although a larger length of the pendulum results in a larger geometric deflection which seems to improve accuracy, this is not true because of the dynamic properties. With careful reading of deflections, the short pendulum of 1.146m length allows an rms error not in excess of at least ± 0.5 mm to be attained. This reading accuracy is sufficient, so no longer pendulum is needed. The shorter pendulum allows more reliable

heel readings due to its better dynamic properties. Longer pendulums are better avoided because they come closer to resonance with short period micro-oscillations of the vessel e.g. from heave and pitch. Fig. 6 shows the calculated transfer function for different length of pendulum, positioned at the bridge of the vessel, from solving the coupled equations of the double pendulum "ship and gauge".

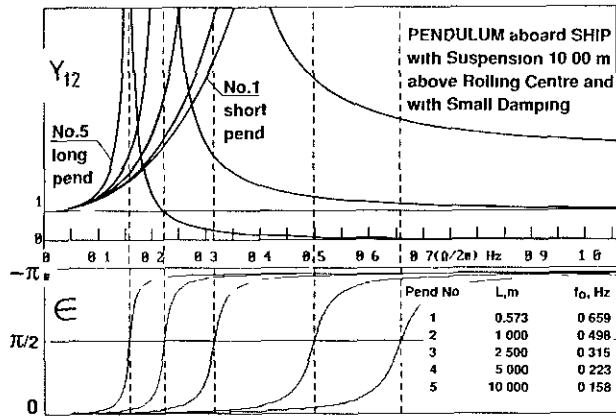


Fig. 6: Calculated Transfer Function of Heel Gauge at different Length of Pendulum

Fig. 7 shows the allowable error in angle measurement, if we ask for a GM-error deviation (rms) of 5 cm not to be exceeded. With small GM, general the case with OSI at the limits of stability, the allowable error standard deviation of the heel readings is more than sufficient with 0.01 deg reading accuracy up to 2.5 m in GM-value. Fig. 7 is an evaluation of the Gaussian law of error propagation applied to equ. (3):

$$e_{GM}^2 = e_p^2 + e_e^2 + e_D^2 + e_{\Phi I}^2 + e_{\Phi II}^2 \quad (4)$$

where e_x ($X = GM, p, e, \Phi_I, \Phi_{II}$) is the ratio of the rms error of the particular quantity x to the true size of the quantity.

In assuming realistic figures for size of quantities and required GM-accuracy, equ. (5) derived from (4) gives the permissible rms-error of the angle measurement versus GM:

$$s_{\Phi perm} = \Phi \cdot e_{\Phi perm} \quad (5)$$

$$= \Phi \sqrt{(0.5(e_{GM}^2 - e_{pe/D}^2))}$$

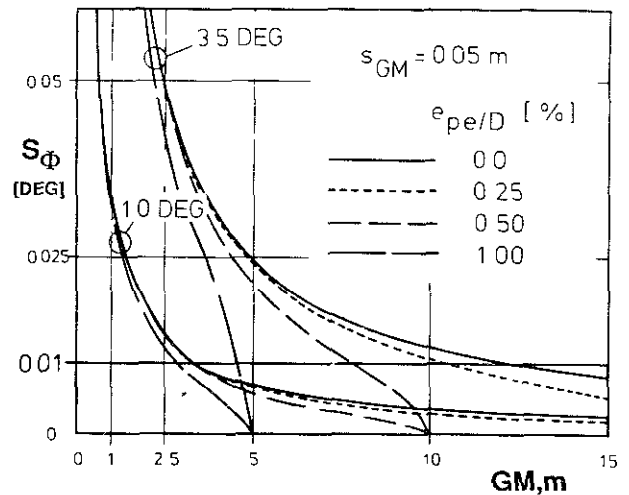


Fig. 7: Allowable RMS Error of Heel Measurement versus GM at Ship Inclining Experiment

Of course, the heel accuracy as in Fig. 7 holds for the lightship inclining test as well (SYD), as discussed by IMO very recently (SLF 34/3/3).

In our Bremen Laboratory for Ship Hydromechanics both a static and a dynamic test bench for inclination gauges and recorders have been developed in order to evaluate measuring equipment objectively [1, 4].

Computer Programs for Stability Control

There are several of reliable computer programs on the market, which with purpose tailored software have brought planning of the ship's statical condition to a high level of reliability, looking at the calculation procedure with respect to trim, structural stresses, and stability. However, this is not the case with the accuracy of the input data. An unknown surplus in the container gross weights has been reported, and it can be estimated in the range of 7% as a world wide average figure, with considerable variations due to region and commodity.

Thus, the weak point is the accuracy of the input data of the cargo. Data from direct in service measurements with the vessel must be used to update calculation results. Updating requires specific input capabilities of the corresponding computer programs.

RESULTS AND CONCLUSIONS

In this project, a careful error estimation was carried out on all the partial errors involved, and on the error propagation for the final outcome of stability.

Input data on loading are very often inaccurate. Measuring the actual stability status by means of the operational ship inclining experiment (OSI) is recommended. A simple chord pendulum of 1.146 m in length is the only gauge required to measure the heel angle accurately during the operational ship inclining experiment. Our tests with different container vessels in different harbours have shown the feasibility of such an approach, see Fig. 8.



Fig. 8: Container ship during loading

Two main points are to be considered in order to improve the accuracy of stability estimates for ships:

(i) updating of stability calculations by operational ship inclining experiments (OSI) during the loading process (and not at the end of it), so it leaves time to adjust the cargo stowage and to take appropriate action.

(ii) development of international standards on the OSI-procedure /2/, in order to measure with enough confidence, and to have a record on the measurement as a base for stability decisions by the master.

In general, the suggested procedure -stability estimates supported by measurement - is evidently useful for any other type of vessel with stability problems from cargo loading, e.g. for Ro/Ro vessels, car ferries, multi-purpose carriers.

NOMENCLATURE

Φ	heel angle
GM	metacentric height
GZ	righting lever
KG	height of ship centre of gravity
KN	normal distance from keel point to buoyancy vector (cross curves of stability)
p	shifted mass at ship inclining
e	horizontal shifting distance
D	ship displacement
Y_{12}	transfer function from ship roll to pendulum
ϵ	phase shift ship-pendulum
s	standard deviation of error (rms-value)
e_x	relative error of quantity x
OSI	operational ship inclining experiment
SYI	ship yard inclining experiment

REFERENCES

1. Kaps, H. and S. Kastner: Beurteilung der Stabilität von Schiffen in der Praxis (On the Judgement of Practical Ship Stability), report for the Federal Ministry of Transport, FE-No. 40199/87, Bremen, February 1989
2. IMO Sub-Committee on Stability and Load Lines and on Fishing Vessels Safety, paper SLF 34/INF.5, London, December 1989
3. Denny, A.: On the Practical Application of Stability Calculations, Transactions, The Institution of Naval Architects, London, 1887
4. Kastner, S.: On the Accuracy of Ship Inclining Experiments. Journal, Ship Technology Research (Schiffstechnik), Vol. 36, Hamburg, June 1989, p. 57/65

CONSIDERATION OF THE INFLUENCE OF A SHIP'S OWN WAVE
SYSTEM ON SHIP STABILITY WHEN MOVING IN FOLLOWING SEAS

Lipis A.V.*, Voitekounski Y.I.**

SUMMARY

The report proposes a method which will allow to take into account influence of ship's own wave system on stability in following seas in linear formulation.

1. INTRODUCTION

The problem of ship stability in following seas, being traditional for small marine ships, has lately become topical also for quite large transport ships due to increasing ship speeds and carriage of deck cargoes (containers).

The today's level of development of methods for ship waves problem solution enables us to consider in stability calculations the hydrodynamic effects and the influence of the hull-generated ship's own wave system on stability.

In its full formulation the hydrodynamic problem of a ship moving in waves is extremely difficult one: it involves consideration of nonstationary flow past solid body crossing the disturbed surface of a viscous liquid. However, for the case of ship movement in following seas with a speed close to the wave propagation speed and with close lengths of waves and hull, which is the most dangerous case regarding

the loss of stability, the hydrodynamic problem can be considerable simplified. This allows to use the results of its solution in practical stability calculation methods.

SHIP STABILITY ASSESSMENT METHOD

The basis for a calculation of ship stability in regular following seas was a method offered by S.N. Blagoveshchensky [1]. The principal assumptions of the method are that the stability moment depends on the projection of gravity and buoyant forces on a frame plane, and that the pressure in a wave is following the hydrostatic law.

The features of implementation of this approach are given in detail in [2]. A set of computer programs allows to define the ship static stability characteristics in following seas when setting an arbitrary shape of wave profile along the ship side.

The consideration of hydrodynamics of flow past ship within the framework of such method will lead to changes in the predicted pressure field on the hull and in the shape of wetted surface due to the altered running ship trim and deformation of free surface by the ship's own wave system. To assess the degree of influence of each of the above factors on stability characteristics, let us consider the hydrodynamic problem of ship movement in following seas assuming that viscosity effects are neglectable.

* Research Scientist

** Professor

Leningrad Shipbuilding Institute
Lotsmanskaya str. 3
Leningrad, USSR

FORMULATION OF THE HYDRODYNAMIC PROBLEM

The ship moves in following seas in the mode permitting static placement of the ship on a wave without intense rolling motions. Assuming the flow to be potential, the problem may be reduced to finding a solution to Laplace equation for velocity potential meeting the boundary conditions of:

- the normal velocity of the flow is zero on the instantaneously wetted hull surface
- disturbance decay far from the hull
- kinematic and dynamic conditions on the disturbed free surface.

It is known that the solution of the problem thus formulated is complicated by non-linearity of boundary conditions and the need to meet them on a surface the shape of which is not known in advance.

A justified linearization of boundary conditions seems to be possible only for ships with sufficiently great percentage elongation as in this case the dangerous navigating condition usually corresponds to an oncoming wave of small relative amplitude; besides, the relative amplitudes of generated waves can also be considered small.

The linearization of boundary conditions allows to present the resultant solution as a superposition of solutions of two special problems:

- of a ship moving in calm water
- of a ship statically placed on the wave.

Then, the pressure field on the hull surface will be the sum of the hydrodynamic component P_w and the hydrostatic component P_s corresponding to the present position of the oncoming wave profile and the hull

$$P = P_s + P_w$$

The complete wave profile along the ship's side will be determined by superposition of the profiles of the following wave and the own wave found from the solution of the first problem. This composite profile will also be in compliance with the ship trim.

METHOD OF SOLUTION OF THE SHIP WAVE PROBLEM

The numerical method of solution of a linearized problem of ship movement in calm water is based on the use of hydrodynamic singularities.

A ship hull determined by hull lines is divided into tetragonal elements by frames and waterlines. Wave-generating sources are distributed over the surface of these elements. Their intensity is assumed constant within each element.

To define the intensities of the sources, the Fredholm's integral equation of the second kind to which the kinematic flow condition on the hull surface is reduced must be solved. In doing so, the flow past the duplicated hull in unlimited liquid is considered and non-wave components of induced velocities are calculated.

After that, the wave components of velocities and the free surface deformations are calculated. To do this, we use analytical expressions for the potential and the velocities induced by uniform distribution of wave-generating sources over a vertical rectangular surface element arbitrary oriented relative to the oncoming flow velocity vector. This method and the results of its proof are presented in detail in Ref.3.

ANALYSIS OF SERIES 60 MODEL FLOW CALCULATION RESULTS

To define the hydrodynamic effects having the greatest influence

on ship stability, let us analyze the results of velocity field calculation for a Series 60 model hull with block coefficient $C_B=0.7$ and Froude number $F_n=0.25$

Fig.1 shows pressure distributions for several frames. The dynamic and hydrostatic components are compared with and without regard to wave profile. It can be seen that the former is significantly smaller, therefore the righting moment caused by it is smaller too. As to the calculation of pressure distribution over the whole surface of the ship hull, it takes much more time than defining the wave profile-shape. This is important for systematic stability calculations.

In this respect it seems possible, in considering the dynamic factors in the calculations of transport ship stability characteristics in following seas, to confine ourselves to introduction of a wave profile along the ship's side with regard to the own wave system.

STABILITY CALCULATION METHOD

The stability calculation for a transport ship was made by the following way.

The most significant component of the righting moment, or the main part according to A.N.Krylov, is defined as [1]

$$M = \int_L m_s(x, Z_{1B}) dx$$

where m_s is the static moment relative to the longitudinal axis of the submerged area of a frame inclined by the angle θ . The area is limited by the relative water level along the ship's side Z_{1B} . In a static calculation, Z_{1B} is defined by the formula

$$Z_{1B} = S_B + T_\theta(x) + Z_B(x)$$

where T_θ is the draft for the section of the ship inclined by the angle θ in calm water at stands-

till.

S_B is the profile of the regular oncoming wave

$$S_B = \zeta_B \cos \frac{2\pi}{\lambda}(x - \Delta)$$

ζ_B is the wave amplitude

$Z_B(x)$ is the wave profile generated by the ship in calm water. This is obtained from the solution of the ship wave problem by the above method.

EXAMPLE OF CALCULATION

As an application example of the proposed method calculations were made for the stability of the containership "Khudozhnik Saryan" ("Merkur 1" Project), with main dimensions of $L=157m$, $L/B=6.5$

$B/T=2.85$ at ship's speed $U=19$

knots ($F_n=0.25$). Following wave parameters were used: $\lambda=L$, $2\zeta_B=8.5m$.

Six main variants of calculation were made

1. in calm water at standstill

$$Z_{1B} = T_\theta$$

2. in calm water with regard to the ship's own wave system at $F_n=0.25$

$$Z_{1B} = T_\theta + Z_B$$

3. on the top of a regular following wave ($\Delta=0$) disregarding the ship wave $Z_{1B} = T_\theta + S_B$

4. on the top of a regular following wave ($\Delta=0$) with regard to the ship wave $Z_{1B} = T_\theta + S_B + Z_B$

5. the same as under (3) but at the trough of a following wave

$$\Delta = \lambda/2$$

6. the same as under (4) but at the trough of a following wave

$$\Delta = \lambda/2$$

The ship moved in a strictly following seas (angle on the bow = 180°). The static stability curves were determined for various values of the ship's longitudinal centre of gravity Z_g , i.e. for various ship loading conditions.

CALCULATION RESULT ANALYSIS

Fig.2 shows wave profiles

along the ship's side as the basic data for the above calculations:

- 1) wave profile generated by the hull moving in calm water,
- 2) profile of an oncoming sinusoidal wave with the top located at the middle of the model,
- 3) the same profile, with the trough at the middle,
- 4) = 1)+2), the result of superposition of the first and the second wave,
- 5) = 1)+3), the result of superposition of the first and the third wave.

It can be seen that the superposition of the ship's own wave system on the following wave changes considerably the form of disturbed free surface near the ship. The nature of these changes depends on the hull's position relative to the waves and on the Froude's number. Thus, in the presented example of calculation, the amplitude and steepness of the wave profile is growing. Flattening can be observed only at the forebody in case of location of the oncoming wave hump at the middle.

These changes affect the nature of the static stability curves accordingly, see Fig.3, at the highest value of $Z_g = 10.41\text{m}$ and draught $T = 8.58\text{m}$.

From the analysis of curves in Fig.3 it follows that:

1. When ship's waves are taken into consideration, in calm water, the maximum righting arm ℓ increases by 2.5%, and the initial metacentric height h_0 , by 5.6%.
2. The decrease of stability at the top of a following wave, disregarding ship's waves, is 33% for ℓ and 28% for h_0 .
3. The same, with regard to ship's waves: 41% for ℓ and 51% for h_0 i.e. 1.24 times higher for ℓ and 1.82 times higher for h_0 .

4. For the ship loading condition in question (permitted according to the USSR Register Rules [4] on the basis of the standard definition of ship stability) the effect of following waves, sea state 7, may result in a decrease of metacentric height lower than acceptable.
5. The range of metacentric height variations in waves is 14% wider with regard to Z_B than disregarding it.

CONCLUSIONS

The analysis of calculation results for transport ship stability characteristics in following seas confirms the need to consider the hull-generated ship's own wave system. From the above example it is clear that disregarding the ship's wave may result in an error on the dangerous side. This is dictated mainly by the peculiarities of the containership hull form (sizeable bulb and inclined side over the whole ship's length) typical for modern fast seagoing ships. For such ships, the deformation of the oncoming wave profile along the side by their own system leads primarily to a reduced waterplane moment of inertia, i.e. to a reduced metacentric radius.

The developed calculation method and the set of computer programs to enable its application allows to consider ship's own waves when assessing stability in following seas.

References

1. A Manual on Ship Theory / Editor: Voitkunsky Y.I. - L.: Sudostro-yeniye, 1985. Vol.1. (in Russian).
2. Bogdanov A. Stability criterion safety speed and wave - to - course angle. Diagram for a ship sailing in storm following seas. // 18th SMSH'89. - 1989. - Varna. Bulgaria, Vol.3.

3. Voitkounski Y.I., Lipis A.V. Numerical solution of the Neuman-Kelvin problem in ship wave theory.//17th SSMH'88. - 1988.- Varna. Bulgaria, Vol.3, p.72.1-72.6.
4. Rules for the Classification and Construction of Sea-Going Ships. USSR Register of Shipping. - L.: Transport, 1985. 328 pp. (in Russian).

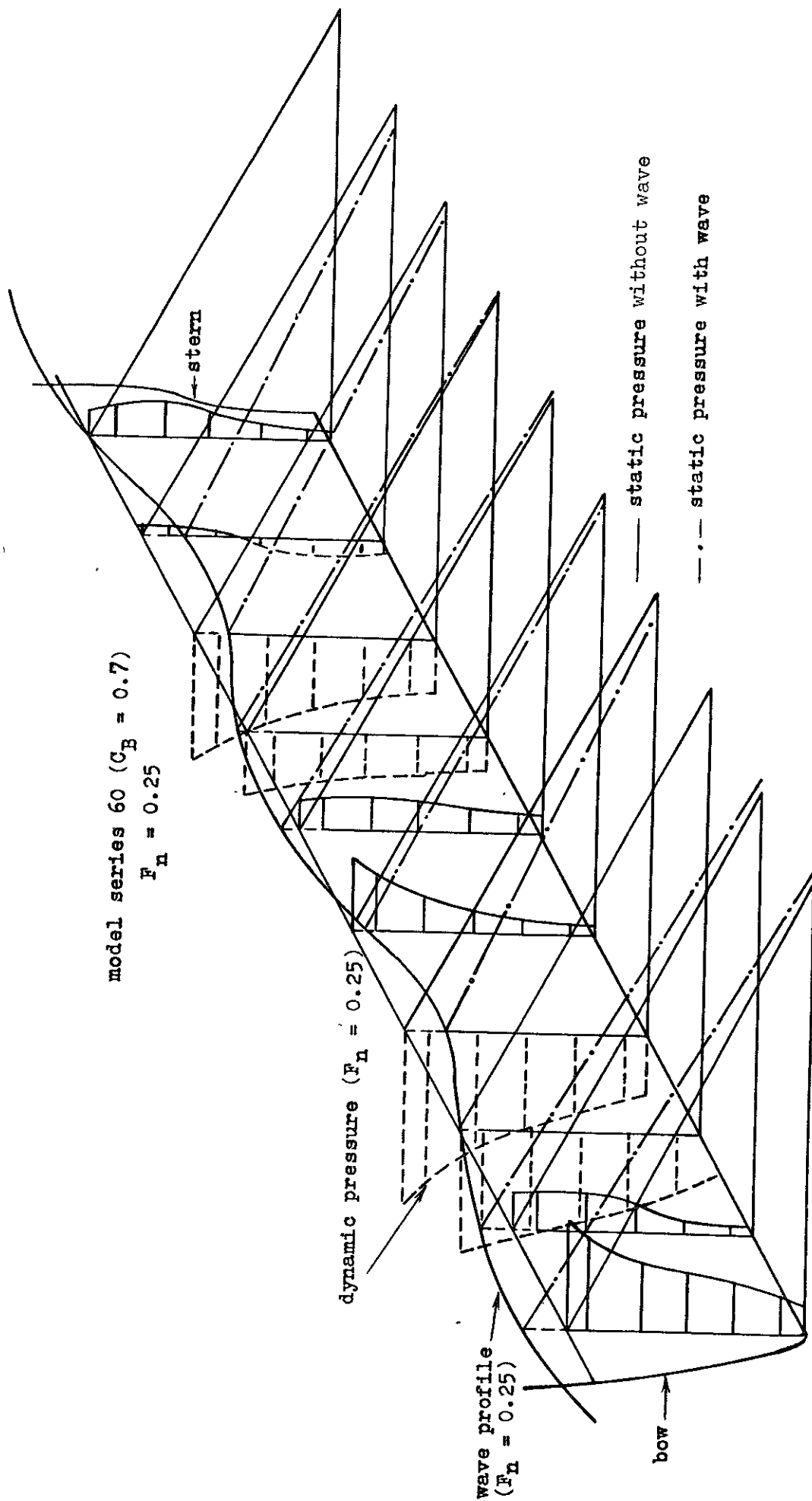


Fig. 1. Distribution of pressure for sections of model

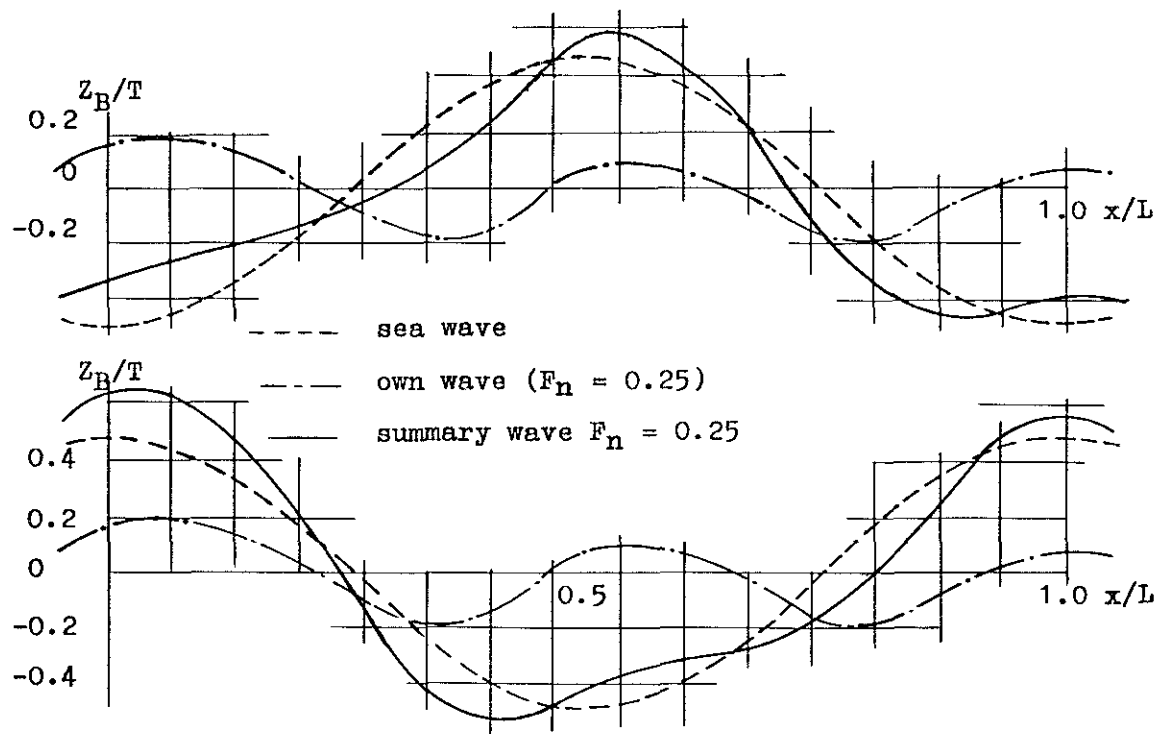


Fig.2. Wave profile along the hull

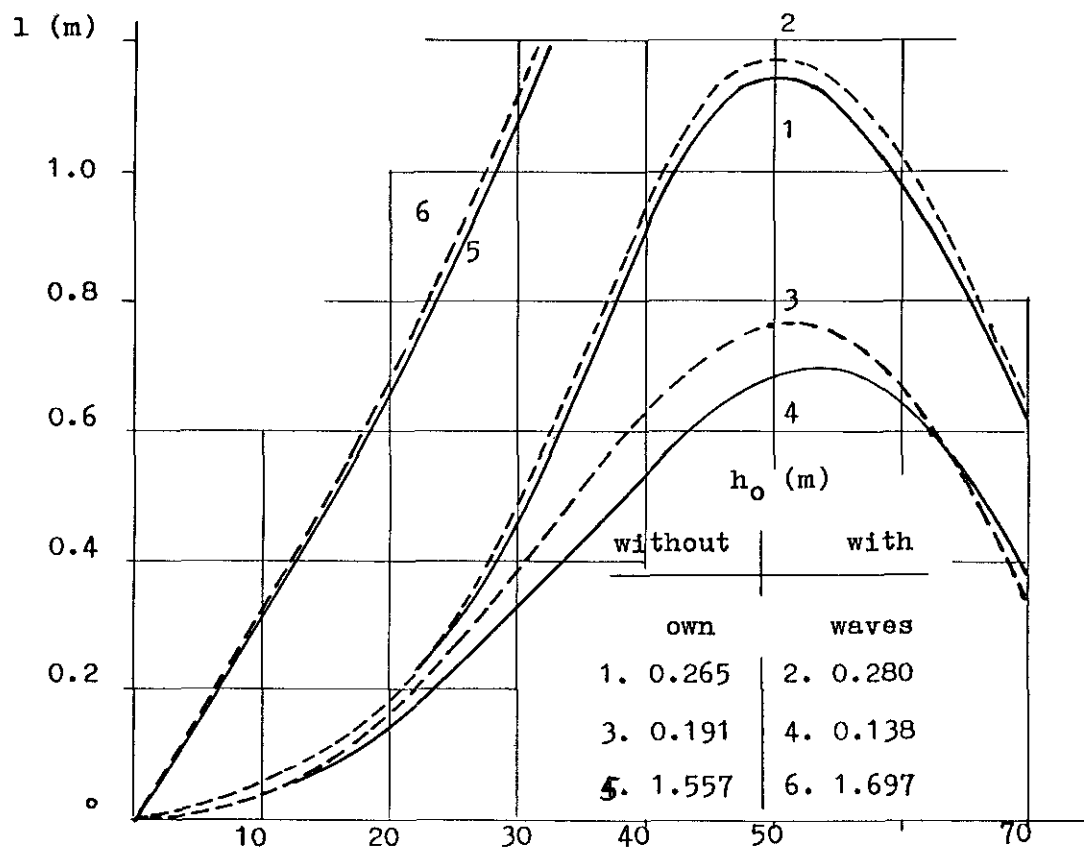


Fig.3. Righting lever curve

A CONTROL OF AN UNSTABLE MOTION OF A SEMISUBMERSIBLE PLATFORM WITH A LARGE LIST ANGLE

Mikio TAKAKI* and Yasushi HIGO*

ABSTRACT

This paper deals with properties of dynamic response of a semisubmersible platform with a large list angle in beam sea condition. In a previous experiment, an unstable motion has occurred at certain wave frequencies. We have made clear a mechanism of the unstable motion. As a result of a numerical simulation of motions, it has become clear that the unstable motion is a subharmonic motion; it is mainly affected by a nonlinear coupling moment and phase lag between motion and wave exciting force.

In addition, we propose a new control device for reducing a list of a platform from a standpoint of safe operation. We have confirmed a validity of the proposed device by a numerical simulation both for a static condition and for a dynamic one of platform. As a result, this device is useful for stabilizing a semisubmersible platform with a large list angle.

1. INTRODUCTION

Up to now, a large number of semisubmersible platforms have been put in operation under a development of subsea oil production in a sea all over the world. And most of semisubmersible platforms are usually being moored to operate in limited areas for a long time, because it has been considered a stable and safe structure on the seas. This mooring system of a semisubmersible platform makes some differences from a conventional ship at a standpoint of a safe operation. Takarada et al. have pointed out that a moored semisubmersible platform may get into danger at a sea condition where a ship floating freely is safe [1],[2]. Furthermore they have made clear the mechanism of capsizing phenomena of a semisubmersible platform [2], and have investigated effects of a fairlead location on a stability and sea-keeping qualities of it [3]. According to their studies, mooring lines restrict a horizontal displacement of a platform, and a reaction force of it, which depends on a fairlead location, induces a heeling moment on a semisubmersible platform. Hence the fairlead location affects not only a stability but also a motion performance of a semisubmersible platform [2],[4].

Takaki et al. have made clear the relation between motions of a semisubmersible platform and a list angle of it [5]. Namely as a list of a semisubmersible platform increases, unstable motions take place. Besides the larger a list of it increases, the larger a rolling amplitude becomes in the low frequency domain in irregular waves. Thereby a semisubmersible platform with a large list angle is unfavorable from a standpoint of a safe operation. This unstable motion, however, disappears, whenever a list of a semisubmersible platform becomes smaller. It is therefore the most important way to keep a small list of a semisubmersible platform at any time for a safe operation.

In this paper, first we make clear a mechanism of unstable motion of a semisubmersible platform with a large list angle in regular waves by the numerical simulations of motions. As a result of it, it follows that the unstable motion is a subharmonic motion; it is mainly affected by a nonlinear coupling moment and phase lag between motion and wave exciting force.

Next, we propose a new control device for reducing a list of a semisubmersible platform from a standpoint of a safe operation. The fairlead location can be easily sifted to reduce a tilt moment due mooring lines to minimum by applying this device. We have confirmed a validity of the proposed device by means of a numerical simulation both for a static condition and for a dynamic one of platform. As a result, this device is useful for stabilizing a semisubmersible platform with a large list angle.

2. UNSTABLE MOTION

2.1 Model and Experimental Result

A model used in this experiment is an usual semisubmersible platform having two lowerhulls, four columns and two horizontal braces. The model is the 1/50 scale model, and its principal dimensions and the natural periods of motions are shown in Table 1 and Table 2 respectively. Fig.1 shows a right handed coordinate system used in this study. The z-axis points vertically upwards, and the x-y plane is coincident with the calm water level. Fig.2 shows the experimental condition, in which a list angle of the model can be changed to the maximum $\pm 20^\circ$ from the up-right condition by adjusting a balance weight on the deck.

Fig 3 shows a typical time histories of a subharmonic motion in our experiment. It follows from this figure that a period of rolling motion is twice the length of a regular incident wave, and the rolling amplitude becomes larger and larger. At the same time, a sinkage of the model increases, whenever

* Hiroshima University, Japan.

Table 1. Principal particulars of model

Length of all	$L = 1.62 \text{ m}$
Breadth of all	$B = 1.42 \text{ m}$
Draught of rig	$T = 0.41 \text{ m}$
Displacement	$\Delta = 0.2095 \text{ m}^3$
Length of lowerhull	$L_L = 1.67 \text{ m}$
Breadth of lowerhull	$B_L = 0.32 \text{ m}$
Depth of lowerhull	$T_L = 0.1472 \text{ m}$
Diameter of column	$D = 0.2672 \text{ m}$
Diameter of brace	$D_B = 0.0767 \text{ m}$
Longitudinal length between columns	$E_{pl} = 1.1 \text{ m}$
Transverse length between columns	$E_{ot} = 1.1 \text{ m}$

Table 2. Test conditions

Initial angle	KG(m)	Radius of gyration R (m)	Air gap ld(m)
Heel $\phi = 10^\circ$	0.412	0.605	0.156
Heel $\phi = 20^\circ$	0.412	0.605	0.052
Natural period (sec)			
	Sway	Heave	Roll
Heel $\phi = 10^\circ$	20.5	2.82	6.69
Heel $\phi = 20^\circ$	19.9	2.83	5.39

*ld : Vertical distance from still water level to under deck

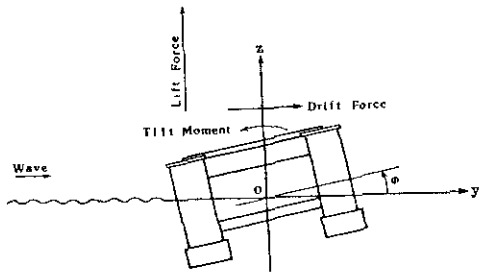


Fig.1. Co-ordinate system

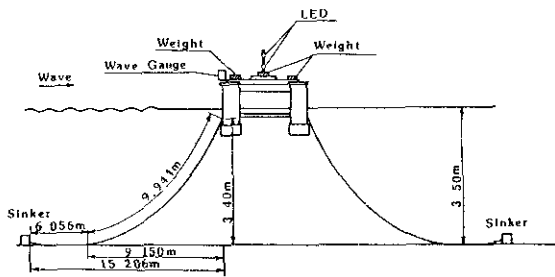


Fig.2. Model set-up

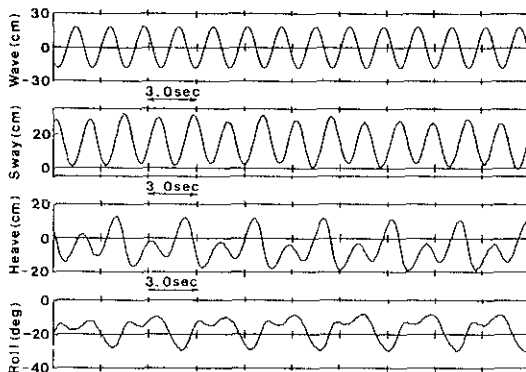
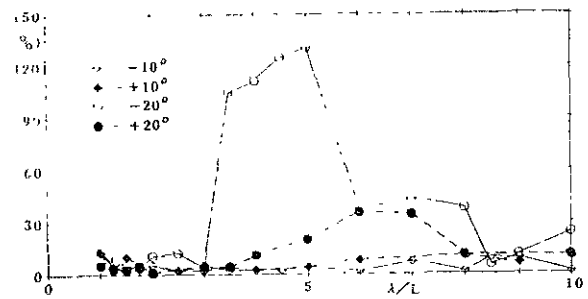
Fig.3. Records of experimental time history ($\phi_0 = -20^\circ, \lambda/L = 5.0$)

Fig.4. Ratios of subharmonic component to fundamental component of rolling motion

a top of one sided lowerhull breaks surface. Fig.4 shows the percentages of the subharmonic component, $\omega/2$, to the fundamental component, ω of rolling motions. The subharmonic component of rolling motion becomes larger near half the natural period of rolling motion. In particular, this unstable motion takes place clearly at the initial list angle of -20° , and its maximum amplitude is almost as large as the amplitude of the fundamental component. On the other hand, the subharmonic component of the initial list angle of $+20^\circ$ is not so large as that of -20° . In the next place, whenever a list of the model decreases less than 10° , its motion becomes stable

Thereby it is of importance to make clear the mechanism of this unstable motion from a standpoint of a safe operation, because this unstable motion induces the dangerous condition such as a small airgap and capsizing.

2.2 Classification of Unstable Motion

So far a many researchers have studied on unstable motions of a ship and/or a semisubmersible platform [7],[8],[9],[10]. These are classified into four categories [6]:

- Asymmetric roll
- Jump phenomenon
- Ultraharmonic resonance and subharmonic resonance
- Parametric oscillation

Let us examine these causes of an unstable rolling motion. The first category (a) is mainly caused by a change of a righting moment arm \overline{GM} . In our experiment, a water plane area of the model is smaller than that of a ship. The change of a righting moment arm therefore is small at every moment. Hence this unstable motion of a semisubmersible platform seems different from an asymmetric rolling motion.

The second category (b) is caused by a shift from one of two stable solutions to another, because the equation of motion has a cubed nonlinear righting moment; there are two stable solutions and one unstable solution. As shown in Fig.4, the time history of our unstable motion is quite different from the jump phenomenon.

The third category (c) is the higher order resonance; it is generally caused by a higher order exciting force with a subharmonic component and

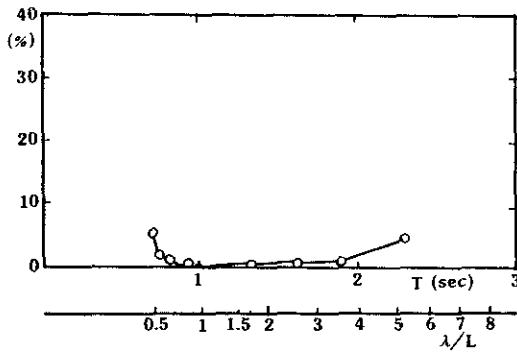


Fig. 5. Ratios of subharmonic component to fundamental component of wave exciting moment at heel angle -20°

an ultraharmonic one. Fig. 5. shows the percentage of the subharmonic component, $\omega/2$, to the fundamental component of the wave exciting moments in our experiment. The wave exciting moment scarcely includes the subharmonic component as shown in Fig. 5. Thereby our unstable motion with the frequency of $\omega/2$ is not caused by the third category (c).

The fourth category (d) is an unstable phenomenon at the condition of $\omega/\omega_0 = n$, where ω_0 is the natural frequency for rolling motion, ω is incident wave frequency, and n is integer. Paulling has showed that the equation of motion can be expressed by Mathieu's equation including the nonlinear hydrodynamic forces on a ship, and has verified experimentally the development of the unstable rolling motion by carrying out the forced oscillation test [7].

Our unstable motion is very similar to that of the category (d). Thereby we assume that our unstable motion of a semisubmersible platform is a kind of the parametric oscillation, and investigate the mechanism of it.

2.3 Mechanism of Unstable Motion

The simultaneous equations for the nonlinear lateral motions due to a parametric oscillation can be generally expressed as follows:

$$\begin{aligned} A_{44}\ddot{\phi} + B_{44}\dot{\phi} + B_{44N}\dot{\phi}|\dot{\phi}| + C_{44}(1 - 2h \sin \omega t)\phi \\ + A_{42}\ddot{y} + B_{42}\dot{y} + C_{42}y \\ + A_{43}\ddot{z} + B_{43}\dot{z} + C_{43}z = M_{\phi e} \end{aligned} \quad (1)$$

$$\begin{aligned} A_{22}\ddot{y} + B_{22}\dot{y} + C_{22}y + A_{23}\ddot{z} + B_{23}\dot{z} + C_{23}z \\ + A_{24}\ddot{\phi} + B_{24}\dot{\phi} + C_{24}\phi = F_{ye} \end{aligned} \quad (2)$$

$$\begin{aligned} A_{33}\ddot{z} + B_{33}\dot{z} + C_{33}z + A_{32}\ddot{y} + B_{32}\dot{y} + C_{32}y \\ + A_{34}\ddot{\phi} + B_{34}\dot{\phi} + C_{34}\phi = F_{ze} \end{aligned} \quad (3)$$

When a semisubmersible platform with a large list angle is loosely moored in waves, the following four items can be considered the causes of the unstable motion:

- (a) Periodic variation of righting moment arm \overline{GM} due to a heaving motion

- (b) Variation of mooring reaction force
(c) Hydrodynamic forces due to asymmetric form of a semisubmersible platform with a large list angle
(d) Asymmetric tilt moment due to a difference between hydrodynamic forces on two lower-hulls Now we examine the effects of the above causes on the unstable motions in the next section.

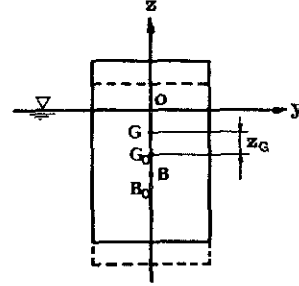


Fig. 6. Simplified model of a heaving body

2.4 Effect of Righting Moment Arm

We consider about the wall sided body shown in Fig. 6, where,

- V_0 : initial displacement,
 I_0 : quadratic moment of water plane area,
 $\overline{B_0 M_0}$: metacentric radius,
 $\overline{G_0 O}$: distance between center of gravity and origin,
 $\overline{B_0 O}$: distance between center of buoyancy and origin,
 A_w : water plane area.

We have the following rolling moment, when the semisubmersible platform is heaving.

$$\begin{aligned} M_1(\phi) &= -W \cdot \overline{GM} \cdot \phi \\ &= -W \cdot \overline{G_0 M_0} \left[1 + \frac{A_w}{V_0} \left(1 + \frac{\overline{G_0 O}}{\overline{G_0 M_0}} \right) z \right] \phi \\ &= -W \cdot \overline{G_0 M_0} (1 + h_{GMR} z) \phi \end{aligned} \quad (4)$$

where,

$$h_{GMR} = \frac{A_w}{V_0} \left(1 + \frac{\overline{G_0 O}}{\overline{G_0 M_0}} \right) \quad (5)$$

h_{GMR} is the nonlinear coupling term from heave into roll.

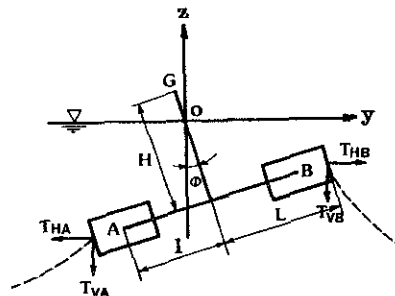


Fig. 7. Simplified model of a semisubmersible platform with a large list angle

When we consider the model of a semisubmersible platform moored shown in Fig. 7, the tilt moment due to the mooring forces can be expressed as follows

$$\begin{aligned}
 M_2(\phi) = & -\{ (T_{VAO}L'_a - T_{VBO}L'_b \\
 & + T_{HAO}L_a + T_{HBO}L_b) \\
 & + (K_{ZZA}L'_a - K_{ZZB}L'_b \\
 & + K_{ZYA}L_a + K_{ZYP}L_b)z \\
 & + (K_{YZA}L'_a - K_{YZB}L'_b \\
 & + K_{YYA}L_a + K_{YYB}L_b)y \} \phi \\
 = & -W \frac{G_0 \bar{M}_0}{(M_{KR} + h_{KZR}z + h_{KYR}y)} \quad (6)
 \end{aligned}$$

where K_{ZZ} , K_{ZY} , K_{YZ} , and K_{YY} are spring constants from heave into heave, from sway into heave, from heave into sway and sway into sway respectively.

$$\begin{aligned}
 M_{KR} = & \frac{1}{W \bar{G}_0 \bar{M}_0} [T_{VAO}L'_a - T_{VBO}L'_b \\
 & + T_{HAO}L_a + T_{HBO}L_b] \\
 h_{KZR} = & \frac{1}{W \bar{G}_0 \bar{M}_0} [K_{ZZA}L'_a - K_{ZZB}L'_b \\
 & + K_{ZYA}L_a + K_{ZYP}L_b] \\
 h_{KYR} = & \frac{1}{W \bar{G}_0 \bar{M}_0} [K_{YZA}L'_a - K_{YZB}L'_b \\
 & + K_{YYA}L_a + K_{YYB}L_b] \\
 \left. \begin{aligned}
 L_a = & L \cos \phi_0 - H \sin \phi_0 \\
 L'_a = & L \sin \phi_0 + H \cos \phi_0 \\
 L_b = & L \cos \phi_0 + H \sin \phi_0 \\
 L'_b = & L \sin \phi_0 - H \cos \phi_0 \\
 \phi_0 : & \text{initial list angle} \\
 & \text{of a semisubmersible platform.}
 \end{aligned} \right\} \quad (7)
 \end{aligned}$$

ϕ_0 : initial list angle of a semisubmersible platform.

Thereby h_{KZR} and h_{KYR} are the nonlinear coupling term of the mooring force from heave and sway into roll

2.6 Tilt Moment Due to Asymmetric Form

The tilt moments are caused by the difference of the hydrodynamic forces on both lowerhulls and the derivatives of added mass on both lowerhulls with respect to z -direction at every moment. Let z_0 and ϕ_0 be initial vertical position of the center of gravity and the initial list angle respectively. Similarly let z and ϕ be a heaving displacement and a rolling one respectively, where $G_0 \bar{O} > 0$, and the center of gravity is upwards of the origin at Fig. 7. z_a and z_b are the positions of the lowerhulls A and B, and z_{a0} and z_{b0} are the initial vertical position of the lowerhulls A and B

Let assume the amplitude of motion very small, and then the added mass M_H for heave on each lowerhull can be expanded about the positions of z_{a0}

and z_{b0} by means of Taylor's expansion as follows

$$\begin{aligned}
 M_H(z_a) = & M_H(z_{a0}) + \frac{\partial M_H(z_{a0})}{\partial z} (z - l_a \phi) \\
 & + O(z^2) \\
 M_H(z_b) = & M_H(z_{b0}) + \frac{\partial M_H(z_{b0})}{\partial z} (z - l_b \phi) \\
 & + O(z^2)
 \end{aligned} \quad (9)$$

where,

$$\begin{aligned}
 l_a = & l \cos \phi_0 - H \sin \phi_0 \\
 l_b = & l \cos \phi_0 + H \sin \phi_0
 \end{aligned} \quad (10)$$

We can express the vertical hydrodynamic forces due to heaving from the equations (9) and (10) as follows.

$$\begin{aligned}
 F_{za} = & -(z - l_a \phi) \left[M_H(z_{a0}) \right. \\
 & \left. + \frac{\partial M_H(z_{a0})}{\partial z} (z - l_a \phi) \right] \\
 F_{zb} = & -(z - l_b \phi) \left[M_H(z_{b0}) \right. \\
 & \left. + \frac{\partial M_H(z_{b0})}{\partial z} (z - l_b \phi) \right]
 \end{aligned} \quad (11)$$

Thereby the tilt moment can be expressed by neglecting the higher order of the equation (11) as follows:

$$\begin{aligned}
 M_3(\phi) = & -F_{za}(l_a - l'_a \phi) + F_{zb}(l_b - l'_b \phi) \\
 = & \left[(M_{Ha} \cdot l_a - M_{Hb} \cdot l_b) \right. \\
 & - (M_{Ha} \cdot l'_a - M_{Hb} \cdot l'_b) \phi \\
 & + \left(\frac{\partial M_{Ha}}{\partial z} l_a - \frac{\partial M_{Hb}}{\partial z} l_b \right) z \\
 & - \left(\frac{\partial M_{Ha}}{\partial z} l_a^2 - \frac{\partial M_{Hb}}{\partial z} l_b^2 \right) \phi \left. \right] z \\
 & + \left[-(M_{Ha} \cdot l_a^2 - M_{Hb} \cdot l_b^2) \right. \\
 & + (M_{Ha} \cdot l_a \cdot l'_a - M_{Hb} \cdot l_b \cdot l'_b) \phi \\
 & - \left(\frac{\partial M_{Ha}}{\partial z} l_a^2 + \frac{\partial M_{Hb}}{\partial z} l_b^2 \right) z \\
 & \left. + \left(\frac{\partial M_{Ha}}{\partial z} l_a^3 - \frac{\partial M_{Hb}}{\partial z} l_b^3 \right) \phi \right] \phi \quad (12)
 \end{aligned}$$

In the above equation, the first and the fifth term are the linear coupling moments. The nonlinear tilt moments due to heaving and rolling therefore can be expressed by

$$\begin{aligned}
 M_3(\phi) = & \left[-(M_{Ha} \cdot l'_a - M_{Hb} \cdot l'_b) \right. \\
 & - \left(\frac{\partial M_{Ha}}{\partial z} l_a^2 - \frac{\partial M_{Hb}}{\partial z} l_b^2 \right) \left. \right] z \phi \\
 & - \left[\frac{\partial M_{Ha}}{\partial z} l_a^2 + \frac{\partial M_{Hb}}{\partial z} l_b^2 \right] z \phi \\
 & + \left[(M_{Ha} \cdot l_a \cdot l'_a + M_{Hb} \cdot l_b \cdot l'_b) \right. \\
 & \left. + \left(\frac{\partial M_{Ha}}{\partial z} l_a^3 - \frac{\partial M_{Hb}}{\partial z} l_b^3 \right) \right] \phi \phi \quad (13)
 \end{aligned}$$

Assuming the periodic motion of ω , we finally have the following equation.

$$M_3(z, \phi) = -W \cdot \overline{G_0 M_0} \cdot [h_{ZZR}z + h_{ZRR}\phi] \quad (14)$$

where,

$$\left. \begin{aligned} h_{ZZR} &= -\frac{\omega^2}{W \overline{G_0 M_0}} \left[(M_{Ha} \cdot l'_a - M_{Hb} \cdot l'_b) + 2 \left(\frac{\partial M_{Ha}}{\partial z} l_a^2 + \frac{\partial M_{Hb}}{\partial z} l_b^2 \right) \right] \\ h_{ZRR} &= \frac{\omega^2}{W \overline{G_0 M_0}} \left[(M_{Ha} \cdot l_a \cdot l'_a + M_{Hb} \cdot l_b \cdot l'_b) + \left(\frac{\partial M_{Ha}}{\partial z} l_a^3 - \frac{\partial M_{Hb}}{\partial z} l_b^3 \right) \right] \\ M_{Ha} &= M_H(z_{a0}) \quad , \quad M_{Hb} = M_H(z_{b0}) \end{aligned} \right\} \quad (15)$$

$$\left. \begin{aligned} l'_a &= l \cos \phi_0 + H \sin \phi_0 \\ l'_b &= l \cos \phi_0 - H \sin \phi_0 \end{aligned} \right\} \quad (16)$$

In the same way as the above equations, the nonlinear tilt moment due to swaying and rolling can be also expressed as follows:

$$M_4(y, \phi) = -W \cdot \overline{G_0 M_0} \cdot [h_{YYR}y + h_{YZR}z + h_{YRR}\phi] \quad (17)$$

where,

$$\left. \begin{aligned} h_{YYR} &= \frac{-\omega^2}{W \overline{G_0 M_0}} \left[(M_{Sa} \cdot l_a - M_{Sb} \cdot l_b) - \left(\frac{\partial M_{Sa}}{\partial z} l_a \cdot l'_a + \frac{\partial M_{Sb}}{\partial z} l_b \cdot l'_b \right) \right] \\ h_{YZR} &= \frac{-\omega^2}{W \overline{G_0 M_0}} \left(\frac{\partial M_{Sa}}{\partial z} l_a^2 + \frac{\partial M_{Sb}}{\partial z} l_b^2 \right) \\ h_{ZRR} &= \frac{-\omega^2}{W \overline{G_0 M_0}} \left[(M_{Sa} \cdot l_a \cdot l'_a + M_{Sb} \cdot l_b \cdot l'_b) - \left(\frac{\partial M_{Sa}}{\partial z} l_a \cdot l_a^2 - \frac{\partial M_{Sb}}{\partial z} l_b \cdot l_b^2 \right) \right] \\ M_{Sa} &= M_S(z_{a0}) \quad , \quad M_{Sb} = M_S(z_{b0}) \quad , \\ M_S &; \text{ added mass for sway.} \end{aligned} \right\} \quad (18)$$

Rearranging the equations (4) to (18), we can get finally the nonlinear tilt moment on a semisubmersible platform with a large list angle as follows:

$$\begin{aligned} M(y, z, \phi) &= -W \cdot \overline{G_0 M_0} \\ &\cdot [(h_{KYR} + h_{YYR}) \cdot y \\ &+ (h_{GMR} + h_{KZR} + h_{ZZR} + h_{YZR}) \cdot z \\ &+ (h_{YRR} + h_{ZRR}) \cdot \phi] \phi \end{aligned} \quad (19)$$

Substituting the above equation into (1), we have

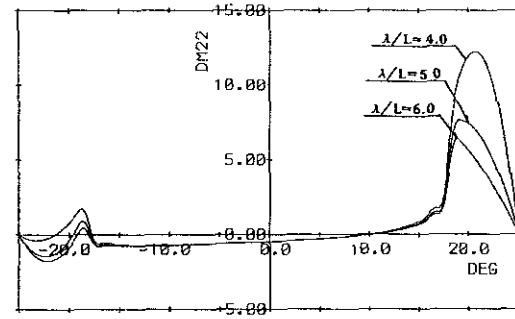
$$\begin{aligned} A_{44}\ddot{\phi} + B_{44}\dot{\phi} + B_{44N}\dot{\phi}|\dot{\phi}| \\ + W \cdot \overline{G_0 M_0} \\ \cdot [1 + M_{KR} + (h_{KYR} + h_{YYR})y \\ + (h_{GMR} + h_{KZR} + h_{ZZR} + h_{YZR})z \\ + (h_{YRR} + h_{ZRR})\phi] \phi \\ + A_{42}\ddot{y} + B_{42}\dot{y} + C_{42}y + A_{43}\ddot{z} + B_{43}\dot{z} + C_{43}z \\ = M_{\phi c} \end{aligned} \quad (20)$$

The equation (20) is Mathieu's equation having the coupling terms and the wave exciting moment.

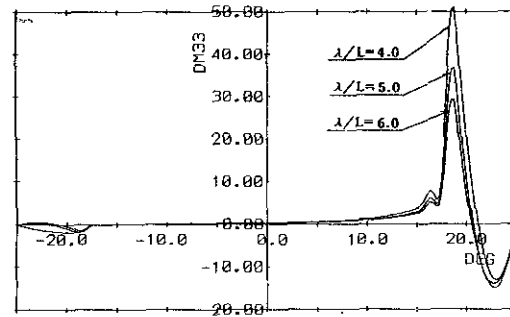
3. NUMERICAL SIMULATION

3.1 Hydrodynamic Force

We have evaluated the hydrodynamic coefficients of the equations (1) to (3) by applying 3-D singular distribution method. One side of the lowerhulls, however, comes near a free surface and its top sometimes breaks surface in waves, when a list of a semisubmersible platform becomes larger. As a result, It has been made clear that the estimation accuracy of the hydrodynamic forces on a submerged body in a vicinity of a free surface becomes worse [11], [12]. Hence by applying a Spline function to the exact hydrodynamic forces, we have approximated them on it with a large list angle. In addition, the vertical derivatives of the added mass with respect to z-direction in the equation (20) are evaluated from the numerical differential of the added mass above estimated.



(a) Sway



(b) Heave

Fig.8. The derivatives of added mass of lowerhull with respect to z-direction

Fig. 8 shows the derivatives of the added mass on the lee-side lowerhull for sway (a) and heave (b) estimated by the above method; the horizontal axis of this figure corresponds to the list angle.

Fig. 9 and Fig. 10 show the absolute values of the unstable parameters, h , in the equation (19) at the list angle of 10° and 20° respectively; the horizontal axis of figures corresponds the ratio of the oscillating frequency to twice the length of the rolling natural frequency. It is clear from these figures that the values of the unstable parameters h_{GMR} due to the change of \overline{GM} and h_{KYR} ,

h_{KZR} due to the mooring forces are small, while h_{ZZR} , h_{ZRR} due to the derivatives of the added mass are large. In particular these values of the list angle 20° are larger than those of the list angle 10° . Thereby the unstable parameters become larger, as the list of platform becomes larger. We have carried out the numerical simulation by making use of the Runge-Kutta-Gill method, and have examined the mechanism of a parametric oscillation.

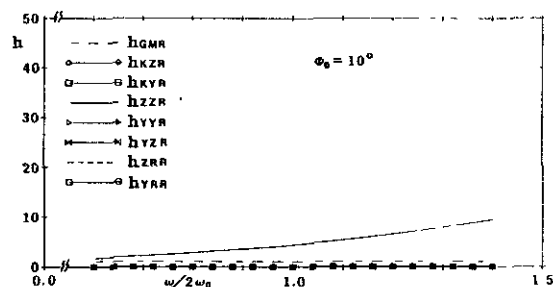


Fig.9. Nonlinear coupling term at heel angle 10°

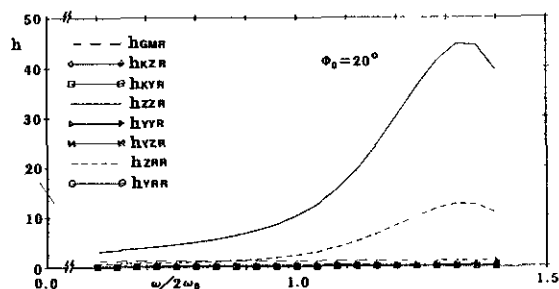


Fig.10. Nonlinear coupling term at heel angle 20°

3.2 Comparison of Simulation and Experiment

Fig. 11 shows the numerical examples with list angle, -20° , at wave length ratio, $\lambda/L = 5$, where the subharmonic motion has occurred intensely in the experiment [13]. The subharmonic motion occurs as large as the experiment as shown in Fig. 3. On the other hand, the motion with the list angle, 20° , is stable as shown in Fig. 12. In addition to these simulations, Fig. 13 shows simulation results with the list angle, -20° , in which the unstable parameter, h , is not taken into account. It follows from this figure that unless the unstable parameter, h , is taken into account, the unstable motion never occurs at the condition where even if the list angle is -20° . It therefore follows that the phase lag between a wave force and motion, and the unstable parameter, h , such as h_{ZZR} and h_{ZRR} affect intensely the subharmonic component of rolling motion.

Fig. 14 shows the comparison between the experimental result and simulation result obtained by Fourier analysis of both the time histories. The bold line and the dotted line correspond to the simulated values with the list angle, -20° and $+20^\circ$ respectively, the white circle and the black circle correspond to the experimental values with the list

angle, -20° and $+20^\circ$ respectively. The simulated values are in qualitative good agreement with the experimental ones. The difference, however, appears at the list of -20° . It is because that we have used the values of the viscous damping B_{4+V} at the rolling natural period in calm water: the values are not useful for simulating exactly the subharmonic motion in waves. The viscous damping, however, affects essentially not the mechanism of the subharmonic motion but the amplitudes of motions.

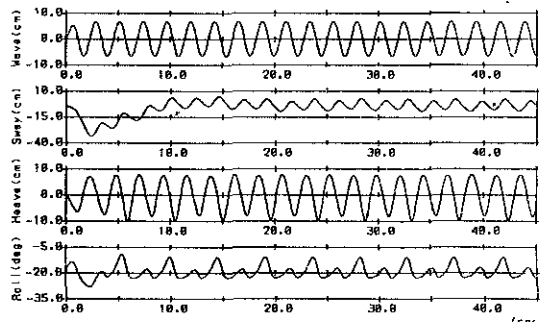


Fig.11. Simulation of motions with unstable parameter ($\phi_0 = -20^\circ$, $\lambda/L = 5.0$)

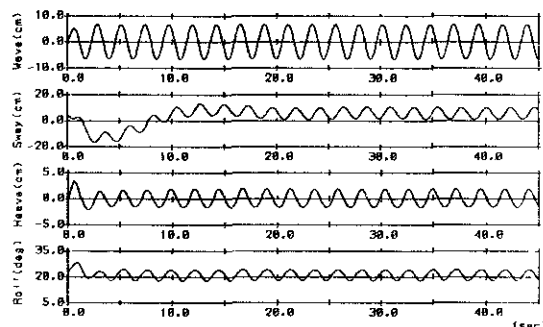


Fig.12. Simulation of motions with unstable parameter ($\phi_0 = 20^\circ$, $\lambda/L = 5.0$)

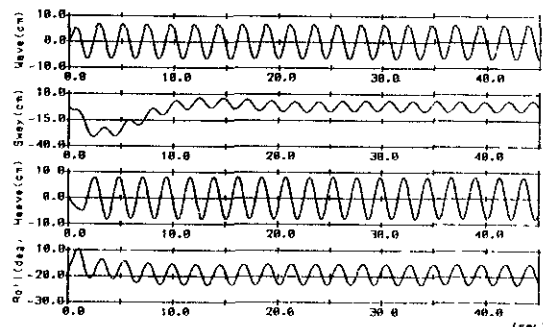


Fig.13. Simulation of motions without unstable parameter ($\phi_0 = -20^\circ$, $\lambda/L = 5.0$)

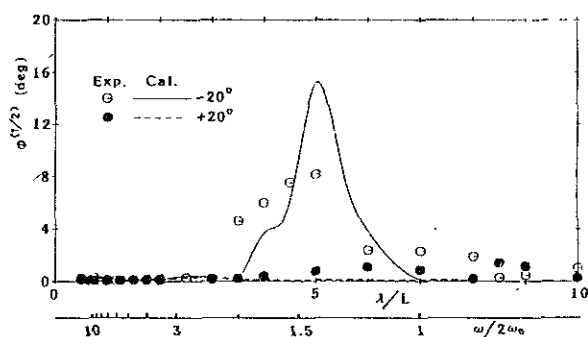


Fig.14. Comparisons of calculated and experimental results for the subharmonic component

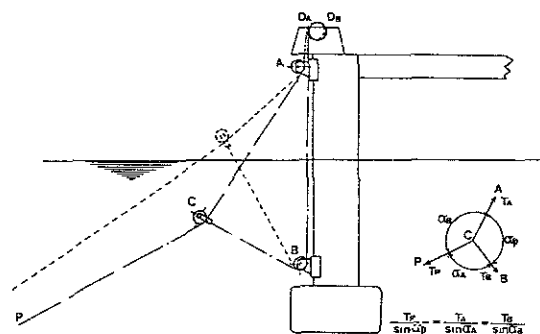


Fig.15. General arrangement of the new mooring system

4. CONTROL OF MOTIONS

4.1 Proposal of Control Device

As mentioned in Chapter 2, as the larger the list of platform increases, the larger the rolling amplitude becomes, and the more dangerous it becomes. The unstable motion, however, disappears, as the list of it becomes smaller. It is therefore of importance to keep a small list from a standpoint of a safe operation. Hence we have developed a new control device of motions of a semisubmersible platform; it can move freely the fairlead location to the most suitable point on a column in order to reduce a tilt moment induced by environmental loads to a minimum.

The control device developed newly is made up of two fixed pulleys A & B and one driving pulley C as shown in Fig.15. The fixed pulleys A & B are set up at both the upper and the lower end of a column, and the mooring line \overline{AP} passing through the driving pulley C is stretched from the fixed pulley A. Let T_P , T_A , T_B be the mooring tensions of lines \overline{PC} , \overline{AC} , \overline{BC} respectively. Then we have the following equations among these tensions and the angles α_P , α_A , α_B .

$$\frac{T_P}{\sin \alpha_P} = \frac{T_A}{\sin \alpha_A} = \frac{T_B}{\sin \alpha_B} \quad (21)$$

We therefore can move the fairlead location C to an arbitrary position between the column length \overline{AB} by changing the mooring tensions T_A and T_B .

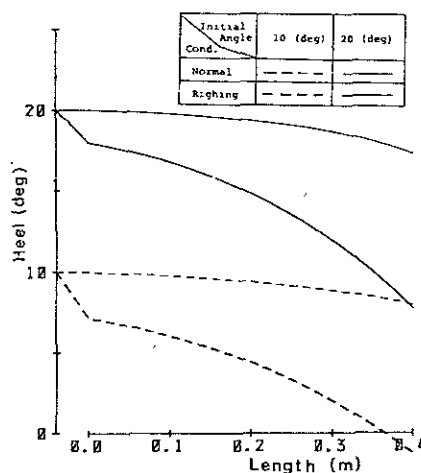


Fig.16. Heel angles in wind-up condition

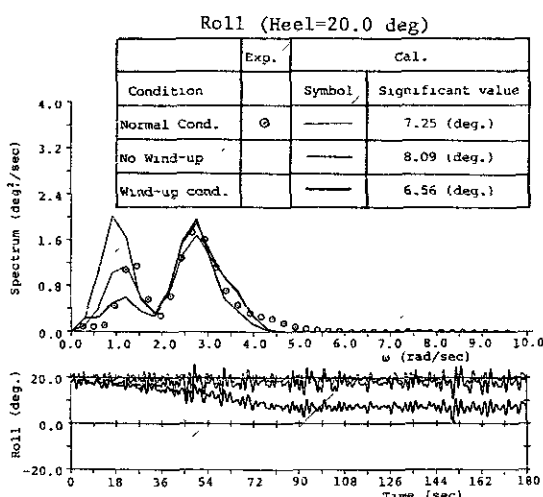


Fig.17. Spectra and time histories of rolling motion

4.2 Control of Static and Dynamic Condition

The model is set up in beam sea condition as shown in Fig. 2. Under this condition, the righting moment on a semisubmersible platform affects intensely its safety performance. We therefore show only heeling angle and rolling motion in irregular waves as one example of using this device.

In Fig. 16, let Normal Condition be that the fairlead location is set up at the design point of 0.31 m upwards from the keel line; let Righting Condition be that two fairleads are set up at both the upper end and the lower end of the column. In Normal Condition, heeling angle slightly reduces by only 1° and 2.5° from the initial list angles of 10° and 20° respectively. While in Righting Condition, this device reduces the list angle larger than 10° from both the initial list. According to the reference [5], the method of adjusting the ballast water can reduce by only less than 3.5° at the same initial list angle, 20° . Thereby it becomes clear that this device is useful for controlling a list of a semisubmersible platform.

Fig. 17 shows the comparison of spectra between the experiment and simulation, and its time

When the device puts in operation, the mooring lines are wound up, the slow rolling amplitudes become smaller and the initial lists of 10° and 20° recover to the mean list angles of -0.06° and 7.11° respectively. It becomes clear from this simulation that the new proposed control device is useful for reducing the oscillating amplitudes of the listing platform as well as that of a static one.

5. CONCLUSION

From the standpoint of the safety operation of a semisubmersible platform, we have made clear the mechanism of the unstable motion and proposed the new mooring system. The main conclusions obtained from this study may be summarized as follows:

- (1) The phase lag between a wave force and motion, and the unstable parameter, h , affect intensely the subharmonic component of rolling motion.
- (2) The unstable parameters become larger, as the list of platform becomes larger. It is because that the difference between hydrodynamic forces on two lowerhulls becomes larger, when one side of the lowerhulls comes near a free surface.
- (3) From a standpoint of a safe operation, the control of the list of a semisubmersible platform is the most important in order to reduce a list and/or to remove the unstable motion.
- (4) We propose the new mooring system to control the list of a semisubmersible platform.
- (5) The validity of this control system is confirmed by the numerical simulation.

ACKNOWLEDGMENT

The authors would like to express to their sincere gratitude to Prof. Takezawa, Yokohama National University, for his useful discussions. They also thanks Dr. Iwashita and the students in the Laboratory of Dynamics of Ocean Environment in Hiroshima University for their considerable assistance and cooperation to carry out the extensive experiments.

REFERENCE

1. Takarada, N. et al., The Stability on Semi-submersible Platform in Waves (On the Capsizing of Moored Semi-submersible Platform), The 2nd International Conference on Stability of Ships and Ocean Vehicles, 1982, pp.589-601.
2. Takarada, N. et al., A Study on the Capsizing Mechanism of Semisubmersible Platform, (1st, 2nd and 3rd Report), Journal of the Society of Naval Architects of Japan, Vol. 155, 156 and 157, 1984, 1985.
3. Takarada, N. et al., Effects of Mooring on Safety and Stability of Offshore Structures, Third Marine Dynamic Symposium, The Society of Naval Architects of Japan, 1986, pp. 217-236.
4. Takezawa, S. and Hirayama, T., SAFETY ON

A MOORED SEMISUBMERSIBLE PLATFORM UNDER EXTREME COMPLEX EXTERNAL LOADS. Proceedings of Fifth International Offshore Mechanics and Arctic Engineering (OMAE) Symposium, Vol. 3, 1986, pp. 29-36.

5. Takaki, M., Higo, Y. et al., A Study on the Stabilizing Method of Semisubmersible Platform with a Large List in Waves", JOURNAL OF THE KANSAI SOCIETY OF NAVAL ARCHITECTS, JAPAN, No. 204, 1987, pp. 1-10.
6. Kan, M. and Yamakoshi, Y., Capsize of Ships in Beam Seas, Safety and Stability of Ships and Offshore Structures -Third Marine Dynamics Symposium-, 1986, pp. 95-124.
7. Paulling, J.R. and Rosenberg, R.M., On Unstable Ship Motions Resulting from Nonlinear Coupling, J.S.R. 3-1, 1956, pp. 36-46.
8. Kyouzuka, Y. et al., On the Unstable Swaying Motions of a Moored Cylinder in Regular Waves, Journal of the Society of Naval Architects of Japan, Vol. 142, 1977, pp. 83-89.
9. Nishihara, S. and Imakita, A., Parametric Excitation in Tension Leg Platform, Journal of the Society of Naval Architects of Japan, Vol. 145, 1979, pp. 219-226.
10. Huang, X. and Naess, A., Dynamic Response of a Heavily Listed Semi-Submersible Platform, 2nd international Symposium on Ocean Engineering and Ship Handle, SSPA Gothenburg, 1983, pp.375-392.
11. Nakamura, I., Takaki, M., Park, R. and Harada, S., Hydrodynamic Loads acting on a Semisubmersible Unit with a Large List angle, Transactions of the West-Japan Society of Naval Architects, No.68, 1984, pp.119-133.
12. Higo, Y., A Study on the Nonlinear Hydrodynamic Forces Acting on a Rectangular Cylinder Oscillation with a Large Amplitude, Journal of the Kansai Society of Naval Architects, Japan, No.199, 1985, pp. 1-9.
13. Nakamura, K. and Fujii, M., A Study on Stability of a Semisubmersible Platform with a large List Angle in Regular Waves, Graduation Thesis of Hiroshima University, 1985.

RESEARCH TOWARDS CRITERIA OF STABILITY OF CIVIL DECK BULK CARGO SHIPS

Yang Dibarg*, Huang Weiping*, Jirg Qilar** and Wu Zhi***

ABSTRACT

In this paper, a suggestion is proposed to set up the criteria of the stability of civil deck bulk cargo ships. It bases on the mechanism of deck cargo slipping, the theoretical analyses and the calculations of added-capsizing moments to ships due to cargo-slipping, the results got from tests of rolling-platform and the tank experiments for models. This suggestion has been accepted by the Register of shipping of the P.R. China (ZC).

INTRODUCTION

In the civil shipping of China, deck bulk cargo ships have a very important position both for amount and deadweight tonnages. They have advantages such as intact structure, light weight, easily to be load on or off, etc, but the gravity centers of cargos are high. The bulk cargos are easily to slip when ships are in rolling, and they aggravate the capsizing of ships, even cause a capsizing mishap[1].

The influences of cargo-slipping to stability of ships are extremely concerned with various countries. Nedrelid T. has made a theoretical analysis to stability of the slopes of bulk cargos[2]. A proposal made by U.S.A. has been sent to IMCO, suggesting a simple step to limit the heights of cargos, so as to guarantee the safety of ships before cargo-slipping[3]. It's also concerned in China that cargo-slipping causes capsizing accidents. But the comprehensive research work to cargo-slipping have not been launched actually. Up to date, the influences of cargo slipping have not been considered in the civil standards of stability of all the countries.

THEORETICAL CALCULATIONAL METHOD OF CARGO-SLIPPING

Although theoretical calculations to cargo-slipping is similar to civil engineering, they have some characteristics as follows:

1. In civil engineering, the slopes are in static states; while the deck cargos

are in motion with the motion of ships, having velocities and accelerations.

2. In civil engineering, its mainly concerned about the stability of slopes; while in calculations of cargo-slipping, further decisions should be made of the slipping conditions of cargo slope, the process of slipping and the shapes after slipping and the added-capsizing moments of ships due to cargo-slipping.

3. It has been observed in experiments that besides losing stability and collapsing, deck bulk cargos would slip wholly or partly along the surface of deck. The dangerous surfaces of bulk cargos appear as two demarcations with different features.

Similar to rock mechanics and civil engineering, we get that the shearing stress which can be supported on any face of cargo, or shearing strength T_f , keeps with Coulomb's formula in certain range.

$$T_f = C + \sigma \cdot \phi \quad (1)$$

where, σ is normal stress on shearing face.

C, ϕ is coherent specific coefficient and frictional angle of cargo separately.

Since there is some water in the void of cargo, when the cargo is compressed there will be a certain void pressure V , which has a relationship with total stress σ and effective stress σ' .

$$\sigma = \sigma' + V \quad (2)$$

The degree of stability on any slipping face of cargo is showed by τ versus T_f , or $F_s = T_f / \tau$. F_s is called as safety coefficient of the face. If $F_s \leq 1$, cargo will slip along the face. The most dangerous face is the face on which F_s gets its minimum.

Fig.1 indicates a certain differential strip of deck bulk cargo. Line 1-3 shows a slope of cargo. Line 2-4 shows a slipping face and dw --gravity

*--Both work in Huazhong University of Science and Technology (HUST) as associate professors, in Wuhan.

**--Graduated from HUST as a Master in 1989, now works in Wuhan Shipbuilding Development & Design Institute, P.R. of China.

***--Graduated from HUST as a Master in 1986, now studies in HUST as a doctor of mechanics.

dN' , dS & dvs --effective normal force, tangential force, void pressure or slipping face, separately

E, T & V --effective normal force, tangential force, void pressure on two sides, separately

dQy , dQz & dMx --inertia force and moment when the strip is in motion with ships roll, sway, heave & pitch

Establish equilibrium equations of the slipping face, and of the moments to the centre of differential slipping strip. Based on the limit dynamic equilibrium theory, we have

$$dS = (C' dy \cdot \sec \alpha + dN' \cdot \tan \phi') / F_s \quad (3)$$

Introduce Morgenstern & Price conditions:[5]

1. shearing stress on the differential strip of slipping face does not exceed shearing strength.

2. Cargo can't stand pulling forces. So the effective resultant line on the differential strip would not be pointed out from the strip.

Amalgamate two equations of the forces and moments, and simplify them. It comes out two nonlinear equation groups which are indeterminated.

$$\begin{aligned} & \left(\frac{dE}{dy} + \frac{dV}{dy} \right) \left(1 - \frac{\tan \phi'}{F_s} \frac{dZ}{dy} \right) + \frac{dQy}{dy} \left(1 + \frac{\tan \phi'}{F_s} \frac{dZ}{dy} \right) \\ & + \left(\frac{dT}{dy} + \frac{dW}{dy} - \frac{dQz}{dy} \right) \left(\frac{\tan \phi'}{F_s} + \frac{dZ}{dy} \right) \\ & + \left[1 + \left(\frac{dZ}{dy} \right)^2 \right] \left(\frac{C'}{F_s} - V \frac{\tan \phi'}{F_s} \right) = 0 \end{aligned} \quad (4)$$

$$\begin{aligned} dT = & \frac{d}{dy} (E \cdot Z_t) - Z \frac{dE}{dy} + \frac{d}{dy} (V \cdot h_t) - Z \frac{dV}{dy} \\ & - \frac{dQy}{dy} (Z_q - Z) - \frac{dMx}{dy} + \frac{dQz}{dy} (Y_q - Y) \end{aligned} \quad (5)$$

where, Y_q , Z_q --coordinates of center of strip's quality

In rock mechanics and civil engineering, two kind of method are used to solve the above equations

1. Bishop's method[6],[7]

Suppose the slipping face is cylindrical. Using an equation of moment to the center of the cylinder surface instead of equation(5), we can make a simplification. The safety coefficient on the slipping face is

$$F_s = \frac{[C' l_i \cos \alpha_i + N_f] / M_{\alpha i}}{[W_i (Y_{oc} - Y_{qi}) + M_q] / R + M_{eu} / R + M_{xi}} \quad (6)$$

where, $N_f = (W_i + Q_{zi} + T_i - T_{i+1} + V_i \cdot l_i \cos \alpha_i) \tan \phi'$
 $M_q = Q_{yi} (Z_{oc} - Z_{qi}) - Q_{zi} (Y_{oc} - Y_{qi})$
 $M_{eu} = (E_a + V_a) (Z_{oc} - Z_a) - (E_b + V_b) (Z_{oc} - Z_b)$
 $M_{\alpha i} = \cos \alpha_i + \tan \phi' i - \sin \alpha_i / F_s$
 l_i --length of differential strip or the slipping face with an order number i

Y_{oc}, Z_{oc} --Center coordinates of cylinder slipping face

E_a, E_b, V_a & V_b --horizontal pulling force and void pressure on two

ends to the slipping body

2. General slip surface (GPS) method.

Slipping face can be formed from any surface. Yet suppose that all the statical forces on a differential strip pass through the resultant point on the slipping face. The point of the horizontal pulling force is located on the lowest of which divide the side of the strip into three equal parts. This supposition is based on large quantity experimental observations, and satisfies the accuracy of engineering calculations. Dispersing equations from (3) to (5), we get a group of equations as follows:

$$T_i = C_i' / F_s + (\sigma_i - V_i) \cdot \tan \phi' / F_s \quad (7)$$

$$\sigma_i = \frac{W_i - Q_{zi} - R_i}{dy_i (1 + \tan \phi' i \cdot \tan \alpha_i / F_s)} \quad (8)$$

$$F_s = \frac{[C_i' + (\sigma_i - V_i) \tan \phi' i] dy_i}{E_a + E_b + [(\sigma_i \cdot \tan \alpha_i \cdot dy_i + Q_{yi} + V_i + V_{i+1})]} \quad (9)$$

$$\begin{aligned} E_{i+1} = & E_i + (V_i - V_{i+1}) + Q_{yi} + (\tan \alpha_i - \tan \phi' i / F_s) \cdot \\ & \sigma_i \cdot dy_i - (C' / F_s - V_i \cdot \tan \phi' i / F_s) dy_i \end{aligned} \quad (10)$$

$$\begin{aligned} T_{i+1} = & [E_{i+1} (Z_{t, i+1} - Z_{ai}) - E_i (Z_{t, i} - Z_{ai}) \\ & + V_{i+1} (h_{t, i+1} - Z_{ai}) - V_i (h_{t, i} - Z_{ai}) \\ & - T_i (Y_{ai} - Y_i) + Q_{zi} (Y_{qi} - Y_{ai}) - Q_{yi} (Z_{qi} - Z_{ai})] / (Y_{i+1} - Y_{ai}) \end{aligned} \quad (11)$$

where, $R_i = (T_i - T_{i+1}) - (C_i' + \tan \phi' i \cdot V_i) dy_i \cdot \tan \alpha_i / F_s$
 Y_{ai}, Z_{ai} --coordinates of the point to the resultant on slipping face

Solve the above five equations by repeat iteration, can get the safety coefficient and various forces.

Using the above theoretical and calculational methods to calculate slipping of deck bulk cargos. We have also got some work mainly as follows:

1. Decide physical and mechanical parameters (load factor, free slope angle and shearing strength) of several common bulk cargos, by the aids of large quantity of tests.

2. Decide motion parameters through theoretical calculations and model tests. The motion is coupled with roll, sway, heave and pitch.

3. It is approved that the safety coefficient F_s , considering the effects of velocity and acceleration to the motions, is still a single kurtosis in the search range. So the iterating process to search the most dangerous slipping face is always convergent, as long as the searching range is appropriate

RESULTS FROM MODEL TESTS AND THEORETICAL CALCULATIONS

1. Static capsizing tests of bulk cargo slipping

Fig.2 and Fig.3 show the results of static capsizing tests for a model loaded

with coal and sand separately. The model is one-tenth scale of a part of a 1000 tons barge, and the part is used to load cargos. The curves showed in the figures are got from theoretical calculations. Mc1 or Mc2 is the capsizing moment counting or not counting cargo-slipping. Curve D is the weight line of model loaded with cargo. It may show the situation of cargo-slipping over railings and falling down. The capsizing moments measured in the tests are also showed in the figures with different symbols. The same kind of tests is carried out to phosphor-ore and Korea-iron-ore. Also, tests and theoretical calculations are carried out on a one-sixteenth scale model. All the tests results show good coincidences with the theoretical calculations.

2. Dynamic capsizing characteristics of bulk cargo slipping

We take out dynamic capsizing tests with amplitude of 60 degrees, half period from 240 to 8 seconds, on a rolling-platform. It shows in the tests that cargos can significantly slip along deck surfaces as whole bodys besides normal collapsing slipping when they slip over the frictional angle between cargos and deck surfaces. The capsizing moments increase rapidly. However, from a whole point, the capsizing moments of cargos are mainly statical ones produced by gravity. The inertia moments are small. They are mainly to decrease initial capsizing moments, delay the falling and make the curves of capsizing postponed. These phenomena are entirely coincident with theoretical calculations.

3. Simulations on the characteristics of bulk cargo slipping for full-scale ships

It has been showed from both theoretical calculations and experiments that because of limitation of model scale, the slipings on two boards, when simulate a full-scale ship's capsizing, are smaller and almost equal. And cargo are made dense and sunk due to rapid motion of ships. This makes capsizing moments decreased largely. In the tests, we mainly measure the limit stable angles of slopes and make a comparison with theoretical calculation. Table 1. is given out when cargos are rolling with magnitude of 12 deg. and loss stability. It shows a good coincidence.

Table 1. Rolling period when the slopes loss stability

kind of cargo	coal	sand	phosphor ore	korea iron-ore
moisture content (%)	9-11	8-11	6-8	6-8
measured period (sec)	1.2-1.4	1.2	1.2	1.4
calculated period (sec)	1.2	1.0	1.0	1.4

4. Model capsizing tests in the tank

Fig.4 shows dynamic stability curves

got from model capsizing tests in HUST tank. The model is one-twenty fifth scale of a 1000 tons barge and carries different amount of sand. Because of rolling damps. The measured values (dashed lines) are much higher than the calculated ones (real lines) of stability at large angles. The maximum of capsizing angles measured in the tests are 27.3 to 30 degrees, while the calculations show the limit stable angles at 35 degrees. So there is no cargo slipping before capsizing from observations. In the tests with the second kind of loadage, by making a forced recovery when the model capsizing to 34 degrees. We can find out the local collapsing occur along cargo slopes. The rifts can be seen clearly on the aft-slope. The sand get separation from the railing at about 4 mm, which is coincident with theoretical calculations

SLIPING CHARACTERISTICS OF DECK BULK CARGOES

Slipping characteristics of 4 kinds of cargos are calculated on 44 kinds active civil ships in China. The loadage distribution of these ships are showed in table 2.

Table 2. Loadage distribution of deck bulk cargo ships which calculated

loadage (tons)	>=1000	>=500	>=250	<250	total
barges without main engines	7	2	9	5	23
ships with main engines	0	3	2	16	21
total	7	5	11	21	44

By analysing the calculated results, we can conclude slipping characteristics of deck bulk cargos as follows.

1. The slipping characteristics of a ship loaded with different cargos are distake. As the load factor of coal is large, the cargo has a high gravity center and can slip easily, and the stability is not very good. As for Korea-iron-ore, it occupies less space, and its gravity center is low. Despite the distance of cargo slipping and the added-capsizing moment is large, the stability within the range of calculated angles is good. Table 3 shows the calculated results of a 1500-ton barge (The entrance angle is 19.5 degrees).

Table 3. Affections to cargo-slipping due to cargo kinds

Kird of cargo	coal	sard	phoshor ore	korea iron-ore
Zg (cargo)(m)	5.319	4.872	4.872	4.778
limited stable angle (deg.)	5	4	6	5
falling angle (deg.)	18	29	37	43
maximum of Ls (m)	.6	.73	.74	.76
correspond angle (deg.)	19.5	19.5	19.5	19.5
maximum of Ls(add) (m)	.12	.19	.18	.20
correspond angle (deg.)	18.0	19.5	19.5	19.5

2. The added capsizing lever are quite different with different grades of loadage carrying same kind of cargo. Before the cargo capsizing over the railing and falling down, the curvature radius of dangerous surface to a bigger loadage is larger, and the added capsizing lever is also larger to make the ship capsizing more easily. Table 4 shows the calculated results of five typical loadages of Korea-iron-ore.

Table 4. Affections to cargo-slipping due to loadage grades

loadage grade (tons)	1500	1000	500	300	100
limited stable angle to cargo slope Qs(deg.)	5	5	7	7	7.5
added statical stab. lever*(m)	.20	.12	.14	.12	.08
added dynamical stab. lever* (m*rad)	.032	.020	.023	.019	.015

*The heeling angle of cargo-slops is 20°

3. With the same loadage grade and the same kind of cargo, due to different deck loading areas the stability of ships has some divergerces. The larger the area of loading deck is and the more spaces can be filled while cargo-slipping. The more difficult for cargo to fall down and the larger added capsizing lever is. Table 5 shows calculated results of three kinds of deck barge loading 1000 tons of coal.

Table 5. Affections to cargo-slipping due to loading areas

kird of barge	1	2	3
length* (m)	46.6	53.4	52.0
width* (m)	8.0	7.7	10.5
high* (m)	1.75	1.8	1.8
falling angle of cargo (deg.)	7	13.5	30

*Deck loading area

4. When capsizing angle is over 30 deg. the variations of stability levers of different kinds of ships and cargos are very complicated and dispersed. Cargos loading on some of ships fall down with large quality. The displacements are decreased, and the form stability levers are increased rotably. The added-capsizing levers of cargo-slipping decrease, ever get negative. In actual slipping, it may appear that recovery of ship after cargo's topple and fall down. Cargos loading on the other ships have not falling. The added-capsizing levers increase rapidly. Fig. 5 and Fig.6 are stability curves for these two kinds of ships. Subscript 2 and 1 indicate the stability levers with or without the affection of cargo-slipping respectively.

5. Based on the above characteristics of cargo-slipping, all of the 188 added-capsizing lever curves have been divided into several groups according to their kinds of cargo and loadage. The curves of added-capsizing lever versus heeling angle, which are arosed by cargo-slipping with different kinds and loadages, can be concluded empirically. Fig.7 shows the added-capsizing lever when loaded with sand. It can be used as a criterion to the stability of deck bulk cargo ships.

SUGGESTIONS ABOUT THE CRITERIA TO STABILITY OF DECK BULK CARGO SHIPS

Based on the above research towards stability of deck bulk cargo ships and characteristics of cargo-slipping, considered the situations in China, suggestions about criteria of the stability of deck bulk cargo ship have been put forwards as follows.

1. When checking stability of a ship, we propose a specific way to the kind of piling up and the limits of the range of cargo's load factor, free slope angle.

2. Considering the affection of cargo-slipping to the stability of a ship, we have to deduce added-capsizing lever of cargo-slipping from statical stability lever, and use the deducted lever to calculate dynamic stability lever. The stability curves after deduction should satisfy the requirements of present standards to ordinary ships.

The aim of above suggestions is to make the present standards of the stability in China more perfect and actual, and to raise recoverability of ships and to avoid large capsizing and cargo-slipping in large scale.

ACKNOWLEDGEMENTS

The theoretical calculations, tests processes and atlas of the research have been authenticated by ZC in June, 1988. They have been accepted and will be used in modifying standards of China civil ships stability in 1990.

Cheng Pir, Ye Lusheng, Jir Darong, Niu Xiehua take part in part work of this research.

REFERENCE

- [1] Yang Dibang, etc, Analysis on Capsizing Mishaps of Deck Bulk Barges in Changjiang River, Reports of the Civil Register of shipping of the P.R.C.(ZC). 1986, Vol. 2. (in Chinese)
- [2] T. Nedrelid, Stability & Safety for Vessels in Rough Weather, 3rd International Conference on Stability of Ship & Ocean Vehicles, 1986.
- [3] IMCO STAB/79, Intact stability of Barges, submitted by the United States.
- [4] Lin Hongbo, etc, Analysis on Capsizing Mishaps of Seagoing Vessels, Science and Technology of ZC, Vol.1.(in Chinese)
- [5] N.R. Morgenstern, V.E.Price, The Analysis of the Stability of General slip surface, Geotechnique, 1965, XV, No.1.
- [6] A.W.Bishop, The Use of the Slip Circles in the Stability Analysis of Slopes, Geotechnique, 1955, Vol.5, No.1.
- [7] W.Fellerius, Calculation of the Stability of Earth dams, Transaction 2nd Congress on Large dams, Washington, D.C. 1986, Vol.4.
- [8] N.Jarbu, Slope Stability Computations, Embankment Dams Engineering, 1973.

Differential strip

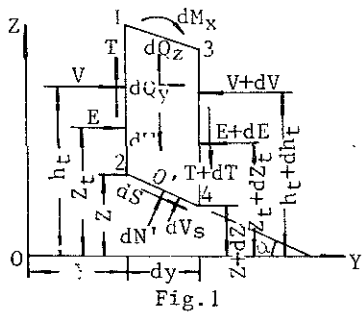


Fig. 1

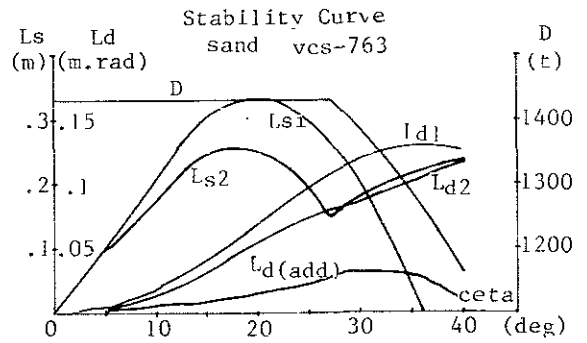


Fig. 5

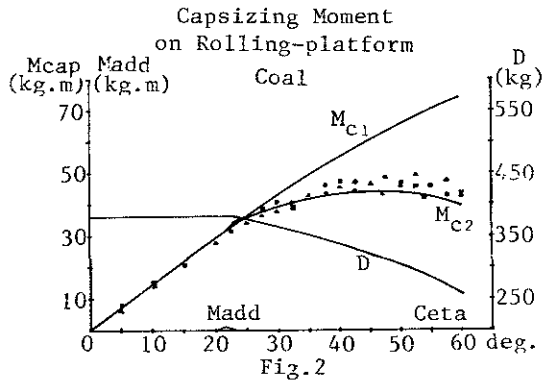


Fig. 2

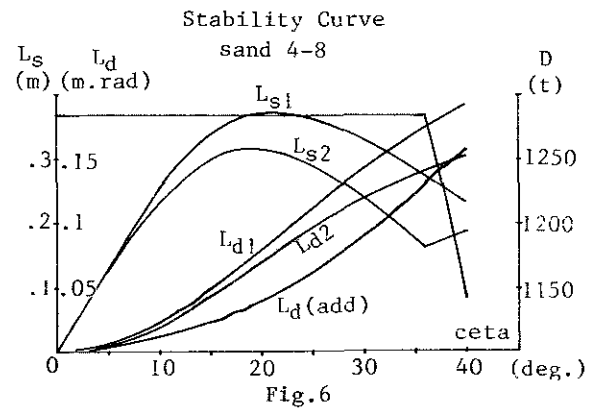


Fig. 6

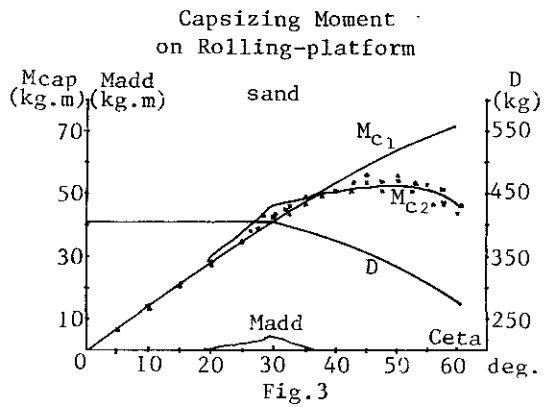


Fig. 3

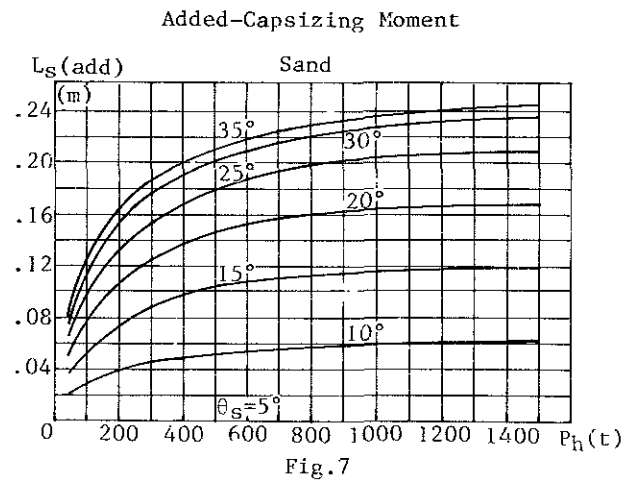


Fig. 7

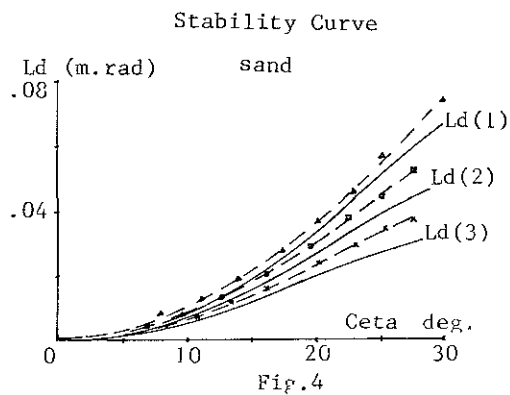


Fig. 4

by A.K. Brook* and R.G. Standing*

ABSTRACT: A review is given of available theoretical methods for determining the roll damping of arbitrary ship forms and their suitability for application to barges with high beam to draught ratios is discussed. Recently, new theoretical methods have been developed to determine the vortex shedding component of the roll damping of a hull section which has an isolated edge and this method is described in the paper. This has been successfully applied to barge sections for a number of beam to draught ratios for a range of bilge keel spans and bilge radii. A correlation is given between the discrete vortex method and selected experimental results which have been obtained for a range of barge sections. For comparison purposes theoretical results are also shown from Tanaka's and Ikeda's empirical methods which are applicable to normal ship forms. From the correlation with the experimental results the discrete vortex method is identified as a reliable method for determining the roll damping of barges. The final part of the paper considers the motion responses of barges in an irregular sea-way. The variation in motion responses for each of the different theoretical roll damping methods is quantified to highlight the sensitivity of barge roll response to the accuracy of the roll damping coefficients.

1 INTRODUCTION

The motion of many large volume displacement vessels in a sea-way can be determined from theoretical methods which assume that the response in a regular wave can be represented by a linear theory. This assumption is valid for all motions with the exception of the roll, where for wave frequencies in the neighbourhood of the vessel's natural frequency, non-linear viscous roll damping effects give a significant contribution to damping the roll motions. Hence, if only the linear potential-flow term is used for the roll damping, large roll responses are predicted at resonant frequencies.

The necessity of including non-linear, viscous roll damping terms has been recognised for a number of years and they are included in the majority of the available seakeeping programs for monohulls, such as that of Salvesen et al [Ref.1]. The non-linear damping terms are usually included in the roll equation as an additional equivalent linear damping term which depends on the roll amplitude. This results in an iterative solution being required to determine the roll response but the harmonic time dependence of the linear equations can still be removed and hence the response amplitudes can be determined for a given regular unit wave amplitude at a particular frequency.

The non-linear roll damping contribution is also important for barges as well as for conventional monohulls. In each case the major contribution to the viscous roll damping arises due to vortices being shed from sharp corners on the bare hull and appendages such as bilge keels. The

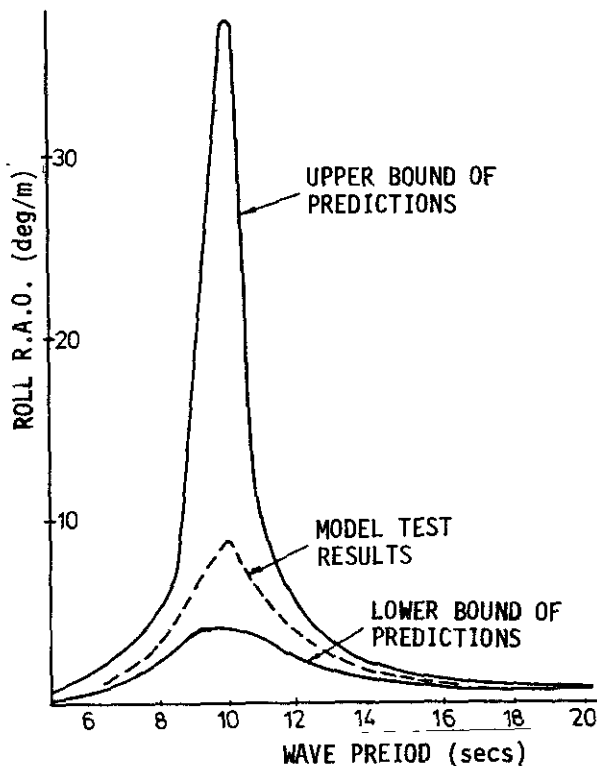


Fig.1 Range of Roll Response Predicted with Different Empirical Methods for the Vortex Roll Damping Component of Barges [Ref.2]

importance of including viscous roll damping effects for barges has been discussed by Stewart [Ref.2]. Figure 1 shows the range of the roll response predicted with different empirical methods for the viscous roll damping. A number of empirical methods are available to determine the viscous roll damping of a vessel and the most notable ones are Ikeda's [Ref.3] and Tanaka's [Ref.4]. In each

* British Maritime Technology, U.K.

case, a two-dimensional stripwise approach is used, where the contribution for a number of selected sections is calculated along the vessel length due to local hull geometry and the presence of appendages such as bilge keels. This approach neglects any interaction effects between sections and this may be significant particularly for vessels at forward speed. In the case of transportation barges, the forward speed will probably be low and hence a two-dimensional strip approach is likely to give reasonable results. However, existing empirical methods have been developed on the basis of limited experimental data for conventional ship forms and an assessment of their general applicability has been given in Ref.[5].

The beam to draught ratio of most transportation barges is larger than conventional hull forms and it is questionable whether existing empirical methods are suitable for such cross-sectional shapes. In fact Fig.1 shows for the programs considered that the theoretical motion response of the barge with viscous roll damping included, can be considerably greater than or less than that measured in model tests. As part of an earlier programme of research the roll damping and motion response of selected barges has been measured and correlated with theoretical methods [Ref.6]. Following this study a new theoretical method was developed by Imperial College and BMT, where the viscous roll damping was determined by modelling the generation of vortices into the neighbouring fluid from sharp corners and appendages. This earlier work was correlated with limited model tests and in order to further assess the reliability of the DVM method a systematic series of model tests has been undertaken on uniform rectangular sections. A range of beam/draught ratios, bilge radii and bilge keel sizes were considered. A summary of the correlation between these experimental results and the theoretical methods is given in this paper following a more detailed discussion of the discrete vortex method.

2 APPLICATION OF THE DISCRETE VORTEX METHOD TO BARGE SECTIONS

The generation of vortices in oscillatory flow has been studied extensively in connection with wave motion around cylinders. The intensity of the vortex shedding depends on a number of factors, such as surface roughness, but primarily on the Keulegan-Carpenter number K_C defined by

$$K_C = \frac{U_m \bar{T}}{D} \quad (1)$$

where U_m is the maximum relative velocity of the fluid, \bar{T} the period of oscillation and D is the body diameter.

If the body is oscillating in a stationary fluid, the shedding of vortices is similar and is related to the value of the

Keulegan-Carpenter number. For an oscillating cylinder in a stationary fluid the vortices do not become detached from the body at low values of K_C , whilst at values between about 8 and 15 the vortices detach at various points in time during the cycle. As K_C increases to 25 the vortices are shed discretely at a greater frequency during the whole of the cycle. A similar phenomenon exists with a rolling ship section which has either sharp corners or bilge keels. The intensity of the vortex shedding depends on a Keulegan-Carpenter number defined in terms of a characteristic length, the roll amplitude and roll period. The bilge radius or bilge keel span is used as the characteristic length where appropriate.

The discrete vortex method (DVM) was applied to rectangular sections by Graham [Ref.7]. Application to barges has been made by Downie [Ref.8] and Cozens [Ref.9], who also extended the method to arbitrary ship sections. A detailed review of this earlier work has been given by Standing et al [Ref.10]. In applying the DVM method to rolling sections the point of flow separation is assumed to be fixed at either the corner, for a rectangular section, or at the bilge keel edge. If a rounded bilge is present with no bilge keel the method is less successful since the point of separation needs to be fixed at some assumed location but in reality its position is uncertain. The DVM involves a time simulation of the separating shear layers which are represented by arrays of isolated point vortices which are introduced into the flow near the separation point. The numerical simulation then represents the formulation of larger vortices from the discretized shear layers and the convection of these vortex groups around the body. Groups of vortices which can be recognised as rolled-up sheets far from the shedding edge are progressively wound into a central core vortex and hence individual vortex elements are effectively destroyed.

Flow visualisation experiments were undertaken by both Downie [Ref.8] and Cozens [Ref.9] using dye which was injected at the assumed shedding edge for a rectangular section which was force rolled. Cozens also compared the numerical simulation of the vortex behaviour with the flow visualisation experiments and a typical comparison is shown in Fig.2 where it can be seen that the correlation between theory and experiment is good.

The force acting on the body due to the vortices can be obtained either by integrating the pressures on the surface using Bernoulli's equation or through the application of the Blasius equation. A drag coefficient is defined by

$$C_D = \frac{3\pi}{4T} \int_0^T \frac{F_v(\tau/T)}{\frac{1}{2} \rho U_m^2 L} \cos \frac{2\pi\tau}{T} d\tau. \quad (2)$$

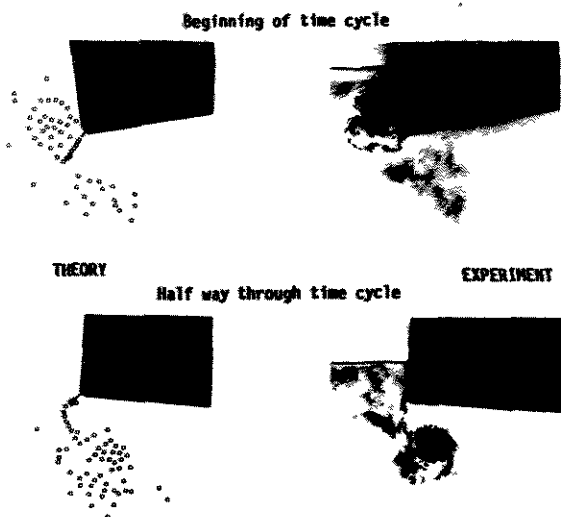


Fig.2 Comparison between Experimental Flow Visualisation and DVM Predictions (Barge with Rounded Edge and Bilge Keels)

$F_v(t/T)$ is the instantaneous force at time t , L is a length scale and the uniform flow is defined by

$$U = U_m \cos \frac{2\pi T}{T} \quad (3)$$

The simulation is undertaken over a number of cycles and the drag coefficient is calculated after each cycle. The drag coefficient converges to a fixed value after typically 5-10 cycles. An inertia coefficient is calculated in a similar manner and, because of the isolated edge assumption, in applying the method to barges the drag and inertia coefficients can be determined for corner sections independent of the local section geometry. Hence the drag and inertia coefficients of a right-angled corner section of infinite extent can be determined for a range of bilge keel radii and bilge keel spans. Figure 3 shows the drag coefficients C_D which have been calculated for a square edge for a range of bilge keel radii and bilge keel spans. The roll damping coefficient of a particular sectional shape is determined from the drag and inertia coefficient and the lever arm between the centre of pressure of the force and the specified roll axis. The bilge keel span and bilge radius are both non-dimensionalised with respect to a length scale which depends on the local sectional geometry and the drag coefficient is obtained from Fig.3 based on these non-dimensional values.

A number of other authors have applied DVM techniques to determine the roll damping of barges. The most notable work is that of Braathen and Faltinsen [Ref.11] who give a comparison of the drag coefficient for a barge with Tanaka's [Ref.4] and Downie's [Ref.8] results as shown in Table 1. The agreement between the two DVM methods is within 4% but the empirical Tanaka method which is applicable to conventional ship forms underpredicts the damping by 25%.

The DVM method which has been developed by Downie [Ref.8] and Cozens [Ref.9] assumes

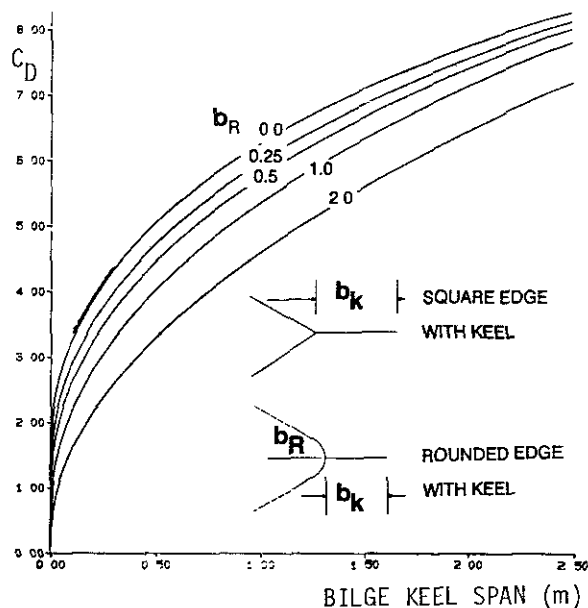


Fig.3 Drag Coefficient C_D for Square Edge of Infinite Extent for a Range of Non-dimensional Bilge Radii and Bilge Keel Spans

that the free surface is rigid. Braathen and Faltinsen [Ref.11] have extended this approach to allow for the effect of the free surface and a comparison is given for selected cases with and without a free-surface as shown in Table 2. $B_{44}(R)$ is the sum of the vortex shedding component from the DVM method with a rigid free surface and the wave damping component obtained from a seakeeping program. $B_{44}(F)$ is the total vortex and wave damping components obtained from the DVM method with a free surface. Except for small roll periods (less than 8 seconds) the results are in reasonable agreement and since the natural roll period of barges is normally between 8 and 16 seconds the inclusion of the free surface, although desirable, does not seem to be critical. The results which are presented in the next two sections are based on the DVM method of Cozens [Ref.9] which assumes a rigid free surface and the wave damping component is obtained from a seakeeping program.

The DVM method is most reliable for cases where a well defined shedding edge is present, and for a section with rounded bilges and no bilge keel the method fails to give stable drag coefficients when a simulation is undertaken over a number of periods of oscillation. The results shown in Fig.3 with $b_k = 0$ have been obtained by extrapolating the data obtained with a bilge keel. Fortunately the method is still reliable for very small bilge keel

Table 1 : Vortex Roll Damping Coefficient for a Barge Section [Ref.11]

Method	Coefficient
Tanaka [Ref.4]	0.40
Downie [Ref.8]	0.50
Braathen [Ref.11]	0.48

Table 2 : Influence of Free Surface in DVM
[Ref.11]

Roll Period (secs)	Roll Amplitude (degs)	$\frac{B_{44}(R)^{\#}}{B_{44}(F)^{*}}$
16	10	1.08
8	10	1.05
8	5	1.09
4	10	1.31
4	5	1.38
2.6	5	1.38

$B_{44}(R)$ - Total damping with rigid free surface.

* $B_{44}(F)$ - Total damping with free surface.

spans so that the curves are well defined close to $b_k = 0$. In the earlier work reported in Ref.[6], however, it was found that these results still gave poor correlation with available model test results as shown in Fig.4 and in order to provide a better estimate Robinson [Ref.12] has formulated an empirical correction for a barge section with rounded bilges and no bilge keel. The correction is applied to the roll damping for a sharp cornered section B_{44C} with no bilge keel and is given by

$$B_{44R} = B_{44C} \left[1 - e^{-0.006K_{CB}^2} \right] \quad (4)$$

where
$$K_{CB} = \frac{\pi r_K \varphi_A \omega}{b_R \omega_N} \quad (5)$$

K_{CB} is the bilge Keulegan-Carpenter number; r_K is the distance from the roll centre to the bilge tangent; φ_A is the roll amplitude; ω is the roll frequency; b_R is the bilge radius and ω_N is the roll natural frequency. Figure 4 shows that this empirical correction gives better agreement

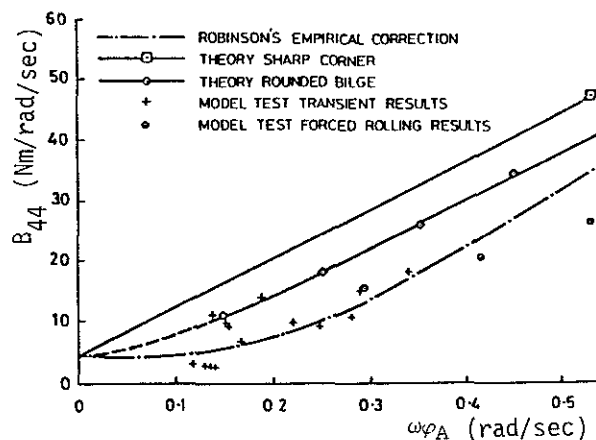


Fig.4 Comparison of Roll Damping Coefficient for Round Cornered Barge from DVM Calculation, Robinson's Correction Method and Experimental Results

Table 3 . Summary of Barge Section Geometries Tested

Draught	40, 60, 120 mm
B/T	15, 10, 5
Bilge Keel Span	0, 10, 20 mm
Bilge Radius	0, 10, 30 mm
Roll Centre	127, 180 mm

with experimental data than applying the DVM method directly to a section with rounded bilges. This method has been further evaluated for the extensive experimental results which have been used to correlate with the DVM method as discussed in the next section.

3 CORRELATION BETWEEN THEORETICAL AND EXPERIMENTAL ROLL DAMPING COEFFICIENTS

An extensive experimental programme of tests has been undertaken on barge sections in order to provide data which can be correlated with the discrete vortex method. Both forced roll and free-decay tests were undertaken and thirty different barge geometries were tested as summarised in Table 3 in order to investigate the effects of draught, bilge keel span, bilge radius and roll centre variations. Forced roll tests were undertaken at the natural frequency and at two other frequencies. The wave damping component was obtained from an analysis of the measured radiated wave. The total damping was obtained from the free decay angles in the case of the free decay tests and the measured roll angles and roll moment for the forced roll tests. An equivalent lineal damping coefficient was obtained in both cases using techniques described in Ref [13]. Figure 5 shows a typical correlation of the wave damping component at three frequencies and the agreement is reasonable between theory and experiment at the two highest frequencies. In addition to a wave damping and vortex shedding component there is a

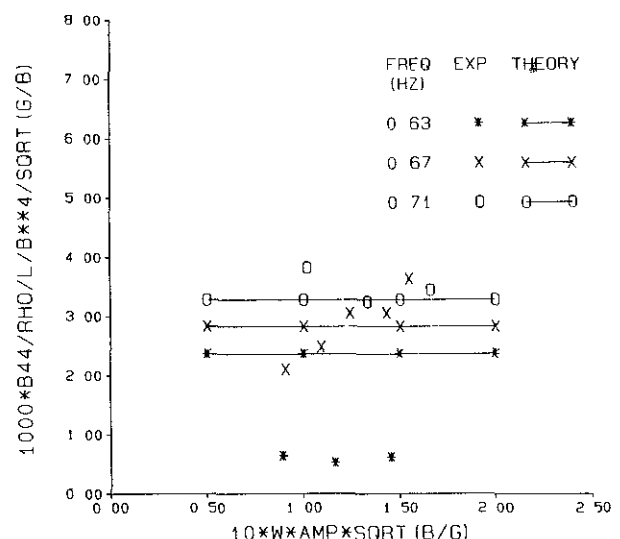


Fig.5 Correlation of Theoretical and Experimental Wave Damping Component for Barge Section (Draft 60mm, Bilge Radius 10mm, Bilge Keel Span 0mm)

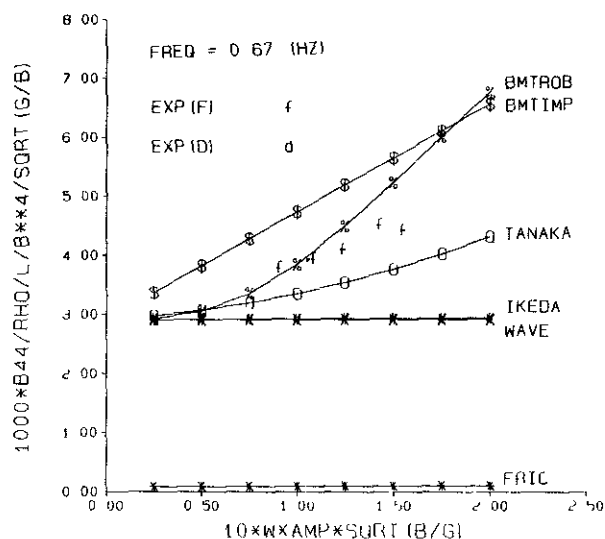


Fig.6 Correlation of Theoretical and Experimental Damping Components for Barge Section (Draft 60mm, Bilge Radius 10mm, Bilge Keel Span 0mm)

small frictional component which has not been measured experimentally as a separate contribution but as shown, in Figs.6 and 7 it is virtually negligible in comparison to the other components. These two figures show the total measured damping for a barge section with a rounded bilge with and without a bilge keel. The theoretical damping from the DVM (BMTIMP), Tanaka's and Ikeda's methods are shown for comparative purposes. The case with no bilge keels (Fig.6) also shows the application of Robinson's empirical correction to the sharp cornered results. From the trend of the forced roll results it is apparent that both the DVM and Robinson's methods both significantly overpredict the damping in this case at large roll amplitudes.

Figure 7 shows that for a rounded section with a bilge keel the DVM method gives good agreement but that both the Ikeda and Tanaka methods significantly overpredict the damping. The free decay and forced roll experimental results are consistent in this case but for some of the experiments the agreement was poor probably due to some bearing friction being present for the forced roll tests. This was particularly pronounced for rounded sections with no keels which have very low damping characteristics. A feature of most of the tests undertaken was that the wave damping component was a significant proportion of the total damping (typically between 50 and 75% depending on such factors as draught and bilge keel dimensions).

Generally the DVM method gave the best correlation for all the conditions tested although in some cases the agreement was not as good as shown in Fig.7. The Ikeda method gave very poor correlation for sections with no bilge keel and as shown in Fig.6 the vortex shedding component was predicted to be negligible for the case considered. On the other hand Tanaka's method was found to consistently overpredict the damping for sections with bilge keels and, as

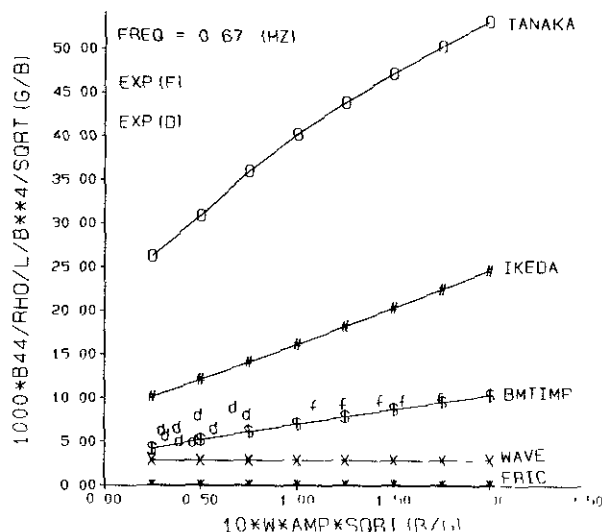


Fig.7 Correlation of Theoretical and Experimental Damping Components for Barge Section (Draft 60mm, Bilge Radius 10mm, Bilge Keel Span 20mm)

demonstrated in Fig.7 this was more pronounced for high beam to draught ratios. For rounded sections with no bilge keels the use of Robinson's empirical correction gives reasonable agreement at small roll amplitudes but overpredicts at large roll amplitudes and neither method is ideal for this case.

From the correlations which were undertaken it has been demonstrated that both Ikeda's and Tanaka's empirical methods are unsuitable for general application to barge sections and that the discrete vortex method provides a more reliable method. A limited number of tests were also undertaken on ship sections and the DVM method has been extended to allow for arbitrary ship sections with and without bilge keels. The correlation was generally poor and either Ikeda's or Tanaka's methods are more suitable for conventional hull forms. Although the DVM could probably be developed further to give better correlation for conventional hull forms it would not be possible to pre-compute the drag and inertia coefficients in the same way as for barges. The difficulties of undertaking extensive simulations to determine the drag of each section of a conventional ship form would probably exclude the method as a practical design tool.

4 ROLL RESPONSE OF TRANSPORTATION BARGES

The roll damping of ocean going transportation barges needs to be determined to a reasonable accuracy in order to determine the roll motion response as shown in Fig.1. The influence of the vortex shedding component has been investigated previously by a number of authors such as Robinson [Ref.12]. Many of the references relate to work undertaken under the earlier Noble Denton Study [Ref.6] but a number of other studies have been undertaken such as that reported by deBord [Ref.14]. A discussion of the intact stability and motion characteristics

Table 4 : Barge General Particulars and Loading Conditions

Lpp (m)	91.5		
B (m)	30.5		
T (m)	3.8		
B/T	8		
Δ (tonnes)	9700		
\bar{T} (secs)	9	12	15
KG (m)	10	13	15
GM (m)	14	11	9
K_{ϕ}/B	0.55	0.65	0.74

of barges from an operator's viewpoint has been given by Kossa [Ref.15] and factors such as the high centre of gravity and shallow draught are discussed.

The roll motion of the barge specified in Table 4 has been calculated for three loading conditions corresponding to natural roll periods of 9, 12 and 15 seconds which are typical operating conditions. The roll damping has been calculated using the discrete vortex method for the barge with a square edge, rounded bilge and a rounded bilge with a bilge keel. Results from Ikeda's and Tanaka's method are shown for comparative purposes in Table 5. The variation of the regular roll response with wave frequency is shown in Fig.8 for the barge with square edges and as expected the Ikeda and Tanaka methods predict significantly larger roll responses than the DVM method. This is also demonstrated in Table 5 by the value of the RMS roll in a 5 metre significant wave height which has an average wave period of 8 seconds (this is close to the natural roll period of 9 seconds). The Ikeda and Tanaka methods give the same damping coefficients for a rounded bilge as a square-edge and this highlights the inadequacies of the methods for applications to barges. The damping coefficients are in much closer agreement for the case with a bilge keel although the damping for the Tanaka method is highest resulting in a lower roll response. These trends are consistent with that shown in Figs.6 and 7 where the Ikeda method

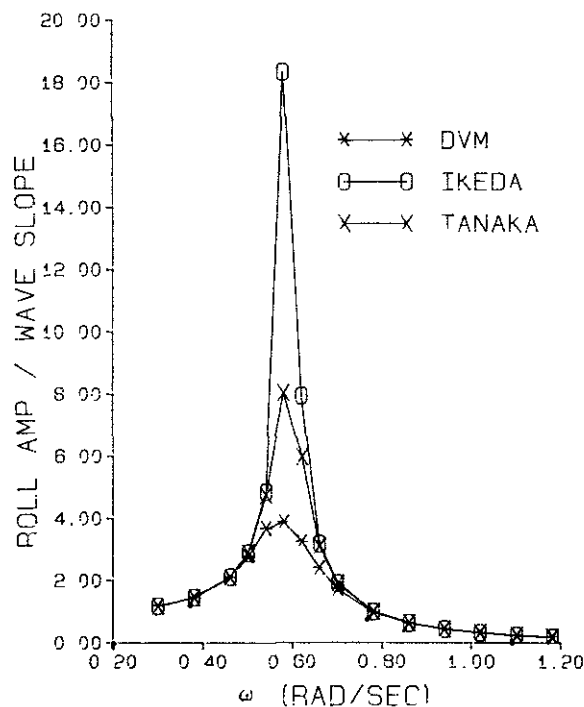


Fig.8 Comparison of Roll RAO with DVM, Ikeda and Tanaka Roll Damping Coefficients

predicted virtually no vortex damping for sections with no bilge keel and the Tanaka method overpredicted the damping for sections with bilge keels. The motion responses shown in Fig.8 and Table 5 emphasize that the ship based damping methods of Ikeda and Tanaka are unsuitable for application to transport- ation barges with shallow draughts and high beam to draught ratios.

The Robinson correction method given by equation (4) has been compared in Table 5 with the direct DVM method and although the non-linear damping is larger the negative linear term results in a slightly larger RMS roll response. The damping coefficients shown in Table 5 exclude the wavemaking damping which is determined in the seakeeping program and a negative damping will not occur in practice when this component is added to the vortex shedding terms. A negative coefficient can occur because B_1 and B_2 are obtained from a least square fit to the equivalent linear damping calculated over a range of roll amplitudes. B_1 represents the intercept at the origin (zero roll amplitude) and B_2 the slope of the equivalent linear damping which arises due to the assumption of a quadratic non-linear damping. In practice the equivalent linear damping does not vary linearly with roll amplitude as shown in Figs.6 and 7, particularly for the Robinson correction (BMTROB) and Tanaka's method. The damping coefficients B_1 and B_2 are consistent with the uncoupled non-linear roll equation

$$(I+a_{44})\ddot{\phi} + (B_w + B_1)\dot{\phi} + B_2\phi = F(t) \quad (6)$$

where I is the moment of inertia, a_{44} is the added mass moment of inertia and B_w is

Table 5 : Roll Damping Coefficients and RMS Responses for Different Theoretical Methods ($\bar{T} = 9$ secs)

Bilge Condition	Method	B_1 $2\omega(I+a_{44})$	B_2 $2(I+a_{44})$	RMS Roll (degs) $\xi_{1/3} = 5m$ $\bar{T}_p = 8$ secs
Square Edge	BMTIMP	0.00	0.86	5.1
	IKEDA	0.00	0.01	13.4
	TANAKA	-0.01	0.22	8.1
Round Edge ($b_R = 0.5m$)	BMTIMP	0.00	0.79	5.2
	BMTROB	-0.04	1.00	5.4
	IKEDA	0.00	0.01	13.4
	TANAKA	-0.01	0.22	8.1
Round Edge with Bilge Keel ($b_K = 0.5m$)	BMTIMP	0.02	1.14	4.4
	IKEDA	-0.01	1.35	4.5
	TANAKA	0.09	1.36	3.3

the wave damping component obtained from a seakeeping program. The vortex shedding damping coefficients shown in Table 5 have been calculated at the natural period of the vessel and since the coefficients vary only slightly with wave frequency they are applied at all frequencies in the seakeeping program in the regular response calculations by obtaining an equivalent damping term

$$B_2 \dot{\phi} \left| \dot{\phi} \right| = \frac{8}{3\pi} \varphi_A \omega \dot{\phi} B_2 \quad (7)$$

The roll damping coefficients for all three loading conditions shown in Table 4 have been determined and the non-linear DVM coefficients vary by at the most 8% whereas the Tanaka coefficient varies by as much as 30% due to the sensitivity of the method to the position of the vertical centre of gravity. The barge's roll response in irregular shortcrested seas is shown in Table 6 for each loading condition for three significant wave heights, using the DVM and Robinson's correction methods where applicable for the vortex damping components. As expected the highest roll response occurs for the condition with the smallest natural roll period since the other conditions have natural roll periods which are much greater than the average wave period.

The results which have been presented are for a barge at zero speed which is probably acceptable due to the low tow speeds used for transportation barges. No reliable methods exists to include the speed effect for the DVM method and as discussed in Ref.[5] the existing methods for including speed effects for conventional monohulls are unreliable and hence should not be applied to barges. The motion responses which have been presented have neglected non-linear effects due to the restoring moment, deck-edge or cargo immersion and non-linear wave loading due to the shallow draught and the possibility of wave impact on overhanging loads as discussed by a number of authors such as Robinson [Ref.12] and Patel [Ref.16]. Other effects such as the accelerations are also important, particularly for large volume cargoes and the accuracy of the horizontal acceleration obviously depends on the reliability of the roll damping.

5 CONCLUSIONS

Previous studies reported in Ref.[6] have indicated that existing theoretical methods for determining the vortex shedding of conventional ship forms are unsuitable for application to transportation barges which have high beam to draught ratios and a large variation in the vertical position of the roll centre. In an earlier study the discrete vortex method was demonstrated to give more reliable damping coefficients for barges with sharp corners or bilge keels [Refs.6 & 12]. A detailed description of the DVM method has been presented in this paper together with a discussion of a correlation which has been undertaken with

Table 6 : RMS Roll Response in Short-Crested Seas for Different Loading Conditions

Bilge Condition	Barge Natural Period (secs)	RMS Roll (degs)		
		$\xi_{1/3}(m)$ $[\bar{T}_p(secs)]$		
		3 [7]	5 [8]	8 [9.5]
Square- * Edge	9	2.6	5.1	8.2
	12	1.0	2.5	5.7
	15	0.5	1.0	2.8
Round- # Edge ($b_R = 0.5m$)	9	2.8	5.4	8.7
	12	1.1	2.8	6.3
	15	0.5	1.0	3.0
Round- * Edge with Bilge Keel ($b_K = 0.5m$)	9	2.3	4.4	7.0
	12	1.0	2.3	4.9
	15	0.5	1.0	2.5
* BMTIMP # BMTROB				

an extensive series of model tests for a range of barge sections with varying beam to draught ratios, roll centres, bilge radii and bilge keel spans.

A practical design method has been developed based on the DVM method so that the vortex shedding component of transportation barges can be determined for a range of beam to draught ratios for a square edge and in addition for a range of bilge radii and bilge keel spans. The Robinson empirical correction [Ref.12] which can be applied to rounded sections with no bilge keel gives reasonable agreement with the direct DVM method which takes account of the bilge radius.

The roll motion of a typical transportation barge has been determined for three loading conditions which represent typical cargoes which have different vertical centre of gravities or natural roll periods. The motion characteristics confirm that the conventional ship based empirical methods of Ikeda and Tanaka are unsuitable for application to transportation barges. The DVM method which has been discussed and evaluated in this paper provides a reliable means of determining the roll damping component due to vortex shedding and it can be used in conjunction with any existing seakeeping program. Alternatively it could be used in a time domain analysis which could be developed to investigate non-linear restoring, wave-load and cargo immersion effects.

ACKNOWLEDGEMENTS

The authors would like to acknowledge BP Engineering Ltd., Elf U.K., Shell Expro and BMT who jointly sponsored much of the work reported in this paper and who authorised publication of the results.

REFERENCES

- [1] SALVESEN, N. et al. Ship Motions and Sea Loads. Trans. SNAME, 1970.
- [2] STEWART, W.P. et al. Non-linear Marine Barge Motion Response. Proc. Conf: 'Offshore Structures - The Use of Physical Models in their Design'. Watford, England, Nov. 1979.
- [3] IKEDA, Y. A Prediction Method for Ship Roll Damping. Report No.00405, Department of Naval Architecture, University of Osaka, Japan, 1978.
- [4] SCHMITKE, R.T. Ship Sway, Roll and Yaw Motions in Oblique Seas. Trans. SNAME, 1978.
- [5] BROOK, A.K. Evaluation of Theoretical Methods for Determining Roll Damping Coefficients. RINA Spring Meetings, April 1989.
- [6] Report on the Prediction of Roll Damping of Transportation Barges, Final Phase - Barge Motions Research Programme for Noble Denton and Associates. NMI Report, Project No.20009, November 1985.
- [7] GRAHAM, J.M.R. Force on Cylindrical Bodies in Oscillatory Flow at Keulegan-Carpenter Numbers. Mechanics of Wave Induced Forces on Cylinders. Ed. by T.L. Shaw, 1979.
- [8] DOWNIE, M.J. et al. Prediction of the Roll Damping of Barges Including the Effects of Vortex Shedding. Dept. of Aeronautics, Imperial College, Report R.188, 1984.
- [9] COZENS, P.D. Numerical Modelling of the Roll Damping of Ships due to Vortex Shedding. PhD Thesis, September 1987, Dept. of Aeronautics Imperial College, London.
- [10] STANDING, R.G. et al. Numerical Prediction of Roll Damping and Response of Ships and Barges, based on the Discrete Vortex Method. Computer Modelling in Ocean Engineering, Ed. B.A. Schrefler and A.C. Zienkiewics. Published by A.A. Balkema, Rotterdam, 1988, p.567-579.
- [11] BRAATHAN, A. and FALTINSEN, O.M. Application of a Vortex Tracking Method to Roll Damping. Advances in Underwater Technology, Ocean Science and Offshore Engineering, Vol.15, Technology Common to Aero and Marine Engineering, 1988.
- [12] ROBINSON, R.W. and STODDART, A.W. An Engineering Assessment of the Role of Non-linearities in Transportation Barge Roll Response. TRINA, 1987.
- [13] SPOUGE, J.R. Non-linear Analysis of Large Amplitude Rolling Experiments. Int. Shipbuilding Progress, 35, No.403, 1988.
- [14] DEBORD, F. et al. Measurement of Full-Scale Barge Motions and Comparisons with Model Test and Mathematical Model Predictions. Trans SNAME, 1987.
- [15] KOSSA, M.M. Stability and Roll Motions of Ocean Barges. Proc. 4th Int. Tug Conv. 1975.
- [16] PATEL, M.H. On the Prediction of Resonant Roll Motions for Flat-Bottomed Barges. TRINA, 1985.

A NOTE ON SURGING AND LOSS OF CONTROL OF SMALL
FISHING VESSELS IN SEVERE FOLLOWING SEAS

M.R. RENILSON¹ G.A. THOMAS²

It has long been established that the behaviour of a small vessel in a following sea is determined by the longitudinal surging and surf riding caused by the waves.

Experiments have been carried out to investigate the surging forces applied by the waves and this is related to the reduction of rudder effectiveness in the waves and hence to the likelihood of broaching.

INTRODUCTION

It is known that vessels travelling in steep following seas can become uncontrollable and broach-to with potentially disastrous consequences (1).

Recently, work done by one of the authors and by others (2,3,4,5) has shown that broaching-to occurs when the wave induced yawing moment exceeds the yawing moment available from the rudder for a sufficient length of time to allow a large yaw-rate to build up. As both the rudder effectiveness and the yawing moment from the wave are functions of the longitudinal position of the vessel in the wave this means that a critical longitudinal position relative to the wave can be identified (6). Hence, if sufficient time is spent in this critical position a broach is likely.

In addition, the wave imposes a longitudinal force on the vessel which is also a function of the relative position of the vessel to the wave. When the encounter frequency is low this longitudinal force can dominate the vessels behaviour causing surging with a mean speed greater than that in calm water. This is because the vessel spends more time in the part of the wave with the greatest forward force. In the extreme case this longitudinal force may cause the vessel to travel at wave speed - a phenomenon known as surf riding.

Unfortunately, for waves between about one to two times the ships length the region where the longitudinal force is greatest also coincides with the largest yawing moment and the lowest rudder effectiveness.

In order to investigate the longitudinal force on the vessel and the loss in rudder effectiveness caused by the wave, captive model experiments were carried out on a trawler model at a low frequency of encounter in steep regular waves.

¹Senior Lecturer, Ship Hydrodynamics Centre, Australian Maritime College, Tasmania, Australia 7250.

²Research Assistant, Ship Hydrodynamics Centre, Australian Maritime College, Tasmania, Australia 7250.

EXPERIMENTAL PROCEDURE

The 1/15 scale model used in the study was that of a Success Class Trawler, this is a 25 metre stern trawler built by Australian Shipbuilding Industries (WA), Fig. 1,2. The model was set up with an adjustable rudder (an all moveable rudder with bottom support). Details of the stern geometry are shown in Fig. 3. At this stage in the investigation the model was not fitted with a propeller.

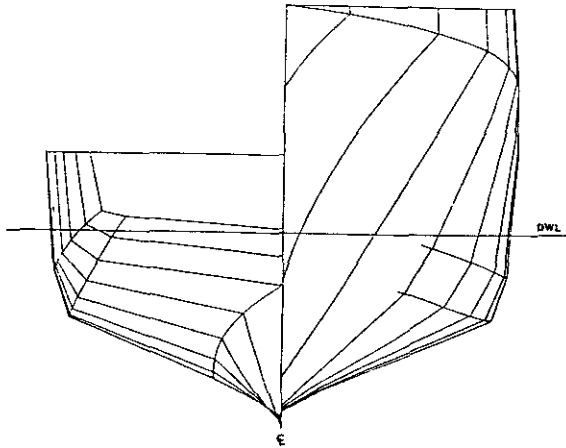


Figure 1 Body Plan

	Full Scale Vessel	Model
Length BP	22.05m	1.470m
Beam W.L.	7.31m	0.487m
Draught	3.00m	0.200m
Displacement	204 tonnes	58.970kg
Longitudinal Centre of Buoyancy	0.74m aft of amidship	0.049m aft of amidship
Rudder Area	2.64m ²	0.0118m ²
Rudder Aspect Ratio	1.838	1.838

Figure 2 Principal Particulars

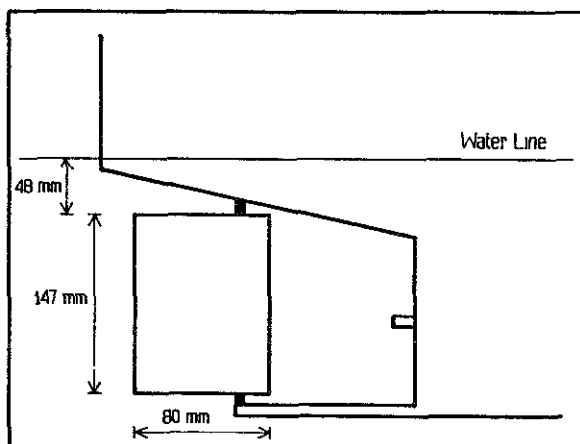


Figure 3 Stern Profile of Model

The tests were carried out in the 60m towing tank of the Ship Hydrodynamics Centre at the Australian Maritime College. (For further details of the Centres facilities see Ref. 7.

The model was free in heave, pitch and roll, thus the forces in surge, sway and yaw were measured. A wave probe was fixed in line with the forward perpendicular of the model in order to measure the wave height and also determine the relative position of the model and the wave crest. The data was recorded using an IBM-PC mounted on the carriage sampling at the rate of 100 samples per second for a period of 15 seconds.

Three waveheights were tested at a constant wave frequency. The wave length chosen corresponded to approximately $\lambda/L = 1.2$ which from previous work has been shown to be that most likely to cause broaching-to. The smallest wave was non-breaking, the next was on the verge of breaking whilst the steepest was a fully breaking wave. Due to the steepness of the waves non-linearities caused the wave celerity and length to vary with height (see Appendix).

$$\omega L/g^{1/2} = 2.255$$

h/λ	λ/L	Fn for $\omega_s = 0$
0.0783	1.310	0.470
0.0968	1.351	0.485
0.1110	1.387	0.498

Figure 4 Principal Wave Particulars

The aim of the experiments was to determine the variation in the values of rudder effectiveness (N_δ) and longitudinal force (X_ξ) over the wave length. In order to avoid any possible frequency effects the model was towed at close to wave speed and hence the encounter frequency was approximately equal to zero. For this reason a number of runs had to be made for each wave to ensure results were obtained over the complete wave length.

RESULTS AND DISCUSSION

Longitudinal Forces

The usual method for non-dimensionalising forces is:-

$$X' = \frac{X}{\frac{1}{2}\rho V^2 L^2} \quad (1)$$

This was felt to be inappropriate in this case as:-

- (i) The longitudinal wave force is deemed to be independent of vessel speed for small encounter frequencies.
- (ii) The wave height and vessel beam would have greater influence, than the vessel length, on the longitudinal wave force.

Thus the following non-dimensionalising method for the Longitudinal force was adopted.

$$X^* = \frac{X}{\frac{1}{2}\rho c^2 h B} \quad (2)$$

In order to determine the longitudinal wave force from the total measured force, the resistance of the model in calm water was deducted as follows:-

$$X_{\text{WAVE}} = X_{\text{MEASURED}} - X_{\text{RESISTANCE}}$$

This was then non-dimensionalised and plotted as a function of the non-dimensional position of the wave crest relative to the ships stern, ($\xi = X_w/\lambda$), see Fig. 5).

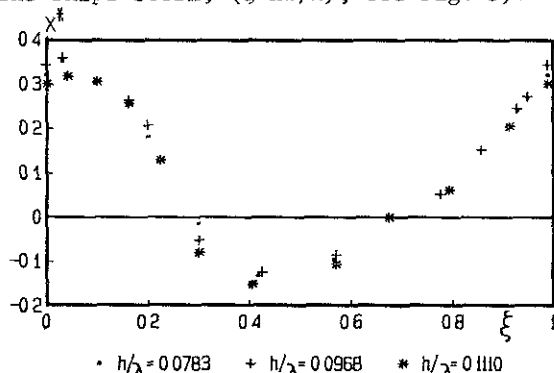


Figure 5 X^* for Varying ξ

As can be seen from this Figure the results from the three different wave heights all collapse essentially to the same curve. Thus for the range of wave heights tested a single curve of X^* against ξ can be drawn, Fig. 6.

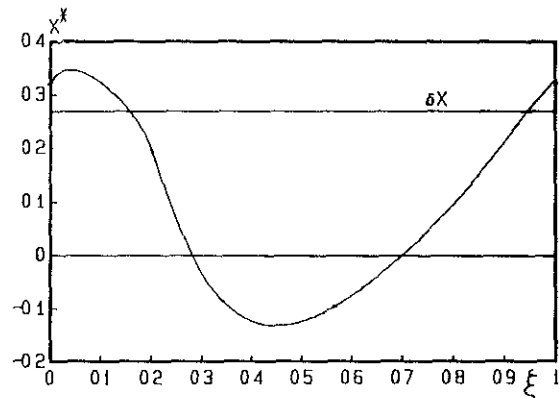


Figure 6 X^* for Varying ξ

From this curve an indication of the vessels behaviour in the wave can be obtained. In order for longitudinal equilibrium to be achieved the force from the wave must balance the difference between the vessel resistance at wave speed and the thrust available from the propeller.

For any given wave height, speed and propeller revs this can be calculated and plotted as a horizontal straight line. From this it is possible to identify any points of longitudinal equilibrium.

$$X^* = \frac{X_{\text{PROPELLER}} - X_{\text{RESISTANCE}}}{\frac{1}{2}\rho c^2 h B} \quad (4)$$

For example Fig. 6 indicates two positions where this occurs: when $\xi = 0.16$ and $\xi = 0.95$. At $\xi = 0.16$ there exists a position of unstable equilibrium since a decrease in ξ results in an increase in X^* thereby increasing the acceleration and hence producing a smaller ξ . Similarly when $\xi = 0.95$ represents a stable position of equilibrium, and is thus the point on the wave that the vessel will spend most time.

Rudder Effectiveness

The values of the rudder derivative obtained from the experimental data were plotted as functions of ξ (see Fig. 7).

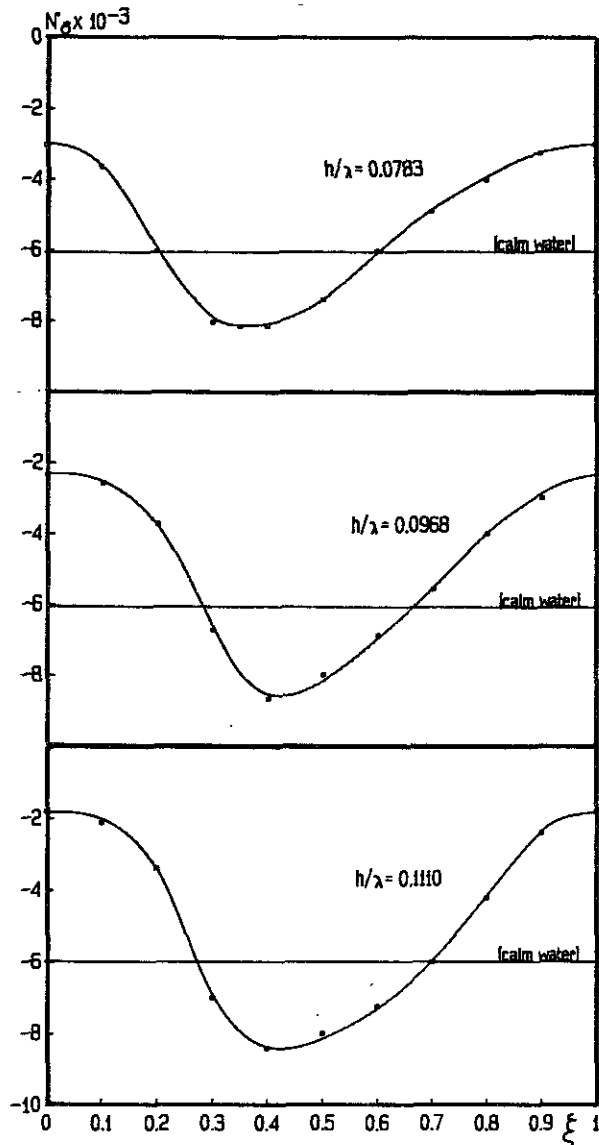


Figure 7 N'_δ for Varying ξ

The curves show the variation of rudder effectiveness for different positions on the wave; the rudder is least effective when the crest is at the stern and most effective just before the trough reaches the stern (as the wave slowly overtakes the vessel). It can be seen that over the whole wave there is a general loss of effectiveness when compared to the calm water value. Fig. 8 indicates that the rudder effectiveness reduction becomes more marked as the steepness of the wave

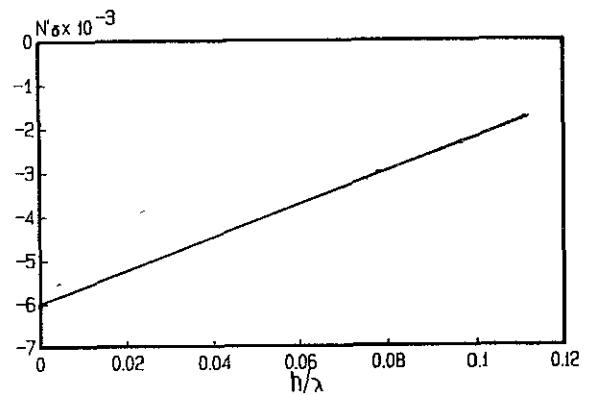


Figure 8 N'_δ for Varying h/λ

increases. It is interesting to note that when the vessel is operating in the wave with the greatest steepness, a severe breaking wave, the rudder effectiveness is reduced by 70% when $\xi = \text{zero}$. This large change in effectiveness can be attributed to the orbital velocities of particles in the wave altering the water velocity over the rudder.

It must be appreciated though, that with a operating propeller in front of the rudder this change is likely to be reduced. As shown above a vessel in a following sea spends most time with the wave crest at its stern, thus seeming to suggest that a vessels inability to avoid broaching is seriously increased by the reduction in rudder effectiveness found with this wave position.

CONCLUSIONS

When a vessel is travelling in a following sea at a low encounter frequency:-

- (i) The wave applies a Longitudinal force which is a function of the Longitudinal position of the vessel in the wave. This force is approximately proportional to the wave height over the range tested.
- (ii) This Longitudinal force will cause surging and the vessel will spend longer at a wave position with the

crest just aft of the transom.

- (iii) The rudder effectiveness varies as a function of Longitudinal position of the vessel in the wave, with the minimum occurring at a wave position with the crest at the stern.

APPENDIX

The Effect of Wave Amplitude on Wave Celerity

It is well known that the celerity of finite amplitude waves is dependent on their height. This is usually ignored, however, as the waves become very steep it must be taken into account. In order to determine the effect of wave height on speed two wave probes were positioned in the tank at a known distance apart (less than a wave length). The wave profile data was recorded using an IBM-PC sampling at 100 samples per second. The celerity was derived by measuring the time for a peak to travel from one probe to the next.

The results were compared with that predicted by the third order correction for wave velocity as outlined by Wehausen and Laitone (8).

$$\text{Where } A = A[1 + 1/8 A^2 m^2] \quad (5)$$

the velocity becomes

$$c = (g/m)^{1/2} (1 + 1/2 A^2 m^2 + \dots). \quad (6)$$

Fig. 9 shows the good correlation between the experimental results and the theory within the non breaking range.

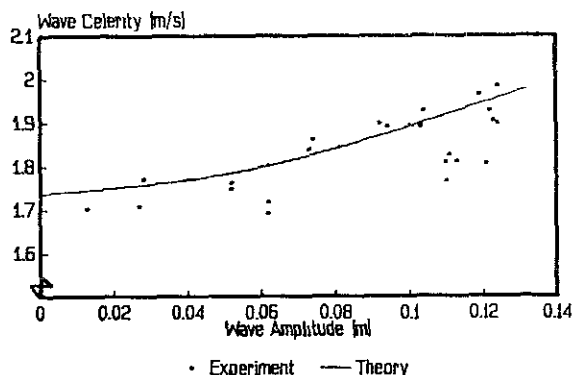


Figure 9 Wave Celerity for Varying Wave Amplitude

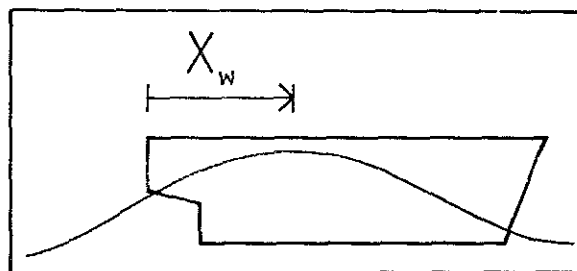


Figure 10 Definition of X_w

NOTATION

L	Ship length
B	Ship beam
V	Ship velocity
c	Wave celerity
λ	Wave length
h	Wave height
X_w	x distance from wave crest to transom, (see Figure 10).
ξ	Non-dimensional wave position
X_ξ	Wave induced surge force
X^*	Non-dimensional surge force
X'	Component of force along x axis
X''	Non-dimensional X force
N_δ	Yaw moment derivative with respect to rudder angle
N'_δ	Non-dimensional Yaw moment derivative with respect to rudder angle
ρ	Mass density of water

REFERENCES

1. Du Cane, P., Goodrich, G.J., "The Following Sea", Broaching and Surging". Trans. R.I.N.A., Volume 104, April 1962.
2. Renilson, M.R., Driscoll, A., "Broaching - An Investigation into the Loss of Directional Control in Severe Following Seas". R.I.N.A. Spring Meetings 1981.
3. Renilson, M.R., "An Investigation into the Factors Affecting the Likelihood of Broaching - to in Following Seas". Second International Conference on

- Stability of Ships and Ocean Vehicles,
Tokyo, October, 1981.
4. Matora, S., Fujino, M., Fuwa, T.,
"On the Mechanism of Broaching to
Phenomena" Second International
Conference on Stability of Ships and
Ocean Vehicles, Tokyo, October 1981.
 5. Fuwa, T., Sugai, K., Yoshino, T.,
Yamamoto, T., "An Experimental Study
on Broaching of a Small High Speed
Boat". Ship Research Institute,
Report Number 66, April 1982.
 6. Renilson, M.R., "The Seabrake A Device
for Assisting in the Prevention of
Broaching to Third International
Conference on Stability of Ships and
Ocean Vehicles, Gdansk, September 1986.
 7. Renilson, M.R., "The Ship Hydrodynamics
Centre at the Australian Maritime
College". Workshop on National Need,
Capabilities and Resources for Off-
Shore Engineering, Monash University,
Melbourne 1986.

DETERMINATION OF CAPSIZING SAFETY OF DAMAGED SHIPS BY MEANS OF MOTION SIMULATIONS IN WAVES

by Fernando Petey

We present a numerical method for simulating the motions of a damaged ship in an irregular seaway and for computing the capsizing probability during a given time.

We are mainly interested in following and head seas because of the oscillations of the righting levers caused by the passage of waves along the ship.

Computations carried out for an example ship show that the internal fluid acts as a very effective roll damping mechanism. We show that a damaged ship subdivided in accordance to the damage stability requirements of the German Navy can be safe during a period of time in the order of magnitude of days even in extremely severe seaways.

THE NUMERICAL METHOD

The classical strip theory is an efficient tool for handling heave, pitch, sway and yaw motions of a ship even in severe seaway conditions. Unfortunately the roll motion is a notoriously nonlinear phenomenon. The righting lever of a ship in still water, for instance, is a highly nonlinear function of the heel angle. Other effects on the righting levers result from the change of the submerged volume during the passage of waves along the ship: in general, the stability of a ship is improved in the sagging and reduced in the hogging condition. Further influences depending nonlinearly on the ship motions are the hydrodynamic roll damping, forces induced by the motion of liquid in tanks or damaged compartments, etc.

Therefore the method combines the simulation of the roll and surge

motions of the ship in the time domain with a treatment of the other four motions by the strip method. Since we are interested in computing ship motions for several loading and damage cases, subdivision arrangements and seaway conditions for extended periods of time, it is of paramount importance to use a model which, being accurate enough, requires a relatively small computational effort. As a result of this consideration, the program represents a compromise of the conflicting requirements for accuracy versus computer demand.

In the program the ship is considered as a six-degree-of-freedom system travelling at a given angle relative to the dominant direction of a stationary short-crested sea. The seaway is represented as the sum of a large

number of regular waves, each having a particular frequency, amplitude, direction and a random phase angle. The wave components are generated by the program from a given sea spectrum (Pierson & Moskowitz, Jonswap or Wallops). Breaking waves, which can be dangerous for small ships, cannot thus be simulated.

We use response amplitude operators for determining the heave, pitch, sway and yaw motions.

Both the wave exciting moment and the roll moment induced by the sway and yaw motions of the ship are determined by response amplitude operators as well. This is justifiable since in following, quartering, bow and head seas they play a much less important role than the oscillations of the righting levers due to the passage of the waves along the ship.

In the roll and surge simulation, time is advanced in small increments. Forces and moments due to the liquid in tanks and damaged compartments may be added to the external forces and moments due to wave excitation, wind etc. In this way we obtain a time domain solution for both ship motions and internal fluid motions.

The program considers particularly the shape of the righting lever curve up to large heel angles and its changes due to the waves and ship motions. We use Grim's "effective wave" /1/ for representing the elevation of the sea surface along the ship's hull. The program is thus capable of simulating the phenomenon of autoparametric excitation which may lead to ship capsizing.

Tanks and damaged compartments are divided into two groups: those with a low and those with a high fill depth of liquid.

The case of low fill depth is governed by a nonlinear hyperbolic system of so-called shallow-water equations. Its solution is obtained numerically, using Glimm's method /2,3/ (random choice method). This method is capable of simulating both two-dimensional and three-dimensional flows, including the frequently occurring cases of hydraulic jumps and of a partially dry bottom.

In the high depth case the greatest natural period of the fluid oscillation is much smaller than the dominant periods of the ship motions. As a result the liquid free surface may be oblique but remains essentially flat. This leads to a simple equation of motion of the center of gravity of the fluid which can be solved in the time domain using the familiar Runge-Kutta's integration scheme /2/.

Water flowing through orifices in the ship's hull is estimated by straightforward relations based on the classical Torricelli's formula, so that the volume of water inside the ship can be corrected at each time step. Since the liquid fill depth in a damaged compartment is variable on account of the flow through orifices, the program is capable of changing automatically between the two above-mentioned flow computing methods during the simulation.

CAPSIZEING PROBABILITY

We examine a ship in a given loading case travelling in a seaway at a given speed and heading. The probability $P(t)$ that the ship does not capsize in the time interval $(0, t)$ is

$$P(t) = \exp(-t/T_k), \quad (1)$$

where T_k is the mean capsizing period.

T_k can be determined, at least in principle, by simulating the ship motions during a certain time d . If the ship capsizes N times during d (after each capsizing we restart the simulation with the ship in its upright position) a good estimate for T_k is

$$T_k = d / N.$$

The starting conditions (roll angle and roll velocity), however, must not have too much influence upon N . Therefore we do not take into account the time immediately after each simulation start.

In the cases of practical interest, however, T_k can have an order of magnitude of years, so that the simulation time $d = N \cdot T_k$ (N should not be less than 5) would be unrealistically long.

Therefore Söding and Tonguc /4/ proposed to simulate the ship motions in a steeper seaway (i.e., with a higher significant wave height H but with the same characteristic period), in which T_k could be determined by the above-mentioned formula, and extrapolate the capsizing probability to less severe seaways. They found that

the dependence of T_k upon H can be estimated by

$$T_k/T_s = \exp(A + B / H^2), \quad (2)$$

where T_s is the characteristic period of the seaway; A and B are constants.

According to the formula above, if we calculate T_k by simulation for a number of wave heights H and plot $\ln(T_k/T_s)$ over H^{-2} we get approximately a straight line from which the constants A and B can be determined easily. The greater the slope B , the safer the ship.

We performed a very large number of simulations which confirmed the validity of the expression (2).

Very interesting is the dependence of the probability P , that the ship does not capsize, upon the significant wave height H (combination of expressions (1) and (2)). If we choose t large enough, so that

$$\lim_{H \rightarrow \infty} P = 0,$$

we see on fig.1 ($A=1.0$) that after keeping practically the value 100% for low wave heights (the ship is thus safe) the curve $P(H)$ falls extremely sharply to around 0% (not safe).

APPLICATION

We present some results for the following example ship:

Lpp	=	146.0 m
Breadth	=	24.6 m
Height to deck 2	=	16.3 m
Height to deck 3	=	9.0 m

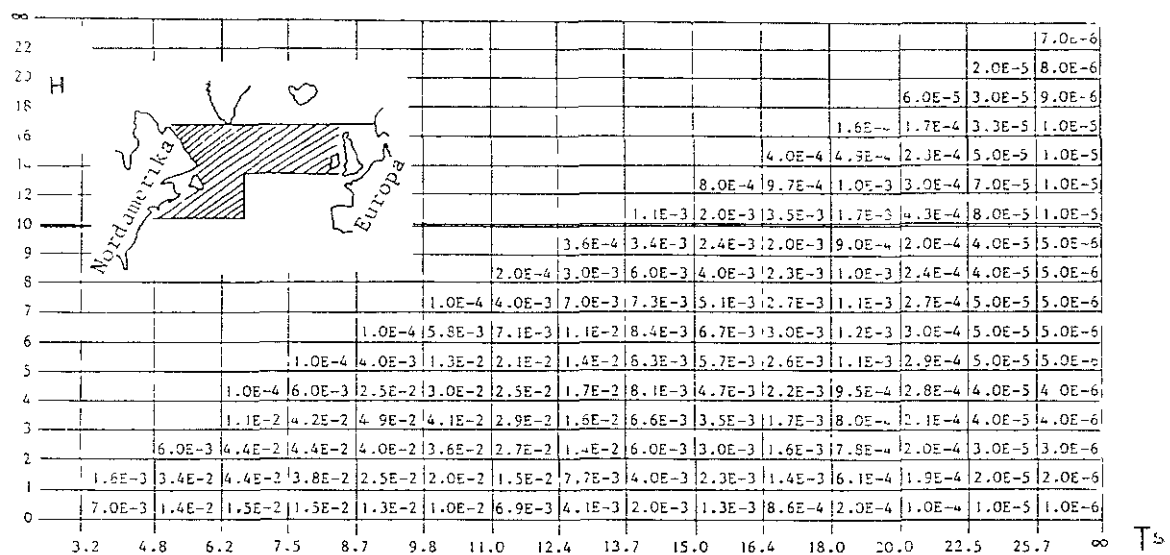


Fig.1: Dependence of the probability P, that the ship does not capsize, upon the significant wave height (in m) according to equations (1) and (2).

17	16	15	14	13	12	11	10	8	Deck 2
27	26	25	24	23	22	21	20		Deck 3

Fig.2: Subdivision

17	18		
27	28		

Fig.3: Damage case 2

Double bottom height = 1.5 m

Situation before damage:

Displacement = 19000 m³

Draught = 8.17 m

Trim = 0.23 m by the stern

Fig.2 shows the subdivision.

We present results for 2 damage cases (symmetrical flooding): number 2 (fig.3, damage at stern) and number 4 (fig.4 damage at amidships). Other cases and details in /5/.

Case	Damaged Compartments	KG'	KG	GM
2a	16 17 26 27	11.76	11.94	0.00
4a	13 14 23 24	12.22	11.15	0.00
4b	13 14 23 24	11.98	10.95	0.20
4c	13 14 23 24	11.76	10.75	0.40

In the table above KG' and KG are the heights (m) of the center of gravity above the keel before and after damage respectively; GM is the residual metacentric height (m).

According to the damage stability regulations of the German Navy /6/ the maximum allowed intact KG' for the subdivision shown on fig.2 is 11.76 m.

The still-water righting lever curves are shown on fig.5 (calculated by the lost-buoyancy method, i.e., displacement taken constant).

RESULTS

The righting levers of a damaged ship are usually very small compared with those of an intact vessel. Its range of stability is reduced. Furthermore the hydrodynamic damping moment is small on account of the low speed of damaged ships (some forward speed is necessary for the sake of manoeuvrability).

In a seaway the righting levers can further be reduced by the passage of waves along the ship's hull causing a capsizing.

In beam seas the righting lever oscillations are relatively small, so that they can be neglected. In following or head seas, however, they can be very severe and must be considered, if sufficient accuracy is to be obtained.

For ships travelling at low speeds there is no danger of capsizing on account of pure loss of stability in the hogging condition, since the encounter period of the slow moving ship with the much faster travelling waves is too short.

In damage cases which result in a very small residual metacentric height GM we expect no danger neither from roll resonance nor from autoparametric excitation since the roll period of the damaged ship (even if it differs somewhat from the theoretical value in still water) is very long.

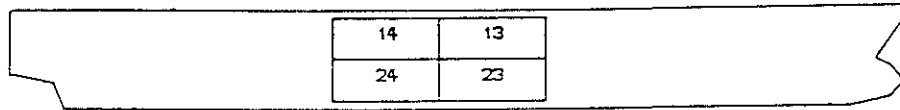


Fig.4: Damage case 4

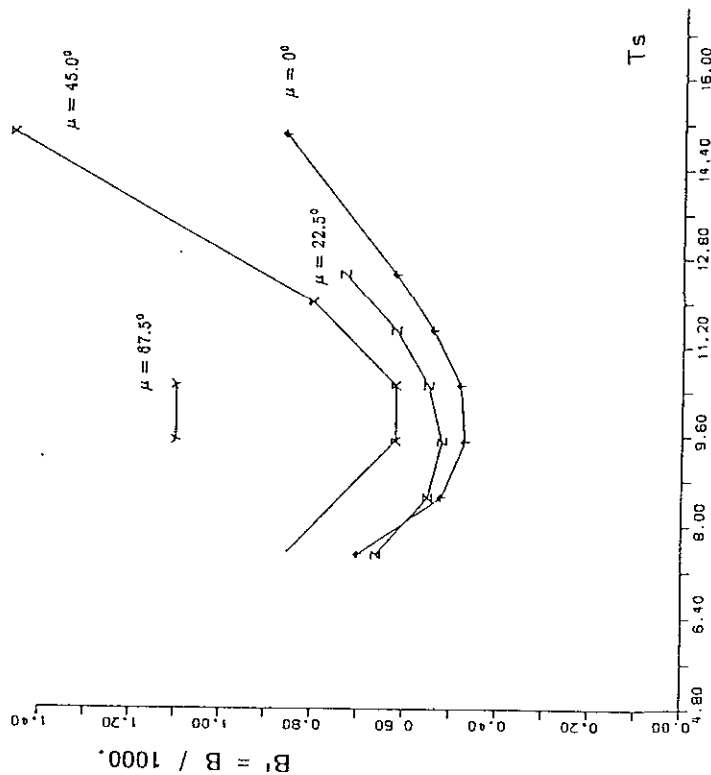
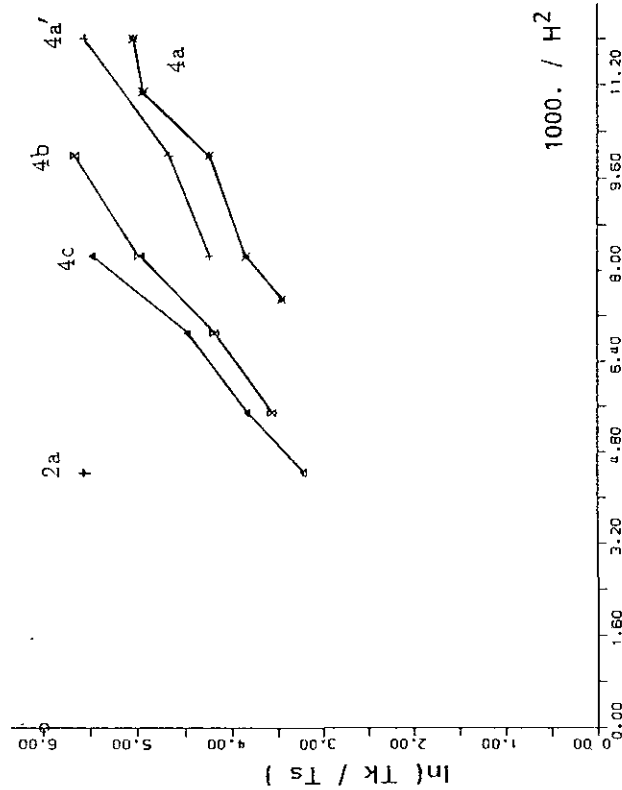
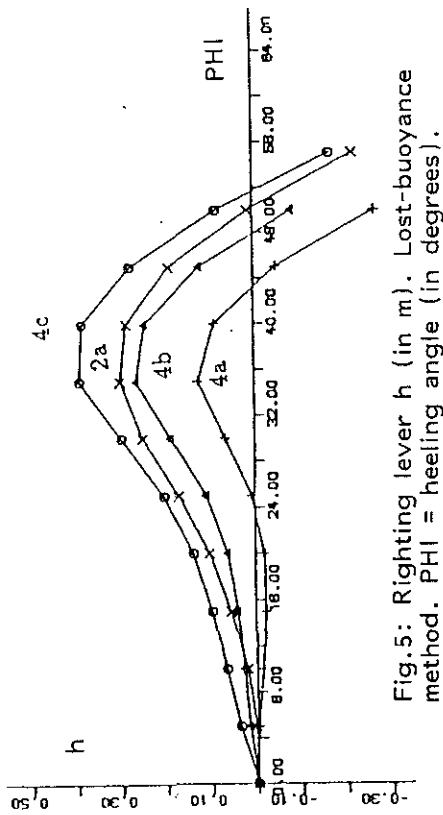


Fig.7: Dependence of the slope B according to equation (2) upon the significant period of the seaway T_s (in s) and upon the dominant wave direction μ ($=0$ in following seas). The greater B , the safer the ship. Damage case 4b.

In all cases investigated in /5/ the water in the flooded compartments was found to act as a very effective damping mechanism, i.e., the dynamic effect of the flooding water was to damp the roll motion, not to excite it. This was a result of the energy dissipation connected with the appearance of hydraulic jumps (shallow water) and the flow of water through the orifices in the ship's hull which causes a shift in the phase between the roll velocity and the moment exerted on the vessel by the flooding water.

Fig.6 shows the dependence of the mean capsizing period T_k upon the significant wave height H for both case 2 and case 4. The ship is travelling at a constant speed of 5 knots in following seas. The short-crested seaway was generated from a Jonswap spectrum and has a significant period $T_s=9.5s$ (cases 2a, 4a, 4b and 4c) or 8.5s (case 4a'). The curves correspond quite well to the expected linear trend according to expression (2). Notice that the greater the residual metacentric height GM in case 4, the greater the slope B (and thus the more stable the damaged ship). The following table shows the dependence of the mean capsizing period T_k upon the residual metacentric height GM for a significant wave height $H=6.5$ m.

Case	GM (m)	T_k (hours)
4a	0.00	20.1
4b	0.20	511.6
4c	0.40	4144.0

The probability, for instance, that

the ship in case 4a does not capsize during 2 days time is according to expression (1)

$$\exp(-48.0 / 20.1) = 9\%.$$

In the limit case 4c ($KG'=11.76m$) we get

$$\exp(-48.0 / 511.6) = 91\%.$$

Other cases investigated in /5/, however, show that an increase in GM need not make the damaged ship safer.

Fig.7 shows for case 4b the dependence of the slope B upon the significant period T_s of the seaway and upon the dominant wave direction μ ($\mu=0$ in following seas). We see that the most dangerous conditions are in following and quartering seas. We could only very seldom observe capsizings in head or beam seas.

Furthermore we see that in following and quartering seas, in turn, the most dangerous condition occurs when the wave spectrum has its maximum value for those waves, the lengths of which closely match the ship's length. In this case are expected the most severe righting lever oscillations.

The pattern shown on fig.7 was found to hold for all other cases we investigated.

Very interesting is the comparison between the cases 2a and 4c. From fig.5 one should expect case 4c to be safer than case 2a. Just the opposite occurs. There is following explanation for this behaviour: the righting lever oscillations in the seaway depend on the form of the

intact part of the ship. If the damaged compartments are located at amidships (case 4a) the oscillations due to the passage of the waves along the ship's hull are severe on account of the triangle-shaped frames at the bow and at the stern. Conversely, these oscillations are much less severe if the damage is located at one or at both ship's ends, so that the damaged ship is safer.

If we now have wave data for a given sea area like, for instance, that shown on table 1 /7/, we can combine this information with that from fig.7 to define a "long term mean capsizing period" T' for this sea area (details in /5/). For the limit cases 2a and 4c we found the value of T' to be much longer than the time the ship needs to reach the nearest harbour, say, 5 days. The damaged ship is thus safe.

For case 4b (KG reduced by 20cm) we found $T' = 1646$ hours (approx. 69 days). If the ship travels during 5 days the capsizing probability in North Atlantic is

$$1 - \exp(-5.0 / 69.0) = 7\%.$$

If we further take into account that the captain of a damaged ship can adjust heading (see fig.7) and speed in order to decrease the danger of capsizing, we can consider this case 4b as safe too.

REFERENCES

/1/ O. Grim, Safety of Ships in a Seaway (in German), Schiff und Hafen, No.6, 1961.

/2/ F. Petey, Calculation of Forces and Moments due to Fluid Motion in

Tanks and Damaged Compartments, STAB 86 Proceedings, Gdansk, 1986.

/3/ J. Dillingham, Motion Studies of a Vessel with Water on Deck, Marine Technology, Vol.18, No.1, 1981.

/4/ H. Söding and E. Tonguc, Computing Capsizing Frequencies of Ships in a Seaway, STAB 86 Proceedings, Gdansk, 1986.

/5/ F. Petey, Numerical Determination of the Capsizing Probability of Damaged Ships in a Seaway (in German), Report No.487 of the Institut für Schiffbau der Universität Hamburg, 1988.

/6/ Stability Regulation No.1033 for Ships of the German Navy (in German), Koblenz.

/7/ H. Söding, Capsizing Risk Analysis by Means of Ship Motion Simulation (in German), Schiffstechnik, Vol.34, No.1, 1987.

AUTHOR

Dr. Fernando Petey, Marinetechnik Gesellschaft, Hamburg, Federal Republic of Germany.

SERIES STAND TESTS WITH PASSIVE STABILIZING TANKS

V. Rakitin ¹⁾, R. Nachev ¹⁾, Tz. Tzvetanov ²⁾

ABSTRACT

The paper presents results obtained by series model tests of "FLUME"- and "FRAME" - type passive stabilizing tanks. The mathematical aspect of the problem and the experimental realization, as well as certain technical aspects of force and stabilizing moment measurements have been described. Some of the results, representing the amplitude and phase characteristics of the measured values in the frequency range, are also presented in this paper. Some particular effects of fluid motion in the tanks, depending on the internal damping coefficient, have been described.

Analytical approximation formulae have been derived on the basis of experimental data. Conclusions have been drawn about the effectiveness of the stabilizing tanks.

INTRODUCTION

The problem of choice of both type and dimensions of the stabilizing tanks, which should be optimum for a particular ship, inevitably occurs in the design process. The solution of this problem is substantially facilitated at availability of objective experimental data for the roll motions of the stabilized ship, the efficiency of the tanks, the fluid motion in them, the influence of the different devices, varying the internal damping coefficient, etc. Such data can be obtained most thoroughly by model experiments.

Due to the interest of the foreign clients and in connection with the prospects for development of the Bulgarian Shipbuilding industry, an extensive programme for investigation of stabilizing tanks of "FLUME" and "FRAME" types, has been developed at BSHC. The programme included perfor-

mance of series model stand tests and tests in regular and irregular waves of ship models equipped with stabilizing tanks. For this purpose a three-component motion simulator and a system for measuring the stabilizing moment and the horizontal force during the tests in waves in the experimental tank, were designed and manufactured. The motion simulator imitates roll, heave and sway motions of the ship. During the experiments the dependence of the generated stabilizing moment on the geometrical characteristics of the stabilizing tanks and their internal damping was investigated. The experimental data obtained in view of its great amount proved to be reliable basis for development of analytical approximation formulae and design procedures of a stabilizing tank for a particular ship. The analysis of the experimental results allowed determination of the extent of influence of the varying parameters on the effective operation of the stabilizing tanks.

1) Naval Architect, Research Scientist

2) Dipl. Ing., Research Scientist

BSHC, Varna 9000, Bulgaria

This paper comments the results of part of the stand model tests performed and it gives the main conclusions drawn from the

investigations, as well as the trends of continuing this activity.

MATHEMATICAL MODEL

It should be noted that in the preparation of the mathematical model describing the stand tests, use was made of the classical theoretical approach based on the simplified theory of roll motions (1,2).

The pure ship roll motions about the longitudinal axis passing through its centre of weight is discussed. In first approximation the equation of such an oscillation can be represented, as follows:

$$I_1 \ddot{\phi} + 2N_{\phi} \dot{\phi} + \Delta h_0 \phi = M_T, \quad (1)$$

where, M_T - some harmonic excitation function.

It can be assumed that the resultant motion after certain period of time, will also become harmonic and will be performed with the same frequency but with a phase lag in comparison to the excitation effect. In the accepted formulation of the problem the total moment M_T consists of the moment of the external excitation effect and the moment generated by the fluid moving in the stabilizing tank. The external excitation moment during the stand tests can be assumed to be strictly harmonic and then the equation of the roll motions has the following form:

$$I_1 \ddot{\phi} + 2N_{\phi} \dot{\phi} + \Delta h_0 \phi = \Delta h_0 \alpha_m \sin \sigma t + M_{ST} \quad (2)$$

where,

$$M_{ST} = m_{ST} \sin(\sigma t + \varepsilon_{ST}).$$

In view of the sinusoidal character of the external excitation the stabilizing moment in the frequency range, interesting from practical point of view, is also a harmonically varying function.

In its normal form eq.(2) can be written in the following form:

$$\ddot{\phi} + 2\nu_{\phi} \dot{\phi} + n_{\phi}^2 \phi = \alpha_m n_{\phi}^2 \sin \sigma t + \frac{m_{ST}}{I_1} \sin(\sigma t + \varepsilon_{ST}), \quad (3)$$

where,

α_m - effective angle of the wave slope,

$n_{\phi} = \sqrt{\Delta h_0 / I_1}$ - natural roll frequency,

ε_{ST} - phase angle of the stabilizing moment.

The equation of roll motions is transformed by transferring the expression for the stabilizing moment to its left side,

$$\begin{aligned} \ddot{\phi} + \frac{m_{ST}}{I_1} \cos \varepsilon_{ST} \sin \sigma t + 2\nu_{\phi} \dot{\phi} + \\ + \frac{m_{ST}}{I_1} \sin \varepsilon_{ST} \cos \sigma t + n_{\phi}^2 \phi = \alpha_m n_{\phi}^2 \sin \sigma t \end{aligned} \quad (4)$$

The solution of eq.(3) is well known and in this case it is sought in the form:

$$\phi = A \sin \sigma t + B \cos \sigma t$$

In the obtained algebraic equation after grouping the terms in the sine and cosine parts, the following is obtained:

$$\begin{aligned} (A(n_{\phi}^2 - \sigma^2) - 2\nu_{\phi} \sigma B - \alpha_m n_{\phi}^2 + \frac{m_{ST}}{I_1} \cos \varepsilon_{ST}) \sin \sigma t + \\ + (B(n_{\phi}^2 - \sigma^2) + 2\nu_{\phi} \sigma A + \frac{m_{ST}}{I_1} \sin \varepsilon_{ST}) \cos \sigma t = 0 \end{aligned} \quad (5)$$

The equalizing of the sine and the cosine parts of this equation leads to the following expressions:

$$\begin{aligned} A(n_{\phi}^2 - \sigma^2) - B 2\nu_{\phi} \sigma &= \alpha_m n_{\phi}^2 - \frac{m_{ST}}{I_1} \cos \varepsilon_{ST} \\ A 2\nu_{\phi} \sigma + B(n_{\phi}^2 - \sigma^2) &= - \frac{m_{ST}}{I_1} \sin \varepsilon_{ST} \end{aligned}$$

And the subsequent transformations allow obtaining of a formula for the roll motions' amplitude of the stabilized ship.

$$\begin{aligned} \phi_{ST}^2 &= A^2 + B^2 = \\ &= \frac{(m_W / I_1)^2 + (m_{ST} / I_1)^2 \cos^2 \varepsilon_{ST} +}{(n_{\phi}^2 - \sigma^2)^2 +} \quad (6) \\ &+ \frac{(m_{ST} / I_1)^2 \sin^2 \varepsilon_{ST} - 2(m_W / I_1)(m_{ST} / I_1) \cos \varepsilon_{ST}}{+ 4\nu_{\phi}^2 \sigma^2} \end{aligned}$$

or

$$\phi_{ST} = \frac{1}{I_1} \frac{\sqrt{m_W^2 + m_{ST}^2 - 2m_W m_{ST} \cos \varepsilon_{ST}}}{\sqrt{(n_{\phi}^2 - \sigma^2)^2 + 4\nu_{\phi}^2 \sigma^2}},$$

where,

$m_W = \Delta h_{0m} \alpha_m$ - excitation moment amplitude,
 m_{ST} - stabilizing moment amplitude.

Eq.(6) is quite simplified but it clearly reflects the stabilizing tank effect on the behaviour of the stabilized ship in pure external harmonic excitation.

EXPERIMENTS

The series model tests have been performed with stabilizing tank models of FLUME and FRAME types at approximate scale $M = 1 : 25$ in comparison to full scale. During the stand experiments the roll and sway motions were simulated. The experimental programme has been developed on the basis of the variation of the following parameters:

- height (breadth) of the connection water channel;
- internal damping coefficient in the tank;
- mass of the water filling the tanks;
- value of the roll angle;
- value of the sway motion;
- frequency of the oscillations generated by the simulator.

The combinations of the varying roll and sway amplitudes and the frequency of motion have been selected, so that they should reflect comparatively most accurately the behaviour of the real ship. During the experiments the phase angle between those two oscillations simulated by the stand, was varied. The tests have been performed in the following two states: "frozen" liquid and "free" stabilizing liquid.

It should be noted that in the development of the force-measuring system of the motions simulator an approach has been accepted, treating the investigated stabilizing tank as a body of six degrees of freedom, so that in the three-dimensional coordinate system this body was subjected to the effects of the external forces, the application points and directions of which are not known and vary during the experi-

ments. This approach makes the measurement complex but it has the following advantages:

- adequate reflection and perception of the forces acting on the stabilizing tanks;
- a possibility for simultaneous measurement of all force components of interest;
- preconditions for increasing the measurement accuracy;
- independence of the different force-measuring elements.

During the tests the following parameters have been measured and controlled:

- moment with regard to the roll axis;
- horizontal force;
- fluid motion in the tank;
- roll and sway motions;
- oscillation frequency.

The data acquisition and preliminary processing of the experimental data has been performed by means of a computer system using IBM PC.

The accepted algorithm of processing the experimental data of the stand tests is based on the method described in (2) and it consists in determination of the amplitudes of the stabilizing moment and the horizontal force and their phase angles, as follows:

$$A_0 = \sqrt{(A_1 \cos \varepsilon_1 - A_2)^2 + (A_1 \sin \varepsilon_1)^2}$$

$$\varepsilon_0 = \arctg \frac{A_1 \sin \varepsilon_1}{A_1 \cos \varepsilon_1 - A_2},$$

where,

- A_0 - stabilizing moment amplitude (horizontal force);
- A_1 - first harmonic amplitude of the measured moment (force) of the open water tests;
- A_2 - first harmonic amplitude of the measured moment (force) in frozen water tests
- ε_0 - phase angle of the stabilizing moment (horizontal force) versus the angular oscillations;
- ε_1 - phase angle of the first harmonic of the moment (force) versus the angular oscillation of the open water tests.

As a result of the experimental data processing the sine (in-phase) and the cosine (quadrature) components of the stabilizing moment are obtained depending on the frequency of the external excitation. Those components are necessary for the determination of the roll amplitude of the stabilized ship in regular waves and the drawing of the amplitude response function of the ship in real sea waves.

TESTS RESULTS

The final processing of the experimental results of the stand tests has been performed on a 32-bit computer, using Fourier analysis program modules. The test results are presented in non-dimensional form, so that the dimensionalizing coefficients depend on the geometrical dimensions of the stabilizing tanks and the oscillation amplitude. On the account of these results generalized graphical relationships have been developed concerning the measured values as a function of the varying parameters. It should be noted that to a great extent the reliability of the results obtained depends on the correct and accurate modelling of the "frozen" water state, expressing in the exact height determination of the mass centre position. The same refers to the modelling of the mass inertia moment of the stabilizing tank. Figs.1-4 give exemplary graphical relationships for the non-dimensional amplitudes and the phase angles of the stabilizing moment and the horizontal force generated by the stabilizing tanks in force motion of the water in them.

The performed analysis of the experimental results obtained allowed evaluation of the influence of the parameters varying during the tests on the measured stabilizing moment, horizontal force and the water oscillations in the tanks.

The free water surface with the FRAME type tank is kept horizontal independently on the oscillation angle up to frequencies

of about 0.2 Hz at lack of sway motion. The sway motions, particularly when they are in a phase with the phase oscillation, lead to strong curving of the water surface in the tank and occurrence of standing waves. In the further increase of the oscillation frequency the height of those standing waves increases and they start breaking. In this case the influence of the roll motions angle is strong. The total breaking of the water surface linearity occurs at angles greater than 8° . It should be noted that the internal damping coefficient significantly influences the behaviour of the water in the tank, so that its increase shifts the strong damping of the water surface in the higher frequency zone of the forced oscillations.

With the FLUME type tank due to the great area of the water surface and the specifics of its internal configuration even at very low oscillation frequencies, surface waves are generated, the amplitude of which quickly increases with the increase of the roll motions angle. The waves start breaking at oscillation angles greater than 10° , so that this breaking occurs very rapidly at presence of sway motions. At oscillation frequencies higher than 0.25Hz the different water levels are clearly formed in the different tank volumes. The internal tank damping influences significantly the water surface shape. At high internal damping coefficients and oscillation frequencies greater than 0.45Hz the occurring waves propagate only in the ranges of each different tank section and they have insignificant height. It should be noted that at those states the generated stabilizing moment is quite small. A typical example of the registered water surface behaviour in the FLUME and FRAME type tanks is shown on Figs.5-6.

The described fluid motion in the tank characterizes the phase variation of the generated stabilizing moment regarding the external excitation. At small oscillation angles this phase increases monotonously with the variation of the frequency

and its determination experimentally is no problem. When the oscillation amplitudes, however, become significant ($>12^\circ$) and the water surface behaviour assumes predominantly expressive nonlinear character (strong wavemaking with subsequent total wave breaking), the determination of the phase angle becomes difficult. This particularly refers to the frequency zone, in which the hydraulic jump occurs. That is why in this region there is certain instability of the experimental results.

The amplitude of the moment, generated by the fluid oscillating in the tank, is influenced most strongly by the frequency of the external excitation effect, so that this relationship appears to be a function of the third power of this frequency at given roll and sway motions and oscillation frequencies higher than 0.45Hz. In the low frequency range the variation of the stabilizing moment is proportional to those frequencies (Fig.7).

The effect analysis of the phase angle oscillation in the whole frequency range of the external excitation shows that the stabilizing moment seems to be a function of the first degree of those amplitudes with the FRAME type tanks and respectively, a function of their second degree with the FLUME type tanks.

The internal damping coefficient influences significantly the amplitudes and the angles of the stabilizing moment generated by the tanks. The increase of the internal resistance leads to considerable increase of the phase angle with the high frequencies of the forced oscillations but the absolute value of the moment amplitude starts decreasing. At low oscillation frequencies the stabilizing moment is in approximately linear dependence on the roll angle.

It should be noted that the phase difference between the forced oscillations, in principle does not influence significant-

ly the distribution by frequencies of the moment generated by the tank and leads only to decrease of the moment amplitudes at dephasing of 90° between roll and sway motions. This reduction of the moment value is most significant at oscillation frequencies higher than 0.30Hz, which is explained by the increase of the share of the stabilizing moment falling to the sway motion and by its direction opposite to the basic component.

During the test performance the effect of the pure sway motion on the stabilizing moment has been investigated too. The analysis of those data shows that up to frequencies in the range of 0.25-0.30Hz this influence seems to be slight but above those frequencies it starts growing (Fig.8).

The phase frequency characteristics of the horizontal force and the stabilizing moment correctly reflect the physics of the fluid motion processes occurring in the stabilizing tanks. The phase shift of the measured values with regard to the phase angle oscillation strongly depends on the internal tank resistance, on the amplitudes and frequencies of the forced oscillations and the phase difference between them. In all those cases, however, the jump of the phase characteristics occurs at attaining of the minimum values of the measured moment and horizontal force. The water level in the tank also influences these phase characteristics.

During all stand tests the tank height position with regard to the oscillation axis does not vary and that is why no conclusions regarding the relationship between the amplitude of the stabilizing moment and the tank position can be drawn.

ANALYTICAL APPROXIMATION

One of the aims of the experimental investigations performed was the obtaining of analytical approximation expressions about the stabilizing moment and its phase, depending on the parameters varying during the tests.

The main requirements towards the analytical approximations were the incorporation of all combinations of the varying parameters and accuracy not less than that of the experimental data results. The standard approach was adopted, at which the approximation function is represented by the following expression:

$$m_{ST} = \sum_{i=1}^N A_i X_i^{a_i}$$

where,

A_i - regression coefficients,

X_i - varying parameters,

a_i - integer power values.

At the systematic analysis of the experimental data the regression coefficients have been obtained with the aid of standard programs for regression analysis (5). There are different regression models developed for the two types of tanks. The full approximation relationships describe quite accurately all experimental results and allow obtaining of the stabilizing moment for any of the parameter combination within their variation ranges. However, as far as the analytical formulae have been intended for practical application in the design of the stabilizing tanks, it is necessary to note the following: the full approximation developed does not give satisfactory result in the determination of the main characteristics of a stabilizing tank designed and accounted for a particular real ship. This disadvantage of the full approximation function is due to the ultimately small number of variations for almost all parameters included in the regression. This has imposed a certain change of the investigation program in the sense of the additional test performance with the purpose of expanding the ranges of some of the varying parameters. In spite of that on the basis of the main and additional investigations two-parameter approximations of the experimental results have been developed for varying frequency of the external excitation effect and one varying parameter and at fixed values of

the rest tank characteristics. It should be noted that this approach has lead to significant improvement of the results from the practical application of the analytical formulae. A calculation procedure has been prepared for determination of the geometric and tank damping characteristics with the use of these formulae and the developed analytical expression for prediction of the stabilizing moment obtained by test results of ship models equipped with passive stabilizing tanks in regular wave or harmonic external excitement (4).

CONCLUSIONS

The model investigations performed with FRAME and FLUME type stabilizing tanks have allowed accumulation of a great deal of experimental data, the multivariant investigation of which gives a possibility to evaluate the effect of a number of parameters on the tank efficiency. That is why the calculation procedure created, including also a computer program for prediction of the stabilized ship behaviour in first approximation, has been considered as a first stage in the creation of a test procedure for design of passive stabilizing tanks.

ACKNOWLEDGEMENTS

The authors would like to express their appreciations to Dr.S.Spasoov, a mathematician from BSHC Seakeeping & Manoeuvring Department, for his valuable consultations and assistance in the development of the analytical approximations of the experimental results discussed in this paper.

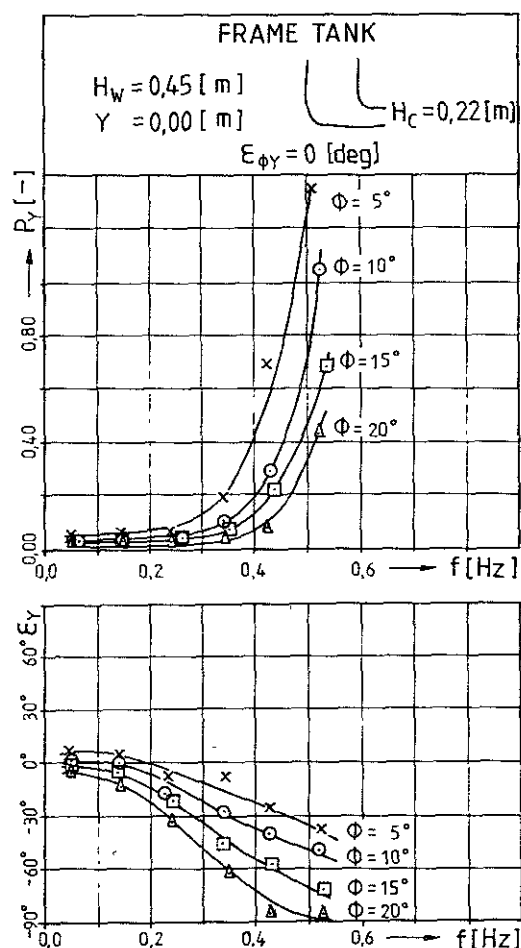
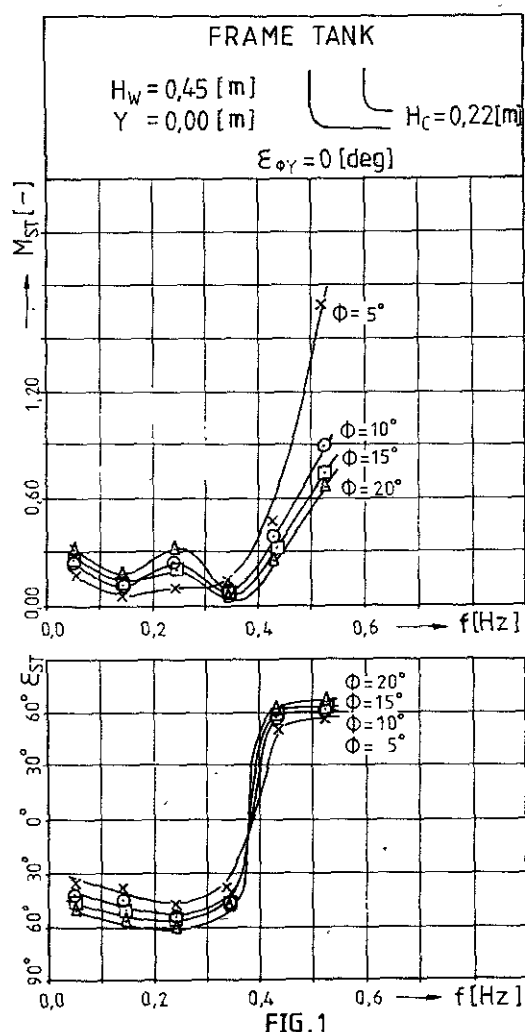
NOMENCLATURE

- f - Oscillation frequency
- h_0 - Metacentric height
- H_w - Water level height
- I_1 - Virtual mass moment of inertia about the roll axis

M_T - Total excitation moment
 M_{ST} - Stabilizing moment
 m_{ST} - Stabilizing moment amplitudes
 m_W - Wave excitation moment
 n_ϕ - Natural roll frequency
 p_Y - Amplitude of the horizontal force, generated by fluid motion in the tank
 WL - Water level oscillation amplitude
 Y - Sway amplitude
 α_m - Effective wave slope
 Δ - Displacement
 ϵ_{ST} - Phase angle of the stabilizing moment
 ϵ_{PY} - Phase angle of the horizontal force
 $\epsilon_{\phi Y}$ - Phase angle between the roll and sway motions
 ν_ϕ - Non-dimensional roll damping coefficient
 σ - Circular wave frequency
 ϕ - Roll amplitude

REFERENCES

1. Bosch, J.J. and Vugts, J.H., Roll Damping by Free Surface Tanks, Shipp.World and Shipbuilder, No.3792, 1966.
2. Zdybek, T., The Use of Bench Test Results for Calculating Roll Response of a Tank Stabilized Ship, International Shipbuilding Progress, April, 1980.
3. Shmirev, A.N., Morensildt, V.A., Ship Stabilizers, Sudostroenie Publ. House, Leningrad, 1972 (in Russian).
4. Rakitin, V. and Tzvetanov, Tz., Computer-Aided Prediction of the Stabilizing Tank Moment, Proceedings of CADMO'88, Southampton, U.K., 1988.
5. Dicson, V.I., BMDP Computer Programs, California University, 1979.



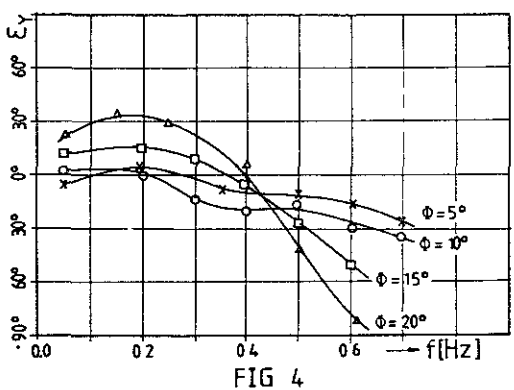
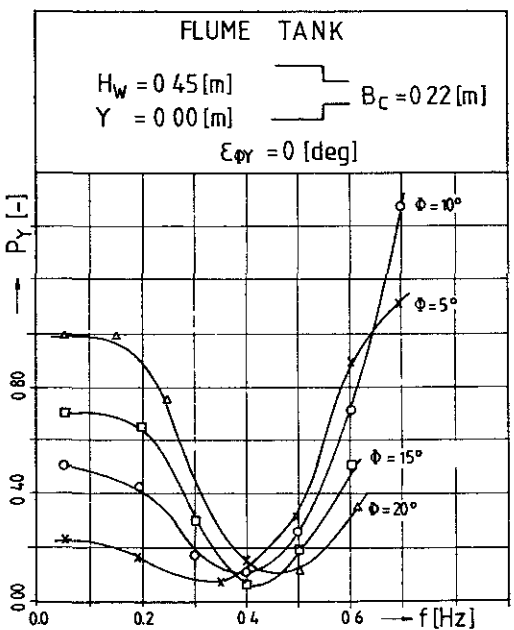
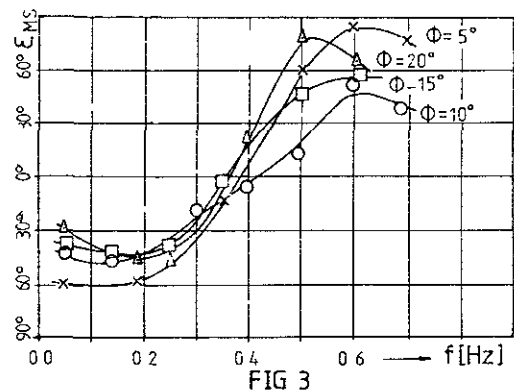
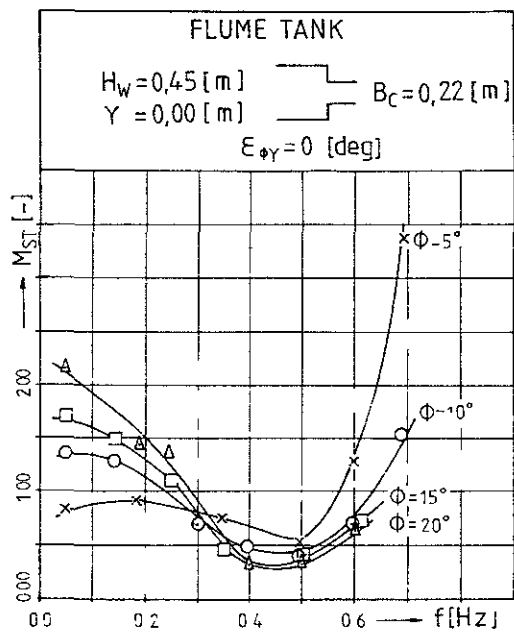


FIG 3

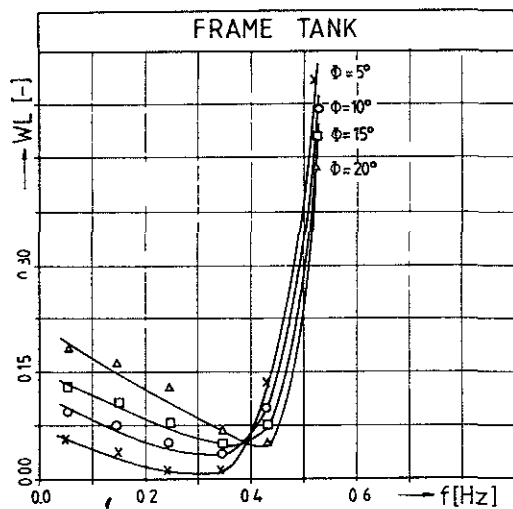


FIG 5

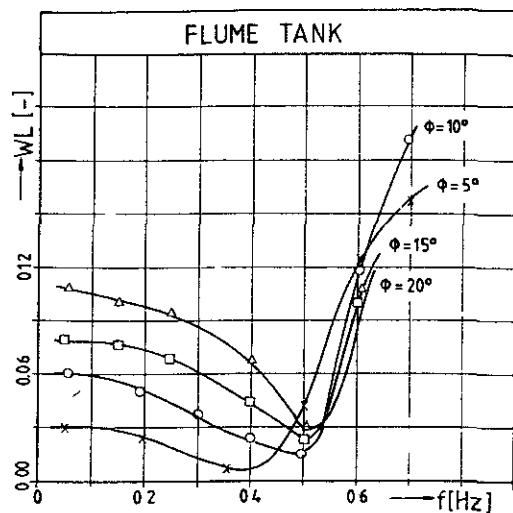


FIG 6

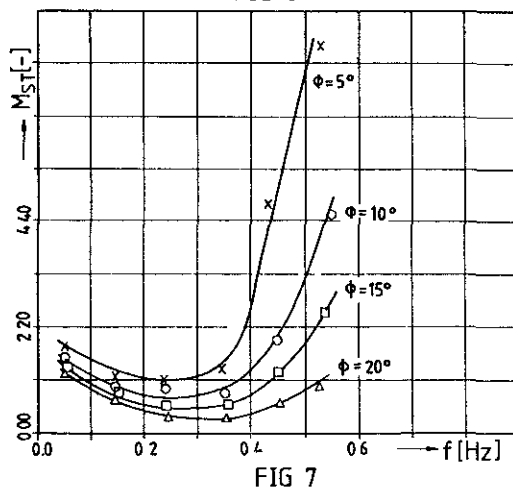


FIG 7

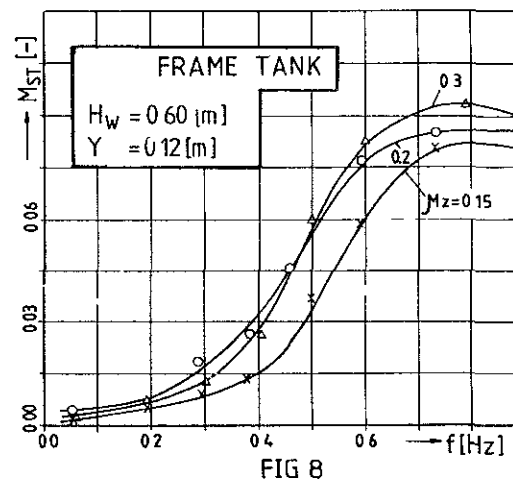


FIG 8

APPROXIMATE METHOD FOR STABILITY ARM EVALUATION AT INITIAL SHIP DESIGN STAGES

S. Dimitrova ¹⁾, R. Kishev ²⁾

ABSTRACT

In this paper a simplified procedure for static and dynamic stability arms calculation at equivolume inclinations is presented, employing the three-parameter Lewis forms technique for reconstruction of the cross sections in a semifixed (rotational) coordinate system, the sectional data being obtained by preceding optimization full form evaluations. The easiness of the procedure, unburdened by excessive inputs, makes it applicable for the purposes of preliminary ship design.

INTRODUCTION

In the process of ship design the static and dynamic stability diagrams are calculated by standardized procedures, approved by the classification societies and requiring detailed description of the ship hull form (2). At earlier (contract) design stages, however, computerized systems for optimum selection by multivariant comparisons could be applied (3), (4), and for stability assessment in the frames of comparative seakeeping calculations express methods, operating with generalized form characteristics, are needed in those systems.

1. OUTLINE OF THE DESIGN PROCEDURE

In (3) an original ranking procedure for stability assessment is outlined and further integrated in the generalized procedure of hull form optimum design by seakeep-

ing considerations (4). The method is based on Bales ranking approach, which searches empirical relationship between certain hull form parameters and the generalized seakeeping estimator defined as an averaged and nondimensionalized complex reaction:

$$R(\hat{D}) \hat{=} R^*(\hat{G}) \quad (1)$$

where, \hat{D} is a set of significant reactions, forming the general ship behaviour in waves, and \hat{G} is a set of geometry parameters most influencing ship seakeeping. In (4) these factors are defined, as follows:

$$\hat{D} = (R_{sw}, R_s, Z_s, P_s, a_s, \tau/\tau_0, k, \alpha_k, l_{dmax}, l_{smax}, \frac{(\theta_m + \theta_f)}{2}, N_{aw}, N_{sh}, N_{sl}, N_{sr}) \quad (2)$$

and hence,

$$\hat{G} = (L/\nabla^{1/3}, B/T, T/L, D/T, C_B, C_W, C_M, LCB, LCF, \frac{(T_a - T_f)}{L}, S_f/S_m, S_a/S_m) \quad (3)$$

(See the list of used nomenclature at the end of the paper).

The optimum complex of design param-

¹⁾ Research Scientist

²⁾ Senior Research Scientist, Ph.D.

BSHC, Varna 9000, Bulgaria

ters is then searched by conditional optimization of eq.(1).

To calculate motion amplitudes and other wave related phenomena, a standard strip theory procedure using conformal mapping of cross sections by Lewis forms could be applied, considering the simplified generation of variant hull forms on the one hand, and the minimum computing time requirements, on the other one.

2. CALCULATION OF SHIP STABILITY CHARACTERISTICS

The authorized procedures for static and dynamic stability arms calculation (5) demand rigorous description of the ship lines. The simplified design approach, however, deals with general form characteristics, such as sectional halfwidths, draughts, areas and consequent static moments obtained as output of the optimization procedure (4). In accord with the well known fact that small local variations of the hull form do not affect significantly ship dynamic characteristics (3),(4), an attempt has been made to calculate stability diagram elements participating in eq.(2) by reconstruction of the cross section contours as analytical Lewis forms.

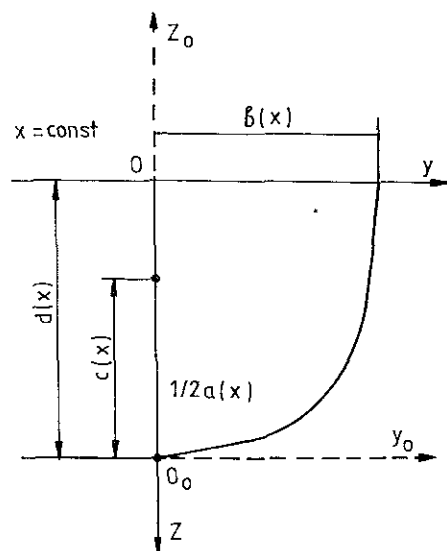


Fig.1. Cross Section Description

The original contour of the i-th cross section, defined on Fig.1 in the fixed coordinate system $O(x)yz$ by the integral parameters -

$a(x)$ - cross section wetted area;

$b(x)$ - halfbeam;

$c(x)$ - vertical position of the section centroid;

$d(x)$ - sectional draft;

is approximately described by (1):

$$\begin{aligned} y &= f_1(\alpha, C_i, i=1 \div 4) \\ z &= f_2(\alpha, C_i, i=1 \div 4) \end{aligned} \quad (4)$$

where, Lewis form coefficients C_i are to be expressed originally by a , b , c and d .

It is suggested, however, that for proper accounting of board entry at inclination, the section geometry parameters have to be evaluated with respect to the deckline rather than the waterline.

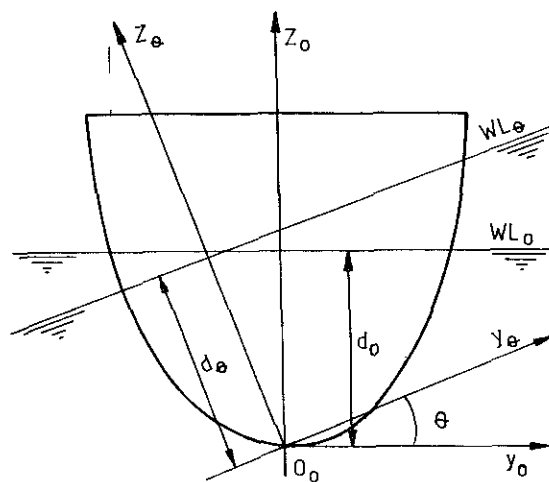


Fig.2. Coordinate Systems

For the inclination description a new coordinate system, $O_\theta(x)y_\theta z_\theta$, is introduced, as shown on Fig.2 with origin lying at the crosspoint of the baseline and the centerline. The index θ corresponds to the angle of inclination, to which the coordinate axes are rotated, following the free surface position ($\theta=0$ corresponds to the upright position).

Obviously,

$$\begin{aligned} \dot{y}_0 &= y \\ z_0 &= z + d(x) \end{aligned} \quad (5)$$

and hence,

$$\begin{aligned} y_\theta &= y_0 \cos \theta + z_0 \sin \theta \\ z_\theta &= z_0 \cos \theta - y_0 \sin \theta \end{aligned} \quad (6)$$

The sectional draft at inclined position, $d_\theta(x)$, is obtained from the equilibrium condition:

$$\nabla_\theta = \nabla_0 \quad (7)$$

by expressing sectional area as a function of $d_\theta(x)$ and successive approximation of eq.(7). Further, the procedure follows the well known routine (5), consecutively evaluating:

- the coordinates of the new CB position with respect to the rotated axes:

$$\begin{aligned} y_{B\theta} &= M_{z\theta} / \nabla_\theta \\ z_{B\theta} &= M_{y\theta} / \nabla_\theta \end{aligned} \quad (8)$$

and their respective values $y_B(\theta)$ and $z_B(\theta)$ in the upright coordinate system, obtained by eq.(6);

- the lever arm of weight stability:

$$l_g(\theta) = (KG - z_B(0)) \sin \theta \quad (9)$$

- the lever arm of form stability:

$$l_f(\theta) = y_B(\theta) \cos \theta + (z_B(\theta) - z_B(0)) \sin \theta \quad (10)$$

- the static stability arm:

$$l_s(\theta) = l_f(\theta) - l_g(\theta) \quad (11)$$

- the dynamic stability arm:

$$l_d(\theta) = \int_0^\theta l_s(\theta) d\theta \quad (12)$$

For calculation convenience the static stability arm curve is approximated by a

power series, as follows:

$$l_s(\theta) = \sum_{i=1}^n a_i \theta^{2i+1}, \quad (13)$$

which makes possible the analytical evaluation of the requested diagram elements l_{smax} , l_{dmax} , θ_m and θ_f .

3. PRACTICAL APPLICATION

The method of approximate evaluation of the stability diagram elements has been applied as an optional procedure in the course of the seakeeping optimization of a container-ship hull form, described in details in (3), and (4). To prove its applicability, comparative calculations of the stability diagrams have been effected applying different techniques, namely:

- rigorous presentation of the ship hull form (up to 30 offset points per section, parabolic interpolation). The program module is authorized by the Bulgarian Register of Shipping;
- widely spaced offsets (up to 9 points per section, linear interpolation). This module is incorporated in the complex program system SEA, which is intended for general seakeeping calculations;
- approximation of the cross section contours by the three-parameter Lewis form, as realized in the computerized design optimization system SEAOPT (3),(4).

The comparison illustrated on Fig.3 for the case of the form stability arm diagram of the basic hull shows quite acceptable coincidence between the predictions obtained by the three techniques. Obviously, the greater discrepancies occur in the region of the maximum stability arms but they never exceed 1.5%. It makes the suggested form approximation applicable for the purposes of ship stability estimation at initial design stages.

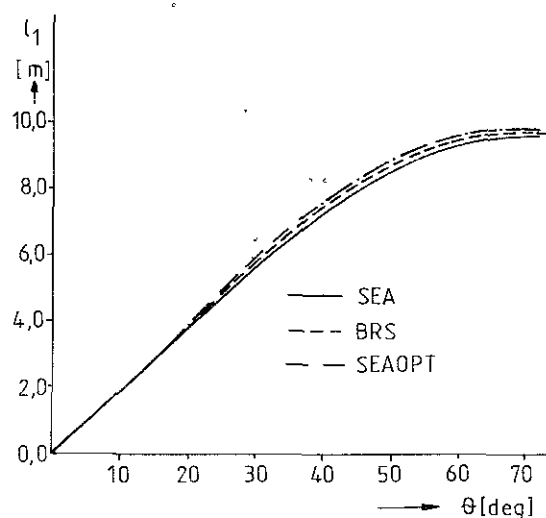


Fig.3. Lever Arm of Form Stability, Calculated by Different Techniques

NOMENCLATURE

a_s	- Significant vertical acceleration at FP
B	- Breadth, moulded
c_i	- Linear regression coefficients
C_B	- Block coefficient
C_W	- Waterline coefficient
C_M	- Middle cross-section area coefficient
D	- Depth, moulded
H_s	- Significant wave height
K	- Weather criterion
KG	- Position of CG above baseline
l_f	- Lever arm of form stability
l_g	- Lever arm of weight stability
l_s, L_d	- Static and dynamic stability arms
L	- Ship length
LCB, LCF	- Longitudinal centres of buoyancy and floatation
M_y	- Static moment of the volume around O_y axis
M_z	- Static moment of the volume around O_z axis
N_{aw}	- Added power in waves
N_{sh}, N_{sl}, N_{sr}	- Numbers of occurrence of deck wetness, slamming and screw racing

P_s, R_s, Z_s	- Significant pitch, roll and heave amplitudes
R_{sw}	- Still water resistance
R	- Rank criterion
S_a, S_f, S_m	- Cross-section area at AP, FP and at the middle
T, T_f, T_a	- Draft average, forward, aft
α_k	- Weather criterion gradient
∇	- Volume displacement
θ	- Heeling angle
θ_m	- Angle of maximum stability lever
θ_f	- Angle of flooding
τ_o	- Natural roll period
τ	- Average period of rolling in waves

REFERENCES

1. Athanassoulis, G., Loukakis, T., An Extended Lewis Form Family of Ship Sections and Applications to Seakeeping Calculations. NIUA, Athens, 1983.
2. Classification Rules of the Bulgarian Register of Shipping. Part IV: Stability. Varna, 1982 (in Bulgarian).
3. Kishev, R., Dimitrova, S., Variational Investigation of a Fast Containership Form for Ensuring Good Dynamic Stability in Waves. Proceedings of the 17th SMSSH. BSHC, Varna, 1988.
4. Kishev, R., Dimitrova, S., Gaberova, M., A Generalized Procedure for Rank Optimization Application to Ship Design. Proceedings of the IVth PRADS Symposium. Varna, 1989.
5. Rozhdestvensky, V., Lugovsky, V., Borisov, R., Mirokhin, B., Ship Statics. Sudostroenie Publ. House, Leningrad, 1986, (in Russian).

ON LARGE ROLLING IN FOLLOWING DIRECTIONAL SPECTRUM WAVES

Seiji TAKEZAWA*, Tsugukiyo HIRAYAMA**, Schivashis Acharrya ***

ABSTRACT

As well as in beam seas, rolling motion of a running ship become large in quartering sea. On the other hand, no rolling motions are expected in following long crested seas within linear theory. But it is known well that nonlinear mechanism induces rolling motions in following seas and in some cases capsizing will occur. Other than this, large rolling seems to be excited in following sea condition of short crest within linear phenomena. Our study is experimental and theoretical study on the rolling motion in following short crested irregular waves expressed by two dimensional spectrum and we call such waves as directional spectrum waves. Such a running experiment could be done owing to the newly developed wave maker installed at the end of long towing tank and such an experiment will be the first time in the world.

INTRODUCTION

Ship rolling in quartering seas is important for her stability and rolling in following seas is also important because encounter wave period become long and there are possibility that the resonant large rolling motions are excited. So, many studies were made on rolling in following long crested waves.

However, study on rolling motion in following short crested irregular seas had not been carried out yet in laboratory. This is mainly because that there did not exist such an experimental tank in which we can conduct a running ship test with generating and controlling such a multi directional seas as we want.

This paper show the experimental and theoretical results about rolling of a running ship in following directional spectrum wave in a long towing tank, and this could be realized by the newly developed wave maker[1] which can generate directional spectrum waves.

Here, we call short crested irregular waves as "directional spectrum waves" because we consider irregular waves that have continuous spectrum in direction as well as in frequency.

* Professor, Yokohama National University, Department of Naval Architecture and Ocean Engineering, Tokiwadai-156, Hodogayaku, Yokohama, JAPAN

** Associate Professor, Do.

*** Student of Post Graduate Course, Do.

EXPERIMENTAL TECHNIQUE

Generation of Directional Spectrum waves and Measurement

Wave generator: Up to this time, it had been considered that generation of directional spectrum waves with arbitrary directional function will be very difficult in a towing or long tank, because of wave reflection at the tank wall. On the other hand snake type wave maker installed in a square basin or rectangular tank can realize only a very small area of uniform directional spectrum wave.

For generating the uniform directional spectrum waves along a long towing tank, a new wave maker was installed at the end of the towing tank of Yokohama National University[1]. The type of this wave maker is so called snake type but the most important point is that this wave maker utilize the tank wall reflection positively as mirror image generators.

Considering infinite number of mirror images of the wave maker, we can understand that uniform wave field will be realized over the long tank.

Schematic description of this wave maker is shown in Fig.1 and an example of generated directional spectrum wave is shown in Photo 1. The wave directional characteristics of this tank are already confirmed [3,4]. Each unit with electric servo motor can be controlled independently according to electric signals through D/A converter. Digital wave

signal is pre-calculated as described in the next section and stored in floppy disk of personal computer.

Wave signal: As an expression of directional spectrum we consider the following expression.

$$S(\omega_0, \chi) = S(\omega_0)D(\chi) \quad (1)$$

ω_0 = absolute wave frequency

As directional spreading function D , next two expressions are familiar and here we adopted those expression.

$$D_1(\chi) = C_1 \cos^{2n} \chi \quad \text{where } -\frac{\pi}{2} \leq \chi \leq \frac{\pi}{2} \quad (2)$$

$$D_2(\chi) = C_2 \cos^{2s}(\frac{\chi}{2}) \quad \text{where } -\pi \leq \chi \leq \pi$$

$$\chi = \text{wave direction} \quad (3)$$

Parameters n and s are both concentration parameter and inverse of those parameters will be called as directional or angular spreading parameter. Between those two parameters there is an approximated relation as $s=4.3n$. C_1 and C_2 are coefficient for normalization.

Based on the expression (1), time history of voltage for wave maker signal are calculated considering transfer functions of wave maker units. As one dimensional wave spectrum we adopted so called P-M type. Significant wave height was adjusted to 6.7 m (7.6 cm in model scale), zero up crossing mean period to 11.3 sec (1.21 sec in model scale), and range of wave direction was limited as ± 90 deg. The number of frequency is 150 to 200. Direction interval is made 2 degrees and time interval is made 0.935 sec (0.1 sec in model scale).

Measurement of directional Wave: Directional spectra are estimated by using so called MLM (Maximum Likelihood Method) [2,3]. For this purpose we used arrays of five wave probes as illustrated in Fig.1 and 3. at rested position.

For the running condition, in case of head seas, we can estimate encounter directional spectrum by introducing small correction into MLM, but in following seas we can not apply MLM because of one to one correspondence in frequency domain can not be realized.

This situation is described in Fig.2. Fig.2(a) is an example of estimated directional spectrum from wave records at standing condition. Abscissa is circular frequency and ordinate is wave direction. On the other hand (b) is directional encounter wave spectrum in following sea condition transformed from (a). This transformation is made by the following formula

$$S(\omega_e, \chi) = \frac{S(\omega_0, \chi, V)}{1 - \frac{2\omega_0}{g} V \cos \chi} \quad (4)$$

The suffix o means absolute and e means encounter. Spectrum in the right hand side does not include V in this case. (Expression (4) including V is used for motion spectrum estimated by the transfer function expressed in absolute wave frequency.)

The relation between absolute wave frequency and encounter wave frequency is given by

$$\omega_e = \omega_0 - \frac{\omega_0^2}{g} V \cos \chi \quad (5)$$

Fig.2(c) shows one of contour curves of spectrum (a), and this curve is transformed into a thick solid curve in Fig.2(d). Others are transformed results of lattice in (c). As can be seen in this figure, corresponding frequency area is modified and folded, so one to one correspondence can not be realized in such a following sea case. So, MLM can not be applied for these following sea case.

From this reason, in following sea case, we adopted directional spectrum estimated at standing condition as input wave spectrum for obtaining response spectrum as shown equation (6)

$$S_z(\omega_0, \chi, V) = |H_z(\omega_0, \chi, V)|^2 S_\xi(\omega_0, \chi) \quad (6)$$

After this, the obtained spectrum is transformed into encounter frequency expression by formula (4).

Model and Experimental Conditions

Model ship: Principal particulars of two meters length model ship used is shown in Table 1. This is container ship type and was adopted in the ITTC's comparative study of ship motion. Two speeds are selected. $Fn=0.2$ (16.1 knots) and 0.275 (22.1 knots)

Experimental setup: Arrangement for model experiment in following sea condition is shown in Fig.3. The model ship is towed through gymbal mounted at the center of gravity of the model, and the heave, pitch and roll motions are measured. This time surge, yaw and sway motions are fixed and theoretical calculations are also made following this condition.

Generally speaking, for obtaining stable statistical values, about 200 encounter cycles are requested in irregular waves, so 8 to 14 times runs were executed for following sea experiment.

RESULTS and DISCUSSION

Example of Timehistory

Example of timehistories of wave and motions measured in following irregular waves are shown in Fig.4. Fig.4(a) corresponds to that in long crested wave and (b) corresponds to that in directional spectrum waves. Directional distribution is cos square. The wave height and absolute mean period are the same in both cases.

Of course encounter mean wave period is changed from that absolute value and become longer in following sea condition. Furthermore, from analysis, encounter mean period of directional spectrum waves becomes shorter than that of long crested irregular waves by about 10% in this case, but this can not be seen accurately in time history.

The most significant feature is that in following directional spectrum waves there appear rolling motion which can hardly seen in long crested following (encounter angle=0 degree) irregular waves except non-linear phenomena. The encounter mean wave period (23 sec) of this case is close to natural period of rolling so about 40 degrees maximum double amplitude can be seen. On the other hand pitch is reduced by 8%.

Example of Theoretical Estimation

Two dimensional spectrum: Left hand side in Fig.5, we show two dimensional frequency response functions and two dimensional spectra. Contour curves in the right hand side corresponds to that of left. Abscissa shows absolute (not encounter) wave frequency and ordinate shows component wave direction. Mean (or main) wave direction corresponds to zero degree.

(a) is "wave slope" spectrum transformed from wave elevation spectrum of Fig.2(a) at standing condition. This expression corresponds to transfer function expressed in wave slope. (c) and (g), each corresponds to theoretical transfer functions of pitch and roll at Froude number of 0.275. Theoretical calculations made by strip method (NSM) is done on the base of absolute wave frequency namely on wave length. Considering experimental condition, sway and yaw are fixed. Roll damping from free roll is used.

Transfer functions of angular motions are expressed by wave slope, so by wave slope spectrum multiplied by square of transfer functions, we can obtain theoretically estimated response directional spectrum as Fig.5(e) and (i), as already described by equation (6).

As can be seen in Fig.5(g), (h), the peak of transfer function of

roll exist not at 90 degrees but at about 60 degrees of following oblique waves. Such characteristic is already referred to, for example in reference [5], and this will results large rolling in following directional spectrum waves.

Comparison of Experimental Results with Estimations

Theoretically estimated two dimensional spectrum, as shown in Fig.5, can not be compared directly with experiment, because measured motion timehistory results in one dimensional spectrum. In other words this is the integrated results of two dimensional spectrum as following equation.

$$S_z(\omega_e) = \int_{-\pi}^{\pi} S_z(\omega_e, \chi) d\chi \quad (7)$$

So, here, comparison between one dimensional spectra is made.

Left hand side of Fig.6 correspond to $Fn=0.2$ and that of right to $Fn=0.275$. Directional function is cosine square type. Cal means calculated results, as already described, using theoretical directional transfer function and directional spectrum of waves estimated from the measured waves at standing condition.

FFT means that the one dimensional spectrum is obtained by Fast Fourier Transformation method and MEM means by Maximum Entropy Method. Results in Fig.6 are averaged results according to run number. Both methods show about the same results but relatively sharp peaks are obtained by MEM than by FFT.

Differences are seen between cal and experiment. Cal is smaller than experiments for rolling and larger for pitching. For the $Fn=0.2$ case, the peak frequency of encounter wave is near to that of natural rolling and large rolling is excited. For the $Fn=0.275$ case there seems two peaks, one correspond to wave and the other to roll natural frequency, so it will be said that resonant rolling motion was induced.

It should be noted that vertical scale of Fig.6 (c) and (f) are different each other and rolling of $Fn=0.275$ case is smaller than $Fn=0.2$ case, because wave period is near but out of roll natural period in case of $Fn=0.275$. In following sea case, pitch natural frequency is far out of wave frequency as shown by downward arrows.

About the reasons why the theoretical estimations show discrepancies with experimental results, discrepancies between wave directional spectrum measured at standing condition and running condition will be one reason. Estimations are made by the wave at standing condition. Secondary, the response spectrum is

the results of multiplication of wave directional spectrum and response function as shown in Fig.7 (this figure is quoted from Fig.5(b) and (h)). So the small estimation error of relative peak position of wave and transfer function will make a large differences.

Effect of angular spreading parameter: To see the effect of wave directional spreading on motions, we show Fig.8. The abscissa is angular spreading factor defined by $1/s$, and s is parameter used in equation (2). Four kind of s is considered. Ordinate is defined by square root of $M_o(\text{motion})/M_o(\text{wave})$. Here M_o means area of spectrum, so if this value equal 6.0 then by a wave with significant height of 1.0 meter, 6.0 degrees significant roll or pitch significant values are excited.

As shown in this figure, cosine square directional function correspond to $1/s=0.2$ approximately. And for pitch motion the effect of angular spreading factor is not large but for roll its effect is very large in experiment and so very important factor. Both for pitch and roll the experimental results show larger change than calculated results.

Statistical characteristics:

Next Fig.9, we show the results by statistical analyses. First, Fig.9 (a) is roll maximum double amplitude in following seas. Abscissa is by spectrum and ordinate is by statistical analysis. In the estimation from spectrum, we used formula for narrow banded spectrum including the dependency on number of peaks of time history. The peak number is about 200. Looking this figure the maximum double roll amplitude is lower than estimation from spectrum, and nonlinear large rolling phenomena as parametric oscillation will not be seen from this figure. Fig.10 correspond to maximum roll single amplitude according to directional spreading factor. This figure is very similar to that Fig.8(b), (d), and this means that the effect of angular spreading factor on maximum roll is similar to that on mean or significant value.

Finally, frequency distributions are presented. Fig.11 is roll double amplitude and Fig.12 corresponds to roll maxima. Solid curve in left is Rayleigh distribution and that in right is calculated by using band width parameter following Longuet-Higgins.

From these figures it will be said that rolling in following directional seas have not so abnormal features within our experiment of this time.

CONCLUSION

Following conclusion will be

made about the rolling motion of a running ship in following directional spectrum waves. We consider that this experiment is the first case conducted in a laboratory. But here it must be noted that the experiments are made under the condition that sway and yaw are fixed. Furthermore nonlinear oscillations like parametric oscillation are not considered here.

(1) In following directional spectrum waves the effect of directional spreading factor on roll is very large and small on pitch. This tendency is more severe than theoretical results.

(2) Even if the main wave direction is not beam or quartering, resonant large rolls about 40 degrees single amplitude were observed in directional spectrum waves as cosine square distribution of with 0 degree main direction, 6m significant wave height, 11sec mean wave period, and at the speed of 16 knots.

(3) Conclusion (1) show the sufficient controlling characteristics of the newly developed directional spectrum water wave maker in a long tank.

Finally, in our experiments the wave conditions are not changed widely so more research will be needed in this field.

Acknowledgement: The authors would like to acknowledge to Mr.K.Miyakawa and Mr.T.Takayama in developing new wave maker and execution of experiment. The authors also acknowledge the contribution of Dr.K.Kobayashi who developed computer program of NSM and prepare digital signals of wave maker.

REFERENCES

- [1] Takezawa, S., Hirayama, T., Miyakawa, K. and Takayama, T., The directional spectrum water wave generator for towing tanks. Journal of Kansai Society of Naval Architects, Japan, (JK SNA JAPAN) No.211, 1989, pp.83-95.
- [2] Maeda, H. & Kasahara, A., Generation and analysis of 2-dimensional irregular water waves. JK SNA Japan, No.202, 1986, pp.13-21.
- [3] Takezawa, S., Kobayashi, K. and Kasahara, A., Directional irregular waves generated in a long tank. Journal of Society of Naval Architects Japan (JSNA JAPAN) No.163, 1988.
- [4] Takezawa, S., Miyakawa, K., Takayama, T. and Itabashi, M., On the measurement of directional wave spectra by the new wave measuring system using laser beams. JSNA Japan, No.166, 1989.
- [5] Takaishi, Y., Yoshino, T., Takagi, M., Saitou, K., On the motions of a high speed container ship with a single screw in oblique waves. JSNA JAPAN, No.129, 1971, pp.67-81.

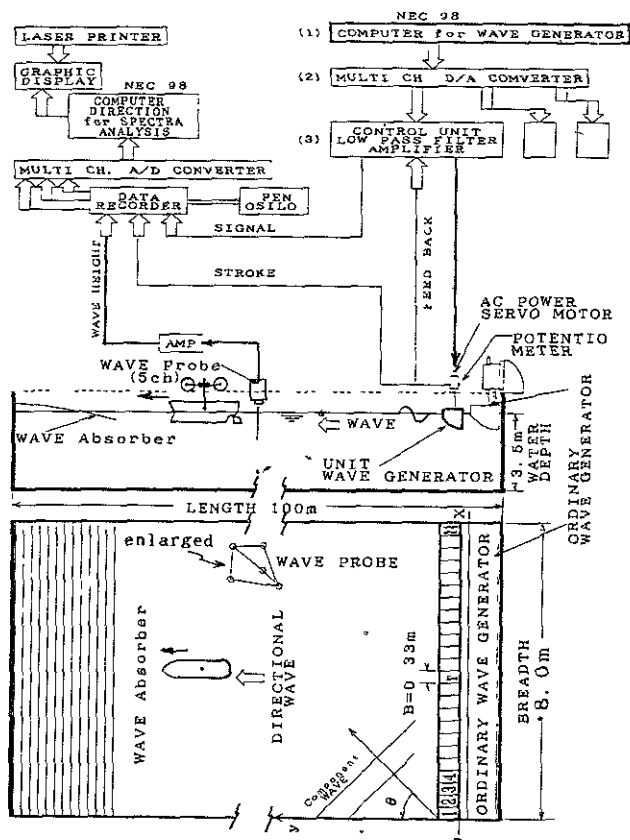


Fig.1 The directional spectrum water wave generator for long towing tank of Yokohama National Univ.



Photo.1 Example of generated wave.

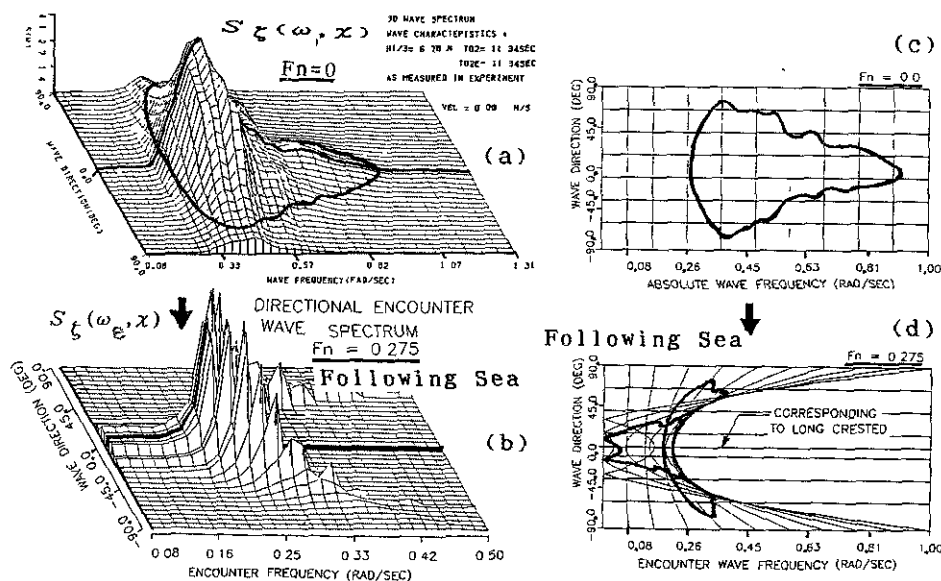


Fig.2 Example of two dimensional spectrum of wave. (a) is estimated at $F_n=0$ and (b) is transformed results from (a) under the condition of following sea ($F_n=0.275$). (d) correspond to transformation of contour curve and mesh of (c). The contour curve of (c) is drawn at 5% level of spectral peak of (a).

Table.1 Principal particulars

ITEMS	SHIP		MODEL*	
	SPECIFIED	VALUE	EXP	VALUE
LENGTH (P.P.)	175.00 (m)	2 000 (m)		
BREADTH	25.40 (m)	0 290 (m)		
DEPTH	15.40 (m)	0.176 (m)		
DRAFT	9.50 (m)	0 1086 (m)		
DISPLACEMENT	24742 (ton)	36.032 (kg)	36 030 (kg)	
BLOCK COEFF.	0.562	0 562		
C.G. FROM KEEL	9.52 (m)	0 1088 (m)	0 10865 (m)	
C.G. FROM DE	-3.164 (m)	-0.0382 (m)		
LONGI. RADIUS OF GYRATION	0 24 L_{KP}	0 24 L_{KP}	0.239 L_{KP}	
TRIM	0.0 (m)	0.0 (m)		
GM	1.0 (m)	0 01143 (m)	0.01154 (m)	
RM	10.52 (m)	0 1202 (m)		
T (PITCH)	$F_n = 0$	7.47 (sec) ←	0.799 (sec)	
	$F_n = 0.2$	7.46 (sec) ←	0.798 (sec)	
	$F_n = 0.275$	7.45 (sec) ←	0.796 (sec)	
T (HEAVE)	$F_n = 0$	7.25 (sec) ←	0.775 (sec)	
	$F_n = 0.2$	7.22 (sec) ←	0.772 (sec)	
	$F_n = 0.275$	7.24 (sec) ←	0.774 (sec)	
T (ROLL)	$F_n = 0$	19.4 (sec) ←	2.07 (sec)	
	$F_n = 0.2$	18.9 (sec) ←	2.02 (sec)	
	$F_n = 0.275$	18.2 (sec) ←	1.94 (sec)	
SCALE	1	2 / 175		

* with bilge keel

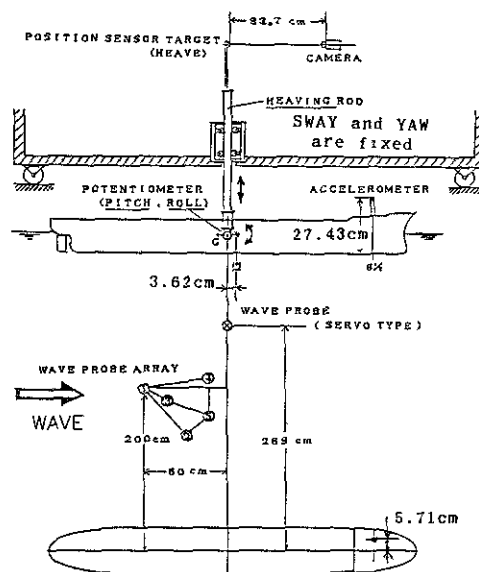


Fig.3 Schematic arrangement for model experiment in following sea condition.

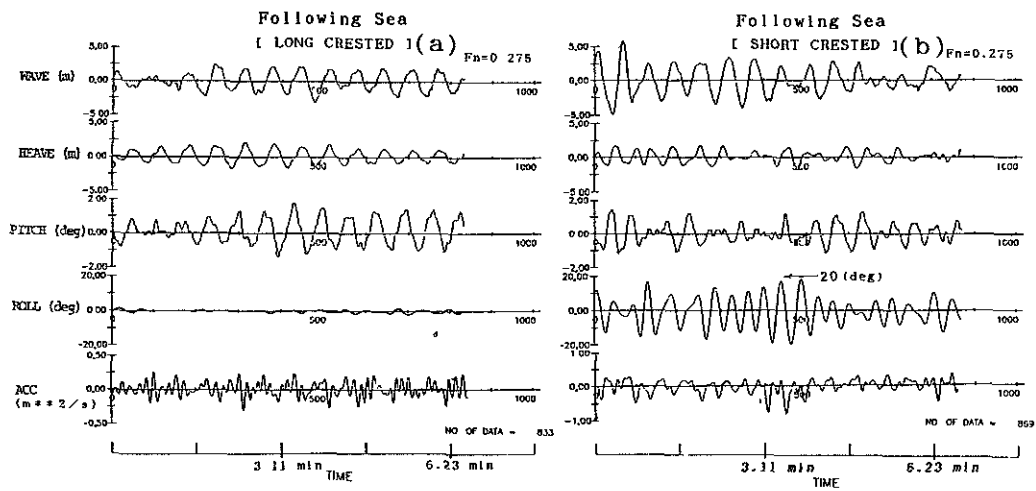


Fig.4 Example of measured timehistory in long crested(left) and short crested(right) irregular waves. Scale is drawn in actual ship scale. $F_n=0.275$. The wave condition is the same in both case: $H_{1/3}=6.78$ m (7.75 cm in model scale), $T_{02}=11.34$ sec (1.2 sec in model scale).

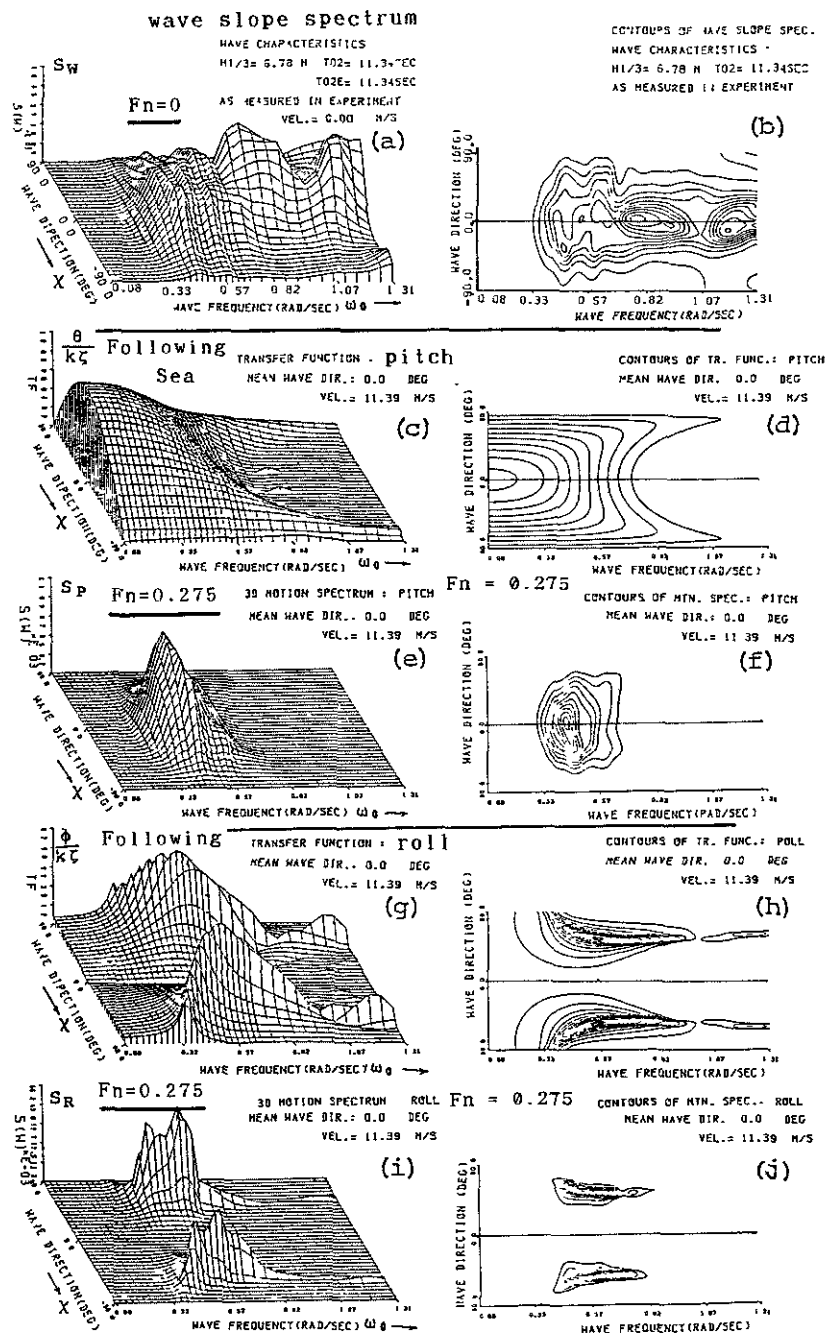


Fig.5 Analyzed directional wave slope spectrum (a) from measured timehistory at $F_n=0$. Theoretical transfer function of pitch(c) and roll(g). Estimated motion spectra of pitch(e) and roll(i). Right hand side correspond to contour curve of left figures. Except waves, Froude number is 0.275 and all are in following sea. All abscissa is drawn in absolute wave frequency.

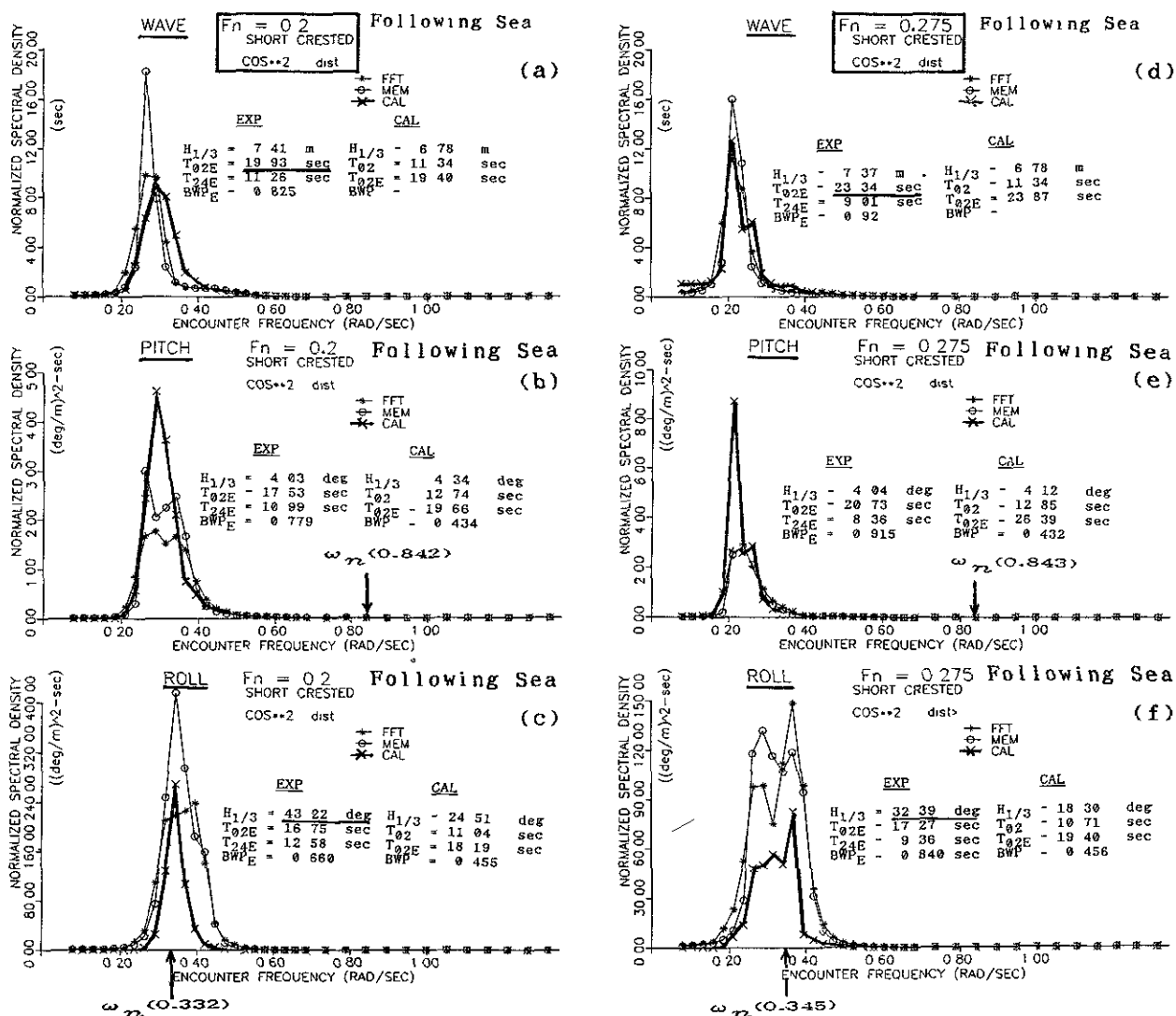


Fig.6 Analyzed one dimensional encounter spectrum of wave(a)(d), pitch(b)(e) and roll(c)(f) from experiment in following sea condition. Left hand side correspond to $F_n=0.2$ and right to 0.275. FFT means by Fast Fourier Transformation method and MEM by Maximum Entropy Method. Cal is estimation by theoretical transfer function and measured wave at standing condition. Natural frequencies of pitch and roll are shown by arrows.

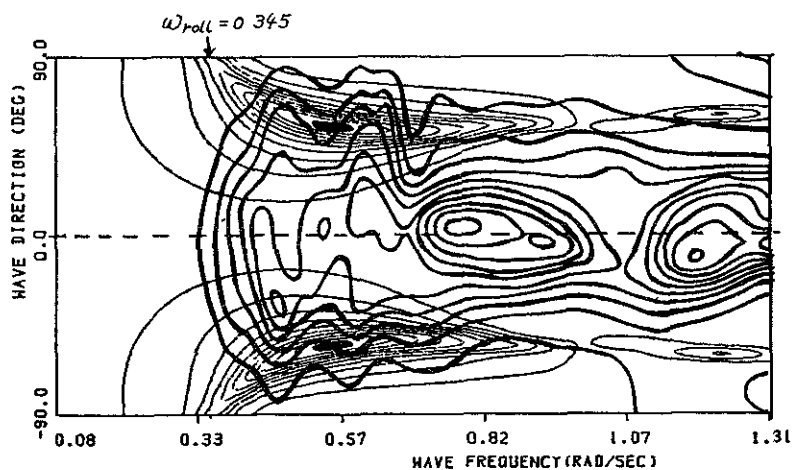


Fig.7 Superposition of contour curves of Fig.5(b) and (h). Multiplication of (b) and square of (h) make the response directional spectrum of roll. The resultant response spectrum will largely different by the small differences between peak position of spectra of wave and transfer function.

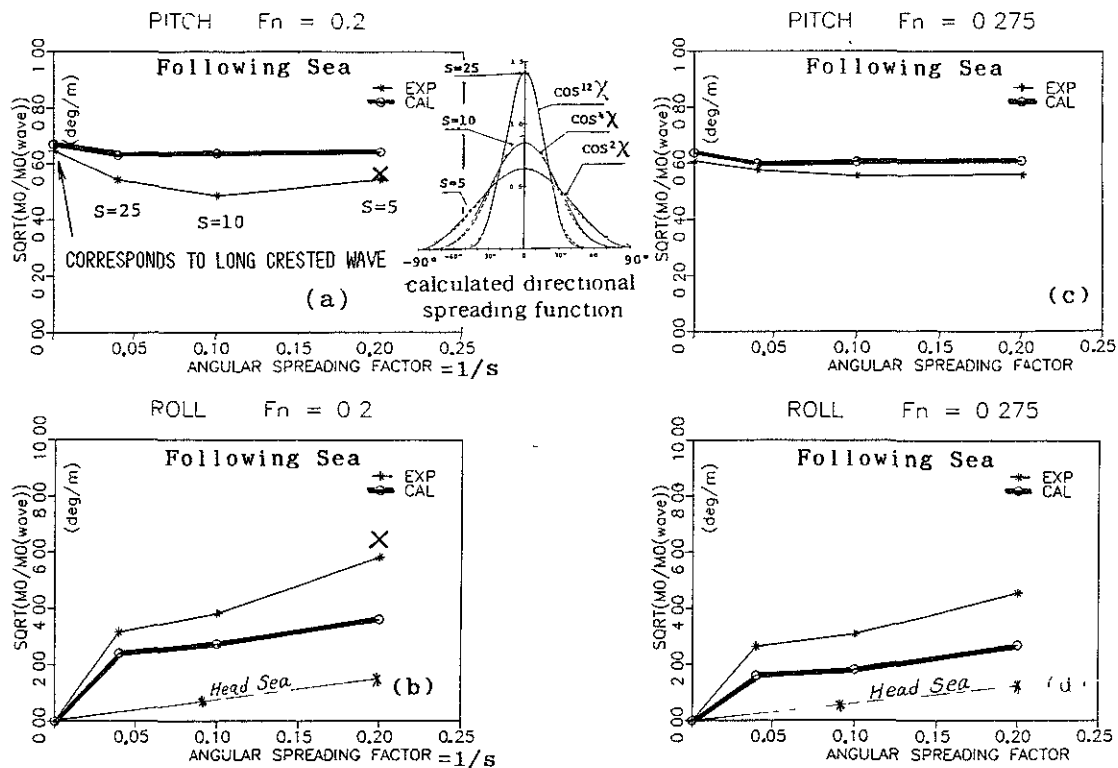


Fig.8 Ratio of root mean square of angular motion and that of wave elevation in ship scale against angular(or directional)spreading factor(=1/s). Significant wave height is around 6.7 m.T02=11.3 sec. Mark x in (a),(b) correspond to the data at low significant wave height (3.5 m) case.

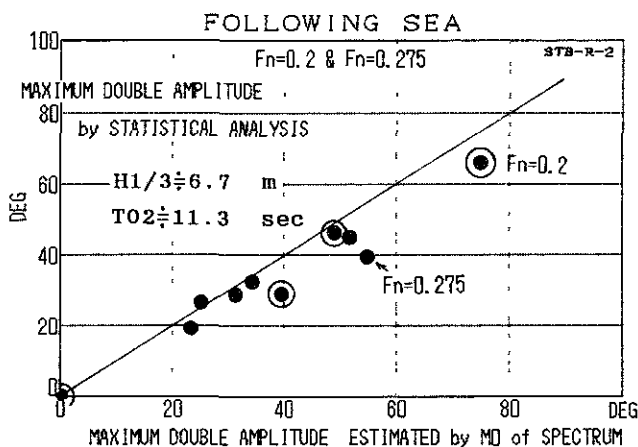


Fig.9 Maximum roll double amplitude by statistical analysis against by spectrum in following sea.

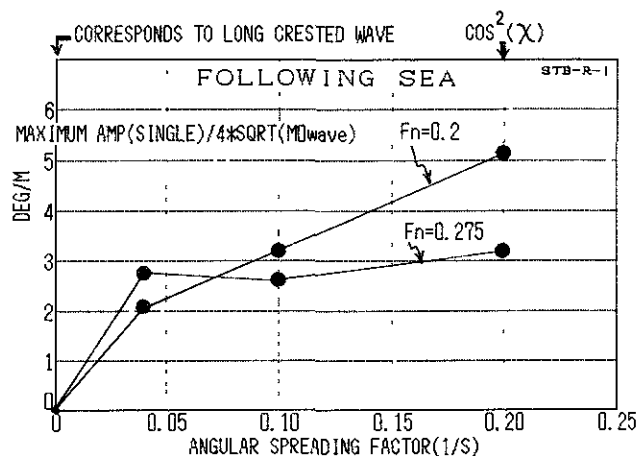


Fig.10 Maximum roll single amplitude against angular spreading factor. Ordinate is divided by significant wave height in ship scale.

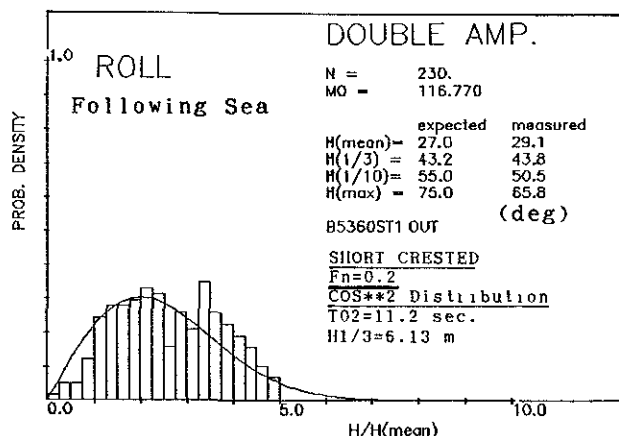


Fig.11 Frequency distribution of roll double amplitude. Solid curve show Rayleigh distribution.

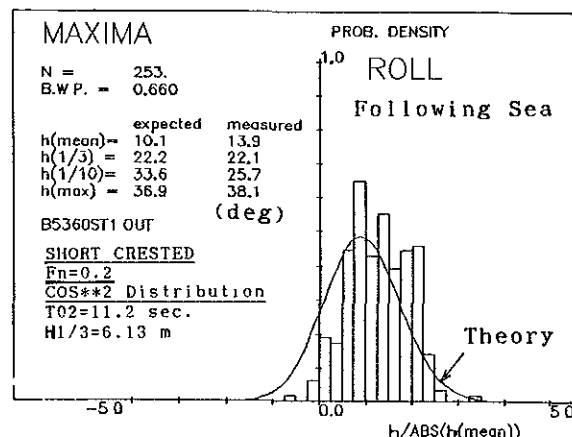


Fig.12 Frequency distribution of roll maxima in probability density scale.

DAMPING EFFECTS OF SAILS ON ROLL MOTION AND EFFECT OF SAIL ON CAPSIZING OF SAIL SHIPS IN GUSTS AND WAVES

N. Takarada

Y. Inoue

(Yokohama National University, Japan)

ABSTRACT

The present paper studies the effect of sail on roll damping of ships. For the analysis, a 26000 dwt bulk carrier with sails as an auxiliary drive is considered. From the results, it is observed that there is considerable reduction in roll amplitudes due to the sails, although there is a slight increase in heel angle. The effectiveness of the sail in roll damping increases with the wind velocity and with the area of the sail. The effect of heel on the hydrodynamic characteristics of the ship is relatively small.

1. INTRODUCTION

Rising oil prices and corresponding increase in operational costs prompted ship owners and shipyards to look for alternative sources of energy. An obvious source was the enormous 'wind power' which was mostly unused for merchant ships after the world war I. A first step in this direction was made in Japan about a decade ago. A sail ship was developed which had the ordinary engine for the main propulsion and an auxiliary propulsion system by sails. This type of sail ship is called 'Sail Assisted Ship'. After the successful development of the first ship, more than 15 ships of the same type were built in Japan. Matsumoto et al⁽¹⁾ reported the effect of sail on roll motion of this type of ships, through first ship model experiments and Takarada et al⁽²⁾ reported roll damping effect by sail in ITTC 87 session 3b.

In this paper the authors would like to present an evaluation method of 'roll damping effect' due to the sail in different wind speeds and different sail areas. Roll motion response functions of ship with and without sail in wind and waves can be estimated by using lift and drag

coefficients. Hydrodynamic behaviour and motion responses of heeled ship without sail are evaluated by 'three dimensional source technique'. And finally the effect of sails on capsize of the ship in gust and waves are discussed on the basis of 'Rules on Stability in Japan'.

2. PRINCIPAL PARTICULARS OF SAIL ASSISTED SHIP

The study has been conducted on a 26,000 DWT sail assisted log and bulk carrier. This ship was built in November 1984⁽³⁾.

Principal particulars are as follows :

Loa	162.00 m
Lbp	152.00 m
B (mld)	25.20 m
D (mld)	14.80 m
d (mld)	10.57 m
Cb	0.7909
GM	1.31 m
T	23.00 s
Sail area/Ld	0.478

3. STABILITY CRITERIA

equivalence of energy in a half period the following equation can be derived.

$$B_e = B_1 + \frac{8}{3\pi} \omega_e B_2 \phi_A \quad \dots (3)$$

B_1 and B_2 are constants obtained from experimental data.

Now, the lateral wind force acting on the sail is given by,

$$F_{SAIL} = \frac{1}{2} \rho_a C_f S_a (V_{wy} + \dot{\eta})^2 \quad \dots (4)$$

ρ_a : density of air

C_f : drag coefficient

S_a : sail area

V_{wy} : wind velocity

η : horizontal displacement of motion of the sail (positive in starboard)

By expansion of (4)

$$F_{SAIL} = \frac{1}{2} \rho_a C_f S_a (V_{wy}^2 + 2 V_{wy} \dot{\eta} + \dot{\eta}^2) \quad \dots (5)$$

Deleting the terms independent of the motion of the sail,

$$N_{S2} \dot{\eta} = \rho_a C_f S_a (V_{wy} \dot{\eta} + \frac{1}{2} \dot{\eta}^2) \quad \dots (6)$$

where

N_{S2} : damping coefficient due to horizontal motion of the sail

From the energy method described above, we obtain,

$$N_{S2} = \rho_a C_f S_a (V_{wy} + \frac{4}{3\pi} \omega_e \eta_A) \quad \dots (7)$$

For the rolling and yawing of ship, the damping coefficients are described,

$$N_{S4} = \rho_a C_f S_a (V_{wy} + \frac{4}{3\pi} \omega_\phi l_z \phi_A) \quad \dots (8)$$

$$N_{S8} = \rho_a C_f S_a \{ V_{wy} + \frac{4}{3\pi} \omega_e l_x \phi_A \} \quad \dots (9)$$

where

l_z : vertical distance from C.G. of ship to the center of sail (positive in downward)

l_x : horizontal distance from C.G. of ship to the center of sail (positive in offward)

η_A : amplitude of swaying motion

ϕ_A : amplitude of yawing motion

Considering now only the lateral motion due to the rolling,

we have,

$$\begin{aligned} \text{lever} \quad y &= \eta + l_z \phi \\ \text{velocity} \quad v &= V_{wy} \dot{\psi} + \dot{\eta} + l_z \dot{\phi} \end{aligned}$$

Now considering both the rolling and yawing,

$$F_{S\eta 1} = N_{S2} (-V_{wy} \dot{\psi} + \dot{\eta} + l_z \dot{\phi} + l_x \dot{\psi}) \quad \dots (10)$$

The damping moment in rolling and yawing motion are given as under.

$$M_{S\phi 1} = N_{S4} l_z (-V_{wy} \dot{\psi} + \dot{\eta} + l_z \dot{\phi} + l_x \dot{\psi}) \quad \dots (11)$$

$$M_{S\psi 1} = N_{S8} l_x (-V_{wy} \dot{\psi} + \dot{\eta} + l_z \dot{\phi} + l_x \dot{\psi}) \quad \dots (12)$$

The formulation presented above applies to the case of single sail. In the case of multiple sails, air damping moment of each of the sail must be calculated and by addition, the damping effect of the sail system can be evaluated.

5. HYDRODYNAMICAL BEHAVIOUR AND MOTION RESPONSES OF HEELED SHIP

The sail ship heels during navigation, due to wind forces. In this situation, underwater hull surface would change to unsymmetrical body. Therefore, heeled navigation would bring about the change of added mass, potential damping, exciting forces. By using three dimensional source technique, hydrodynamic behaviours of heeled condition is investigated here. The hull wetted surface is divided into 250 panel elements and heeled angles are taken as 0, 10 & 20.

Roll damping coefficient 'N', obtained by these calculation are observed to be about 1/4th of total damping, that is around 0.003. On the other hand, the roll damping coefficient obtained from free roll tests is above 0.01. Hence, the wave damping is considered to be relatively small in comparison with the total damping in roll motion (ref. Fig. 4 & 5). In the present discussion, only 'increase of damping due to wind force is taken into consideration, neglecting increase of wave damping due to heel.

6. SAIL EFFECT ON STABILITY CRITERIA

From the results of the calculation the following effects on stability characteristics are observed.

The sail contributes significantly to the roll damping. However, there is a slight increase in the heel angle due to the sail. (ref. Fig. 2 & 3). In figures, two cases of GM - metacentric height - is considered. It can be observed that the damping due to the sail is more for the case with low GM value. As a result of this, for small GM values also, the increase in rolling amplitude is very little.

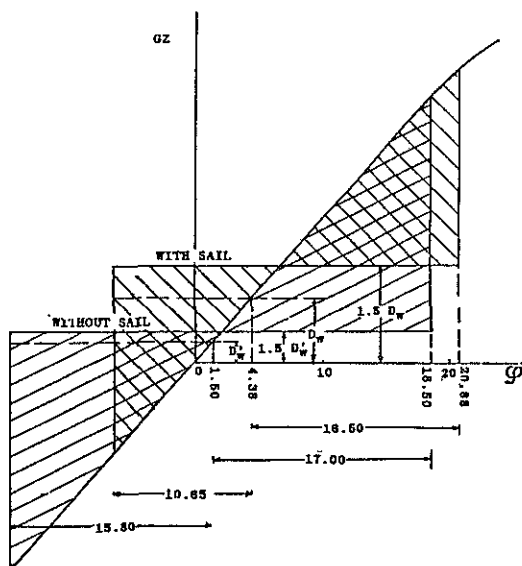


Fig. 2 Stability with and without Sail

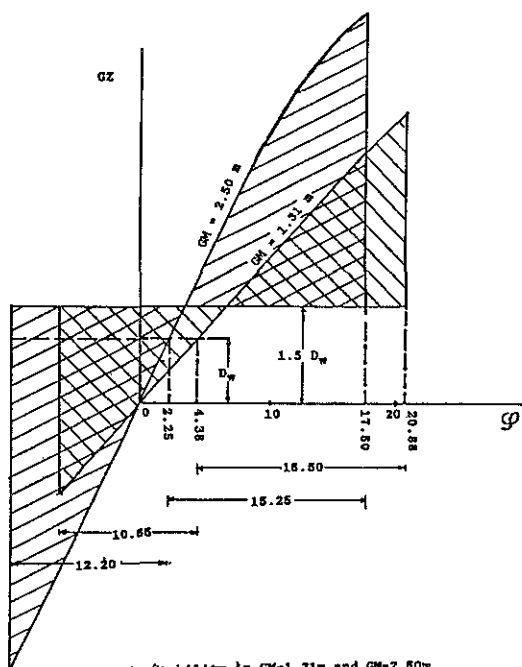


Fig. 3 Stability in GM=1.31m and GM=2.50m

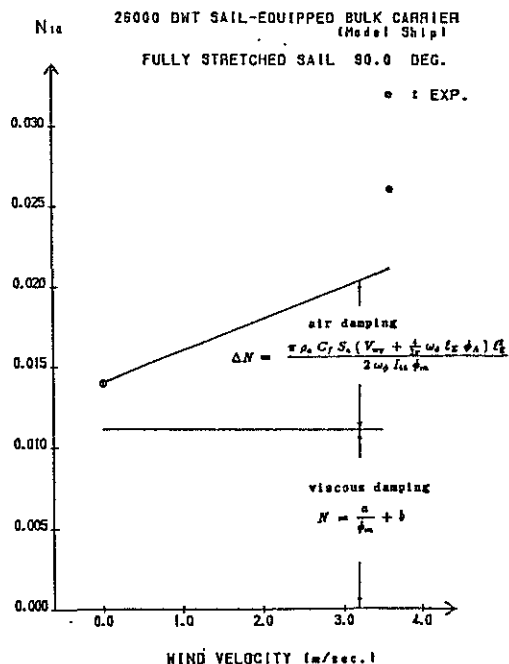


Fig. 4 Variation of N Coefficient with Wind Velocity

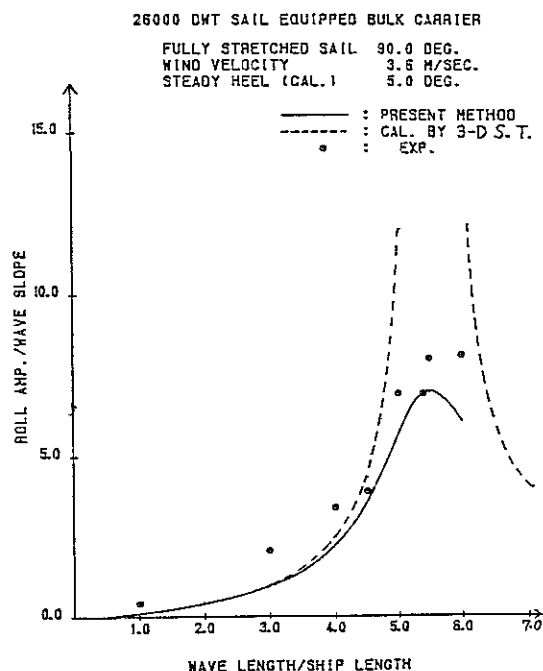


Fig. 5 Roll Motion Response

REFERENCES

1. N. Matsumoto, M. Inoue, M. Sudo : Operating Performance of a Sail Equipped Tanker in Waves and Wind, STB' 82.
2. N. Takarada, J. Obokata: Model Test of a Sail Training Ship, ITTC' 87.
3. Report of the Model Tests of Sail Characteristics and Roll Motion of a 28000 DWT Bulk Carrier, SUMITOMO HEAVY INDUSTRIES, JAPAN, February, 1982.

A FAST NUMERICAL SOLVER FOR LARGE AMPLITUDE SHIP MOTIONS SIMULATIONS

Bradley K. King ¹

ABSTRACT

The theoretical study of large amplitude ship motions is very complex. While it is desirable to obtain global criteria for ultimate stability assessment, the present understanding of such phenomena is insufficient to obtain valid limits. A viable method of investigation currently available consists of performing nonlinear time domain ship motions simulations in near capsize conditions.

The paper discusses a program to perform these large amplitude simulations. The governing equations are presented, and the numerical schemes employed to efficiently resolve the resulting nonlinear differential equation system are discussed. The methods used to make the approach rapid and reliable will be presented. The results of certain simulations will be presented and compared with experiments.

INTRODUCTION

Linear seakeeping theories have been widely developed and verified for a number of years. Among the most popular is the strip theory of Salvesen, Faltinsen, and Tuck [9]. These theories are very useful for studying the seakeeping performance of ships, but provide little information about large amplitude motions and near capsize conditions. Many researchers have considered specific motions problems in greater detail to allow for certain nonlinear effects; for example, Neyfeh [6] has studied extensively the effects of certain nonlinearities on roll motions. Several years ago Oakley, Paulling, and Wood [7] developed a program to perform time domain simulations of the large amplitude motions of a ship. Their method was quite successful and demonstrated the practical advantages of such an approach.

Time domain simulations allow for many nonlinear effects to be taken into account in a straightforward manner. While such methods cannot give global ship stability criteria directly, they are useful for studying accidents and critical cases or for performing systematic studies in the same manner as experiments.

The approach presented here does not deviate significantly from that taken by Oakley et al. and many others, for example Elsimillawy [2]. The goal of the present work is to perform the nonlinear simulation of the motions with the best information currently available, and to develop a method that is reliable and sufficiently rapid to allow significant validation and comparison with experiments. By this approach, the aspects that are not well modeled may be singled out and improved in the future.

THEORETICAL APPROACH

The approach taken is described in the following sections. The exact kinematic and dynamic model of the ship motions presents no particular difficulty and is fully retained. The exciting forces, especially those due to the fluid flow field, must be modeled approximately.

The incident waves are regarded as a sum of sinusoidal waves that satisfy the linearized free surface boundary condition. The linear wave approach does not model large breaking waves or wave impact, but the nonlinear models currently available are also incapable of modeling these important phenomena. It was decided that the complexity of implementation

¹Visiting Researcher, Bassin D'Essais des Carènes, 8 Bd. Victor, 75732 Paris CEDEX 15, FRANCE.

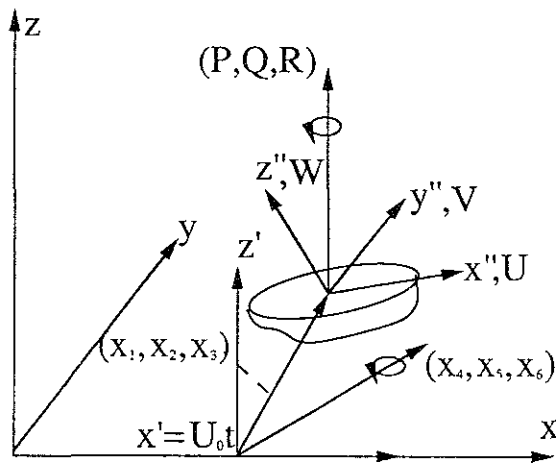


Figure 1: Coordinate Systems

of nonlinear models for the incident waves, especially in the case of irregular seas, prevented their use at the present time.

Kinematics

For a floating body or a ship, three coordinate systems are defined. The first system is a fixed system defined by its origin and the three coordinates (x, y, z) (Figure 1). Next a coordinate system in steady translation with speed U_0 is defined by the coordinates: (x', y', z')

$$\begin{aligned} x' &= x + U_0 t \\ y' &= y \\ z' &= z. \end{aligned}$$

The center of gravity of the ship is the origin of the third system denoted by: (x'', y'', z'') . The origin of this system with respect to the steady translating system is given by the vector (x_1, x_2, x_3) . The rotation of the ship is given by the vector (x_4, x_5, x_6) , also measured with respect to the translating system. In this manner a point in the ship-fixed system with the displacements, $(x_1, x_2, x_3, x_4, x_5, x_6)$ may be represented in the absolute system by a transformation of coordinates (see for example [3]):

$$\begin{Bmatrix} x \\ y \\ z \end{Bmatrix} = \begin{Bmatrix} x_1 + U_0 t \\ x_2 \\ x_3 \end{Bmatrix} + [T] \begin{Bmatrix} x'' \\ y'' \\ z'' \end{Bmatrix} \quad (1)$$

$$[T] = \begin{bmatrix} c_5 c_6 & s_4 s_5 c_6 - c_4 s_6 & c_4 s_5 c_6 + s_4 s_6 \\ c_5 s_6 & s_4 s_5 s_6 + c_4 c_6 & s_4 s_5 s_6 - s_4 c_6 \\ -s_5 & s_4 c_5 & c_4 c_5 \end{bmatrix}$$

$$\begin{aligned} c_n &\equiv \cos x_n \\ s_n &\equiv \sin x_n \end{aligned}$$

The velocities in the steady translating system are linked to the velocity vectors \vec{V} and $\vec{\omega}$ by:

$$\begin{Bmatrix} \dot{x}_1 \\ \dot{x}_2 \\ \dot{x}_3 \end{Bmatrix} = [T] \begin{Bmatrix} U \\ V \\ W \end{Bmatrix} \quad (2)$$

$$\begin{Bmatrix} \dot{x}_4 \\ \dot{x}_5 \\ \dot{x}_6 \end{Bmatrix} = [S] \begin{Bmatrix} P \\ Q \\ R \end{Bmatrix}$$

$$[S] = \begin{bmatrix} 1 & s_4 \tan x_5 & c_4 \tan x_5 \\ 0 & c_4 & -s_4 \\ 0 & s_4/c_5 & c_4/c_5 \end{bmatrix}$$

The velocities \dot{x}_i presented in this manner represent the motions of the ship with respect to the steadily advancing coordinate system. The integral of these velocities represent the position of the ship in the same coordinate system, linked to the absolute system by a simple translation of coordinates at steady velocity.

Dynamics

The dynamic equation is written in the ship-fixed system as:

$$\begin{Bmatrix} \vec{F} - m\vec{\omega} \wedge \vec{V} \\ \vec{\Gamma} - \vec{\omega} \wedge \vec{h} \end{Bmatrix} = [M] \begin{Bmatrix} \dot{U} \\ \dot{V} \\ \dot{W} \\ \dot{P} \\ \dot{Q} \\ \dot{R} \end{Bmatrix} \quad (3)$$

$$[M] = \begin{bmatrix} \begin{bmatrix} m & 0 & 0 \\ 0 & m & 0 \\ 0 & 0 & m \end{bmatrix} & [0] \\ [0] & [I] \end{bmatrix}$$

$$[I] = \begin{bmatrix} I_{xx} & 0 & -I_{xz} \\ 0 & I_{yy} & 0 \\ -I_{xz} & 0 & I_{zz} \end{bmatrix}$$

where $\vec{V} = \{U, V, W\}$ represents the ship velocities in the instantaneous ship-fixed system and $\vec{\omega} = \{P, Q, R\}$ represents the angular velocities of the ship system with respect to the coordinate system in translation. M is the generalized mass matrix, m being the mass of the ship. Written in this manner, the moments of inertia, I_{jk} , do not depend on the motions. The forces denoted by \vec{F} and $\vec{\Gamma}$ represent the sum of all forces acting on the ship.

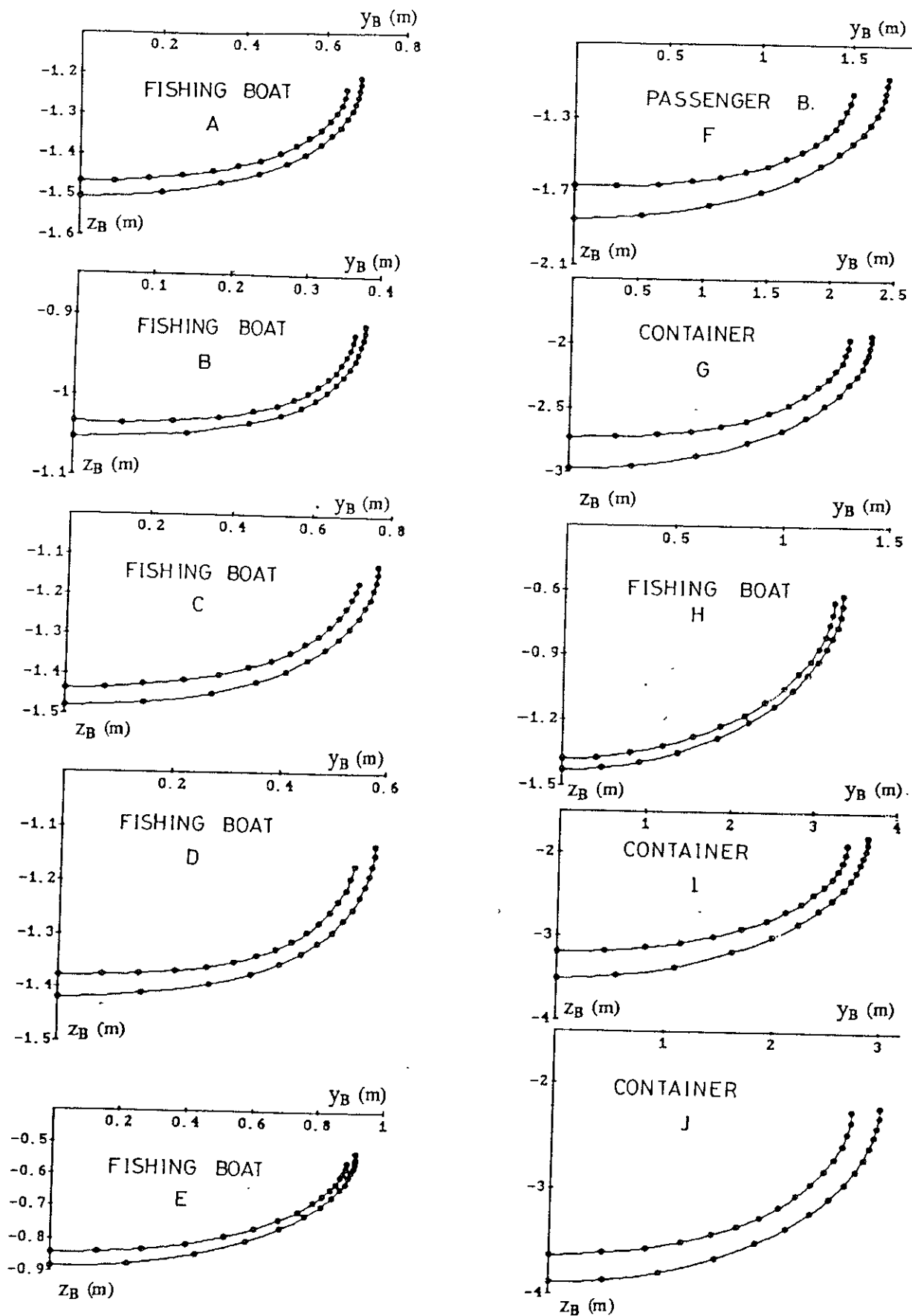


Fig. 5 Trajectories of center of buoyancies in still water and wave at crest amidship

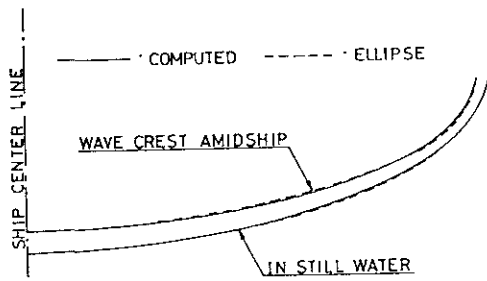


Fig. 6 Trajectories of C.B. and ellipses for Ship E

a_s and a_w shown in Figs. 7 and 8, denote the long axes in still water and at wave crest amidship and b_s, b_w the short axes respectively. Non-dimensional values of these axes are introduced as follows:

$$\begin{aligned} \text{non-dimensional long axis} &= (a_s \text{ or } a_w)/B \\ \text{non-dimensional short axis} &= (b_s \text{ or } b_w)/d \end{aligned} \quad (10)$$

The non-dimensional long and short axes are deeply concerned with F_E/d . F_E/d is a newly defined hull form parameter which means a ratio of effective freeboard to draft derived as:

$$F_E/d = (\text{volumes of main hull between L.W.L. and upper deck}) / (\text{water plane area} \times d) \quad (11)$$

In Figs. 7 and 8, the long and short axes keep linear relations for the F_E/d in all cases.

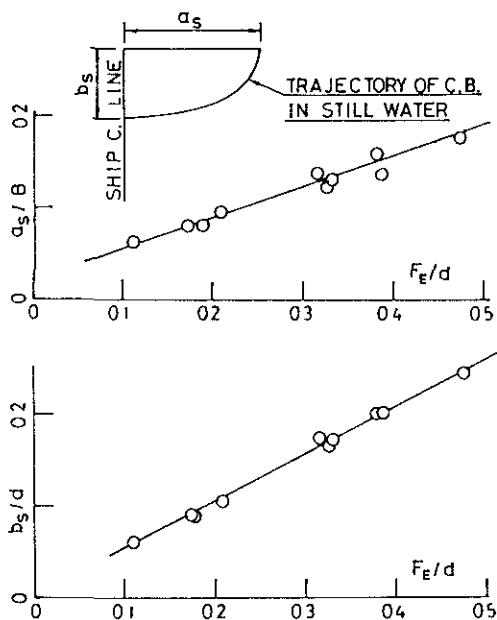


Fig. 7 Long and short axes of trajectories of C.B. in still water

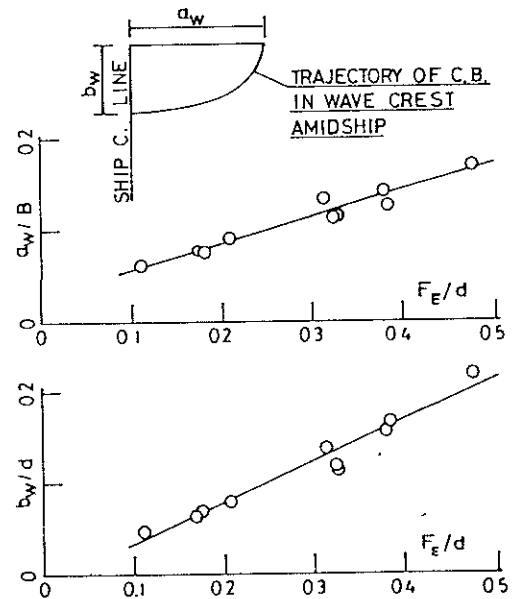


Fig. 8 Long and short axes of trajectories of C.B. at wave crest amidship

4. BR AND BR_w

Fig. 9 shows an inclined condition of a ship in still water. The center of buoyancy moves from B to B_s . The buoyancy force at B_s acts upward to water surface. BR is a horizontal lever between B and B_s . This BR is represented as:

$$BR = y_{BS} \cos \phi + (z_B - z_{BS}) \sin \phi \quad (12)$$

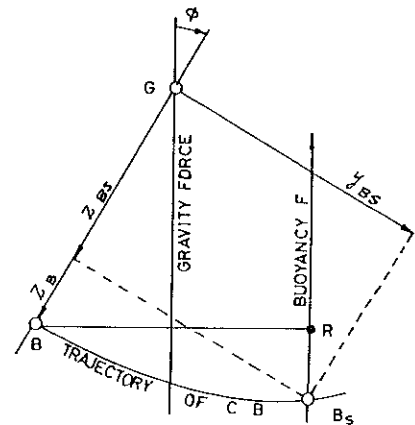


Fig. 9 B_s and BR in inclined condition

In the same way, BR_w for wave crest amidship can also be represented as

$$BR_w = y_{BW} \cos \phi + (z_B - z_{BW}) \sin \phi \quad (13)$$

Both BR and BR_w were calculated for the trajectories of center of buoyancy shown in Fig. 5. The results are shown in Figs. 10 and 11. Now we will explain with some

External Forces

The exciting forces acting on the body are divided somewhat unconventionally. The hydrostatic forces and radiated wave forces are typically identified as spring stiffness, damping, and added mass. Here they are considered as being external forces in order to retain the generality of the differential equation system. The external forces consist of the following:

- Incident wave forces, including the hydrostatic forces
- Diffracted wave forces
- Viscous forces (primarily for roll motions)
- Forces due to lifting surfaces: rudders, stabilizing fins or the entire body at an angle of attack
- Eternally imposed forces, mooring systems, wind, etc.
- Ship resistance and propulsive forces at forward speed

Incident wave forces: The forces due to the incident waves are the result of the integration of the pressure field created by the undisturbed incident wave potential. The forces may be written in the following manner:

$$\begin{aligned}\vec{F}_I &= \iint_{S_e} dS \vec{n} p_I \\ \vec{\Gamma}_I &= \iint_{S_e} dS \vec{r} \wedge \vec{n} p_I\end{aligned}\quad (4)$$

with:

S_e = the hull wetted surface

\vec{n} = the hull normal

\vec{r} = the vector between the center of gravity and the integration variable

p_I = the pressure due to the incident wave

$$p_I(\vec{x}, t) = -\rho \frac{\partial}{\partial t} \phi_I - \rho g z$$

$$\phi_I(\vec{x}, t) = ig \sum_n \frac{\eta_n}{\omega_n} e^{k_n z} e^{i k_n (x \cos \beta_n + y \sin \beta_n)} e^{i \omega_n t}$$

P_I and ϕ_I are taken as the real parts of the expressions.

To facilitate the integration of the pressure on the hull surface, the incident wave potential may be written in the coordinate system linked to the hull center of gravity.

$$\begin{aligned}p_I(\vec{x}'', t) &= \rho g \sum_n \eta_n e^{i \omega_n t} e^{\gamma_n} \prod_{j=1}^3 e^{\alpha_{nj} x''_j} \\ &\quad - \rho g \left(x_3 + \sum_{j=1}^3 T_{3j} x''_j \right)\end{aligned}\quad (5)$$

$$\alpha_{nj} = k_n (T_{1j} \cos \beta_n + T_{2j} \sin \beta_n + T_{3j})$$

$$\gamma_n = k_n (x_3 + i((x_1 + U_0 t) \cos \beta_n + x_2 \sin \beta_n))$$

The pressure is first integrated along each ship section at x''_1 constant, then along the ship length. By assuming that each ship section may be represented as a series of straight line segments, it is possible to integrate (4) analytically for each section. This integration is performed up to the surface $z = 0$ or the surface $p(\vec{x}'', t) = 0$. Linearized theory indicates that the integrations should be performed up to the calm water plane instead of the exact free surface. There is much controversy about the appropriate expression for the pressure above the calm water plane (see [10]); for this reason the two options are made available for investigation.

Diffracted wave forces: The forces due to the diffracted incident waves are determined from a linear seakeeping calculation, either of strip theory nature or a three-dimensional diffraction code. This computation, if performed for the mean hull position and the non-linear change due to the changing hull position, is not taken into account. The forces take the form:

$$\vec{F}_D = \sum_n \eta_n \vec{X}_D(\omega_n, \beta_n) e^{i \omega_n t}$$

$$\vec{\Gamma}_D = \sum_n \eta_n \vec{Y}_D(\omega_n, \beta_n) e^{i \omega_n t}$$

with

\vec{X}_D = Diffraction force at frequency ω_n with wave direction β_n

\vec{Y}_D = Diffracted wave moment.

The values of \vec{X}_D and \vec{Y}_D are considered as program inputs, and their determination is not discussed here. The effect of a change of body position on the diffraction force remains a point of further investigation.

Radiated wave forces: The waves created by the ship motions are taken into account, as in the case of the diffracted waves, by the use of results of a linear computation at the mean hull position. Ignoring the effect of the changing body orientation, the radiated wave force may be written in the form:

$$\vec{F}_j(t) = -\mu_{jk}\ddot{x}_k(t) - \int_0^t d\tau h_{jk}(\tau)\dot{x}_k(t-\tau) \quad (6)$$

$$h_{jk}(t) = \frac{2}{\pi} \int_0^\infty d\omega B_{jk}(\omega) \cos \omega t \quad (7)$$

$$\mu_{jk} = \frac{1}{2} A_{jk}(\omega^*) + \frac{1}{4\sqrt{\omega^*}} \int_0^{\omega^*} d\xi \frac{A_{jk}(\xi)}{\sqrt{\xi}} \quad (8)$$

h_{jk} represents the impulse response function for the force in direction j due to an impulsive motion in the direction k

μ_{jk} represents the infinite-frequency added mass.

The formula for the infinite-frequency added mass is the result of an asymptotic development by Greenhow [5] using the Kramers-Kronig relations; ω^* is the highest frequency for which A_{jk} is known. In the case of monochromatic waves and linearized motions, this general expression may be simplified to added mass and damping for harmonic motion, but when the equations are nonlinear the response is not necessarily monochromatic and the general form as given should be retained.

Viscous forces: In the case of roll motions it is clear that this formulation is insufficient for the representation of the forces due to the motion. In the roll direction it is imperative that the viscous forces are taken into account. There is currently no rational means of reliably predicting the viscous damping. One of the most frequently used expressions takes the form:

$$F_{viscous} = -b_1\dot{x}_4 - b_2\dot{x}_4|\dot{x}_4| \quad (9)$$

The values of the damping coefficients are usually taken as the values found experimentally at the resonance frequency, knowing that the damping is most important near the resonance peak.

Lifting surface forces: For a ship that is free to sway and yaw in waves, a system is needed to maintain the heading. For this purpose a fairly simple autopilot model has been

implemented. The rudder angle requested is given by the command law:

$$\delta_d(t) = k_P x_6 + k_D \dot{x}_6 + k_I \int_0^t dt x_6 \quad (10)$$

The rudder force is modeled by the simple formulas:

$$\begin{aligned} F_1(t) &= D & L &= 1/2\rho V^2 C_L \\ F_2(t) &= L & D &= 1/2\rho V^2 C_D \\ F_3(t) &= 0 & C_L &= \frac{2\pi\mathcal{R}}{2+\mathcal{R}} \\ \Gamma_4(t) &= (z_{cg} - z_{cp})L & C_D &= \frac{C_L^2}{\pi\mathcal{R}} \\ \Gamma_5(t) &= 0 & \mathcal{R} &= \frac{(2 \cdot \text{span})^2}{\text{area}} \\ \Gamma_6(t) &= -(x_{cg} - x_{cp})L \end{aligned} \quad (11)$$

\mathcal{R} is the effective rudder aspect ratio

(x_{cp}, y_{cp}, z_{cp}) is the rudder's center of effort.

The rudder inflow velocity is assumed to be $U_0 + \dot{x}_1$ with its direction remaining parallel with the ship. It is obvious that the influence of the propeller, the incident waves, the yaw angle, and other phenomena play an important role, but their influence is left to further investigation.

Resistive and propulsive forces: The ship resistance and propeller thrust, which become unsteady with the ship motions in waves, are extremely difficult to model realistically. The effect of the incident waves on the propeller forces and the added resistance in waves are examples of the effects that cannot be modeled accurately at present. For these reasons no model is currently implemented, and the ship is either given a steady forward speed or allowed to deviate from its steady speed without restriction.

The Differential Equation System

With the kinematic and dynamic equations, as well as the external force components explained above, it is possible to establish a system of 12 coupled first-order differential equations to be resolved:

$$\begin{Bmatrix} \dot{x}_1 \\ \dot{x}_2 \\ \dot{x}_3 \\ \dot{x}_4 \\ \dot{x}_5 \\ \dot{x}_6 \end{Bmatrix} = \begin{bmatrix} [T] & [0] \\ [0] & [S] \end{bmatrix} \begin{Bmatrix} U \\ V \\ W \\ P \\ Q \\ R \end{Bmatrix} \quad (12)$$

$$\begin{Bmatrix} \dot{U} \\ \dot{V} \\ \dot{W} \\ \dot{P} \\ \dot{Q} \\ \dot{R} \end{Bmatrix} = [[M] + [\mu]]^{-1} \begin{Bmatrix} \vec{F}^* - m\vec{\omega} \wedge \vec{V} \\ \vec{\Gamma}^* - \vec{\omega} \wedge \vec{h} \end{Bmatrix} \quad (13)$$

$\vec{F}^*, \vec{\Gamma}^*$ represent all external forces with the exception of the infinite-frequency added mass, which is added directly to the generalized mass matrix. It should be noted that all 12 equations are coupled, because the right hand sides depend on the unknown positions and velocities.

THE COMPUTER PROGRAM

A computer code for the resolution of equations 12 and 13 was written in the FORTRAN programming language. The approach used is straightforward; the extrapolation method of Stoer and Burlisch was used for the simultaneous resolution of the differential equations (see [11]).

The integration scheme differs from the typical Runge-Kutta time-step optimizing methods or predictor-corrector schemes. In brief, the approach taken is to consider a large time step that is systematically subdivided. The results of the time step at each level of discretization is extrapolated to an infinitely small time step. When the extrapolation error is less than a fixed value, the integration is considered to be converged to the extrapolated value for the large time step, and the integration continues. This approach has the advantages of being simple to program, stable, and efficient in most cases. The program that currently runs on an Alliant FX-80 computer is faster than real time, even for the irregular seas cases where a sea state with 19 wave components is used.

The majority of the computer time is spent computing the right-hand side of equation 13. A method for reducing the number of function evaluations necessary for integrating the system was found that is quite successful in many cases. The ship position is predicted one time step in advance, and the external forces are computed for this position. The forces found are linearly interpolated to give the values at the necessary intermediate times. In this way the number of calls to the subroutine that determines the exciting forces for a specific ship position is greatly reduced.

The method of prediction is the maximum entropy or all poles method (see [8]). The linear predictor takes the form:

$$x_n = \sum_{k=1}^N d_k x_{n-k} \quad (14)$$

where the d_k are determined using the maximum entropy method based on the past history of the motions. Since the prediction is performed for only one time step beyond known values, the prediction is, in general, very accurate. The program runs five to ten times faster by this method with only a slight change in the results.

RESULTS

The program was run for a variety of ship shapes. The values of the added mass, damping, and diffraction forces are taken from a strip theory computation. The first case presented (Figure 2) is for a simple two-dimensional form. Several V hull forms were tested at the Bassin des Carènes that present interesting nonlinear behavior. The hulls were three meters long. The result shown is a roll decay test performed with an initial heel angle of 20 degrees. The viscous damping term was chosen to make the amplitudes of the roll decay correspond approximately. The most interesting feature is the dependence of the natural period on the amplitude of roll. While the nonlinear simulation does not match exactly, it models the roll behavior much more correctly than the linear model. Later in the simulation the cumulative small errors cause the simulations to be out of phase with the experiment. The next graph (Figure 3) is an interesting case of varying the incident wave amplitude. The curves for the different amplitudes are dimensional and are not normalized by the wave amplitude. It is quite interesting to note that the peak frequency depends on the wave amplitude and that, for the smaller periods, the roll amplitude does not depend on wave height. The time domain simulations do not match the experiments exactly; however, the nonlinear behavior is modeled. It is also very interesting to note that the simulation results were obtained without the addition of viscous damping terms. It is clear that in this case the linear approximation for the hydrostatic forces creates an artificial need for "viscous" damping to limit the roll angles. A

linear theory result for the same case yields 100 degrees of roll for the 100mm wave height.

The second set of results are for a trawler with a length of 25 meters; experiments were performed on a 1:7.5 scale model for a fishing boat-stability study in cooperation with IFREMER. The viscous damping term was taken as 20 % of critical damping as an average value for similar hull forms [4]. The results are for a irregular following sea ITTC spectrum with a 2.5 meters wave height, a peak period of seven seconds, and a ship speed of five knots. At the present time only qualitative comparisons can be made because synchronized wave and motion signals were not available. The response spectra (4) for the pitch motions agree reasonably well between the experiments and the computer code, but in the following seas case it is difficult to perform accurate spectral analysis. The next two cases (Figures 5 and 6) are examples of a more extreme sea state (a significant wave height of six meters) than was tested in the model bassin. It may be noted that the only difference between the capsized and the uncapsized case is that in the uncapsized case the ship heading was maintained. This result agrees well with observations from 1:20 scale model tests that were performed to obtain phenomenological information about ship capsize. These experiments that capsize were most generally preceded by a large change in heading, a large roll angle that is maintained during one or more wave cycles, and, finally, the capsize.

CONCLUSIONS

The paper presents a simulation approach that has the advantage of being rapid enough to allow numerous simulations to be performed allowing for significant parameter variation. It is clear that certain aspects of the problem remain to be addressed. Perhaps the most important point in terms of ship capsize is the influence of water on the deck. Dillingham and Falzarano [1] presented a solid approach to treating the dynamics of water on deck. Nothing preclude the inclusion of the effect of deck water in the code, but many questions are still outstanding. The amount of water trapped on the deck depend on the action of breaking waves, relative motions, and the hydrodynamic behavior of freeing ports. Other important factors that are not well modeled are surfing on waves, oscillatory propulsive forces, and

low-frequency horizontal motions. With ever-increasing computer speeds the direct simulation of the complete hydrodynamics problem with a nonlinear free surface will one day be feasible. At the present time a simulation code as discussed here is a realistic step in that direction. The results indicate that the simulations performed by the program realistically model important nonlinear phenomena and point out weaknesses in linear models. In particular, the results for the V-hull cylinders indicate that, in part the important influence of the empirical viscous damping term in the roll equation is an artifact of the linearizing assumptions.

ACKNOWLEDGEMENTS

The author wishes to thank the Bassin d'Essais des Carènes for its support of the project. In addition the author profited from the results of the cooperative stability program of SEMER, IFREMER, BECP, SIRHENA ENSM/LNH, and Bureau Veritas.

References

- [1] Dillingham, J.T. and Falzarano, J.M., Three dimensional simulation of green water-on-deck. In *Proceedings of the Third International Conference on the Stability of Ships and Ocean Vehicles*. Gdansk, 1986.
- [2] Elsimillawy, N. and Miller, N.S., Time simulations of ship motions: A guide to the factors degrading dynamic stability. In *Transactions Naval Architecture and Marine Engineering*, 1988, vol. 94, pp. 215-40.
- [3] Etkin, B., *Dynamics of Atmospheric Flight*. John Wiley & Sons Inc., New York, 1972.
- [4] Goudey, C.A. and Venugopal, M., Roll damping on two new england trawlers: An experimental study. In *Marine Technology*, 1989, vol. 26, no. 2, pp. 160-67.
- [5] Greenhow, M., High- and low-frequency asymptotic consequences of the Kramers-Kronig relations. In *Journal of Engineering Mathematics*, Martinus Nijhoff Publishers, Dordrecht, Netherlands, pp. 293-306.

- [6] Neyfeh, A.H. and Sanchez, N.E., Chaos and dynamic instability in the rolling motion of ships. In *Proceedings of the Seventeenth Symposium on Naval Hydrodynamics*, National Academy Press, Washington, D.C., 1989, pp. 617-31.
- [7] Oakley, O.H., Paulling, J.R., and Wood, P. D., Ship motions and capsizing in astern seas. In *Proceedings of the Tenth Symposium on Naval Hydrodynamics*, Office of Naval Research, Washington, D.C., 1974, pp. 297-350.
- [8] Press, W.H., Flannery, B.P., Teukolsky, S.A., Vetterling, W.T., *Numerical Recipes the Art of Scientific Computing*. Cambridge University Press, Cambridge, 1986.
- [9] Salvesen, N., Faltinsen, O., and Tuck, E.O., Ship motions and sea loads. In *Transactions Society of Naval Architects and Marine Engineers*, 1970, vol. 78, pp. 250-79.
- [10] Shjekkbreia, J., Tørum, A., Berek, E., Gudmestad, O.T., Heideman, J., Spidsøe, N., Laboratory measurements of regular and irregular wave kinematics. E & P Forum Workshop on Wave and Current Kinematics and Loading, Institut Français de Pétrole, Rueil Malmaison., France, October 1989.
- [11] Stoer, B. and Bulirsch, R., *Introduction to Numerical Analysis*, Springer-Verlag, New York, 1980.

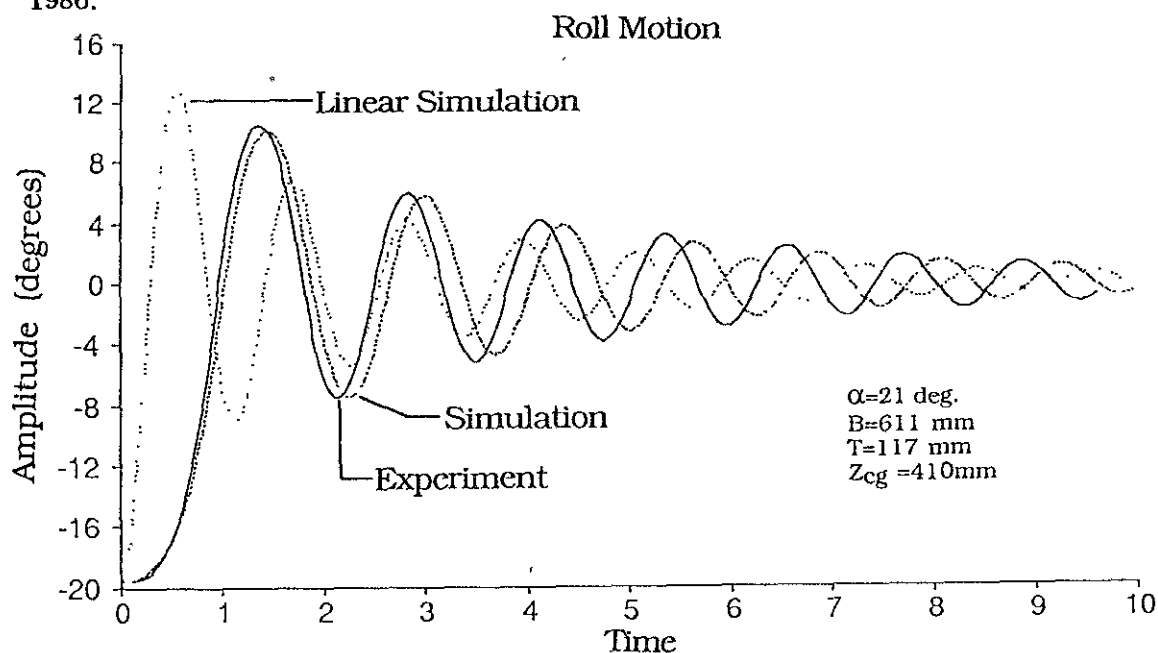


Figure 2: V-Hull Roll Decay

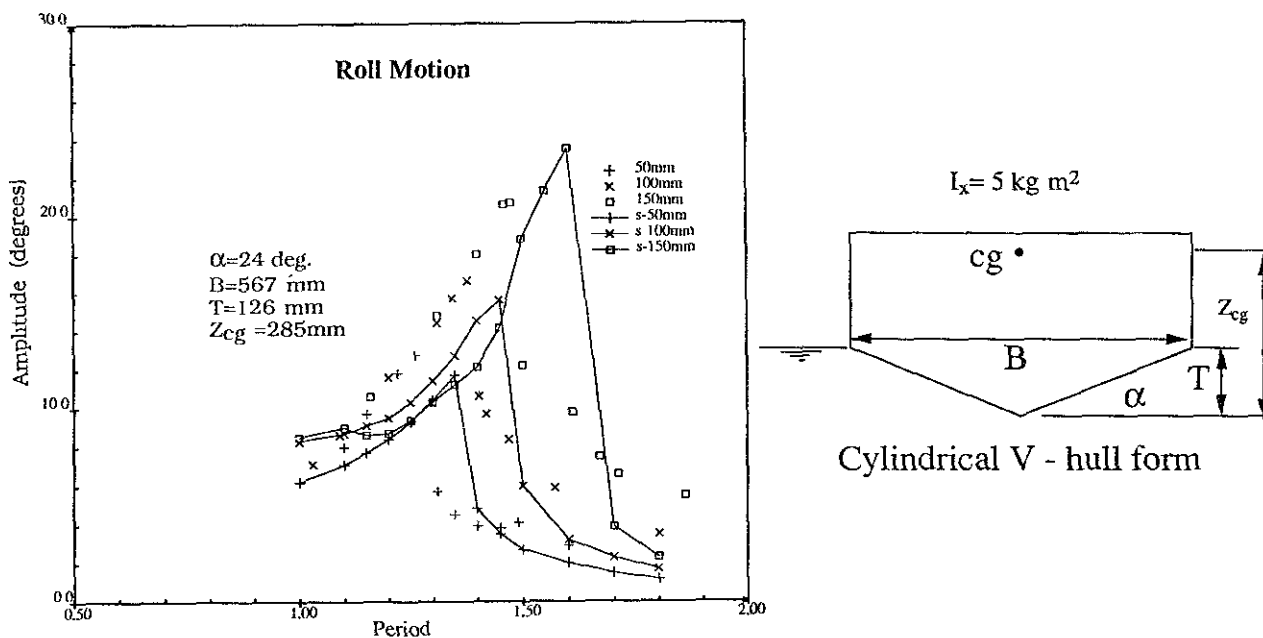


Figure 3: V-Hull Roll Motions

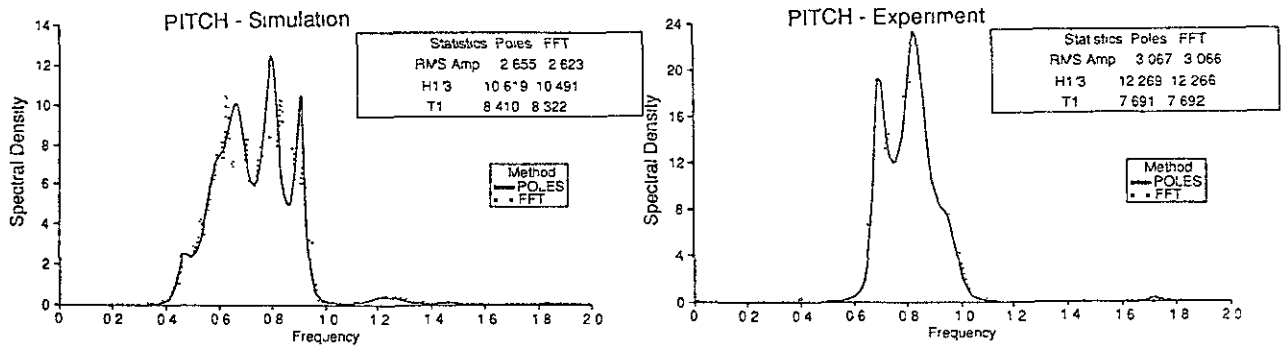


Figure 4: Trawler Motions Pitch Response Spectrum

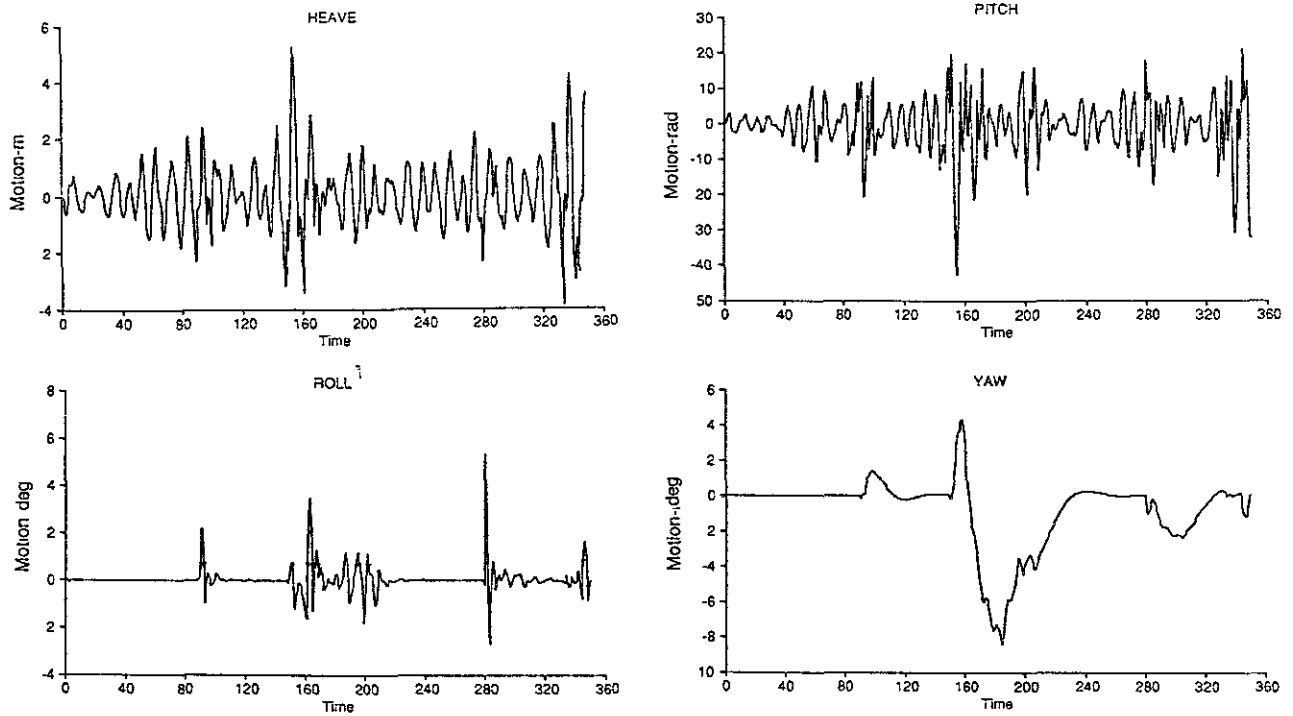


Figure 5: Large Amplitude Trawler Motions - Simulation with Auto-Pilot

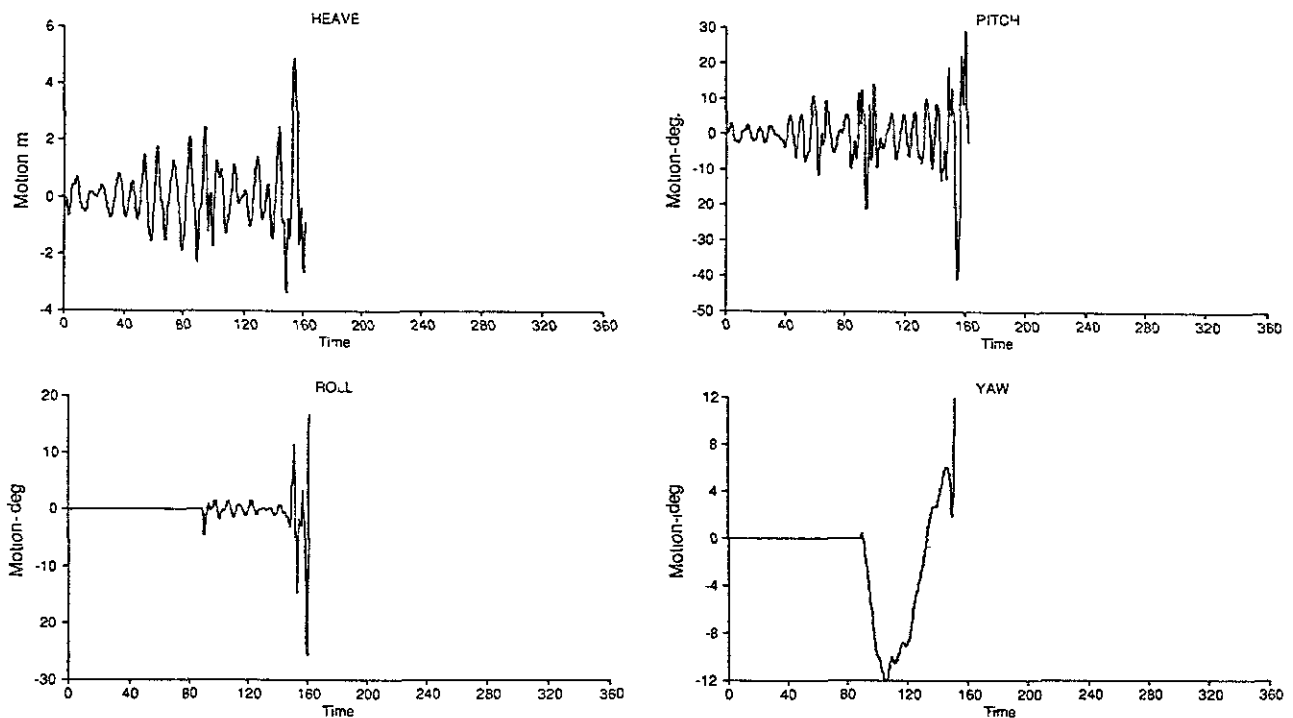


Figure 6: Large Amplitude Trawler Motions - Simulation with Capsize

REVIEW OF THE NEW SOLAS DAMAGE STABILITY REQUIREMENTS
FOR PASSENGER SHIPS

P. L. Carrigan, U.S. Coast Guard Headquarters, Washington, DC
J. S. Spencer, U.S. Coast Guard Headquarters, Washington, DC

The views expressed herein are the opinions of the authors and not necessarily those of the U.S. Department of Transportation or the U.S. Coast Guard.

ABSTRACT

This paper reviews the recently adopted passenger ship damage stability amendments to the International Convention for the Safety of Life at Sea, 1974. The development of international damage stability regulations and the new amendments is discussed. Knowledge gained from the United States (U.S.) Stability Control Verification Program in 1987-89 is addressed as well. The contents of the amendments are reviewed, with emphasis on those areas that may be subject to interpretation. The general effect of the amendments on both the U.S. and the world passenger ship fleets is examined. The paper presents the status of a U.S. study on the effect of implementing the new amendments on small passenger vessels in the U.S. Finally, future goals regarding international passenger ship subdivision and damage stability regulations are discussed.

BACKGROUND AND HISTORY

1) Damage Stability Regulation Prior to 1974

The 1912 collision of the "unsinkable" SS TITANIC with an iceberg initiated recognition of the need for international ship safety standards to reduce loss of life at sea. The TITANIC casualty led to the world maritime nations gathering in London in 1913-1914 to develop the first International Safety of Life at Sea Convention (SOLAS, 1914). The SOLAS Convention details specific features, construction standards, and safety measures applicable to passenger ships that make international voyages. Because of the onset of World War I, SOLAS, 1914 did not come into force, although some maritime nations used portions of the Convention in their domestic laws.

In 1929, a new SOLAS Convention, SOLAS, 1929, was drafted. SOLAS, 1929, like its predecessor, SOLAS, 1914, contained a simple subdivision standard for passenger ships. This standard did not consider damage stability concerns, such as unsymmetrical flooding or specific extents of damage. The standard was based on a factor of subdivision and assumed that by decreasing the spacing

distance between bulkheads, the level of safety attained by a ship would be increased. Portions of this subdivision standard are still contained in the current SOLAS Convention, SOLAS, 1974.

The first attempt to address comprehensive damage stability problems, such as unsymmetrical flooding, appeared in SOLAS, 1948. Passenger ships subject to SOLAS, 1948 are required to have sufficient metacentric height (GM) to limit heel to 7 degrees for one-compartment flooding and 15 degrees for two-compartment flooding.

In 1959, a specialized agency of the United Nations, now called the International Maritime Organization (IMO; originally IMCO - Inter-Governmental Maritime Consultative Organization) was formed. The IMO is an international technical body which has two main functions; (1) the safety of life at sea and (2) the prevention of pollution from ships. The IMO became the forum used by the world maritime nations to discuss and approve standards, such as the already existing SOLAS Conventions, for the international shipping community and to facilitate the international movement of ships.

During the development of SOLAS, 1960, a number of countries including the Federal Republic of Germany, Italy, Japan, Union of Soviet Socialist Republics, and the U.S., advocated various changes to improve the deterministic damage stability and subdivision standards contained in SOLAS, 1948. Progress in ship design since the standard's origin with SOLAS, 1914 failed to ensure the level of safety afforded by the deterministic method of calculating damage stability and subdivision. However, even though it was acknowledged that "improvement of these regulations was desired"; SOLAS, 1960 contained the same deterministic damage stability standard as SOLAS, 1948 with a few minor modifications.

As a consequence of the attempt to revise the subdivision and damage stability requirements during the development of SOLAS, 1960, an international evaluation of the validity of probability-based damage stability requirements was initiated in 1962 under the auspices of the IMO. This study used actual passenger ship casualty data as a basis and in evaluating the existing subdivision of passenger ships and their

damage stability. The study concluded that deficiencies in the subdivision and damage stability standard in SOLAS, 1960 led to an incorrect measure of a ship's safety. The study also stated that "the method used in SOLAS, 1960 calls two ships equally safe if they have the same factor of subdivision even though these ships may have quite different actual capabilities to withstand damage." In 1973, after more than ten years of theoretical and experimental research, including a limited number of model tests with two damaged ships in a seaway, Resolution A.265(VIII), the probabilistic approach to damage stability, was published as a recommended standard that was equivalent to and acceptable as a total alternative to the deterministic standard in SOLAS, 1960. Following the publication of A.265, no agreements were reached on further revisions to the deterministic standard in SOLAS, 1960 in order to assure an equivalent level of safety to that of A.265 for all passenger ships.

2) Development of New Amendments

As the 1974 amendments to the International Convention for the Safety of Life at Sea (SOLAS, 1974) were being developed, some concern was expressed over the need for residual damage stability requirements in the SOLAS deterministic damage stability regulations for passenger ships. Agreement could not be reached on specific regulations for residual stability, so the matter was left, in general terms, to the discretion of each country.

The concept of residual righting energy, as described by a range of positive stability after damage and a minimum specified residual righting lever within that range, is contained in several international codes for ships, including those for bulk chemical carriers (1985), liquefied gas carriers (1983), tankers (1973), cargo ships with reduced freeboard (1966), special purpose ships (1983), and others. By 1983, the need for similar regulations for passenger ships was recognized by most countries, and work on the subject began in earnest at the IMO.

The Sub-Committee on Stability and Load Lines and on Fishing Vessels Safety (SLF), is the body at IMO responsible for developing residual stability requirements for passenger ships. At its 29th session in January 1984 (SLF 1929), the Sub-Committee developed a framework for regulations, which included (1) a range of positive stability in the final condition of flooding, (2) maximum angle of heel before equalization, (3) angle of heel in the final condition, and (4) stability in intermediate stages of flooding. Except for item (3), where it was decided that the final angle of heel should be not more than 7 degrees, agreement was not reached on specific numerical requirements.

The basic problem was that SLF could

not agree on, "How much is enough?"

There were neither casualty data nor studies to provide clear guidance, and there were two schools of thought on the matter. For example, in discussing range of stability and righting lever, one group believed that criteria already used by some countries (7 degree range, 0.05 meter righting lever) had proven satisfactory, as evidenced by the large number of ro/ro ships in service which were built to those standards. The other group favored requirements similar to those already established for tankers and certain other ships (20 degree range, 0.1 meter righting lever), arguing that the requirements for passenger ships should not be less than those for other types of ships.

At SLF 30 in February 1985, the debate continued. There was a wide range of opinion on the factors which should be taken into account concerning residual stability, such as the effects of wind, cargo shift, movement of passengers to life-saving stations, and embarkation of lifeboats. SLF decided that additional studies were needed concerning the impact of any new standards on future designs, the overall level of safety of passenger ships, and the relative safety of such ships compared to other types of ships.

SLF 31 met in June 1986. Although additional information was presented, it was clear that there were still two different opinions on the matter which were very far apart. There were matters of principle involved which appeared to leave little room for compromise. SLF agreed that the effects of passenger movement, deployment of life-saving appliances, and wind should be considered in an assessment of residual stability, and that residual stability criteria should be expressed in terms of righting lever, range of stability, and area under the righting lever curve. However, as for actual numerical criteria, SLF could not find a basis for agreement, primarily because of the two different philosophies behind the criteria being proposed.

One philosophy stated that residual stability should be treated in a manner based on an analytical approach to the physical aspects of the problem. This approach required that the residual stability of a vessel be adequate to withstand probable heeling moments imposed on the vessel in the worst damage case specified by SOLAS, 1974. The residual stability criteria which were adopted by IMO for liquid cargo vessels required to meet damage stability standards and for special purpose ships carrying special personnel were proposed also for passenger ships, with a possible reduction in the range of positive stability after equilibrium. The residual stability of the vessel should be sufficient to withstand the overturning moment due to the effects of passenger movement, deployment of life-saving appliances, and wind, applied in a manner to simulate a realistic situation. The group supporting this

philosophy proposed, in the final stage of flooding, a righting lever of at least 0.10 meter, a positive range of at least 15 degrees, and an area under the righting arm curve of at least 0.02 meter-radian.

The other philosophy pointed to existing passenger ships which were known to operate successfully with a different standard of residual stability, which was met in the worst damage case. The residual stability standards taken in conjunction with the standards used for extent of damage, intermediate stages of flooding, permeability, and other factors, were considered to provide an adequate level of safety in the worst case. The coincidence of damage occurring in the worst loading conditions and at the deepest draught was thought to be remote. For all other loading conditions and damage locations, the margin of residual stability after damage would be increased. Experience indicated that in this situation, many of the damage cases would in fact achieve a significantly greater residual lever. It was contended that it is a basic principle that many of the assumptions related to the damage requirements in SOLAS were determined implicitly having regard to the probability of their occurrence. Furthermore, it was suggested that there was no evidence to show that the survival criteria used were inadequate. The group supporting this philosophy proposed, in the final stage of flooding, a righting lever of at least 0.05 meter, a positive range of at least 7 degrees, and an area under the righting arm curve of at least 0.006 meter-radian.

The differences in points of views might never have been reconciled, except for the unfortunate fact that on 6 March 1987, the passenger ro/ro ferry HERALD OF FREE ENTERPRISE capsized just outside the harbor at Zeebrugge, Belgium. That accident, in which 194 people were killed, brought the subject of passenger ship safety and stability sharply into focus with considerable public interest. There was some continued discussion of the two philosophies at SLF 32 in September 1987, but the Sub-Committee decided to recommend amendments to SOLAS, 1974 consistent with the higher level of residual stability. The Sub-Committee prepared draft amendments that included detailed requirements for heeling moments due to passenger movement, launching of life-saving appliances, and wind pressure, and margins of safety to be applied.

The proposed amendments were debated by the IMO Maritime Safety Committee (MSC), the body responsible for approving tacit amendments to SOLAS, 1974, in April 1988. As in the SLF meetings, the same two points of view emerged, and there were some attempts to study the matter further by returning it to SLF or not applying it to certain vessels such as ro/ro ships. The MSC decided to circulate the draft amendments with minor changes, with a view to adopt them at its

next session. With minor additional changes, the proposed amendments were adopted by the MSC in October 1988. According to IMO procedures, they were deemed accepted a year later, and they entered into force for new passenger ships on 29 April 1990.

3) U.S. Stability Control Verification Program

There are nearly 100 foreign flag passenger cruise ships that operate in and out of U.S. ports during most of the year. Some of these ships can accommodate upwards of 2000 passengers per voyage. On many of these voyages, most of the passengers are U.S. citizens.

By international agreement passenger ships from flag states that are a party to SOLAS are required to comply with the safety standards set out in the SOLAS Convention. The SOLAS Convention provides the authority to its signatory parties to exercise port state control over all ships operating within their jurisdiction for the purpose of verifying compliance with SOLAS. Prior to 1987, the U.S. accepted the flag state's assurance that each ship met the appropriate stability requirements of SOLAS and carried out inspections only to verify that each ship met the fire protection and life saving requirements of SOLAS before departing a U.S. port with U.S. passengers.

Following the highly publicized passenger ship casualty of the British ferry, HERALD OF FREE ENTERPRISE, the U.S. and the rest of the world began to reexamine more closely the damage stability standards of passenger ships. At the 32nd session of the SLF in September 1987, the U.S. noted that there might be differing interpretations by different Administrations of current SOLAS passenger ship stability requirements. The U.S. was concerned that methods of calculating damage stability could result in a broad variation in the level of safety attained from ship to ship.

The possible interpretative differences, combined with the passenger ship casualties, and the realization that U.S. citizens represent 70-80% of the cruise ship passengers worldwide, resulted in the U.S. Coast Guard initiating the Stability Control Verification Program. In November 1987, the U.S. gave worldwide notification of the extended program at the 55th session of the MSC. The program was initially limited to foreign passenger ships operating from a U.S. port for the first time. It was decided that, if interpretation differences resulted in substantiated concern about a reduced level of safety on foreign flag passenger ships operating from U.S. ports, then the program would be extended to all foreign flag passenger ships.

Between November 1987 and April 1989, the U.S. Stability Control Verification Program reviewed more than fifteen foreign flag passenger ships.

Approximately one-third of these ships were older existing cruise ships coming to the U.S. for the first time, and the rest were newly built modern passenger ships. As part of the review process, the ships were also checked against the new standard for residual stability that was approved by the MSC and subsequently adopted into SOLAS in 1989.

The U.S. was able to conclude that there were no broad differences in interpretation of the SOLAS stability requirements by different Administrations, so it ended the Stability Control Verification Program on 11 April 1989. However, the U.S. and the maritime community did benefit greatly from the program as described below.

As the verification program progressed, it soon became apparent that instead of interpretation problems, there existed an ever increasing inadequacy of the residual damage stability regulations. Comparison of the design of new passenger vessels reviewed during the program with older passenger vessels substantiated the U.S. belief that the damage stability standard of SOLAS, 1974 could no longer ensure an acceptable level of safety. Some new cruise ship designs which met the requirements of SOLAS, 1974 did not provide sufficient reserve stability to survive passenger movement, launching of lifecraft or moderate wind and waves. The review of some of these new designs revealed typical righting levers on the order of 0.02 meters. Ranges of positive stability that were considerably less than ten degrees were characteristic in many damage cases, not just the worst ones. One modern cruise design failed the new damage stability amendments in nearly 70% of the damage cases using the existing SOLAS extents of damage. At the opposite extreme, the review of older passenger ships of similar size and service were found to fully comply with the new damage stability standard.

It became very clear that using the SOLAS minimum GM of 0.05 meter as the only measure of a ship's stability after damage was dangerously misleading. For the older passenger ships with large freeboards and whose hull forms generate intact righting arm curves that are concave upward at small angles of heel, minimum GM was an acceptable indicator of sufficient stability. A ship with this type of righting arm curve will continue to list to an acceptable angle as the initial stability reduces to zero. However, for the more modern passenger ships with smaller freeboards, the righting arm curve can be concave downward at small angles of heel and have a short range of stability which diminishes very quickly as GM gets smaller. This type of righting arm curve can quickly become negative with degradation of stability to an unsafe level. A ship with this type of righting arm curve could capsize without warning as stability is reduced by damage or other factors.

Some owners of new foreign flag passenger ships were introduced to the new damage stability requirements that were under consideration and subsequently adopted by IMO during the stability control verification program. Many of the owners of new passenger ships in the design stage accepted U.S. Coast Guard's advice and decided to ensure their new ships met the requirements even though they were not yet formally applicable. There were only a few problems encountered in meeting the new amendments if the new ship was early in the design process. Residual stability was increased by relocating downflooding points inboard, using symmetric flooding, installing partial bulkheads above the bulkhead deck to gain additional buoyancy, raising the bulkhead deck in some areas, and by minor rearrangement of tanks, bulkheads, and decks. All were found to be practicable methods of meeting the new residual stability requirements without a major impact on passenger convenience or utility of the ship.

REVIEW OF THE AMENDMENTS

The amendments that were adopted in October 1988 at MSC 56 contained revisions to the deterministic damage stability standard in SOLAS, 1974. These revisions set specific requirements and revised the very general standard in Part B, Chapter II-1/8 of the SOLAS, 1974, as amended. For the first time range of positive stability, as well as sufficient positive righting lever and righting energy, were included. Provisions were also included to assure limited survivability for the crowding of passengers to one side, launching of fully loaded survival craft, and beam winds. The effective date for the new amendments was 29 April 1990. The specific provisions of the new damage stability amendments are described below.

1) Righting Energy, Range of Stability and Angles of Heel

The new amendments set minimum acceptable levels of righting energy, range of stability, and angles of heel for passenger ships in intermediate stages of flooding and in the final condition of flooding as well. These requirements of the new amendments are outlined below.

1. A passenger ship in the final condition, after all flooding and after equalization where it is provided, must attain:

1. Minimum range of stability of 15 degrees beyond the angle of equilibrium.
2. For one-compartment flooding, the area under the righting arm curve measured from the angle of equilibrium to the lesser of the angle at which downflooding occurs or 22° measured from the upright must be greater than or equal to 0.015 meter-radian.
3. For two-compartment flooding, the area under the righting arm curve

measured from the angle of equilibrium to the lesser of the angle at which downflooding occurs or 27° measured from the upright must be greater than or equal to 0.015 meter-radian.

II. A passenger ship in intermediate stages of flooding must attain:

1. Minimum range of positive stability of 7 degrees.
2. The maximum righting lever within the required range of positive stability must be at least 0.05 meter.

In all intermediate cases of flooding, only one breach in the hull and only one free surface need be assumed.

III. The maximum angle of heel after flooding but before equalization must be less than 15 degrees.

IV. In the final condition, after flooding and after equalization in the case of unsymmetrical flooding; the angle of heel must not exceed:

1. 7 degrees for one-compartment flooding.
2. 12 degrees for simultaneous flooding of two or more adjacent compartments.

2) Heeling Moments

The new amendments require that new passenger ships be able to survive heeling moments due to a light wind, launching of survival craft, and movement of passengers for each assumed damaged condition. The specific composition of the heeling moments is outlined below.

Each passenger ship in the final condition after damage and after equalization where provided must demonstrate a righting lever within the required 15 degree range of stability that is equal to or greater than each of the heeling moments divided by the ship's displacement plus 0.04 meter. The required righting lever must always be greater than 0.10 meter.

$$GZ(m) = \frac{\text{Heeling Moment}}{\text{Displacement}} + 0.04 \text{ m} \quad (1)$$

When calculating the heeling moments, the following assumptions must be used:

I. For passenger crowding heeling moment:

1. 4 people per square meter;
2. 75 kilograms mass per person;
3. People must be distributed on the available deck areas towards one side of the ship on the decks where muster stations are located and in a manner that produces the most adverse heeling moment.

II. For moment due to launching of fully loaded davit-launched survival craft on one side:

1. All life boats and rescue boats fitted on the side to which the ship has heeled after sustaining damage shall be assumed to be swung out fully loaded and ready for lowering;
2. For lifeboats which are arranged to be launched fully loaded from the stowed position, the maximum heeling during launching must be used;

3. A fully loaded davit-launched lifecraft attached to each davit on the side to which the ship has heeled after sustained damage shall be assumed to be swung out ready for lowering;

4. Persons not in the life saving appliances which are swung out shall not provide either additional heeling or righting moment;

5. Life saving appliances on the side of the ship opposite to which the ship has heeled shall be assumed to be in the stowed position.

III. For wind heeling moment:

1. A wind pressure of 120 N/m^2 must be applied;
2. The applicable windage area shall be the projected lateral area of the ship above the waterline corresponding to the intact condition.
3. The moment arm shall be the vertical distance from a point at one-half of the mean draft corresponding to the intact condition to the center of gravity of the lateral area.

3) Areas Subject to Interpretation

Because there were some owners of new passenger ships who decided to meet the new amendments during the U.S. Stability Control Verification some problems with the uniform application of the new amendments soon came up. One of the methods used to meet the new regulations was to provide increased reserve buoyancy above the bulkhead deck by using well placed partial bulkheads. The new amendments do not specifically define the acceptable watertight integrity of partial bulkheads above the bulkhead deck so a clarification was needed in regulations II-1/8 and II-1/20 of SOLAS, 1974. There was some question as to whether or not weathertight closures above the bulkhead deck could provide buoyancy if they were submerged in the intermediate but not final stage of flooding. By definition, achieving the range of stability and righting energy specified by the new amendments required that watertight integrity above the bulkhead deck be maintained for volumes to be part of the increased buoyancy. In response to owners requesting the U.S. position with respect to this provision, the U.S. suggested that any opening submerged above the bulkhead deck, such as doors in partial bulkheads, that were within the range of residual stability should be watertight. The U.S. deferred to flag Administrations until IMO could address the issue.

Further problems in applying the new amendments resulted because, by allowing credit for watertight volumes above the bulkhead deck, fire doors might have to serve as watertight doors. The number of watertight doors above the bulkhead deck that must also be used as a means of escape under regulation II-2/28 is therefore increased. Since the means of escape for fire protection must not be compromised, the U.S. recommended at

SLF 34 the extension of existing requirements for escapes below the bulkhead deck to watertight areas above the bulkhead deck. However, at least one of the escapes must be independent of watertight doors.

At SLF 34, the U.S. set forth those interpretations and proposed that SOLAS, 1974 regulations II-1/8 and II-1/20 be amended to ensure that the new damage stability standard would be uniformly applied. The U.S. proposed that regulation II-2/28 be referred to the Sub-Committee on Fire Protection because of concerns with escapes above the bulkhead deck. SLF 34 essentially agreed that clarifications were needed to ensure uniform application of the new amendments. SLF 34 sent amendments of regulations II-1/8 and II-1/20 forward for consideration at MSC 58 and recommended that the clarifications of these two regulations be distributed by Circular to member nations. Revisions to regulation II-2/28 were referred to the Sub-Committee on Fire Protection.

EFFECT OF IMPLEMENTATION ON DESIGN

1) General Design Variations

Over the last two decades, passenger ships have undergone significant changes in their hull forms and general arrangements. The traditional passenger liners typically had fine lines forward and aft, deep watertight bulkheads, and a limited number of decks above the bulkhead deck. As a consequence of the prevailing effort to accommodate as many passengers as possible, modern passenger ships have long full mid-bodies, low bulkhead decks, and many levels of structure and deadweight above the bulkhead deck. As was seen in the U.S. Stability Control Verification Program, to achieve the standards set by the new damage stability amendment, new passenger cruise ships will be redesigned by moving downflooding points inboard, using symmetric flooding, installing partial bulkheads above the bulkhead deck, and/or raising the bulkhead deck. Careful consideration of damage stability will be needed early in the design process to allow desired arrangements of tanks, bulkheads, and decks. With forethought and good design, meeting the new requirements is attainable without impacting on passenger convenience or utility.

Passenger ship operating companies want long, slow rolling for passenger comfort, and concern was expressed by some member nations at IMO, that the only method of complying with the new amendments was by increasing GM and consequently, increasing roll period. However, none of the information gained from the U.S. Stability Control Verification Program substantiated the idea that the only method to meet the new standard was by increasing intact GM beyond an operationally acceptable level. Designing to only an intact GM requirement is not the solution intended

to comply with the new amendments. Another concern expressed, during the discussions at IMO, regarded increased freeboards resulting from complying with the new amendments. Particularly, that new ro/ro passenger ferries complying with the new amendments would be unable to use the existing shoreside facilities because of their increased freeboard. However, even though this concern is valid, the effect on shoreside facilities is not an acceptable reason for not requiring sufficient residual stability.

2) U.S. Study on Small Vessels

The U.S. flag passenger vessel fleet of some 5100 vessels is mainly comprised of those less than 100 gross tons. These vessels carry anywhere from 6 to more than 1000 passengers per voyage. About 4000 of these vessels are less than 65 feet in length. At least 25 new small passenger vessels are built each year for service in the U.S.

The U.S. passenger vessel fleet met a higher stability standard than that of SOLAS, 1974, prior to the new damage stability amendments. U.S. small passenger vessels were designed to a damage standard similar to what existed in SOLAS, 1974 as well as an intact wind and passenger movement criteria. The U.S., through its domestic regulatory process, is proposing to apply the new SOLAS damage stability requirements to all new domestic passenger vessels, regardless of size or route. This action will maintain the level of damage stability safety of U.S. domestic passenger vessels equivalent to that of SOLAS vessels. The U.S. Coast Guard, the responsible government agency for passenger vessel safety in the U.S., believes that the need to require passenger ship survival after damage should not be a function of service or route, and that the hazard this standard seeks to prevent is present on domestic as well as international voyages. To substantiate this position, the U.S. Coast Guard undertook a study through the U.S. Department of Transportation's Transportation Systems Center to evaluate the effect of the new standard on the domestic passenger vessel fleet. Sixteen existing vessels have been examined so far to determine the effect of these regulations.

The U.S. passenger vessel fleet is extremely diverse with some vessels built over 100 years ago as well as newly built high speed craft. The major types of new small passenger vessels are party fishing boats, paddlewheelers, dinner/excursion boats, passenger/car ferries, and converted offshore supply vessel hulls. There are also a number of passenger/car ferries of greater than 100 gross tons. Because of their prevalence, the U.S. study is concentrated on those five types of vessels.

The study is divided into two parts. The first is to determine whether or not each vessel meets the new criteria. For those vessels which do not meet the

criteria, the necessary design changes required for a new vessel to comply with the criteria are to be determined, and the cost of these changes in construction and lost operating capacity are to be calculated.

The majority of the vessels examined to this point have had little difficulty in meeting all requirements for range of stability, righting levers, and righting energy. Two vessels failed because they had low downflooding angles. For both vessel designs, the downflooding points could be relocated without high cost, provided the vessel is in a design stage.

Few U.S. small passenger vessels carry davit-launched lifecraft. One vessel checked that does have this type of lifecraft easily complied with all provisions of the new standard. The wind loading consideration in the new standard was also satisfied by all of the vessels examined, with the exception of three light displacement vessels (a ferry and two paddlewheelers).

By far the most difficult part of the criteria to comply with is the passenger crowding to one side. Seven of sixteen vessels examined failed this provision, some by wide margins. Preliminary analysis showed it was the lighter displacement vessels which have greater difficulty complying with this portion of the new standard, and the worst damage case was usually the engine room. For about half of the failures, design changes similar to those used by the SOLAS vessels, such as moving bulkheads, locating downflooding points inboard, careful placement of tanks, etc., allow them to fully comply with the new standard. Economic evaluations of the major design changes needed have not been completed. A more detailed analysis of the failures, design changes, and economic impact will be available when the study concludes.

FUTURE OF PASSENGER SHIP DAMAGE STABILITY REGULATIONS

During future meetings of the SLF Sub-Committee, considerable review of the passenger vessel damage stability requirements of SOLAS will be undertaken. Important issues, such as the future direction of the SOLAS damage stability regulations (deterministic, probabilistic or both in parallel), will be decided by the world maritime nations. Some of the issues under consideration are discussed in detail here.

1) The Deterministic Method

The deterministic subdivision and damage stability methods in Part B, Chapter II-1 of the SOLAS, 1974 Convention with its accompanying subdivision standard, part of which originated back with SOLAS, 1929, are scheduled for review by the SLF Sub-Committee. Many countries believe the subdivision standards in Regulations II-1/4 through II-1/7 have become outdated and do not ensure the same level of safety for modern passenger ship designs as the new damage stability

amendment. The basic difference is that for the subdivision regulations, transverse watertight bulkheads must extend from sideshell to sideshell, but for damage stability only to the B/5 penetration limit. Although it may be thought that the subdivision regulations provide a higher level of safety for damage conditions that exceed the B/5 transverse damage penetration limit, subdivision does not account for residual stability for the off-center flooding which is most certain on modern passenger ship designs. Although the U.S. is generally supportive of measures that can ensure a higher level of safety, it appears that the provisions of regulations 4 through 7 that address floodable length and permissible length are misleading, or at best, redundant, so this outdated standard should be removed.

In concert with this change, other revisions are also under consideration at SLF including relating the degree of flooding protection to the number of passengers carried rather than the size or arrangement of the vessel, revising the permeabilities based on current research, and eliminating the margin line concept.

2) The Probabilistic Method

Even after the publication of A.265, the majority of SOLAS passenger ships continued to be designed to the deterministic subdivision and damage stability standard of SOLAS, 1960 and SOLAS, 1974. One of the major reasons for not making use of the probabilistic standard was the ship designer's familiarity with the deterministic standard and unfamiliarity with the probabilistic approach. The fact that A.265 was only a recommended alternative and not required by the SOLAS Convention further de-emphasized the application of the new standard.

Many believe that because Resolution A.265 attempted to correct the deficiencies found in SOLAS, 1960, it required a higher level of safety for modern passenger ships than that of the existing deterministic subdivision and damage stability standard in SOLAS, 1974. In the minds of the owners and operators of passenger ships, a higher level of safety usually translates to higher costs. Because of this reasoning, A.265 has not been put to full use by ship designers, although it has been proven to be a better and more flexible standard.

Resolution A.265 is similar to the deterministic method in SOLAS, 1974 in that it depends heavily on an initial upright GM, however, it is modified by ratios of beam and effective freeboard and by ratios of constants determined from model tests conducted in the U.S. and United Kingdom. The constants used in the formulae of A.265 are minimums to prevent capsizing in a light seaway, but they may need to be modified to account for wind, passenger movement, and launching of survival craft. Also, the tests were never varied to account for

changes in vessel proportions even though vessel proportions can affect the floodability of the hull from both a buoyancy and stability viewpoint. There is a danger in the A.265 assumption that all ships have a righting arm curve that is concave upward. The relationship between GM and survivability was based on hull forms that still had a significantly high amount of area under the righting arm curve when GM was equal to zero.

Resolution A.265 should be updated with research using modern cruise ship hull forms with due consideration for the effects of varying vessel proportions and accounting for sufficient residual stability. The United Kingdom has made important progress in this area subsequent to the HERALD OF FREE ENTERPRISE casualty. Knowledge gained from the dry cargo ship probabilistic standard which has been under consideration at IMO should be incorporated into the formulae and organization of A.265. The best course for the future would be a melding of the deterministic and probabilistic methods into a single required damage stability standard that would provide an acceptable level of safety. At the least, Resolution A.265 needs to be given a higher profile as an acceptable alternative standard to the present deterministic standard that will ensure a similar level of safety.

3) Other Stability Related Areas

Flooding Protection - Means of Escape -

Considerable research and technical knowledge have gone into formulating the SOLAS Conventions. These efforts go a long way to assure the survival of a ship in the flooding scenarios described in SOLAS, 1974. However, SOLAS, 1974 does not consider the survival of passengers or crew who are accommodated in spaces located within the damage extent described in SOLAS, 1974. From the passenger ships examined during the U.S. Stability Control Verification Program, it was discovered that current design practice accommodates large numbers of passengers and crew on and below the bulkhead deck, where, in the event of damage as prescribed by SOLAS, 1974, persons in those spaces may be entrapped by flooding waters that will displace air in the spaces and escape routes. This means that, while the current requirements of SOLAS may ensure survival of the ship, the passengers and crew accommodated in the flooded spaces may be doomed.

The dangers of entrapping persons in spaces that could be completely flooded in the required flooding damage scenarios has been addressed by some of the classification societies and by the

domestic regulations of some of the world maritime countries, including the U.S. However, an international standard for flooding protection of both passengers and crew is needed.

A new regulation should be added to SOLAS to ensure that accommodation spaces for large numbers of persons be sized and located to ensure rapid vertical escape or be arranged to ensure a suitable and accessible volume of air to allow for evacuating the spaces within a reasonable period of time. The United Kingdom has stated that regulations should provide for escape from vessels at very large angles of heel. In future revisions of the damage stability requirements of SOLAS, this important issue should be given serious consideration.

CONCLUSIONS

While the SOLAS Conventions have done much since their beginning in 1914 to increase the safety of life at sea, there is much that remains to be accomplished in the area of passenger ship damage stability. The new revisions to the deterministic damage stability standard in SOLAS, 1974 go a long way towards ensuring the safety of passengers and passenger ships. However, further revisions of SOLAS, 1974 Chapter II/1 to remove the redundant subdivision standards and to base the degree of flooding protection on the number of passengers carried rather than on the design of the hull must continue, so that the safety standards of modern cruise ships can be improved. As passenger ship designs change, so must the SOLAS Convention. We must be wary of those regulations which become outdated or misleading. From recent work at SLF, the real future of damage stability regulations lies in the more scientific and casualty based methods of the probabilistic approach to damage stability rather than the archaic deterministic method.

REFERENCES

1. Twenty-Ninth through Thirty-Fourth Meetings of the IMO Sub-Committee on Stability, Load Lines and Fishing Vessels Safety, Passenger Ship Damage Stability Papers.
2. Fifty-Fifth through Fifty-Eighth Meetings of the IMO Maritime Safety Committee, Passenger Ship Damage Stability Papers.
3. International Safety of Life at Sea Conventions since 1914.
4. Resolution A.265(VIII), "Regulations on Subdivision and Stability of Passenger Ships as an Equivalent to Part B of Chapter II of the International Safety of Life at Sea, 1960."

Michel K. Ochi

ABSTRACT

This paper discusses the significance of low frequency turbulent winds over a seaway which induce very large drag forces that may seriously affect the stability of ships and ocean structures. The spectral energy density obtained from measurements over a seaway is much greater at low frequencies than that computed by any of the currently available formulations. The magnitude of extreme turbulent wind-induced drag force with a risk parameter of 0.01, which is highly recommended for design consideration, is much greater than that of the mean wind drag force.

INTRODUCTION

A recent study on turbulent wind spectra over a seaway indicates that the magnitude of turbulent wind energy is quite large at low frequencies of less than approximately 0.02 Hz [1]. To elaborate on the low frequency turbulent wind components, Figure 1 taken from Reference [2] shows an example of a time history of wind speed. As can be seen in the figure, wind velocity consists of a variety of frequencies. High frequency turbulence often called "gust winds" appear to be severe in the figure but, in reality, their energy is

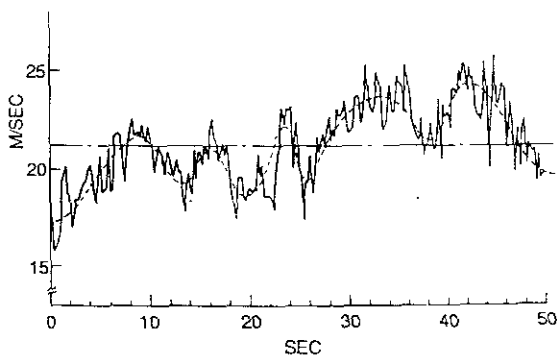


Figure 1: Example of time history of wind speed (from Ref. 2).

small. On the other hand, low frequency components as indicated by the dotted line carry substantially larger amounts of energy, especially over a seaway. Nevertheless, it is common practice not to consider turbulent wind energy in the design of marine systems. Furthermore, the natural response frequencies of some marine systems such as those of surging or yawing motions of a tension-leg platform or a moored ship appear to be in the frequency domain where very large turbulent energy is observed. When this is the case, turbulent winds may induce resonance in addition to that produced by rough waves resulting in a critical condition during storms.

This paper presents the significance of low frequency turbulent winds over a seaway; information vital for evaluating stability characteristics of marine systems. The paper discusses (i) turbulent wind spectra to be considered for evaluating drag force and (ii) some results of a comparison of the extreme turbulent wind drag forces with the commonly known mean wind-induced drag force.

TURBULENT WINDS

Professor, University of Florida
Coastal & Oceanographic Engineering Department, 336 Weil Hall, Gainesville, Florida 32611, U.S.A.

Energy of turbulent winds is a function of the severity of mean wind speed, wind shear velocity, height above the sea

level and frequency; hence, the energy spectrum is often presented in the following dimensionless form:

$$S(f_*) = f S(f) / u_*^2 \quad (1)$$

$$\text{where } f_* = fz/\bar{u}_z \quad (2)$$

f = frequency in cps

z = height above sea level in meters

\bar{u}_z = mean wind speed at height z in m/sec

$S(f)$ = spectral density function in m^2/sec

u_* = shear velocity in m/sec.

Although a variety of formulae are available for mean wind speed at height z above sea level and for friction velocity u_* , the following formulae are used in the present study. These are,

$$\bar{u}_z = \bar{u}_{10} + 2.5 u_* \ln(z/10) \quad (3)$$

$$u_* = \sqrt{C_{10}} \bar{u}_{10}, \quad (4)$$

where

\bar{u}_{10} = mean wind speed at 10 m height in m/sec

C_{10} = surface drag coefficient evaluated from wind measurements at 10 m height.

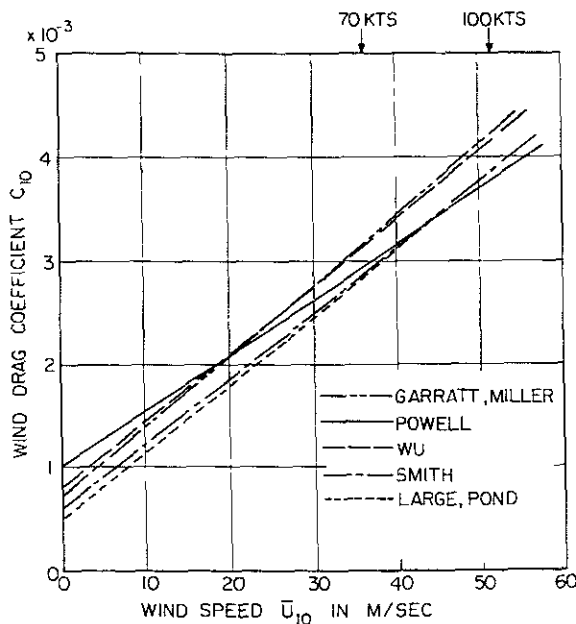


Figure 2: Wind drag coefficient C_{10} as a function of mean wind speed at height $z = 10$ m (from Ref. 1).

The surface drag coefficient, C_{10} , depends on mean wind speed, \bar{u}_{10} . The results of several studies on this subject are summarized and shown in Figure 2. Among others, Wu's results [3] are based on data obtained for a wide range of wind velocities over a seaway which may be expressed by

$$C_{10} = (0.77 + 0.066 \bar{u}_{10}) \times 10^{-3} \quad (5)$$

From Eqs.(3) and (5), the ratio of the mean wind speed at height z and that at 10 meter height, \bar{u}_z/\bar{u}_{10} , which may be called the height coefficient can be calculated. It is a function of \bar{u}_{10} as shown in Figure 3.

Figure 4 shows a compilation of available turbulent wind spectra obtained from wind speed measured over a seaway at different geographical locations [1]. In the figure, the upper and lower bounds are given for Eidsvik's spectra covering 15 spectra developed from an extensive analysis of measured data [4]. As can be seen, Eidsvik's upper and lower bounds encompass most of the other spectra derived from analysis of data obtained elsewhere. We draw the average curve of all measured spectra shown in Figure 2 (except for Smith's result) and represent it approximately by the following formula shown in Figure 5.

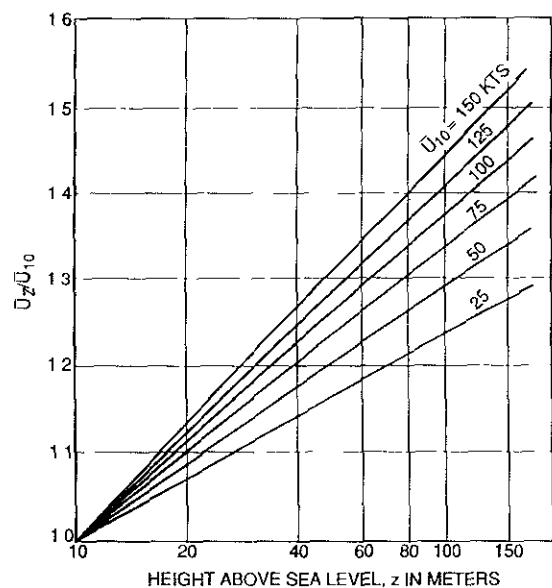


Figure 3: Height coefficient \bar{u}_z/\bar{u}_{10} as a function of height above sea level.

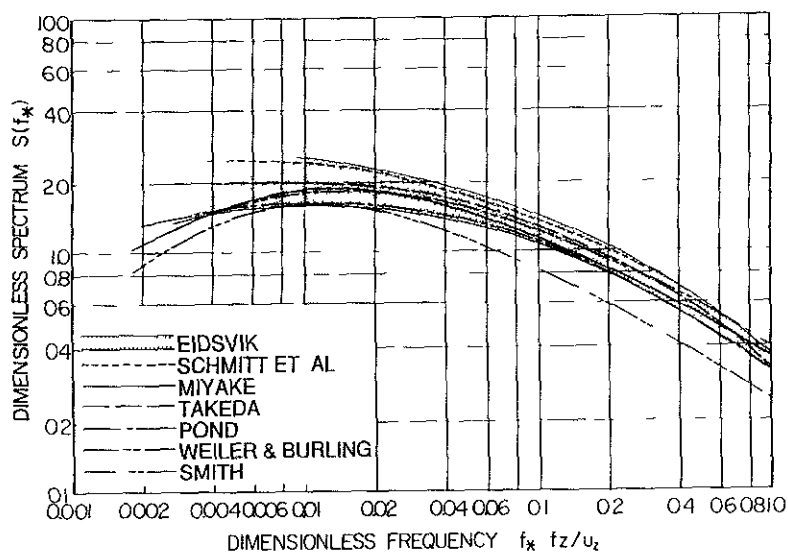


Figure 4:
Comparison between dimensionless turbulent wind spectra obtained from data measured over a seaway (from Ref. 1).

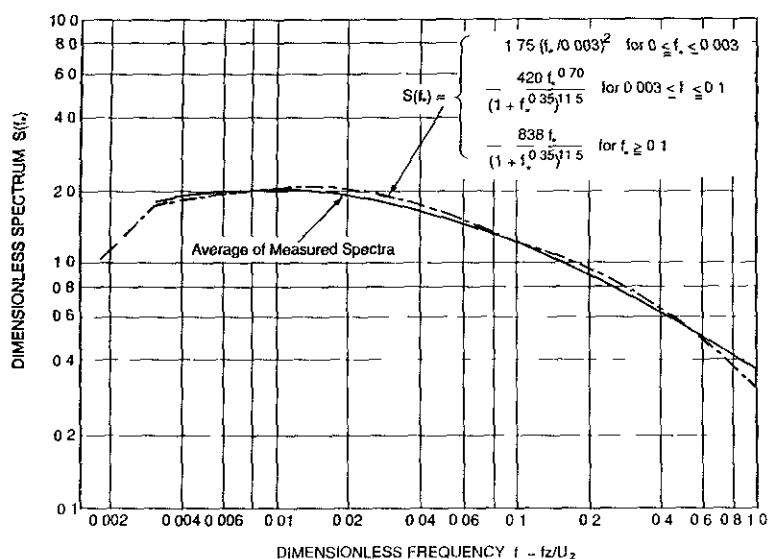


Figure 5:
Mathematical presentation of average of measured wind spectra over a seaway (from Ref. 1).

$$S(f_*) = \begin{cases} 1.75 (f_*/0.003)^2 & \text{for } 0 \leq f_* \leq 0.003 \\ \frac{420 f_*^{0.70}}{(1 + f_*^{0.35})^{11.5}} & \text{for } 0.003 \leq f_* \leq 0.1 \\ \frac{838 f_*}{(1 + f_*^{0.35})^{11.5}} & \text{for } f_* \geq 0.1 \end{cases} \quad (6)$$

The dimensional wind spectrum as a function of frequency ω becomes

$$S(\omega) = \begin{cases} 4925 u_*^2 (z/\bar{U}_z)^2 \omega & \text{for } 0 \leq \omega \leq 0.0189(\bar{U}_z/z) \\ \frac{420 u_*^2 (\omega z/2\pi\bar{U}_z)^{0.70}}{\omega \{1 + (\omega z/2\pi\bar{U}_z)^{0.35}\}^{11.5}} & \text{for } 0.0189(\bar{U}_z/z) \leq \omega \leq 0.628(\bar{U}_z/z) \\ \frac{838 u_*^2 (z/\bar{U}_z)}{2\pi \{1 + (\omega z/2\pi\bar{U}_z)^{0.35}\}^{11.5}} & \text{for } \omega \geq 0.628(\bar{U}_z/z) \end{cases} \quad (7)$$

It is noted that due to a minor simplification made in the conversion from f_* to ω , there is approximately 0.5% difference in $S(\omega)$ computed by the first and second equations at $\omega = 0.00189(\bar{U}_z/z)$. It is also noted that no data is available at present for the energy spectrum at frequencies less than $f_* = 0.003$. Hence, the spectral formulation is given such that the energy reduces linearly to zero at $\omega = 0$ (in dimensional form) for frequencies less than $f_* = 0.003$.

Figure 6 shows the turbulent wind spectra $S(\omega)$, computed by Eq.(7) for various mean wind speeds at height $z = 10$ meters. The figure demonstrates that the turbulent wind energy increases substantially at low frequencies and the increase is particularly pronounced for large mean wind speeds. These low frequencies are in the domain of natural surging and yawing

frequencies of tension-leg platforms and mooring ships; hence, there is a possibility that the turbulent wind may induce resonant motion responses.

Figure 7 shows an example of the effect of height above sea level on the intensity of energy spectra. As can be seen, for the mean wind speed $\bar{U}_{10} = 100$ knots (51.4 m/sec), there is no significant difference in the intensity irrespective of the height above the sea level for frequencies ω greater than 0.15.

It may be of interest to compare the average of the spectral density functions obtained from measurements over a seaway with currently available turbulent wind spectral formulations. As stated in the Introduction, currently available spectral formulations are developed based on data measured primarily over land in an attempt to formulate turbulent wind energy for rel-

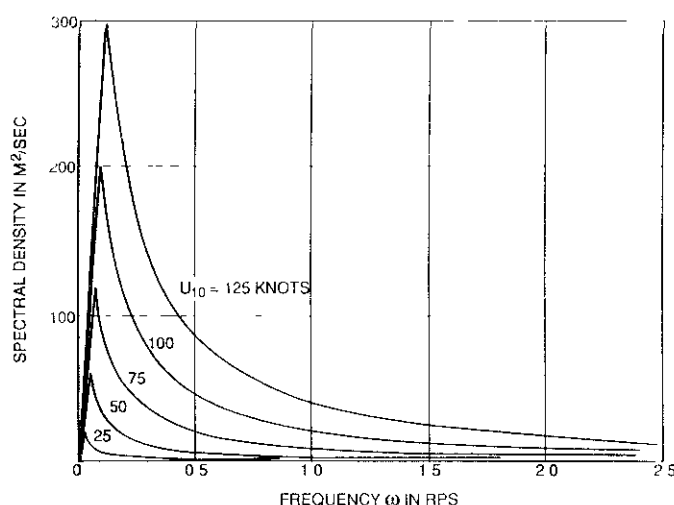


Figure 6:
Turbulent wind spectra for various wind speeds at height $z = 10$ m.

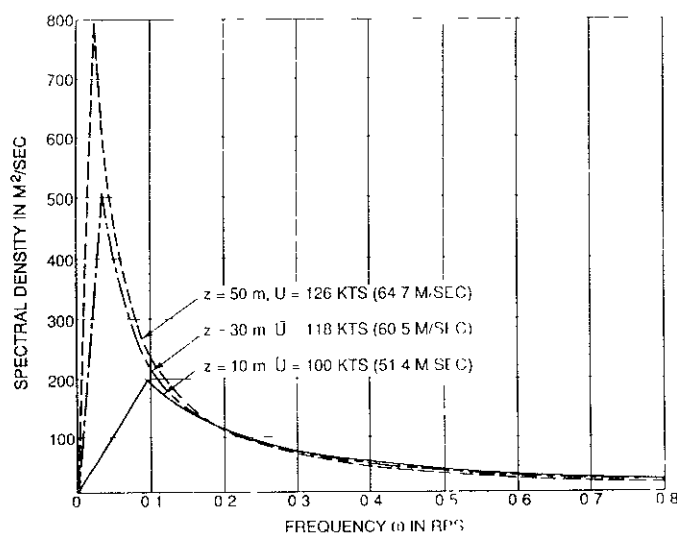


Figure 7:
Effect of height above the sea level on intensity of energy spectra for $\bar{U}_{10} = 51.4$ m/sec (100 knots).

atively high frequencies, say $f_* > 0.1$. However, extension of the formulations is made here to see if they are still valid in the low frequency range of interest for the design of offshore structures.

As can be seen in Figure 8, spectral energy density obtained from measurements over a seaway is much greater than that computed by any of the formulations at low frequencies, smaller than $f_* = 0.01$. The dimensionless frequency 0.01 is equivalent to a period of 19.6 sec at 10 m and 49.5 sec at 30 m height, respectively, for a mean wind speed of 100 knots (51.4 m/sec).

WIND-INDUCED DRAG FORCE

The incident wind speed as shown in Figure 1 consists of two components; one a constant mean speed, \bar{U} , the other a randomly fluctuating turbulent wind speed, $w(t)$. We may write

$$U(t) = \bar{U} + w(t). \quad (8)$$

Then, the wind-induced drag force acting on offshore structures can be written by

$$\begin{aligned} F_D(t) &= \frac{1}{2} \rho C_D A \{U(t)\}^2 \\ &= \frac{1}{2} \rho C_D A \bar{U}^2 + \rho C_D A \bar{U} w(t) + \frac{1}{2} \rho C_D A \{w(t)\}^2, \end{aligned} \quad (9)$$

where ρ = air density, C_D = drag coefficient, A = projected area of structure.

The first term of Eq.(9) is called the mean drag force, denoted by \bar{F}_D , the second term is the linear turbulent wind-induced drag force, while the third term is the nonlinear turbulent wind-induced force. It may be well to write Equation (9) as follows:

$$F_D(t) = \bar{F}_D \left[1 + \frac{2}{\bar{U}} w(t) + \frac{1}{\bar{U}^2} \{w(t)\}^2 \right], \quad (10)$$

$$\text{where } \bar{F}_D = \frac{1}{2} \rho C_D A \bar{U}^2.$$

In order to find the significance of turbulence in wind-induced drag force, the last two terms in Eq.(10) including the nonlinear term should be considered. It was found, however, that the linear term is the major contributor to the drag force [5]. Hence, in the following analysis we will evaluate the extreme magnitude of the linear turbulent drag force and compare it with the magnitude of the mean wind drag force.

We assume that the turbulent wind speed is a non-narrow-band Gaussian random process with mean value zero and with variance σ^2 , where the variance is equal to the area under the turbulent wind energy spectrum. Then, the extreme magnitude of the peaks (or troughs) of the turbulent wind speed expected to occur in T-hours with a risk parameter α , denoted by $\eta_{\text{ext}}(\alpha)$, can be evaluated by [6],

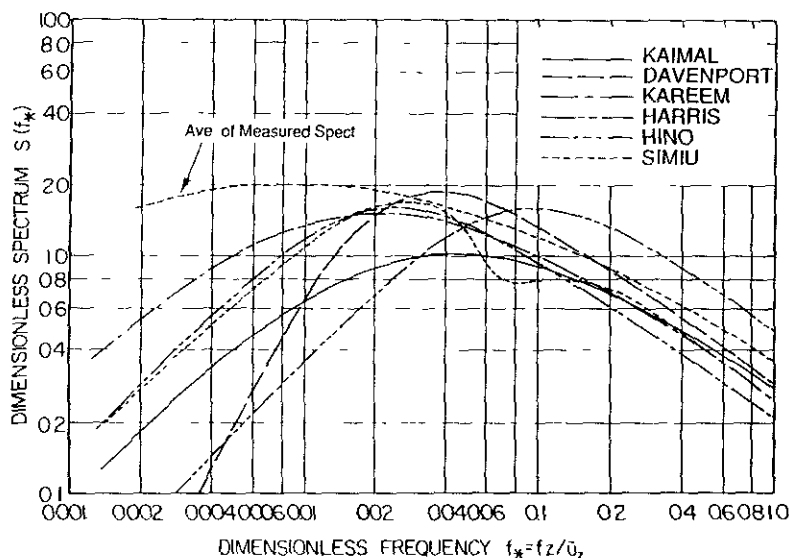


Figure 8:
Comparison of various dimensionless wind spectral formulations (from Ref. 1).
(Davenport formulation is non-dimensionalized for $\bar{U}_{30} = 44.7$ m/sec. at height $z = 30$ m).

$$\eta_{\text{ext}}(\alpha) = \sqrt{2 \ln \left\{ \frac{(60)^2 T}{2\pi\alpha} \sqrt{m_2/m_0} \right\} m_0} \quad (11)$$

where m_j = j-th moment of the turbulent wind energy spectrum, and $\alpha = 1$ yields the most probable extreme value.

Computations of the extreme values $\eta_{\text{ext}}(\alpha)$ are made for $\alpha = 1$ and 0.01 for various mean wind speeds at 30 meter height above the sea surface on an offshore structure having a projected area $A = 2,000 \text{ m}^2$. By multiplying the computed extreme values of $\eta_{\text{ext}}(\alpha)$ by $2 \bar{F}_D / \bar{U}_z$, we can evaluate the magnitude of the peaks (or troughs) of turbulent wind-induced drag force. In computing the mean drag force, \bar{F}_D , the drag coefficient C_D is taken as unity, while the air density ρ is taken as 1.2 kg/m^3 .

The results of the computations are shown in Figure 9. Included also in the figure is the mean drag force for comparison. As can be seen in the figure, the magnitude of the probable extreme turbulent

drag force expected in one hour is of the same order as that of the mean wind drag force. It is noted that the probability that the extreme drag force will exceed the probable extreme value is rather large — theoretically $1 - e^{-1} = 0.632$. Hence, it is highly desirable to evaluate an extreme value for which the probability of being exceeded is very small: for example, the risk parameter α equal to 0.01. The magnitude of the extreme turbulent drag force for $\alpha = 0.01$ is much greater than that of the mean drag force, particularly for large mean wind speeds. For example, the former is 33 percent greater than the latter for a mean wind speed of 60.5 m/sec at 30 meter height which corresponds to 100 knots at 10 meter height above the sea surface.

CONCLUSIONS

This paper discusses the significance of low frequency turbulent winds over a seaway which induce very large drag forces that may seriously affect the stability of ships and ocean structures. The turbulent wind energy spectral densities obtained from data measured over a seaway are very large at low frequencies (less than 0.02 Hz) — much greater than those evaluated by any of the currently available spectral formulations. The low frequencies are in the domain of some natural response frequencies of marine systems; hence, there is a high possibility that the turbulent wind will induce resonant motion responses.

The magnitude of turbulent wind-induced force acting on marine structures appear to be significant and thereby extreme care must be taken to include the turbulent wind-induced force in evaluating stability criteria of ships and offshore structures. Results of the computations show that the probable extreme value of the peaks (or troughs) of the turbulent wind-induced force is of the same order as that of the force associated with the mean wind speed. The magnitude of extreme drag force

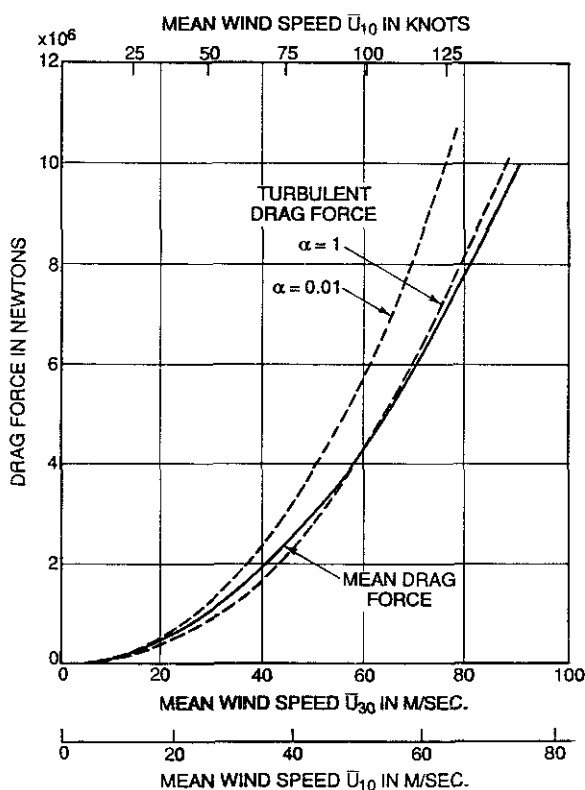


Figure 9: Comparison between extreme turbulent wind-induced drag force and mean drag force for various wind speeds at height $z = 30 \text{ m}$.

with risk parameter $\alpha = 0.01$ is much greater than that of the mean drag force. For example the former is 33 percent greater than the latter for a mean wind speed of 60.5 m/sec at 30 meter height which corresponds to 100 knots at 10 meter height above the sea surface.

REFERENCES

1. Ochi, M.K. and Shin, Y.S., Wind turbulent spectra for design consideration of offshore structures. Proc. Offshore Tech. Conf. OTC 5736, 1988, Vol.2, pp.461-468.
2. Shiraishi, N., Aerodynamic response of bridge to natural winds, Wind Effect on Structures, Univ. of Tokyo.
3. Wu, J., Wind-stress coefficients over sea surface from breeze to hurricane, J. Geophys. Res. 1982, Vol.87, pp. 9704-9706.
4. Eidsvik, K., Large-sample estimates of wind fluctuations over the ocean, J. Boundary-Layer Meteorol., 1985, Vol.32, pp. 103-132.
5. Ochi, M.K. and Murer, Y., Estimation of extreme wind force for offshore structure design, Univ. of Florida, Tech. Rep., UFL/COEL- TR/81, 1989.
6. Ochi, M.K., On prediction of extreme values, J. Ship Res., 1973, Vol.17 No.1, pp. 29-37.

STABILITY OF HIGH SPEED VESSELS

Egil Jullumstroe, Senior Research Engineer,
MARINTEK A/S, Norway.

Abstract

The paper discusses present state of the art regarding the possibility of developing complete stability rules and regulations for high speed vessels.

Compared to conventional ships and their stability recommendations, safety codes of high speed vessels need to include further requirements. By their nature high speed vehicles are much more sensitive to problems associated with motions, transverse and longitudinal stability, control and behaviour in different wave situations and wave directions.

Reflecting the fact that static stability data alone are not sufficient for future rules and recommendations, MARINTEK A/S has initiated a research programme which incorporate the dynamics of high speed vehicles with respect to stability on an overall basis.

In this programme, transverse stability is investigated in beam and oblique sea conditions, longitudinal stability is investigated in following wave conditions. Investigations concerning operational aspects such as loss of stability, loss of lift, dangerous situations are carried out both for long-crested and short-crested waves. Stability as a function of manoeuvring, are investigated in calm water as well as in waves.

The work within the research programme is based on a combination of experiments and theoretical work to obtain a complete understanding of the stability problem of high speed vehicles.

The results and the methodology derived from the research programme will be put forward to national (Norwegian, NMD) and International (IMO) governmental organizations.

Examples of results and stability recommendations based upon these are presented.

1. INTRODUCTION.

Over the later years, the operational pattern of high speed vehicles has changed quite a lot. Vessels are designed for all kinds of tasks within transportation services, and they are operating in very rough sea conditions compared to what until now were acceptable conditions. As a result of this, the safety margins have changed and become more critical due to reduction of safety factors.

Advanced high speed vessels are poorly developed with respect to stability rules and regulations compared to conventional vessels. There are several reasons for this. One important factor is that there are many different types of high speed vehicles, and many different solutions within each category. Thus, a generalization of rules and regulations is difficult. Another factor is that there is poor understanding of different phenomena affecting ship stability, both longitudinal and transverse stability. A better understanding of these phenomena is necessary for developing of future rules.

The "Code of Safety for Dynamically Supported Craft" is the international safety standard of IMO developed for high speed vehicles. High speed vessels in this context could be SES, hydrofoils, catamarans, ACV's et cetera. With respect to stability, both static and dynamic stability in the transverse direction is described for hydrofoils, however, most other vehicles are not dealt with in detail. With the trend of today towards hydrofoils, SES and catamarans there are at least two concepts that should be developed parallel to the hydrofoil concept. The recommendations of the hydrofoil concept in itself is inadequate, however, the framework for future rules are laid through the IMO-recommendation.

Future stability and safety rules should be based upon different thinking and methodology, rather than by using traditional precedents. Instead of extending conventional ship standards readily available, methods from the aircraft industry should be applied and developed. Through the Norwegian Research Programme of High Speed Vessels, one of the main goals is to develop safety standards for SES, catamarans and hydrofoils.

2. STABILITY AND SAFETY REGULATIONS.

The IMO-recommendation concerning stability of high-speed crafts are laid down in resolution A.373(x), "Code of Safety for Dynamically Supported Craft", the stability rules can briefly be described as follows:

- * A single paragraph covers all types of high speed vehicles.
- * Transverse stability recommendations are given for hydrofoil vessels. The framework for future recommendations is laid, however the specific stability demands should be adjusted.
- * Transverse stability recommendations for vessels other than hydrofoils are not covered by A.373(x).
- * Longitudinal stability recommendations do not exist.
- * Coupling of transverse and longitudinal stability is not described.
- * "Active", safety demands such as operation manuals are not included.
- * The stability requirements are in accordance with the requirements of conventional, displacement ships.

Though the safety record of high-speed vehicles has been excellent, there is no doubt that new safety standards should be worked out for all kinds of high-speed craft. With respect to stability, each major class of vessels should each have a paragraph covering specific characteristics for different types of vessels. This also applies for other safety standards than pure stability, for instance fire safety, design features, buoyancy and subdivision, damage etc.

The IMO-Code is a minimum safety standard, a future minimum standard should, in the author's opinion cover at least the above mentioned aspects. As to the code of today, it is only mandatory for international voyages. A future code should have binding rules also for international services.

As a consequence of developing and taking new rules into use, a thorough documentation of vessel characteristics is also necessary. All technical data and details of construction affecting stability of the vessel should be presented. Performance data should be obtained for the relevant situations. If the performance data does not comply with the rules, action should be taken.

3. RESEARCH PROGRAMME.

The Norwegian Research Programme for High Speed Vessels is a four year programme, it was started medio 1989 and will be finalized in 1993. The programme is sponsored by The Norwegian Council of Science & Research (NTNF) and Norwegian Industry. Among several topics within the programme, the following sub-projects are mentioned since they are related to the overall safety of high-speed vessels, and due to the fact that they will contribute to the working out of new safety recommendations.

- * Cockpit-project.
- * Seakeeping Prediction Programme.
- * Safety regulations for high-speed vessels.

The Cockpit-project is run in order to provide efficient and safe operation of high-speed vessels, by developing bridge systems, procedures for operation, equipment systems, simulation/training systems and accidents/evacuation procedures.

The Seakeeping Qualities Project is run in order to work out tools that predict sea loads and motions of high-speed vessels. This means that for SES, hydrofoils and catamarans, the limitations of today's numerical prediction models are reduced.

The Safety Regulation Project identifies important areas where rules and regulations should be improved and/or extended. Hereunder stability in a broad sense. The work described in the following chapters is carried out in this sub-project.

A catamaran and a hydrofoilcatamaran vessel are investigated in beam and following seas with respect to stability. In respect to beam seas results one should bear in mind that a SES off-cushion behaves quite similarly to a catamaran and that the GZ-curve is reduced in on-cushion compared to off-cushion condition. The beam seas test results are judged against the existing stability recommendations of high-speed vessels.

For longitudinal stability, no recommendations exist to this day. This is rather astonishing, the documentation made by this project and experience from full scale, fully confirms that this problem must be taken seriously. Concerning high-speed vessels, the probability of major accidents due to low longitudinal stability is very high.

4. TRANSVERSE STABILITY - PROBABILITY OF CAPSIZE.

A catamaran hull has been tested with various righting moment curves. The variation in the righting moment was obtained by altering the superstructure, thus the metacentric height GM_T and VCG-values were equal to those of full scale designs. Increase of VCG-values to decrease the initial stability and to alter the roll resonance period towards longer periods was not regarded of interest. The tests carried out were therefore an investigation upon the shape of the GZ-curve and the requirements of having a positive GZ-value to a certain heeling angle. Figure 1 shows GZ-curves for catamarans with small/normal superstructures and for a catamaran with a large superstructure.

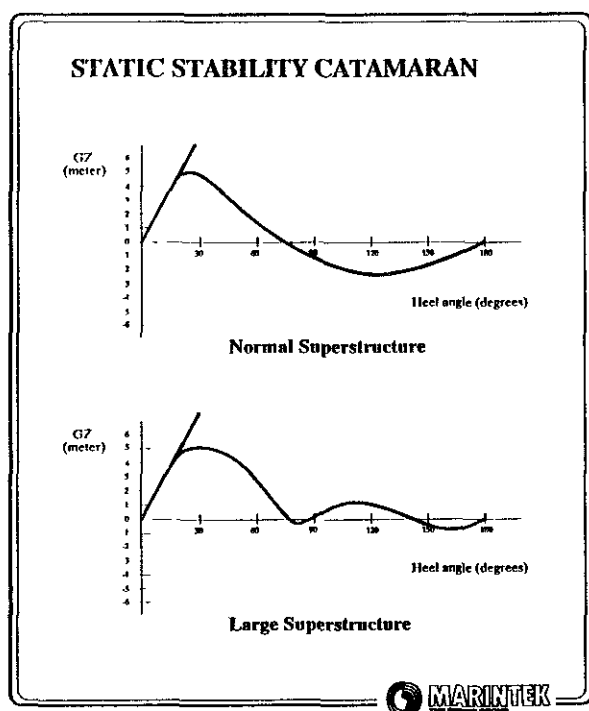


Figure 1. - Static stability curve for catamarans.

Tests were performed in regular waves (resonant capsize), irregular wavetrains (capsize due to breaking waves and

groupiness in the wavetrain), and in steep plunging breakers (capsize when hit by the breaker). The tests were carried out in hullborne condition, speed equal to zero, incoming waves as beam seas and with the model completely free to move in 6 degrees of freedom. As indicated above, there are different hypothesis for typical situations in which capsizing might occur, however most tests were performed in plunging breakers. This is in accordance with a test philosophy and procedures developed at Marintek for stability research with conventional hull-forms, i.e. for cargo vessels and fishing vessels.

A general conclusion from the test programme can briefly be described as follows:

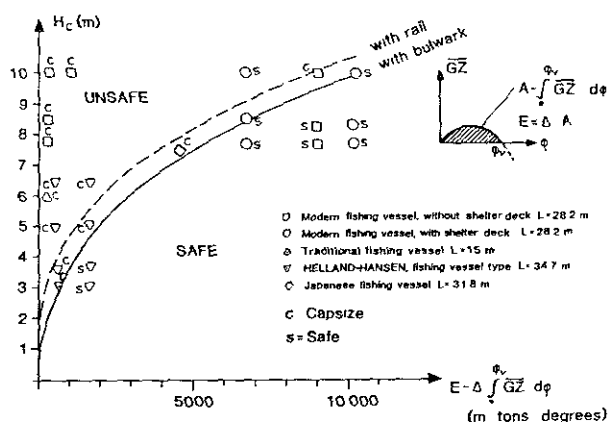
The catamaran hull with large superstructure, i.e. with GZ-curve positive to a large heel angle, did not capsize in any wave situation.

The catamaran hull with a normal small superstructure, that is with a GZ-curve having a distinctive angle of vanishing stability at approx. 70 degrees, and large negative GZ-values from 70 to 180 degrees, did not capsize as a result of resonant rolling, nor in irregular wave trains. However, capsizing occurred in plunging breakers when wind load was applied.

A large number of tests were run with varying wind loads, varying wave heights and with variation in prehistory of the plunging, breaking wave. A well defined limit for occurrence of capsizing was established through these tests.

The probability of capsize in steep and high waves from the side for small vessels is evaluated by E.Aa. Dahle, D. Myrhaug and S.J. Dahl in ref. [1], based on the Sevastianov method ref. [2]. In this evaluation, the critical height of a near-breaking wave H_c is defined as a function of the significant wave height, and a probability of extreme waves for given sea states are calculated. The probability of capsize as a function of H_c is expressed versus the internal work $E = \Delta \int \phi^v GZ d\phi$ until GZ becomes zero. Further, it is shown that capsizing frequency derived from model tests shows good agreement with full scale accidents.

As an example, the results from the present study is compared with results from earlier investigations, mainly fishing vessels, this is done to express the difference in probability between a catamaran hull and mono-hulls.



Probability of capsizing (from Dahle and Myrhaug 1986).
 □ Nedreid *et al.* (1983) ▽ Dahle and Kjarland (1980)
 ○ Miyawaki and Yamashita (1985) / IMO (1983)

Figure 2. Probability of capsizing for fishing vessels.

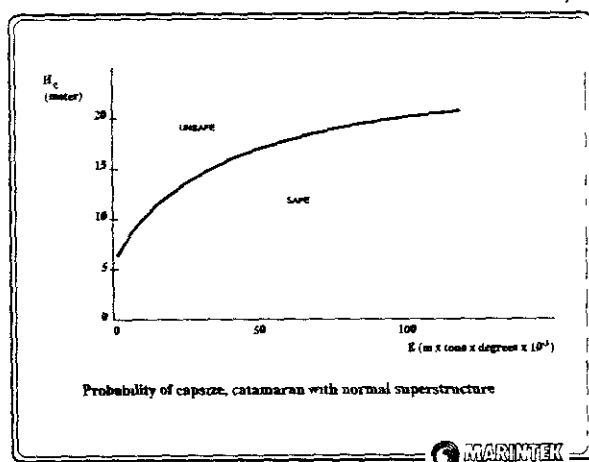


Figure 3. Probability of capsizing for catamaran hull (hullborne).

By comparing the curves in Fig. 2 & 3, the following should be observed:-

- The probability of capsizing for a catamaran hull is much less than for monohull of similar size, nevertheless, there is a probability of capsizing catamarans.
- The probability of capsizing for catamaran hulls on international voyages is significant, small vessels i.e. displacements less than 750-1000 tonnes should be carefully studied with respect to stability to avoid capsizing.

- The difference in righting moment expressed as GZ-curves is for a catamaran as compared to a monohull enormous, however, the heeling moment due to wave loads will also be much higher for a catamaran than for a monohull.

Discussing stability of catamarans and multihulls out from monohull stability recommendations are due to this irrelevant.

- As for monohull capsizing safety, the shape of the GZ-curve beyond 40 degrees heeling angle is of great importance, as is also the angle of vanishing stability.

- A relevant requirement for the GZ-curve for small catamaran vessels is that the curve is positive to a heeling angle of 80 degrees.

Another safety aspect which is very important with catamaran hulls is the magnitude of roll motion and accelerations with respect to cargo and cargo shifting. In general, roll motions and vertical accelerations at the ship's side will be much higher than for a monohull. This means that cargo is much more exposed to shifting. According to this, the cargo securing recommendations should be strengthened.

5. LONGITUDINAL STABILITY - DECK DIVING.

A catamaran and a foil-catamaran hull are investigated with respect to longitudinal stability in following seas. The investigations were carried out as model tests and as computer calculations. The objective of this work is to evaluate the probability of deck diving at high speed.

Tests and computations were performed with various speeds, with variation in wavelength/shiplength and in waveheight/wavelength. Tests were carried out in regular waves, the model was free to surge, pitch and heave. "Bowdive", a Marintek developed program was used in computations.

The background for these investigations is that high speed vessels in most cases are designed and built with slender forebodies, in order to reduce wave impacts. As a result of this the buoyancy of the foreship is reduced, while the afterbody is normally highly buoyant oscillating in a seaway.

The combination of high speed, hull design and wave situations might lead to different dangerous situations. This study is related to following sea situations and safety. In following seas, loss of foil lift is also very pronounced.

The main conclusions from this work are:-

- The probability of deck diving of today's design of catamarans, mono-hull and foilcatamarans and high-speed vehicles is very high.
- Deck diving might occur in very small wave heights. If wave length and ship speed is unfavourable in combination, deck diving becomes a problem even for 2-3 metres wave height.
- Deck diving occurs frequently for wave length/ship length ratios between 1.0 and 2.0. That is, similar situations that lead forward to broaching situations.
- Deck diving is critical for ship speed equal to or greater than wave speed.
- Model tests and computer calculations of deck diving in a wave situation shows good agreement.
- Reduced foil-lift due to waveparticle velocity, ventilation, out of water situations and pitch angle close to or larger than zero-lift angle may lead to deck diving.

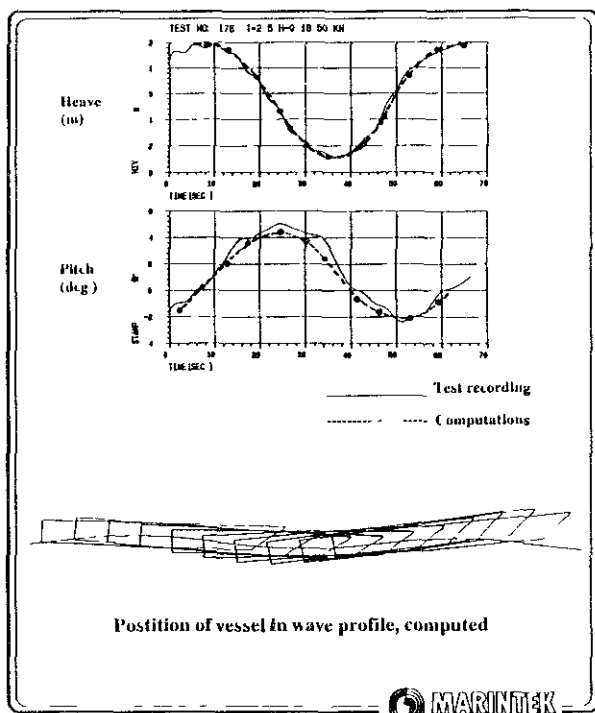


Figure 4. Time series from tests and from computations of heave and pitch in a following wave.

Position of bow in relation to wave profile.

When deck diving occurs, the following scenarios are possible:

- Deck/superstructure goes into the water, total buoyancy of submerged volume is sufficient to bring the vessel to an upright position. Speed is reduced as a function of diving depth, equipment on deck and parts of superstructure may be damaged.
- Deck/superstructure goes into water and the total buoyancy of the foreship is insufficient to raise the forebody out of the water. Speed is reduced to zero, large longitudinal acceleration occurs, superstructure will be violently submerged and possible destroyed. The possibility of having flooded compartments is high.

Both scenarios include high risks for small vessel safety and must be avoided.

6. FUTURE RECOMMENDATIONS.

The future high-speed craft industry will be a high risk business similar to the aviation industry. Thus, many of the same challenges that the aircraft industry meet will have to be dealt with in a similar manner for high-speed craft. This will be also be the situation in regard to safety rules, hereunder stability and safe operation of vessels. The results obtained so far in this project clearly state the necessity for improved rules and recommendations, and also for operation. A good example in this context is the deck diving situation that might occur in following seas. It is very difficult to design and operate a vessel for international voyages that will not be exposed to deck diving. The risk of deck diving should be evaluated at the design stage. However, in extreme weather conditions procedures for safe operation are needed. To build up systems and procedures similar to those of the aviation industry is the only reasonable way to go.

Adopting systems and procedures from the aircraft industry, does not mean that vessels shall be classified as aircraft. Ship and waterway regulations must apply. The first step in the sketched direction for IMO will be to recognize that this is the way to go, secondly, separate paragraphs should be worked out to cover all types of high-speed vessels in a correct manner. Further, a third step required prior to the implementation of the rules, is to develop safety standards and procedures covering the different paragraphs.

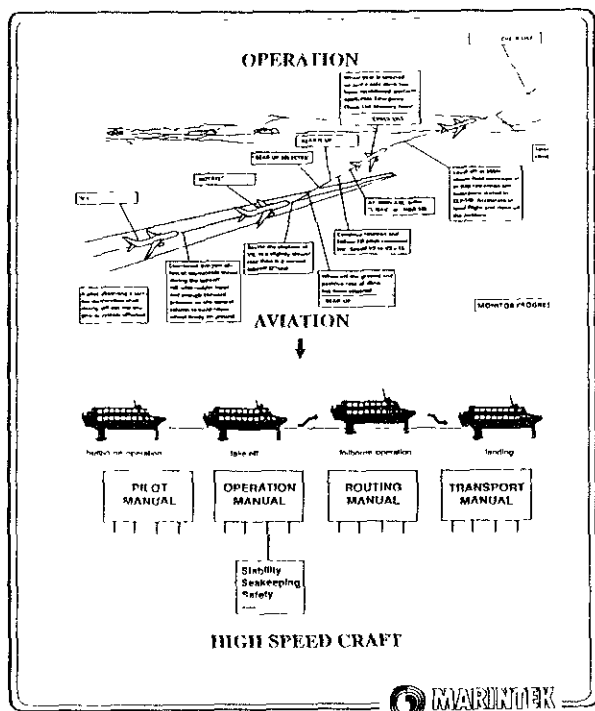


Figure 5. Safety System For High-Speed Craft Based On Aviation Industry System.

7. CONCLUSIVE REMARKS.

Development of safety standards and stability recommendations for high-speed craft will be one of the great challenges for IMO and other institutes during the nineties.

Stability recommendations for high-speed craft other than monohull, based on conventional ships' code are inadequate.

Transverse stability and safety of SES's and catamarans are highly dependant upon the extension of the GZ-curve and the area under the curve for heel angles greater than 50 degrees.

Capsizing of multihull vessels is possible, in spite of high initial stability and righting moment curve, this possibility should be associated with critical wave heights.

Longitudinal stability, expressed as deck diving probability, is a very serious problem. To this day this problem has not yet been paid attention, in the future it will be necessary to treat this problem as equally important as the transverse stability problem. Accidents due to lack of longitudinal stability can have the same outcome as capsizing accidents with respect to loss of lives and vessels.

REFERENCES.

- [1] E.Aa.Dahle, D.Myrhaug & S.J.Dahl: "Probability of capsizing in steep and high waves from the side in open sea and coastal waters". Ocean Eng.Vol.15,No.2, pp.139-151, 1988.
- [2] Sevastianov, N.B.: "Practical and Scientific Aspects of the stability Problem for Small Fishing Vessels". Int. Conf. on Design Considerations for Small Craft, RINA,LONDON 1984.
- [3] International Maritime Organization, IMO-resolution A.373(x) -"Code of Safety for Dynamically Supported Craft" - 1977.
- [4] Kristiansen, Svein et al - Efficient and Safe Transport of High Speed Craft. MARINTEK Reports January 1990.
- [5] Holden, K.O.: -Summary report of activities within High Speed Craft Programme NTNf-report HRAP1/1990.02.14.
- [6] Jullumstrø, Egil.: -Stability of High Speed Craft. - NTNf-reports 600006-01, 600006-02, 600006-03 March 1990.

PROBABILISTIC STUDY ON SHIP CAPSIZING DUE TO PURE LOSS OF STABILITY
IN IRREGULAR QUARTERING SEAS

Naoya Umeda,¹⁾ Yasuyuki Yamakoshi¹⁾ and Tsutomu Tsuchiya²⁾

ABSTRACT

This study presents a theoretical method for calculating probabilities of capsizing due to pure loss of stability for a ship running in short crested waves and fluctuating wind. The aim was to develop stability criteria of a ship in quartering seas making use of the risk analysis. We divide the ship motions into the steady motions and the unsteady motions. Then we integrate the probability density function, which is given by the steady random process theory, on the safe domain that is determined by separatorices of the unsteady dynamic system. The reduction of restoring moment when a wave crest moves into the center of gravity of the ship is fully considered by Grim's effective wave concept. Numerical example is shown for a coastal trawler.

INTRODUCTION

Stability criteria against capsizing in following or quartering seas are required besides the IMO weather criterion for a ship in beam seas. [1] Because many seamen have lost their lives in quartering seas and naval architects observed capsizing of radio-controlled models mainly in quartering waves. [2] In particular, the pure loss of stability is the most critical phenomenon among the capsizing modes in quartering seas. [3] This means that the transverse stability of a ship in quartering seas is drastically reduced when a wave crest moves into the center of gravity and the ship easily capsizes.

To develop practical stability criteria, we should assess the capsizing in irregular seas. Because, the risk and reliability analysis requires the probability of capsizing of a ship to compare this with the acceptable risks. [4,5] However, we have few studies to assess the probability of capsizing due to the pure loss of stability in irregular following seas. [6,7,8] As to the capsizing in irregular quartering seas we find very few studies besides model experiments and numerical simulation those use a kind of the Monte Carlo technique.

Therefore, the authors did propose a method to assess the probability of capsizing due to the pure loss of stability in irregular quartering seas to develop stability criteria by using risk analysis. In addition, an assessment of a ship in following seas or beam seas can be included as a limit of this method.

BASIC CONCEPTS OF THIS STUDY

We assume that a ship is running with a constant averaged speed and a constant averaged course in wind and waves. The wind velocity changes with time around the averaged velocity U_T and has the Davenport spectrum $S_{uu}(\omega)$; ω is a circular frequency [4]. The wind generates short crested waves. The significant wave height $H_{1/3}$ and the mean wave period T_{01} are given by the Pierson-Moskowitz formulae :

$$H_{1/3} = 0.0214 U_{7.5}^2 \quad (1)$$

$$T_{01} = 3.86 \sqrt{H_{1/3}} \quad (2)$$

$$U_{7.5} = U_T (7.5/10)^{1/7} \quad (3)$$

The spectral density of the fully developed waves is greater than that of the developing waves. Thus we use the ITTC (1978) directional spectrum $S(\omega, \alpha)$ for the fully developed waves. [9] Here α is an angle of the component wave to the principal wave direction. Further, we assume that the wind direction coincides with the principal wave direction.

Next, we should consider ship motions including capsizing in the wind and waves. In the final stage for capsizing, the ship motions are completely non-linear and unsteady. Thus to predict capsizing is very difficult besides random simulation in time domain. Since a non-linear dynamic system depends on initial conditions, we must employ all possible combinations of the initial conditions to carry out the random simulation. In the meanwhile, except for this final stage, it is often reported that linear and steady seakeeping theories can predict irregular ship motions in even heavy seas. [10] Therefore, we divide the

1) National Research Institute of Fisheries Engineering; Hasaki, Kashima, Ibaraki, Japan

2) President, FRP Fishing Boat Research Association of Japan; Tokyo, Japan

ship motions into the steady motions and the unsteady motions those include capsizing (See Fig.1). First the steady motions are statistically predicted by a linear theory in frequency domain. Then we regard the predicted steady motions as initial conditions for the unsteady problem and integrate non-linear equations of motion in time domain. The correlation between the steady and the unsteady motions is reflected by the continuity of physical variables on bounds. This concept was previously used by Blocki [11] for the low cycle resonance in beam seas where the bounds selected are when roll angle is zero. In this study the bounds selected are when a wave moves into the center of gravity because the pure loss of stability is a trigger for the capsizing in quartering seas.

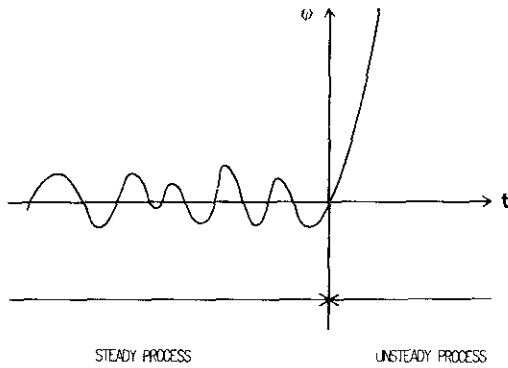


Fig.1 Scheme of capsizing

STEADY MOTIONS

Motions due to wind

When a ship runs with her velocity V in the wind whose velocity is U_T and angle is $\bar{\chi}$, the apparent wind velocity and angle on the ship are calculated as follows: (See Fig.2)

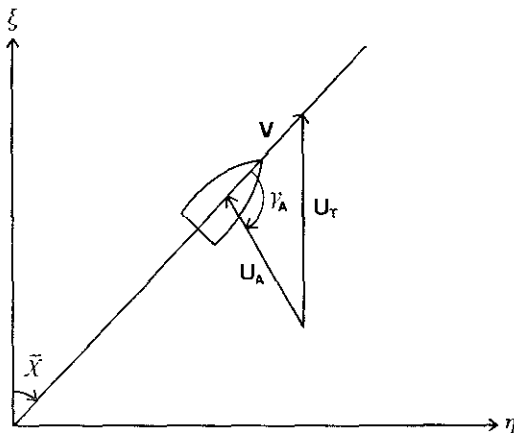


Fig.2 Apparent wind

$$U_A = \sqrt{V^2 + U_T^2 - 2VU_T \cos \bar{\chi}} \quad (4)$$

$$\gamma_A = \cos^{-1} \left(\frac{V^2 + U_A^2 - U_T^2}{2VU_A} \right) \quad (5)$$

We rewrite U_T and U_A

$$U_T = \bar{U}_T + \tilde{U}_T \quad (6)$$

$$U_A = \bar{U}_A + \tilde{U}_A \quad (7)$$

Here \bar{U}_T and \bar{U}_A are averaged velocity and \tilde{U}_T and \tilde{U}_A are variations of the velocity and change with time. Substituting Eqs. (6)-(7) into Eqs. (4)-(5),

$$\tilde{U}_A = \left(\frac{\tilde{U}_T}{\bar{U}_A} - \frac{V}{\bar{U}_A} \cos \bar{\chi} \right) \tilde{U}_T \quad (8)$$

$$\sin^2 \gamma_A =$$

$$(\sin \gamma_A)^2 \left[1 + \left(\frac{\cos \gamma_A}{\sin \gamma_A} \right)^2 \left\{ \frac{2}{\bar{U}_A^2} (\bar{U}_T - V \cos \bar{\chi}) + \frac{2 \cos \bar{\chi}}{\bar{U}_A \cos \gamma_A} \right\} \tilde{U}_T \right] \quad (9)$$

The aerodynamic lateral force due to averaged wind F_A is given by

$$F_A = \frac{1}{2} \rho_A A_A C_{DA} \bar{U}_A^2 (\sin \gamma_A)^2 \quad (10)$$

Here ρ_A is air density, A_A is a transverse projected area of the ship above water, C_{DA} is an aerodynamic drag coefficient and h_A is a distance of the center of the force from a water surface. Since this aerodynamic force induces a hydrodynamic force whose magnitude is same and direction is opposite and a distance of the center of the hydrodynamic force from a water surface is h_H , the inclining moment, $F_A (h_A + h_H)$, acts on the ship. Thus, a heel angle of the ship, ϕ_0 , is obtained by the following equation of equilibrium.

$$F_A (h_A + h_H) - W G Z(\phi_0) = 0 \quad (11)$$

The roll moment due to wind is assumed to be given by

$$K_A(t) = \frac{1}{2} \rho_A A_A C_{DA} h_{AG} U_A^2 \sin^2 \gamma_A \quad (12)$$

Here h_{AG} is a distance of the center of the wind force from the center of gravity of the ship. Then we separate variations of the moment, $\tilde{K}_A(t)$, only from $K_A(t)$.

$$\tilde{K}_A = \rho_A A_A C_{DA} h_{AG} \left\{ \left(\bar{U}_T - V \cos \bar{\chi} \right) + \bar{U}_A \cos \gamma_A \cos \bar{\chi} \right\} \tilde{U}_T \quad (13)$$

Neglecting the coupling effects, we can obtain an equation of one-freedom roll motion due to the wind as follows:

$$(I_{44} + A_{44})\ddot{\phi} + B_{44}\dot{\phi} + C_{44}\phi = \ddot{K}_A(t) \quad (14)$$

where I_{44} is the moment of inertia of the ship, A_{44} is the added moment of inertia, B_{44} is a linearized roll damping coefficient and

$$C_{44}(\phi_0) = W \left(\frac{dGZ_0}{d\phi} \right)_{\phi=\phi_0} \quad (15)$$

Here W is the weight of the ship; GZ_0 is a righting lever of the ship in still water. Hence the transfer function of the roll whose input is the fluctuating wind velocity is given by

$$H_{\phi}^{WIND}(\omega) = H_{\phi c}^{WIND} + i H_{\phi s}^{WIND} \quad (16)$$

where

$$H_{\phi c}^{WIND} = \frac{\omega_0^2 - \omega^2}{(\omega_0^2 - \omega^2)^2 + a^2\omega^2}$$

$$\frac{\rho_A A_{44} C_{DA} h_{4G}}{I_{44} + A_{44}} \{ (\bar{U}_T - V \cos \bar{\chi}) - \bar{U}_T \cos \bar{\gamma}_A \cos \bar{\chi} \}$$

$$H_{\phi s}^{WIND} = \frac{-a\omega}{(\omega_0^2 - \omega^2)^2 + a^2\omega^2}$$

$$\frac{\rho_A A_{44} C_{DA} h_{4G}}{I_{44} + A_{44}} \{ (\bar{U}_T - V \cos \bar{\chi}) - \bar{U}_T \cos \bar{\gamma}_A \cos \bar{\chi} \}$$

$$\alpha = \frac{B_{44}(\phi_0)}{I_{44} + A_{44}(\phi_0)} \quad \omega_0 = \sqrt{\frac{C_{44}(\phi_0)}{I_{44} + A_{44}(\phi_0)}}$$

Motions due to waves

It is well-known that linear strip methods can predict steady ship motions due to waves. Lee & Kim applied a strip method for the sway-heave-pitch-roll-yaw motions of a ship with a heel angle. [12] Though we can use their result, we temporarily use the transfer function of one-freedom roll motion due to waves, as follows: [13]

$$H_{\phi}(\omega, \chi) = H_{\phi c} + i H_{\phi s} \quad (17)$$

where

$$H_{\phi c} = \frac{a\omega_e}{(\omega_0^2 - \omega_e^2)^2 + a^2\omega_e^2} \frac{C_{44}\gamma(\omega^2/g) \sin \chi}{I_{44} + A_{44}}$$

$$H_{\phi s} = \frac{(\omega_0^2 - \omega_e^2)}{(\omega_0^2 - \omega_e^2)^2 + a^2\omega_e^2} \frac{C_{44}\gamma(\omega^2/g) \sin \chi}{I_{44} + A_{44}}$$

$$\omega_e = \omega - \frac{\omega^2}{g} V \cos \chi$$

and γ is an effective wave slope coefficient. As to the surge motion, the transfer function $H_x(\omega, \chi)$ can be obtained in the same manner. [14]

CHANGE IN GZ DUE TO WAVES

It is difficult to predict restoring moment in irregular quartering seas because the

relation between the restoring moment and wave is non-linear. [8] To bypass this difficulty, Grim [6] proposed the concept of an effective wave where an irregular wave profile around the ship is replaced with a regular wave called "the effective wave". The length of the effective wave is equal to the ship length L_{pp} and the crest or the trough of the wave is situated at the center of gravity (See Fig.3). Since the relation between GZ and the effective wave is not only non-linear but also non-memory, we can discuss the probabilistic properties of GZ . Though Grim presented formulae for the ship in long-crested following seas, we presented formulae for the ship in short-crested quartering seas shown in Fig.4.

If sea surface elevation is assumed to have a Gaussian distribution, it is represented as follows:

$$\zeta_w(\xi, \eta, t) = \int_0^\infty \int_{-\pi}^{\pi} \sqrt{2S(\omega, \alpha)} d\omega d\alpha \cos(\omega t - k\xi \cos \alpha - k\eta \sin \alpha + \psi) \quad (18)$$

where $\chi = \alpha - \bar{\chi}$ and ψ is a random number. The effective wave is defined as follows:

$$\zeta_{eff}(x, t) = a(t) + \zeta_{eff}(t) \cos \frac{2\pi}{L} x \quad \left(-\frac{L}{2} < x < \frac{L}{2} \right) \quad (19)$$

Making use of the least square method, the transfer function H_{ζ} whose input is ζ_w and output is ζ_{eff} is given by

$$H_{\zeta}(\omega, \chi) = H_{\zeta c} + i H_{\zeta s} \quad (20)$$

where

$$H_{\zeta c} = \frac{\frac{\omega^2 L}{g} \cos \chi \sin \left(\frac{\omega^2 L}{2g} \cos \chi \right)}{\pi^2 - \left(\frac{\omega^2 L}{2g} \cos \chi \right)^2}$$

$$H_{\zeta s} = 0$$

Further, the righting lever is rewritten

$$GZ(\phi, t) = GZ_0(\phi) + GZ_w(\phi, t) \quad (21)$$

where $GZ_0(\phi)$ is the righting lever in still water; $GZ_w(\phi, t)$ is the variation of the righting lever in waves. We would calculate $GZ_w(\phi, t)$ for only the effective wave. The effect of the frequency ω and χ is taken into account by Eq.(20). We examined the effective wave concept by comparison with direct stability calculations [15] shown in Figs.5-6. In this study the stability calculation for the effective wave is based on the Froude-Krylov hypothesis without the Smith effect and integrates water pressure up to the actual free surface. [16]

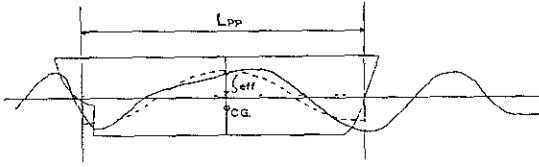


Fig.3 Effective wave concept

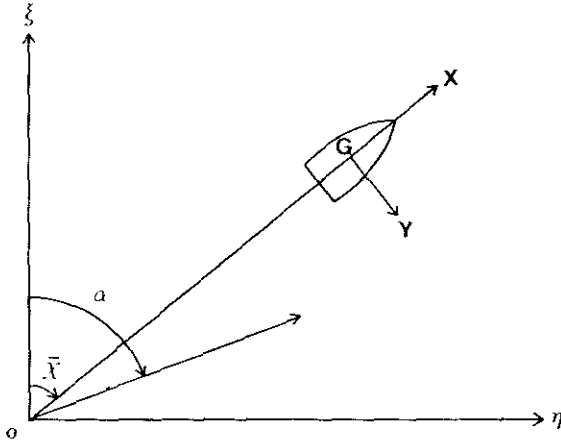
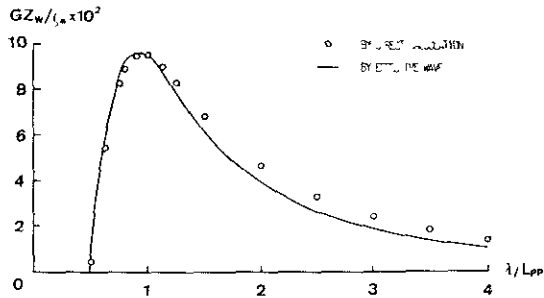
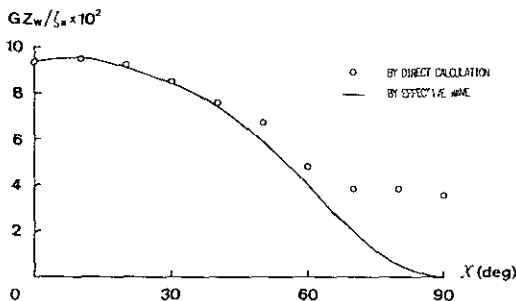


Fig.4 Coordinate systems


 Fig.5 Loss of stability for a Japanese drift netter ($H/L_{pp}=0.05$, $\chi = 0$, $\phi = 30^\circ$, wave crest at C.G.)

 Fig.6 Loss of stability for a Japanese drift netter ($H/L_{pp}=0.0866$, $\lambda/L=1.0$, $\phi = 30^\circ$, wave crest at C.G.)

The restoring moment of a ship decreases when a wave crest moves into the center of gravity. At the same time the velocity of the ship becomes almost a maximum and the relative velocity to the wave phase velocity becomes small. Then the restoring moment of the ship decreases for a prolonged period of time because of frequency modulation due to surge. Though we can express the frequency modulation by an infinite series of trigonometric functions and the Bessel functions [14], this paper uses a simple approximation with a square wave model shown in Fig.7. An interval when the restoring moment decreases, τ_c , is approximated by

$$\tau_c(\chi) = \frac{\pi}{\omega_L - (\omega_L^2/g)(V + \dot{\chi})\cos\chi} \quad (22)$$

where

$$\omega_L = \sqrt{\frac{2\pi g}{L\cos\chi}}$$

and χ is surging velocity.

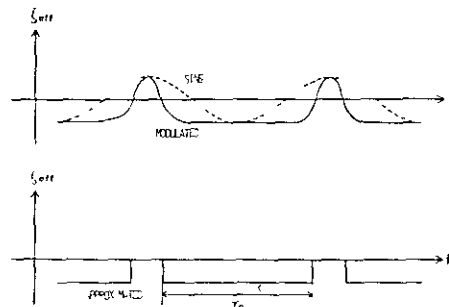


Fig.7 Approximation of Change in the effective wave

The selected bounds between the steady and unsteady motions are the moment when a wave crest comes into the center of gravity, that is, the effective wave becomes a minimum. At the same time the wave exciting roll moment that is independent of a roll angle is almost zero. Therefore, the equation of the roll can be obtained as follows:

$$(I_{44} + A_{44})\ddot{\phi} + B_{44}\dot{\phi} + W G Z(\phi, \zeta_{eff}(t)) = K_A \quad (23)$$

where

$$\zeta_{eff}(t) = \begin{cases} \zeta_{eff}^* & 0 \leq t \leq \tau_c \\ 0 & \tau_c < t \end{cases}$$

and $t=0$ means the bounds. K_A^* , $\dot{\chi}^*$, ϕ^* , $\dot{\phi}^*$ are values of K_A , $\dot{\chi}$, ϕ , $\dot{\phi}$ when $t=0$. These are statistically predicted by a steady random process theory; ϕ^* and $\dot{\phi}^*$ are used for initial conditions of Eq.(23). In addition, for simplicity sake, we use an approximation for the wind moment as follows:

$$K_A^* \doteq F_A (h_A + h_H) \quad (24)$$

Then we would numerically integrate Eq.(23) with the initial conditions of ϕ and $\dot{\phi}$. Drawing separatorics on the phase plane is efficient to show properties of a dynamic system because the number of trajectories is infinite. The separatorics are passing through unstable equilibrium points. [17] This is the same method as one of the authors used for the surf-riding. [18] That is, we start to integrate Eq.(23) from unstable points of equilibrium with $\dot{\phi}=0$. Then we can find a safe domain on the phase plane. All trajectories within the safe domain tend to stable points of equilibrium. All trajectories outside the safe domain tend to capsizing. Numerical examples for $\tau_c \rightarrow \infty$ are shown in Figs. 8-11.

When an amplitude of the effective wave increases, the safe domain shaded on the phase plane becomes smaller. When $\zeta_{eff}/L > 0.08$, the safe domain does not exist and the ship capsizes regardless of initial conditions. Furthermore, the safe domain for $\tau_c < \infty$ is obtained by integrating the equation from the separatorics where $\zeta_{eff} = 0$ for the period τ_c . Therefore, we can obtain the safe domain if $\zeta_{eff}, \dot{x}, \phi$ and $\dot{\phi}$ are given.

PROBABILITY OF CAPSIZING

If the initial conditions of Eq.(23) are selected within the safe domain S , the ship never capsizes when she meets the wave crest. In the meanwhile, the probability density of the initial conditions, that is, $\zeta_{eff}, \dot{x}, \phi$ and $\dot{\phi}$ can be predicted by a steady random process theory. Thus we obtain the probability of capsizing when the ship meets a wave crest, p , by integrating the probability density of the initial conditions on the safe domain as follows:

$$p = 1 - p_e \int_{-\infty}^{\infty} \int_{-\infty}^{\infty} \int \int S(\zeta_{eff}, \dot{x}, \phi, \dot{\phi}) f(\zeta_{eff}, \dot{x}, \phi, \dot{\phi}) d\dot{\phi} d\phi d\dot{x} d\zeta_{eff} \quad (25)$$

where f is the probability density function of \dot{x}, ϕ and $\dot{\phi}$ when the center of gravity meets a minimum of the effective wave. (See Appendix.) In addition, p_e is the probability of a minimum of the effective wave when the ship meets a wave crest.

$$p_e = \sqrt{\frac{m'_4 m_2}{m'_2 m_4}} \quad (26)$$

where

$$m_n = \int_0^{\infty} \int_{-\pi/2-\bar{\chi}}^{\pi/2-\bar{\chi}} \omega_e^n S(\omega, \chi) d\omega d\chi$$

$$m'_n = \int_0^{\infty} \int_{-\pi/2-\bar{\chi}}^{\pi/2-\bar{\chi}} \omega_e^n |H_{\zeta}(\omega, \chi)|^2 S(\omega, \chi) d\omega d\chi$$

Moreover, annual risk of capsizing for a ship can be calculated by making use of both p and the statistics for sea states. [5] Then we will compare the annual risk with the acceptable risk. The results enable us to develop stability criteria and present an operational manual for the master of a ship.

Numerical example

We presents a numerical example of the described procedure. The ship used is a Japanese coastal trawler whose principal particulars are shown in Table 1 and whose body plan and general arrangement are shown in Figs.12-13. Fig.14 shows the probability of capsizing drastically increases when the wind velocity exceeds about 10 m/sec. This increase is due to mainly the increase of the effective wave amplitude. When the wind velocity increases more, the probability of capsizing continues to increase. The heel due to wind plays a significant role for this tendency instead of the effective wave. For simplicity sake, we neglect the effects of the surging motion in this example. This means that τ_c equals infinite. Thus the probability of capsizing for the ship may be somewhat overestimated in this example.

We will continue to calculate the probability of capsizing of ships after submitting this paper. How the ship velocity, the encounter angle, the metacentric height and the ship length affect the capsizing is an urgent problem to be solved. When the encounter angle tends to $\pi/2$, this method may examine the acceptable risk of the IMO weather criterion. Then we may discuss the stability criteria for a ship in quartering seas with the same acceptable risk. Further numerical results will be appeared as soon as possible.

CONCLUSIONS

On the basis of this study the following conclusions can be drawn:

- (1) We examined that the effective wave concept is useful to predict the restoring moment in waves by comparing with direct stability calculations.
- (2) We showed that the safe domain on the phase plane becomes smaller when an amplitude of the effective wave increases.
- (3) We presented a theoretical method to evaluate the probability of capsizing due

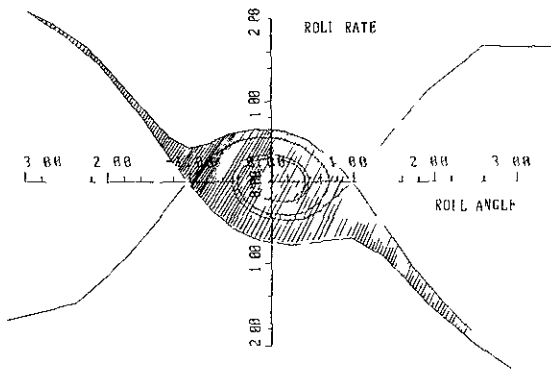


Fig.8 Safe domain for the coastal trawler ($\zeta_{\text{eff}}/L_{\text{PP}}=0.0$, $U_T=20\text{m/sec}$, $\chi=30^\circ$, $F_n=0.3$, $\tau_c=\infty$)

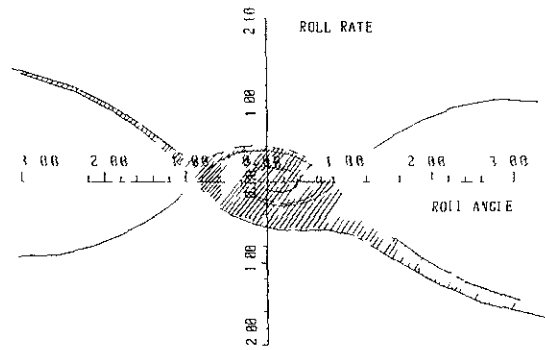


Fig.9 Safe domain for the coastal trawler ($\zeta_{\text{eff}}/L_{\text{PP}}=0.025$, $U_T=20\text{m/sec}$, $\chi=30^\circ$, $F_n=0.3$, $\tau_c=\infty$)

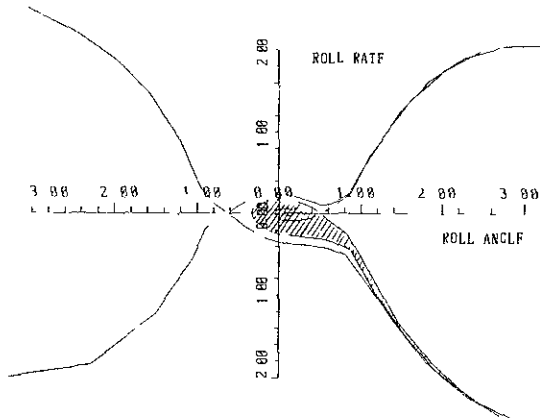


Fig.10 Safe domain for the coastal trawler ($\zeta_{\text{eff}}/L_{\text{PP}}=0.05$, $U_T=20\text{m/sec}$, $\chi=30^\circ$, $F_n=0.3$, $\tau_c=\infty$)

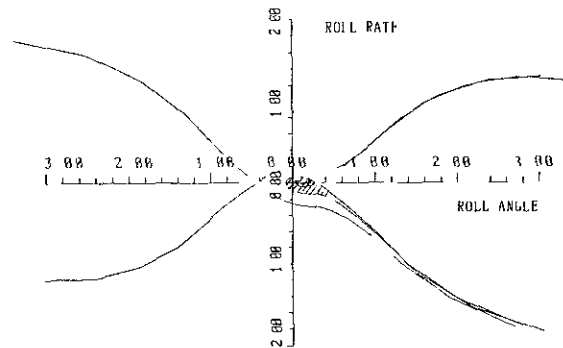


Fig.11 Safe domain for the coastal trawler ($\zeta_{\text{eff}}/L_{\text{PP}}=0.075$, $U_T=20\text{m/sec}$, $\chi=30^\circ$, $F_n=0.3$, $\tau_c=\infty$)

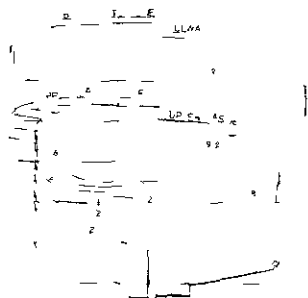


Fig.12 Body plan of the coastal trawler

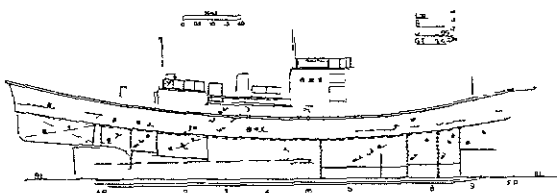


Fig.13 General arrangement of the coastal trawler

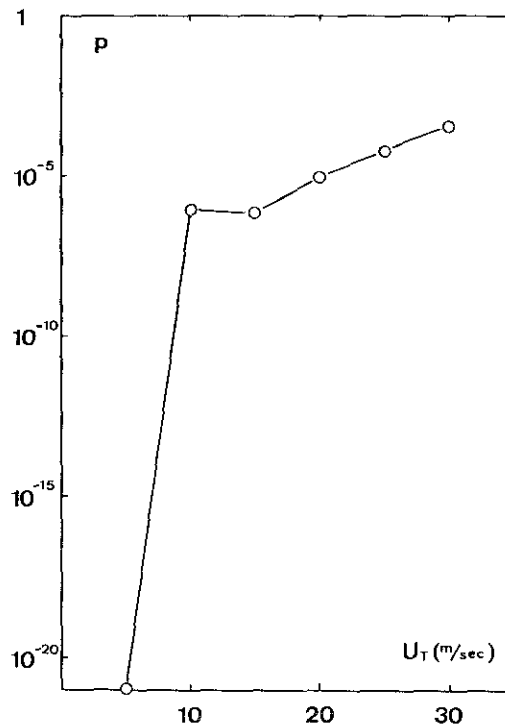


Fig.14 Probability of Capsizing for the coastal trawler when the ship meets a wave crest ($\chi=30^\circ$, $F_n=0.3$, short crested wave)

to pure loss of stability for a ship running in both short crested quartering waves and fluctuating wind.

(4) The calculated results show that the probability of capsizing for a coastal trawler drastically increases when the wind velocity exceeds about 10m/sec.

(5) We should continue to calculate the probability of capsizing under various conditions by the present method.

We would like to thank Prof. M. Hamamoto of Osaka University for his effective advice. We also acknowledge informative discussions with members of RR24 panel. The computations were carried out by AGOS 930 at the Computing Center for Research in Agriculture, Forestry and Fisheries.

REFERENCES

- 1) Plaza, F. & Petrov, A. A., Further IMO Activities in the Development of International Requirements for the Stability of Ships, Proc. 3rd Int. Conf. Stab., Gdańsk, Vol.2, 1986, p7.
- 2) Oakley, O. H., Paulling, J. R. & Wood, P. D., Ship Motions and Capsizing in Astern Seas, Proc. 10th Symp. Nav. Hydro., Cambridge, 1974, p297.
- 3) Kan, M., Saruta, T., Taguchi, H. & Yasuno, M., Capsizing of a Ship in Quartering Seas (Part 1), J. Soc. Nav. Arch. Japan, Vol.167, 1990, p81, (in Japanese).
- 4) Schuëller, G. I., Einführung in die Sicherheit und Zuverlässigkeit von Tragwerken, Wilhelm Ernst & Sohn, 1981.
- 5) Caldwell, J.B. & Yang, Y. S., Risk and Reliability Analysis Applied to Ship Capsize, Proc. Int. Conf. Safeship Project, London, 1986.
- 6) Grim, O., Beitrag zu dem Problem der Sicherheit des Schiffes im Seegang, Schiff und Hafen, Heft 6, 1961, p490.
- 7) Krappinger, O., Über Kenterkriterion, Schiffstechnik, Bd 17, Heft 88, 1970, p145.
- 8) Umeda, N. & Yamakoshi, Y., Experimental Study on Pure Loss of Stability in Regular and Irregular Following Seas, Proc. 3rd Int. Conf. Stab., Gdańsk, Vol.1, 1986, p93.
- 9) ITTC, Report of Seakeeping Committee, 15th ITTC, 1978.
- 10) Yamakoshi, Y., Takaishi, Y., Kan, M., Yoshino, T. & Tsuchiya, T., Model Experiments on Capsize of Fishing Boats in Waves, Proc. 2nd Int. Conf. Stab., Tokyo, 1982, p199.
- 11) Blocki, W., Ship Safety in Connection with Parametric Resonance of the Roll, Int. Ship Prog., 27-306, 1980, p36.
- 12) Lee, C. M. & Kim, K.H., Prediction of Motion of Ships in Damaged Condition in Waves, Proc. 2nd Int. Conf. Stab., Tokyo, 1982, p287.
- 13) Watanabe, Y., Some Contributions to the theory of Rolling, Tran. R. Int. Nav. Arch., 1938, p408.
- 14) Umeda, N. & Kohyama, T., Surf-riding of a Ship in Regular Seas, J. Kansai Soc. Nav. Arch. Japan, Vol.213, 1990, p63, (in Japanese).

15) Hamamoto, M., Transverse Stability of Ships in a Quartering Sea, Proc. 3rd Int. Conf. Stab., Gdańsk, Vol.1, 1986, p7.

16) Hamamoto, M. & Nomoto, K., Transverse Stability of Ships in a Following Sea, Proc. 2nd Int. Conf. Stab., Tokyo, 1982, p215.

17) Sato, C., Non-linear Vibration, Asakura Books, Tokyo, 1970, p24, (in Japanese).

18) Umeda, N., Probabilistic Study on Surf-riding of a Ship in Irregular Following Seas, Proc. 4th Int. Conf. Stab., Naples, 1990, (to be appeared).

19) Price, W. G. & Bishop, R. E. D., Probabilistic Theory of Ship Dynamics, Chapman and Hall, 1974.

APPENDIX

The minima of the effective wave ζ_{eff} are defined as the points which satisfy the conditions $\dot{\zeta}_{\text{eff}}=0$ and $\ddot{\zeta}_{\text{eff}}>0$. Hence a combined probability function of the minima of the effective wave, roll, roll rate and surge velocity is described as [19]

$$f(\zeta_{\text{eff}}, \phi, \dot{\phi}, \dot{X}) = \int_0^\infty \ddot{\zeta}_{\text{eff}} g(\zeta_{\text{eff}}, 0, \ddot{\zeta}_{\text{eff}}, \phi, \dot{\phi}, \dot{X}) d\ddot{\zeta}_{\text{eff}} / \int_{-\infty}^\infty d\zeta_{\text{eff}} \int_{-\infty}^\infty d\dot{X} \int_{-\infty}^\infty d\phi \int_{-\infty}^\infty d\dot{\phi} \int_0^\infty \ddot{\zeta}_{\text{eff}} g(\zeta_{\text{eff}}, 0, \ddot{\zeta}_{\text{eff}}, \phi, \dot{\phi}, \dot{X}) d\ddot{\zeta}_{\text{eff}} \quad (27)$$

Here g is a combined probability function of $x_1 (= \zeta_{\text{eff}})$, $x_2 (= \dot{\zeta}_{\text{eff}})$, $x_3 (= \ddot{\zeta}_{\text{eff}})$, $x_4 (= \phi)$, $x_5 (= \dot{\phi})$ and $x_6 (= \dot{X})$ and given by

$$g(x_1, x_2, x_3, x_4, x_5, x_6) = \frac{1}{(2\pi)^3 |\Delta|^{1/2}} \exp \left[\frac{-1}{2|\Delta|} \sum_{j=1}^6 \sum_{k=1}^6 |\Delta|_{jk} (x_j - E[x_j])(x_k - E[x_k]) \right] \quad (28)$$

Because, we assumed that the effective wave, the roll and the surge are Gaussian Process. Further, Δ denotes a covariance matrix whose element is C_{jk} ($j, k \leq 6$). $|\Delta|$ denotes the determinant of Δ ; $|\Delta|_{jk}$ denotes the determinant of a cofactor of Δ .

We find the variance or covariance C_{jk} as follows:

$$C_{jk} = \int_0^\infty \left[\int_{-\frac{\pi}{2}}^{\frac{\pi}{2}} |H_j(\omega, \chi)| |H_k(\omega, \chi)| S(\omega, \chi + \bar{\chi}) \cos\{\varepsilon_k(\omega, \chi) - \varepsilon_j(\omega, \chi)\} d\chi \right. \\ \left. + \delta_{jk} \int_0^\infty |H_j^{\text{WIND}}(\omega)|^2 S_{uu}(\omega) d\omega \right] \quad (29)$$

where

$$|H_j(\omega, \chi)| = \sqrt{H_{jc}^2 + H_{js}^2}$$

$$\varepsilon_j(\omega, \chi) = -\tan^{-1}(H_{js}/H_{jc})$$

$$H_j^{WIND}(\omega) = \sqrt{(H_{jc}^{WIND})^2 + (H_{js}^{WIND})^2}$$

and δ_{jl} is Kronecker's delta. Here we assume that the wind is uncorrelated with waves.

Neglecting higher order effects due to wind and waves, we find the mean $E[x_j]$ as follows:

$$\begin{aligned} E[x_j] &= 0 & (j = 4) \\ &= -\phi_0 & (j = 4) \end{aligned} \quad (30)$$

Substituting Eq.(28) into Eq.(27) and integrating analytically, we can obtain f as follows:

$$\begin{aligned} f(\zeta_{eff}, \phi, \dot{\phi}, \dot{x}) &= 2\pi \sqrt{\frac{m^2}{m^4}} \frac{1}{(2\pi)^3 |\Delta|^{1/2}} \frac{1}{2\alpha''} \left(1 - \frac{\beta''}{2} \sqrt{\frac{\pi}{\alpha''}} \exp\left(\frac{\beta''^2}{4\alpha''}\right) \right) \\ \times \exp \left[-\frac{|\Delta|_{11}}{2|\Delta|} \zeta_{eff}^2 - \frac{1}{|\Delta|} \left(|\Delta|_{14}(\dot{\phi} + \phi_0) + |\Delta|_{15}\dot{\phi} + |\Delta|_{16}\dot{x} \right) \zeta_{eff} \right. \\ &\quad \left. - \frac{1}{2|\Delta|} \left(|\Delta|_{44}\dot{\phi}^2 + |\Delta|_{55}\dot{\phi}^2 + |\Delta|_{66}\dot{x}^2 \right) \right. \\ &\quad \left. - \frac{1}{|\Delta|} \left(|\Delta|_{45}\dot{\phi}\dot{\phi} + |\Delta|_{46}\dot{\phi}\dot{x} + |\Delta|_{56}\dot{\phi}\dot{x} \right) \right] \end{aligned} \quad (31)$$

where

$$\alpha'' = \frac{|\Delta|_{33}}{2|\Delta|}$$

$$\beta'' = \frac{1}{|\Delta|} \left\{ |\Delta|_{13}\zeta_{eff} + |\Delta|_{34}(\phi + \phi_0) + |\Delta|_{35}\dot{\phi} + |\Delta|_{36}\dot{x} \right\}$$

Table 1 Principal particulars of the coastal trawler

Length B.P.	L_{PP} [m]	14.40
Breadth	B [m]	3.05
Depth	D [m]	1.38
Draft	d [m]	0.875
Trim	τ [m]	1.05
Displacement volume	V [m ³]	27.56
C.G. from midship	l_{cb} [m]	1.28
Metacentric height	GM [m]	0.152
Rolling period	T_R [sec]	10.2

Naoya Umeda¹⁾

ABSTRACT

This study deals with surf-riding of a ship to develop stability criteria against broaching-to. The author discusses limits of the surf-riding in regular following seas by using separatorices on the phase plane of the longitudinal motion. Furthermore, a theoretical method is presented for calculating probabilities of surf-riding for a ship self-propelled with constant revolution in irregular seas. The results indicate that the probability for a type of the surf-riding, that never occurs in regular seas, is not so small in irregular seas.

INTRODUCTION

Stability criteria for ships in following seas are required to prevent capsizing of small ships like fishing boats. The stability criteria should consider three modes of capsizing, that is, broaching-to, low cycle resonance and pure loss of stability. In addition, like a weather criterion for ships in beam seas, practical criteria are desired to take irregularity of actual waves into account. However, we have very few studies on these capsizing modes in irregular following seas, especially for the broaching-to [1][2].

A ship in waves usually runs with periodic surging motions. However, in heavy following seas she may be accelerated and run with a wave velocity [3], which is called as surf-riding and can be regarded as a kind of non-linear phenomenon. Under the surf-riding condition the ship may suddenly yaw her desired course despite application of maximum opposite rudder. This is known as broaching-to and possibly causes even a capsize. Hence, the surf-riding is a prerequisite for the broaching-to to happen.

Since the surf-riding is completely non-linear, a phase plane of the dynamic system is an appropriate tool to analyze the surf-riding [4]. Following a pioneer work in USSR [5], the present work analyzes the surf-riding for a ship in regular seas by using the phase plane.

We would further study the surf-riding for a ship in irregular following seas to develop practical stability criteria. Recently Grim studied the surf-riding for a ship in irregular following seas by using a deterministic approach [2]. However, a probabilistic approach is more suitable to develop the criteria because we can only forecast ocean waves as random process.

Therefore, this study presents a method to predict probability of the surf-riding for a ship in irregular following seas.

SURF-RIDING IN REGULAR SEAS

Equation of motion

An overview of the coordinate systems for a ship running in regular following seas is shown in Fig.1. The inertial system, defined by $O\xi\zeta$ translates with a wave trough at the wave phase velocity C . The local system Gxz is fixed in the ship with the origin G being located at the center of gravity. ξ_G is a horizontal distance between O and G .

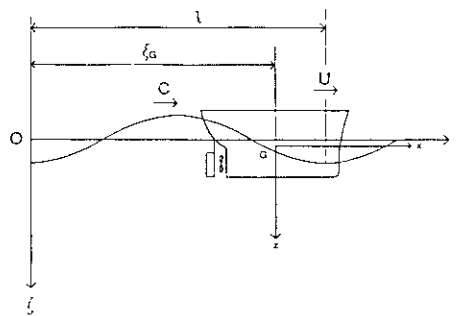


Fig. 1 Coordinate systems

Since the ship is slender, the coupling effect on the surging motion is negligible. Thus we can use an one-freedom equation of the surging motion as follows:

$$m\ddot{\xi}_G = F_X - R + T + VM \quad (1)$$

Here m is the mass of the ship, F_X is the wave force acting on the ship in x direction, R is the resistance of the ship in still water, T is the thrust due to the propeller and VM is inertia force due to the virtual mass of the ship.

1) National Research Institute of Fisheries Engineering; Hasaki, Kashima, Ibaraki, JAPAN

As to the wave force, the Froude-Krylov hypothesis is effective. Under the surf-riding condition where the ship velocity U equals to the wave velocity c , this Froude-Krylov force can be regarded as the first order approximation for an exact potential theory and be explained as the interaction between ocean waves and ship generating waves [6].

$$F_X = -\rho g \zeta_w k \int_{AE}^{FE} e^{-kd(x)} S(x) \sin(k\xi_G + x) dx \\ = -\rho g \zeta_w k \sqrt{F_c^2 + F_s^2} \sin(k\xi_G + \epsilon) \quad (2)$$

where

$$F_c = \int_{AE}^{FE} e^{-kd(x)} S(x) \cos kx dx \\ F_s = \int_{AE}^{FE} e^{-kd(x)} S(x) \sin kx dx \\ \epsilon = \tan^{-1}(F_s/F_c)$$

Here $S(x)$ is local sectional area of the ship, $d(x)$ is its local depth, AE is an aft end of a submerged hull of the ship and FE is a fore end of that. ξ_w , λ and k are wave amplitude, wave length and wave number, respectively. The ship resistance, the thrust and the virtual mass may be estimated by experimental results in still water as the first order approximation.

$$R = R(c + \dot{\xi}_G) \quad (3)$$

$$T = (1 - t_p) \rho n^2 D_p^4 K_T [(c + \dot{\xi}_G)(1 - w)/n D_p] \quad (4)$$

$$VM = -m_x \ddot{\xi}_G \quad (5)$$

Here t_p is a thrust deduction fraction, w is a wake fraction, n is a revolution number of the propeller, D_p is a diameter of the propeller, K_T is a thrust coefficient, m_x is a virtual mass of the ship. The wave phase velocity c is calculated by the dispersion relation as follows:

$$c^2 = g/k (1 + k^2 \zeta_w^2) \quad (6)$$

Substituting Eqs.(2)-(5) for Eq.(1), one can obtain the equation of motion as follows:

$$m \ddot{\xi}_G = -\rho g \zeta_w k \sqrt{F_c^2 + F_s^2} \sin(k\xi_G + \epsilon) \\ - R(\dot{\xi}_G + c) + (1 - t_p) \rho n^2 D_p^4 K_T [(1 - w)(\dot{\xi}_G + c)/(n D_p)] - m_x \ddot{\xi}_G \quad (7)$$

Since $\dot{\xi}_G$ is the relative velocity of the ship to the wave, $\dot{\xi}_G$ equals to zero under the surf-riding condition. Defining $\dot{\xi}_0$ as velocity of the ship running steady in still water, an equation of the equilibrium is given by

$$0 = -R(\dot{\xi}_0 + c) + (1 - t_p) \rho n^2 D_p^4 K_T [(1 - w)(\dot{\xi}_0 + c)/(n D_p)] \quad (8)$$

Subtracting Eq.(8) from Eq.(7) and expanding R and K_T near c , one can finally obtain the following equation.

$$\ddot{\xi}_G + \mu \dot{\xi}_G + f \sin(k\xi_G + \epsilon) = b \quad (9)$$

where

$$\mu = \frac{1}{m + m_x} \left[\frac{\partial R}{\partial V} - (1 - t_p) \rho n^2 D_p^4 \frac{\partial K_T}{\partial J} \frac{1 - w}{n D_p} \right]_{V=c} \\ f = \frac{\rho g \zeta_w k}{m + m_x} \sqrt{F_c^2 + F_s^2} \\ b = \frac{1}{m + m_x} \left[\frac{\partial R}{\partial V} - (1 - t_p) \rho n^2 D_p^4 \frac{\partial K_T}{\partial J} \frac{1 - w}{n D_p} \right]_{V=c} \dot{\xi}_0$$

Phase plane

Since an equation of the motion like Eq.(9) is non-linear, we cannot easily find an analytical solution of the equation. Therefore, we numerically integrate Eq.(7) and present the results as phase trajectories. The ordinate of the phase plane is instantaneous velocity of the ship, U/c , and the abscissa is relative position of the ship to wave, ξ_G/λ . Drawing

separatrices is efficient to show properties of a dynamic system because the number of trajectories is infinite. The separatrices are trajectories passing through unstable equilibrium points, namely, saddle points or cusps.

The dynamic system described by Eq.(7) may have two points for equilibrium in one cycle; one is stable and the other is unstable. Near the stable point trajectories are converged to the point. On the contrary, trajectories close to the unstable point are dispersed. Since separatrices pass through the unstable point, it is difficult to determine them. To bypass this difficulty, we start to integrate the differential equation from points, those are at short distance apart from the unstable point in the eigen direction, in place of the unstable point itself. We must integrate it usually four times per unstable point, because an unstable point has usually two eigen directions. [14]

A ship used for this study is a Japanese offshore trawler whose lines are shown in Fig.2 and principal particulars are shown in Table 1.

The phase trajectories are presented in Figs.3-6 for the regular waves whose length equals to the ship length and steepness is 0.1. The revolution number of the propeller is constant during simulation in each figure.

The phase trajectories for $F_n = 0.2846$ are shown in Fig.3. Here the Froude number F_n represents the revolution number of the propeller that causes the ship to run in still water with its Froude number. We can

find a periodic attractor that means surging motion with an encounter frequency. All trajectories are gathered in the attractor. That is, the ship is successively overtaken by waves and does not suffer the surf-riding.

When the propeller thrust increases, the equilibrium of longitudinal force may exist. In Figs.4-6 the trajectories passing through only two unstable points are shown for simplicity sake. In Figs.4-5 all trajectories within shaded zone converge to the stable equilibrium points. All trajectories outside the zone are gathered in the periodic attractor. That is to say, while the ship suffers the surf-riding under certain initial conditions, the ship may be successively overtaken by waves under other initial conditions. We can conclude that the ship, whose initial speed is lower than the periodic attractor, with constant revolution in regular seas does never suffer the surf-riding.

In Fig.6, when the propeller thrust increases more, the trajectory from the unstable equilibrium point to the left is captured in the stable equilibrium point and the periodic attractor does not exist. Thus all trajectories in the phase plane converge to the stable equilibrium points. That is to say, the ship suffers the surf-riding under any initial conditions.

Though we found three different patterns for the longitudinal motion of a ship in regular following seas, this fact had already been pointed out by a Russian paper and the present paper confirmed its results.

Results and discussion

The critical condition for "the surf-riding under certain initial conditions" is whether equilibrium of the longitudinal force exists or not. Further, the critical condition for "the surf-riding under any initial conditions" is whether the trajectory from the unstable point to the left is captured in the stable equilibrium point. The latter critical condition can be solved as a two-point boundary value problem by using an iterative method. Grim[7] proposed that limits of the surf-riding are characterized by the fact that after exceeding the unstable position of equilibrium with relative velocity zero and after travelling through the entire following wave train, the ship arrives once again in the new unstable position of equilibrium with the velocity zero. We can see that his proposal is identical to the present explanation for the latter condition.

Figs.7-8 show critical velocity of the ship for the surf-riding in regular waves. Besides results calculated by the described method, experimental results for the same ship by Kan et al.[8] were plotted. Since Kan's model with constant revolution of its propeller was accelerated from almost $U=0$, the experimental critical velocity corresponds to the critical velocity for "the surf-riding under any initial conditions." Thus we concluded that agreement between the experiments and the theory is fairly good for the critical condition of "the surf-riding under any initial conditions."



Fig. 2 Lines of the trawler

Table 1 Principal Particulars of the trawler

		ship	model
length	L_{pp} [m]	30.58	2.548
breadth	B [m]	7.38	0.615
fore draft	d_f [m]	1.62	0.135
mean draft	d_m [m]	2.62	0.218
aft draft	d_a [m]	3.62	0.302
center of buoyancy	LCB [m]	2.71	0.226
block coefficient	C_b	0.779	0.779
wetted surface area	S [m ²]	334.1	2.32
maximum velocity	U_{max} [kt]	12.0	
propeller diameter	D [m]	2.30	0.186
rudder area ratio	A_r/L_d	1/27.3	1/27.3

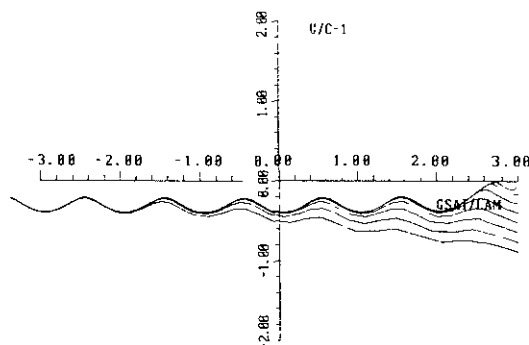


Fig.3 Phase trajectories
($H/\lambda=0.1$, $\lambda/L=1.0$, $F_n=0.2846$)

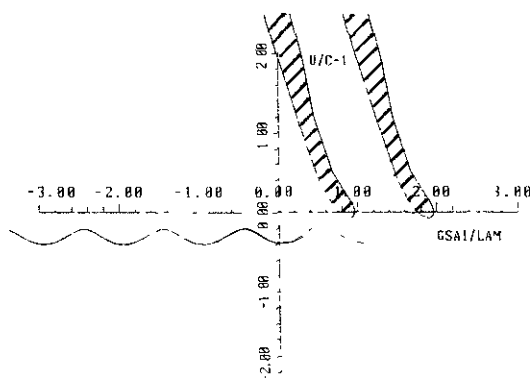


Fig.4 Phase trajectories
($H/\lambda=0.1$, $\lambda/L=1.0$, $F_n=0.2866$)

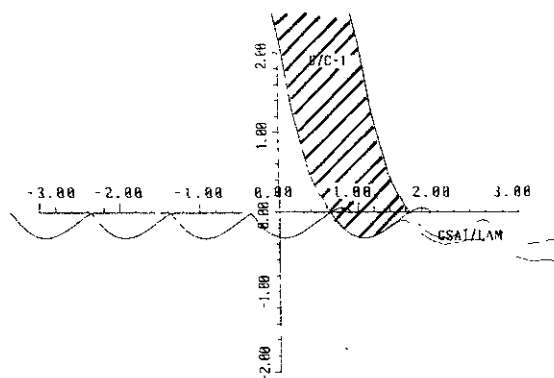


Fig.5 Phase trajectories
($H/\lambda=0.1$, $\lambda/L=1.0$, $F_n=0.3397$)

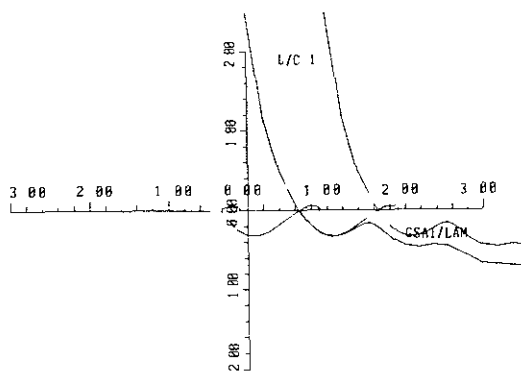


Fig. 6 Phase trajectories
($H/\lambda=0.1$, $\lambda/L=1.0$, $F_n=0.3416$)

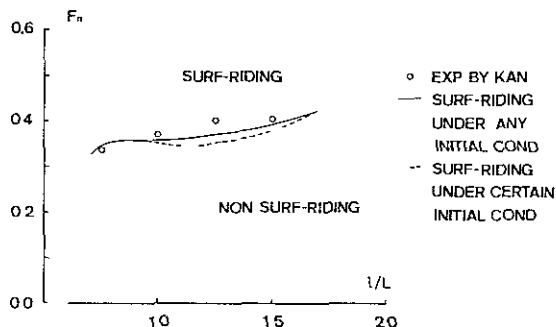


Fig. 7 Critical velocity for surf-riding
($H/\lambda=1/20$)

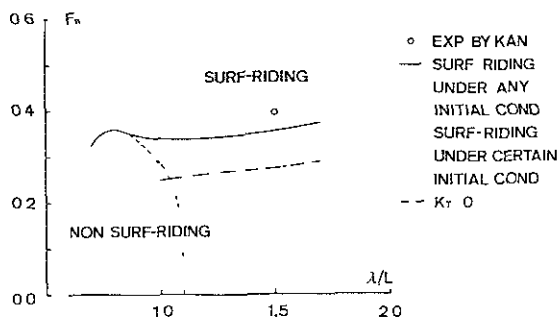


Fig. 8 Critical velocity for surf-riding
($H/\lambda=1/10$)

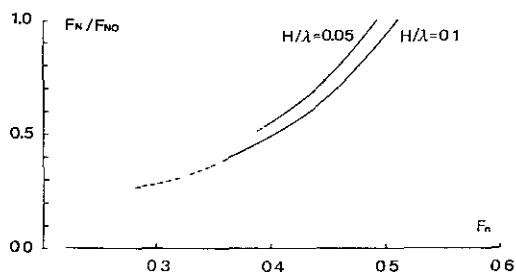


Fig. 9 Normal force of rudder under surf-riding condition
($\lambda/L=1.5$; F_{n0} means normal force of rudder in still water for the same Froude number)

Under the surf-riding condition the propeller thrust decreases because the ship is accelerated by a wave and the advance coefficient increases. The reduction of the thrust reduces rudder force. Because, the rudder force F_N is proportional to a square of the inflow velocity, u_R ; u_R is estimated as follows: [9]

$$\left(\frac{u_R}{u_P}\right)^2 = \epsilon_R^2 \left(1 + K_R \frac{8K_T}{\pi J^2}\right) \quad (10)$$

Here u_P is inflow velocity at a propeller.

Experimental constants were determined by steering experiments; $\epsilon_R=0.885$ and $K_R=0.617$. Fig. 9 shows ratio of the rudder normal force under the surf-riding condition to that in still water for the same Froude number. Calculated results indicate that the rudder force drastically decreases under surf-riding condition. This fact can cause the broaching-to.

A ship self-propelled with a constant revolution in regular waves suffers the surf-riding when she exceeds the critical velocity of "the surf-riding under any initial conditions." Then, if a master of the ship reduces the revolution of the propeller to almost the critical condition for "the surf-riding under certain initial conditions," the ship can escape from the surf-riding. In Fig. 8 where $H/\lambda=1/20$, it is easy to escape from the surf-riding by reducing the propeller revolution because a difference between the two critical conditions is small. However, in Fig. 9 where $H/\lambda=1/10$, it is impossible for the ship once captured by a wave to escape from the surf-riding by only reducing the propeller revolution because even the propeller revolution zero is satisfied with the condition for "the surf-riding under certain initial conditions." Moreover, since the reduction of propeller revolution reduces the rudder force, the ship attempting to escape from the surf-riding may tend to broach.

SURF-RIDING IN IRREGULAR SEAS

Probabilistic theory

We can obtain the critical wave height for the surf-riding in the regular waves by using the described method. The critical wave height for "the surf-riding under any initial conditions" is H_c^* ; that for "the surf-riding under certain initial conditions" is H_N^* . In this chapter the probabilistic theory for the surf-riding in irregular seas is formulated.

If sea surface elevation is assumed to have a Gaussian distribution, it is represented as follows:

$$\zeta(t) = \sum_{n=1}^{\infty} a_n \cos(2\pi f_n t + \epsilon_n) \quad (11)$$

When the spectrum of the elevation is narrow-banded, we can rewrite Eq.(11) as follows:

$$\zeta(t) = R(t) \cos[2\pi \bar{f}_n t + \phi(t)] \quad (12)$$

where \bar{f} denotes the carrier frequency:

$$f = \frac{\bar{\omega}}{2\pi} = \frac{m_1}{m_0} \quad (13)$$

and m_n denotes the n th moment of the spectral density $S(f)$:

$$m_n = \int_0^\infty f^n S(f) df \quad (14)$$

We shall adopt the narrow-banded hypothesis, that is,

$$v^2 \ll 1 \quad \ddot{R}^2 \ll 1 \quad \dot{\phi}^2 \ll 1 \quad (15)$$

where

$$v = \frac{1}{\bar{\omega}} \left(\frac{\mu_2}{m_0} \right)^{1/2} \quad (16)$$

$$\hat{\mu}_2 = (2\pi)^2 \mu_2 \quad (17)$$

$$\mu_2 = \int_0^\infty (f - \bar{f})^2 S(f) df = m_2 - \frac{m_1^2}{m_0} \quad (18)$$

Thus a random process described by Eq.(12) mainly depends on the random variables, that is, R , \dot{R} , ϕ and $\dot{\phi}$. A combined probability density p is obtained by [9]

$$p(R, \phi, \dot{R}, \dot{\phi}) = \frac{R^2}{4\pi^2 m_0 \mu_2} \exp\left[-\frac{R^2}{2m_0}\right] \exp\left[-\frac{\dot{R}^2 + R^2 \dot{\phi}^2}{2\mu_2}\right] \quad (19)$$

The probability for "the surf-riding under any initial conditions" corresponds to probability for a ship to meet a peak-to-peak wave whose height H and length λ are satisfied with the condition for the surf-riding in regular waves. Since Longuet-Higgins [11] presented the joint distribution of wave height and periods and confirmed that his theory can express the general feature of the observed data, the probability for surf-riding can be estimated by making use of his approach. Under the assumption $v \ll 1$, the local wave period T can be approximated by [11]

$$T \approx 2\pi / (\bar{\omega} + \dot{\phi}) \quad (20)$$

Applying the dispersion relation of water waves, we find,

$$\lambda = \frac{gT^2}{2\pi} = \frac{2\pi g}{(\bar{\omega} + \dot{\phi})^2} \quad (21)$$

Under the assumption $v \ll 1$, the local wave height H can be approximated by

$$H = 2R \quad (22)$$

Thus we represent R and ϕ by H and λ .

$$R = H^*/2 \quad \dot{\phi} = -\bar{\omega} + \sqrt{\frac{2\pi g}{\lambda^* L}} \quad (23)$$

where

$$\lambda^* = \lambda/L \quad \text{and} \quad H^* = H/L \quad (24)$$

Then substituting Eq.(23) for Eq.(19) and integrating ϕ out, we can obtain

$$p(H^*, \lambda^*, \dot{R}) = \frac{\sqrt{g} T^{5/2}}{16\sqrt{2} m_0 \mu_2} H^{*2} \lambda^{*3/2} \exp\left[-\frac{\dot{R}^2}{2\mu_2}\right] \exp\left[-\frac{L^2 H^{*2}}{8} \left\{ \frac{1}{m_0} + \frac{1}{\mu_2} \left(-\bar{\omega} + \sqrt{\frac{2\pi g}{\lambda^* L}} \right)^2 \right\}\right] \quad (25)$$

The probability for "the surf-riding under any initial conditions" when the ship meets the local wave whose length is λ^* , $p_1(\lambda^*)$, is given by

$$p_1(\lambda^*) = \frac{\int_{-\infty}^{\infty} \int_{-\infty}^{\infty} p(H^*, \lambda^*, \dot{R}) dH^* d\dot{R}}{\int_{-\infty}^{\infty} \int_{-\infty}^{\infty} p(H^*, \lambda^*, \dot{R}) dH^* d\dot{R}} = \frac{1}{\tilde{p}(\lambda^*)} \int_{-\infty}^{\infty} H^{*2} \exp\left[-\frac{\dot{R}^2}{2\mu_2}\right] d\dot{R} \left\{ \frac{1}{m_0} + \frac{1}{\mu_2} \left(-\bar{\omega} + \sqrt{\frac{2\pi g}{\lambda^* L}} \right)^2 \right\} \quad (26)$$

where

$$\tilde{p}(\lambda^*) = \frac{\sqrt{g} T^{5/2}}{16\sqrt{2}} \left\{ \frac{1}{m_0} + \frac{1}{\mu_2} \left(-\bar{\omega} + \sqrt{\frac{2\pi g}{\lambda^* L}} \right)^2 \right\} \quad (27)$$

Next, to estimate the probability for "the surf-riding under certain initial conditions", we must consider not only the peak-to-peak wave that the ship instantaneously meets but also the preceding motion of the ship. Since the preceding surging motion of the ship for the surf-riding is non-linear, we cannot use a linear theory to predict the surge motion. In the meanwhile, the non-linear surge motion rapidly converges to the forced oscillation, shown in Fig.3. Thus we consider the preceding peak-to-peak wave cycle in place of the preceding motion itself.

R and ϕ between the peak-to-peak wave that ship meets and the preceding peak-to-peak wave can be regarded as constant because \ddot{R} , $\ddot{\phi} \ll 1$. This means that the wave length and the changing rate of wave height are approximately constant between the two peak-to-peak waves. Therefore we can say that "the surf-riding under certain initial conditions" occurs when the phase trajectory of the preceding motion intersects the surf-riding zone on the phase plane.

When the surf-riding zone extends below the self-propulsion velocity in still water, $U_0/c-1$, and the wave height of the preceding wave is less than a certain value, shown in Fig.10, the surf-riding occurs. The critical height of the preceding wave is denoted by H_{NP}^* . When the surf-riding zone does not extend below $U_0/c-1$, the surf-riding does not occur regardless of the wave height of the preceding wave. For form's sake, we denote that $H_{NP}^* < 0$. Though the lower end of the surf-riding zone generally differs from the minimum of the surging motion in phase, the difference between the two becomes zero when H_{NP}^* tends to H_c^* . (See Figs. 4-5.)

We can relate R with the preceding wave height, H_P^* and the height of the wave that the ship meets, H^* , as follows :

$$H^* - H_P^* = \frac{2\dot{R}}{L\bar{f}} \quad (28)$$

Thus, the condition for "the surf-riding under certain initial conditions" is given by

$$\dot{R} - \dot{R}_{min}(H^*) \quad (29)$$

$$\dot{R}_{min}(H^*) = \frac{\{H^* - H_{NP}^*(H^*)\}L\bar{f}}{2} \quad \begin{matrix} H_{NP}^* \geq 0 \\ H_{NP}^* < 0 \end{matrix} \quad (30)$$

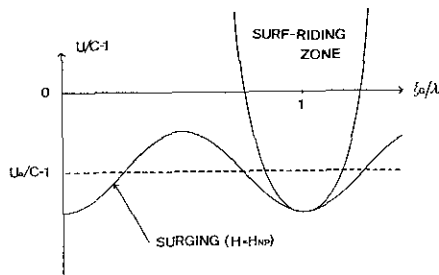


Fig.10 Explanatory sketch for the relation between surf-riding zone and surging trajectories ($H_{NP}^* \geq 0$)

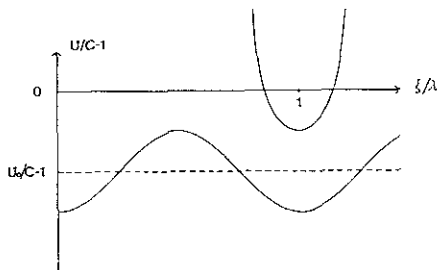


Fig.11 Explanatory sketch for the relation between surf-riding zone and surging trajectories ($H_{NP}^* < 0$)

Therefore, the probability for "the surf-riding under certain initial conditions" when the ship meets the local wave whose length is λ^* , $p_2(\lambda^*)$, is given by

$$p_2(\lambda^*) = \frac{\int_{H_N^*}^{H_c^*} \int_{\dot{R}_{min}(H^*)}^{\dot{R}} p(H^*, \lambda^*, \dot{R}) d\dot{R} dH^*}{\int_0^\infty \int_{-\infty}^\infty p(H^*, \lambda^*, \dot{R}) d\dot{R} dH^*} \\ = \frac{1}{\sqrt{\pi} \tilde{p}(\lambda^*)} \int_{H_N^*}^{H_c^*} \text{Erfc} \left\{ \frac{\dot{R}_{min}(H^*)}{\sqrt{2} \tilde{\mu}_2} \right\} \\ \times H^{*2} \exp \left[-\frac{L^2 H^{*2} \lambda^{*2}}{8} \left\{ \frac{1}{m_0} + \frac{1}{\tilde{\mu}_2} \right. \right. \\ \left. \left. + \left(-\tilde{\omega} \tau \sqrt{\frac{2\pi g}{\lambda^* L}} \right)^2 \right\} \right] dH^* \quad (31)$$

In the meanwhile, we find the probability density to meet the local wave whose length is λ^* as follows: [11]

$$p_w(\lambda^*) = \frac{\int_{-\infty}^\infty \int_0^\infty p(H^*, \lambda^*, \dot{R}) dH^* d\dot{R}}{\int_{-\infty}^\infty \int_0^\infty \int_0^\infty p(H^*, \lambda^*, \dot{R}) d\lambda^* dH^* d\dot{R}} \\ = \frac{\sqrt{g} L^{\frac{5}{2}}}{8\sqrt{\mu_2} m_0} \left(1 + \frac{1}{\sqrt{1+\nu^2}} \right)^{-1} \lambda^{*- \frac{5}{2}} \tilde{p}(\lambda^*) \quad (32)$$

Finally, the probability for the surf-riding when the ship meets a certain local wave, p , is given by

$$P = \int_{\lambda_{min}^*}^{\lambda_{max}^*} p_w(\lambda^*) \{p_1(\lambda^*) + p_2(\lambda^*)\} d\lambda^* \quad (33)$$

Here λ_{max}^* and λ_{min}^* can be determined in the light of the broaching-to.

Results and discussion

The probability for the surf-riding of the trawler is calculated by the formulae above. The revolution number of the propeller is maximum in service and can propel the ship in still water with 12 knots ($Fn=0.35$). The irregular wave is related with the Beaufort scale and its spectrum was defined by the ITTC (1978) spectrum. [15]

Fig.12 shows the conditional probability of the surf-riding when the ship meets the local wave whose length is $\lambda^* = \lambda/L$. We can find that the conditional probability for "the surf-riding under certain initial conditions", p_2 , is comparable with the conditional probability for "the surf-riding under any initial conditions", p_1 , though "the surf-riding under certain initial conditions" does not occur for a ship self-propelled in regular seas. It is the reason why we should consider the surf-riding in irregular seas.

Fig.13 shows the probability of the surf-riding for the Beaufort scale. The range of wave length used for the calculation is 1.0-1.75 because of the previous experiments for broaching-to. [12] The present theory can consider the effect of the band parameter ν besides the significant wave height and the mean wave

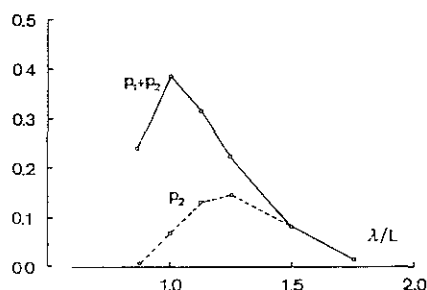


Fig.12 Conditional probability of surf-riding
(Beaufort No.6; $F_n=0.35$)

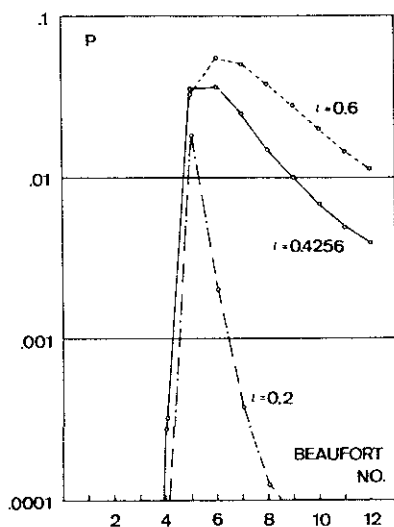


Fig.13 Probability of surf-riding
($F_n=0.35$)

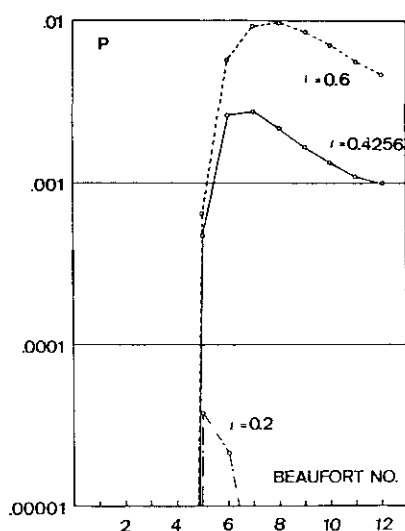


Fig.14 Probability of surf-riding
($F_n=0.30$)

period. Though theoretical value of ν is 0.4256 for Pierson-Moskowitz type spectrum, measured values of ν are distributed within about 0.2-0.6. Thus numerical results for $\nu=0.2$ and 0.6 are added. When sea states exceed beyond the Beaufort scale No.5, that is, wind velocity about 10m/sec, the probability for surf-riding drastically increases. Since the probability is greater than 0.01, the ship can suffer surf-riding once when she runs for some minutes.

The author also calculated the probability for the ship whose propeller revolution can propel in the still water with 10 knots ($F_n=0.30$) to indicate the effect of the reducing speed. Fig.14 shows that the probability for $F_n=0.30$ is about one-tenth of that for $F_n=0.35$. That is, the ship can suffer surf-riding once when she runs for some hours. Therefore we conclude that the reducing speed is very effective to prevent surf-riding. Though the stability criterion proposed by GDR and Poland [13] prohibits for ships running in following seas with $F_n \geq 0.23$, the theoretical basis is not presented. However, the present method to predict the probability of surf-riding can theoretically and quantitatively show the maximum velocity to prevent broaching-to.

CONCLUSIONS

On the basis of this study the following conclusions can be drawn:

- (1) The author confirmed, in the light of separatorices on the phase plane, that the longitudinal motion of a ship is divided among the periodic surging motion, the surf-riding under certain initial conditions and that under any initial conditions.
- (2) A ship self-propelled with constant revolution in regular seas does not suffer "the surf-riding under certain initial conditions."
- (3) The critical velocity of "the surf-riding under any initial conditions" predicted by separatorices agreed with that measured by free running model experiments.
- (4) The calculated results show that the rudder force is remarkably reduced under the surf-riding condition as the propeller advance coefficient increases.
- (5) "The surf-riding under certain initial conditions" does not occur in regular seas but does in irregular seas.
- (6) The slight reduction of propeller revolution drastically reduces the probability of surf-riding in irregular following seas and is a good measure to prevent the surf-riding.
- (7) However, once a ship captured by a wave, reducing the propeller revolution is not always be a good measure to escape from the surf-riding.

The author would like to thank Dr. T. Kohyama of Shiga University for his guidance in the light of theoretical physics. The computations were carried out by ACOS 930 at the Computing Center for

REFERENCES

1. Boese, P., Über die Erhöhung der Sicherheit eines im achterlichen Seegang fahrenden Schiffes im Hinblick auf die Steuerfähigkeit, Schiff und Hafen, Heft 2/1970, 22. Jahrgang, p109.
2. Grim, O., Das Schiff in von achtern Kommendem Seegang, Schiffstechnik, Bd. 30, 1983, p84.
3. Cane, P.D. & Goodrich, G.J., The Following Sea, Broaching and Surging, The Royal Institution of Naval Architects Quarterly Transactions, Vol.104, No.2, 1962, p109.
4. Sato, G., Non-linear Vibration, Asakura Books, Tokyo, 1970, p24.
5. Soviet delegation, Stability of a Fishing Vessel in a Seaway, IMCO, PFV X/8/1, 1970.
6. Umeda, N., On the Surf-riding of a Ship, J. Soc. Nav. Arch. Japan, Vol.152, 1983, p192, (in Japanese), and also available, Bull. of Nat. Res. Inst. Fish. Eng., No.5, 1984, p185, (in English.)
7. Grim, O., Das Schiff in von achtern auflaufender See, Jahrbuch der Schiffbautechnischen Gesellschaft, Vol.45, 1951, p264, (DTMB Translation, 313, 1965.)
8. Kan, M., Saruta, T., Yasuno, M., Yamakoshi, Y. & Suzuki, S., Surging of Large Amplitude and Surf-riding of Ships in Following Seas, J. Soc. Nav. Arch. Japan, Vol.162, 1987, p152, (in Japanese.)
9. Nakato, M., Kose, K. & Saeki, T., Experimental study on Accelerating and Decelerating Ship Motions (2nd Report), J. Soc. Nav. Arch. Japan, Vol.144, 1978, p50, (in Japanese.)
10. Goda, Y., Random Seas and Design of Maritime Structures, University of Tokyo Press, Tokyo, 1985, p221.
11. Longuet-Higgins, M.S., On the joint distribution of wave periods and amplitudes in a random wave field, Proc. R. Soc. Lond, A389, 1983, p241.
12. Nicholson, K., Some Parametric Model Experiments to Investigate Broaching-to, Proc. of Int. Symp. on the Dynamics of Marine Vehicles and Structures in Waves, London, 1974, p160.
13. GDR & Poland, Improvement of Stability Requirements of resolution A.167 (ES.IV), IMCO, STAB XXVI/4/7, 1981.
14. Umeda, N. & Kohyama, T., Surf-riding of a Ship in Regular Seas, J. Kansai. Soc. Nav. Arch. Japan, Vol.213, 1990, p63, (in Japanese).
15. Umeda, N., Surf-riding of a Ship in Irregular Seas, J. Kansai. Soc. Nav. Arch. Japan, Vol.213, 1990, p75, (in Japanese).

ON THE STABILITY OF A SWATH FERRY IN CALM WATER AND IN WAVES

A. PAPANIKOLAOU*), G. ZARAPHONITIS**),
C. KOSKINAS***), J. SAVVAS***)

ABSTRACT

Theoretical and experimental results on the stability of a high-speed SWATH passenger/car ferry in calm water and in waves are presented. The hydrostatic analysis concerns the intact and damaged stability of the projected vessel and the assessment of the obtained results in view of existing or newly proposed stability criteria, as they pertain to conventional or advanced marine vehicles. The hydrodynamic analysis includes theoretical calculations of the ship's motion behaviour in waves and the validation of the theoretical results by model experiments. The influence of properly selected stabilizing fins on the dynamic stability of the moving vessel with high speed in waves is shown to be of great importance. On the basis of the obtained results, it is concluded that the designed prototype vessel, namely the 'Aegean Queen', has acceptable hydrostatic and hydrodynamic characteristics to operate safely in the Aegean Sea on the route from Piraeus to Crete.

1. INTRODUCTION

In recent years the interest of naval architects in high performance advanced marine vehicles increased substantially. The introduction of new concepts, like SWATH ships, went together with the developments of new design approaches. As far as the stability of SWATH vessels is concerned, it was necessary to reconsider the applicability of conventional ship stability criteria. Especially, depending on the possible hazards to which these unconventional vessels may be subjected, it is essential to consider on a case basis, what compromises in the design have to be accepted, in case of failing to meet anticipated or desired stability and buoyancy standards.

The smallness of the waterplane area of SWATH ships, together with the twin-hull configuration, has significant influence on the overall hydrostatic and hydrodynamic performance of this type of vessels, in comparison to single-hull ships of equal displacement. The natural periods of heave, pitch and roll are much longer for the SWATH ships, thus, considerably longer waves are required for

exciting large motions. Also, due to the submergence of the buoyancy providing, lower hulls, wave-exciting forces and moments are significantly reduced and the employment of stabilizing fins there proves to be very efficient for controlling the ship motions at resonant frequencies.

On the other side, the small waterplane area may have some undesirable effects on the SWATH performance, like reduced restoring ability for trim and sinkage and vertical plane instabilities at high speeds. However, these effects can be overcome by efficient ballast control systems, the employment of horizontal, stabilizing fins and by proper hull design, as to the extent of smallness, form and moment characteristics of the waterplane area of a projected SWATH ship.

It is nowadays accepted that the stability of a SWATH ship is mainly governed by the following two critical items:

- Damaged stability performance, when flooding of adjacent compartments occurs and simultaneously the ship is rolling, due to beam seas and heeling due to an assumed storm side wind.
- Dynamic vertical plane instabilities due to the action of the so-called Munk's moment for vessels moving at high-speed and design of

National Technical University of Athens

Dept. of Naval Architecture & Marine Engineering

*) Professor, **) Res. Assistant,

***) Graduated Students.

proper stabilizing fins.

Comparably, little work has been done until now to systematically evaluate the validity of proposed stability criteria for SWATH ships. This is mainly due to the fact that only few ships of this type have been constructed to date. However, because of the involvement of the U.S. Navy in the development of SWATH Navy ships (see e.g. T-AGOS 19, construction [1]), certain stability criteria have been discussed by various authors, especially as to the application to naval ships (see [2]) or research vessels (see [3]).

Also, as to the vertical plane stability of SWATH ships, when with high speed in waves, and the design of stabilizing fins many efforts have been done before, starting with the work by C.M. Lee and R.M. Curphey [4] and many others in the following. In any case, though a fairly detailed theoretical analysis of the pitch instabilities problem exists, the required systematic experimental work for validation of the theoretical data and optimization of the size and position of the fins remains to be done in the future.

In the present paper, that summarizes partial results of a recently completed NTUA research project dealing with the design of a high-speed passenger-car ferry for the Aegean Sea, the hydrostatic and dynamic stability of the designed vessel are discussed. This is done in view of operational and stability criteria set by the owner's requirements, or the proposed stability of the U.S. Navy respectively, adjusted for the local conditions in the Aegean Sea. The hydrostatic analysis includes the intact and damaged stability of the ship in calm water, that is considered as two-compartment ship in the sense of the SOLAS regulations. The dynamic analysis concerns the quasi-static approach of the ship's stability in beam and following seas, hydrodynamic calculations of the ship motion behaviour in waves through a strip theory approach, alternatively a 3D diffraction theory and the design of stabilizing fins on the basis of a vertical plane stability analysis. The dynamic motion behaviour of the vessel in head waves has been validated by model experiments at the Towing Tank of NTUA.

2. OUTLINE OF VESSEL'S REQUIREMENTS

The objective of the designed prototype vessel, to be discussed in the following, is to operate as a link in a rapid marine transit system, connecting the Greek mainland (port of Piraeus) with the island of Crete (port of Heraklion).

Following a three-stage, technoeconomical optimization (see [5]), according to a realistic scenario of requirements for the specific route, a vessel with the following characteristics has been developed.

Box Length (m)	51.5
Box Breadth (m)	31.7
Strut Length (m)	37.6
Strut Breadth (m) (locally)	2.60
Lower Hull Length (m)	50.0
Lower Hull Diameter (m) (locally)	3.80
Draft (m)	5.00
Side Depth to Main Deck (m)	9.46
Displacement (t)	1060
DWT (t)	226
Number of Passengers (one class)	752
Number of Cars (one deck)	80 (+ 4)
Speed (kn)	30.0
Main Machinery Power (MCR)	MTU 16V 1163 TB 63 MCR 5000PS each 1100 rev/min
Gross Tonnage (Intern.)	2544 GRT
Net Gross Tonnage (Intern.)	763 NRT

Table I: Main characteristics of prototype high-speed ferry 'Aegean Queen'.

On the operational side the vessel is required to be able to operate without loss of efficiency in all sea conditions, typical to the Aegean Sea, up to and including Sea State 5-6 (sign. wave height $H_s \leq 2.5$ m for South West Aegean Sea). Efficiency means here that the vessel will be able to maintain its course at not significantly reduced service speed of at least 28 kn and the corresponding seakeeping behaviour should characteristically consider the following criteria of the U.S. Navy, as proposed for hydrographic vessels [7]

- significant amplitude of roll ≤ 3 deg.,
- significant amplitude of pitch ≤ 3 deg.,
- Vertical acceleration at any point of deck ≤ 0.2 g.

On the damaged stability side, it is required the vessel to be adequate in terms of the SOLAS criteria with any two adjacent compartments flooded. Because the present design considers the main machineries, that should be of Diesel type, to be installed in the lower hulls, what resulted to large machinery rooms, it was expected that the simultaneous flooding of the two-compartment machinery rooms on each side of the vessel would lead to the worst damaged stability case. The remaining quasistatic stability criteria, as to the combined wind-roll motion loads, have been taken according to L.L. Goldberg and R.C. Tucker [2].

The dynamic stability of the vessel with speed in waves, as to the vertical plane modes pitch and

heave, together with the design procedure of the employed stabilizing fins is based on the method proposed by C.M. Lee and R.M. Curphey [4] and leads here to speeds for the inception of pitch instabilities of well over 40 kn.

3. STABILITY IN CALM WATER

3.1. Intact Stability

The intact stability of the designed vessel was investigated for various conditions, namely at design displacement (departure) of 1060 tons, light ship displacement of 915 tonnes (incl 81 tonnes ballast for zero trim) and overload displacement of 1300 tonnes. The weight characteristics of the ship in the design condition are given in the following table

Weight Group	Weight (t)	LCG (m)	KG (m)
Structure	517 000	25 740	7 529
Machinery Equipment	212 000	16.110	2 330
Outfitting	105.000	30.106	10 346
DWT	226.000	32 321	9.418
Total	1060.000	25.650	7.317

The intact righting arms of the 'Aegean Queen' for the aforementioned conditions are shown in Fig. 1a. The calculations are performed by use of the ARCHIMEDES software [8]. As it is expected for a SWATH ship, the area under the intact stability curves and the corresponding restoring energy is very large. Characteristically, the maximum GZ is nearly 11,0 m (at approx. 20 degrees), GM equals 12.206 m and the range of stability extends to nearly 80 degrees. It is of interest to note here that the stability characteristics of the discussed ship do not change significantly for the three studied conditions, though they can be considered as extreme cases.

The applied intact stability criteria are according to Goldberg and Tucker [2], though not clearly defined there as criteria, but at least as guidance. The heeling arms, due to high beam winds of 80 knots speed, have been calculated herein exactly to account for the actually shaded area of the inclined SWATH structure. Characteristically, the maximum wind moment occurs at angles different from zero. As shown in Fig. 1b, it is apparent that the vessel is not in danger, even if this side wind is combined with a rolling motion of amplitude 7 degrees (in the worst case at resonance period, see 4.2). Further to it, the effect of crowding of passengers and personnel to one side will produce

here a heeling arm of approximately 1,75 m at zero angle, thus, the ship can be considered safe in the intact stability case.

3.2. Damaged Stability

The damaged stability of SWATH type vessels is usually affecting significantly the overall design. This is due to the fact, that subject to the most probably unsymmetrical underwater flooding, the extent of which can be taken according to the expected hazzards, the SWATH ship may heel and trim with ease, because of her small waterplane area.

Before discussing the damaged stability of the herein presented ship, some of her characteristics must be commented, because of the differences to other typical SWATH vessels. Due to the set owner's requirements (see 1), the projected vessel has the installed diesel machinery, providing 4x5000 HP horse power, in the lower hulls. The selected 2x2 MTU engines have been placed in the compartments B and C, as shown in Fig. 2, thus, the engine room is subdivided by a watertight bulkhead. The lower hull diameter and the strut's beam are locally enlarged for the engines to fit through for service or installation. This resulted to a comparably large waterplane area for the present SWATH, the GM of which is quite high, namely 12.206 m (departure condition). Also, the longitudinal metacentric height is herein comparably low, namely 7.144 m. As will be shown later (see 4.2), by that the eigenperiods for heave and pitch of the 'Aegean Queen' are quite separated even without the employment of fins, what is desired from the seakeeping point of view.

The damaged stability of the projected vessel has been studied systematically on the basis of the criteria set in [2] for 'two compartment' SWATH's and for various combinations of the defined compartments A to H, shown in Fig. 3. In Table II the most critical cases are outlined.

There it is shown (case 1) that simultaneous flooding of compartment A (after peak) and B (after machinery room) is the worst overall case. It can be balanced by e.g. counterflooding compartment Hh (lower hull) and Hb (58.3 t in box). Also, case No.2 (flooding of B and C) requires counterflooding of e.g. compartment Hh. In Fig. 3a the righting arm curve for case No. 3 (flooding of C and D) is shown, where no counterflooding is necessary.

In this latter case a static heel angle of 8 degrees results, that is considered acceptable. The damage

CASE	FLOODED COMPARTMENT	DRAFT MEAN [m]	PORT SIDE		STARBOARD		HEEL [deg]	TRIM [%L]
			T _F [m]	T _A [m]	T _F [m]	T _A [m]		
1	A.95 B.75 Hh.95 Hb 58.3l	6.009	6.496	5.048	6.969	5.522	-0.855	2.810
2	B.75 C.75 Hh.95	7.118	4.999	6.491	7.744	9.236	-4.949	-2.898
3	C.75 D.95	6.610	4.159	5.215	8.004	9.006	-6.915	-2.050
4	D.95 E.95	5.186	4.449	2.814	7.557	5.922	-5.600	3.176
5	E.95 F.95	4.119	4.663	1.110	7.122	3.570	-4.435	6.890
6	F.95 G.95	3.526	4.675	0.131	6.920	2.376	-4.050	8.824
7	G.95 H.95	2.989	4.705	-0.600	6.578	1.270	-3.382	10.304
8	A.95 Hh.95	6.377	5.486	6.580	6.173	7.267	-1.242	-2.123
9	B.75 Hh.95	5.123	5.614	4.050	6.189	4.631	-1.040	3.026
10	C.75 Hh.95	5.440	5.407	3.988	6.890	5.472	-2.679	2.755

- N.B. : 1. The drafts T_F and T_A are measured at the leading and trailing edges of a box with (L x B x T).
2. The flooded compartments A, B, ..., H are designated acc. to their assumed permeability, e.g. A.95 means comp. A flooded to 95%.
3. Additional designation to flooded compartments, e.g. Hh or Hb, means hull (h) or box (b) location.

Table II : Drafts, Heel and Trim after Flooding of Compartments of SWATH-'Aegean Queen'.

waterlines are shown in Figs. 3b and 3c. The vessel meets the criteria laid down in [2], including consideration of a 60 kn beam wind (or more) and 7 degrees of roll motion due to beam waves. The latter is determined by calculations with relevant computer programs (see 4.2). Finally, it should be noted that the reserve buoyancy of the projected vessel, as given by the watertight box structure, is sufficient to carry the total weight of the ship, in case of total loss of buoyancy of the structure's legs. However, it must be assumed that any openings in the sponson-box interface (longitudinal WT bulkhead) have to be closed in time to prevent flooding into the undamaged box area.

4. DYNAMIC STABILITY

4.1. Quasi-Static Approach

The stability of the projected vessel in waves has been studied at first by the common quasi-static approach, namely by balancing the weight of the ship with her displacement at various relative wave positions.

As to the beam seas condition, after having determined analytically the maximum expected roll angle of approximately 7 degrees, the common

criteria for the quasi-dynamic stability of ships or offshore structures have been applied, imposing certain conditions as to the relative magnitude of the areas below the righting and heeling arms. In view of the characteristics of Fig. 1b, it is evident that the area below the righting arm curve of the 'Aegean Queen', corresponding to the available restoring energy, is more than sufficient to counteract the heeling work imposed to the ship by the wind or rolling action. The 40% margin to account for gusts or calculation inaccuracies is also fulfilled.

The present ship has been investigated in addition for the case of following seas, by considering a trochoidal, design wave of length 112,5 m and height 5 m. For various relative positions of the wave crest of the selected wave, assuming its passing from the bow to the stern of the ship (t=0: node through to crest amidships), the restoring arm of the projected SWATH has been calculated by use of the ARCHIMEDES software [8]. As shown in Fig. 4, remarkably the GZ curve of the 'Aegean Queen' seems to be unaffected by the given wave excitation. This is mainly due to the fact that typically SWATH vessels have vertical struts of almost constant waterplane area around the waterline, thus, unless a 'huge' wave of extreme wave height is applied,

hitting the bottom of the box structure or letting the lower hulls emerge, no significant effects can be expected. In the present case, since a 5m wave is considered sufficient for the design of a ship to operate in the S.W. Aegean Sea (probability of occurrence of waves over 5.5 m is approx. $p=0.0002$ [9]), it is concluded that the projected vessel will safely operate on its route to Crete. Of course, it must be remembered that the quasi-static approach does not account for the motions of the ship in waves, considered in the following.

4.2. Hydrodynamic Analysis

The hydrodynamic behaviour of the projected vessel in waves has been studied systematically by use of existing and newly developed computer programs, relying on the strip theory approach, alternatively a 3D diffraction theory method.

The employed strip theory is based on the method proposed by C.M. Lee and R.M. Curphey [4]. Thereby the quasi two-dimensional, strip theory approach, formulated for the hydrodynamics of SWATH like, slender hull forms, accounts for the effects of viscous damping and of stabilizing fins on the ship's motion behaviour. Based on this method, the original NSRDC computer program for monohull vessels, given in [10], has been modified to account for twin-hull vessels and later on for SWATH-like hull forms [11].

An alternative 3D pulsating source distribution method has been developed at NTUA to account for the forward speed effects of moving slender ships in waves. The method is exact for the zero forward speed problem and includes effects of forward speed in the manner of a slender body theory by assuming that the frequency of encounter is relatively high and/or the speed of advance of the vessel small. The derivatives in the longitudinal direction are assumed also small in the sense of a slender body assumption. Based on this, the dependence of the required Green's function on the forward speed can be shown to be small and the problem is solved using the zero speed 3D Green's function. It should be added, that the method has been successfully tested for the loads and motions prediction of various hull forms, like container ships [12], and has been modified to account for the viscous damping and fins of SWATH ships. The details of the method are given in [12], whereas the related computer program is described in more details in [13]. Herein, the SWATH has been discretized by 2×256 surface elements and the obtained results are considered very satisfactory, despite the high service speed of the projected vessels that violates a

basic assumption for the development of the formulas.

The motion responses in 6 DOF of the projected vessel have been studied systematically for various wave conditions, angles of incidence and vessel's speed. The influence of stabilizing fins has been checked also systematically, both theoretically, as well as experimentally, in the Towing Tank of NTUA using a 1:17 ($L=3,0$ m) model.

In the following figures 5 to 8 some typical examples of the obtained theoretical and experimental data of the seakeeping behaviour of the 'Aegean Queen' are shown. Starting with the zero speed, head seas, heave/pitch responses, it is evident from Fig. 5a and b that the projected vessel exhibits two pronounced resonance regions, namely one corresponding to the heave eigenperiod for wave periods near 8 sec and the second one corresponding to the pitch eigenperiod for waves near 12 sec. Both regions are outside of the range of typical periods of the S.W. Aegean Sea, where the vessel is assumed to operate, (mean period considerably less 6 sec). The influence of stabilizing fins at zero forward of the ship is consequently very limited (not for active fins!), though it is evident that the heave and pitch resonances are shifted to higher wave periods. The theoretical prediction of the heave response at zero speed, with the fins included, fails as to the resonance peaks, probably due to the fact that the employed formulas [4] for the influence of the fins on the hydrodynamics of the vessel are less meaningful at zero forward speed.

In the following figures 6 ($U=15$ kn) and 7 ($U=30$ kn), it is clearly shown that the projected vessel, designed with fins and operating at seas with period typically less than 6 sec, will exhibit a superior seakeeping behaviour, without any remarkable motion for its passenger-deck structure. For 15 kn the agreement between theoretical predictions and experiments is excellent. Because of the lack of experimental data for the 30 kn case, the calculated responses by the 2D strip theory have been validated only by 3D theoretical predictions according to [13]. The superior seakeeping behaviour of the 'Aegean Queen' model, when moving with full scale 30 kn in regular or irregular waves at the Towing Tank of NTUA, has been captured at least at a video film, to be shown at the conference meeting.

Finally, in the last two figures (Fig. 8a and b) the roll and sway response of the vessel at zero forward speed and beam seas is shown. Because typical seaways in the S.W. Aegean Sea are characterized by

waves with length much less than 100 m ($\lambda \approx 2L$), it is not expected that the projected vessel will run into trouble even in case of involuntary stop on the route to Crete.

In the following seas case, not shown here for the sake of brevity, some further interesting results are obtained. There it is shown that the occurrence of the critical, zero frequency of encounter, case, happens for the projected SWATH, when running with 30 kn, at following seas of length 152 m.

Because the typical wave lengths of the Aegean Sea are much less than this limit, the projected vessel is going to overtake the any probable following wave without being in danger of coming into resonance ('platforming' mode).

Concluding the seakeeping behaviour of the 'Aegean Queen' seems to be fully satisfactory according to the set owner's requirements (sec 2). The worst case proved to be the zero forward speed case. The employment of stabilizing fins improves the seakeeping of the vessel at high speeds significantly.

4.3. Design of Fins

When an elongated body, like a submarine, is moving in a non-viscous fluid at an acute angle of attack (α) between its longitudinal axis and its path, it would not experience any force, but an unstable deviating moment, the so-called Munk-moment [14]. This moment is proportional to the difference of the added mass coefficients for the transverse and axial flow components, the velocity head and the sinus of the double angle of attack $\sin(2\alpha)$.

For a SWATH ship it is of interest to consider the Munk-moment related to the pitch-heave motion, because of the reduced restoring ability of the SWATH in the pitch mode related to the inherent small waterplane area of this type of vessels. It can be shown that, beyond a certain threshold forward speed, a SWATH ship becomes unstable, due to the reduction of the effective pitch restoring coefficient C_{55} to become less than zero. Also, it is probably of interest to study in the future the horizontal plane stability of SWATH ships due to the coupled

FIN SIZE		MODE	DAMPING RATIO		NATURAL PERIOD [sec]	
AFT	FWD		15 kn	30 kn	15 kn	30 kn
0.00	0.00	HEAVE (H)	0.01	0.00	6.70	6.45
		PITCH (P)	0.28	1.00	27.56	0.00
0.60	0.00	H	0.19	0.36	6.95	7.27
		P	0.35	0.88	17.88	43.81
0.80	0.00	H	0.25	0.54	7.14	8.18
		P	0.34	0.52	16.43	17.58
1.00	0.00	H	0.31	0.69	7.39	8.58
		P	0.33	0.27	15.19	14.40
1.20	0.00	H	0.38	0.77	7.68	8.64
		P	0.30	0.13	14.14	13.72
1.40	0.00	H	0.46	0.82	8.00	8.76
		P	0.26	0.04	13.34	13.50
1.60	0.00	H	0.53	0.85	8.29	9.00
		P	0.22	UNS	12.83	UNS
1.80	0.00	H	0.59	0.88	8.55	9.41
		P	0.17	UNS	12.54	UNS
2.00	0.00	H	0.65	0.91	8.81	10.06
		P	0.14	UNS	12.39	UNS
1.20	0.80	H	0.35	0.59	7.12	7.79
		P	1.00	1.00	0.00	0.00
1.40	0.60	H	0.41	0.80	7.48	11.23
		P	0.81	1.00	29.70	0.00
1.60	0.40	H	0.49	0.89	7.99	10.81
		P	0.58	0.53	18.21	22.66
1.70	0.30	H	0.53	0.89	8.28	10.14
		P	0.47	0.28	15.75	18.12
1.80	0.20	H	0.58	0.90	8.52	9.86
		P	0.36	0.12	14.20	16.06
1.90	0.10	H	0.61	0.90	8.69	9.83
		P	0.26	UNS	13.20	UNS

N.B. : 1. Basic fin size (1.0): Chord 3.77 m, Span 4.52 m,
Location: inboard side at 0.15L (aft) and 0.765L (forward).
2. Natural periods: UNS means unstable,
0.0 means damping ratio equals 1.0.

Table III : Stability Characteristics of SWATH-'Aegean Queen'

sway-yaw motion and in view of the absence of restoring forces, but with the action of Munk's moment in this plane as well.

Initial studies of the projected vessel have shown that the threshold velocity of the 'Aegean Queen' is about 20.5 kn. Thus, for a service speed of about 30 kn it was required to select proper stabilizing fins with the aim to increase the threshold velocity, but also improve the overall seakeeping of the vessel by shifting its eigenperiods to higher values, outside the range of interest for common seaways.

The selection procedure of the proper fins for a specific SWATH vessel is based on the analysis of the stability of the coupled heave-pitch motion equations, according to the well known Routh's criteria [4]. A summary of this analysis for various fins combinations is given in table III.

The finally selected fin pair, having the characteristics of 1.60 times the basic size aft and 0.40 forward, resulted acceptable natural periods in heave and pitch of over 10 sec resp. 20 sec and a threshold velocity of over 40 kn. The details of this analysis cannot be shown here, since of the limited space available.

Though the employment of stabilizing fins improves greatly the seakeeping behaviour of the vessel, it should be remembered that the calm water resistance of the ship will appreciably increase. In this present case, this increase was approx. 8% at service speed according to the Towing Tank experiments. However, the stern flow to the propeller of the ship has been significantly stabilized by the employment of the fins, thus, it can be expected that the overall propulsive efficiency of the ship with fins is comparable, if not better, than for the bare hull condition. An optimization of the proper location and size of the fins with respect to the least added resistance and maximum propulsive and stability efficiency remains to be addressed in the future.

5. CONCLUSIONS

The present paper dealt with the hydrostatic and hydrodynamic analysis of a prototype high-speed passenger-car SWATH ferry. The obtained theoretical and experimental results relieved certain peculiarities of the stability of SWATH type vessels:

1. The intact stability of SWATH ships is usually more than sufficient.
2. The damaged stability may cause certain problems, when simultaneous flooding of large

adjacent compartments occurs. These problems can be usually treated by counterflooding of undamaged compartments, or by shifting the bulkheads.

3. Wind loads or other heeling moments are usually not seriously affecting the stability of SWATH vessels.
4. The dynamic stability of SWATH ships in waves does not present insurmountable problems, because of the excellent SWATH seakeeping behaviour.
5. The employment of fins (stationary or active) is essential for high-speed SWATH ships to be operated beyond their threshold speed.
6. The stability criteria, laid down in [2], or as they are known from similar regulations for offshore structures, are sufficient for SWATH ships. However, they can be improved by better accounting for the actual wind moments on the inclined SWATH and the damaged stability criteria for the asymmetrical flooding of compartments and the resulting damage waterlines.

6. ACKNOWLEDGEMENTS

The present paper is based on results of a recently completed research project of NTUA, dealing with the 'Preliminary Design of a SWATH Passenger/Car Ferry for the route Piraeus-Crete'. This project was financed by the Greek Secretary General for Research and Technology (project IIPONE 86Γ924) and partially supported by the Hellenic Shipyards.

REFERENCES

- [1] J.A. Watson, W.M. Hayden, "Overview of Coast Guard Plan Review for High-Tech Ship Design", Journ. Marine Techn., Vol. 27, 1990, p. 47 ff.
- [2] L.L. Goldberg, R.G. Tucker, "Current Status of Stability and Buoyancy Criteria Used by the U.S. Navy for Advanced Marine Vehicles", Journ. Naval Engineers, Vol. 87, 1975, p. 33 ff.
- [3] D.L. Smith et al, "SWATH Design-A Shipbuilders View and a Practical Example", Proc. RINA Conf. on SWATH Ships and Advanced Multi-Hulled Vessels, 1988.
- [4] C.M. Lee, R.M. Curphey, "Prediction of Motion, Stability and Wave Load of Small-Waterplane-Area, Twin-Hull Ships", Trans. SNAME, Vol. 85, 1977, pp. 94-130.
- [5] A. Papanikolaou, "Hydrodynamic and Technoeconomical Optimization of a High-Speed SWATH Passenger/Car Ferry", Journ. Tecnica Italiana, 1989.

- [6] A. Papanikolaou et al, "Preliminary Design of a High-Speed SWATH Passenger/Car Ferry", Proc. 5th IMAEM Conf., Athens, May 1990.
- [7] G.R. Lamb, "Influence of Seakeeping Requirements on SWATH Ship Geometry", SNAME Chesapeake Section, June 1987.
- [8] H. Söding, "Manual for ARCHIMEDES", publ. SET GmbH, Hamburg, 1989.
- [9] A. Papanikolaou, H. Nowacki et al, "Concept Design and Optimization of a SWATH Passenger/Car Ferry", Proc. RINA-IMAS'89 Conf., reply to questions by Kriketos/Pastras (MAREDEC), May 1989.
- [10] W.G. Meyers, D.J. Sheridan, N. Salvesen, "Manual for the NSRDC Ship-Motion and Sea-Load Computer Program", NSRDC Rep. 3376, Feb. 1975.
- [11] A. Papanikolaou, G. Zaraphonitis, A. Kapotas, I. Savvas, "Modifications of the NSRDC Ship Motion and Sea Load Computer Program for Twin-Hull Vessels", NTUA Internal Report, 1987/1990.
- [12] A. Papanikolaou, G. Zaraphonitis, T.T. Schellin, "A 3D-Method to Evaluate Motions and Loads of Ships with Forward Speed in Waves", Pres. at the 5th IMAEM Conf., Athens, May 1990.
- [13] A. Papanikolaou, G. Zaraphonitis, "Computer Program NEWDRIFT V.6", NTUA Internal Report, 1989.
- [14] M.M. Munk, "Aerodynamics of Airships", Div. Q. in 'Aerodynamic Theory', Vol. VI, ed. by W.F. Durand, publ. J. Springer, Berlin, 1936.

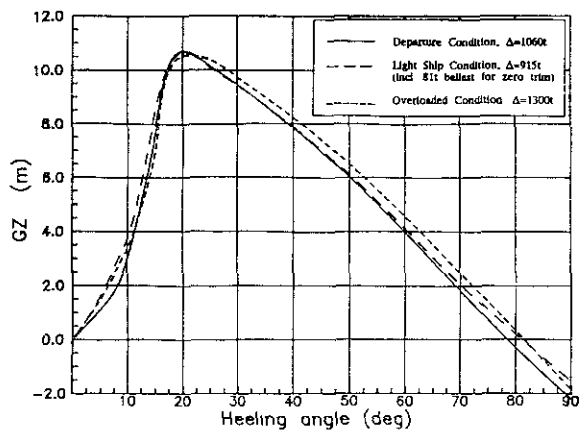


Fig. 1a : Intact Stability Righting Arms

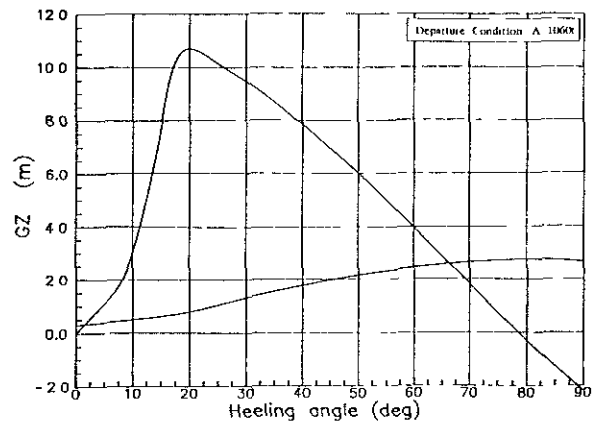


Fig. 1b : Intact Stability Righting Arms with 80kn Beam Wind

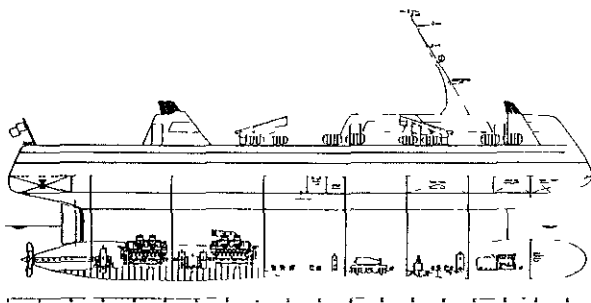


Fig. 2 : Compartmentation and Machinery Arrangements

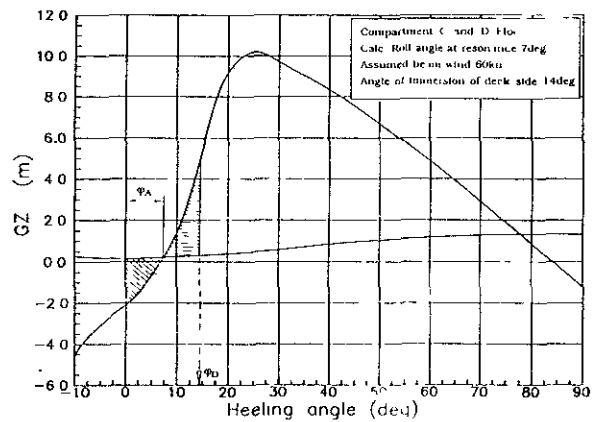


Fig. 3a : Damaged Righting Arm in Beam Seas and Side Wind

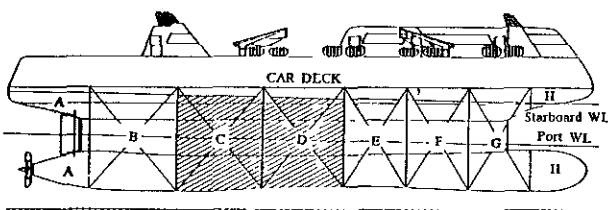


Fig. 3b : Waterlines in Damaged Condition Flooded Compartments 'C' and 'D'

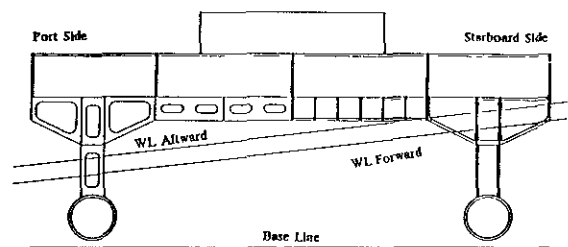


Fig. 3c : Waterlines in Damaged Condition Flooded Compartments 'C' and 'D'

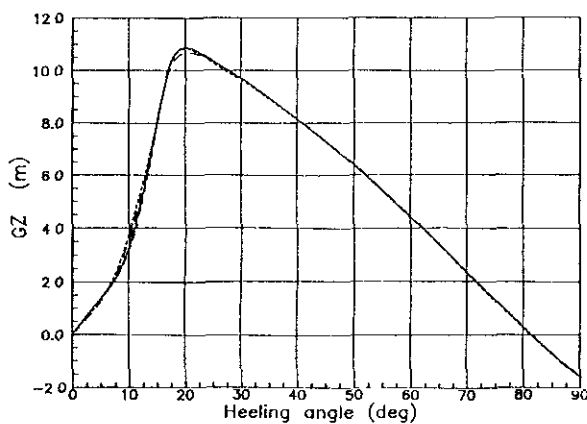


Fig. 4a : Intact Righting Arms in Following Seas. Quasi-Static Approach

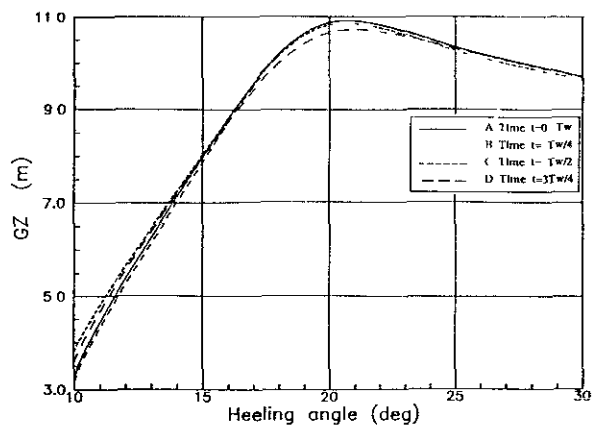


Fig. 4b : Intact Righting Arms in Following Seas. Quasi-Static Approach

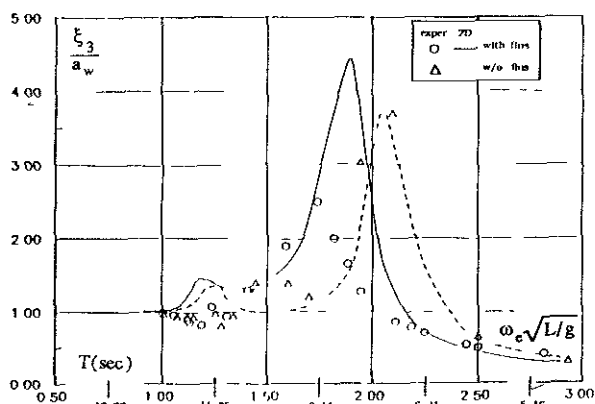


Fig. 5.a : Heave Motion Response in Head Seas, U=0kn

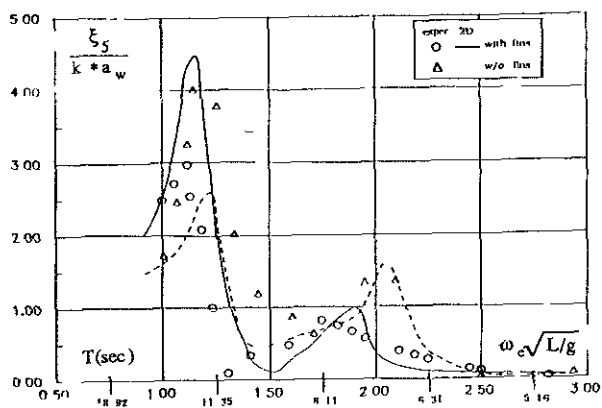


Fig. 5.b : Pitch Motion Response in Head Seas, U=0kn

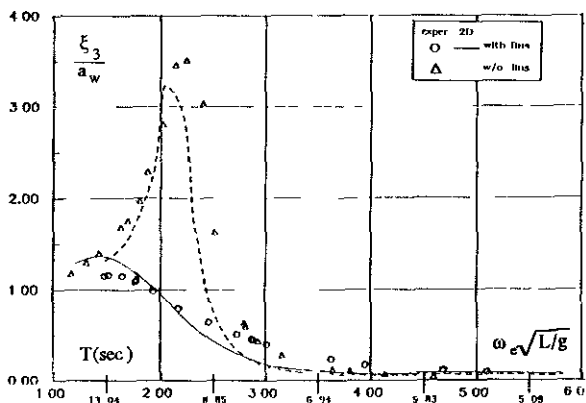


Fig. 6.a : Heave Motion Response in Head Seas, U=15kn

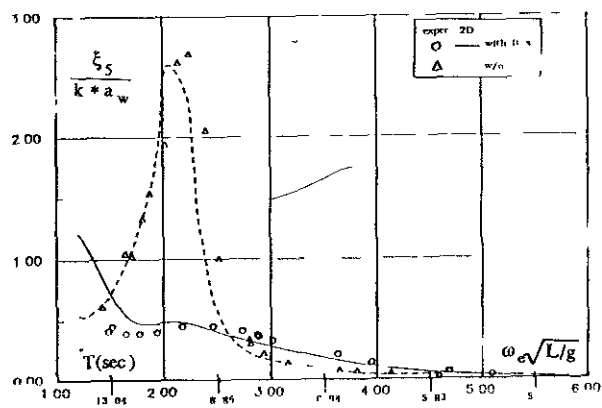


Fig. 6.b : Pitch Motion Response in Head Seas, U=15kn

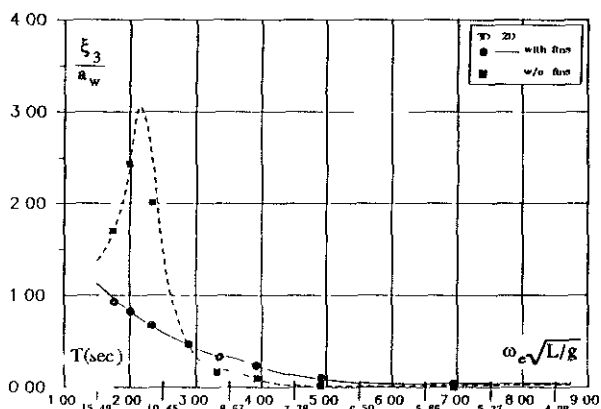


Fig. 7.a : Heave Motion Response in Head Seas, U=30kn

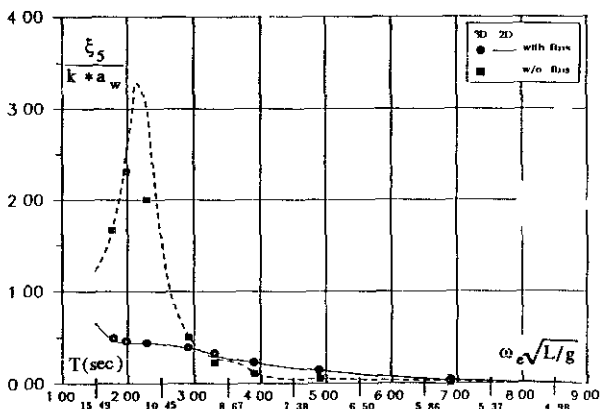


Fig. 7.b : Pitch Motion Response in Head Seas, U=30kn

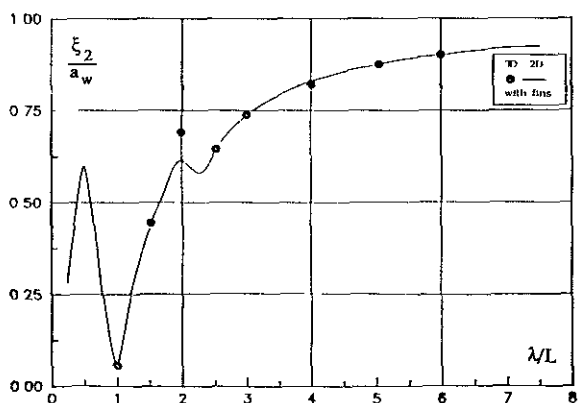


Fig. 8.a : Sway Motion Response in Beam Seas, U=0kn

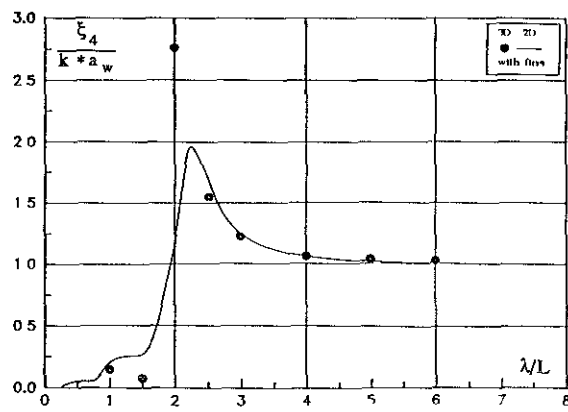


Fig. 8.b : Roll Motion Response in Beam Seas, U=0kn

by Masami Hamamoto*, Toru Shirai**, Norihiro Wakiyama***

ABSTRACT

An analytical approach has been developed for the numerical simulation of ship motions leading to capsizing in order to investigate the influences of the loss of transverse stability on the capsizing of a ship in severe following seas. The equations of motion with respect to the horizontal body axes are presented for analyzing a large amplitude motion. The results simulated by this mathematical model are compared with the results observed in experiments for the check of accuracy. Finally critical metacentric height leading to capsizing is discussed for several kinds of ship.

1. INTRODUCTION

The transverse stability of a ship running in severe following seas is considerably modified by the change in water plane area due to the relative position of ship to wave, alternately in the crest or trough of a wave. As well known, a reduction takes place while the crest of a wave is amidship and an increase takes place when the trough is amidship with ends buried in the crest. The loss of transverse stability may cause a large heel due to external disturbances and the ship motions leading to capsizing. Thus the loss of transverse stability has been considered as an important index for the safety against capsizing.

The main objective of this work is to investigate the influences of the loss of transverse stability on the capsizing of ship in severe following seas. From results of the experiments using radio-controlled

ship models, several modes of capsizing were observed and characterized as pure loss of stability, parametric excitation and broaching-to.

In general, the ship motions leading to capsizing are in a large amplitude with all six degrees of freedom of motion so that there are fundamental problems to be considered for the analytical approach.

First, a coordinate system has to be considered for describing the equations of motion. For this purpose, there are three candidates which are called Earth axes, General body axes and Horizontal body axes. The Earth axes and General body axes are well known coordinate systems and accepted commonly. However, the surface ship is considerably limited in the matter of displacement and angular motions arising from heave, pitch or roll and effects of hydrostatic force are dominant with respect to the seakeeping motion in following seas because the encounter frequency of ship to waves is very low. And also the maneuvering motion in heeled condition is almost limited in the horizontal plane. Thus in this paper the Horizontal body axes is discussed and used for the description of ship motions leading to capsizing.

Next, in regard to the hydrodynamic

* Department of Naval Architecture and Ocean Engineering, Osaka University

** Mitsubishi Heavy Industries, Ltd.

*** Graduate School, Department of Naval Architecture and Ocean Engineering, Osaka University

problem, it is still difficult to predict the added masses and damping coefficients in large amplitude motion both of ship and waves. So that the hydrodynamic forces will be approximately obtained from the linearized theory. Here in engineering sense, the added masses and damping coefficients can be estimated from Tasai's practical formula¹⁸⁾ for seakeeping motion, and Motora's chart⁴⁾ and Inoue's practical formula¹⁹⁾ for maneuvering motion. On the other hand, the hydrostatic forces including the Froude-Krylov force are obtained from the integration over the instantaneous immersed surface to taking into account a large motion of ship.

Finally, on the basis of the equations of motion, the ship motions leading to capsizing are simulated for several kinds of ship and the critical metacentric height of the ship in severe following seas is predicted from the results of simulation.

2. EQUATIONS OF MOTION FOR SIMULATION

In this section, we discuss the basic ground work for the analysis of ship motions. A ship is assumed to behave as a rigid body having six degrees of freedom. For the ship with the origin of the body axes at the ship's center of mass as shown in Fig.1, Euler's equations of motion are usually described as follows:

Translate motions and forces

$$\begin{aligned} m(\dot{u} + wq - vr) &= -mg \sin\theta + X \\ m(\dot{v} + ur - wp) &= mg \cos\theta \sin\phi + Y \\ m(\dot{w} + vp - uq) &= mg \cos\theta \cos\phi + Z \end{aligned} \quad (1)$$

Angular motions and moments

$$\begin{aligned} I_{xx}\dot{p} - I_{zx}\dot{r} - (I_{yy} - I_{zz})qr - I_{zx}pq &= K \\ I_{yy}\dot{q} - (I_{zz} - I_{xx})rp - I_{zx}(r^2 - p^2) &= M \\ I_{zz}\dot{r} - I_{zx}\dot{p} + (I_{yy} - I_{xx})pq + I_{zx}qr &= N \end{aligned} \quad (2)$$

Where u, v and w are the velocities along the x, y and z axes which are oriented in the ship with x forward, y out the starboard and z out the bottom and p, q and r about each axis, m and g are the mass of the ship and gravitational acceleration, I_{xx}, I_{yy}, I_{zz} and I_{zx} are the principal moments

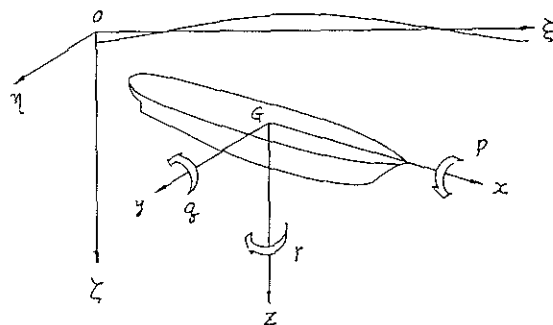


Figure 1. Earth axes and General body axes

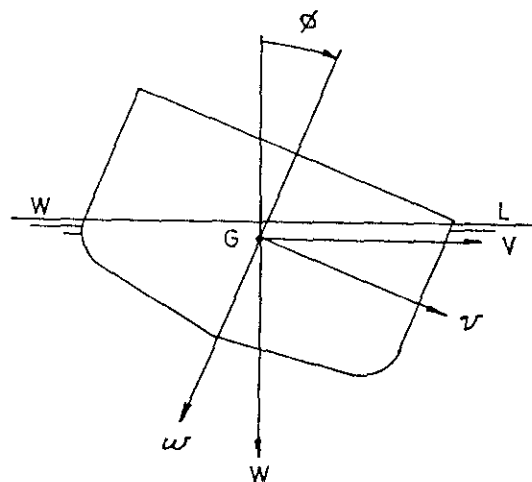


Figure 2. Horizontal body axes

of inertia and productive moment of inertia about the body axes of the ship, ϕ, θ and ψ are Euler's angles to describe the situation of ship in the space fixed axes and also connected with angular velocities as follows:

$$\begin{aligned} p &= \dot{\phi} - \dot{\psi} \sin\theta \\ q &= \dot{\theta} \cos\phi + \dot{\psi} \cos\theta \sin\phi \\ r &= \dot{\psi} \cos\theta \cos\phi - \dot{\theta} \sin\phi \end{aligned} \quad (3)$$

Here, we would like to make some considerations about Equations (1) and (2) for an analysis of a heavy rolling up to capsizing of the ship in water surface. First of all, we shall try to rewrite the equations of motion with the linear velocities U, V and W in the horizontal and vertical plane to the water surface as shown in Fig.2 instead of v and w along the body axes as connected by :

$$V = v \cos \phi - w \sin \phi \quad (4)$$

$$W = -u \sin \theta + v \cos \theta \sin \phi + w \cos \theta \cos \phi$$

And also the trim angle is limited to the small angles of 2 or 3 degrees and it may be assumed that $\theta \approx 0$, Equation (4) reduced to:

$$\begin{aligned} U &\approx u \\ V &\approx v \cos \phi - w \sin \phi \\ W &\approx v \sin \phi + w \cos \phi \end{aligned} \quad (5)$$

and in the same way

$$\begin{aligned} p &\approx \dot{\phi} \\ q &\approx \dot{\theta} \cos \phi + \dot{\psi} \sin \phi \\ r &\approx \dot{\psi} \cos \phi - \dot{\theta} \sin \phi \end{aligned} \quad (6)$$

Substituting Equations (5) and (6) into Equations (1) and (2), we obtain

Translate motions and forces

$$\begin{aligned} m(\dot{U} - V\dot{\psi} + W\dot{\theta}) &= X \\ m(\dot{V} + U\dot{\psi}) &= Y \cos \phi - Z \sin \phi \\ m(\dot{W} - U\dot{\theta}) &= Z \cos \phi + Y \sin \phi + m g \end{aligned} \quad (7)$$

Angular motions and moments

$$\begin{aligned} I_{xx}\ddot{\phi} - (I_{yy} - I_{zz})\left[\frac{1}{2}(\dot{\psi}^2 - \dot{\theta}^2)\sin 2\phi + \dot{\theta}\dot{\psi}\cos 2\phi\right] &= K \\ (I_{yy}\cos^2\phi + I_{zz}\sin^2\phi)\ddot{\theta} &+ (I_{yy} - I_{zz})\left[\left(\frac{1}{2}\dot{\psi} - \dot{\phi}\dot{\theta}\right)\sin 2\phi + \dot{\phi}\dot{\psi}\cos 2\phi\right] + I_{xx}\dot{\phi}\dot{\psi} \\ &= M \cos \phi - N \sin \phi \end{aligned} \quad (8)$$

$$\begin{aligned} (I_{zz}\cos^2\phi + I_{yy}\sin^2\phi)\ddot{\psi} &+ (I_{yy} - I_{zz})\left[\left(\frac{1}{2}\dot{\theta} - \dot{\phi}\dot{\psi}\right)\sin 2\phi + \dot{\theta}\dot{\phi}\cos 2\phi\right] - I_{xx}\dot{\theta}\dot{\phi} = N \cos \phi + M \sin \phi \end{aligned}$$

where the productive moment of inertia I_{zx} is neglected

On the other hand, the force and moment acting on a ship which moves in free water surface are decomposed into the hydrostatic force including Froude-Krylov force and the hydrodynamic force consisting of the added mass and damping force.

The hydrostatic force and moment may be obtained by integrating the pressure p over the entire wetted surface of the ship. By applying Gauss's theorem, the force and moment are given by integrals of the pressure gradient over the submerged volume V of the ship. The components of the force and moment in the body axes G - x, y, z are

Froude-Krylov forces

$$\begin{aligned} X_{F.K}(\xi_G, \zeta_G, \psi, \theta, \phi) &= \iiint_V \frac{\partial p}{\partial x} dV \\ Y_{F.K}(\xi_G, \zeta_G, \psi, \theta, \phi) &= \iiint_V \frac{\partial p}{\partial y} dV \\ Z_{F.K}(\xi_G, \zeta_G, \psi, \theta, \phi) &= \iiint_V \frac{\partial p}{\partial z} dV \end{aligned} \quad (9)$$

and Froude-Krylov moments

$$\begin{aligned} K_{F.K}(\xi_G, \zeta_G, \psi, \theta, \phi) &= \iiint_V \left(\frac{\partial p}{\partial z} y - \frac{\partial p}{\partial y} z \right) dV \\ M_{F.K}(\xi_G, \zeta_G, \psi, \theta, \phi) &= \iiint_V \left(\frac{\partial p}{\partial x} z - \frac{\partial p}{\partial z} x \right) dV \\ N_{F.K}(\xi_G, \zeta_G, \psi, \theta, \phi) &= \iiint_V \left(\frac{\partial p}{\partial y} x - \frac{\partial p}{\partial x} y \right) dV \end{aligned} \quad (10)$$

The hydrostatic pressure p including that of a sinusoidal wave ζ_w

$$\zeta_w = a \cos k(\xi - ct) \quad (11)$$

at any time t and position ξ in the space fixed axes O - ξ, η, ζ is given by

$$p = \rho g \zeta - \rho g a \cos k(\xi - ct) \quad (12)$$

where ρ is the density of water, k is wave number, a is the amplitude of the wave and c is the phase velocity of the wave. In Equation (12), the so-called Smith's effect due to the orbital motion of water particles is neglected. Since set of transformation between the space and body axes is

$$\begin{aligned} \xi - \xi_G &= x \cos \psi \cos \theta + y (\cos \psi \sin \theta \sin \phi - \sin \psi \cos \phi) + z (\cos \psi \sin \theta \cos \phi + \sin \psi \sin \phi) \\ \eta - \eta_G &= x \sin \psi \cos \theta + y (\sin \psi \sin \theta \sin \phi + \cos \psi \cos \phi) + z (\sin \psi \sin \theta \cos \phi - \cos \psi \sin \phi) \\ \zeta - \zeta_G &= -x \sin \theta + y \cos \theta \sin \phi + z \cos \theta \cos \phi \end{aligned} \quad (13)$$

ξ and ζ can approximately written in the forms

$$\begin{aligned}\xi - \xi_G &\doteq x \cos \psi - (y \cos \phi - z \sin \phi) \sin \psi \\ \zeta - \zeta_G &\doteq -x \theta + y \sin \phi + z \cos \phi\end{aligned}\quad (14)$$

Accordingly, the expression of the pressure p in the body axes is obtained as follows

$$\begin{aligned}p &= \rho g (\xi_G - x\theta + y \sin \phi + z \cos \phi) \\ &\quad - \rho g a \cos [\xi_G + x \cos \psi \\ &\quad - (y \cos \phi - z \sin \phi) \sin \psi - c t]\end{aligned}\quad (15)$$

Substituting Equation (15) into Equations (9) and (10), Froude-Krylov forces and moments are computed as a function of ξ_G , θ , ϕ and ψ .

Hydrodynamic Forces

As mentioned previously, it is still difficult to evaluate the hydrodynamic coefficients for large amplitude motions. In following seas, the encounter frequency is very low and the dynamic effects associated with added mass and damping are considerably small and stationary. So, as a first approximation, the results based on the linearized theory may be available.

The hydrodynamic forces for maneuvering motion can be estimated from Motora's chart for the added masses and Inoue's practical formulas for the hydrodynamic derivatives of sway and yaw as follows:

$$\begin{aligned}Y(\dot{V}, V, \dot{\psi}) \cos \phi - Z(\dot{V}, V, \dot{\psi}) \sin \phi \\ = -m_y \dot{V} - Y_v V + Y_r \dot{\psi}\end{aligned}\quad (16)$$

$$\begin{aligned}N(V, \dot{\psi}, \psi) \cos \phi + M(V, \dot{\psi}, \psi) \sin \phi \\ = -J_{zz} \ddot{\psi} - N_r \dot{\psi} - N_v V\end{aligned}$$

$$\begin{aligned}m_y &= \frac{\pi}{2} \rho d^2 \int_L C(x) dx \\ J_{zz} &= \frac{\pi}{2} \rho d^2 \int_L x^2 C(x) dx\end{aligned}\quad (17)$$

$$\begin{aligned}Y_v &= \frac{1}{2} \rho L d U \left(\frac{1}{2} \pi k + 1.4 C_b \frac{B}{L} \right) \\ N_v &= \frac{1}{2} \rho L^2 d U k \\ Y_r &= -\frac{1}{2} \rho L^2 d U \frac{\pi}{4} k \\ N_r &= \frac{1}{2} \rho L^3 d U (0.54 k - k^2)\end{aligned}\quad (18)$$

where Y_v, N_v, Y_r and N_r denote the Hydrodynamic derivatives, k is the aspect ratio of ship $2d/L$ and $C(x)$ the added mass coefficient of Lewis form section.

The hydrodynamic coefficients for seakeeping motion can be estimated from Tasai's practical formula. In this case, it is necessary to express the equations of coupled motion of heaving and pitching in terms of the orientation parameter ξ_G and θ , an expression must be found for W as

$$W = \xi_G + U \theta \quad (19)$$

According to Tasai's practical formulas, the hydrodynamic coefficients of heave and pitch are given as

$$\begin{aligned}Z_{Hy}(\xi_G, \dot{\xi}_G) \cos \phi + Y_{Hy}(\xi_G, \dot{\xi}_G) \sin \phi \\ = -m_z \ddot{\xi}_G - Z_w \dot{\xi}_G \\ M_{Hy}(\ddot{\theta}, \dot{\theta}) \cos \phi - N_{Hy}(\ddot{\theta}, \dot{\theta}) \sin \phi \\ = -J_{yy} \ddot{\theta} - M_q \dot{\theta}\end{aligned}\quad (20)$$

$$\begin{aligned}m_z &= 0.8(B/2d)(\Delta/g)C_w \\ J_{yy} &= 0.83(B/2d)C_p^2(0.25L)^2(\Delta/g) \\ Z_w &= [5.4(C_w/C_p)(B/2d)^{1/2} \\ &\quad - 4.7] \Delta/(gL)^{1/2} \\ M_q &= 0.08(B/2d)\Delta L^2/(gL)^{1/2}\end{aligned}\quad (21)$$

where L denotes ship length, B breadth, d draft, Δ the displacement, C_w water plane area coefficient and C_p prismatic coefficient.

The hydrodynamic moment of roll motion can be described in the approximate equation

$$K_{Hy}(U, \ddot{\phi}, \dot{\phi}) = -J_{xx} \ddot{\phi} - K_{\phi} \dot{\phi} \quad (22)$$

and the damping coefficient K_{ϕ} is given by Takahashi's formula taking into account the effect of ship speed U as follows:

$$\begin{aligned}K_{\phi} &= 2(I_{xx} + J_{xx})[1 + 0.8(1 - e^{-10Fn})] \\ \alpha_e &= \frac{2\pi}{T} N_{\phi m} \\ T &= \frac{2.01 k_{xx}}{GM^{1/2}}\end{aligned}\quad (23)$$

where α_e is the equivalent damping

coefficient, F_n the Froude number, N the extinction coefficient equal to 0.02, ϕ_m the equivalent heel angle, T the natural frequency of roll and k_{xx} the radius of gyration equal to 0.35B

The resistance in the surge motion is based on the instantaneous forward velocity. Assuming that the thrust is constant, the relation between the resistance and thrust can be expressed by

$$T(1-t)-R=\frac{1}{2}\rho C_t S U_0^2[1-(\frac{U}{U_0})^2] \quad (24)$$

where T is the thrust, t the thrust reduction, R the resistance, C_t the total resistance coefficient, S the wetted surface of hull, and U_0 the initial forward velocity of ship.

Substituting the results of the Froude-Krylov forces and hydrodynamic forces into Equations (7) and (8), the equation of motion with respect to the horizontal body axes can be described as follows:

Translate motions and forces

$$\begin{aligned} m(\ddot{U}-V\dot{\psi}+\xi\dot{\theta}+U\dot{\theta}^2) &= -m_x\ddot{U}+m_yV\dot{\psi}-m_z(\xi_G+U\dot{\theta})\dot{\theta} \\ &+X_{FK}(\xi_G,\zeta_G,\psi,\theta,\phi)+T(1-t)-R \\ m(\ddot{V}+U\dot{\psi}) &= -m_y\ddot{V}-m_xU\dot{\psi}+Y_vV+Y_r\dot{\psi} \\ &+Y_{FK}(\xi_G,\zeta_G,\psi,\theta,\phi)\cos\phi \\ &-Z_{FK}(\xi_G,\zeta_G,\psi,\theta,\phi)\sin\phi \\ m\ddot{\xi}_G &= -m_z\ddot{\xi}_G-Z_w\dot{\xi}_G \\ &+Z_{FK}(\xi_G,\zeta_G,\psi,\theta,\phi)\cos\phi \\ &-Y_{FK}(\xi_G,\zeta_G,\psi,\theta,\phi)\sin\phi \end{aligned} \quad (25)$$

Angular motions and moments

$$\begin{aligned} I_{xx}\ddot{\psi}-(I_{yy}-I_{zz})[\frac{1}{2}(\dot{\psi}^2-\dot{\theta}^2)\sin 2\phi &+ \dot{\theta}\dot{\psi}\cos 2\phi] \\ &= -J_{xx}\ddot{\psi}-K_{\phi}\dot{\phi}+K_{FK}(\xi_G,\zeta_G,\psi,\theta,\phi) \\ &- \rho \nabla B G \sin\phi \\ (I_{yy}\cos^2\phi+I_{zz}\sin^2\phi)\ddot{\theta} &+ (I_{yy}-I_{zz})[\frac{1}{2}(\dot{\psi}^2-\dot{\phi}^2)\sin 2\phi \\ &+ \dot{\phi}\dot{\psi}\cos 2\phi]+I_{xx}\dot{\phi}\dot{\psi} \\ &= -J_{yy}\ddot{\theta}-M_{\phi}\dot{\phi}+M_{FK}(\xi_G,\zeta_G,\psi,\theta,\phi)\cos\phi \\ &- N_{FK}(\xi_G,\zeta_G,\psi,\theta,\phi)\sin\phi \\ (I_{zz}\cos^2\phi+I_{yy}\sin^2\phi)\ddot{\phi} & \end{aligned}$$

$$\begin{aligned} &+ (I_{yy}-I_{zz})[\frac{1}{2}(\dot{\theta}^2-\dot{\phi}^2)\sin 2\phi \\ &+ \dot{\theta}\dot{\phi}\cos 2\phi]-I_{xx}\dot{\theta}\dot{\phi} \\ &= -J_{zz}\ddot{\phi}+N_r\dot{\psi}+N_vV \\ &+ N_{FK}(\xi_G,\zeta_G,\psi,\theta,\phi)\cos\phi \\ &+ M_{FK}(\xi_G,\zeta_G,\psi,\theta,\phi)\sin\phi \end{aligned} \quad (26)$$

3. COMPARISONS BETWEEN SIMULATION AND EXPERIMENT

In the basis of the mathematical model introduced in the previous section, the numerical time domain computations are carried out for the 5000GT class of container ship. Characteristics of the ship and stability curves at the crest of a wave amidship are shown in Fig.3. Two examples of motion are compared with the observations of free running model experiments. In this computation, the equations of motion are solved by numerical integration in the time domain. The integration is performed by using standard algorithms to integrate the equation leading to a step-by-step approximation of the ship motion.

	Ship	Model
L (m)	115.	2.5
B (m)	19.	.413
d (m)	6.4	.139
V (m ³)	9859.	.101

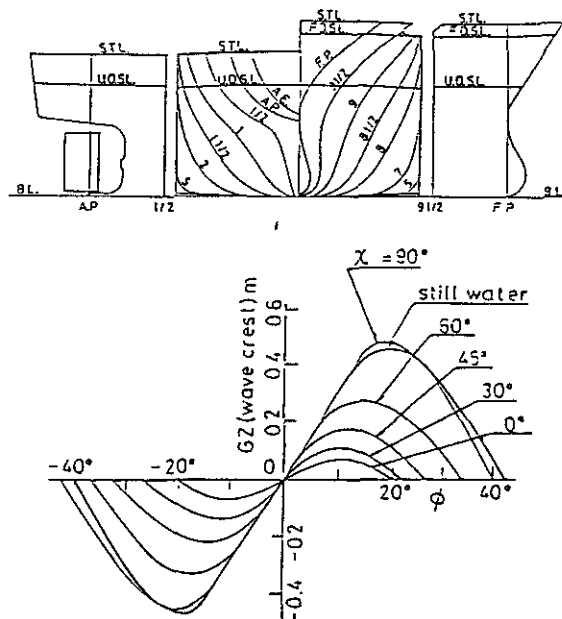


Figure 3. Principal dimensions and stability curves of the ship

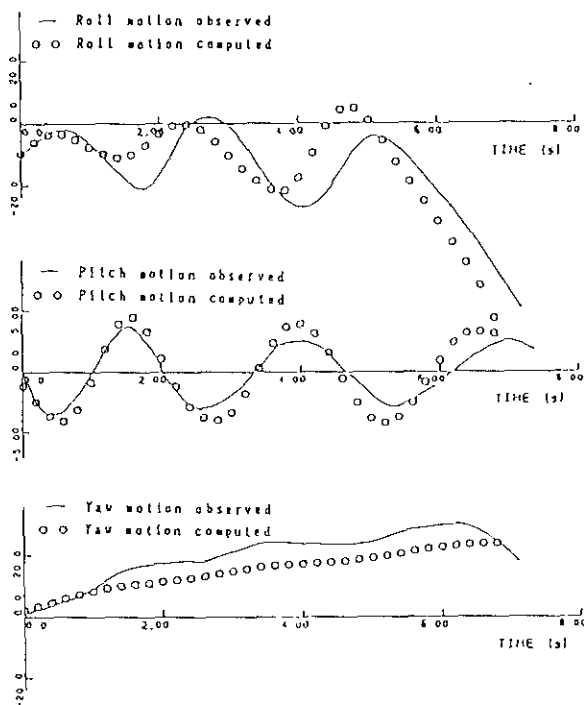


Figure 4. Time domain simulations of roll, pitch and yaw (capsized)

The first example shown in Fig.4 is for the model capsized in following waves, of which the wave length to ship length ratio is equal to 1 and the wave height to wave length ratio $1/25$. The initial heel angle is 9.5 degrees to port. The pitch recorded may be used to judge the number of wave encounters. In this example, rolling frequency is about the same as that of the wave encounter frequency and rolling amplitude builds up rapidly with the heading deviation to starboard. The model capsizes to port when the wave crest came amidship.

The next example shown in Fig.5 is for the model not capsized in quartering waves, where the wave to ship length ratio is about the same as the first example but the wave height to wave length ratio is $1/30$. The initial heading angle is 17 degrees to starboard and the model is travelling in the same direction. Rolling again occurs at the wave encounter frequency. The amplitude is gradually decreased and appears to be stabilized there after. Numerical simulations seem to be in good agreement with the observations of free running model experiments. This may give us a cue for analyzing the capsize of ship in severe following seas, even if examples are a few in this stage.

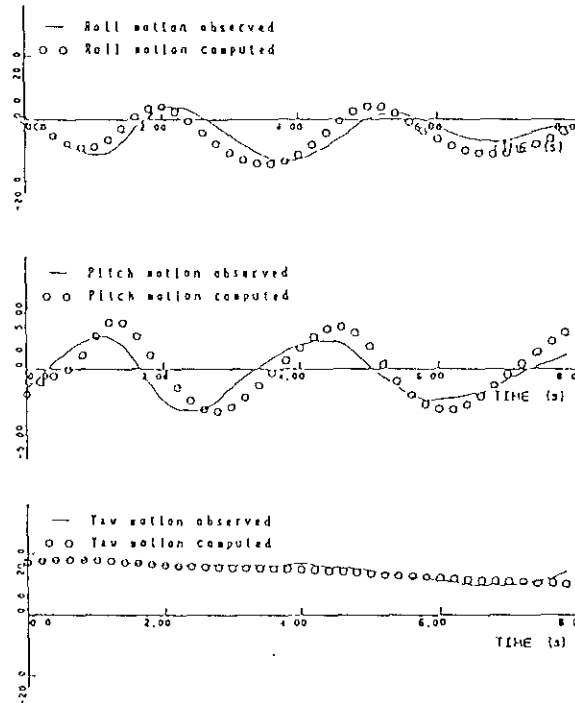


Figure 5. Time domain simulations of roll, pitch and yaw (not capsized)

4. NUMERICAL SIMULATIONS FOR SEVERAL HULL FORMS

Four different hull forms have been chosen for the comparative study. Ship A shown in Fig.6 has a container hull form with bulbous bow and long parallel body. Ships B, C and D shown in Fig.6 represent conventional hull forms of fishing boat. Ship B has the smallest freeboard in three fishing boats, Ship C the middle one and Ship D the largest one. Fig.7 shows the form stability curves BR and the trajectories of center of buoyancy for each ship respectively. And also, while the crest of a wave is amidship, reduction of the form stability is relatively large for Ship B, small for ship D and not so much small for Ship A and C. Reductions of the form stability BR are computed for those ships in cases that wave height to length ratio is equal to $1/20$ and wave length to ship length ratio 1.

Numerical simulations of ship motion are carried out to find the critical metacentric height GM leading to capsizing in several ship speeds. Time histories similar to ones shown in Fig.4 and 5 are obtained from this numerical simulation instead of experiment, to judge whether a

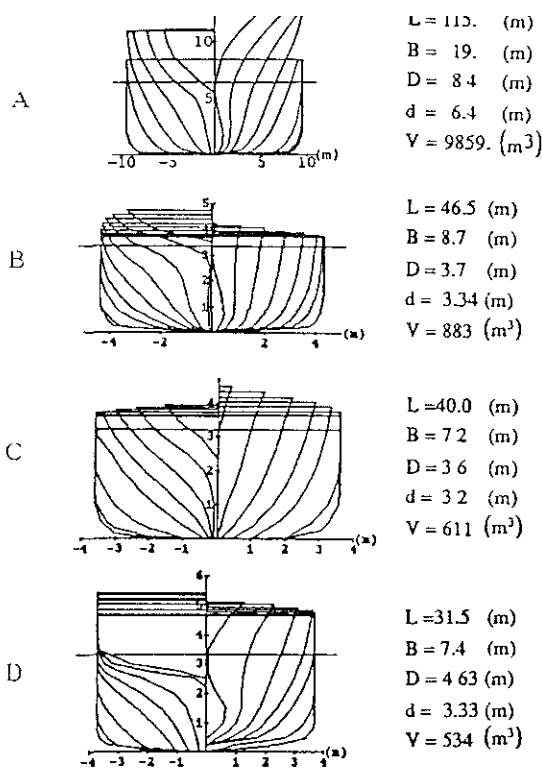


Figure 6. Studied hull forms

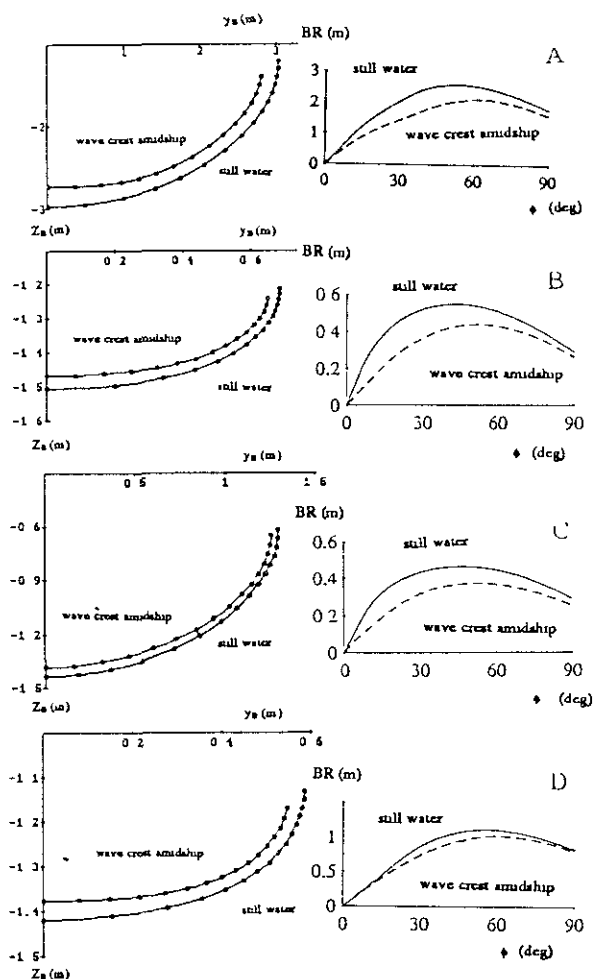


Figure 7. Trajectories of center of buoyancy and form stability curves

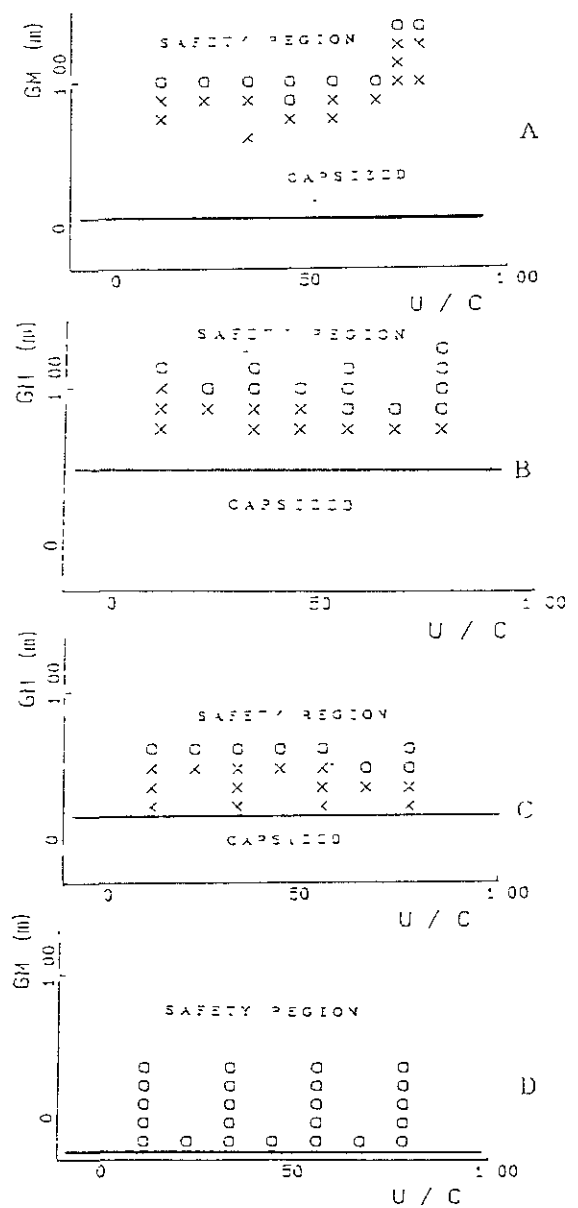


Figure 8. Critical metacentric height of four different ships

ship capsizes or not. For the cases of different metacentric height and forward velocity of a ship. Accordingly, the results capsized or not are obtained for different hull forms as shown in Fig.8. In this figure, circle marks indicate the case not capsized, cross marks the case capsized and solid lines the weather criterion satisfying IMO Resolution A562. From the comparison of different hull forms following things are found. Despite Ship A, B and C satisfy the weather criterion A562 in beam sea condition, they capsize in severe following sea condition that the wave height to length ratio equal to 1/20 and wave to ship length ratio 1. But ship D is safe in both condi-

tions.

In regular waves with length equal to the ship length, the reduction of BR at wave crest amidship for Ships A,B and C are much larger than Ship D with a large freeboard. The magnitude of the reduction significantly depends on the freeboard and hull form. The ships motions leading to capsizing seem to be significantly affected by the reduction, metacentric height and ship speed.

5. CONCLUDING REMARKS

The equations of motion with respect to the horizontal body axes are presented to describe the ship motions leading to capsizing in severe following seas. The simulations of ship motion are performed with a quasistatic time step procedure that takes into account non-linear instantaneous buoyancy, linear damping and added mass forces. And also simulated time histories of ship motion are in fairly good agreement with the experimental results.

The comparative study carried out here for four different hull forms shows that the critical metacentric height leading to capsizing has significant effect on the loss of stability, hull form and speed of the ship travelling with a high Froude number, close to 0.4 as for phase velocity of wave.

REFERENCES

1. Watanabe, Y., On the Dynamic Properties of the Transverse Instability of a ship due to Pitching, J. of Soc. of Naval Arch., Vol.53, 1934.
2. Grim, O., Rollschwingungen, Stabilität und Sicherheit im Seegang, Schiffstechnik, 1952.
3. Kerwin, J.E., Notes on roll in longitudinal waves, I.S.P., Vol.2 (16), 1955.
4. Motora, S., On the Measurement of Added Mass and Added Moment of Inertia for Ship Motion, J. of Soc. of Naval Arch., Vol.105-107, 1959, 1960.
5. Paulling, J.R., The Transverse Stability of a Ship in a Longitudinal Seaway, J. of Ship Research, SNAME, Vol.4, No.1, March, 1961.
6. Dr-Ing. O. Grim, Beitrag zu dem problem der Sicherheit des Schiffes in Seegang, Schiff und Hafen, heft 6, 1961.
7. Du Cane, P., Goodrich, G.G.J., The Following Sea, Broaching and Surging, Trans.RINA, Vol.104, April, 1962.
8. Boses, P., Steuern eines Schiffes im Schweren Achterlichen Seegange, J.S.T.G., Bd, 1971.
9. Price, W.G., The Stability of Ship in a Simple Sinusoidal Wave, J. of Mechanical Engineering Science, Vol.14, 1972.
10. Chou, S. J., Oakely, O.H., Paulling, J. R., Van Slyke, R., Wood, P.D., Zink, V.F., Ship Motions and Capsizing in Astern Seas, Dep. of Transportation United States Coast Guard, Rep. No. CG-D-103-75, 1974.
11. Remilson, M.R., Driscoll, A., Broaching- an Investigation into the Loss of Directional Control in Severe Following Seas, Spring Meeting RINA, 1981.
12. Motora, S., Fujino, M., Fuwa, T., On the Mechanism of Broaching-to Phenomena, STABILITY'82, 1982.
13. Hamamoto, M., Nomoto, K., Transverse Stability of Ship in a Following Sea, STABILITY'82, 1982.
14. Hamamoto, M., Transverse Stability of Ship in a Quartering Sea, STABILITY '86, 1986.
15. Ohkusu, M., Prediction of Wave Forces in a ship Running in Following Waves with Very Low Encounter Frequency, J. of Soc. of Naval Arch. Vol.159, 1986.
16. Hamamoto, M., Akiyoshi, T., Study on Ship Motions and Capsizing in Following Seas (1st Report), J. of Soc. of Naval Arch., Vol.163, 1988.
17. Kuo, C., Vassalos, D., The Strathclyde Approach to Practical Ship Stability Criteria, Workshop on Stability, Germanischer Lloyd, 1984.
18. Tasai, F., Damping Force and Added Mass of Ships Heaving and Pitching (Continued), Trans. of the West-Japan Soc. of Naval Arch., Vol.21, 1961
19. Prediction of Ship Manoeuvrability and its Applications, 4th Marine Dynamics Symposium, 1987.
20. Jan G. de Kat, J.Randolph Paulling, The Simulation of Ship Motions and Capsizing in Severe Seas, The Society of Naval Architects and Marine Engineers, 1989.

by Hisayoshi Tatano*, Jin Ahn Kim**, Yoon Soo Kim***

ABSTRACT

As well known, when a ship comes into the crest of a wave, the center of buoyancy moves to upward from the position of that in still water and then form stability are considerably reduced. The form stability depends on location of center of buoyancy and the location is affected by principal dimensions and hull forms of ship. From such a point of view, several kinds of ships are chosen for this study. These trajectories are quite similar to ellipses and the long and short axes of the ellipses were represented as linear functions of a newly defined hull form parameter, F_E/d . Through the trajectories, the amount of pure loss of stability were also obtained for each ship.

1. INTRODUCTION

There are some approaches for the pure loss of stability of ships at wave crest amidship. In early 1961, Pauling already showed us remarkable reductions of righting arm of Series 60.¹⁾ Lately, Hamamoto and Akiyoshi have discussed on the pure loss of stability of ships in quartering seas and showed a way to obtain righting arms of ship in a following wave.²⁾ The results says that the severe loss of stability occurs at the crest of a wave of which length equals to the ship length. Huss studied on the variation of initial stability of large modern ships in waves.³⁾ The study shows that both, the sectional forms of the hull and the breadth and draft ratio has a significant influence on the stability in a wave. As well known, when a ship comes into the crest of a wave, the center of buoyancy moves to upward from the position of that in still water and then form stability are considerably reduced. The

purpose of this paper is to obtain trajectories of center of buoyancy of ships at wave crest amidship of which length equals to the ship length and height is fixed as $1/20$ of wave length and trajectories were represented as a function of hull form parameters.

2. COMPUTATION FOR LOSS OF STABILITY

In order to compute loss of stability, space fixed axes and body axes are used. As shown in Fig. 1, a co-ordinate system, $0-\xi, \eta, \zeta$ is fixed in space with the origin O located at an arbitrary point in the calm water surface. In the system, a sinusoidal wave ζ_W is expressed as:

$$\zeta_W = a \cos k(\xi - ct) \quad (1)$$

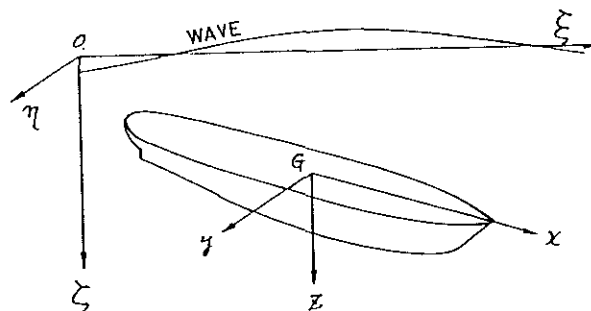


Figure 1. Two co-ordinate systems

where, ζ_W = instantaneous wave height at a certain time, t

* Dept. of Naval Architecture and Ocean Engineering, Osaka University, Japan

** Department of Naval Architecture, Pusan National University, Korea

*** Graduate School, Department of Naval Architecture and Ocean Engineering, Osaka University, Japan

c = phase velocity of the wave

The origin of the body co-ordinate system, $G - x, y, z$ is fixed at the center of gravity. Transformation set between the space and the body axes are as follows:

$$\begin{aligned}\xi - \xi_G &= X \cos \psi \cos \theta \\ &\quad + Y (\cos \psi \sin \theta \sin \phi - \sin \psi \cos \phi) \\ &\quad + Z (\cos \psi \sin \theta \cos \phi + \sin \psi \sin \phi) \\ \eta - \eta_G &= X \sin \psi \cos \theta \\ &\quad + Y (\sin \psi \sin \theta \sin \phi + \cos \psi \cos \phi) \quad (2) \\ &\quad + Z (\sin \psi \sin \theta \cos \phi - \cos \psi \sin \phi) \\ \zeta - \zeta_G &= -X \sin \theta + Y \cos \theta \sin \phi + Z \cos \theta \cos \phi\end{aligned}$$

where, ψ, θ, ϕ : Euler's angles between the
two co-ordinate systems.

For a displacement type ship, the pitching angle θ is very small. Thus, Formula (2) can be represented in the approximate forms:

$$\begin{aligned} \xi - \xi_G &\doteq x \cos \psi - (y \cos \phi - z \sin \phi) \sin \psi \\ \zeta - \zeta_G &\doteq -x \theta + y \sin \phi + z \cos \phi \end{aligned} \quad (3)$$

Substituting Formula (3) into (1), the wave height is represented by the body axes as follows:

$$\xi_W = a \cos[\xi_G + x \cos\psi - (y \cos\phi - z \sin\phi) \sin\psi - ct] \quad (4)$$

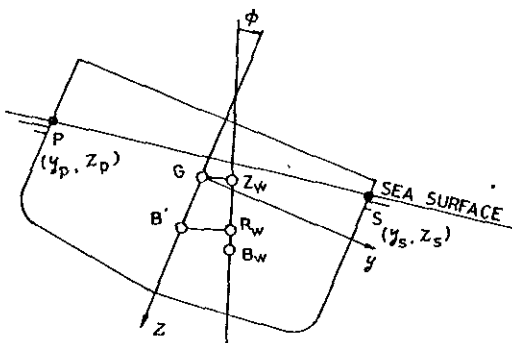


Figure 2. Cross section in wave

In this case, as shown in Fig.2, $P(y_p, z_p)$ and $S(y_s, z_s)$ are exact intersections with wave surface at starboard and portside. Substituting Formula (4) into the second Formula of (3) with the $P(y_p, z_p)$ and $S(y_s, z_s)$, the following Formula is obtained

$$\begin{aligned} \zeta_W(y_P, z_P) &= \zeta_G^{-x} \theta + y_P \sin \phi + z_P \cos \phi \\ \zeta_W(y_S, z_S) &= \zeta_G^{-x} \theta + y_S \sin \phi + z_S \cos \phi \end{aligned} \quad (5)$$

Gradients of water pressure acting on the hull surface of an immersed body differ slightly from the case of still water. This difference is caused by the orbital motions but this might be thought as negligibly small. Accordingly, the following Formulas are obtained:

$$\int_L A(x) dx - \nabla = 0 \quad (6)$$

$$\int_L x A(x) dx - \nabla B \cdot G \sin \theta = 0$$

where, $A(x)$ = sectional area as a function of x

∇ = displacement volumes

θ = trim angle

The first Formula of (6) shows a balance in the displacement of ship while the other one shows moment respectively.

When a ship is inclined in the wave, (y_B, z_B) is the position of the center of buoyancy of the ship. Thus the GZ_w as

$$GZ_H(\phi) = y_B \cos \phi - z_B \sin \phi \quad (7)$$

Then, BR_w becomes

$$BR_W(\phi) = y_B \cos \phi - z_B \sin \phi + BG \sin \phi \quad (8)$$

As shown in Fig. 3, GZ and GZ_w are obtained as follows

$$\begin{aligned} GZ &= BR - BG \sin \phi \\ GZ_w &= BR_w - BG \sin \phi \end{aligned} \quad (9)$$

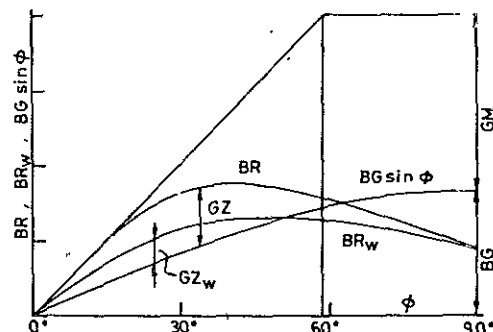


Figure. 3 Relations among BG, GM, GZ, GZ_W
BR and BR_W

The BR and BR_H depend on the ship's hull form and dimensions. $BG\sin\phi$ depends by the height of the center of gravity of the ship.

3. CENTER OF BUOYANCY IN STILL WATER AND AT WAVE CREST AMIDSHIP

Computations mentioned in the previous section were performed for 10 ships, 3 containers, 1 passenger and 6 small sized ships. Fig. 4 shows body plans with principal dimensions of the ships. In this figure, F_E/d for all ships are also shown.

Locations of the center of buoyancy were obtained as shown in Fig. 5. All of the trajectories of center of buoyancy look like ellipses. In cases of wave crest amidship, trajectories are slightly smaller than the ones for still water but shapes are quite similar with the ones for still water. In Fig. 6, ellipses are shown with dotted lines for Ship E and there are very small differences between the trajectories of center of buoyancy and ellipses. This fact shows that shapes of computed trajectories are in good agreement with real ellipses.

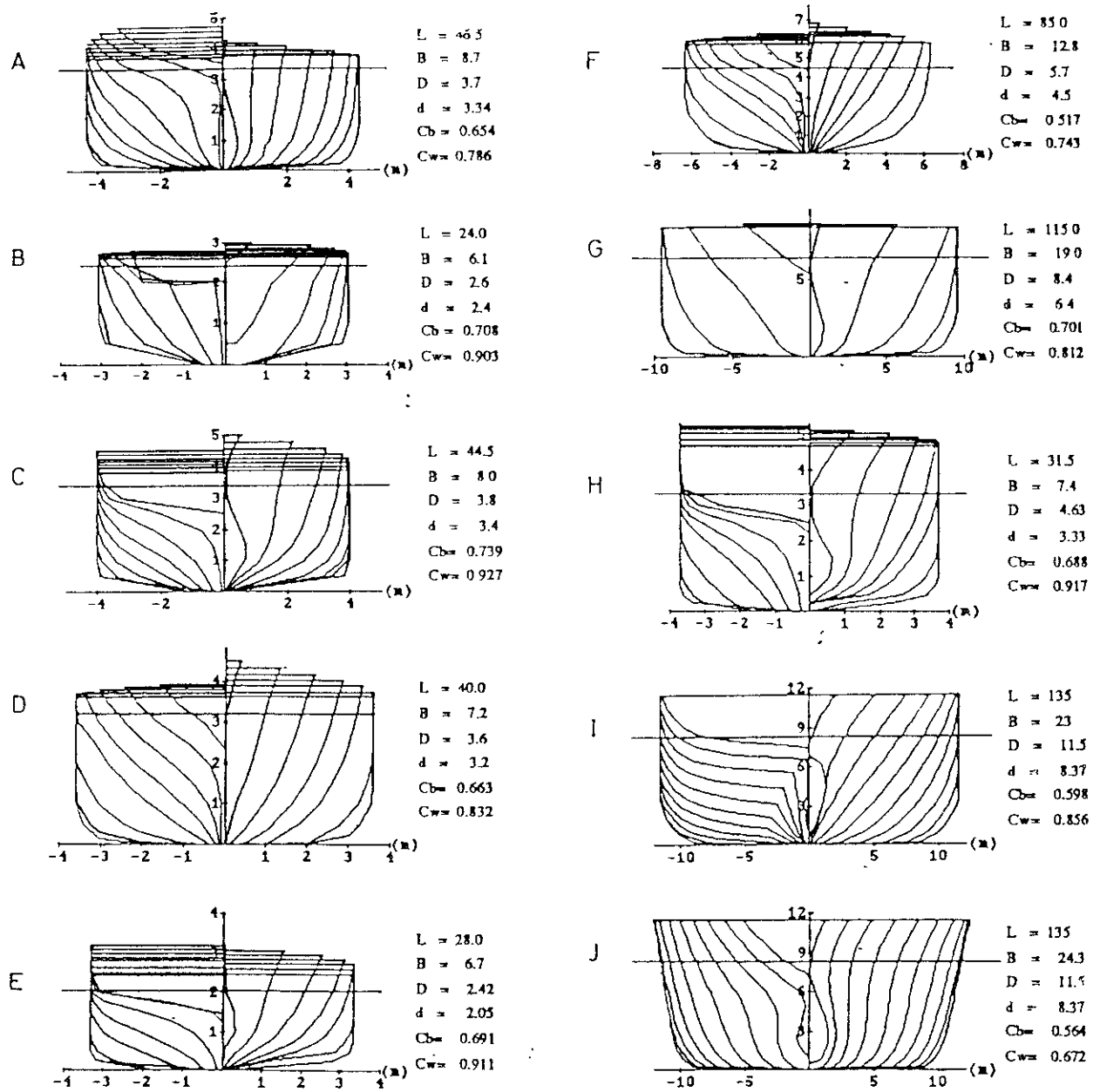


Fig. 4 Body plan, principal dimensions and F_E/d for all ships

typical ships.

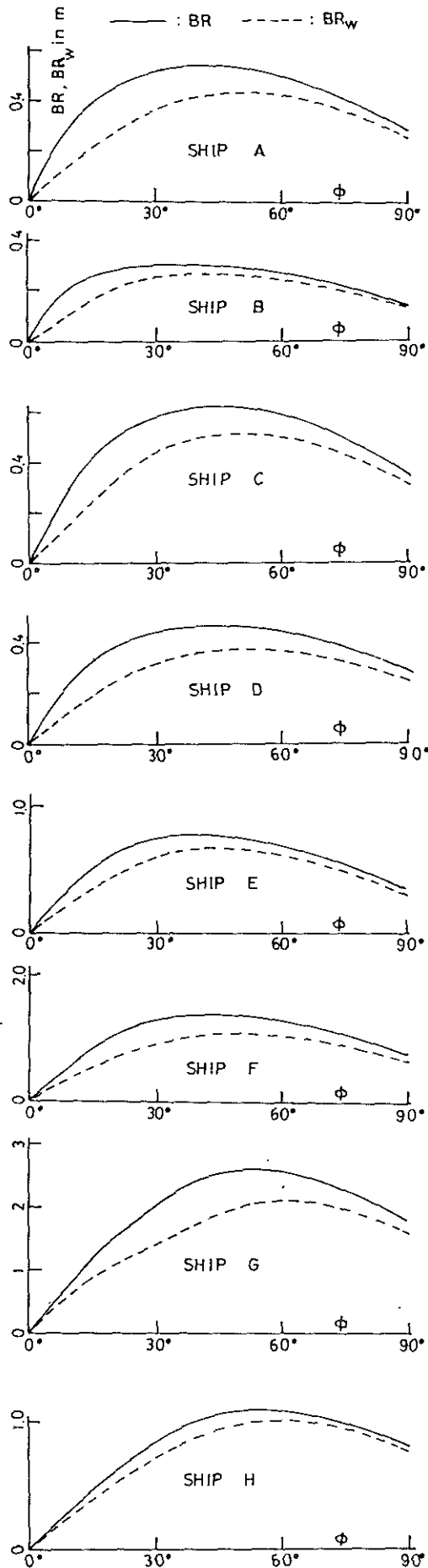


Fig. 10 BR and BR_W curve for Ships A - H

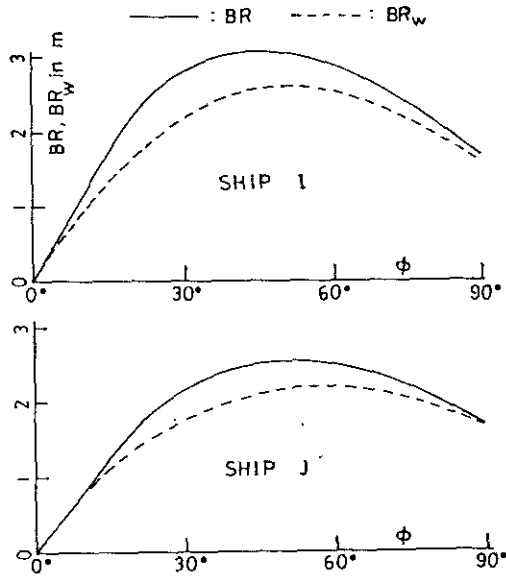


Fig 11. BR and BR_W curve for Ships I and J

Table 1 shows hull form parameters for Ship B and H. Even though most of parameters show similar values each other, Ship B shows small BR and BR_W , and Ship H shows large. For this reason, the difference of F_E/d is thought.

Table 1. L and some hull form parameters for Ships B and H

SHIPS	L m	L/B	B/d	BM/B	C_B	C_W	F_E/d
B	24.0	3.93	2.54	.24	.708	.902	.112
H	31.5	4.26	2.22	.23	.691	.911	.474

Table 2 is for Ships I and J which have similar dimensions each other but different frame line shapes. In these cases, Ship I has larger breadth and C_W than them of Ship J. Therefore, BR and BR_W for Ship I shows larger values than Ship J.

Table 2. L, B and some hull form parameters for Ships I and J

SHIPS	L m	B m ¹⁾	L/B	B/d	C_B	C_W	F_E/d
I	135	230	5.87	2.75	.598	.856	.381
J	135	222	6.08	2.65	.617	.736	.386

1) : BREADTH AT WATER LINE

At wave crest amidship with small inclined angles, Ship J which has unconventional frame lines inclined to outsides, the breadth of water line at around amidship

increases slightly while decreasing at the bow and stern. Accordingly, the moment of inertia of water plane will increase at around amidship while decrease at the bow and stern. As the results, there are no change on the amounts of moment of inertia of water plane and then BR and BR_w are almost the same.

5. CONCLUSION

Computations were performed for 10 ships in the most severe condition, at wave crest amidship, where the wave length equals to the ship length and the wave height ratio, $1/20$ is used. By comparing with the other results obtained in still water, the following conclusions can be made.

1) Trajectories of the center of buoyancy are obtained for still water and at wave crest amidship. Shapes of these trajectories are quite similar to ellipses and non-dimensional long and short axes can be represented as a linear function of F_E/d . F_E/d is a newly defined hull form parameter which means a ratio of effective freeboard to draft.

2) Horizontal levers, BR and BR_w were obtained through the trajectories of the center of buoyancy. The difference between the two is the pure loss of transverse stability for the most severe condition of wave crest amidship.

ACKNOWLEDGEMENT

Acknowledgement is made of professor M. Hamamoto of Osaka University for his invaluable advices.

REFERENCES

1. J. R. Paulling : Transverse Stability of a Ship in a Longitudinal Sea Way, Jour. of Ship Research, SNAME, Vol. 4, No. 4, March, 1961
2. M. Hamamoto and T. Akiyoshi : Pure Loss of Stability of Ships in a Quartering Sea and Its Theoretical Prediction, Jour. of Kansai Society of Naval Architects, Japan No. 205, June 1987 in Japanese
3. Mikael Huss : The Stability of Ships in Wave ; A Comparative Study of Modern Hull Forms with Large B/T Ratio, Report TRITA-SKP 1060, The Royal Institute of Technol-

ogy, Devision of naval architecture,
STOCKHOLM, Sweden

INDEX

AUTHOR'S INDEX

Abicht W.	117
Acharrya S.	287
Adee Bruce H.	620
Ahn Kim J.	362
Alexander J.M.	142
Alexandrov M.	512
Amagai Kiyoshi	175
Armenio V.	401
Arndt B.	487
Balestrieri R.	573
Bardis L.	493
Bass D.W.	217
Bishop Red	150
Blume P.	452
Boccardo G.	556
Bogdanov P.	409
Boroday I.K.	441
Brook A.K.	253
Burcher R.K.	82
Cao Zhenai	167
Carrigan P.L.	307
Cassella P.	556
Cumming D.	159
Dahl S.	191
Dahle E.	191
Dimitrova S.	283, 409
Don Lei Yuan	51
Falzarano J.	565, 647
Frakowiak M.	19
Francescutto A.	401
Fujii I.	378
Fujino M.	378
Gal A.	512
Graham A.	591
Graham R.	159
Grochowalski S.	470
Haddara M.R.	159
Hao Jin	51
Hamamoto M.	354
Hayden W.	535
Helas G.	543
Higashi S.	378
Higo Y.	239
Hirayama T.	287

Hodges S.	604
Holland D. J.	629
Hormann H.	548
Huang W.	247
Huang D.L.	102
Impagliazzo D.	573
Inoue Y.	295
Ishida S.	10
Jullumstroee E.	322
Kan M.	109, 90
Kaplan P.	125
Kaps H.	226
Kastner S.	226
Kimura N.	175
King B.	299
Kishev R.	283, 409
Kobylinski L.	501
Koskinas C.	344
Kuo C.	527, 653
Lipis V. A.	232
Lipis V.B.	66
Loukakis T.A.	493
Magill C.M.	629
Miller A.F.	416
Molinari R.	26
Myrhaug D.	191
Nabergoj R.	597
Nakato M.	378
Natchev R.	275
Nedrelid T.	208
Nehrling B.C.	433
Nekrasov V.	74
Noble P.G.	613
Ochi M.K.	315
Okuyama T.	378
Ozkan R.	460
Pantazopoulos J.	58
Papanikolau A.	344
Parker E.M.	535
Paulling J.R.	386, 395
Pawlowski J.S.	217
Plaza F.	1
Penno C.	26
Pergaev E.	40
Petey F.	267
Price W.G.	150
Quilan J.	247
Rainey R.C.	613
Rakhmanin N.	132
Rakitin V.	275
Randall G.	535
Remez Y.	98
Renilson M.R.	261

Rezzoagli C.	26
Salov V.	66
Saruta T.	109
Savvas J.	344
Semenov V.Y.	1
Shestopal V.	98
Shin C.	479
Shin J.S.	395
Shirai T.	354
Sizov V.	40
Soares G.C.	582
Soliman M.S.	183
Soo Kim Y.	362
Spencer J. S.	307
Spyrou K.	519
Standing R.G.	253
Stasiak J.	424
Steindl A.	647
Suzuki I.	378
Taguchi K.	109
Takaishi M.	10, 109
Takaki M.	239
Takezawa S.	287
Tam G.	613
Tatano H.	362
Taylan M.	32
Temarel P.	150
Thomas G.A.	261
Thompson J.M.T.	613
Tikka K.K.	386
Trincas G.	637
Troger H.	647
Troesch A.V.	565,
Trovao M.F.S.	647
Tsuchiya T.	582
Twizell E.H.	328
Tzvetanov Tz.	150
Umeda N.	275
Van Binh Ho	328, 336
Vassallo C.	19
Vassalos D.	573
Vermeer H.	142, 519, 527
Virgin L.N.	369
Voytkounski Y.	45
Vorobyov Yu	232
Vouros C.A.	40, 200
Wakiyama N.	493
Wu Z.	354
Yang Dibang	247
Yamakoshi Y.	247
Yasuno M.	328
Zaraphonitis G.	109
Zborowski A.	344
Zhukov Y.	32
	512

ARTI GRAFICHE LICENZIATO
Napoli - Via Pasquale Scura, 11
Tel. 081/551.26.56